Quantifying and upscaling surface and subsurface runoff and nutrient flows under climate variability

By

Vesna Tripkovic BSc MSc

School of Civil Engineering and Geosciences,
Newcastle University,
Newcastle upon Tyne,
NE1 7RU,
UK.

A thesis submitted for the Degree of Doctor of Philosophy (Ph.D) at Newcastle University

November 2013

Declaration

I certify that no part of the material offered in this thesis has been previously submitted by me for a degree or other qualification in this or any other University.

Vesna Tripkovic

Newcastle upon Tyne, UK

Abstract

Understanding and predicting the impacts of runoff on nutrients under different climate conditions within an unsaturated zone of soils is a fundamental challenge in hydrological research. The aim of this study is to provide new understanding of surface and subsurface hydrological controls on nutrient fluxes within mineral soils at the hillslope and catchment scales, and how these are influenced by climate variability.

The study covers three nested spatial scales: the Blind Beck catchment (9.2 km^2), the sub-catchment (0.09 km^2) and the plot scale (2 m^2) within the hillslope located in the Upper Eden basin, Cumbria, UK. The methodology combines field experiments and sampling, laboratory analysis and modelling approaches. Runoff experiments were conducted on two hillslope runoff plots to identify runoff processes and to quantify nutrient fluxes, one under perturbed (i.e. increased rainfall) and another under control plot. The SHETRAN physically-based hydrological model was then used to simulate runoff and nutrient flux for climate scenarios. These represent current and future (intensified hydrological cycle) conditions and were generated using the UKCP09 weather generator.

Analyses of flow for different climate conditions within the unsaturated zone suggested: i) overland flow varied from 14% in dry conditions (before treatment) to more than 64% in the enhanced rainfall conditions of the total measured overland flow, ii) lateral subsurface flow dominates hillslope runoff during the transition period, iii) overland flow occurs in the winter during periods of frozen soil as Hortonian flow and iv) nutrients were most concentrated in the topsoil. In extreme climate conditions, saturation excess overland flow is probably a major contributor to storm flow followed by the subsurface flow. The results have shown that sensitivity of different runoff processes to different types/size of storms can support analysis of impacts of enhanced climate variability. The enhanced rainfall treatment in the overland flow reduced the DOC concentration 1.7 times, while increasing the NO_3^- concentration 2.5 times. Under the enhanced rainfall treatment at the perturbed plot, C losses are lower in the overland flow (9.7 kg/ha) compared with the subsurface flow (22 kg/ha). This indicates enhanced loss of the DOC by the subsurface leaching pathway relative to losses through the overland flow. Decreases in the mean rainfall between 0.6% and 2.6% for the 2020 and

2050 period of the A1B emission scenario are modelled to decrease annual runoff 0.4% and 3.4 %. For the A1FI emission scenario, a decrease in rainfall between 1.2% and 3.2% is modelled to decrease annual runoff by 3.4% for the 2020 period and by 4.8% for the 2050 period.

Acknowledgements

Sincere thanks go to my supervisors Dr Geoff Parkin and Professor Thomas Wagner for their guidance, suggestions and support throughout this thesis. I also wish to thank my supervisors Professor Hayley Fowler and Professor Chris Kilsby for their help and guidance with climate change modelling. I would also like to thank Dr Stephen Birkinshaw for his assistance and guidance with SHETRAN modelling. Thanks also go to the farmer Mr Steve Wharton who allowed me to set up a hillslope experiment and do hydrometry on his land at Sykeside Farm.

I would like to thank the staff of Civil Engineering and Geosciences, Newcastle University for field and laboratory assistance during my research.

A final thank you goes to my family and friends for all their support throughout writing this thesis.

Abbreviations

AWS	Automatic Weather Station
BD	Soil Bulk Density
C	Carbon
CBE	Charge Balance Error
CEC	Cation-Exchange Capacity
CHASM	Catchment Hydrology And Sustainable Management
CPOM	Coarse Particulate Matter
DEFRA	Department for Environment, Food and Rural Affairs
DEM	Digital Elevation Model
DIN	Dissolved Inorganic Nitrogen
DO	Dissolved Oxygen
DOC	Dissolved Organic Carbon
DOM	Dissolved Organic Matter
DON	Dissolved Organic Nitrogen
DSC	Differential Scanning Calorimetry
EA	Environmental Agency
EC	Electrical Conductivity
EPA	Environmental Protection Agency
EU	European Union
FPOM	Fine Particulate Organic Matter
GCM	General Climate Model
GIS	Geographical Information System
HadRM3	Hadley Centre Regional Model
HF	Hydrofluoric Acid
HOST	Hydrology Of Soil Types
ICP	Inductively Coupled Plasma
IC	Inorganic Carbon
IPCC	Intergovernmental Panel on Climate Change
LAM	Limited Area Models
LCMGB	Land Cover Map of Great Britain database
Met Office	Meteorological Office
N	Nitrogen
NH_4NO_3	Ammonium Nitrate
NITS	Nitrate Integrated Transformation component for SHETRAN
NO_3^-	Nitrate

NVZ	Nitrate Vulnerable Zone
OC	Organic Carbon
OM	Organic Matter
P	Phosphorus
PDF	Probability Distribution Function
PET	Potential Evapotranspiration
PRMS	Precipitation-Runoff Modelling System
QMS	Quadrupole Mass Spectrometer
RCM	Regional Climate Models
SAAR	Standard Annual Average Rainfall (1961 – 1990)
SHE	Système Hydrologique Europèen
SOC	Soil Organic Carbon
SOM	Soil Organic Matter
SRES	Special Report on Emissions Scenarios
SSF	Subsurface Stormflow
SWAT	Soil and Water Assessment Tool
SWG	Stochastic Weather Generator
SZ	Saturated Zone
TAR	Third Assessment Report
TC	Total Carbon
TG	Thermogravimetry
TIN	Triangular Irregular Network
TN	Total Nitrogen
TOC	Total Organic Carbon
TP	Total Phosphorus
UK	United Kingdom
UKCIP	United Kingdom Climate Impact Programmes
UZ	Unsaturated Zone
WG	Weather Generator
WMO	World Meteorological Organization
WRSRL	Water Resources Systems Research Laboratory

Table of Contents

List of Figures

List of Tables

Chapter 1. Introduction

1.1 Problem statement

Projected future climate variability is expected to cause considerable changes in water quality, flow regime, nutrient flux and soil quality, with widely differing consequences for different regions and climate zones. In Europe it is predicted that more frequent extreme precipitation events are likely to increase, with implications for the leaching and mobilization of pollutants (organic matter and nutrients) from soils and overflows to water bodies (Solheim et al. 2010). This may result in (Solheim et al. 2010):

- *Increased water colour* in rivers, due to increased input of humic substances as dissolved organic carbon (DOC) from catchments,
- *Increased nutrient load* in rivers, due to increased mineralisation and releases of nitrogen, phosphorus and carbon from soil organic matter and enhanced runoff and erosion, and
- *Increased eutrophication* with more harmful algal blooms, reduced water transparency and declining oxygen concentration.

In 2008, DEFRA (The Department for Environment, Food and Rural Affairs, a government department in the UK) has identified an increased interest in UK soils that contain huge amounts of carbon as the major chemical constituent of organic matter (soil organic matter typically contains up to 58% carbon) and an essential component of functioning terrestrial ecosystems. Soil organic matter (SOM) increases the capacity of soils to bind chemicals, buffers the release of pollutants, regulates the supply of nutrients, improves soil structure and makes the soil more resistant to drought and erosion, but due to loss of soil carbon these soil functions will be detrimentally affected (DEFRA 2008). In some agricultural as well as upland organic (peat) soils there is evidence that carbon levels are indeed declining as a result of carbon dioxide that is being released into the atmosphere, contributing to global warming (DEFRA 2008). These observations indicate that climate change will lead to an increase in the loss of soil carbon and nutrients in the UK and many other parts of the world.

Intense agricultural activities are the major source of nutrients such as nitrogen (N) and phosphorus (P), in addition to natural sources such as atmospheric deposition. Increased mobilization of N and P through enhanced runoff directly leads to eutrophication in

streams. Solheim et al. (2010) point out that storm rainfall and snowmelt events increase the nitrate load to surface waters, as nitrate bypasses the biological sinks (Battarbee et al. 2008; Futter et al. 2009) resulting in a positive effect on nitrate leaching. On the other hand, decreasing precipitation may reduce downward infiltration and leaching. According to Davies et al. (2005) and Monteith et al. (2000) nitrate leaching has been shown to increase due to soil freezing and drought (Adamson et al. 1998), but the quantitative importance of these effects is still debated (Borken and Matzner 2009; Matzner and Borken 2008; Solheim et al. 2010).

Solheim et al. (2010) postulated that drought seasons and soil frost may stimulate DOC production through increased fine root and microbial mortality, increased fragmentation of soil organic matter and fresh litter, and increased aggregate instability (e.g. Fitzhugh et al. 2001; Lundquist et al. 1999; Schimel et al. 2007; Tierney et al. 2001). In recent years there has been considerable debate about the main drivers of the observed DOC increases including the role of climate in these trends (e.g. Evans et al. 2005; Freeman et al. 2001a; Freeman et al. 2004; Monteith et al. 2007; Tranvik and Jansson 2002). The discussion of control of climatic variables on the DOC concentrations and fluxes is still ongoing (Solheim et al. 2010). Climate change has already started to show impacts on the surface waters across Europe and on their biodiversity and ecological status, and it is expected that first symptoms will increase over the coming years. The urgent need to counteract these negative impacts of climate change on surface water processes and quality has recently been identified by the European Environmental Agency (Solheim et al. 2010).

To quantify catchment and hillslope scale nutrient fluxes and leaching from the soil, it is important to understand the processes of runoff generation. Recent research has focused on the rainfall-runoff relationship using hydrological modelling or field investigations. For a long time hydrologists have suggested that isolating definable catchment units is a valid approach to constrain and predict runoff (e.g. Sidle et al. 2000, McGlynn et al. 2004; van Verseveld 2007; Bier 2004). Bonell (1993) for example, argues that hillslopes are the fundamental units of upland catchments, and subsurface flow is the dominant runoff mechanism in many forested upland catchments around the world, and also that rainfall-runoff processes at the hillslope scale are intrinsically complex. Detailed studies of runoff processes at the small scale can, in principle, be used to transfer the results from the hillslope to the catchment scale. The hillslope is often identified as the smallest possible elementary unit representing the

catchment scale runoff dynamics across different catchment sizes (e.g. Freese et al. 2011; McGuire et al. 2005). Weiler et al. (2005) contend that understanding of runoff generation in hillslopes is of central interest because runoff pathways and the timing of runoff ultimately determine the chemical composition (quality) and quantity of stream flow. However, far more research has been conducted on overland flow as compared to subsurface flow. Tromp-van Meerveld et al. (2008) suggested that subsurface storm flow is a runoff enigma because *"... it is very difficult to observe and seemingly different at locales with contrasting driving conditions. Part of this enigma relates to the extreme difficulty in acquiring subsurface stormflow data - intensive site investigations, such as a hillslope trench and internal water level measurements, are a precondition for defining internal controls on flow generation"*.

This study aims to address this research gap, and to provide new original data that can be used to interpret flow generation mechanisms in the surface and subsurface in support of assessments of the influence that future climate variability has on nutrient losses from soils. The research question is expressed as a testable hypothesis:

Hypothesis 1 - The subsurface leaching pathways for nutrient losses from soils are enhanced relative to losses through overland flow under an intensified hydrological cycle predicted for continued global warming.

Several studies have evaluated the hydrological controls on nutrient losses from hillslopes (McHale et al. 2002; McKnight et al. 2002; McGlynn et al 2003; Inamdar and Mitchell 2006; Ocampo et al. 2006; Park et al. 2007; van Verseveld et al. 2007). In general, these field experiments were conducted on different types of soil, especially peat and upland forest catchments. Fierer and Gabet (2002) identified C and N losses by overland flow following changes in vegetation; however, they did not consider subsurface flow.

This study aims to address dominant flowpath controls and flushing processes on the DOC and the NO_3^- at the hillslope scale to provide an understanding of delivery mechanisms of key labile nutrients (DOC and NO_3^-) to streams of catchments. Dissolved organic carbon (DOC) plays an important role as an energy source to bacteria and some algae in streams (Kaplan and Newbold 1993). In addition, the DOC absorbs UV-radiation (Morris et al. 1995) that can damage aquatic organisms. Nitrates (NO_3^-) are essential plant nutrients, but in excess amounts, they can cause significant water

quality problems (EPA, 2012). The research question is expressed as a testable hypothesis:

Hypothesis 2 – Labile nutrient (DOC and NO_3^-) sources in the soil solution are preferentially depleted under an intensified hydrological cycle.

Runoff generation is considered to be an important process in catchment hydrology. To be able to identify storm and seasonal runoff pathways that are crucial for understanding and modelling of nutrient transport, there is a need for reliable flow separation. This can be achieved by continuous monitoring of hydrochemistry, using electrical conductivity (EC) as an inexpensive tracer providing high frequency information that can be combined with hydrometric measurements. Hugenschmidt et al. (2010) used chemically based hydrograph separation with electrical conductivity and silica as tracers to analyse stream water in a tropical, mountainous headwater catchment in northern Thailand. Geochemically based hydrograph separation techniques have been carried out to assess the hydrological pathways at different spatial scales in a meso-scale Scottish catchment (Soulsby et al. 2003). One of the most useful tools in studying catchment hydrology is the use of isotopic tracers (Kendall and McDonnell 1998), which can give insights into the age, pathway, and the origin of water in hydrologic systems. The use of isotopic tracers in catchment hydrology has a long history, and is well documented by Dinçer et al. (1968) who used stable isotopes of hydrogen and oxygen to determine the water balance of lakes situated in a subhumid climate in southwestern Turkey, and Kendall et. al. (1998) who used isotopes for tracing sources and cycling of nitrogen in forested catchments. Early work on flow separation of Pinder and Jones (1969) was based on the baseflow contribution to runoff by mass balance of dissolved ions, which were used to infer the chemical signatures of overland runoff and subsurface water from sampling discharge at high and low flows. Tardy et al. (2004, 2005) suggested a hydrochemical model, using hydrograph separation, developed for the Niger basin and applied it in the Amazon basin for studying large-scale basin dynamics. This study demonstrated applicability of using the hydrochemical model across scale and its potential as a simple model. A recent study used hydrochemical and isotope tracers in identifying the runoff contributing sources at different scales in a catchment in Tanzania (Bohté et al. 2010**)**. This study used the hydrochemical tracers to calculate runoff contributions for the sub-catchments and found that they are in agreement with the catchment size and rainfall contributions.

This study aims to test the utility of continuous monitoring of EC together with a simple flow separation model for interpretation of flow pathways. This is expressed as the following hypothesis:

Hypothesis 3 - Hydrochemical flow separation using continuous measurement of variables (EC) at the catchment outlet can provide quantitative estimates of surface and subsurface components of flow.

This study aims to test the scale effect on flow. This will combine the results of field measurements and observations, hydrochemical separation and conceptual models developed in this study together with a modelling approach. The research question is expressed as a testable hypothesis:

Hypothesis 4 - With increases of scale, subsurface flow increase relative to overland flow.

1.2 Outline of experimental approach

Studies of the evolution of the dominant runoff and nutrient processes at the plot scale linked to the hillslope and catchment scales can demonstrate how runoff generation can be linked across different spatial scales. This study covers three nested spatial scales: the hillslope (2 m^2), the sub-catchment (0.09 km^2) and the Blind Beck catchment (9.2 km^2) located in the Upper Eden basin, Cumbria, UK. The Upper Eden has been studied for many years by Newcastle University under the CHASM (Catchment Hydrology and Sustainable Management) project (Bathurst 2001; Walsh 2004; Mayes et al. 2006; Wilkinson 2009). It has been selected as the CHASM study area representative of northwest England. This basin is one of the most instrumented in the UK that provides a structure for the study of scale effects in hydrological response.

The central focus of this study is to develop and implement a novel concept of a climate experiment that allows quantification of the influence of climate variability in terms of precipitation perturbation on both soil quality and nutrient release, and flow. In order to achieve this, the methodology proposed here intends to combine field experiments and sampling, laboratory analysis and modelling approaches. The field experiment consists of a hillslope runoff experiment that was conducted on two hillslope runoff plots to identify runoff processes and to quantify nutrient fluxes, one under perturbed (i.e. enhanced rainfall) and another as a control plot. For improving the understanding of

changes in runoff and nutrient flux process at different scales and the impact of climate change scenarios on simulated runoff, a modelling approach is selected with the use of the SHETRAN physically-based hydrological model. The SHETRAN model is chosen because of its capability to represent the integrated overland and subsurface flows at the small scale, and since it can simulate nutrient transport processes integrated with the water flows. The modelling strategy for this project is to:

- Develop numerical flow and transport models,
- Run models of stream flow and nutrient fluxes at catchment and sub-catchment scales as well as runoff at the hillslope scale,
- Estimate water balances at the three scales,
- Run a runoff simulation under current and future climates.

This study will provide:

- An analysis of hydrological controls on nutrients at the hillslope and catchment scale that can be used to constrain hydrological models,
- A new conceptual model of flow pathways and nutrient flushing from the hillslope and within the catchment that explains the transport of nutrients,
- A hydrological model for predicting runoff at different scales and prediction of spatial nitrate concentrations and fluxes,
- An assessment of the impact of climate scenarios on hillslope runoff that can be used for future water management and farm planning.

1.3 Aim and objectives

The aim of this study is to provide new understanding of surface and subsurface hydrological controls on nutrient fluxes within mineral soils at the hillslope and catchment scales in Cumbria (UK), and how these are possibly influenced by future climate variability.

Objective 1: Identification and quantification of runoff processes at the catchment and hillslope scales using field experiments.

Objective 2: Determination of hydrological controls on soil C and N storage and transport using geochemical analyses.

Objective 3: Construction of a conceptual model of storages and fluxes of water and nutrients from the hillslope to the catchment scales.

Objective 4: Development and testing of numerical flow and transport models, and application of models using probabilistic future weather projections (UKCP09) to simulate possible impacts of precipitation variability on runoff.

1.4 Structure of thesis

This study links experimental (field and lab work) and modelling approaches in order to improve model prediction. This thesis is divided into 12 chapters.

Chapter 1 is an introduction to the general context of the research presented in this thesis. This chapter identifies the significance of climate variability, and the hillslope as a fundamental unit of the catchment that requires further research. The aim, objectives and key hypothesis are defined to address identified problems and knowledge gaps.

Chapter 2 provides a comprehensive literature review of catchment and hillslope hydrology, nutrient pathways and processes, and climate variability.

Chapter 3 introduces the Upper Eden basin in Cumbria (UK) in terms of geographical location and physical characteristics such as geological and geomorphologic conditions, land use and climatic context. It also presents the installed instrumentation.

Chapter 4 gives a description of the field sites and methods that were used in the collection and analysis of samples, monitoring campaigns, as well as the modelling approaches. This chapter focuses on the detailed description of plot scale runoff experiments at the hillslope using soil profiles and enhanced rainfall. The key objective is to quantify overland and subsurface flows in response to natural and perturbed precipitation in combination with nutrient export from the hillslope to the stream of the sub-catchment.

Chapters 5, 6 and 7 present the results collected from the catchment, sub-catchment and hillslope monitoring and experimental studies. The results are presented, and hydrological controls on C and N transport at three nested spatial scales are discussed. Chapter 5 presents hydrological processes at the catchment and sub-catchment scales in

relation to flooding and nutrient export. Chapters 6 and 7 identify runoff processes and quantify nutrient fluxes under the perturbed (i.e. increased rainfall) and control plots.

Chapter 8 identifies changes in physical and chemical properties of soil at the hillslope scale by comparing the responses during the enhanced rainfall treatment (wet condition) and unchanged/natural conditions (dry condition).

Chapter 9 presents new conceptual models for flow paths and nutrient storage and transport for the hillslope scale. The end of chapter 9 summarizes the results collected from three scales and discusses the issue of nutrients in terms of upscaling.

Chapter 10 is devoted to hydrological modelling. It describes how the model was set up and applied to simulate the hourly discharge from the outlet flows at the catchment and sub-catchment scales, and the model validation. In addition, it presents the soil moisture and the nitrate outputs from the model. It also presents the modelling of runoff at the hillslope scale.

Chapter 11 gives predictions of potential climate change impacts on runoff at a hillslope scale.

Chapter 12 summarizes the main findings of this study. It also discusses whether the objectives were met and the key hypotheses answered. Finally, this chapter identifies research limitations and concludes with the directions for future research.

Chapter 2. Literature review

2.1 Introduction

A comprehensive search of the literature was conducted to identify and review similar studies that have been done to date. To address the research questions and test the hypotheses outlined in Chapter 1, a comprehensive literature review was carried out of (2.1) catchment and hillslope hydrology, (2.2) nutrient sources and transport, and (2.3) climate change and variability.

To introduce the process of flow paths in a catchment and to predict how patterns and processes can change across scales, an overview of theoretical concepts, supported by detailed fieldwork over the last 50 years, is provided.

2.1.1 Hydrological pathways in the catchment systems

Horton introduced theories on infiltration capacities versus rainfall intensity and the traditional view of the overland flow generation in 1933, updated in 1945, where storm runoff is produced by infiltration-excess overland flow. Horton explained that overland flow begins when rainfall intensity exceeds the infiltration capacity of the soil (its capacity to absorb and transport the received water), while saturated overland flow is generated when the soil's storage capacity is exceeded, and the soil is effectively saturated. Horton defined infiltration capacity as "the maximum rate at which rain can be absorbed by a given soil at a given condition" (Horton 1933: 453). However, Horton's study failed to include subsurface flow during an individual storm event, which according to him was overland flow. Another limitation is that Horton was not working in forested environments, therefore the Hortonian overland flow is strictly applicable only in arid and semi-arid regions or in paved areas but not necessarily in any given forest setting. Sometimes the overland flow is also called unsaturated overland flow. Horton pointed out that infiltration-excess overland flow would occur uniformly across the catchment area, while Betson (1964) argued that this is not necessary suggesting the variable source area model of overland flow generation (Figure 2-1). Many researches (Kirkby and Chorley 1967; Tischendorf. 1969; Rawitz et al. 1970; Freeze 1972) have shown that Hortonian overland flow is rare or even absent when there is appreciable soil and a vegetative cover (Hofer 2007). Kirkby (1988) suggested that surface water variability could be predicted without the need to refer to overland

flow, but could be generated purely by subsurface flow (Sørbotten 2011). Infiltration excess overland flow can produce large flood peaks and soil erosion despite its restricted extent, both in time and space/area. In the catchment, the residence time is short and contact between the flowing water and the soil is limited. Therefore, the concentration of solute content of infiltration-excess overland flow will be low and it is likely to retain the characteristics of rainfall even when it reaches the stream and it is characterized as "new water" (Burt and Pinay 2005).

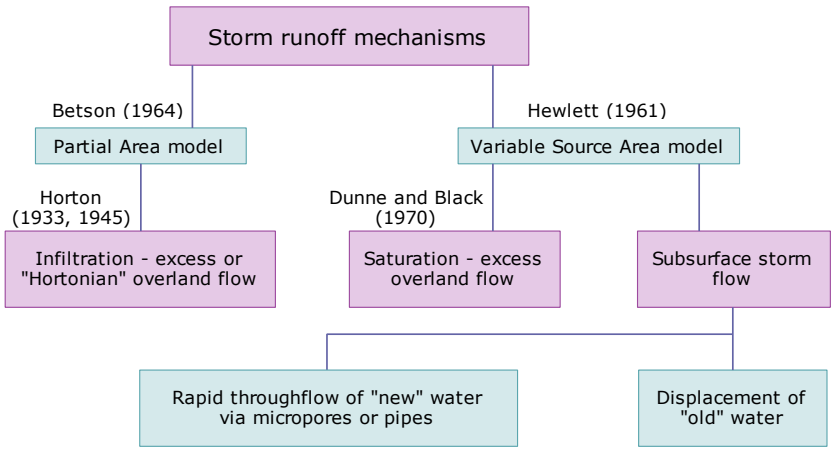

Figure 2-1 *Storm runoff mechanisms (source: originally published in Burt (1989) and modified by the author)*

In 1919, Engler recognizes the importance of subsurface stormflow after making detailed measurements of infiltration and soil properties including porosity, water content, soil texture and hydraulic conductivity (summarized in Weiler et al., 2005). Hewlett and Hibbert (1963) were the first to recognize the importance of unsaturated flow, which could not be ignored in hydrograph analysis. Weyman (1973) later published a study in which he describes the main mechanism in the production of significant quantities of subsurface stormflow (or throughflow), which is produced by saturated conditions within the soil profile, in effect a perched water table, often called the "saturated wedge" from its characteristic downslope shape. In the soil, movement of subsurface stormflow may be generated through the soil matrix, by flow macropores, or by a mixture of both. In this case contact between the flowing water and the soil is longer, so subsurface solute content has a high concentration and it is characterized as "old" water, where macropore flow can be sufficiently rapid to retain the "new" water characteristics. Dunne and Black (1970) pointed out the way in which saturation-excess overland flow is produced. According to them, soil profiles become completely saturated, which involves also a mixture of "return flow" (exfiltrating "old" soil water) and "direct runoff" ("new" rainfall unable to infiltrate the saturated surface. Hewlett

(1961) defines the variable source area in his model of stormflow generation because the extent of the zone of saturated ground varies seasonally and during storm events. It was recognized that infiltration capacities are rarely, if ever, exceeded in forest soils and the variable source area concept was extended to incorporate the idea of an expansion and contraction of saturated areas that affect direct runoff of rain falling on those areas (Hewlett and Hibbert, 1967). Finally, subsurface flow during storm events was recognized as being an important contribution to event based stream discharge.

In order to explain hydrological pathways in the catchment system in this study, it is necessary to review the findings of previous work at the selected study sites. A perceptual model of water movement in a Blind Beck catchment is shown in Figure 2-2. This view is developed by Ockenden (2010) based on observations and analysis of shallow and deep pathways from stream water chemistry. Accordingly, the model represents a range of pathways that may bring water into contact with different types of subsurface strata (soil, drift, rock); different pathways have different short and long residence times and hence different contact times with the matrix. This author offers an explanation using Figure 2-2, which indicates that some water is taking a shallow pathway, passing only through the drift geology and some water is taking a deeper pathway where the water infiltrates into the limestone and then passes through the sandstone before returning to the surface.

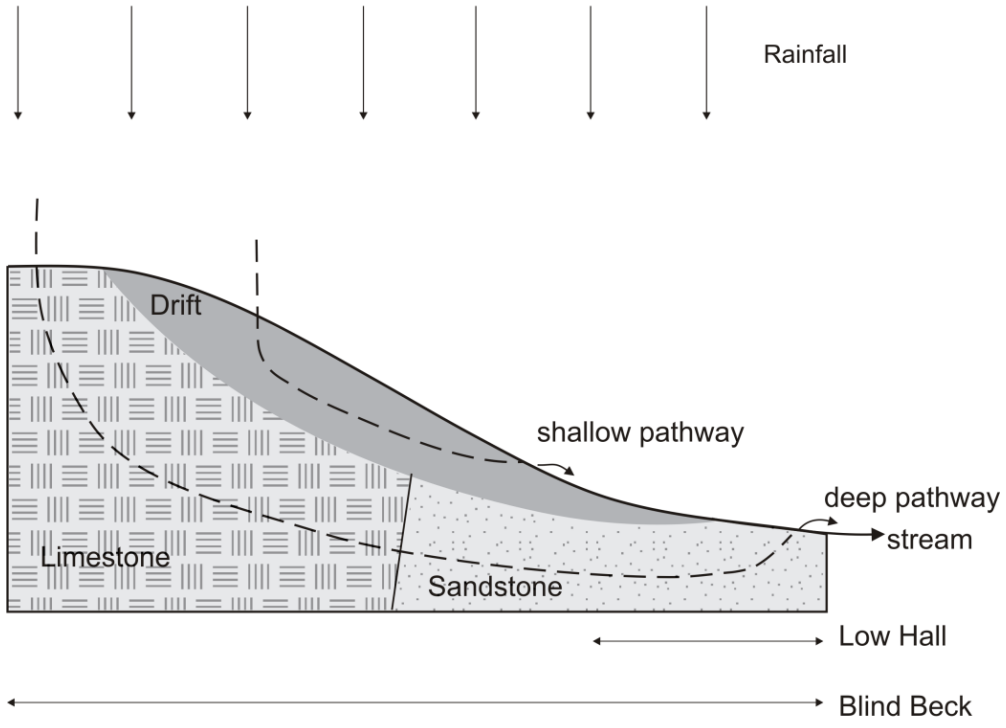

Figure 2-2 *Perceptual model of water pathways in the Blind Beck catchment (source: Ockenden 2010)*

Runoff generation in catchment systems depends on the following factors:

- Atmospheric conditions over the catchment (wind speed, direction, temperature, humidity etc.),
- The surface cover (type, distribution, interception, take up, evapotranspiration, etc.),
- Surface soil (type, permeability, porosity, etc.),
- Terrain (slope, surface texture, etc.), and
- Geology (structure distribution, permeability, porosity, groundwater levels, etc.).

2.1.2 The hillslope runoff processes

Hillslope runoff processes are mainly concerned with the fate of precipitation and the movement of water through the hillslope vegetation and soils (Sørbotten 2011). However, there is little understanding of what drives runoff delivery through the rapid flow paths during large precipitation events. Figure 2-3 shows an overview of the most important water fluxes of the hillslope hydrological cycle. According to that, some water is lost through evapotranspiration (evaporation and transpiration), through interception and from the soil after infiltration, while some water percolates to the groundwater and contributes to storage, and some water moves as throughflow and contributes to stream flow. Water that does not infiltrate is partitioned between overland flow, either Hortonian (also called 'infiltration excess') or saturation, subsurface flow and return flow (Kirkby 1988) (Figure 2-4).

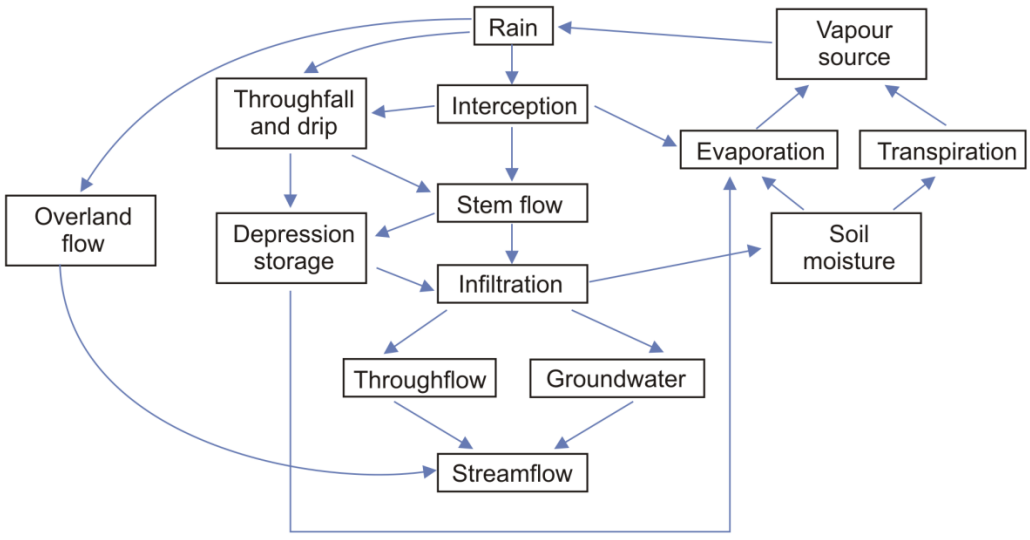

Figure 2-3 *The hillslope hydrological cycle (source: modified after Selby 1993)*

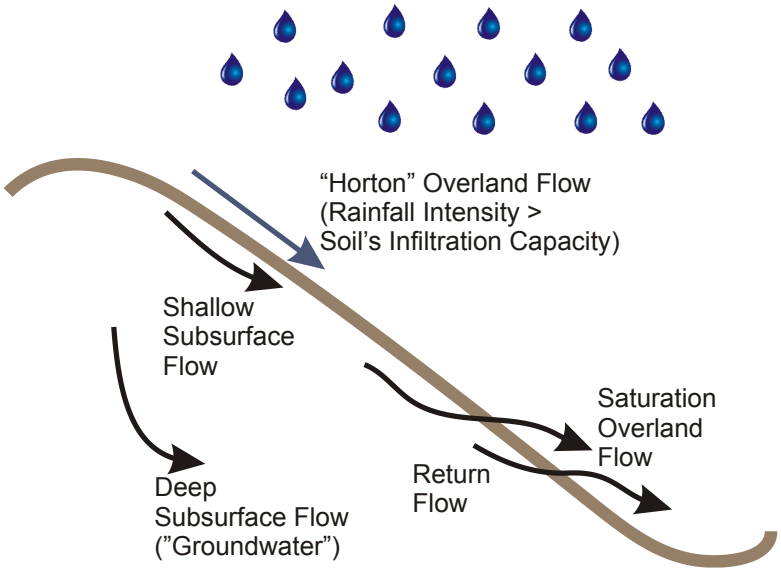

Figure 2-4 *Hillslope runoff processes*

Different approaches have been developed to describe the runoff generation processes on hillslopes. These approaches consist of various field measurement techniques and modelling concepts. Soil infiltration capacity, the rate at which soils absorb rainfall, determines whether water flows on the surface or through the subsurface. Water percolating vertically through the soil eventually reaches the groundwater table.

The runoff process is well described in the literature (e.g. Bonell 1993, 1998). In summary, flow that runs across the surface of the catchment downslope to the stream, generally occurs:

1) When the rate of rainfall on a surface exceeds the rate at which water can infiltrate the ground. This is called *infiltration excess overland flow* or *Hortonian overland flow* as first described by Robert E. Horton (1933).
2) When the soil is saturated and therefore not able to absorb excess water. This runoff is called *saturation excess overland flow* or *saturated overland flow* SOF (Kirkby and Chorly 1967).
3) After water infiltrates the soil, flowing through the soil and re-emerging at the surface because it reaches an impermeable barrier, such as an area of saturated soil or ice. This is called *subsurface return flow* or *return flow* (Dunne and Black 1970).

Overland flow depends on highly variable interactions between geomorphology, soil type, field management, climate and hydrological controls, all contributing to a *variable source area* in which limited areas of a landscape contribute to basin runoff (Gburek and Sharpley 1998).

As mentioned in sub-section 2.1.1, overland flow may be generated either by infiltration excess or saturation excess. Nash et al. (2002) pointed out that saturation excess flow includes both rain and soil water, while infiltration excess flow is comprised predominantly of rain water.

Shallow subsurface flow or throughflow is the movement downslope by gravity of water through the soil within an unsaturated zone parallel to the ground surface.

Deep subsurface flow of deep exfiltration of groundwater is drainage from water stored as groundwater and usually presents baseflow.

Subsurface flow

In the soil matrix, subsurface flow may occur under both saturated and unsaturated conditions and in the vertical and the lateral direction. Movement of soil moisture in all cases occurs in response to a gradient of hydraulic potential, which is the sum of three components: a gravitational potential, a matric potential (or pressure potential or tension) and an osmotic potential (Atkinson 1978). The osmotic potential component is often ignored, and the total hydraulic potential per unit weight of water, h_w is:

$$h_w = z + \psi$$

where: z = the height of a point with consideration to the base of the slope, i.e. the gravitational potential, ψ = the matric potential in centimetres

In the soil matrix, water flow is considered to be laminar and is described by Darcy's law (Darcy 1856) which describes flow per unit area, q.

The Darcy law for vertical flow in unsaturated soils was modified by Buckingham (cf. Flühler and Roth 2004) to:

$$q = -k(\theta_w)\left(\frac{d(z+\psi)}{dz}\right) = -k(\theta_w)\left(\frac{d\psi}{dz} + 1\right)$$

where: k(θw) = the hydraulic conductivity dependent on volumetric soil water content

To calculate the rate of change in the amount of water stored in a block of soil, the continuity equation and Darcy's law can be combined to:

$$\frac{d}{dt}\theta_w = \frac{d}{dz}\left(k(\theta_w)\left(\frac{d\psi}{dz} + 1\right)\right)$$

where: θw = the soil water content

Arnell (2002) defines this process as the difference between the inflow to the block and the outflow from it. This equation, valid for unsaturated soils, is known as the *Richards equation* (Richards 1931).

In order to understand the runoff generation processes, Kienzler and Naef (2008) studied subsurface stormflow (SSF) in an unsaturated zone at four different hillslopes during controlled sprinkling experiments and natural rainfall events. In order to determine event and pre-event water fractions, they used artificially traced sprinkling water with ^{222}Rn as natural tracer. They concluded that when precipitation feeds directly into preferential flow paths, SSF responds quickly and contains low pre-event water fractions. Conversely, when it is fed indirectly via large saturated zones of soil, the SSF response is delayed and consists mainly of pre-event water. Kienzler and Naef (2008) also suggest that the fast flow components from the hillslope, such as overland flow and fast subsurface flow, may produce rapid discharge responses and deliver substantial amounts of pre-event water to the stream.

In summary, the following processes are usually identified in catchment and hillslope hydrology:

- Evapotranspiration at the surface,
- Surface infiltration,
- Overland flow,
- Unsaturated zone flow,
- Saturated zone flow (groundwater).

Understanding and predicting overland and subsurface flow processes at the hillslope scale is highly important in terms of flood prediction, transport of nutrients, sediments and contaminants, slope stability, and soil-atmosphere-vegetation exchange processes.

2.1.3 Flow paths and flow chemistry within the hillslope

Buttle (1994) reviewed the processes responsible for conveying pre-event water rapidly to the channel during storm events: ridging, translation flow, macropore flow, saturation-excess overland flow, kinematic waves and release of water from surface storage (Burt and Pinay 2005). Not all processes occur in all catchments but, whichever dominates, the focus seems inevitably on the near-stream saturated zone (Cirmo and McDonnell 1997; Burt and Pinay 2005).

Figure 2-5 gives one version of solute and nitrate transport during storm events on a two-dimensional hillslope, based on Burt (1986). The slope profile is a low-gradient near-stream zone. Water reaches the ground as precipitation that may flow off directly into the streams as dilute ('new') event water either as infiltration excess overland flow, or as direct runoff from saturated areas. Burt and Pinay (2005) suggest that a water table rises above its pre-event location because of recharge by matrix or macropore flow, possibly aided by capillary fringe effects. Once this happens, flow within the formerly unsaturated zone becomes lateral (Burt 1986; Burt and Pinay 2005). As the water table further rises, concentrated ('old') pre-event water is immediately displaced into the stream by a translatory flow (Hewlett and Hibbert 1967; Anderson and Burt 1982) and solutes are flushed from previously unsaturated soils (Burt 1979; Hornberger et al. 1994). Puckett et al. (2002) suggest that translatory flow may also allow deeper groundwater to contribute to stream flow, depending on its flow path chemistry and age. Channel flow is a mixture of different source of waters according to Burt and Pinay (2005), but it may be impossible to infer the hillslope processes from stream flow dynamics due to the decoupling of biogeochemistry and hydrology in the near-stream zone.

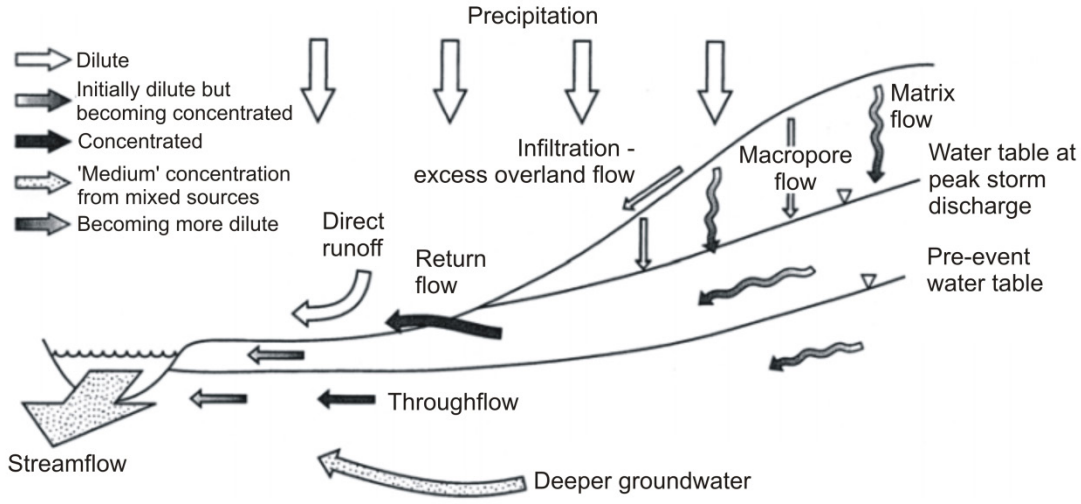

Figure 2-5 *A schematic diagram of solute and nitrate transport within the hillslope (source: Burt (1986) and Buttle (1994))*

Burt and Pinay (2005) pointed out that nitrate may be produced in the near-stream zone by mineralization and rising water tables that can be flushed into the stream. In addition, there is the process of immobilization and denitrification, which can remove nitrate temporarily or permanently.

2.2 Nutrient sources, transport – pathways and processes

The dominant nutrients within the catchment system are in forms of nitrogen (N), phosphorous (P) and carbon (C). This study only discusses N and C.

2.2.1 The carbon cycle

Sources and forms of carbon in soils and sediments

Schumacher (2002) reported three forms of carbon in soils and sediments: (1) elemental, (2) inorganic and (3) organic carbon.

1) **Elemental carbon forms** include soot, graphite, charcoal and coal. In soils and sediments, the primary sources for elemental carbon are incomplete combustion products of organic matter (i.e., charcoal, graphite, and soot), from geologic sources (i.e., graphite and coal), or dispersion of these carbon forms during mining, processing, or combustion of these materials.
2) **Inorganic carbon (IC)** originates from geologic or soil parent material sources. In soils and sediments, inorganic carbon is present as carbonates. The most common carbonate minerals present in soils and sediments are calcite ($CaCO_3$) and dolomite ([$CaMg(CO_3)$] but other minerals may also be present, such as siderite, $FeCO_3$ or other forms depending on where the soils were formed or where the sediment source was located. It is possible that calcite and to some extent, dolomite, may be present in soils and sediments due to agricultural input (i.e., liming practices).
3) **Organic carbon (OC)** originates from the decomposition of plants, bacteria and animals. In soils and sediments, organic carbon composition ranges from freshly deposited litter (e.g., leaves, twigs, branches) to highly decomposed forms such as humus. The vast majority of soil microbes requires organic carbon compounds (these are called organotrophs) to oxidize for energy and to build the organic constituents of their cell bodies.

Sediment organic matter and nutrients

Total Organic Carbon (TOC) refers to the amount of organic matter (OM) preserved within the sediment. Sediment nutrients are assessed as Total Nitrogen (TN) and Total Phosphorus (TP) concentrations, and have inorganic as well as organic sources. The amount of organic matter found in sediment is a function of the amount of various

sources reaching the sediment surface and the rates at which different types of organic matter are degraded by microbial processes during burial.

Phosphorus readily sorbs to sediments and is primarily transported to streams and lakes in overland flow with eroded sediment (USEPA 1999). Nitrogen does not sorb as strongly to sediment as compared to P and is transported to aquatic systems in both particulate and dissolved phases in runoff (USEPA 1999).

Sediment carbon and nutrient content can be altered due to:

- Organic matter breakdown (mineralisation) which reduces sediment carbon and nutrient concentrations,
- Enhanced sediment transport caused by erosion in catchments, which can lower sediment TN and TOC concentrations because inorganic constituents (minerals and clays) can dilute organic matter concentrations (Radke 2002).

Organic matter is a source of food and energy, and its nutritional balance (TOC:TN:TP ratio) plays an important role in material flow through ecosystems. Enriquez et al. (1993) state that decomposition rates of organic matter increase as nitrogen and phosphorus contents increase, and consequently TOC/TN and TOC/TP ratios decrease (Thomann 1972). 'Labile' is the term used to describe sediment organic matter with low TOC:TN ratios that break down easily, whereas 'refractory' organic compounds (woody debris made of lignin and cellulose) have a very high TOC:TN ratios and are highly resistant to degradation. Twilley et al. (1999) point out that organic matter with very high TOC:TN ratios consume more dissolved oxygen, supporting the less denitrification and release of fewer nutrients to the water column (Rivera-Monroy et al. 1996). The decomposition of organic matter with very high TOC:TN ratios can even be nutrient controlled, meaning that it can cause the uptake of dissolved inorganic nitrogen (DIN) from the water column (Grebmeir et al. 1988).

The adsorption process helps to preserve the organic matter (CSIRO Huon Estuary Study Team 2000), and gives rise to a generally positive correlation between TN or TOC and % silt-clay. Sites of organic matter accumulation in water bodies are therefore controlled to a large extent by processes that govern the transport and deposition of fine sediment.

Total organic carbon (TOC) content in sediments has been used as an indicator of pollution and to predict the likelihood of eutrophication (Folger 1972; EPA 2002). High

organic carbon content is considered as a sign of frequent algae blooms, the blooms being a result of increased nutrient (nitrogen and phosphorus) supply into the system.

2.2.2 Dissolved organic carbon (DOC)

Definition of DOC

Malcom and Leenheer (1973) define the term "dissolved organic carbon" (DOC) as a measure of that part of the total organic carbon (TOC) (TOC = DOC + SOC; SOC = suspended organic carbon) in water that passes through a 0.45 micrometre silver membrane filter (Hughes et al. 1974). Hope et al. (1997) use the DOC export from 85 British rivers where the samples were not filtered prior to analysis to highlight that the difference between the DOC concentration between samples that were filtered and unfiltered was less than 5%. Previous studies of the DOC concentrations used GF/F filters in Cumbrian lakes and streams (Tipping et al. 1988) and also in the Moisie River, Quebec (Ford et al. 1990). Later, Fraser (2001) used 0.45 μm filters for water samples from the Mer Bleue bog, Ontario, Canada. Difficulties arise, however, when an attempt is made to compare the DOC concentration between different studies due to the varying filter types. In this study, samples were filtered using Whatman 0.45 μm membrane filter paper.

Sources of DOC

Within a stream, the DOC sources are classified as being of external (allochthonous) or internal (autochthonous) origins, that is derived either from the basin or from within the stream. Allochthonous inputs are derived from soil organic matter and decomposed plant debris (Mash et al. 2004) and can enter a system through precipitation and leaching. Autochthonous inputs are derived from aquatic biota such as algae and macrophytes (Aiken and Cotsaris 1995).

Allochthonous DOC is generally linked to precipitation that mobilizes particles from the vegetation (throughflow and stream flow) and/or leaches soluble carbon from the litter (Peuravuori and Pihlaja 1989). The highest concentration of organic carbon is in the upper soil horizon resulting from decomposing leaf litter and organic material (Cronan and Aiken 1985; Thurman 1985; Bertilsson and Jones 2003). To determinate the effects of the DOC, Cory et al. (2002) simulated leaching from soils; their results confirm that the DOC in streams can have the same composition as soil water in upper soil horizons.

Table 2-1 shows the three main categories of the organic carbon fluxes, and their individual contributions to total organic carbon. Some of these inputs originate from the stream (such as dying macrophytes, animal faeces, extracellular release of dissolved compounds) and some transported into the stream from outside (such as leaf fall, soil particulates and compounds dissolved in soil water) (Allan 2001).

Table 2-1 *Sources of organic matter to running waters. The majority originates from outside the water body, the sources marked with an asterisk arise from energy fixed by photosynthesis within the water bodies that then enters heterotrophic pathways (Allan 2001)*

Sources of Input	Comments
Coarse Particulate Matter (CPOM)	
Leaves and Needles	Major input in woodland streams, typically pulsed seasonally
Macrophytes during die-back	Locally important
Woody debris	May be a major biomass component, very slowly utilized
Other plant parts (flowers, fruit, pollen)	Little information available
Other animal inputs (faeces and carcases)	Little information available
Fine Particulate Organic Matter (FPOM)	
Breakdown of CPOM	Major input where leaf fall or macrophytes provide CPOM
Faeces of small consumers	Important transformation of CPOM
From DOM by microbial uptake	Organic microlayers on stones and other surfaces
From DOM by physical-chemical processes	Flocculation and adsorption, probably less important than microbial uptake route
Sloughing of Algae*	Of local importance, may show temporal pulses
Sloughing of organic layers	Little information available
Forest floor litter and soil	Influenced by storms causing increased channel width and inundation of floodplain, affected by an overland *versus* subsurface flow
Stream bank and channel	Little is known, likely related to storm events
Dissolved Organic Matter (DOM)	
Groundwater	Major input, relatively constant over time, often highly refractory
Subsurface flow or interflow	Less known, perhaps important during storm events
Surface flow	Less known, perhaps important during storm events
Leacate from the detritus of terrestrial origin	Major input, pulsed depending upon leaf fall
Throughfall	Small input, dependent on contact of precipitation with canopy
Extracellular release and leachate from algae*	Of local importance, may show seasonal and diel pulses
Extracellular release and leachate from macrophytes*	Of local importance, may show seasonal and diel pulses

DOC retention and release in soils

The DOC concentration that is available to be released from the catchment to streams varies with the soil type. Accordingly, catchments with a high proportion of organic soil have a large potential to source DOC into streams, such as peatland and forest planted on drained catchments in the UK (Hargreaves et al. 2001). In peatland catchments, carbon accumulates in soil because of low decomposition rates (Grieve and Marsden 2001). Table 2-2 shows examples of different catchments type with the DOC exports.

The DOC concentrations and fluxes in the mineral soil decrease with depth because of metabolization by micro-organisms (Allan 2001). The DOC can also be absorbed to clay minerals, controlled by soil water pH, Jardine et al. (1989) found that the maximum adsorption of DOC within loamy soils occurred at ~ pH 4.5.

Table 2-2 *DOC exports (g C $m^{-2}yr^{-1}$) and annual mean precipitation (mm) from a range of catchments (source: Wearing 2008)*

Site	Catchment type	DOC export (g C m^{-2} yr^{-1})	Annual mean precipitation (mm)	Reference
Hubbard Brook, New Hampshire, USA	Temperate Deciduous Forest	2	1310	McDowell and Likens (1988)
Luquillo Mountains, Puerto Rico	Tropical Evergreen Forest	3.25	3500	McDowell (1998)
Troutbeck catchment, Moorhouse, UK	Upland Peat	4-7.4	1953	Worrall et al. (2006)
Maimai, Westland, New Zealand	Temperate Evergreen Forest	6.8	2400	Moore (1989)
Ochil Hills, Scotland	Upland Peat	8	1200-1500	Grieve (1984)
Mer Bleue bog, Ontario, Canada	Bog	8.3	910	Fraser et al. (2001)
Upper Hafren, Wales	Upland Peat	8.4	2726	Dawson et al. (2002)
Loch Ard, Burn 11, Scotland	Temperate Evergreen Forest	15	2000-2500	Grieve (1994)
Loch Ard, Burn 10, Scotland	Temperate Evergreen Forest	16	2000-2500	Grieve (1994)
Brocky Burn, Scotland	Upland Peat	16.9	1164	Dawson et al. (2002)
Larry River, Westland, New Zealand	Wetland (Moss/fern/scrub vegetation)	65.1	2500	Moore and Jackson (1989)

Significance of DOC in stream water and soil

The dissolved organic carbon (DOC) is a fundamental component of biogeochemical processes in small catchments (Kalbitz et al. 2000; Hope et al. 1994) that affects the food web structure (Jansson et al. 2007) and the carbon balance (Cole et al. 2007; Nilsson et al. 2008). The importance of the DOC is as a small but vital component of the global carbon. Also, the significance of the DOC lies in its role of being able to carry carbon hydrologically between different pools in the ecosystem. The DOC concentrations depend on multiple factors, including the catchment soil carbon storage, vegetation, and local climate, principally precipitation and temperature.

In soil and in stream water, the DOC can reach concentrations of 50 mg/l or more (Dalva and Moore 1991). The DOC can influence the water acidity, nutrient availability, metal solubility, mobility and toxicity of metal.

2.2.3 The nitrogen cycle

The nitrogen cycle represents one of the most important nutrient cycles, which involves many processes that make the N in manure, fertilizer, and soil available to plants. Figure 2-6 shows the major conversion processes in the soil N cycle.

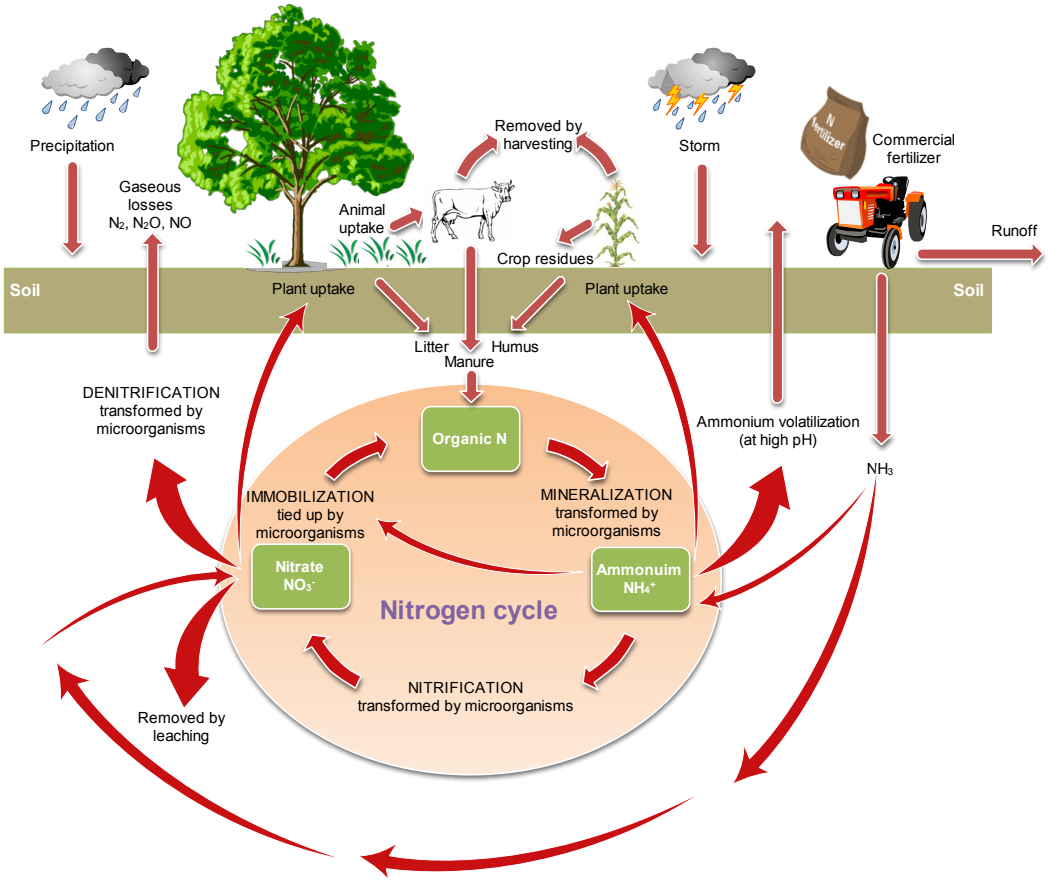

Figure 2-6 *The farm nitrogen cycle (source: the author)*

In the soil, nitrogen (N) comes in both organic and inorganic forms. Inorganic N consists mostly of ammonium (NH_4^+) and nitrate (NO_3^-), and is already available to plants. Organic N (manure, crop residues and soil organic matter) must first be converted to inorganic forms before it can be taken up. This process is called *mineralization*, which is completed by soil microbes as a by-product of organic matter decomposition.

Mineralization

$$Organic\ N \rightarrow Ammonia\ (NH_3^+) \rightarrow Ammonium\ (NH_4^+)$$

The *nitrification* process consists of two steps:

Nitrification

step 1: ammonium-N is converted into nitrite-N by ammonium-oxidizing bacteria

$$Ammonium\ (NH_4^+) \rightarrow Nitrite\ (NO_2^-)$$

step 2: nitrite-N is converted into nitrate-N by nitrite-oxidizing bacteria

$$Nitrite\ (NO_2^-) \rightarrow Nitrate\ NO_3^-$$

Soil micro-organisms use nitrate and ammonium nitrogen when decomposing plant residues. The *immobilization* process occurs when these forms are temporarily "tied-up" (incorporated into microbial tissue). This process is the reverse of mineralization.

Immobilization

$$Organic\ N \leftarrow (NH_4^+)(NO_3^-)$$

Both immobilization and mineralization processes can have a direct impact on water quality.

The process of *denitrification* is the loss of nitrogen (NO_3^-) through metabolic reduction into various gaseous forms of N such as dinitrogen (N_2), nitrous oxide (N_2O) and nitric oxide (NO) gas. These gases then diffuse into the atmosphere and are not available to plants.

Denitrification

$$2NO_3^- \rightarrow 2NO_2^- \rightarrow Nitric\ oxide(2NO) \rightarrow Nitrous\ oxide(N_2O) \rightarrow Nitrogen\ gas\ (N_2)$$

The air we breathe consists of 78% of dinitrogen (N_2) while nitrous oxide (N_2O) and nitric oxide (NO) gases are considered as greenhouse gases. The process of denitrification that can occur within two or three days in poorly drained soils under wet conditions can result in large losses of nitrate type fertilizer.

The process of *volatilization* is the production and loss of ammonia (NH_3^-) from ammonium (NH_4^+).

Volatilization

$$NH_4^+ \rightarrow NH_3^-$$

High soil pH (pH greater than 7.5) and conditions favourable for evaporation can cause large amounts of NH_4^+ to be lost from soils by conversion to NH_3^- gas.

Plants can absorb only ammonium-N and nitrate-N, so the rate of nitrification markedly influences nitrogen absorption efficiency by plants. Nitrate-N (NO_3^-) is very soluble and has a negative charge so it does not attach to soil particles, therefore it is easily lost from the soil system by leaching. The most critical time for the NO_3^- leaching is the beginning of the winter or during heavy rainfall. In overland flow water, only small amounts of inorganic nitrogen are usually present because of nitrogen solubility and the tendency to move into the soil with the first rainfall.

Excess nitrogen in the environment is associated with many large-scale environmental concerns, including, eutrophication of surface waters, toxic algae blooms, hypoxia, acid

rain, nitrogen saturation in forests, and global warming. Eutrophication, as a process of nutrient enrichment primarily phosphorus and nitrogen has numerous undesirable symptoms (see Figure 2-7).

Eutrophication causes an:

- Increase in primary production either as algae or macrophytes
- Reduction in water clarity
- Replacement of submerged macrophytes by phytoplankton
- Increased dominance by blue-green algae which are liable to
- Form surface algal blooms and produce algal toxins
- An increasing respiratory demand for dissolved oxygen causing an
- Increased potential for fish kills and reduction in biodiversity at all trophic levels
- Increase in water treatment costs to remove
    - Taste and odour problems
    - Algal toxins which can

  Threaten public and animal health
- Damage to recreational potential and amenity

Figure 2-7 *Potential impacts of eutrophication (source: adapted from Foy 2005)*

In order to reduce N losses from the farm there are a number of management options based on the strategic use of N fertilizer and improved N recycling within farming systems (Burt et al. 1993; Haygarth and Jarvis 2002). The Nitrates Directive (91/676/EC), adopted by the European Union in 1991, aims to reduce water pollution caused by nitrogen from agricultural sources (Heathwaite et al. 1993) and to prevent such pollution in the future. It seeks to limit nitrogen levels to 50 mg/l in ground and surface waters throughout the EU. The Nitrates Directive requires countries to identify waters that are or could become polluted by nitrates and to designate as Nitrate Vulnerable Zones (NVZs) all land draining to those waters and contributing to the pollution.

Table below summarises Nitrate concentrations (mg/l) in surface waters for the North West region. The General Quality Assessment (GQA) carried out by the EA in 2006 (Table 2-3), revealed that 10% of watercourses in the region were in the high' to 'very

high' N concentrations and 10% were in the 'moderate' N concentration bracket (Barber 2008).

Table 2-3 *Environment agency nitrate concentration guide for North West region (source: adapted from EA 2006)*

EA Nitrate Concentration Guide (mg/l)					
Very Low	Low	Moderately Low	Moderate	High	V High
< 5	> 5 - 10	> 10 - 20	> 20 - 30	> 30 - 40	> 40

The key for the future is to develop sustainable farming management to cause minimal pollution to the environment.

2.2.4 Nutrient loss and leaching

Many studies have shown that most of the N lost from both grasslands and crop fields moves through subsurface flow rather than in overland flow (Andersen et al. 2001a; Heathwaite et al. 1993; Barber 2008). Exceptions can occur after application of fertilizer or manure during heavy rainfall, or when they are applied to frozen soil (Fawcett 2005).

Vertical leaching through the soil profile was determined by Haygarth and Jarvis (2002: 15): "via matrix flow through the whole soil body in light textured soils, or through bypass flow in large macropores and cracks in heavy textured soils".

Leaching of nutrients from the soil occurs mainly during storm events of long duration. During the winter months in the UK, some or all the nitrate that was initially present in the soil will have displaced to below the root zone (DEFRA 2007b). Percolation of surplus water is referred to as "drainage water" or "excess winter rainfall". DEFRA (2007b) found that on soils, the nitrate concentrations in drainage water are typically relatively high in the early winter, and declined over time as the nitrate in the soil is displaced and diluted (Figure 2-8). In the case of retentive soils, such as deep silts, the water content of the soil is greater, and it requires more rainfall to move the soil nitrate below the root zone (DEFRA 2007b). Rainfall is therefore one of the most important climate factors affecting the nitrate levels. Heavy rain causes an initial peak when infiltrating water flushes nitrate from the soil.

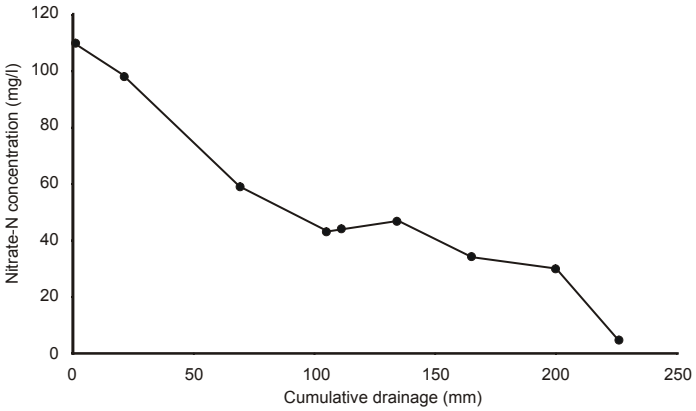

Figure 2-8 *Nitrate concentrations in leachate from the sandy soil in a moderately wet winter (source: DEFRA 2007b)*

Figure 2-9 shows the nitrate concentrations in drainage from clays that tends to fluctuate depending on the rainfall, and concentrations during low flow periods that are greater, because the water has equilibrated with the soil nitrate (DEFRA 2007b). DEFRA (2007b) gave information that in much of the arable clay land, concentrations during low flow periods may exceed 50 mg/l nitrate, while concentrations tend to be smaller during heavy rain. During storm events, on these soils, the rapid overland flow could increase the risk that pollutants in surface applied materials may be rapidly transferred to water bodies (DEFRA 2007b). The nitrate leaching is also possible from loamy soils although nitrate can be retained more effectively in this type of soil with large amounts of organic carbon.

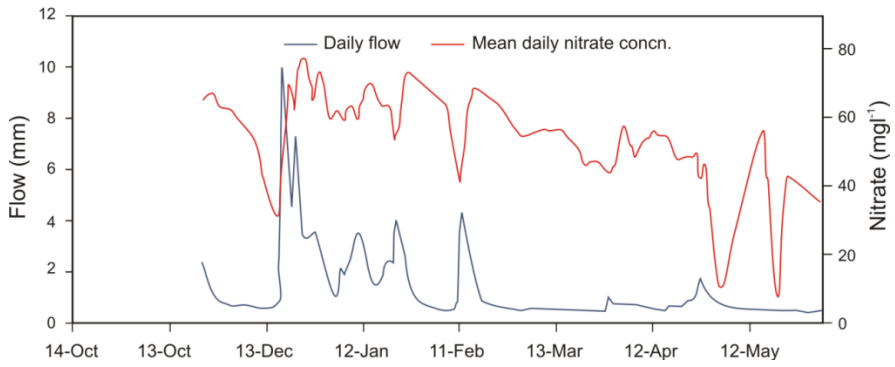

Figure 2-9 *Nitrate concentrations in water draining from grassland in western England, winter 2005/6, showing dilution during heavy rainfall; and a gradual decline in concentrations over winter (source: DEFRA 2007b)*

Specific agricultural activities contribute substantially to losses of N, which include the ploughing of permanent pasture that releases large amounts of N through the mineralisation of soil organic matter, leaving land fallow over the winter, and application of animal manures or N fertilisers during the autumn when plant uptake is low and over-winter rainfall will increase leaching (Addiscott et al. 1991; Skinner et al. 1997).

The risk of flow carrying pollutants to a stream is increased (DEFRA 2007b):

- During heavy rain,
- On soils which are impermeable or where structural damage has reduced the rate of infiltration,
- On bare soils without crop cover,
- On steep slopes,
- On converging slopes, even with moderate slope angles, and
- Where the distance to a ditch or stream is small and there is little physical barrier to flow (e.g. hedge, vegetated headland, buffer strip etc.).

In case of leaching of nitrates, the soil depletes in other nutrients such as Ca^{2+}, Mg^{2+} and K^{+}. Gowariker (2009) mentions that liming generally reduces the leaching of potassium. Havlin (1999) points out that sulphate is also leached from surface soils, where the losses being highest in soils dominated by monovalent cations (potassium, sodium) and lowest in soils with high amounts of aluminium.

DEFRA (2007b) has been found that nutrients carried down through the percolation soil solution are necessarily electrically neutral indicating that anions are leached together with equivalent amounts of cations.

The nitrate concentrations in waters are monitored by the Environment Agency and show the integrated effect of all land uses and other inputs at the abstraction point (DEFRA 2007b). 70% of the N entering English waters is estimated to come from agricultural land (DEFRA 2007b). The experimental results of Haygarth and Jarvis (2002) have shown that in the UK most N is lost from arable farms by leaching during the autumn and the winter, but most by denitrification in the spring. Hatch et al. (2002) claimed that large concentrations of DON have been found in drainage waters leaving grassland lysimeters in Devon, England.

Overland flow can transport large quantities of nutrients from the soil in both dissolved and sediment-bound forms (Gifford and Busby 1973; Lowrance and Williams 1988; Fierer and Gabet 2002).

Kleinman et al. (2006) found that loss of soil nutrients in runoff accelerates eutrophication of surface waters along a single hillslope. They found that significantly greater nutrient losses were under the high intensity rainfall due to larger runoff volumes.

DEFRA (2007a) estimates agriculture's contribution to water pollution in England and Wales to be:

- 60% of nitrate emissions to water,
- >80% of ammonia gaseous emissions,
- 25% of phosphorus emissions to water,
- 5-10% of ammonium-N in water standard failures.

More intense rainfall events and change in rainfall patterns and intensities due to climate change may result in greater amounts of overland flow and a concomitant increase in the quantities of C and N removed from a hillslope (Edwards and Owens 1991). Pimentel and Kounang (1998) indicate that any increase in nutrient removal from the soil may possess long-term consequences for soil quality and ecosystem productivity (Fierer and Gabet 2002). Furthermore, Crosson (1985) indicates that an increase in hillslope nutrient loss may reduce the quality of regional stream waters.

Van Verseveld (2007) gives an overview of nutrient flushing, a term which has been used to describe the movement of solutes in relation to hydrological processes (Burns 2005). Numerous studies have attempted to explain the flushing of nutrients qualitatively by (1) a rising water table that intersects high nutrient concentration in the upper soil layer (Hornberger et al. 1994; Boyer et al. 1997), (2) vertical transport of nutrients by preferential or matrix flow through the (deeper less bio-active) soil to the soil-bedrock interface and then laterally downslope (Hill et al. 1999; Buttle et al. 2001; Creed et al. 1996), and (3) vertical transport of nutrients into the soil and then laterally within the soil profile (e.g. Gaskin et al. 1989). Van Verseveld (2007) indicates that several attempts have been made to move away from this two-dimensional view of catchments and have focused on spatial sources of stream nutrients by dissecting the catchment into different geomorphic units (for example hillslope vs. riparian zone).

Rainfall intensity affects overland flow generation as well as concentration of nutrients in runoff (Kirkby 1978; Srinivasan et al. 2001). Infiltration excess overland flow requires sufficient rainfall intensity and duration for the soil infiltration capacity to be exceeded, whereas saturation excess flow may occur at extremely low rainfall intensities. Determining subsurface flow behaviours across different antecedent wetness conditions is a major research gap in hydrology (Sivapalan 2003) and is a pre-requisite for identifying dominant hydrological controls on stream nutrient patterns. Studies of the hydrological controls on stream concentrations and quality of dissolved organic

carbon (DOC) and nitrate have improved our understanding of flushing and draining process of nutrients at the catchment scale, but quantifying spatial sources of these nutrients during storm events and across seasons remains poorly understood (van Verseveld 2007).

2.3 Climate variability

The following question is addressed: "What is the difference between *climate change* and *climate variability*? According to the World Meteorological Organization (WMO), "climate variability is the term used to describe a range of weather conditions that, averaged together, describe the 'climate' of a region" (WMO 2008). In some parts of the world or in any region for certain time periods or parts of the year, this variability can be weak - i.e. there is not much difference in the conditions within that time period". At the global level, climate change refers to the long-term change, in weather conditions.

2.3.1 Climate change effects on the soil

On 24 September 2009, the EU Agriculture Commissioner and UK Environment Secretary Mr Hilary Benn stated: "Soil is one of the building blocks of life. Good quality soils are essential for a thriving farming industry, a sustainable food supply, and a healthy environment. Britain's soils hold more carbon than all the trees in Europe's forests - and their protection is critical whether we are to successfully combat climate change" (Soil Association 2009).

The "Safeguarding Our Soils: A Strategy for England" document (DEFRA 2009) mentions that England's soils faces three main threats:

- "Soils erosion by wind and rain. Erosion affects both the productivity of soils but also water quality and aquatic ecosystems,
- Compaction of soil reduces agricultural productivity and water infiltration, and increases flood risk through higher levels of runoff,
- Organic matter decline. The loss of soil organic matter reduces soil quality, affecting the supply of nutrients and making it more difficult for plants to grow, and increases emissions to the atmosphere".

All these threats could be influenced by climate change. The latest UK Climate Projections (DEFRA, 2009) show that the influence of climate change in the UK is

likely to result in extreme weather occurrences such as heat waves, dry spells, heavy rain and flooding. This has the potential to significantly affect UK soils and increase the risk of their degradation and increase costs and lost production. Changes in the soil due to change of temperature and moisture of soil may speed up the decomposition of organic matter, reducing the amount of carbon in the soil and increased emissions to the atmosphere. The UK Climate Projections (UKCP09) provide an opportunity to examine the nature and scale of climate change impacts on the soils of England and Wales. This research enables the effects of climate change on the soil to be estimated in order to support agricultural productivity and soil management practices to adapt to climate change.

2.3.2 Climate change effects on nutrients

Climate change affects the soil by variations in temperature and rainfall including the soil loss and degradation as well as changes in nutrient and carbon cycling and budgets.

Kirschbaum (1999) addressed whether changes in soil organic carbon would consequently act as positive or negative feedbacks on climate change. He suggested it could lower the build-up of CO_2 in the atmosphere and reduce further warming. On the other hand, a loss of organic carbon with warming would constitute a positive feedback by further adding to the build-up of CO_2 in the atmosphere.

Knowledge of the factors controlling the soil carbon storage is essential for the understanding the changing global carbon cycle. According to that the Intergovernmental Panel on Climatic Change (IPCC) reports (IPCC 2001) indicate that even small changes in such a large pool of C can be expected to have dramatic feedbacks on the CO_2 concentration in the atmosphere and as a consequence on the global climate system. Bouraoui et al. (2002) published a study that documents the impact of potential climatic change on nutrient loads from agricultural areas to surface water in the Yorkshire Ouse catchment, UK. This study used six climate change scenarios to cover a wide range of climate change predictions using the Soil and Water Assessment Tool (SWAT) model. One of the major conclusions is that all six climate scenarios would affect, significantly, not only water quality and nutrient loads from agricultural areas but also crop growth patterns and will increase the nutrient losses to surface water.

Kaipainen et al. (2008) carried out a quantitative assessment of the impact of climate change on nutrient flows using a modelling procedure in the Kokemäenjoki river basin, Finland. Nutrient loading was modelled in an area that covers 26% of the entire catchment. The Rossby Centre coupled Regional Climate Model was used for the climate scenarios and emission scenarios (A2 and B2) from the IPCC's Special Report on Emissions Scenarios (SRES). According to the scenario simulations or climate model, annual nutrient loading sums will increase.

Climate change and DOC production

The influence of climatic variables on the DOC concentration has been extensively investigated, with the primary focus on temperature (Freeman et al. 2001b) and precipitation patterns (Tranvik and Jansson 2002). It is well established that hydro-climatic conditions control much of the episodic (Boyer et al. 1997), seasonal (Dawson et al. 2008) and inter-annual variability of the DOC (Köhler et al. 2008), but also long-term trends (Erlandsson et al. 2008). A number of studies have found that a warmer and wetter climate would result in an increase in stream DOC concentrations (de Wit and Wright 2008; Köhler et al. 2009; Sebestyen et al. 2009).

However, other studies argue that climate change has no influence in the DOC change, for example, Hruška et al. (2009) investigated temporal trends in DOC concentration and flux at two geochemically distinct forested catchments in the western Czech Republic. They suggest that climate change has played no role in the changes in the DOC where temperature, precipitation and discharge showed no statistically significant trends during the study period (1993 to 2007).

2.3.3 Climate variability in the UK and North West England

Across the UK, annual average temperatures have risen since 1961 by between 1^{o}C and 1.7^{o}C depending on the region. Nine of the ten warmest UK years on record have occurred since 1990. The summer rainfall has declined by up to 17% since 1961, while the winter rainfall has increased in all parts of the UK.

The UK climate has changed over the 20th Century, which is consistent with the warming in global climate (Hulme et al 2002). Hulme et al. (2002) reported that over the last 200 years winters have become wetter throughout the UK and more frequent the summer heat waves, fewer frosts and the winter cold spells have also been measured.

Temperature in Central England has increased by about 1^{o}C since the 1970s, with 2006 being the warmest on record (Jenkins et al. 2008).

The United Kingdom Climate Impacts Programme (UKCIP) highlights that throughout the 21st century, the UK will be subject to progressively (Jenkins et al. 2008):

- Warmer and wetter winters,
- Hotter and drier summers,
- More extreme rainfall events,
- Sea level rise,
- Reduction in soil moisture, especially during the summers,
- Increased wind speeds and atmospheric depressions.

Climate variability has had significant impacts in recent years. In the North West of UK, for example, extreme climate variability has resulted in flooding in Carlisle in January 2005, heavy rainfall record and flooding in June and July 2007, floods in Cumbria in November 2009, heavy rainfall and flooding in Cornwall in November 2010 and snow and low temperatures in December 2010.

Table 2-4 presents changes in mean daily, maximum and minimum temperature in the North West of England. Between 1914 and 2006, annual daily temperatures have shown an increase of 0.88°C, through the autumn, the summer and the spring (0.89 to 1.19°C). The changes for the shorter 1961 to 2004 climatic period, illustrate an even larger mean annual increase of 1.4°C (significance level 95%), with the most rapid change been observed since 1985 (Jenkins et al. 2008). Comparison between the 1914-2006 and 1961-2006 North West temperature data suggest that there have been greater minimum temperature increases during the winter than the summer for 1961-2006, while the opposite case is true for 1914-2006. For the period 1914 to 2006, maximum temperatures have risen by 0.71°C, and annual minimum temperatures have increased by 1.06°C. For the period 1961 to 2006, maximum temperatures have risen by 1.55°C, while minimum annual temperatures have increased by 1.29°C. Sanderson et al. (2008) concluded that during the winter, minimum and maximum temperatures have increased more when compared to the summer increases between 1961 and 2006, whilst for 1914 to 2006 the reverse is true.

Table 2-4 *Observed changes in daily mean, maximum and minimum temperature (°C), according to season from 1961 to 2006 and 1914 to 2006 for North West England. Shaded values are significant at the 95% level (source: Jenkins et al. 2008)*

Variable	1961-2006	1914-2006
	Change Daily Mean Temperature (°C)	
Spring	1.44	0.89
Summer	1.45	0.91
Autumn	1.07	1.19
Winter	1.81	0.66
Annual	1.40	0.88
	Change Daily Maximum Temperature (°C)	
Spring	1.67	0.59
Summer	1.63	0.67
Autumn	1.13	0.95
Winter	1.93	0.77
Annual	1.55	0.71
	Change Daily Minimum Temperature (°C)	
Spring	1.25	1.19
Summer	1.31	1.10
Autumn	1.03	1.47
Winter	1.7	0.60
Annual	1.29	1.06

Table 2-5 shows the percentage change in precipitation and rainy days in millimetres for North West England. Between 1961 and 2006 precipitation increased by 43.0% during the winter, whilst during the summer it decreased by 13.2%. For the period 1914 to 2006, precipitation significantly decreased by 21.6% during the summer.

Table 2-5 *Observed changes in precipitation amount and rain days, according to season from 1961 to 2006 and 1914 to 2006 for North West England. Shaded values are significant at the 95% level (source: Jenkins et al. 2008)*

Variable	1961-2006	1914-2006
	Precipitation amount (%)	
Spring	6.3	15.7
Summer	-13.2	-21.6
Autumn	5.6	3.5
Winter	43.0	-0.5
Annual	8.8	-2.4
	Days of Rain > 1mm (Days)	
Spring	0.4	
Summer	-1.1	
Autumn	2.9	
Winter	6.8	
Annual	7.5	

Kazmierczak and Carter (2010) reported that the current climate of the North West of England is classified as mid-latitude oceanic with warm summers, cool winters and plentiful precipitation throughout the year. They note that the 2009 autumn heavy rainfall and floods in Cumbria exposed the region's vulnerability to intense rainfall events (Kazmierczak and Carter 2010).

Predicted climate changes in the UK and North West England

Climate change scenarios are plausible descriptions of how things may change in the future (Hulme et al. 2002). There has been considerable debate about the use of the terms "prediction", "projection" and "scenario", and the Intergovernmental Panel on Climate Change (IPCC) in their Third Assessment Report (TAR), (IPCC 2001), chose to abandon the word "prediction" in favour of "projection".

The most up to date and detailed projections are from the UK Climate Impacts Programme (UKCIP) produced by the Met Offices Hadley Centre regional model (HadRM3), who published climate change scenarios available in the UK. The UK Projections (UKCIP09) are presented for three different future scenarios representing high, medium and low greenhouse gas emission.

To look at the risk to the internal environment, the latest probabilistic projections from the United Kingdom Climate Impacts Program (UKCP09) can be used to create probabilistic future weather (UK Climate Projections 2009). UKCP09 contains a weather generator which is able to output both daily and consistent hourly weather data on a 5 km grid over the UK for the historic period (1961-1990) and future time slices in decadal steps from the 2020s up to the 2080s (with each encompassing a separate thirty year period) (Jones et al. 2009).

Key findings for the UK, for the highest changes by the 2080s are (UK Climate Projections 2009):

- Under medium emissions, the central estimate of increase in the winter mean temperature is 3.1ºC; it is very unlikely to be less than 1.7ºC and is very unlikely to be more than 4.8ºC,
- Under medium emissions, the central estimate of increase in the summer mean temperature is 4.2ºC; it is very unlikely to be less than 2.2ºC and is very unlikely to be more than 6.8ºC,
- Under medium emissions, the central estimate of change in annual mean precipitation is +2%; it is very unlikely to be less than –3% and is very unlikely to be more than +14%,
- Under medium emissions, the central estimate of change in the winter mean precipitation is +33%; it is very unlikely to be less than +9% and is very unlikely to be more than +70%,

- Under medium emissions, the central estimate of change in the summer mean precipitation is +1%; it is very unlikely to be less than –8% and is very unlikely to be more than +10%.

Key findings for North West England are presented as changes by the 2050s (UK Climate Projections 2009):

- Under medium emissions, the central estimate of increase in the winter mean temperature is 2.0ºC; it is very unlikely to be less than 1.0ºC and is very unlikely to be more than 3.0ºC. A wider range of uncertainty is from 0.8 to 3.3ºC,
- Under medium emissions, the central estimate of increase in the summer mean temperature is 2.6ºC; it is very unlikely to be less than 1.2ºC and is very unlikely to be more than 4.1ºC. A wider range of uncertainty is from 1.1 to 4.7ºC,
- Under medium emissions, the central estimate of change in annual mean precipitation is 0%; it is very unlikely to be less than –4% and is very unlikely to be more than +6%. A wider range of uncertainty is from –6% to +7%,
- Under medium emissions, the central estimate of change in the winter mean precipitation is +13%; it is very unlikely to be less than +3% and is very unlikely to be more than +26%. A wider range of uncertainty is from 0% to +27%,
- Under medium emissions, the central estimate of change in the summer mean precipitation is –17%; it is very unlikely to be less than –34% and is very unlikely to be more than +1%. A wider range of uncertainty is from –36% to +8%.

The UK Climate Projections (2009) show that under a medium greenhouse gas emissions scenario for the 2080s the climate of the North West is projected to change significantly and experience (UK Climate Projections 2009):

- An increase in average summer temperatures with a central estimate of 3.7 degrees,
- 21% less rainfall in the summer, possibly leading to lower crop yields and water stress,
- 16% more rainfall in the winter increasing the threat of the winter flooding, transport disruption and risks to urban drainage,
- Sea level rise in Liverpool of 30-32cm.

2.4 Summary

Methods for runoff and nutrient flux estimation have also been reviewed, with an emphasis on identifying aspects, which will be important to this research project. Understanding the limits and advantages of current methodologies allows for an assessment of where improvements might be made over current methods.

Chapter 3. General description of the Upper Eden basin

3.1 Introduction

According to the selection criteria required to meet the overall objectives of this study, a catchment, a sub-catchment and a hillslope were selected in the Upper Eden basin. This chapter introduces the Upper Eden in terms of its location, topography, solid and drift geology, hydrogeology, vegetation, land use, soils, hydro-climatic conditions and instrumentation.

The Upper Eden basin (322 km^2) above Appleby is one of four meso-scale basins (order 100 km^2) under the Catchment Hydrology and Sustainable Management (CHASM) programme (Figure 3-1). The CHASM research programme has been established to gain new understanding of the hydrological and ecological functioning of meso-scale catchments and of how catchment response changes with scale, and to translate this new knowledge into enhanced predictive capability. The four meso-scale catchments are being instrumented at the patch/hillslope, micro-catchment (1 km^2) and mini-catchment (10 km^2) scales. In addition, there are soil and groundwater monitoring systems.

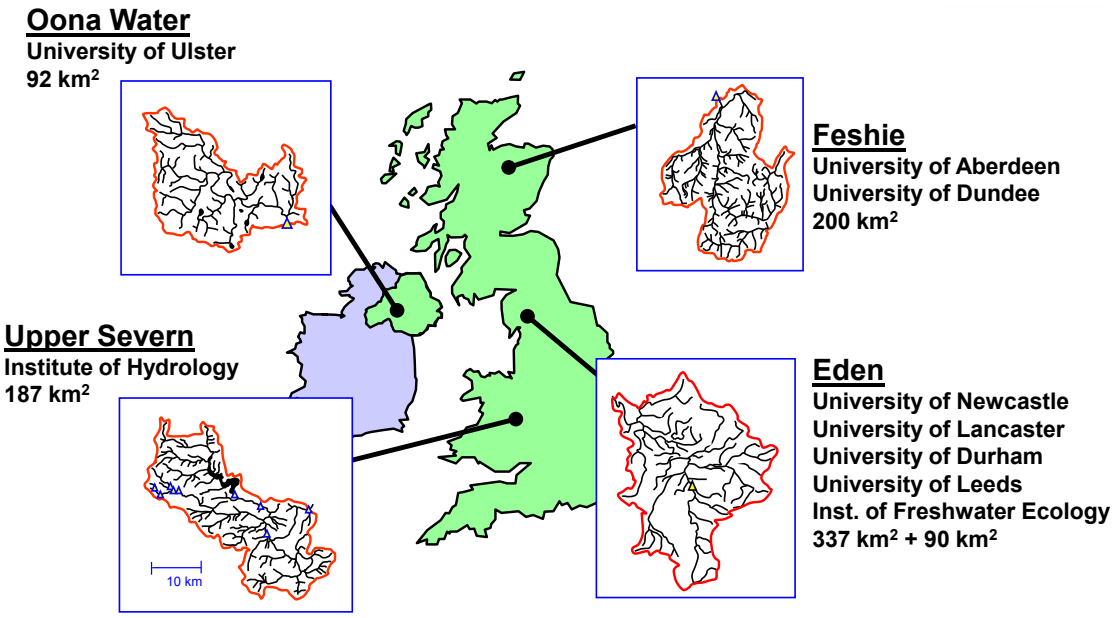

Figure 3-1 *The four instrumented meso-scale catchments across the UK which form the CHASM network (source: University of Newcastle Upon Tyne 2000)*

3.2 Geographical localization and topography

The Eden basin is located in Cumbria in the north west of the UK and is bordered by upland areas of the Pennines to the east and the Lake District to the west (Figure 3-2). It lies at an altitude of 10 to 715 m a.s.l. (latitude 54 36 19 N, longitude 02 49 58 W). The Eden basin is 86 km long, 64 km wide and the Upper Eden basin is 27 km long, 22 km wide. It is limited by the upland areas of the Lake District to the south-west, by the Pennines to the east and the Northumbria National Park to the north. The River Eden rises south of Kirkby Stephen on predominantly limestone fells uplands and then flows northwards through the towns of Kirkby Stephen, Appleby-in-Westmoreland and the city of Carlisle, before discharging into the Irish Sea on the Solway Firth. The Eden receives inputs from of the five key watercourses, the Lowther, Eamont, Irthing, Petteril and Caldew Rivers. This study focuses on Blind Beck and predominantly Sykeside Farm of the Upper Eden basin.

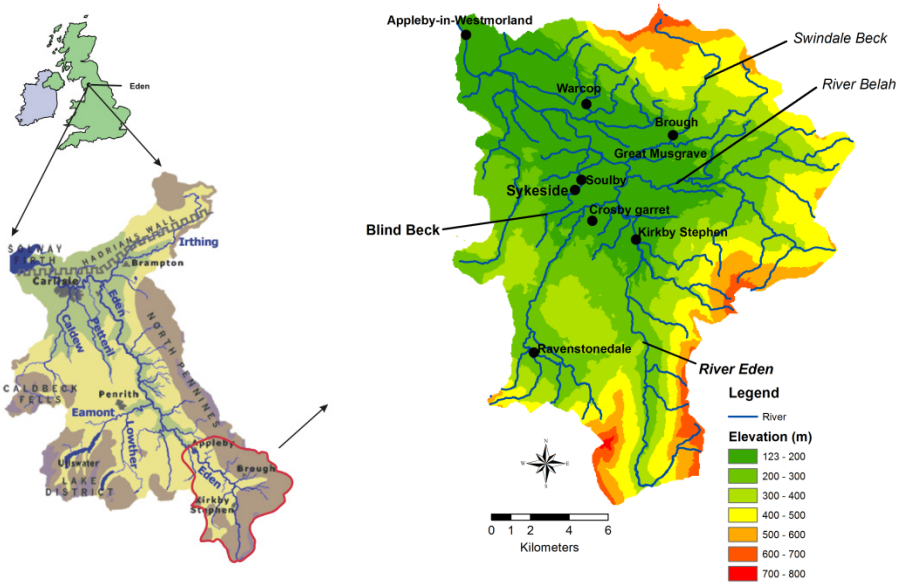

Figure 3-2 *Geographical localization of the Eden (the Upper Eden basin boundary is shown in red) and a Digital Elevation Model (DEM) of the Upper Eden basin*

3.3 Geology and Hydrogeology

The Eden Valley is made up of a half-graben of Permian, Triassic sandstones overlying the Carboniferous series and Jurassic rocks (see Appendix A1). It is separated from the Carboniferous rocks of the Pennine Hills by the Pennine fault (Taylor 2003; Walsh 2004).

In the Eden basin there are seven major hydrostratigraphic units (Younger and Milne 1997; Bathurst 2001; Walsh 2004):

1) The Carboniferous Limestone (aquifers)
2) The Millstone Grit (aquifers and aquitards)
3) The Penrith Sandstone (including the Brockram breccias, and silicified and non-silicified aeolian sandstones) (mainly aquifers)
4) The Eden Shales (aquitards)
5) The St Bees Sandstone (aquifer)
6) The Armathwaite Dyke (aquifer)
7) Quaternary Drift sediments (variable hydrostratigraphy).

Figure 3-3 illustrates a solid geology map with hydrostratigraphic units of the Upper Eden basin.

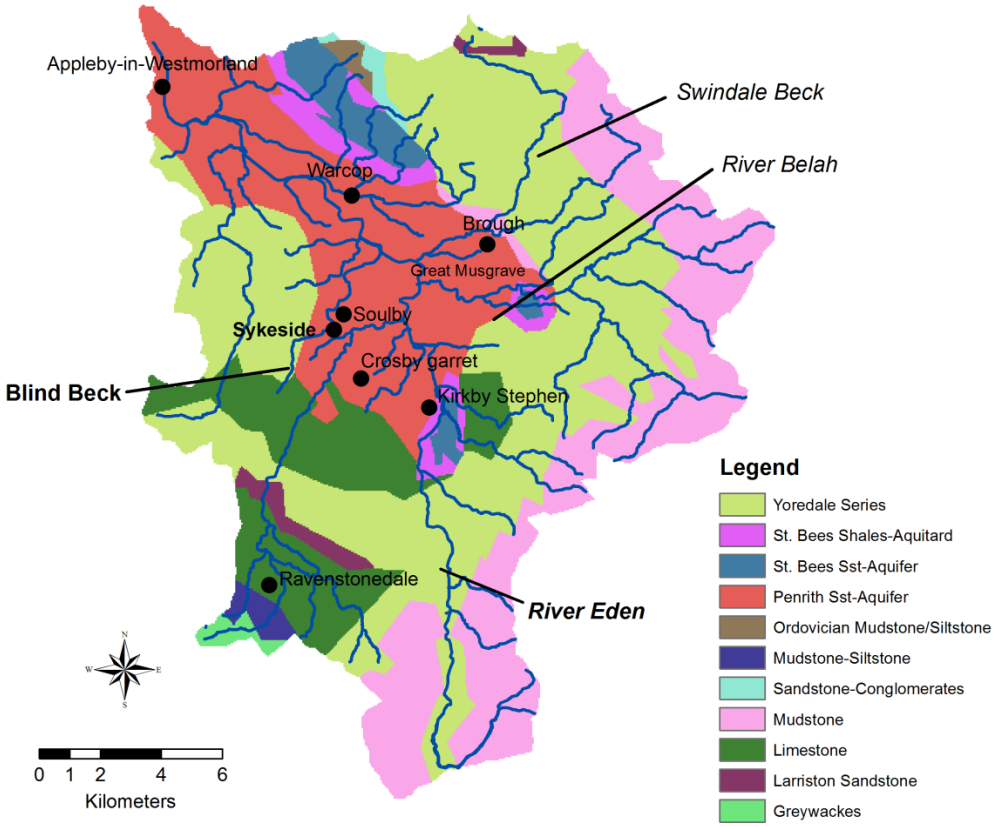

Figure 3-3 *Solid geology with hydrostratigraphic units of the Upper Eden basin*

The major aquifers on the valley floor are the Penrith and St Bees sandstones, which sit on top of the limestone series. The Penrith sandstone is the largest sandstone in the Upper Eden basin and shale separating both of sandstones is defined as aquitard. The valley sides are mainly of Carboniferous limestone and limestone layers, with the exception of the headwater catchment of Gais Gill in the south-west of the basin, which consists of an impermeable greywacke.

Butcher et al. (2003) found that the Permo-Triassic Sandstone has a core hydraulic conductivity of 0.8 m/d for the Penrith Sandstone and 0.24 m/d for the St Bees Sandstone. For both the aquifers, the transmissivity and storage coefficient were given as 240 m^2/d and 1.4 x 10^{-4} respectively. Younger et al. (1997) described the complex hydrostratigraphy of the overlying quaternary deposits, which have a hydraulic conductivity of 0.16 m/d.

Drift geology

A variable thickness of Quaternary drift is present on the valley floor. The drift geology of the Upper Eden is shown in Figure 3-4, where glacial till includes poorly sorted mixtures of diamicts, clays, silts, sands and gravels of hummocky moraines and drumlins interspersed with alluvial deposits. According to Parkin (2000), these may act locally to prevent recharge to the underlying aquifers.

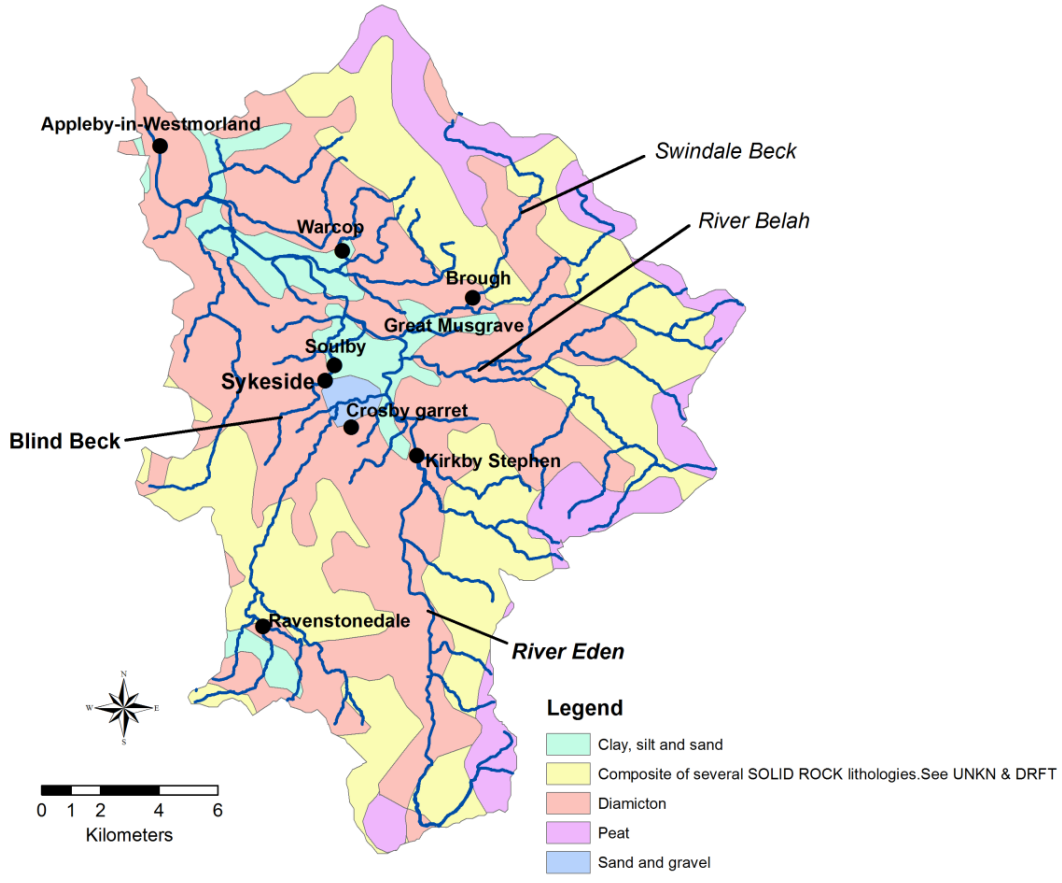

Figure 3-4 *Drift geology of the Upper Eden basin*

3.4 Vegetation and Land use

Upland areas of the Upper Eden consist mainly of rough moorland and unimproved pasture, while lowland areas are generally improved pasture.

The Land Cover Map of Great Britain database (LCMGB) was prepared using available satellite images and aerial photos. Appendix A2 shows a map of 25 different types of land use that have been identified, and the description of each type is given in Table 3-1. In the interests of clarity, a land use map of the major groups has been produced and presented in Figure 3-5. Maps show areas of land as polygons, each with attributes such as land cover class, area and boundary length. Land use types of the Upper Eden basin can be grouped into 13 major groups (Figure 3-5), namely mown, grazed turf, meadow, verge and semi-natural area is the main type with 48%.

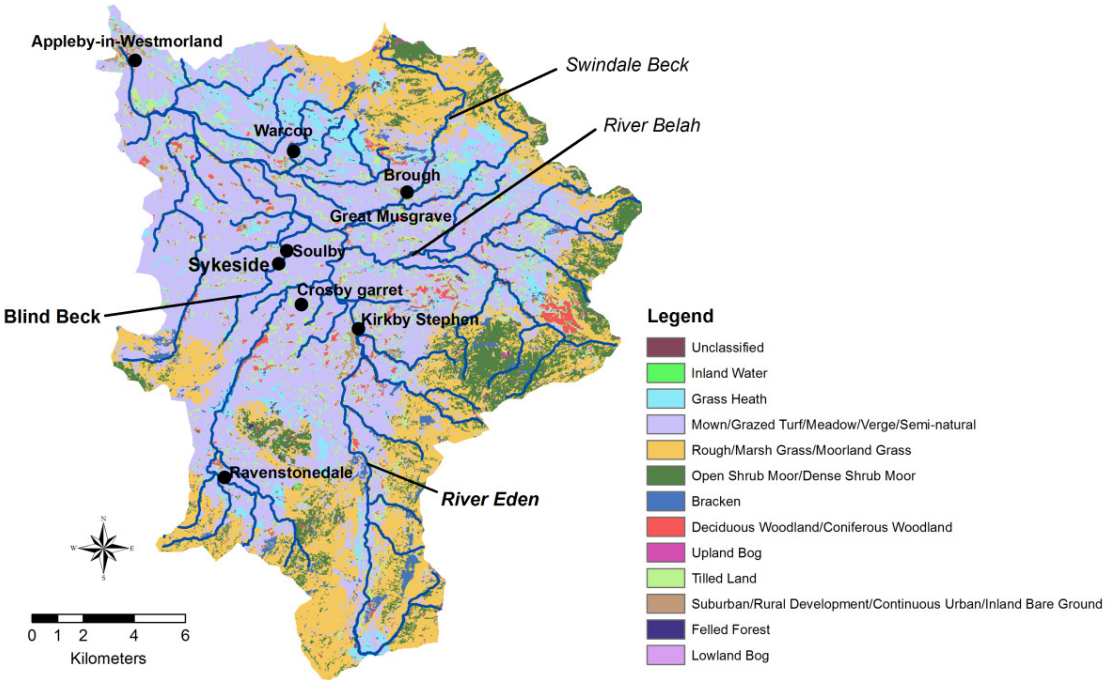

Figure 3-5 *Land Cover Map of major group of the Upper Eden basin*

In the uplands, livestock densities are relatively low, and are continuing to decrease as the entry level single farm payments (and some stewardship schemes) encourage low stock density on the fells, while in the lowlands they are relatively high as the good grasses are ideal for stock rearing. Arable farming occupies a very small proportion of the Upper Eden mainly around the Appleby area, while it increases around the Temple Sowerby area. In the basin there is no coniferous forestry and small patches of deciduous woodland can be found in parts. There are no major settlements in the basin apart from two small market towns of Appleby and Kirkby Stephen. In the basin, there is no major industrial activity and a portion of the north of the catchment is owned by the MoD (Ministry of Defence) and is an infantry training ground; this does not affect the land use vegetation (moorland) but does affect access.

Table 3-1 *The correspondence between the 25 'target' cover-types and the 17 'key' cover types of the Land Cover Map of Great Britain (source: Centre for Ecology and Hydrology, Land Cover Map of Great Britain 1990)*

LAND COVER CATEGORY (17 class system)			TARGET CLASSES (25 class system)	
Aa	1b	Sea / Estuary	1c	Sea / Estuary
B	2	Inland Water	2	Inland Water
C	3	Beach / Mudflat / Cliffs	3	Beach and Coastal Bare
D	4	Saltmarsh	4	Saltmarsh
E	5	Rough Pasture / Dune Grass / Grass Moor	5	Grass Heath
			9	Moorland Grass
F	6	Pasture / Meadow / Amenity Grass	6	Mown / Grazed Turf
			7	Meadow / Verge / Semi-natural
G	7	Marsh / Rough Grass	19	Ruderal Weed
			23	Felled Forest
			8	Rough / Marsh Grass
H	8	Grass Shrub Heath	25	Open Shrub Heath
			10	Open Shrub Moor
I	9	Shrub Heath	13	Dense Shrub Heath
			11	Dense Shrub Moor
J	10	Bracken	12	Bracken
K	11	Deciduous / Mixed Wood	14	Scrub / Orchard
			15	Deciduous Woodland
L	12	Coniferous / Evergreen Woodland	16	Coniferous Woodland
M	13	Bog (Herbaceous)	24	Lowland Bog
			17	Upland Bog
N	14	Tilled (Arable Crops)	18	Tilled Land
O	15	Suburban / Rural Development	20	Suburban / Rural Development
P	16	Urban Development	21	Continuous Urban
Q	17	Inland Bare Ground	22	Inland Bare Ground
			0	Unclassified

[a] class reference within the 17 'key' cover-type categorisation.
[b] 'band' within the 17 'key' cover-type 1 x 1 km summary data.
[c] label value within the 25 'target' cover-type 25 x 25 metre data.

3.5 Soil types

The characteristic soils of the Upper Eden basin are presented in Figure 3-6. A semi-fibrous black peat surface with a reddish brown coloured peat deeper down (Winter Hill Association) is present at the upland moors of Mallerstang Common and the Pennine Hills. The basin around Kirkby Stephen and the sides of the valley are covered by typical brown earth soils (Eardiston 1 and Wick 1 Association), described as reddish well drained coarse loamy, fine silty soils and dark-yellow brown, slightly stony sandy loam or sandy silt soil; and are common in northern England. From Kirkby Stephen to

Temple Sowerby the valley bottom and low lying areas are covered by typical stagnogley soils (Clifton Association and Brickfield 3 Association), with patches of alluvial soils. The Winter Hill series mentioned above is generally a poor draining soil and is susceptible to waterlogging, the stagnogley soils typically have a slowly permeable lower subsoil, which may make them prone to waterlogging, while the other soil series are fairly good to good draining soils.

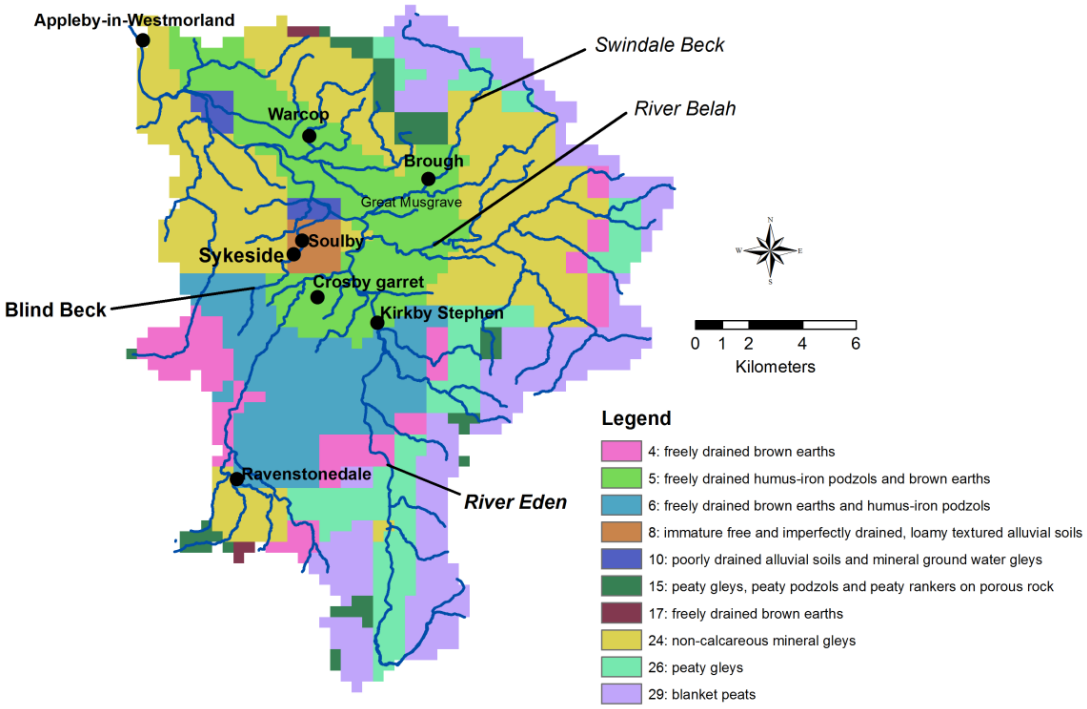

Figure 3-6 *HOST soil classification map of the Upper Eden basin (Appleby)*

Table 3-2 shows the percentage distribution of HOST cover categories over the Upper Eden. The basin is dominated by non-calcareous mineral gleys (28.5%). HOST descriptions are given in Appendix A3.

Table 3-2 *HOST class percentage cover in the Appleby catchment; legend for HOST class is shown in Figure 3-6*

HOST CLASS	Percentage cover of the Upper Eden
4	7.3
5	16.0
6	13.1
8	1.3
10	1.2
15	3.2
17	0.3
24	28.5
26	10.4
29	18.7

3.6 Hydro-Climatic conditions

The Upper Eden basin receives a yearly average precipitation of 735 mm to 2590 mm (SAAR 1961-1990), although there are large differences across the basin due to differing elevations and to rain shadow effects from the local hills and the Lake District Mountains to the west.

According to Walsh (2004) rainfall totals in the Upper Eden vary from less than 650 mm per year in the valley bottom to over 2000 mm per year on the fells and have been linearly related to elevation. Wilkinson (2009) reported that snow cover in the winter months at elevations above 400 m can be significant (15-30 snow days a year); however, for the majority of the Upper Eden there are usually 0-5 snow days a year. The same author indicates that there has been significantly less snow since 2000 compared with snowfall in the 1990s, which may be a result of climate change.

During the winter 2009 and 2010, there was a significant snow cover with long snow days and observed frozen soil. From the National River Flow Archive, mean flow at Temple Sowerby is 14.6 m^3/s.

3.7 The Upper Eden instrumentation

This section introduces the Upper Eden instrumentation in terms of Automatic Weather Stations (AWS), stage recorders and raingauges.

3.7.1 Automatic weather station (AWS)

CHASM Automatic Weather Stations

In the Upper Eden basin, the Warcop Range AWS (NY733197) at an elevation of 227 m has a record dating back to 1983, while the next AWS is Shap (NY557120) outside of the Temple Sowerby basin at an elevation of 255 m, with a record dating back to 1982. Table 3-3 gives details about CHASM AWS that were refurbished systems produced by Environmental Measurements Ltd, Sunderland. Locations of the CHASM AWS are given in Figure 3-7. In January 2005, all weather stations were upgraded to use Campbell CR10X loggers.

Table 3-3 *Automatic weather stations installed in the Eden basin under the CHASM programme*

Station	Coordinate		Elevation (m)	Date installed
	X	Y		
Gais Gill	371400	500900	400	AWS installed 28/7/03
Hill Top Farm (Great Musgrave)	375700	513800	155	AWS installed 9/9/03
Barras	385300	511600	440	AWS installed 01/4/04

Figure 3-7 *Location of all weather stations in the Upper Eden basin*

Data from AWS have been nearly continuously recorded since January 2005 to late 2006, with some problems with sensors. At Gais Gill the temperature and relative humidity measurements have been affected by power fluctuations at certain times of the year, which makes the data set erratic for small time periods (Wilkinson 2009). The same author indicates that following the complete failure of the anemometers and thermometers, Barras and Gais Gill have been offline since November 2006.

The multi-parameter CHASM weather stations record rainfall, wind speed (min, max and average), direction, net radiation, relative humidity and temperature (at 15 minute intervals), and battery voltage of the logger and rain.

3.7.2 Stream gauges

Environment Agency (EA) Stream Gauges

There are only two the Environment Agency gauging stations in the Upper Eden basin. One of them, Kirkby Stephen (NY77300970) is the longest recording gauging station: it

was constructed in November 1971 and has a catchment area of 69.4 km^2. According to data of the Environment Agency, in 2007, the weir structure is a non-standard compound broad crested weir, built to stabilise the bed and act as a low flow control.

The second gauging station was constructed in July 2000 at Great Musgrave, 7 km downstream of the Kirkby Stephen gauging station and is the most recent of the Environment Agency's Upper Eden stations (NY76481313). At this location, the weir is a non-standard shallow V weir, 30 m across.

CHASM Stream Gauges

In Table 3-4, the details of the CHASM gauge stations that were constructed in 2002/03 can be seen.

Table 3-4 *Gauging stations in the Upper Eden basin*

Station	Coordinate		Type	Date installed
	X	Y		
Eden, Appleby	368200	520300	Shaft-encoder and Horizontal Acoustic Doppler Current Profiler	18/12/2002 (H-ADCP installed December 2004)
Scandal Beck, below Ravenstonedale	372100	504600	Shaft-encoder	05/09/2002
Artlegarth Beck, Artlegarth House	372600	502300	Shaft-encoder	16/09/2002
Artlegarth Beck, Gais Gill	371400	501100	Pressure Transducer-Diver	28/07/2003
Helm Beck	370400	514100	Shaft-encoder	18/09/2003
Blind Beck at Little Musgrave	375400	513100	Shaft-encoder	18/07/2003
Scandal Beck at Smardale	373500	508500	Shaft-encoder	18/09/2002
Tributary entering Blind Beck at Smithfield	375300	513000	Pressure Transducer-Diver	10/07/2003

3.7.3 Raingauges

The CHASM raingauges have a network of 21 point-rainfall gauging stations (all tipping-bucket raingauges recording at 0.2 mm increment on event basis). Among them seventeen are located inside and four outside of the Upper Eden basin, as shown in Figure 3-8. The overview of the CHASM raingauges is described in Table 3-5. Data were obtained from Newcastle University.

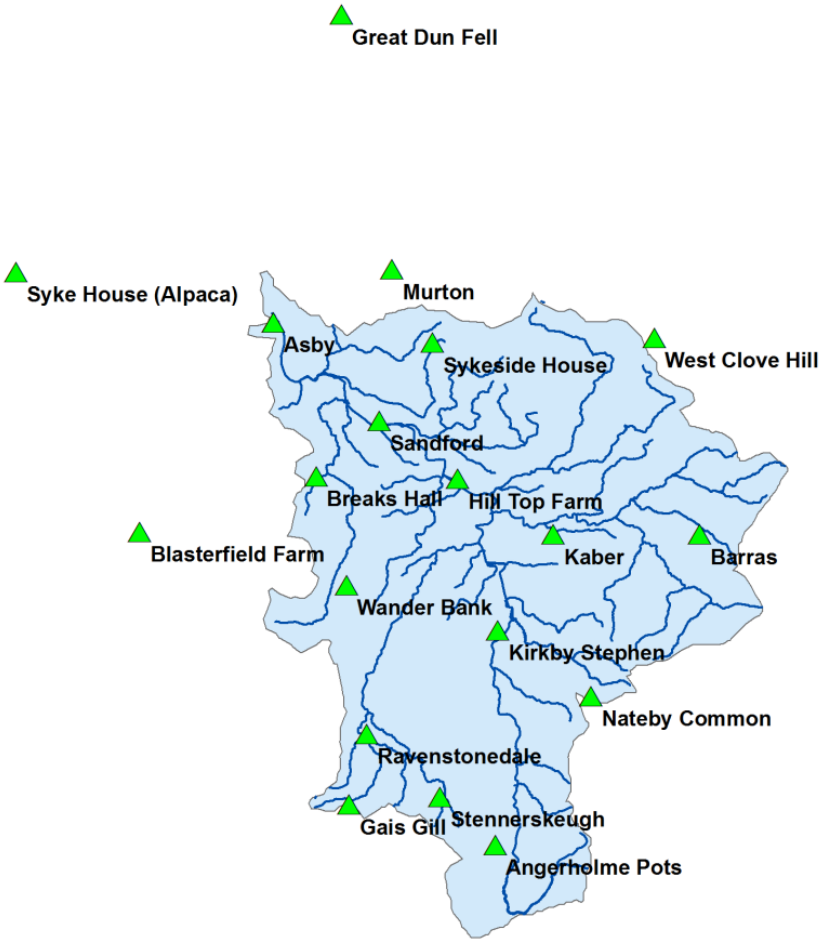

Figure 3-8 *Location of all raingauges in and surrounding the Upper Eden basin*

The longest precipitation data record is from the Appleby Castle raingauge back to 1891.

Table 3-5 *Detail and their dataset of the CHASM gauging stations*

Station	Coordinate		Elevation (m)	Date installed
	X	Y		
Angerholme Pots	377200	499300	480	07/08/2003
Appleby Castle	368400	520000	148	27/2/04
Asby	368400	520000	250	24/10/2003
Barras	385300	511600	440	24/2/04
Blasterfield Farm	363100	511700	330	05/07/05
Breaks Hall	370100	513900	175	22/10/03
Gais Gill	371400	500900	400	28/07/2003
Great Dun Fell	371100	532200	868	01/08/05
Hill Top Farm	375700	513800	155	31/07/2003
Kaber	379500	511600	170	07/09/05
Kirkby Stephen	377300	507800	190	27/11/03
Lunds Fell	380600	596700	650	27/11/03
Murton	373100	522100	275	24/11/03
Nateby Common	381000	505200	500	27/1/04
Ravenstonedale	372100	503700	270	28/10/2002
Sandford	372600	516100	150	07/09/05
Stennerskeugh	375000	501200	380	06/01/2003
Syke House (Alpaca)	358200	522000	120	05/07/05
Sykeside House	374700	519200	180	20/11/04
Wander Bank	371300	509600	315	24/10/03
West Clove Hill	383500	519400	510	16/3/04

3.8 Summary

This chapter presents a brief summary of the location, topography, geology, hydrogeology, vegetation, land use, soils, hydro-climatic conditions and instrumentation of the Upper Eden basin. Within the CHASM programme, the Upper Eden basin is considered as one of the most instrumented at the meso-scale. The Upper Eden basin was found to be the most appropriate where data from this network are available to meet the aim and objectives of this study. In the next chapter, the study sites, hillslope experiment, field sampling, monitoring, analysis and the model setup required are presented.

Chapter 4. Methods

4.1 Introduction

This chapter will examine a series of field investigations, laboratory experimental procedures and a modelling approach. In this study, the methods used will illuminate the central questions about the influence of runoff processes at a hillslope under perturbed climate conditions and a catchment scale with respect to nutrient fluxes. Collected and analysed data will be used to build models across different scales.

In this study, the overall experimental design is proposed to investigate flow and water chemistry across three scales: the Blind Beck catchment (9.2 km^2), the sub-catchment (0.09 km^2) and the plot scale (2 m^2) within the hillslope located in the Upper Eden basin, Cumbria, UK. Runoff experiments are conducted on two hillslope runoff plots to identify runoff processes and to quantify nutrient fluxes, one under perturbed (i.e. increased rainfall) and another under control plot.

4.2 Overall methodology approach

The research methodology consists of three main activities as follows (Figure 4-1):

1) Field work (sampling and monitoring)
2) Laboratory analysis
3) Modelling.

To address the project aims and test the proposed hypotheses (Chapter 1), a field experimental design was used. The field experiment finds its justification in terms of meeting the study aims of improving understanding of hydrological controls on nutrient fluxes, and analysing the influence of future climate variability on nutrient losses from soils. This is generally part of broader research aimed to show scale effects in runoff and nutrient fluxes. Therefore, research methods and criteria for selecting experimental design have been well defined in the literature with the largest amount of research performed using runoff plots to provide specific information about hydrologic processes, for example to test soil erodibility and runoff generation on small plots under simulated rainfall (Messer 1980) or to determine the relationship between soil loss, runoff and slope angle (Djorovic 1980). The plot method has also been carried out to determine nutrient loss in drainage and surface flow from grazed cattle pastures

(Monaghan et al. 2000). Slaymaker (1991) states that most of the runoff plot experiments do not provide suitable data because they are too large or too small to permit very detailed observations during storm events, or because the monitoring system is insufficiently precise to provide detailed formation on process control. Many studies used plots that have varied in shapes, length and width, depending on the process being studied, for example from the 1 m^2 to 10 m^2 plots used by Bagayoko (2006) in the province of Kompeinga, West Africa. There is an argument about the influence of the length, width and slope of the runoff plot on the rate of water and sediment delivery. In practice, it is difficult to suggest an adequate length of the plot (Slaymaker 1991). The advantage of runoff plots is that they give the researcher control over some variables, while the disadvantage is that data cannot be directly translated to a whole basin (Striffler 1965).

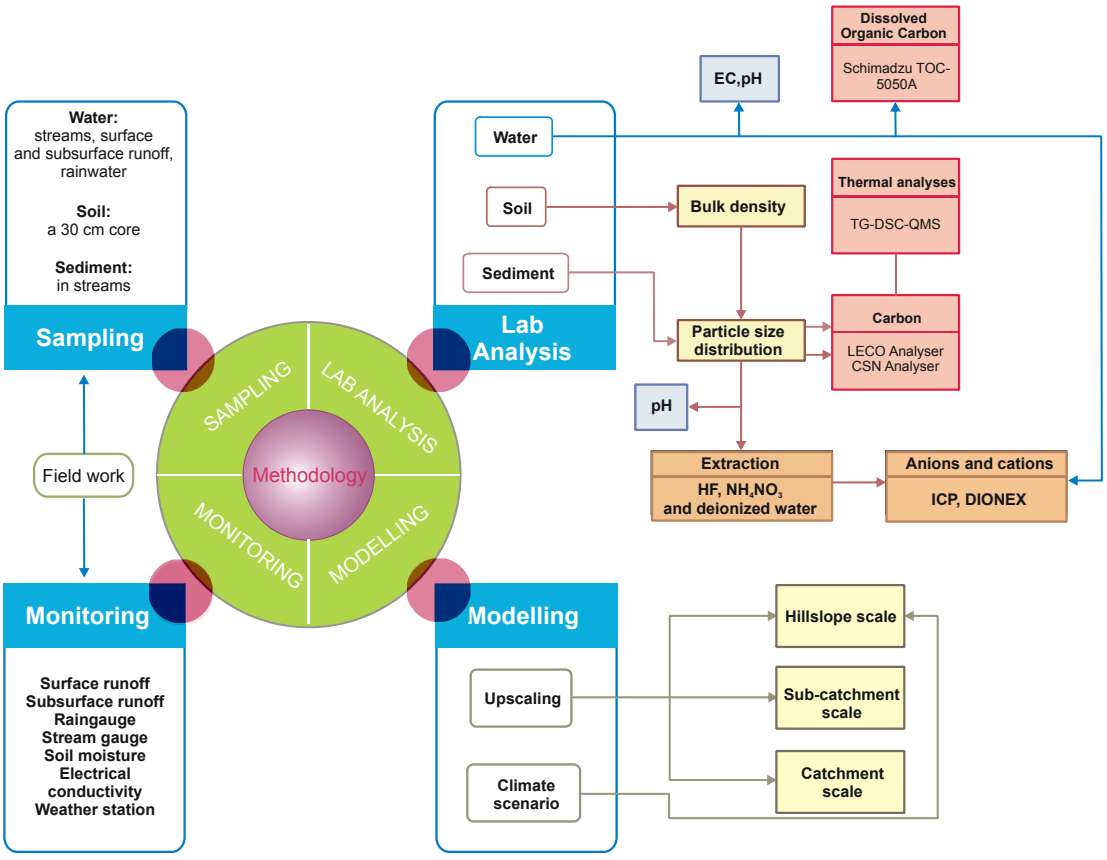

Figure 4-1 *Flow diagram showing main steps in the methodology*

The main focus of this study is on high-resolution experiments at the runoff plot scale, to provide detailed and controlled insights into how precipitation perturbs soil quality and nutrient release. However, since impacts of farming and other land use activities are generally at catchment scales, there is need for the study to obtain information at larger scales. Therefore, an experimental design was devised to investigate hydrological and

hydrochemical behaviour across scales, from a hillslope plot then at sub-catchment and small catchment scales. Modelling studies help to interpret the data at each scale, and are used to generalize the results for other catchments. This design defines the necessary instrumentation, which is focussed on capturing runoff processes in small experimental plots on a hillslope, in a monitored sub-catchment nested within a tributary catchment of the River Eden. Three runoff plots were sited within the sub-catchment to allow discharge measurements. Runoff plot dimensions were 2 by 1 m with wooden sheets on three sides. The downstream section of each plot was fitted with a gutter. The runoff from the plot was led into a tipping bucket raingauge, then into a storage container until it can be measured, sampled and recorded.

Suction lysimeters are the types of equipment used to collect samples of the soil water solution, in order to determine nutrients in subsurface flow. Soil water content was measured with a Soil Moisture Logger DL6. The soil moisture probes were installed at 3 depths (10, 20 and 30 cm) at the upper and the bottom of the hilslope to determine the relationship between soil moisture storage and rainfall infiltration. A trench was constructed to measure a subsurface flow and the DOC and the NO_3^- concentration during different climate conditions. This experimental design was set up to provide data sets at the plot and hillslope scales on runoff, soil and nutrient fluxes. The advantage of using the plot scale studies is the possibility for detailed process monitoring on a small scale, and providing a basic description of the most relevant aspects (Michaelides et al. 2009). Data from the experimental design are used as reference in modelling approach, calibration and validation.

4.3 Site selection

To understand the surface and subsurface hydrological controls on nutrient fluxes, three sites were selected for intensive observation in the Upper Eden basin. The selected sites are the Blind Beck catchment, the Hollow sub-catchment and a hillslope, both at Sykeside Farm. Figure 4-2 shows that Sykeside Farm is located in the Upper Eden basin, about 8 km south-west of Brough and about 7 km north-west of Kirkby Stephen.

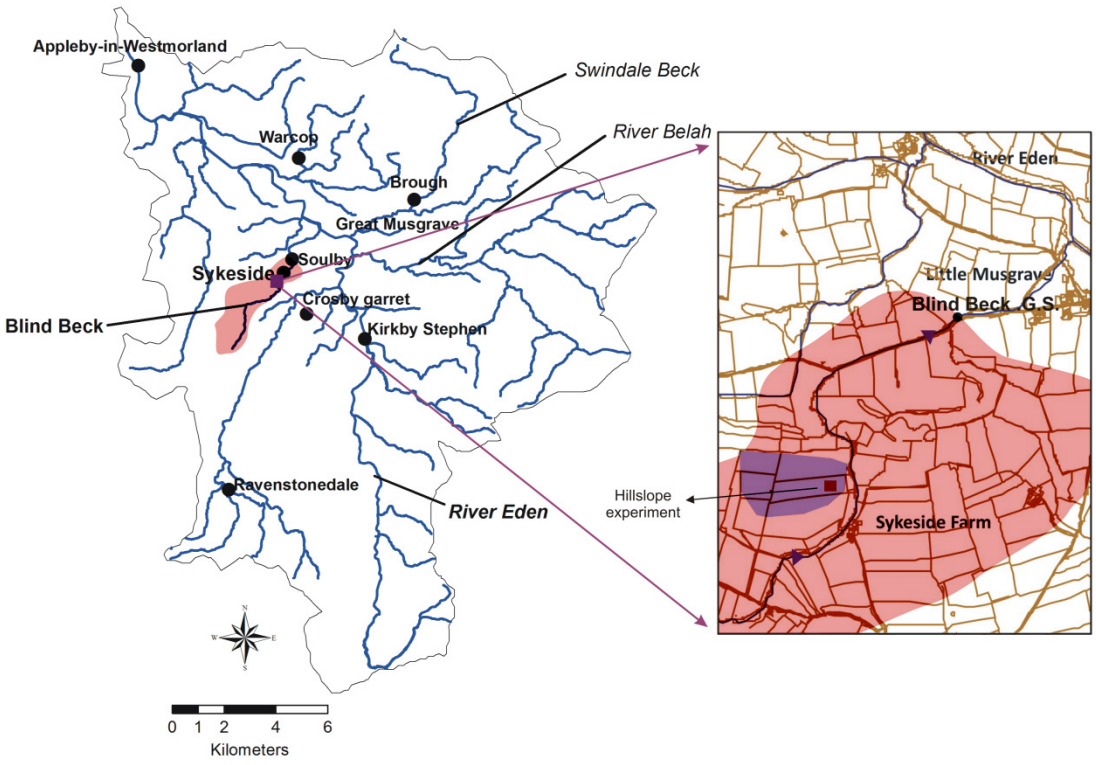

Figure 4-2 *Location of the three study sites. The Blind Beck catchment is shown in the red shaded area; the Hollow sub-catchment is shown in violet shaded area*

The purpose of this study at the catchment/sub-catchment scale is to: a) obtain initial estimates of hydrological and hydrochemical behaviour at catchment/sub-catchment scale and b) test scale variability.

4.3.1 The Blind Beck catchment

The Blind Beck catchment covers 9.22 km^2 and contains a small stream that flows past Little Musgrave Farm (Figure 4-2). The boundary of the catchment and the stream network were delineated from a 50 x 50 m^2 grid cell Digital Elevation Model (DEM) using hydrological functions of ArcGIS, Figure 4-3.

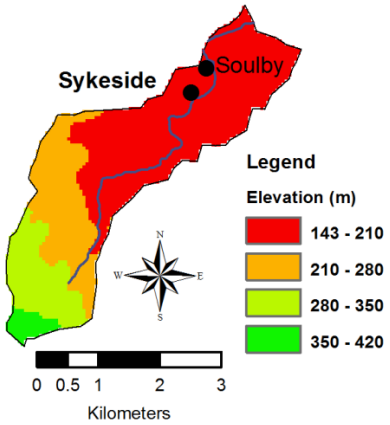

Figure 4-3 *Digital Elevation Model (DEM) of the Blind Beck catchment*

Geology

The main formations in the study area consist of Penrith Sandstones and limestones (Figure 4-4, Table 4-1). It can be seen from Figure 4-5 that most of the study area falls within the till deposits of the Devensian. Lower elevation areas are associated with alluvium deposits. On the west of the stream is fine to medium textured lodgement till (formerly boulder clay), glaciolacustrine and estuarine deposits. Further details of the geology are given in the geology chapter of the Upper Eden basin (Chapter 3).

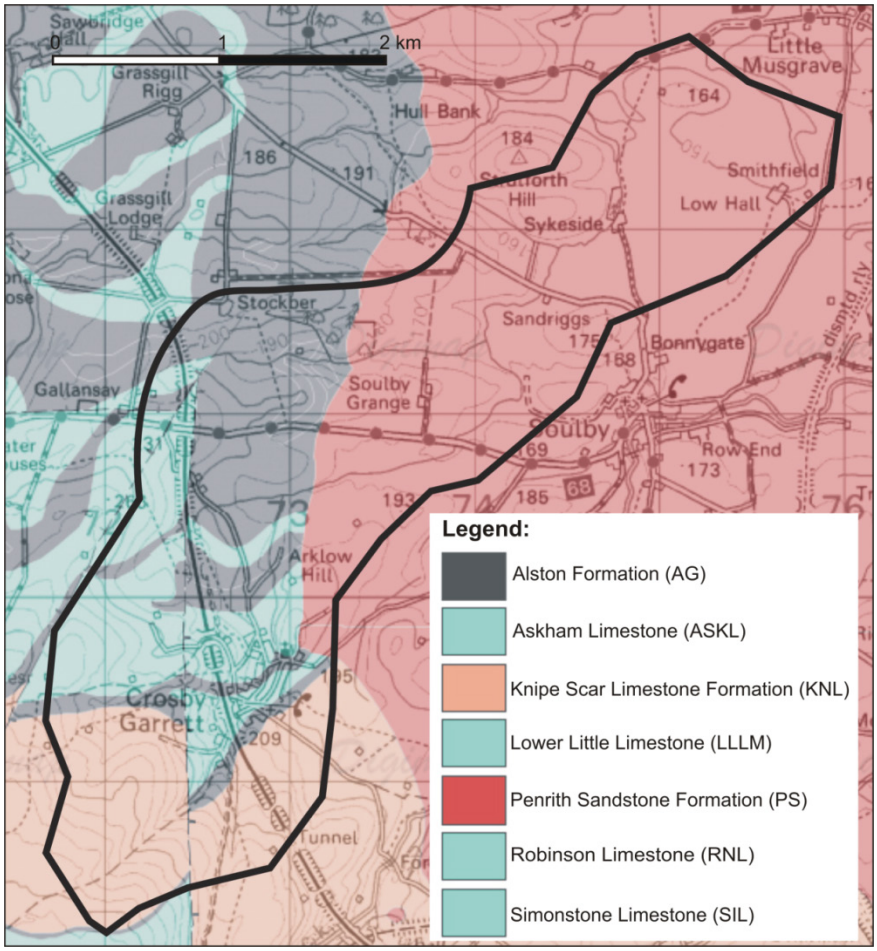

Figure 4-4 *Geology map of the Blind Beck catchment (source: Edina Digimap 2008 and modified by the author)*

Table 4-1 *Rock description of the Blind Beck catchment geology map (source: Edina Digimap)*

Map code	Description	Max age	Min age	Lithology description	Thickness
AG	ALSTON FORMATION	Asbian	Pendleian	Bioclastic limestones, sandstones, mudstones, siltstones and rare coals typically in regular cyclothemic sequence.	c.340m
ASKL	ASKHAM LIMESTONE MEMBER	Asbian	Brigantian	Limestone, dark grey, well-bedded, wackestone and packstone, porcellanous in parts. Prominent layers with algal oncoliths and coral colonies. The member is split into 2 leaves by a thin layer of red-brown mudstone.	12 - 14.7m.
KNL	KNIPE SCAR LIMESTONE FORMATION	Asbian		Pale grey, scar-forming limestones, mostly thick-bedded biosparites and biopelsparites commonly pseudobrecciated, and probable thin siliciclastic bed, not exposed at type section.	61m seen, but top 16 metres of formation not present
LLLM	LOWER LITTLE LIMESTONE	Brigantian			
PS	PENRITH SANDSTONE FORMATION	Early Permian		Coarse-grained cross-bedded aeolian sandstone.	up to c. 100m
RNL	ROBINSON LIMESTONE	Asbian			
SIL	SIMONSTONE LIMESTONE	Brigantian			

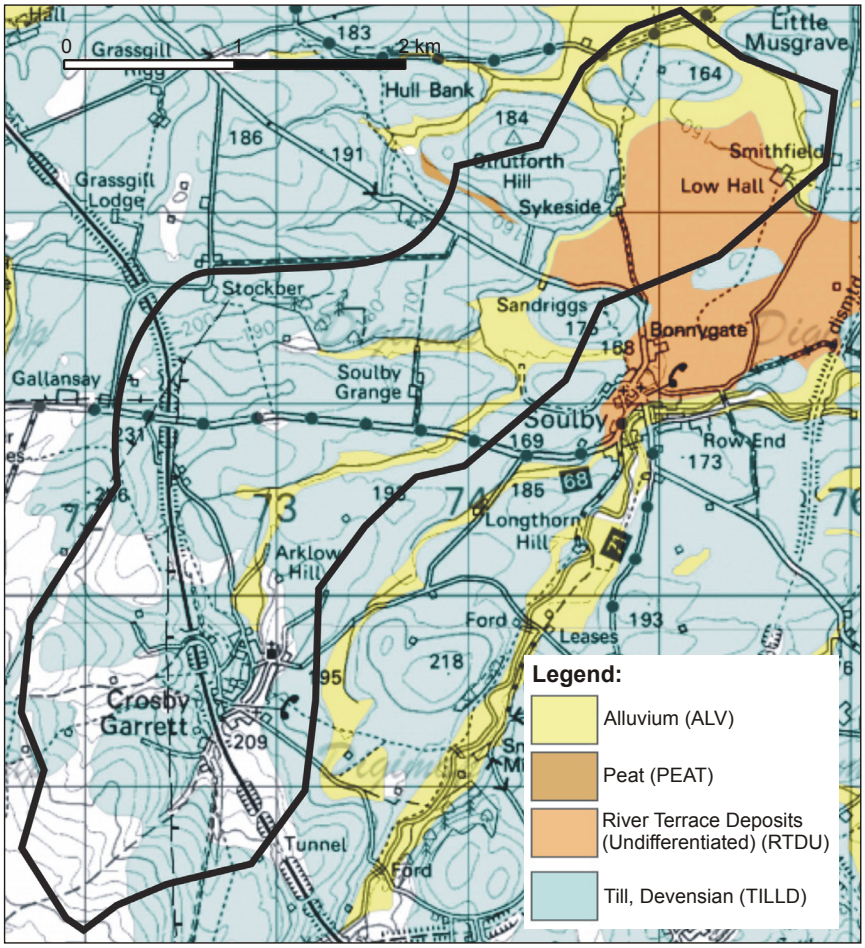

Figure 4-5 *Superficial deposits map of the Blind Beck catchment (source: Edina Digimap 2008 and modified by the author)*

Vegetation and land use

A map of 25 different types of land use is presented over the study area. This map was reclassified into twelve (12) categories of land cover, as shown in Figure 4-6. The vegetation of the Blind Beck catchment is represented essentially by meadow (58%) and mown, grazed turf (24%).

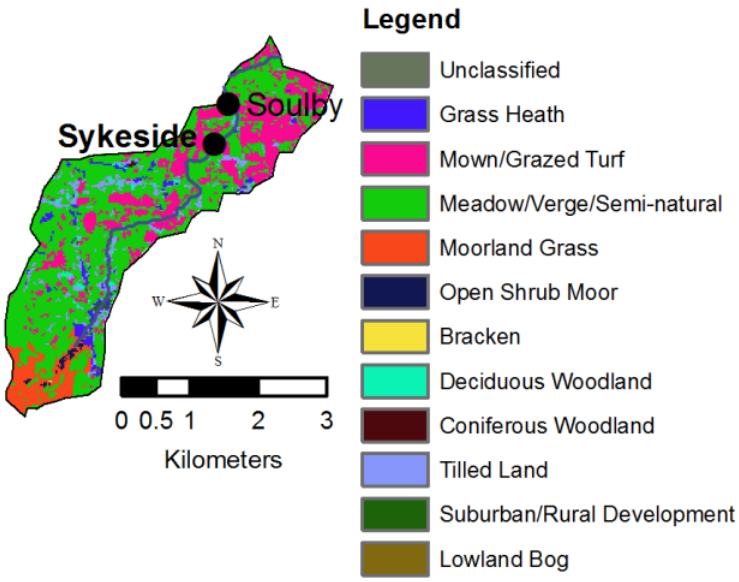

Figure 4-6 *The Land Cover Map of the Blind Beck catchment*

Soil types

The spatial distribution of the main types of soil can be seen in a soil map (Figure 4-7). The soils in this area are predominantly freely drained brown earths and humus-iron podzols (43%) and loamy textured alluvial soil (27%) in the lower part of the catchment with wetness class I – III (Figure 4-8). Loamy textured alluvial soil has a thick top layer and a higher infiltration capacity, making it less susceptible to erosion. On the west, the soil type is non-calcareous mineral gleys with wetness class III or IV (Appendix A3). This clay soil is characterised by poor infiltration with a shallow layer of topsoil that makes it more prone to overland flow and soil erosion.

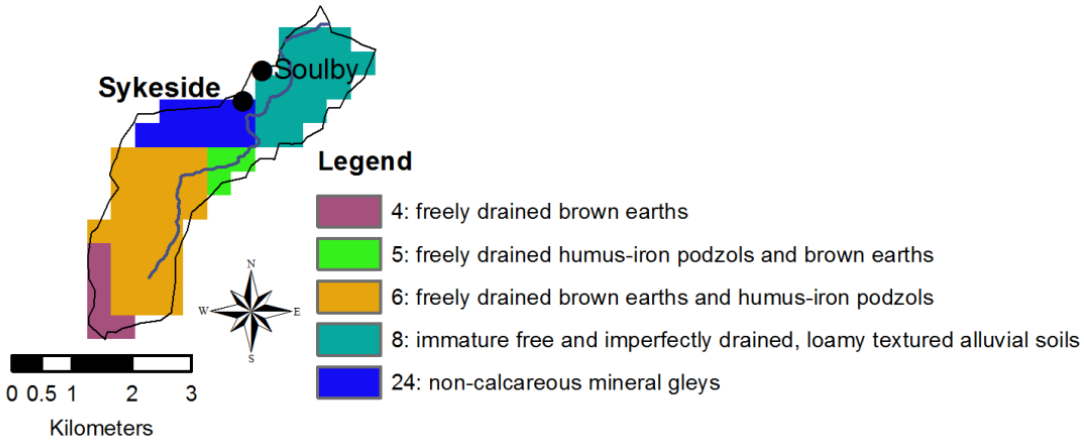

Figure 4-7 *The HOST map of the Blind Beck catchment*

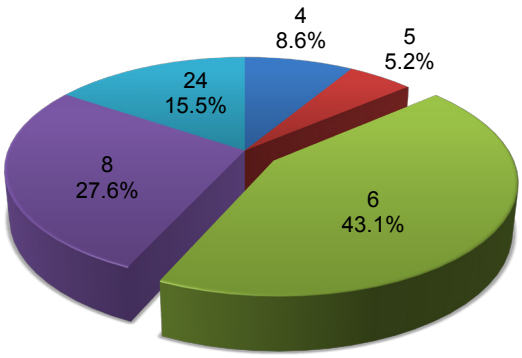

Figure 4-8 *The HOST class percentage cover for the Blind Beck catchment 4: freely drained brown earths, 5: freely drained humus-iron podzols and brown earths, 6: freely drained brown earths and humus-iron podzols, 8: immature free and imperfectly drained loamy textured alluvial soils and 24: non-calcareous mineral gleys*

The Blind Beck catchment instrumentation

Instruments at the outlet of the Blind Beck catchment include a multi-parameter water quality station recording a selection of physico-chemical variables (including pH, conductivity, turbidity, and dissolved oxygen (DO)). This station was installed in July 2005. Unfortunately, it has become broken since 2008 and there are no data available for our study period. The site is also equipped with a stream gauge. Stream flow is logged at 15 minute intervals. Figure 4-9 shows the permanent equipment of the Blind Beck stream.

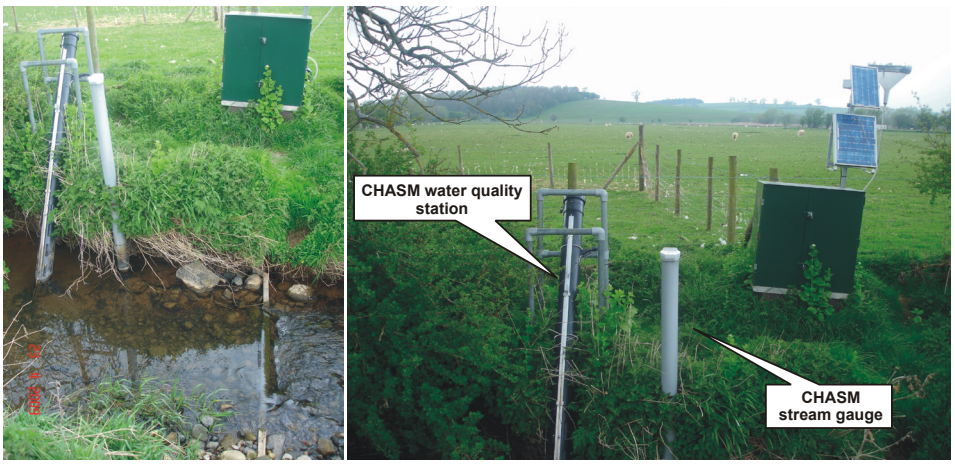

Figure 4-9 *The Blind Beck catchment: permanent equipment*

4.3.2 The Hollow sub-catchment

The Hollow sub-catchment is located at Sykeside Farm with an area of 0.09 km^2 with a small ephemeral stream, which was chosen as the flow observation point (Figure 4-2). The lowest elevation of the sub-catchment is about 150 m (east side) at its outlet to stream and its peak reaches an elevation of 184 m above sea level (a.s.l.) in the southwest part at Strutforth Hill.

Barber (2008) mentions Sykeside Farm in his thesis as an example of a sediment and nutrient loss mini-catchment 'hotspot' within the Upper Eden basin. It is also characterised by a flashy response during storms. This site was selected because of good relations with the landowner, an arranged land agreement, installed equipment for the CHASM project, and good position of the sub-catchment. The boundary and topography of the Hollow sub-catchment were obtained using GPS surveying equipment.

Field survey

A survey of the sub-catchment area was undertaken by the author. This was done using the Leica 1200 GPS (base station and rover) to provide a close resolution topographic survey and to map visible features (Figure 4-10). A control point was established on high ground (184 and 173 m). The GPS operator walked across the entire area, recording points at a distance of approximately 20 m intervals.

Figure 4-10 *The author taking points in the Hollow sub-catchment*

Satellite reception proved to be problematic in the areas of higher vegetation. Very dense, overhead vegetation can block or weaken the signal. In that case, it is helpful to take data points in a nearby area to obtain a clearer satellite signal.

A total of 512 points was collected over the sub-catchment area. These points were then transferred to an Excel spread sheet to facilitate analysis and GIS mapping. The X and Y data were then used to automatically plot the points onto a map in ArcGIS (Figure 4-11). These point data were then interpolated to create a triangulated irregular network (TIN) using *3D Analyst-Create/Modify TIN*, Figure 4-12.

Figure 4-11 *Data points recorded over the sub-catchment*

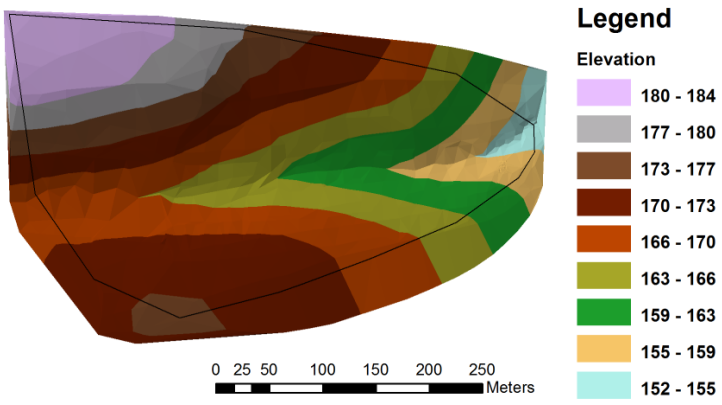

Figure 4-12 *Triangulated Irregular Network (TIN) of the Hollow sub-catchment*

A Digital Elevation Model (DEM) of the sub-catchment was constructed using the TIN model.

Geology

On Sykeside Farm, the dominant rock type is Penrith sandstone (Figure 4-13, Table 4-2).

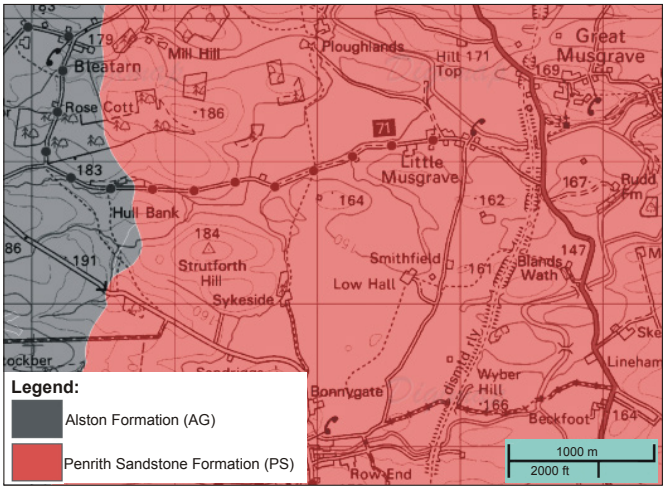

Figure 4-13 *The geology map of Sykeside Farm (source: Edina Digimap 2008 and modified by the author)*

Table 4-2 *Rock description of Sykeside geology map (source: Edina Digimap 2008)*

Map code	Description	Max age	Min age	Lithology description	Thickness
AG	ALSTON FORMATION	Asbian	Pendleian	Bioclastic limestones, sandstones, mudstones, siltstones, and rare coals typically in regular cyclothemic sequence.	c. 340m
PS	PENRITH SANDSTONE FORMATION	Early Permian		Coarse-grained cross-bedded aeolian sandstone.	up to c. 100m

Figure 4-14 presents superficial deposits with dominant till and alluvial deposits from the Permian and the Jurassic.

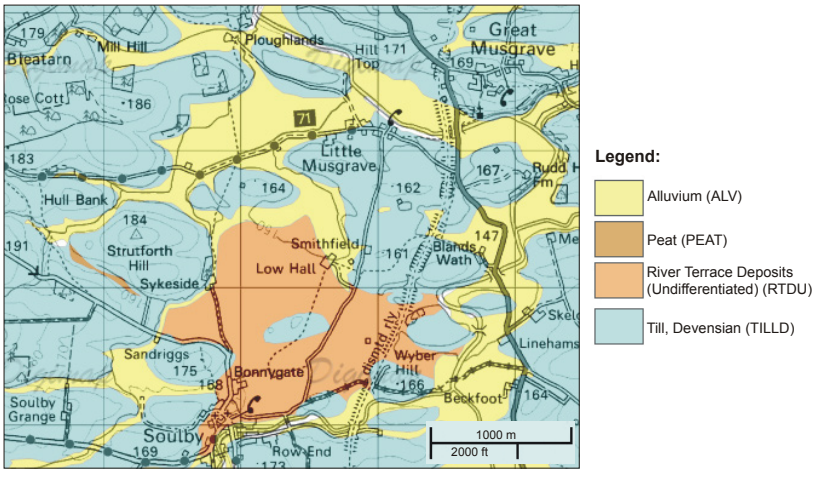

Figure 4-14 *Superficial deposits of Sykeside Farm (source: Edina Digimap 2008 and modified by the author)*

Vegetation and land use

The vegetation of Sykeside Farm covers about 26 ha of the field with wetlands, permanent pasture and temporary grass field, Figure 4-15. The Hollow sub-catchment is represented by permanent pasture. Livestock farming is the predominant activity at Sykeside Farm, with the rearing of animals such as cattle and sheep. In the northern part of the field, as at the lower end of the farm, wetland has been under the stewardship for some years.

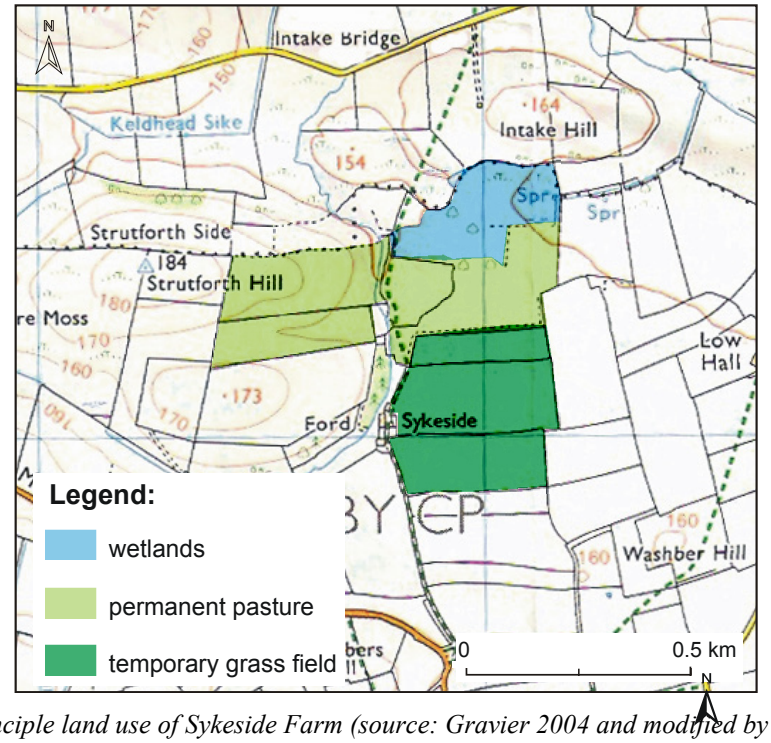

Figure 4-15 *Principle land use of Sykeside Farm (source: Gravier 2004 and modified by the author)*

The unimproved and naturally boggy north part of the farm (represented at the top of Figure 4-15) is used intermittently for sheep grazing.

Soil types

Soils are classified according to the HOST Classification (The Macaulay Institute 2008). As can be seen in Figure 3-6 for the Upper Eden basin, Sykeside Farm is classified as the HOST type 8 and 24. The HOST type 8 corresponds to the immature free and imperfectly drained, loamy textured alluvial soils and the HOST Type 24 corresponds to the non-calcareous mineral gleys.

Sub-catchment instrumentation

Rainfall data were collected using a raingauge installed at the outlet of the Hollow sub-catchment (Figure 4-16 and 4-17). This raingauge has been operational since 1996 and measurements are taken automatically at 0.2 mm increments on an event basis.

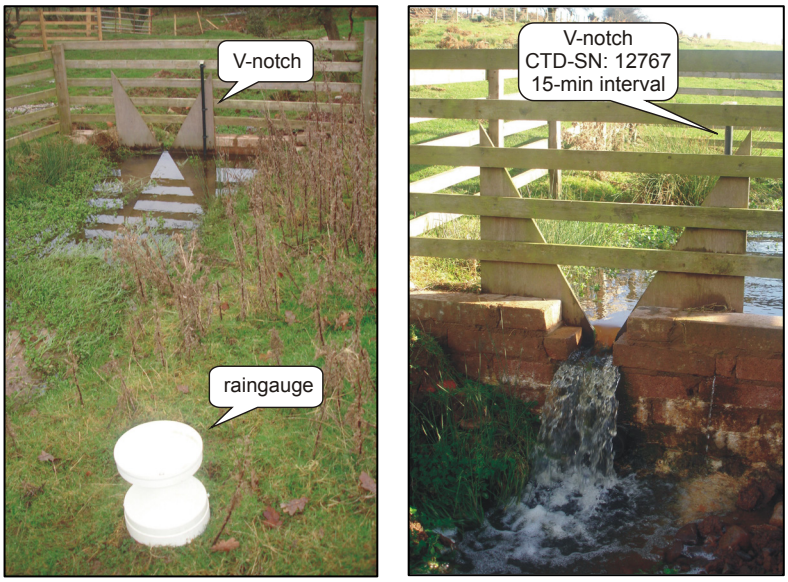

Figure 4-16 *The Hollow catchment: permanent equipment*

Discharge data used in this study have been provided by an existing data logger at 15 minute intervals on the 60° V-notch weir at the outlet of the sub-catchment Hollow (Figure 4-16). Details about the construction and maintenance of the weir can be found under section "Monitoring" later in the text. Figure 4-16 presents the permanent instruments that are installed at the outlet of the catchment.

The X, Y and Z data obtained from GPS survey were used to plot 3-dimensional surface of the Hollow sub-catchment by SURFER software (Figure 4-17).

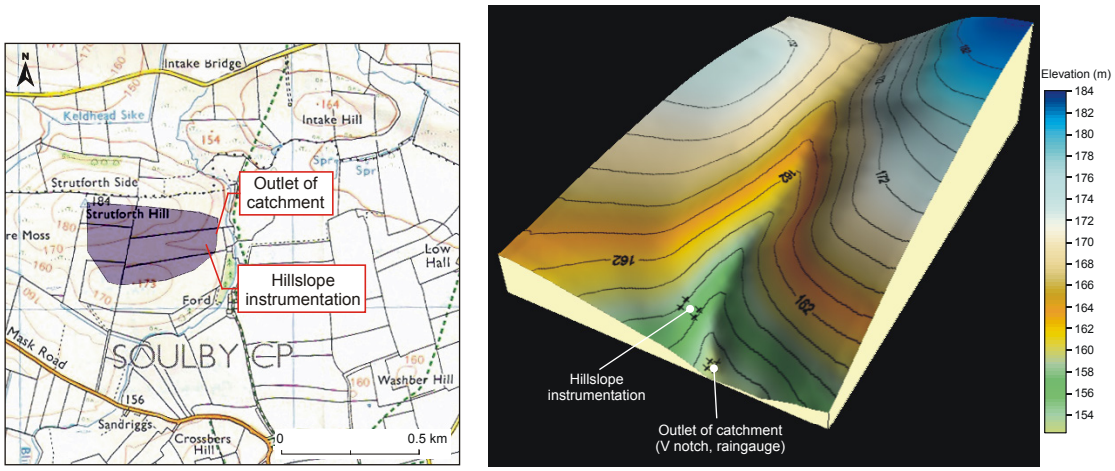

Figure 4-17 *Location of the Hollow sub-catchment and the hillslope instrumentation*

4.4 Hillslope experiment

4.4.1 Field site and soil

The location of the hillslope experiment is presented in Figure 4-17 in the Hollow sub-catchment. The soil profile was observed when a trench was dug to excavate and

repair a drainage pipe running through the middle of the sub-catchment area, Figure 4-18 (see Appendix B). This mineral soil profile shows:

Litter – (O horizon) the top, made up of humus (decomposed organic matter),

Organic-rich topsoil – (A horizon) the topsoil, plant roots grow in this dark-coloured layer, made up of humus mixed with mineral particles,

Compacted inorganic layer – (E horizon) the leaching layer, light in colour. It is made up mostly of sand and silt, while below is the subsoil (B horizon) layer which consists of clay and mineral deposits (such as calcium carbonate). In the process of leaching, this layer has lost most of its minerals and clay as water percolates through the soil,

Gravel and stones – regolith (C horizon) consists of slightly broken-up bedrock. Plant roots do not penetrate into this layer, very little organic material is found in this layer.

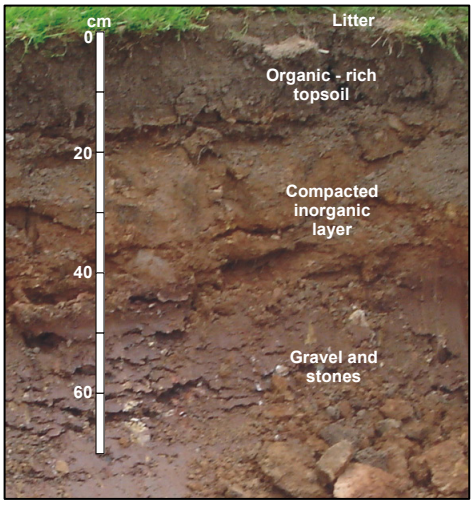

Figure 4-18 *A soil profile in the Hollow sub-catchment open pit*

4.4.2 Experimental design

Experimental runoff plots were set up in April 2009 at the hillslope of Sykeside Farm. The location of these plots within the sub-catchment is shown in Figure 4-17. A wooden fence measuring 9.5 m x 11 m has been placed at the hillslope to prevent cattle accessing the plot, and to protect the hillslope instrumentation. A list of material and instruments used for runoff plot installation is shown in Table 4-3.

The Mini Diver is a data logger for the measurement of temperature and water level. The CTD Diver is a datalogger for measurement of conductivity, temperature and water level. The Baro Diver is designed to measure the atmospheric (barometric)

pressure for a particular area in order to compensate the Diver range of Loggers. When used in conjunction with the MiniDiver and CTD Diver, the data collected is compensated using the DiverOffice software wizard to provide correct water level readings.

Table 4-3 *Material and instrument list required for experimental runoff plots*

No.	Material - Instruments - Data collection system
10	2 m wooden board
7	1 m wooden board
3	1 m plastic gutter
6	gutter corners
2	1 x 2 m plastic sheet
	polyethylene pipe
2	1 m perforated PVC pipe
2	47 x 64 x 50 cm containers
4	Tipping bucket collector 3.5l
2	Tipping bucket collector 10l
1	Rainwater collector
6	MiniDiver
2	CTD Diver
2	Baro Diver
4	Lysimeter
1	Soil Moisture Data Logger DL6 with 6 Theta Probes
	Pocket PC
	Grass trimmer

The purpose of the study at the runoff plots is to: a) test experimental methods and b) obtain initial estimates of hydrological and nutrient responses of plots under natural and altered climate conditions.

Plot characteristics

At the hillslope of Sykeside Farm, three pairs of 1 m wide by 2 m long runoff plots have been isolated on the upper three sides by wooden frames driven 5 cm into the soil and extending 5 cm above the soil with the long axis orientated down the slope (Figure 4-19 and 4-20). A 1 m gutter was installed at the base of each plot to collect overland flow; inserted 5 cm into the soil to the upper edge level with the soil surface at the lower end of each plot. Special care provided for minimal soil disturbance in the installation of the gutters and runoff plots. The gutters were equipped with polyethylene pipe, which firstly directs the rainfall into a small plastic bottle with a CTD Diver (250 ml) and then into a runoff collector (in general tipping buckets) of 3.5 l (MiniDiver) and 10 l placed in the ground (Figure 4-19). One Baro Diver was placed in the bucket at the hillslope while one surplus Baro Diver was installed at the outlet of the Hollow sub-catchment as

a backup. The start time of the runoff (runoff discharging from the gutter to a collection bucket) is recorded by a MiniDiver installed in the bucket. The 10 l runoff collectors were cleared of sediment and water after each rainfall event. As the rain falls, the first plastic bottle fills up and then overflows into the second one and so on, until it reaches the last one for collecting runoff samples through the pipe fitted to the wall of the bucket. When the last tipping bucket is full, the rainfall then overflows through the pipe fitted in the lid. The tipping buckets were covered with a plastic lid to prevent the catching of external precipitation and to prevent the evaporation of the collected runoff water. The loss of runoff into the tipping buckets was minimal due to continuously checking of possible air in the pipes due to visual evidence of the air bubbles in the small plastic bottle with CTD Diver (250 ml). For removing air from pipes, first the gutter was cleaned, then the pipe fitted to the wall of the bucket was removed, and the water amount was increased into the gutter to force the air out or by the second method of blowing through the pipe to dislodge the lock. The gradient of runoff plots was matched to the gradient of the hillslope (a gradient of 13%) on which they were set up. These runoff plots were placed close enough to each other (a distance of 1 m between them) to avoid the influence of the soil spatial variability and rainfall runoff monitoring (Figure 4-20). According to this, the soil was uniform and the soil physical characteristics of an area of 9.5 m x 11 m were similar. Table 4-4 shows the summary of the soil physical characteristics collected outside and around on the fence at four points. Samples were taken with a hammer auger at the 7.6 cm depth and 3.3 cm diameter before fencing. Figure 4-19 shows the layout of the hillslope instrumentation.

The plots were named A, B and C; A and B were selected to present perturbed climate conditions (double rainfall input) with installed irrigation pipes, while C was a control plot, so that the natural (unperturbed) climate conditions can be presented. In order to not disturb runoff plot A, plot B was used for taking the soil samples. It is assumed that additional rainfall for the perturbed plot is proportional to the area of the rainfall catcher.

Table 4-4 *Physical properties of soil in site*

Site	Bulk Density (g/cm^3)	% Sand	% Clay + Silt	Soil Class*
1	1.47	80.40	19.17	Loamy sand
2	1.46	83.82	15.86	Loamy sand
3	1.38	84.52	15.26	Loamy sand
4	1.43	84.56	15.12	Loamy sand

*Based on the particle size distribution triangle, the UK system

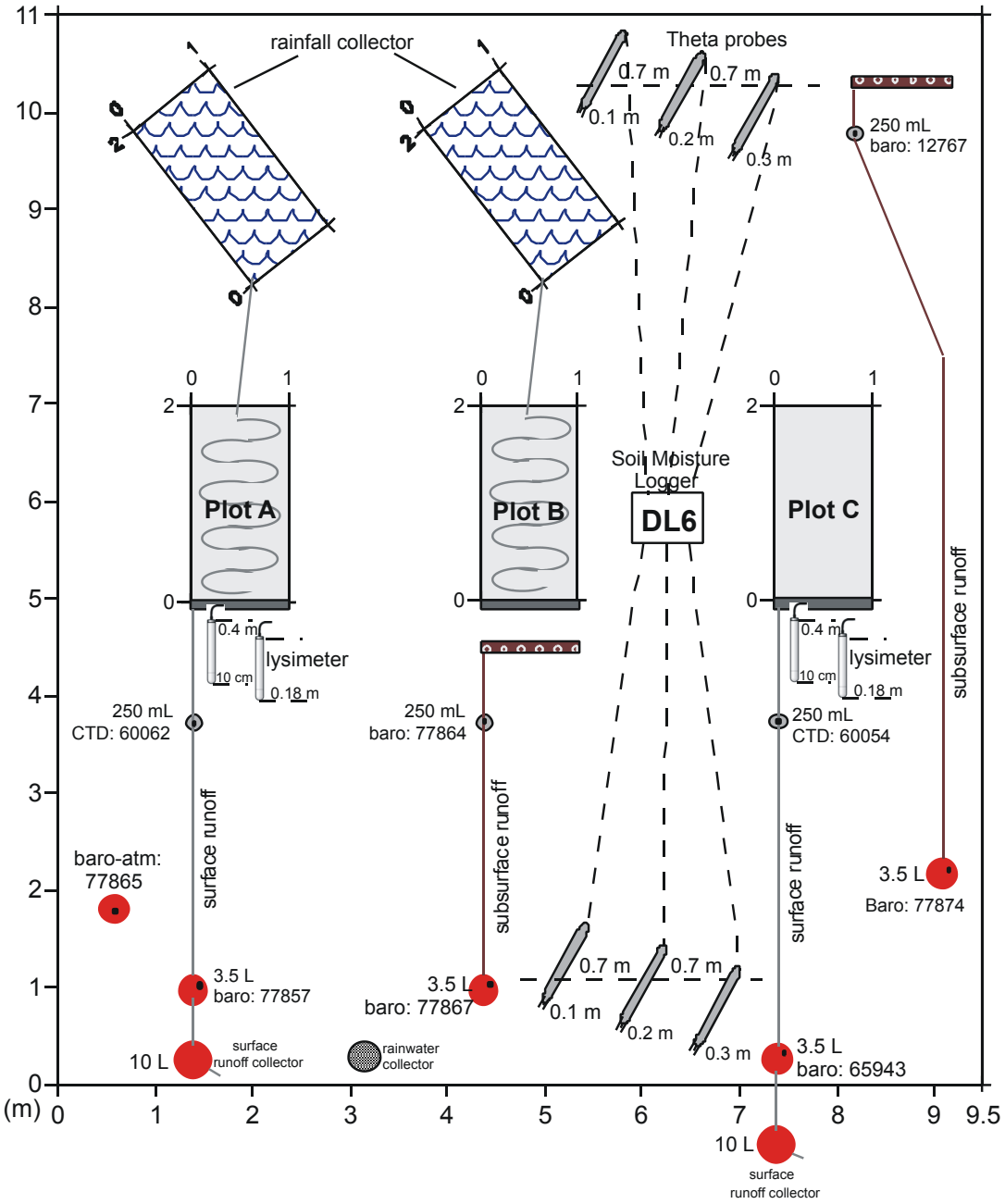

Figure 4-19 *Layout of the hillslope instrumentation*

Plots were assigned as follows:

- Perturbed plot => Double rainfall # A
- Perturbed - sample plot => Double rainfall - soil samples # B
- Control plot => Natural # C

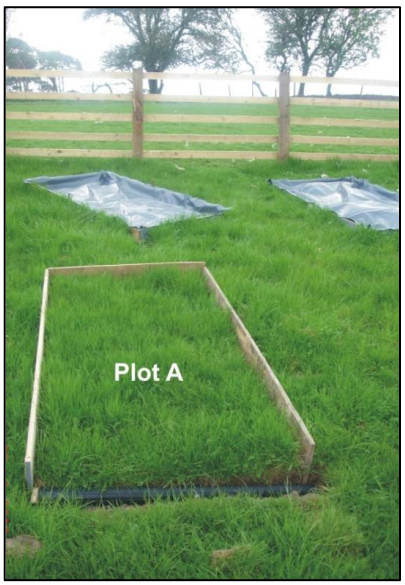

Runoff plot A when freshly constructed

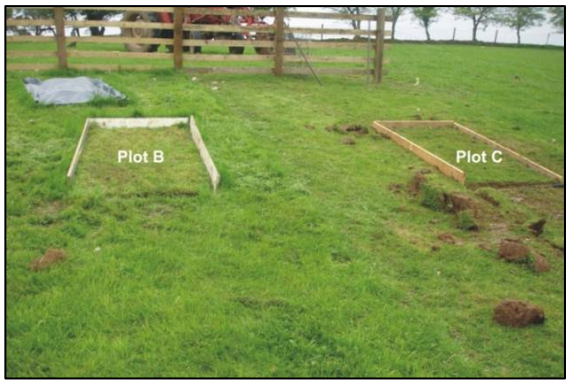

Runoff plots B and C when freshly constructed

Perturbed plots A and B with installed irrigation pipes when freshly constructed

Figure 4-20 *Runoff and rainfall plots in picture*

Considering that the runoff coefficient from a grass plot due to each storm would be in the range of 0.05 - 0.35 meaning that they only contribute 5% - 35% of their rainfall to overland flow, it is assumed that a figure of 30% runoff coefficient would be reasonable. From historical data, it is estimated that the highest amount of rain for each storm event would be about 100 mm. Therefore, a design rainfall figure of 125 mm would be sufficient. In a case of a 2 m^2 runoff plot, the runoff generated from each storm would be equal to 75 litres.

Rainfall simulator

Water used in the enhanced rainfall was obtained from rainfall collectors. It was necessary to collect small volumes of rainfall water, instead of trying to collect larger volumes of rainwater in a bigger tank over a longer period, as this would encourage the blooming of algae. Each collector consisted of rainfall plot, measuring 1 m by 2 m, isolated by wooden frames, with the bottom being covered by a plastic sheet (Figure 4-20). These collectors were connected to the perturbed plots using

polyethylene irrigation pipes. Later on, containers were used with size 47 x 64 x 50 cm for collection of rainfall of larger volume.

Application of the enhanced rainfall was made on 27 August 2009 to 18 March 2010, and then started again on 15 July 2010 to 19 August 2010. On 15 July 2010, containers were used to collect additional rainfall to perturbed plots (A and B).

4.4.3 Rainfall and runoff measurements (non-recording raingauge)

A modified rainfall collector was placed between plots to monitor the rainfall volume and to take rainwater samples (Figure 4-19 and Figure 4-21). A 10 litre tipping bucket is attached to a UV resistant plastic funnel, diameter of 254 mm. A plastic mesh is placed in the funnel to prevent blocking.

Figure 4-21 *A rainfall collector devices*

The total rain and runoff from runoff plots was measured by emptying the tipping bucket into a measuring cylinder. The main disadvantage of this method was that cumulative runoff from several rainfall events could be attributed to one rainfall event. For example, during the night several rainfall events can take place after which only one reading is made.

4.4.4 Soil moisture measurements

Prior to the field experiment, grass had been grown on the hillslope. The grass was removed with minimal disturbance to the soil surface. The soil moisture content was observed at 10, 20 and 30 cm depths on the top and the bottom of the hillslope with the use of a Soil Moisture Logger DL6 (Figure 4-19 and Figure 4-22). The soil moisture content was recorded at 15 min intervals at three depths. A Theta Probe was inserted

into the ground at a 45 degree angle. It measures volumetric soil moisture content (θv) by responding to changes in the dielectric constant (ε) of the soil.

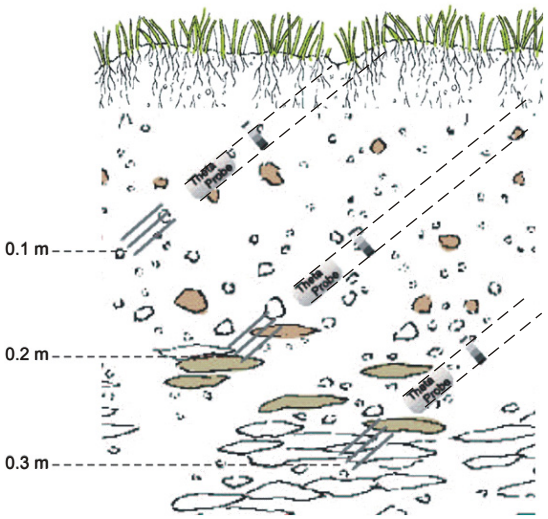

Figure 4-22 *The Theta Probes installed at three depths*

4.4.5 Suction lysimeters

The perturbed (A) and control (C) plots were instrumented with soil water samplers, also known as lysimeters (1900L12-B02M2 SOIL WATER SAMPLER, 12 inch length) at shallow (10 cm) and deep (18 cm) soil profile position above clay layer. Soil water was extracted by an extraction kit at time intervals of once per month. On each plot, two samplers were placed approximately 0.40 m away from each other and 0.30 m away from the left and right edge of the plot (Figure 4-23).

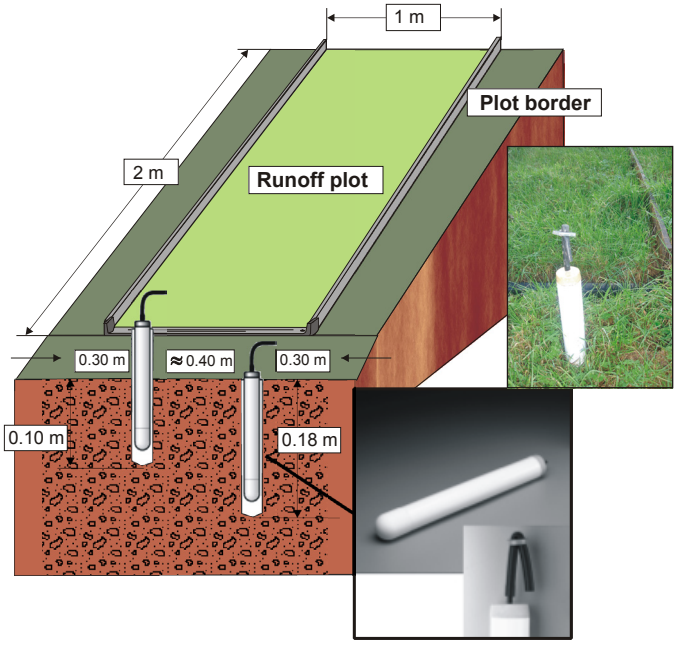

Figure 4-23 *Installation of 1900 soil water sampler*

The soil water samplers are simple, consisting of a porous ceramic cup and a sample collection tube. In order to create a vacuum in the sampler, a vacuum pump was used, which draws water from the soil matrix through the ceramic cup and into the sampler. The lysimeters were sampled monthly and analysed for pH, EC, DOC and ions in the chemistry laboratory at Newcastle University.

4.4.6 Subsurface drainage installation

Prior to installation, a trench was dug that was roughly twice the width of a drainage pipe and deep enough so the drainage pipe would be below the frost level (Figure 4-24). The subsurface drainage systems consisted of a 150 mm diameter, 1 m perforated PVC (Polyvinyl chloride) pipe placed at 18 cm depth. Two PVC pipes were installed horizontally, first under runoff plot B and second above control (natural) runoff plot (C) as shown schematically in Figure 4-19. Drainage pipes were connected with a small diameter pipe to tipping buckets completed with MiniDivers to monitor subsurface flow. This approach of installation was used in order to provide a low level of soil disturbance.

Figure 4-24 *Subsurface drainage pipe installation*

4.4.7 The trimming program of vegetation

The experimental area together with runoff plots were cut in June 2009 and July 2010. The grass was cut from the field using a grass trimmer and a shear held at 5 cm above ground level.

4.5 Monitoring

The three study sites (the Blind Beck catchment, the Hollow sub-catchment and the hillslope) were monitored by the author between 2009 and August 2010. This was done by establishing the following monitoring program:

- Stream gauge which recorded water depth at 15 min intervals,
- Continuously monitoring discharge on the outlet of sub-catchment,
- CTD and MiniDiver data loggers which recorded water level and electrical conductivity (EC) of runoff at 15 min intervals,
- Meteorological measurements,
- Soil moisture equipment.

The following section will provide details of how this monitoring program was established to provide stream discharge and runoff for the purpose of monitoring water quality and nutrients through the catchment, the sub-catchment and the hillslope.

4.5.1 Stream gauge at the catchment scale

Continuous records of stream flows were derived from a stream gauge record. An electronic datalogger was installed in July 2003 owned by the CHASM project, to record flow at Blind Beck. This logger stores readings in its memory, and the data are downloaded every one to two months. It takes around five to ten minutes to download the data at a stage gauge. Proper maintenance and handling of the stream gauge ensures that if a problem did occur with a logger, then the data gap would be kept to a minimum. The maintenance of a gauge includes the removing of debris and vegetation around the gauge and to check the logger stage value with a tape measure on the outside. At this site, the stage gauge has an associated rating curve, which is regularly checked with a spot gauging.

In the field, stream data is transferred onto a tough book laptop. The Hydrolog database is developed to store the raw data extracted from the laptop. The database is designed to

automatically convert the raw data into discharge using the rating curve equation stored into mentioned database. The Hydrolog is a fully integrated tool for storing hydrological data, performing data quality checks, performing corrections and can be used for producing reports and exports of data.

4.5.2 Discharge measurement at the sub-catchment scale

The main discharge data that have been used in this work was provided by the existing runoff gauge and a V-notch weir at the Hollow sub-catchment.

Construction and maintenance of V-notch weir

The design, construction and maintenance of the weir are based on the criteria of the British Standard (BSI 1981) as shown in Table 4-5.

Table 4-5 *Construction and maintenance of the weir according to the British Standard (BSI 1981)*

Weir component	Criteria to meet	Achieved
Weir Plate	Constructed of a material that cannot be damaged or distorted	Yes
	The upstream face of the plate to be smooth within a distance of ~ 0.02 m of the crest (Ackers et al. 1978)	Yes
	The surface of the notch should be planed surfaces, forming sharp edges where it intersects with the upstream face of the weir plate	Yes
	The width of the notch surface should be between 1-2 mm, if greater than it should be chamfered on the downstream edges at an angle of no less than 45°. To help prevent water clinging to the downstream face of the weir at low heads than a chamfer of 60° is recommended (Dodge 2001)	Yes
Weir Plate Installation	The plate should be perpendicular to the walls of the channel	Yes
	The weir plate should be water tight where it intersects with the wall and floors of the channel.	Yes
	The centre of the notch should be in the centre of the stream channel	Yes
	The nappe should only touch the upstream faces of weir plate and downstream the channel should be a sufficient vertical distance to ensure free discharge where the discharge is independent of the downstream water level and there must be atmospheric pressure underneath the nappe of the flow over the weir	Yes
Maintenance	The weir plate must be cleaned and silt, vegetation and any obstructions up or downstream of the weir removed	Yes continuous maintenance

The V-notch weir has an angle of 60-degree at the sub-catchment outlet, and was constructed using wood, bricks and concrete (see Figure 4-16). The stream's water level was determined using a gauge installed at the base of the stream behind the weir plate. A gauge was equipped with a CTD Diver, which takes measurements automatically at 15 minutes time intervals. The MiniDiver was installed on 15 January 2009. The data were downloaded every month. Figure 4-25 shows a schematic of the weir plate used. The illustrated weir can measure up to a head height of 0.95 m measuring discharge up

to 710 l/s. During 2009 there was a loss of water from around the V-notch, which was immediately fixed.

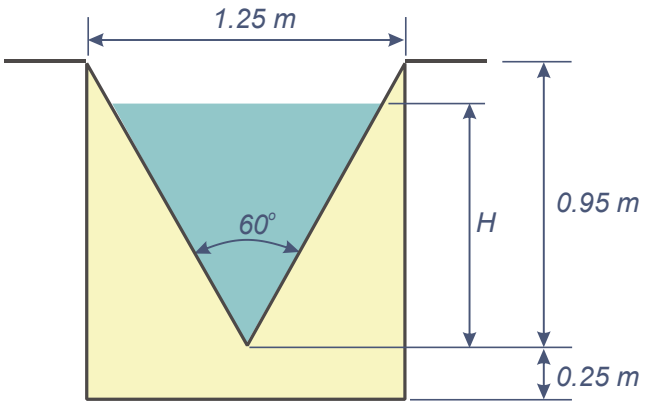

Figure 4-25 *Schematic of 60° V-notch weir plate*

Calculation of V-notch discharge

The Baro Diver is installed above the water level and measures the atmospheric pressure, (Pb) and the MiniDiver under water measures the total pressure including the water pressure. The CTD Diver measures water pressure (Pw) with a built-in pressure sensor. After data (in cm) are downloaded from the Diver, so that pressure can be converted to depth, the difference between the water pressure (Pw) and barometric pressure (Pb) gives the depth of the water passing over the V-notch, PW = (Pb + Pw) - Pb. At the zero gauge of the weir, the gauge reading corresponds to the level of the crest, which was 30 cm above the pressure of water. The discharge Q of V-notch is directly related to the height of the upstream flow, above the crest. To determine the depth of water, 30 cm was subtracted from all depth measurements. The water level value is termed *H* and used in the discharge equation. For the given V-notch weir of angle 60°, the Kindsvater-Shen formula is used:

$$Q = \frac{8}{15} Cd \sqrt{2g}\, tan\left(\frac{\theta}{2}\right) H^{5/2}$$

where: Q = the volume rate of flow (m^3/s), Cd = the coefficient of discharge; g = the acceleration due to gravity (m/s^2), θ = the notch angle i.e. the angle included between the sides of the notch in degrees (60°), H = height above notch base (m)

Weir calibration

To check that the discharge calculation presented above was producing accurate discharges, a calibration check was performed. The water level readings were calibrated by taking manual measurements by using a stopwatch and capturing and measuring the weir flow. For this site, several stream manual discharge measurements were made to

define a stage-discharge rating curve plotted in Figure 4-26. According to the rating curve, discharge can be calculated from height using the following equation:

$$Q = 0.0081H^{2.4978}$$

where: Q = discharge (l/s), H = the measured height above notch base (cm)

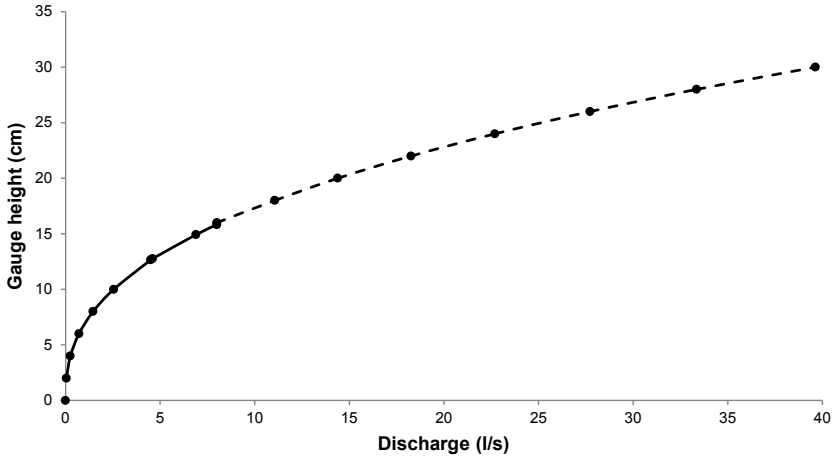

Figure 4-26 *Rating curve for the Hollow sub-catchment stream shown by solid line; extrapolated the relationship of the stage-discharge as shown by the dashed line*

As the field measurements did not cover all discharges, higher discharges were extrapolated.

4.5.3 Hillslope monitoring

Hillslope monitoring deals with runoff flow, electrical conductivity and soil moisture processes within mineral soils. The tipping buckets were equipped with the data loggers (see Figure 4-19) that recorded runoff at 15 min time intervals. Overland flow was monitored during the period March 2009 - August 2010 and subsurface for the period September 2009 - August 2010.

Soil moisture

Soil moisture Theta Probes were set up for measuring and monitoring the soil moisture content at three depths at the top and the bottom of the hillslope. The sampling frequency was at 15 minute intervals. They were used from October 2009 up to August 2010. During the observed period, both wet and dry periods were observed.

A generalised calibration equation for mineral soil was used to convert the dielectric constant to volumetric soil moisture content (θv) as a ratio of volume of water to volume of sample (m^3m^{-3}). A typical error for this calibration is ± 0.05 m^3m^{-3} (Theta

Probe 1999). A third order polynomial has been used to convert the voltage output from the Theta Probe (V) to the square root of the dielectric constant (ε).

$$\sqrt{\varepsilon} = 1.07 + 6.4V - 6.4V^2 + 4.7V^3 \qquad (R^2 = 0.998)$$

or by linear relationship

$$\sqrt{\varepsilon} = a_0 + a_1\theta_v$$

where: a_0 =1.6, a_1 =8.4 for a general mineral soil, θ_v is in m^3m^{-3}

Electrical conductivity

The electrical conductivity (EC) was recorded at two study sites: the outlet of the sub-catchment for the period January 2009 - August 2010 and the hillslope for the period March 2009 - August 2010.

At the outlet of the Hollow sub-catchment together with the gauge level, the EC of discharge water was recorded using the CTD Diver at 15 minute time intervals. Data from the EC are given in mS/cm, and after being downloaded are converted to µS/cm. The EC values have been used as a geochemical tracer for hydrograph separation of runoff components.

At the hillslope, the EC of overland flow was measured with CTD Divers installed in the 250 ml tipping buckets close to the perturbed and control runoff plots. This gives support to the idea of using the EC as a tracer to have knowledge of the different sources of runoff during low and high flow as the relationship between runoff and dissolved ions.

4.5.4 Raingauge stations

Rainfall data of three tipping bucket raingauge stations for the period 2009 - 2010 were obtained from Sykeside, Asby and Great Musgrave sites. Figure 4-27 shows the locations of these stations.

Rainfall was recorded using a tipping bucket system linked to the datalogger. Raw data are input as event rainfall (i.e. the time of the tip of 0.2 mm of rain) then put into Hydrolog data base which converts data into time series rainfall (from 1 min to 1 year).

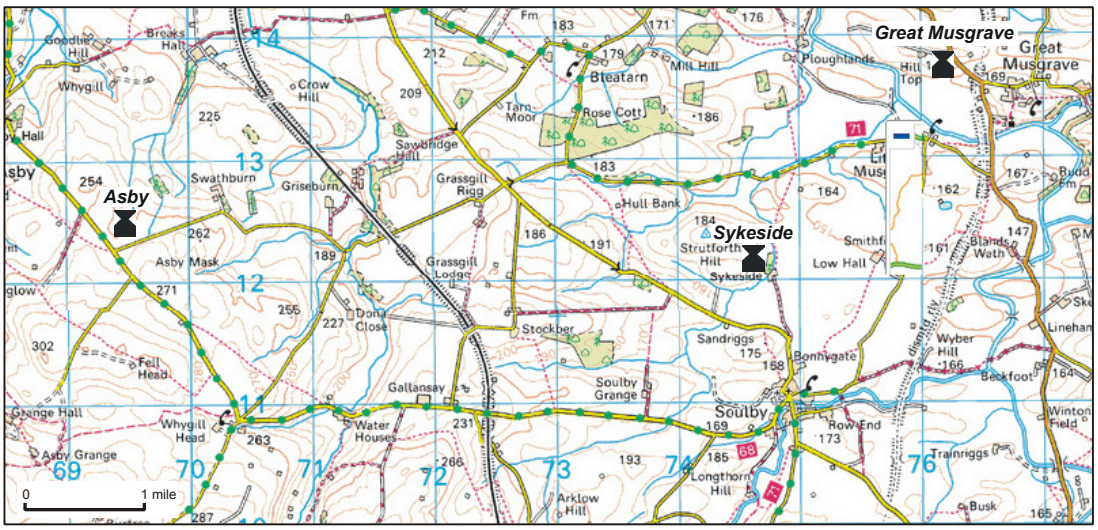

Figure 4-27 *Location of raingauge stations*

Figure 4-28 *Downloaded raw rainfall data from raingauge at Asby by the author*

Rainfall data processing and filling of missing values

Missing data in hydrology are a common problem. Rainfall and evapotranspiration data are the most important input variables in all hydrological models. To obtain appropriate the model results, data accuracy is crucial. Data accuracy is also crucial for checking the water balance, agricultural demand and the effects of the climate changes.

There was missing rainfall data for Sykeside raingauge station for the years of 2009 and 2010. Data completion was carried out by linear regression using stations that have shown significant correlation. The method is based on fitting the best straight line through observations. To obtain a good quality of fit, the coefficient of determination should be a number between 0 and 1, where 1 represents perfect fit.

Using linear regression, a mathematical relationship can be defined between data of a base station and other stations of the form (de Laat 2005):

$$Y = C + C_1X_1 + C_2X_2 + C_3X_3 + etc.$$

where: Y = a series of values of the base station (dependent variable), X_i = a series of values of neighbouring station i (independent variable), C = the equation's constant, C_i = the equation's coefficients

Multiple regressions mean that more than one neighbouring station (independent variable) is regarded. In the case of a base station and one neighbouring station, the equation reduces to:

$$Y = C + C_1X_1$$

This equation was performed between Sykeside (dependent variable) and neighbouring stations (independent variable):

- Asby for data collected between July and November 2009,
- Great Musgrave for data collected between February and October 2010.

Double mass curve analysis

Using a double mass curve analysis, in homogeneities and inconsistencies in the time series can be detected. This is indicated in the curve of the double mass plot showing an inflection point in the straight line. The deviation from the straight line is mainly due to the change of observer, change of measurement method, location change to new site, etc. The principle of double mass analysis is to plot accumulated values of a station under investigation against accumulated values of other stations over the same period of time. The principle of double mass curve analysis is exercised through plotting accumulated 15 min time interval rainfall for one certain period over the year for raingauge of observation for station Sykeside against the mean of the other two stations (Figure 4-29 and 4-30).

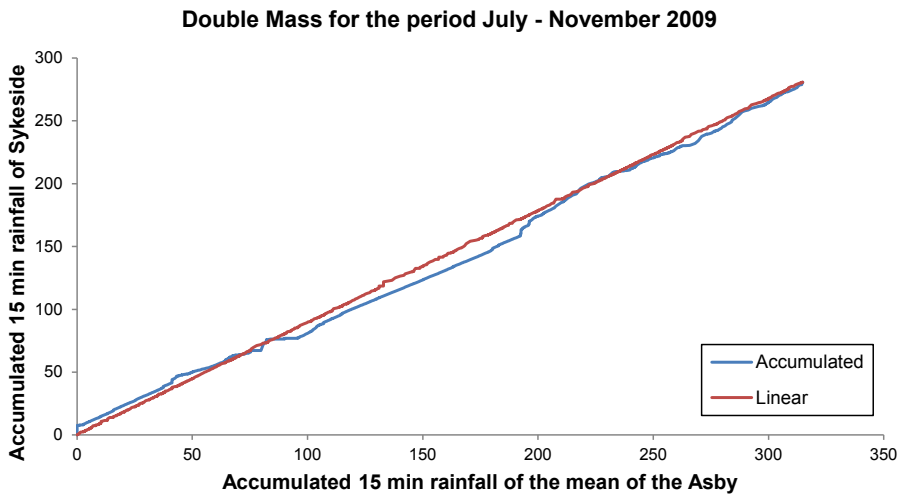

Figure 4-29 *Double mass analysis of 15 min rainfall between Asby and Sykeside raingauge stations*

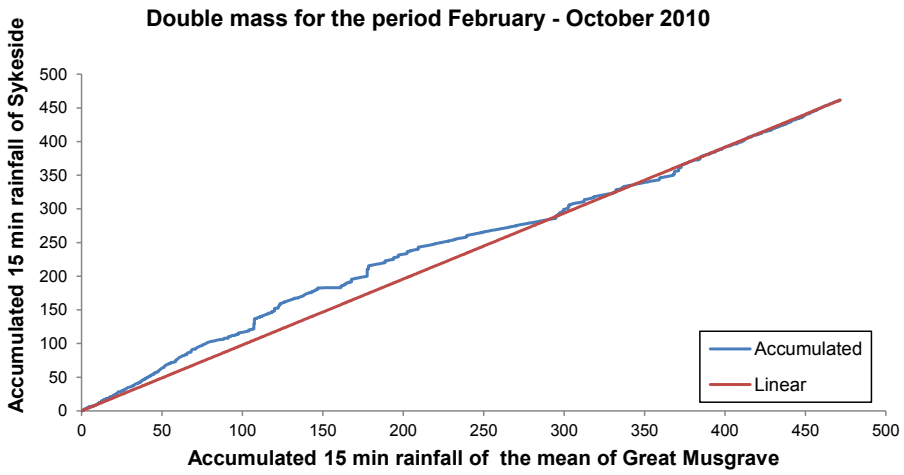

Figure 4-30 *Double mass analysis of 15 min rainfall between Great Musgrave and Sykeside raingauge stations*

The double mass curve as shown in Figures 4-29 and 4-30 can be interpreted as follows:

- an upward deviation from the linear relation indicates relative high values of Sykeside raingauge station
- a parallel line indicates a constant relation between station Asby or Great Musgrave and Sykeside
- a downward deviation from the linear relation indicates relative low values of Sykeside raingauge station.

The double mass curve analysis shows that during the study period rainfall at three raingauge stations was nearly the same. These results show that the close proximity of the Sykeside raingauge to the Asby and Great Musgrave raingauge minimized the differences in gauge catch due to spatial variation in rainfall intensity or occurrence.

It is not necessary to plot the residuals and to continue with the analysis, as there is no significant deviation and the data are homogenous.

4.5.5 Weather station

An automatic weather station was established at Hill Top Farm (Great Musgrave) in September 2003 as a part of AWS network under the CHASM Project in the Upper Eden basin. Location and details of the station are presented in sub-section 3.7.1. The station was installed on the hill at a 155 m elevation where no obstacles were present, which could potentially affect the readings. It is powered by solar cells, which charge a 12v battery internally. This station was a refurbished system produced by

Environmental Measurements Ltd, Sunderland that resulted in patchy data for a period of 18 months. Later, it was upgraded with a Campbell's CR10X logger in January 2005. Air temperature, wind speed average over 15 minutes (min, max and average), wind direction, net radiation, relative humidity, and battery voltage of the logger were recorded. From September 2003 to October 2010, data from the weather station has been near continuous, except for a gap between October 2008 and February 2010, when it was offline.

4.6 Field Sampling

4.6.1 Plot soil core program

For the estimation of nutrients, the normal sampling depth is about 15 cm (6 in.) because most plant roots grow and tillage mixes most nutrients into the soil to about 15 cm deep (Reid 2006). If the sampling is deeper than 15 cm (6 in.), the subsoil is normally much lower in nutrient content, and the sample is not representative of the field. For the sampling of nitrates, a depth of 30 cm (1 ft.) will provide a more accurate indication of the amount of nitrate available to the crop, since nitrate will move more easily in soil water than other nutrients (Reid 2006). According to this, it was decided that the best depth to adopt for soil investigation in terms of nutrients was 30 cm.

The soil samples were taken in the spring 2009 (April 30) before wetting (enhanced rainfall) and in the autumn 2009 (October 8) and the summer 2010 (August 19) after wetting from perturbed (B) and control plot (C).

The soil cores were extracted using an auger that is manufactured by the Ejkelkamp firm, with a diameter of 6.0 cm (Figures 4-31 and 4-32). From each plot, four soil samples were collected (6 cm diam., 30 cm deep). Extra care was taken not to disturb the hydrological effects at the hillslope. Due to this, samples from the perturbed plot (B) was collected inside the plot, and samples from the control plot (C) were taken adjacent to the plot. The hole created by soil core removal was filled with soil. After collection, the samples were preserved in PVC tubes, being wrapped in cellophane (Figure 4-33) to protect from drying out whilst being transported to the laboratory prior to analysis.

Figure 4-31 *The author obtains a soil core at the hillslope adjacent to plot*

Figure 4-32 *An auger used to sample soil core*

Figure 4-33 *A 40 cm soil core obtained and, wrapped in cellophane*

Layout of soil cores obtained from two plots at the hillslope

To obtain a representative sample or "representative value" for a soil property, a number of samples need to be taken over the area. In the case of a plot, the samples are analysed separately. The position of the soil cores was chosen by adapting the sampling strategy used in UK agriculture, which is to walk along a "W" shaped path, as shown in Figure 4-34 for a field (Rowell et al. 1994).

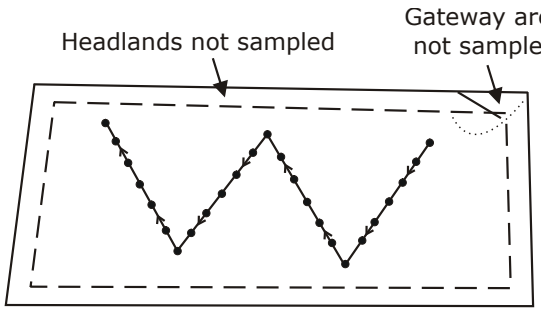

Figure 4-34 *A soil sampling strategy for a field area (source: Rowell 1994)*

Layout of soil cores are presented in Figures 4-35, 4-36 and 4-37.

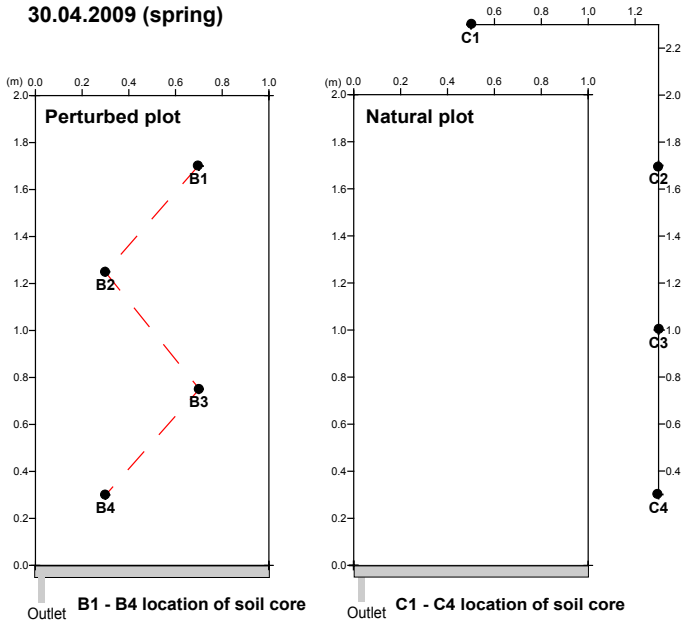

Figure 4-35 *Layout of runoff plots, illustrating the location of the 30 cm cores used to evaluate the soil properties of each plot before wetting, the spring 2009*

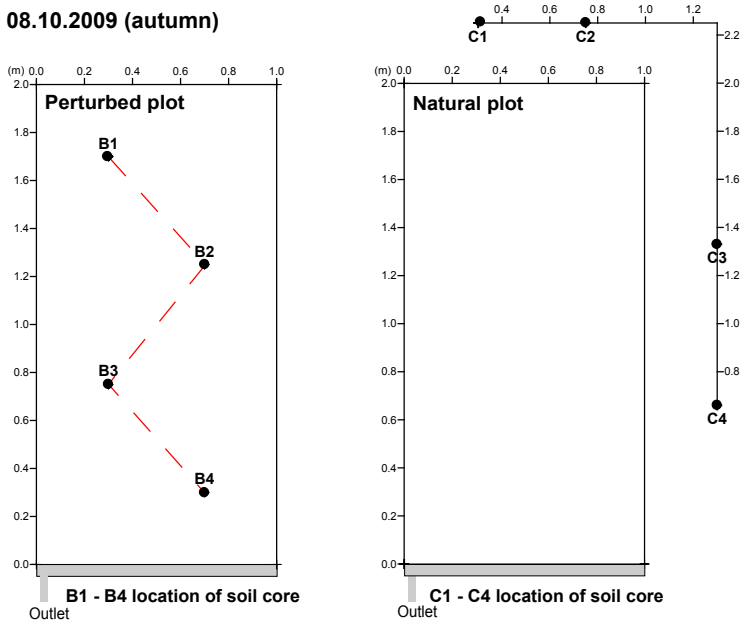

Figure 4-36 *Layout of runoff plots illustrating the location of the 30 cm cores used to evaluate the soil properties of each plot, after wetting, the autumn 2009*

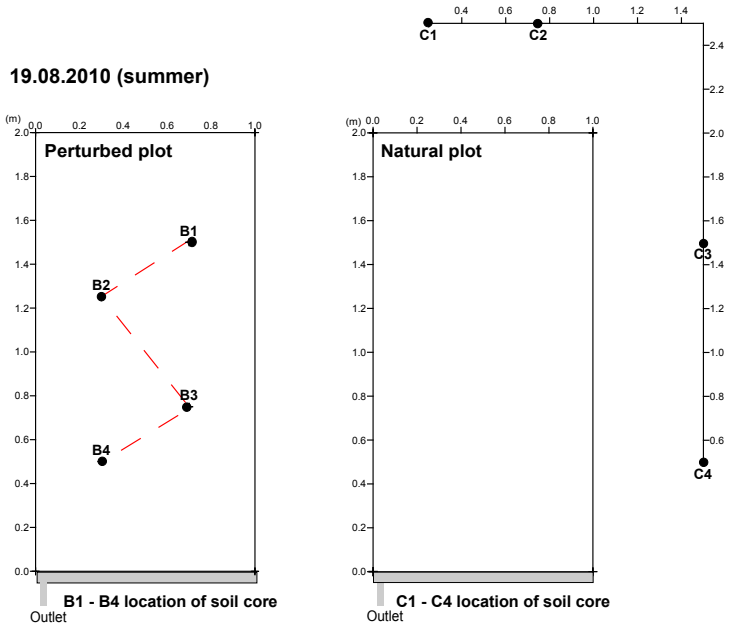

Figure 4-37 *Layout of runoff plots illustrating the location of the 30 cm cores used to evaluate the soil properties of each plot, after wetting, the summer 2010*

4.6.2 Catchment water and sediment sampling program

Site selection and sampling location

Prior to collection of samples, a walk through the study site was conducted to identify sample locations. As a result of visual observations, five sample site locations of stream water and sediment were selected, Figure 4-38. The stream sampling program is based on monthly samples and more frequent sampling during some episodes such as storm events.

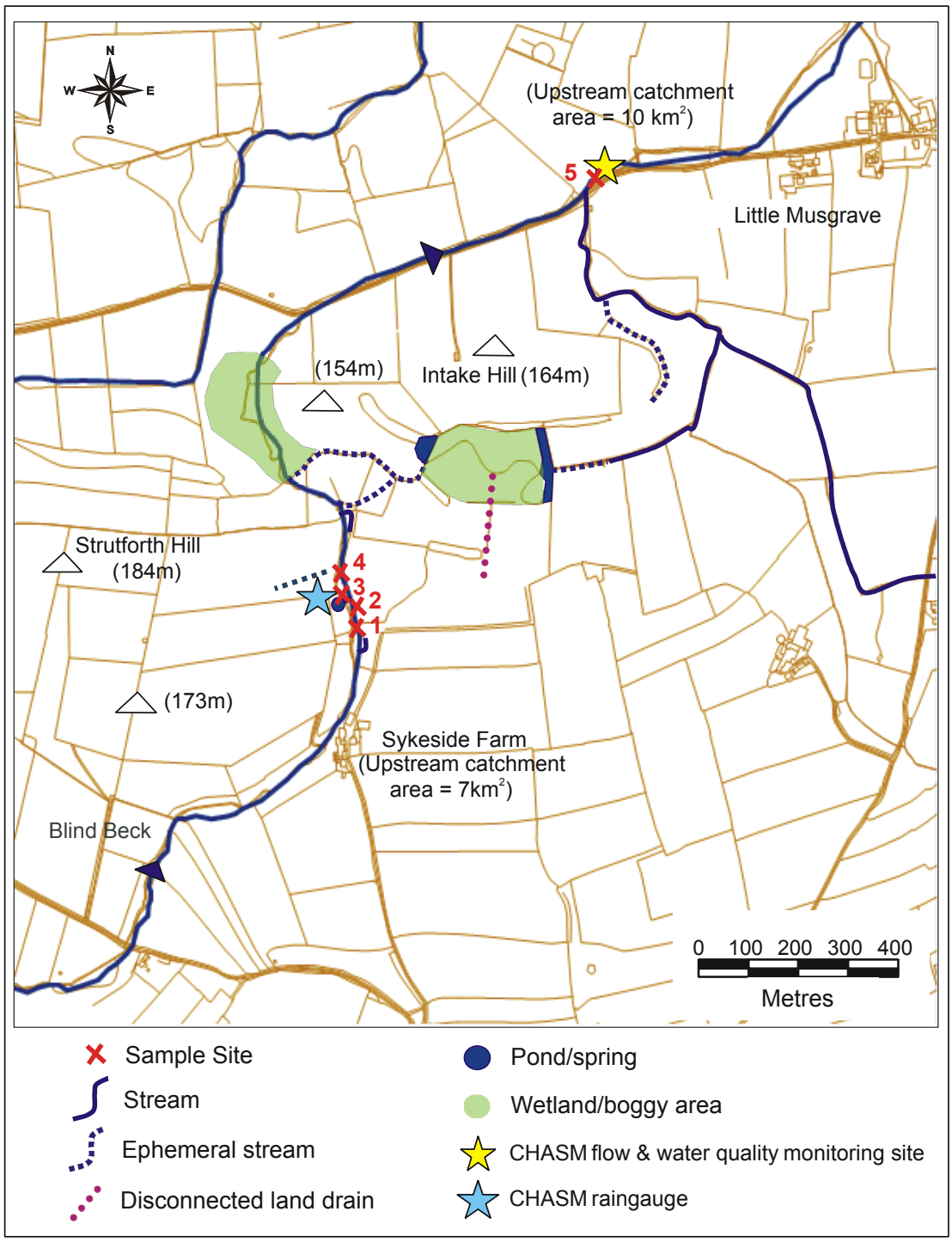

Figure 4-38 *Plan view showing sample locations and instrumentation*

Site 1: Downstream of Sykeside Farmyard

Site 1 is located at Sykeside Farm, approximately 150 m downstream from the farmyard. Figure 4-39 shows the wider channel and pathway where a farmer used to cross a stream called the Beck with farm machinery.

Figure 4-39 *Photograph showing sample site 1: directly downstream of Sykeside Farmyard (flow left to right)*

The selected area is used for sheep grazing where animals have easy access to Blind Beck itself. In addition, animals have a drinking pond, which is directly connected to the stream. Approximately 20 m from the east of this site there is a hard standing, which is used for the temporary shelter for cattle and storage of animal feed. Water is carried by a man-made drain directly from the hard standing to Blind Beck. At this site, the water contains high levels of suspended sediment and has large areas of algae growing on the bed.

Site 2: Directly upstream of CHASM raingauge

Site 2 is located downstream of site 1 and upstream of ephemeral spring and a CHASM raingauge. Figure 4-40 shows a large gully that drains the improved field further uphill. During the storm event, there is evidence of tramlines running perpendicular to the hillslope and surface runoff directly to Blind Beck.

Figure 4-40 *Photograph showing sample site 2: Directly upstream of CHASM raingauge (flow right to left)*

Site 3: Downstream of ephemeral spring (upstream of buffer strip area)

Figure 4-41 shows the location of site 3 approximately 150 m downstream of site 1 where the Beck flows at the foot of Strutforth Hill. The uphill fields are drained by natural gullying and man-made drainage ditches running into the stream.

The fields are a mixture of improved grassland and grazing. Figure 4-41 shows a pipe that drains the area in between the two hills and emerges as a small ephemeral spring that flows into Beck just 10 m upstream at the sample point.

Figure 4-41 *Photograph showing sample site 3: directly downstream of ephemeral spring (view in upstream direction)*

On the eastern bank, the Beck is fenced off from the fields, and there is a small amount of riparian vegetation. At this site, the stream is rather shallow approximately 15-20 cm deep. The stream bed is heavily presented with areas of algal growth and turbid water. The riparian area is approximately 120 m downstream of site 3.

Site 4: V-notch at the outlet of the Hollow sub-catchment

The sampling site 4 is located at the outlet of the sub-catchment (Figure 4-42). This was to obtain representative samples of water and sediments for whole sub-catchment.

Figure 4-42 *Photograph showing sample site 4: V-notch at the outlet of the Hollow sub-catchment*

Site 5: CHASM sampling site on the Blind Beck

Site 5 is located at the Blind Beck catchment outlet, where the Beck flows by the side of the road in a ditch that becomes heavily vegetated in the summer. This site is also a CHASM monitoring site (water quality and stream flow), Figure 4-43.

Figure 4-43 *Photograph showing sample site 5: furthest downstream monitoring site near Little Musgrave Farm (flow left to right)*

This site is characterized by improved grassland to the north and heavily grazed, unimproved land to the south. The stream is very fast and bed is considerably less silted than further upstream at Sykeside Farm where there is algal growth.

Sampling type and sampling schedule

One schedule was followed for water quality and sediment sampling: monthly point values. Figure 4-44 provides a sampling period of stream water, rainwater and sediments. Data collection took place between April 23, 2009 and August 19, 2010. Travel time required 1 day to visit all sites. Table 4-6 lists the sampling schedule and the parameters analysed for each site.

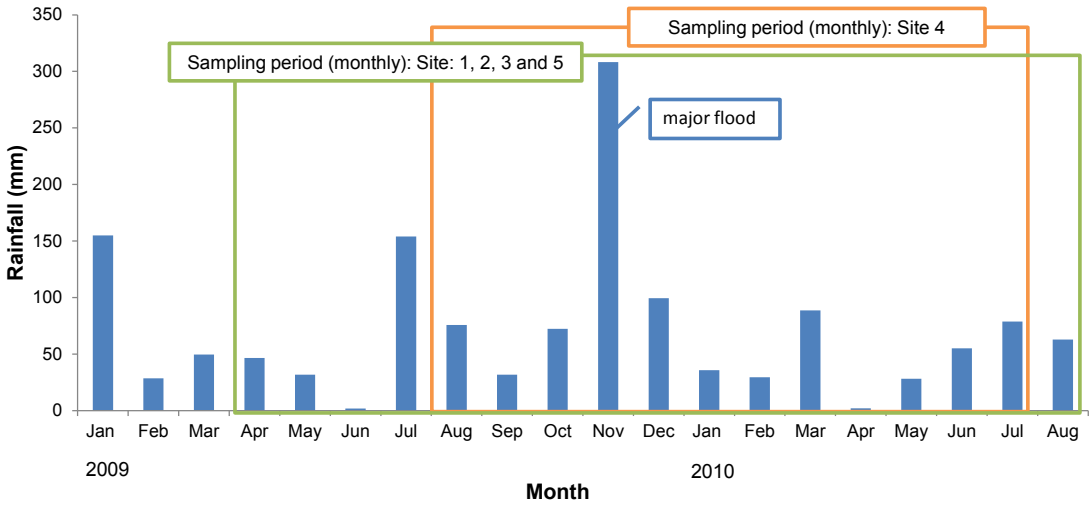

Figure 4-44 *Sampling period of stream water, rainwater and sediments*

Table 4-6 *Sampling schedule and parameters analyses at monitoring stations*

Site	1		2		3		4		5	
Monthly	water	sediment	water	sediment	water	sediment	water	sediment	water	sediment
Parameter	A	B	A	B	A	B	A	B	A	B

A: [pH, EC
Anions: chloride, nitrate, sulphate, hydrogen carbonate
Cations: calcium, magnesium, sodium, potassium
Dissolved organic carbon (DOC)]

B: [Particle size distribution (PSD)
Total organic carbon (TOC)
Total carbon (TC)and total nitrogen (TN)]

Figure 4-45 presents the measured rainfall at the outlet of the Hollow sub-catchment, the periods of enhanced rainfall on the perturbed plot, soil and water sampling calendar in the 2009 and 2010 year for the hillslope plots.

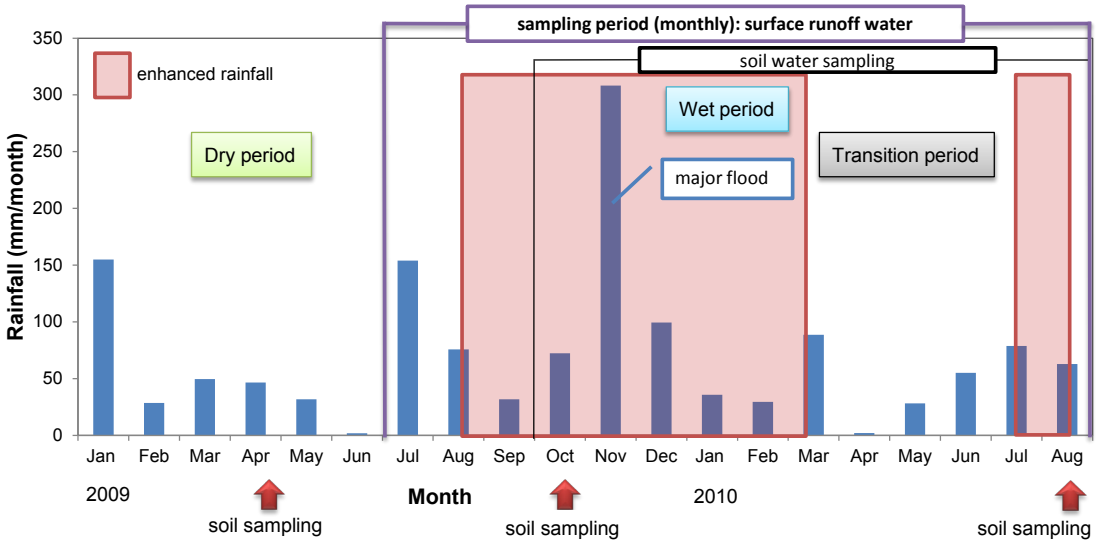

Figure 4-45 *Monthly rainfall, enhanced rainfall periods, and sampling calendar for the hillslope plots*

4.6.3 Field data quality assurance/quality control

Quality assurance (QA) is defined as a system of management activities to ensure that a process, item or service is of the type and quality needed by the user.

Data validation

Field observations, activities and sample sites were noted in a field book. Monthly visits included a description of the vegetation, precipitation, flow level, condition of V-notch weir, raingauges, stream gauges, runoff plots and irrigation pipes, tipping buckets, pipe connectors, divers, Theta Probes and any problems that occurred. Photographs were

taken to document experiment set up, topographic survey, sampling activities and stream flow.

Accuracy

Accuracy is defined as a measure of the closeness of the measured value to the "true value". In the field this means following standardized techniques and procedures to minimize sampling error.

Comparability

Comparability is used to measure how well one data set can be considered as similar to another.

Completeness

During sampling, the procedure followed a sampling plan to collect all of the designated samples. Changes of the sampling plan were made before visiting the field after discussion. All necessary samples were collected, transported to and analysed by the laboratory.

Quality control

The quality control measures used in the field include but are not limited to:

- Proper cleaning of sample tipping buckets and sampling equipment,
- Maintenance, cleaning and calibration of field equipment/kits per the manufacturer's and/or laboratory's specifications,
- Proper field sample collection and analysis techniques,
- Correct sample labelling and data entry,
- Proper sample handling and transport techniques,
- One field duplicate per set of 10 samples (minimum of 1).

4.7 Soil and sediment analysis

Physical and chemical properties of soil and sediment samples were characterised by standard UK procedures.

In the laboratory soil cores obtained from field were photographed (Figure 4-46) then pushed out from PVC tubes. After that, they were divided into segments of 0-10, 10-20 and 20-30 cm and used for further analysis.

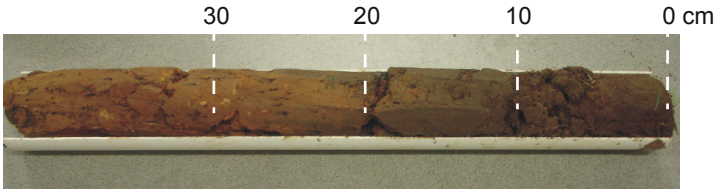

Figure 4-46 *Example of soil core, taken from the hillslope; numbers indicate cm below surface and cut segments*

4.7.1 Determining Soil – water by the gravimetric method

Soil bulk density is a measure of how dense and tightly packed a sample of soil is. This was determined via the core method (Blake and Hartage 1986) by taking four undisturbed soil cores from the perturbed and control plots before and during enhanced rainfall from 0-10, 10-20 and 20-30 cm soil depths. The soil samples were dried at 105^{o}C for 24 hours in a forced-air oven, weighed and bulk density calculated as the weight of oven-dry soil divided (Wds) by the volume of soil (Vs) before drying, expressed in g/cm^3.

$$BD = \frac{Wds}{Vs}$$

$$Volume_{core}\ Vs = \frac{3.14 \cdot inside\ diameter^{squared} \cdot Height}{4}$$

$$Vs = \frac{3.14\ d^2\ H}{4}$$

Soil total porosity was calculated utilizing a modification of the Water Desorption Method described by Danielson and Sutherland (1986):

$$TP(\%) = [1\text{-}(bulk\ density/d)] \cdot 100$$

where: d = the specific gravity of the solid constituents of the soil; it = estimated to be 2.65 g/cm^3 for an average soil, 2.4 for a highly calcareous soil, 2.0 for a humiferous soil and 1.5 for a peaty soil.

In general, porosity values typically are in the range from 30% in very fine textured soils to 80% in peat.

4.7.2 Particle Size Distribution

A dried soil sample's lumps were broken into small particles with an agate mortar, homogenized by shaking, stirring and pulverizing using a blender to remove plant debris and root matter before they were passed through the sieves, Figure 4-47. Particle size analysis was determined by sieve analysis using a set of sieves (2 mm – passing

0.063 mm) in a sieve shaker and weighed each fraction separately, Figures 4-48 and 4-49. The milled sample was then mixed and placed in a labelled, glass sample bottle, while representative homogenized powder soil sample for thermogravity analysis in small labelled glass bottle.

Figure 4-47 *Mortar and pestle used to crush the soil*

Figure 4-48 *Set of sieves in a sieve shaker*

diameter: 1.18 mm diameter: 0.212 mm

Figure 4-49 *Sediments being sieved*

The percentage of gravel, sand, silt and clay size particles presented in the soil were obtained from a particle size distribution curve. A soil and sediment texture triangle was used to classify the texture class defined by the UK classification (Figure 4-50).

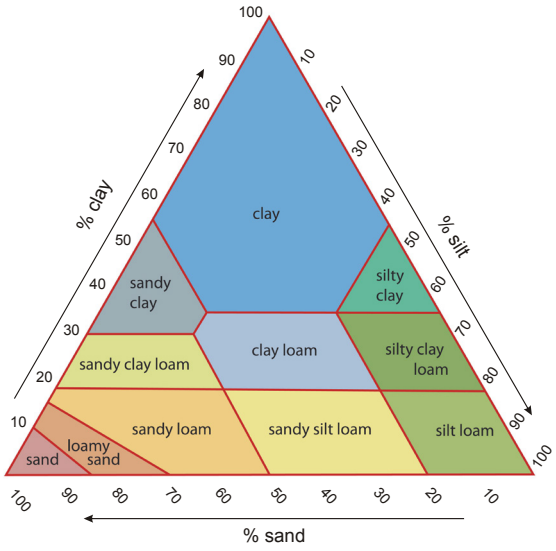

Figure 4-50 *The particle size distribution triangle, the UK system (source: Land Inforamtion Systems 2013 and modified by the author)*

Definition of particle size classes

The particle size classes of the soil (< 2 mm) are defined as follows (FAO 2006):

Clay < 2 µm
Silt 2 – 63 µm
Sand 63 – 2000 µm

Classification of the surface sediments based on grain size

The final dry samples were screened with a set of sieves arranged into a uniform database containing percentages for silt+clay content (grain size <63 µm), sand (grain size between 63 µm and 2000 µm) and gravel (grain size >2000 µm). The classification system used to distinguish sediment type and the sorting index were carried out in accordance with FAO (2006).

4.7.3 Quantification of total organic carbon (TOC) by LECO TOC analyser

Total organic carbon was determined using the direct method. Direct determination consists of previous removal of any carbonates present by treating the soil with hydrochloric acid.

The dried and homogenized soil or sediment samples were analysed for TOC in duplicate. Samples were weighed (about 100 mg) in a porous crucible and in-situ acidified with sufficient dilute hydrochloric acid (4.0 mol/l) to remove carbonates. After the acid has drained from the crucibles, these samples were put in the oven and dried at 65^{o}C overnight. Total organic carbon (TOC) of oven dried samples were determined using a LECO Carbon/Sulphur Analyser, previously calibrated with standard steel rings of certified carbon content. The ceramic crucible was placed in a radio frequency furnace and the sample combusted in a stream of carbon dioxide-free oxygen. The residual carbon (organic) was oxidised to carbon dioxide by combustion in a stream of oxygen, and the CO_2 produced was quantified by infra-red detection.

4.7.4 Quantification of total carbon (TC) and total nitrogen (TN) by CNS analyser

Total soil C and N were determined by the CNS analyser (Vario EL, Elementar Analysensysteme GmbH, Hanau, Germany). The analyses were carried out on 100 mg of crushed samples in a crucible without previous decarbonation. The CNS Analyser gives a rapid analysis of total carbon, which includes organic carbon and carbonates. Total Nitrogen (TN) is a measure of both inorganic and organic forms of nitrogen. Total C and N are expressed as a percentage.

Calculation of $CaCO_3$

The total inorganic carbon (TIC) was determined by difference:

$$TIC\ (wt\%) = TC(wt\%) - TOC(wt\%)$$

To express TIC as a percentage calcium carbonate ($CaCO_3$), the following equation was used:

$$(TC - OC)\ \cdot 8.33 = CaCO_3(wt\%)$$

Quality assurance: duplicate sample analysis

$$RPD = \frac{\left|\left(Carbon_{sample1} - Carbon_{sample2}\right)\right|}{\left(\frac{\left(Carbon_{sample1} + Carbon_{sample2}\right)}{2}\right)} \cdot 100$$

4.7.5 Thermal analysis of soil (TG-DSC-QMS)

Thermal analysis was conducted using a Netzch Simultaneous Thermal Analyzer STA 449C Jupiter equipped with a Thermogravimetry (TG) - Differential scanning calorimetry (DSC) sample carrier type S supports a PtRh10-Pt thermocouple.

Approximately 30 mg of soil passing 63 μm was placed in an Al_2O_3 crucible. Samples were heated continuously from 40 to 900°C at a heating rate of 20°C min^{-1} under flowing 20% oxygen (to maximise oxidation of evolved carbon gas species to CO_2) in helium (30cm^3/min).

For Quadrupole Mass Spectrometer (QMS) analysis, mass/charge (m/z) values from 10 to 300 were collected and *m/z* intensities of interest 12 (C), 18 (H_20) and 44 (CO_2 and N_2O) were reported.

A reference soil, humus, was used for calibrating the temperature axis and the corresponding enthalpy output.

The TG QMS instrument failed on October 10th, 2008. The problem was resolved by engineers from Germany and the 13th of November 2009 was the last time the equipment was serviced. After this period quadrupole mass spectrometer (QMS) instrument continued to work up to December 2010.

4.7.6 Soil extraction

In order to quantify the elemental composition of a soil, two extraction schemes were used: Ammonium Nitrate (NH_4NO_3) and Hydrofluoric Acid (HF).

Sample preparation for ICP

Extraction with an Ammonium Nitrate (NH_4NO_3)

The commonest extraction of soil is with ammonium nitrate. Approximately 10 g of sieved soil samples were extracted with 50 ml 1.0 mol/l NH_4NO_3, shaken on the shaking machine for 30 minutes, and filtered through a 125 mm Whatman No. 2 filter paper (MAFF 1986) (Figure 4-51). NH_4NO_3 soil extracts due to their high concentration of nitrate were not suitable for ICP. According to that, a dilution was made using 5 ml of extract and 25 ml of deionised H_2O. Samples were stored in a cold room at 5°C prior to ICP analysis.

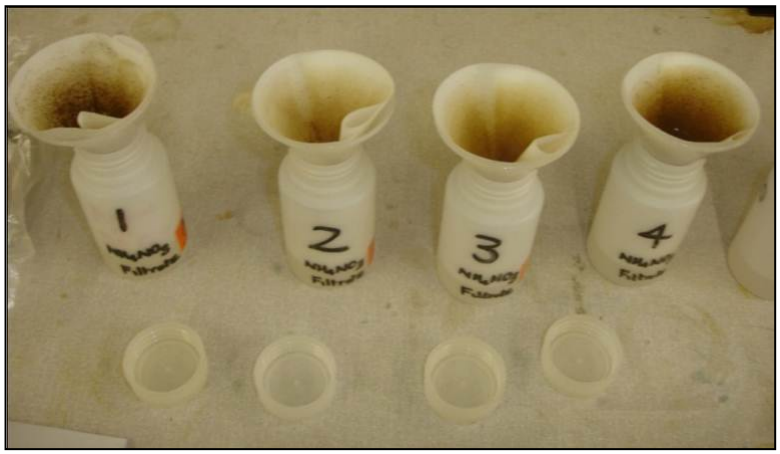

Figure 4-51 *Filtering of soil extracts through a 125 mm Whatman No. 2 filter paper*

This extraction is mainly developed for agriculture and it is not suitable for "total" element analysis.

Extraction with Hydrofluoric Acid (HF)

Extraction with HF means a known weight of soil is dissolved in a known volume of concentrated acid at high temperature and pressure. To understand a complete dissolution of soil, 4 different concentrated acids were used: HF (hydrofluoric acid) used to break silicate bonds, concentrated perchloric acid used to break down the organic matter (heated becomes a strong oxidizer) and also effectively removes excess HF from the sample, boric acid used to dissolve rare-earth fluorides that may be present and HCl (hydrochloric acid) used for dissolution of metals.

Approximately 300 - 400 mg of oven dried powdered soil samples were ashed at 550^{o}C overnight in porcelain crucibles. Sediment samples were transferred into teflon crucibles and any remaining sediment was washed with 2.5 ml concentration of nitric acid, and a further 2.5 ml concentration of nitric acid was added to the teflon crucible. Samples were extracted with 5 ml concentration of HF, placed on a hotplate, and several drops of concentrated perchloric were added and left to evaporate to dryness at approximately 130^{o}C for 24 hours. After 24 hours, 5 ml of boric acid was added and left to evaporate to dryness at the same temperature for 6 to 8 hours. Evaporation was repeated to ensure that all HF residual was removed from the matrix. Then the inside walls of the crucible were rinsed carefully with 5 ml of 50% HCl, heated to near boiling to dissolve all salts (probably ~ 70^{o}C), added to a 100 ml volumetric flask and made up to volume. Solutions were then analysed for cations using ICP spectrometry.

Sample preparation for DIONEX (anion)

Extraction with deionised water (DI)

A first batch of soil samples (collected in April, 2009) was extracted with a soil:extract ratio of 1:10 using approximately 2.5 g of sieved soil (Figure 4-52) with 25 ml of deionised water in 50 ml bottles. A second batch of samples (collected in August, 2010) was extracted with a soil:extract ratio of 1:5 using approximately 2 g of sieved soil with 10 ml of deionised water in conical tubes. The reason for changing the extract ratio was due to a high concentration of fine particles in extraction. Samples were shaken overnight at 300 RPM on an orbital shaker. Then the first batch of extracts were decanted and filtered through a 125 mm Whatman No. 2 filter paper. Samples with high concentrations were vacuum-filtered through a filter Glass-Microfibre Discs Grade MGA Dia 70 (Figure 4-53). The second batch of extracts in tubes was centrifuged at 6,000 rpm for ten minutes. After centrifugation, the extracts were decanted and filtered. Filtered extracts were stored at 5^{o}C for analysis by DIONEX.

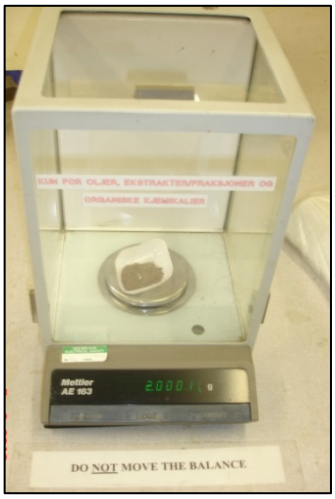

Figure 4-52 *Electronic balance with the dried soil*

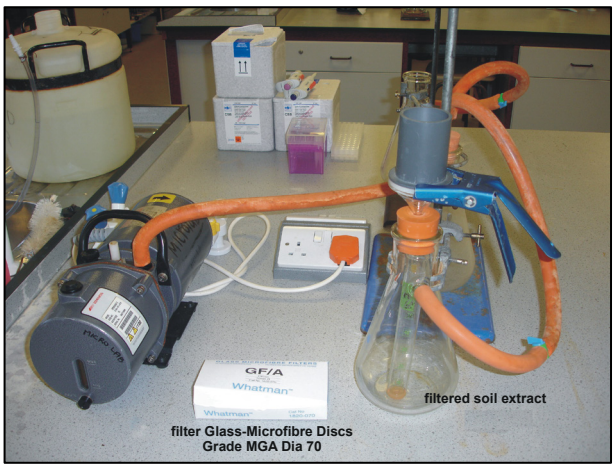

Figure 4-53 *Vacuum-filtered soil extract*

DIONEX Ion - Chromatography Model ICS - 1000

Anion analysis by DIONEX of the soil samples was performed by the Newcastle University laboratory, School of Civil Engineering and Geosciences.

0.5 ml of extraction with 0.45 ml of deionised water was put into DIONEX vials (5 ml) for analysis of anions in soil. Then soil samples, blanks and check-standards in vials were placed in the autosampler of DIONEX machine, Figure 4-54.

Figure 4-54 *Dionex DX-100 Ion Chromatography*

4.7.7 Measurement of soil pH

Soil pH was determined in 1:5 suspension using a pH Meter 3310 JENWAY. 5 ml of soil was weighed into a plastic tube and 25 ml of deionised water from measuring cylinder were added. The suspensions were first stirred for 15 seconds, and then placed in a mechanical shaker for 15 minutes. The samples were left to stand for overnight. The pH value was determined using a pH meter previously calibrated using 4.0 and 7.0 buffer solutions.

4.7.8 Soil Organic matter (SOM)

Soil organic matter (SOM) encompasses a wide range of organic compounds, and no analytical method allows SOM to be accurately determined from direct measurement (Sleutel 2005). The organic carbon measurements were used to indirectly determine soil organic matter (SOM) through the use of a conversation factor 1.724 based on the assumption that SOM contains 58% carbon (Kerven et al. 2000):

$$\%Organic\ C \times 1.724 = \%SOM$$

The "Van Bemmelen factor" of 1.724 has been used for many years although the literature indicates that the proportion of organic carbon in SOM for a range of soils is very variable (Soil Survey Lab Staff 1996).

4.8 Water sample collection and analysis

4.8.1 Sample handling and filtration

Water samples were collected with clean 0.5 l capacity plastic bottles and labelled. Prior to collection, the plastic bottles were cleaned by washing, rinsing with tap water, then rinsing with distilled water and put into the oven to dry.

Stream water

During sampling, sample bottles were rinsed with the sampled water three times and then filled to the brim (Figure 4-55).

Figure 4-55 *Sampling of stream water by the author*

Surface runoff water and rainfall

Samples were collected in 10 l plastic containers. The collection was carried out by careful immersion of the sample containers deep inside the water.

Subsurface (soil solution) runoff water

The subsurface water sample was extracted from the collection tube using an extraction kit of 50 ml (Figure 4-56) and taken to the laboratory for chemical analysis.

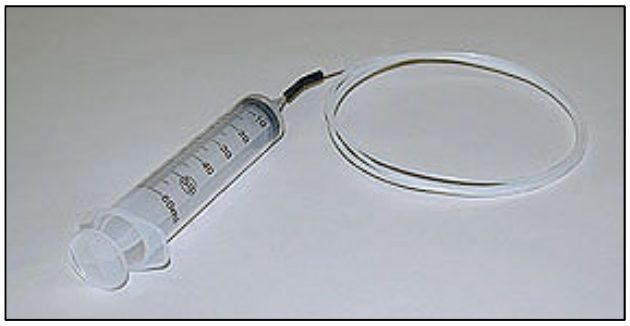

Figure 4-56 *Extraction kit (50 ml)*

Notes were kept on volume of surface and subsurface (soil solution) runoff and rainfall. When the collected sample volume was insufficient, analyses were done first for the DOC. The samples were transported to the Laboratory as soon as possible and stored in the refrigerator at 5^{o}C prior to analysis. After collection, raw waters were filtered to remove particulate matter using a vacuum type filtration apparatus with a conditioned Whatman 0.45 μm membrane filter paper.

4.8.2 Determination of pH and Electrical Conductivity (EC)

Standard methods were followed in the determination of pH and EC. pH was measured using a pH meter (model: 3310 JENWAY). The pH meter was calibrated using buffers of pH 4.0 and 7.0. pH was measured immediately after the samples reached the laboratory.

Electrical conductivity (EC) is a measure of dissolved salts in the water and therefore an indicator of salinity. Yusop et al. (2006) suggested that the EC value could be used as an indicator of the overall ionic content or concentration of dissolved salts. The EC was measured using a hand held EC meter. It was calibrated using standard salinity solution prior to use.

4.8.3 Determination of dissolved organic carbon (DOC) by TOC Analyser

The DOC determination was performed by the Newcastle University laboratory, School of Civil Engineering and Geosciences. Dissolved organic carbon (DOC) concentrations were analysed in filtered water samples using a Shimadzu TOC-5000A total organic carbon analyser (Figure 4-57). The instrument is capable of measuring inorganic carbon and total carbon separately. Filtered samples were put into cartridges and put in TOC analyser with the first blank sample.

Figure 4-57 *A Shimadzu TOC-5000a total organic carbon analyser*

4.8.4 Major cation analysis

Inductively coupled plasma (ICP) optical emission spectroscopy (OES)

Ion chromatography (Vista MPX, CCP Simultaneous ICP-OES, Varian) allows detection and measurement of cations in solution to ppb levels. Cation analysis by ICP optical emission spectroscopy of soil samples was performed by the Newcastle University laboratory, School of Civil Engineering and Geosciences. In case where Ca^{2+} and Mg^{2+} were not detected, dilutions were made for every sample with dilution factor 1:10 using standardized volumetric flasks and deionised water. Blanks, standard checks and replicates were run every 15 samples. The ICP-OES was recalibrated when the standard check differed by more than ±5%.

4.8.5 Major anion analysis

DIONEX Ion - Chromatography Model ICS - 1000

1 ml of filtered water sample was put into vials with 4 ml of deionized water, duplicate for every sample (a and b) and labelled dilution factor 1:5 (Figure 4-58). 5 ml of filtered sample was used in case where concentrations of NO_3^- and PO_3 were not detected. Blank and check-standards were placed in the first three places. Samples were placed in a DIONEX machine.

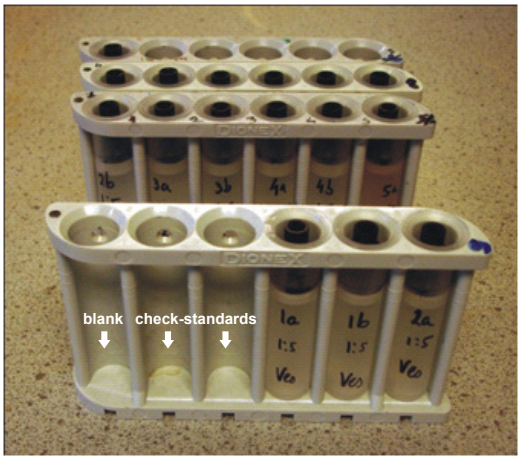

Figure 4-58 *5 ml vials with filter caps used for the automated sample*

4.8.6 Lab quality assurance

Quality Control in laboratories includes the following:

- Laboratory instrumentation calibrated with the analytical procedure,
- Laboratory instrumentation maintained in accordance with the instrument manufacturer's specifications, the laboratory's (QMP) and Standard Operating Procedures (SOPs),
- Method Blanks, Matrix spike/matrix spike duplicates, sample duplicates, etc. per the laboratory's QMP.
- Laboratory data verification and validation.

Charge Balance Error (CBE)

The first step of the water quality of data was calculating the balance of positive and negative ions. The equation for ion balance is shown below:

$$Charge\ balance\ error = \frac{\sum cations - \sum anions}{\sum cations + \sum anions} \cdot 100\%$$

An error up to ±10% is tolerable for surface water. A significant imbalance in the charge balance indicates that additional constituents are present or that an error has been made in the analysis of one or more of the ions.

4.9 Modelling: SHETRAN model description

4.9.1 Theory behind the model

The SHETRAN modelling system has been developed by the Water Resources Systems Research Laboratory (WRSRL) at the Newcastle University. SHETRAN (Ewen et al.

2000; Ewen et al. 2002) has its origins in the Système Hydrologique Europèen (SHE) (Abbott et al. 1986a, b) and is a fully distributed, physically based model for water flow, sediment and contaminant transport in river basins. Figure 4-59 shows the SHETRAN representations of catchment hydrological processes and consequently requires a considerable quantity of data to describe the properties of the catchment. In SHETRAN the catchment is divided into a horizontal orthogonal grid network and in the vertical direction by a column of horizontal layers at each grid square. The channel system is represented on the boundaries of the grid squares (Nasr et al. 2004). Each grid cell carries a piece of information for the catchment at that point. This information includes a specific surface elevation and model components for interception, evapotranspiration, snowmelt, and one-dimensional vertical unsaturated zone flow where appropriate (Ewen et al. 2000). The water flow component is able to simulate overland and channel water flow on the ground surface and in the stream channels, and soil-water and ground-water flow in the unsaturated and saturated zones, including systems of unconfined and perched aquifers (Ewen et al. 2000; Walsh 2004). Each grid element represents a rectangular area of ground surface and vegetation, and the part of the unsaturated and saturated zones directly below the ground surface (Walsh 2004).

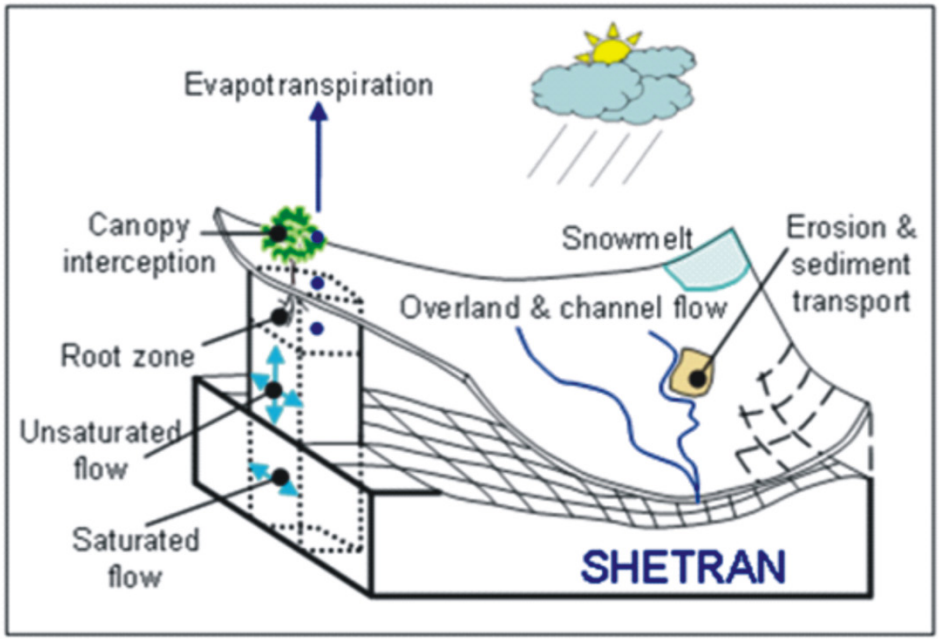

Figure 4-59 *Schematic illustration showing SHETRAN column and its (Sub-Column) cells (source: created by Ewen 2000, modified by Bovolo 2006)*

SHETRAN gives a detailed description in time and space of the flow and transport in the basin, which can be visualized using animated graphical computer displays (Ewen et al. 2000). This makes it a powerful tool for studying the environmental impacts of land

erosion (e.g. Wicks and Bathurst 1996), pollution (Birkinshaw and Ewen 2000a), the effects of changes in land use and climate (Parkin et al. 1996) and also in studying surface water and ground water resources (Parkin et al. 1996) and management (Adams et al. 1995; Walsh 2004). SHETRAN can be applied to a wide variety of spatial scales from large (2,500 km^2) contiguous river basins with multiple sub-basins, to single or partial basins, to individual hillslopes and catchments (0.94 km^2) (Bathurst et al. 2004).

Flow and infiltration in an unsaturated zone (UZ) are modelled using Richard's equation which is governed by the soil-hydraulic parameters (soil matrix potential and the hydraulic conductivity that is calculated using the equation of Brooks and Corey 1964) and this zone presents an integral part of subsurface flow where subsurface flow and transport are coupled directly to surface flow and transport. Interception is calculated using the Rutter (1971/1972) equation, which depends on ground cover areas, canopy drainage and storage capacity and transpiration, is accounted for by a root density function. Actual evapotranspiration can be calculated, using either the Penman-Monteith equation or observed evaporation data (e.g. pan evaporation), as a function of soil tension (water potential; e.g. Feddes et al. 1976). The process governs the generation of runoff and is coupled to a saturated zone (SZ). Overland flow (runoff) can be generated by excess of rainfall over infiltration capacity (Horton flow) or by excess of saturation (Dunne flow) (Figueiredo and Bathurst 2007). Transport capacity can be calculated using the equations of Yalin (1963) or Engelund and Hansen (1967). The 3D solute transport equations were used to simulate the leaching and transport of nitrate. A nitrogen transformation model has been integrated into SHETRAN, so spatially distributed river catchment modelling simulations of coupled flow and nitrate transport can be made (Birkinshaw and Ewen 2000a). In terms of simulation time step, SHETRAN can simulate at any time step from one minute up to one day.

4.9.2 Data required by the model

The spatial data required by SHETRAN includes a Digital Elevation Model (DEM), land use map and soil map. The meteorological variables include rainfall and potential evapotranspiration data. For nutrient modelling, a time series of nitrate application loads is required. Time series of observed discharge and nutrient concentrations are vital for calibrating and validating the models.

A more detailed description of the equations and nature of SHETRAN, covering its strengths and weaknesses, its data requirements, and its wide range of applications, is available elsewhere in the literature (Ewen et al. 2000; Birkinshaw et al. 2010) and it is not repeated here.

4.10 Summary

This chapter is designed to define the main field and laboratory methods used to determine the runoff, water quality parameters, chemical and physical characteristics of soil as well as modelling approach. The case study sites are described and laboratory methods to determine the nutrients, such carbon and nitrate are also discussed. The results for each aspect of the methods described here are presented in the next chapters.

Chapter 5. Hydrological and nutrient behaviour at the catchment and sub-catchment scale

5.1 Introduction

The following chapter provides insights for a better understanding of hydrological processes at a catchment and sub-catchment scale in relation to nutrient export. To address this issue, manually collected water samples and sediment data from the stream are summarised and discussed in relation to the nutrient status of the water and the sediments.

The results of this study aim to answer the following questions: 1) What are the major hydrological pathways in the sub-catchment? 2) How do the concentrations of nutrients (DOC and NO_3^-) in stream water and sediments vary with season and discharge? 3) How does the catchment size affect carbon and nitrogen variations in the sediments?

5.2 Precipitation and discharge relationships of the Blind Beck catchment

The period from 2009 to 2010 is used in this study. As in most of UK catchments, the Blind Beck catchment and the Hollow sub-catchment were subject to two rainy seasons; one in the autumn and another in the spring (Figure 5-1). The winter of 2009 - 2010 was unusually cold in the UK with heavy snowfalls from December to January. The Met Office (Meteorological Office; the United Kingdom's national weather service) website provides information about the winter 2009-2010 in the UK (Appendix C1). This source reported that: “from Thursday 17 December 2009 to Friday 15 January 2010 the UK experienced a spell of very low temperatures and significant snowfalls which affected almost the whole country. With daytime temperatures often failing to rise above freezing, little thawing occurred so fresh snowfalls added to previous accumulations. Snow depths of 10 to 20 cm were widespread across England and Wales, whilst across upland areas of northern England and in the Scottish Highlands, depths exceeded 30 cm in many areas. By 7 January, the UK was covered by lying snow, almost without exception, to significant depths in many areas” (source: Met Office 2012) (Appendix C2). Long drought periods occurred in May and June 2010 at both locations.

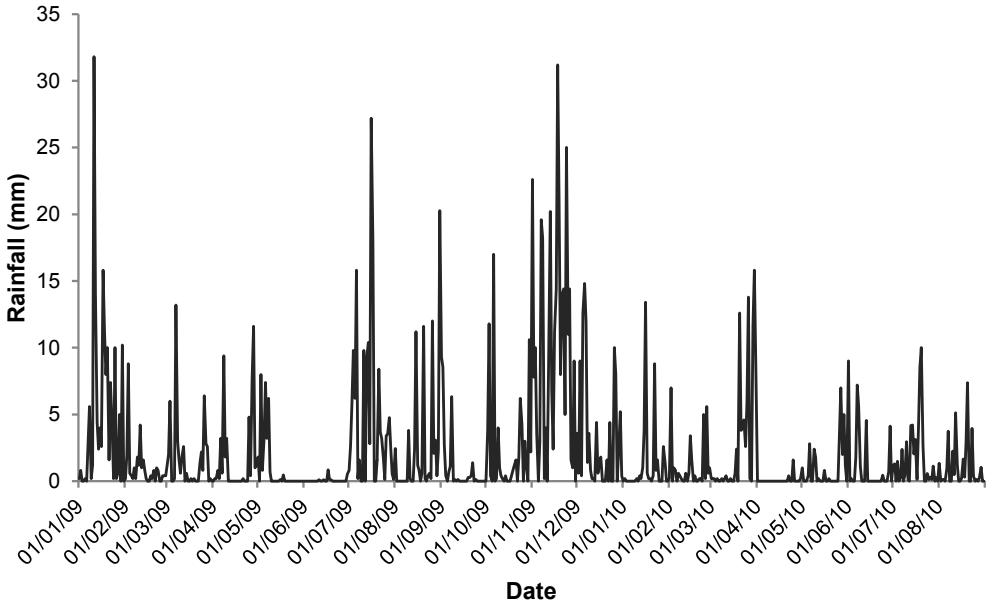

Figure 5-1 *Daily rainfall (mm) from 1/1/2009 to 31/08/2010*

Table 5-1 gives a positive water balance (Precipitation- PET) for the wet period in the autumn and the winter, while for the dry season there is a negative water balance in the spring. The total precipitation from 1 January to 31 August was 542 mm and 311 mm for 2009 and 2010 respectively. This shows that 2009 was a relatively wet period and, conversely, 2010 was a drier period. Precipitation data were provided from the Hydrolog data base. Potential evapotranspiration (PET) values were calculated using a weather generator as described in sub-section 7.3.2.

Table 5-1 *Water balance data for seasons of 2009 and 2010*

Season	Winter (DJF)	Spring (MAM)	Summer (JJA)	Autumn (SON)	Winter (DJF)	Spring (MAM)	Summer (JJA)	Autumn (SON)
Year	2009				2010			
Precipitation (mm)	249	125	232	412	164	119	197	N/A
PET (mm)	26	164	228	78	28	163	192	N/A
Water balance (mm) (Precipitation-PET)	223	-39	4	334	136	-44	5	N/A

N/A: not available; J-January, F-February, M-March, A-April, M-May, J-Jun, J-July, A-August, N-November, D-December

Figure 5-2 shows a time series of rainfall and stream flow with five storm events. Precipitation data were obtained from the Sykeside raingauge, while discharge data were from the stream gauge at the outlet of the Blind Beck catchment. The total precipitation from 1 May 2009 to 31 August 2010 was 1084 mm, and discharge was 537 mm. November 2009 was the most eventful month with many discharge peaks that reflect significant rainfall inputs. A total of 228 mm of rain fell in the catchment during five storm events, which are named in following E1 to E6. There have been four minor (E1, E2, E4 and E5) and one large flooding event (E3). Of the five events, the event of

November 18, 2009 (E3 in Table 5-2) produced the largest amount of rainfall (99.6 mm). Discharge rates decreased from April 2010 to August 2010, which was likely due to lower total rain, higher evapotranspiration, and decreased water table level.

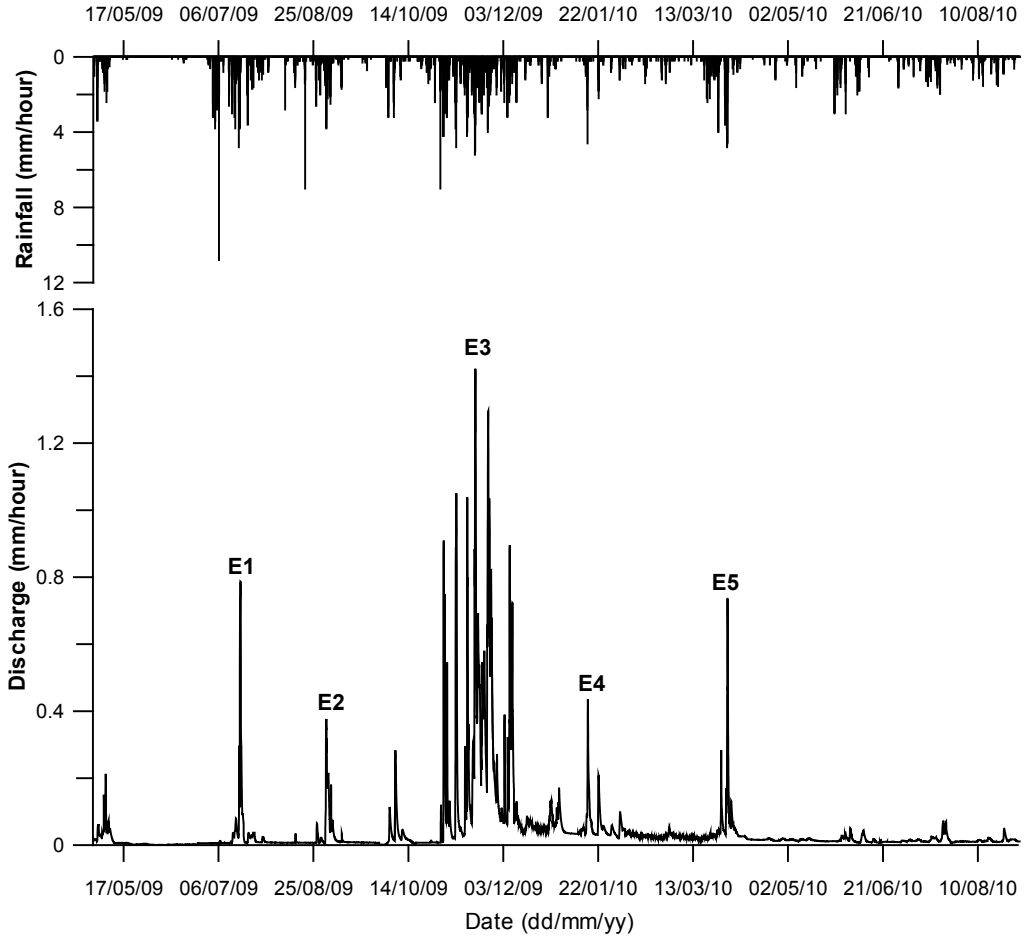

Figure 5-2 *Rainfall and stream flow discharge for the study period from May 2009 to August 2010 for Blind Beck. The five selected storm events are indicated*

Total storm runoff is considered to be the total hydrograph volume minus the baseflow volume for the storm event. Since precise definition of a storm duration is difficult for multiple-peaked hydrographs, a pragmatic choice of the start and end of each storm was made based on visual inspection of the hydrograph.

Table 5-2 *Hydrologic parameters for the five selected storm events over the study period of May 2009 to August 2010 for Blind Beck. APT_7 is the antecedent precipitation total (mm) for 7 days prior to the event*

Event #	Day of the event	Rainfall total (mm)	Hourly peak rainfall (mm)	API_7 (mm)	Runoff depth (mm)	Hourly peak runoff (mm)	Runoff ratio
E1	17-18/7/2009	37	4.8	60	18	0.79	0.49
E2	30-31/8/2009	38	3.8	19	11	0.38	0.29
E3	16-21/11/2009	100	5.2	53	66	1.42	0.66
E4	15-17/1/2010	18	4.6	6	10	0.44	0.56
E5	29/3/-1/4/2010	36	4.8	31	14	0.74	0.39

Table 5-2 summarizes hydrologic characteristics associated with the five storm events during the study period of May 2009 to August 2010. The runoff ratio is one indicator

of the water balance in a catchment (Tockner and Robinson 2009). Runoff ratios have been calculated for individual events with values ranged from 0.30 to 0.66. Thus, the runoff ratio (total runoff as a proportion of total available precipitation) values were slightly variable between storm events E1, E2, E4 and E5 except for the large flooding event in November 2009, E3. This distribution suggests that there is variability of the storm duration, total precipitation, rainfall intensity or antecedent wetness conditions. However, the variability of runoff ratio is well documented in the literature but with no clear conclusion about which factors govern this variability (e.g. Gottschalk et al. 1998; Wainwright et al. 2002; Longobardi et al. 2003). There are also several variables related to catchment characteristics that affect the runoff ratio, which control mechanisms such as evapotranspiration, soil infiltration and groundwater abstraction (Burt 1992; Gustard 1992; Tockner and Robinson 2009). Longobardi et al. (2003) indicated that rainfall-runoff transformation is a non-linear process, and proposed that the dependence of runoff ratio on antecedent conditions could be assessed by means of a conceptual framework. They estimated the runoff coefficient as the ratio between quick flow and rainfall volume on an event basis, and as a function of the initial catchment state conditions prior to an event, such as pre-event soil moisture and pre-event base flow. In this study, detailed antecedent soil moisture conditions have not been measured at the catchment and sub-catchment scale, as this requires many point measurements to represent the antecedent catchment state adequately, so antecedent precipitation totals are used as a proxy.

The November 16th - 21st 2009 (which from here on will be called the November 2009 flood, E3) was the largest flood event to be recorded by the instrumentation and visual observation in Blind Beck as can be seen in Figure 5-3 at sampling site 1 and Figure 5-4 downstream at sampling site 5.

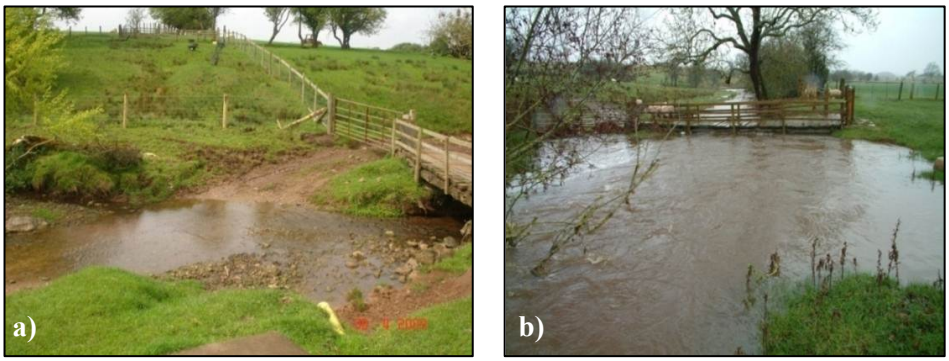

Figure 5-3 *Blind Beck stream at sampling site 1: a) April, 2009 and b) flood event, November 18th 2009 photo taken by Nick Barber 2009)*

Figure 5-4 *Blind Beck at sampling site 5: a) April 2009 and b) flood event, November 22th 2009 (photo taken by James Bathurst 2009)*

The main cause of the November 2009 flooding was the large amount and the intensity of the rainfall occurring on a saturated soil that resulted in high overland flow rates. Figure 5-5 shows the November flood hydrograph.

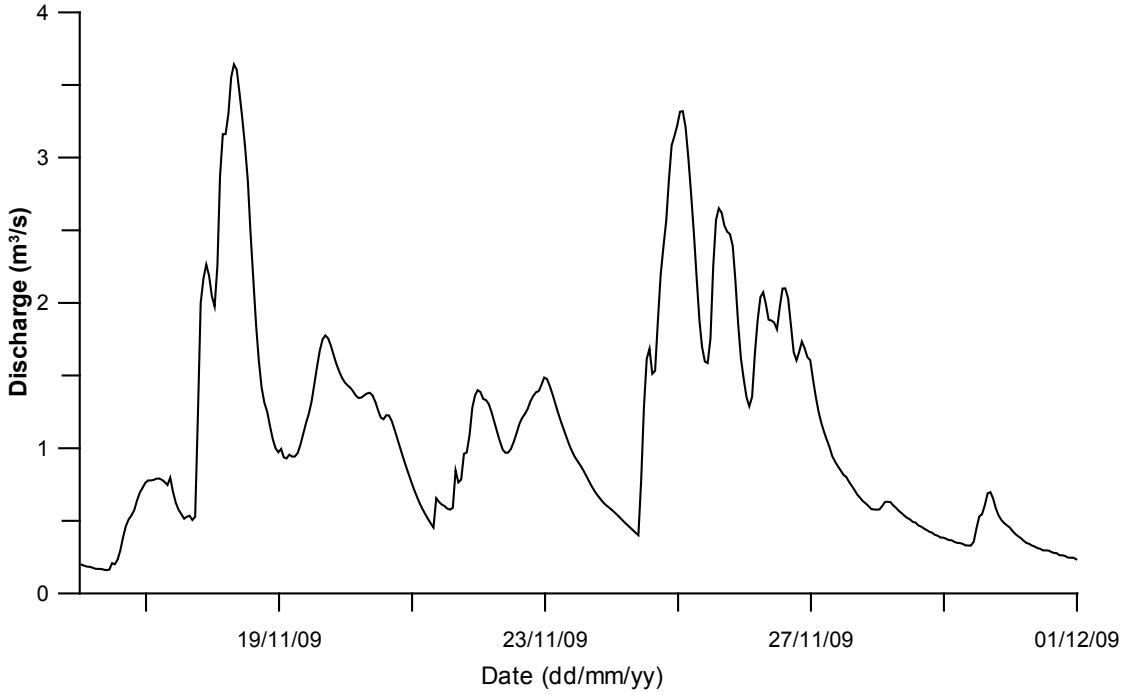

Figure 5-5 *Flood hydrograph at the Blind Beck catchment during the November 2009 flood event*

5.3 Electrical conductivity, precipitation and discharge relationship of the Hollow sub-catchment

The Hollow sub-catchment in a pasture landscape consists of large open surfaces (Figure 5-6) that contribute to the large volume of runoff during months of high rainfall. The total annual precipitation from 1 June 2009 to 31 July 2010 was 1019 mm, and 6.11×10^7 litres or 680 mm of water flowed past the V-notch weir. Precipitation and discharge data were obtained from the raingauge and data logger on the 60^o V-notch weir at the outlet of the Hollow sub-catchment.

Figure 5-6 *The Hollow sub-catchment*

Figure 5-7 shows the relationship between precipitation and discharge from June 2009 to July 2010. For the mentioned period, the minimum recorded flow was zero. The maximum recorded hourly flow was 56 mm during the period from 17 to 19 November 2009 associated with the storm event with large discharge peaks that reflect the significant rainfall inputs. The left photo in Figure 5-8 shows no flow over the weir on 6 August 2009, and the right photo shows the flood event on 17 November 2009.

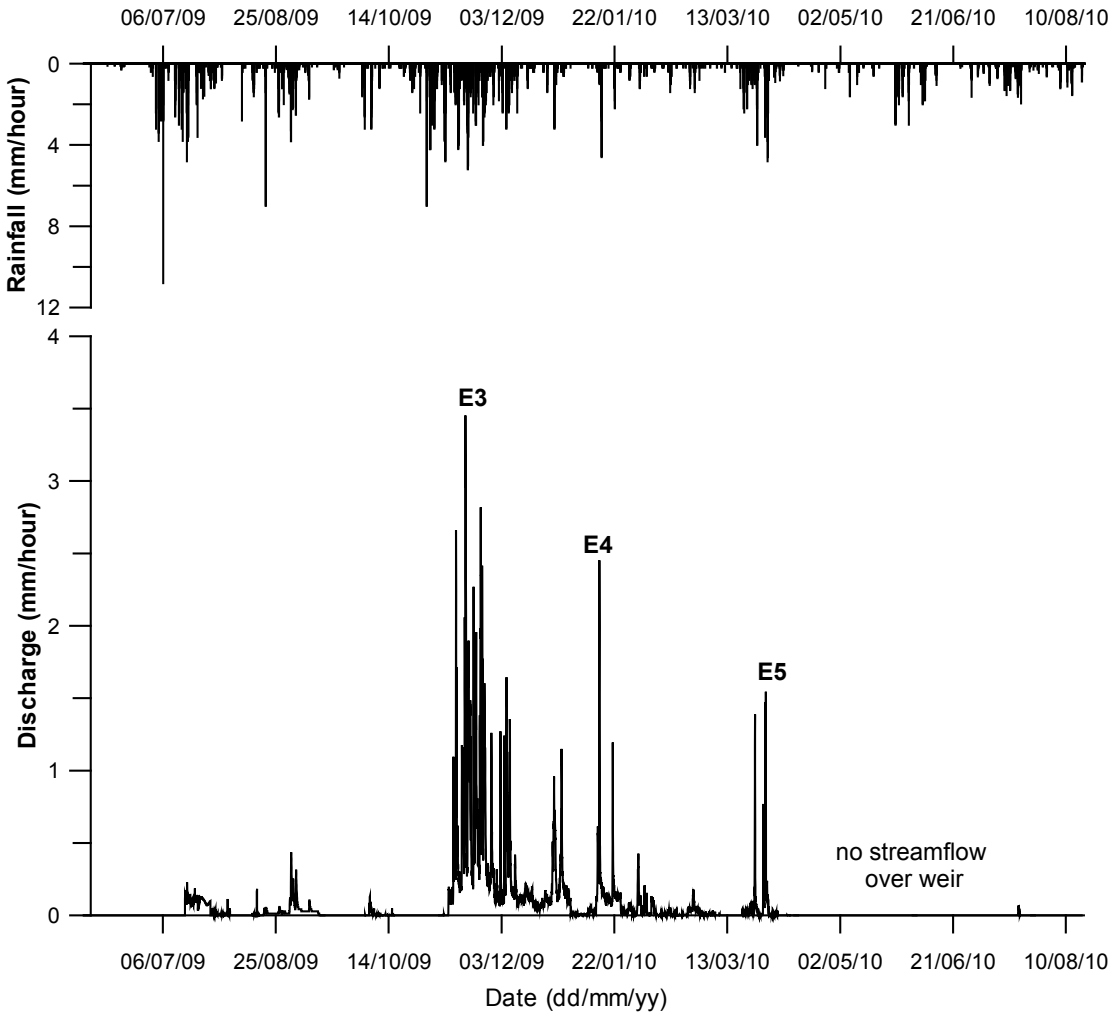

Figure 5-7 *Rainfall and streamflow, at the Hollow sub-catchment for the study period of June 2009 to July 2010. The three storm events are indicated. Dry conditions resulted in no streamflow (zero values) over the V-notch weir*

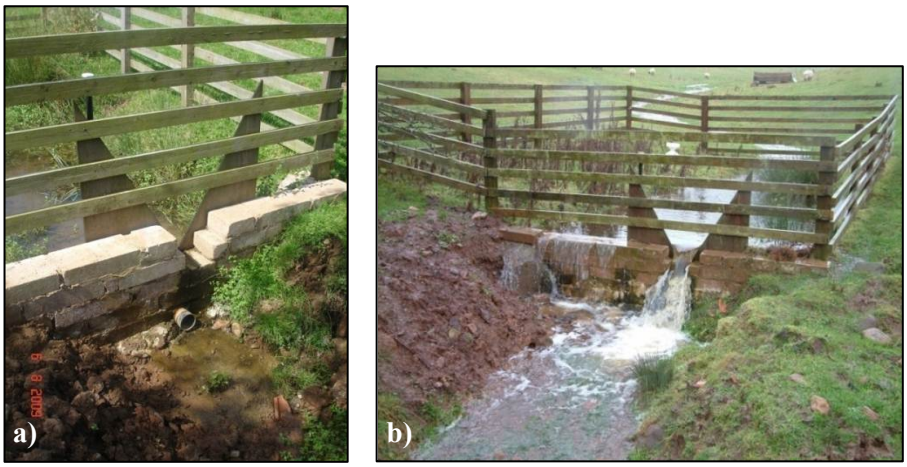

Figure 5-8 *Hollow at sampling site 4: a) no flow over the V-notch weir, August 2009 and b) flood event, November 17th 2009*

In total three storm events were monitored for stream flow discharge at the outlet of the Hollow sub-catchment. Table 5-3 summarizes the main hydrologic characteristics associated with the three events for the Hollow sub-catchment. The runoff ratio is also presented with values ranged from 0.28 to 0.85. Runoff ratios were variable between catchment and sub-catchment with no evident relationship to catchment size (Tables 5-2 and 5-3). In event 3, the runoff ratio was 0.85 for the Hollow and a smaller value of 0.66 for Blind Beck. The timing of runoff response to rainfall was directly related to catchment size (Figures 5-2 and 5-7) with the sub-catchment reacting most quickly.

Table 5-3 *Hydrologic parameters for the five selected storm events over the study period of May 2009 to August 2010 for the Hollow sub-catchment. APT_7 is the antecedent precipitation total (mm) for 7 days prior to the event*

Event #	Day of the event	Rainfall total (mm)	Hourly peak rainfall (mm)	API_7 (mm)	Runoff depth (mm)	Hourly peak runoff (mm)	Runoff ratio
E3	17-19/11/2009	66	5.2	53	56	3.5	0.85
E4	15-17/1/2010	18	4.6	6	5	2.5	0.28
E5	30/3/-1/4/2010	25	4.8	31	9	1.5	0.36

In event 4, the runoff ratio was smaller than event 3, being 0.28 for the sub-catchment and a larger value of 0.54 at the catchment scale. The lag in initial response between sub-catchment and catchment was 28 h. Similar to event 3, the sub-catchment reacted most quickly to precipitation. In event 5, runoff ratios were almost the same between the Hollow sub-catchment and Blind Beck (Tables 5-2 and 5-3). A 26 h lag is recorded between the sub-catchment and catchment scales.

Tockner and Robinson (2009) indicate that the runoff ratio normally decreases with a catchment area because the catchment size is an indicator of the path length a raindrop to travel from the headwaters before leaving the catchment downstream. Differences in

runoff ratios and timing between the catchment and sub-catchment showed that the large storm event (E3) with wet antecedent conditions resulted in less lagged timing.

Figure 5-9 shows the rainfall, discharge and the behaviour of electrical conductivity (EC) during the November storm event. In the sub-catchment, the electric conductivity (EC) of the runoff was measured at 15 min intervals. The November 2009 event (E3) was selected as a representation of the relationships between the EC and discharge because it was the largest storm event. At the outlet of the sub-catchment, the EC of stream water responds quickly to stream flow (Figure 5-9).

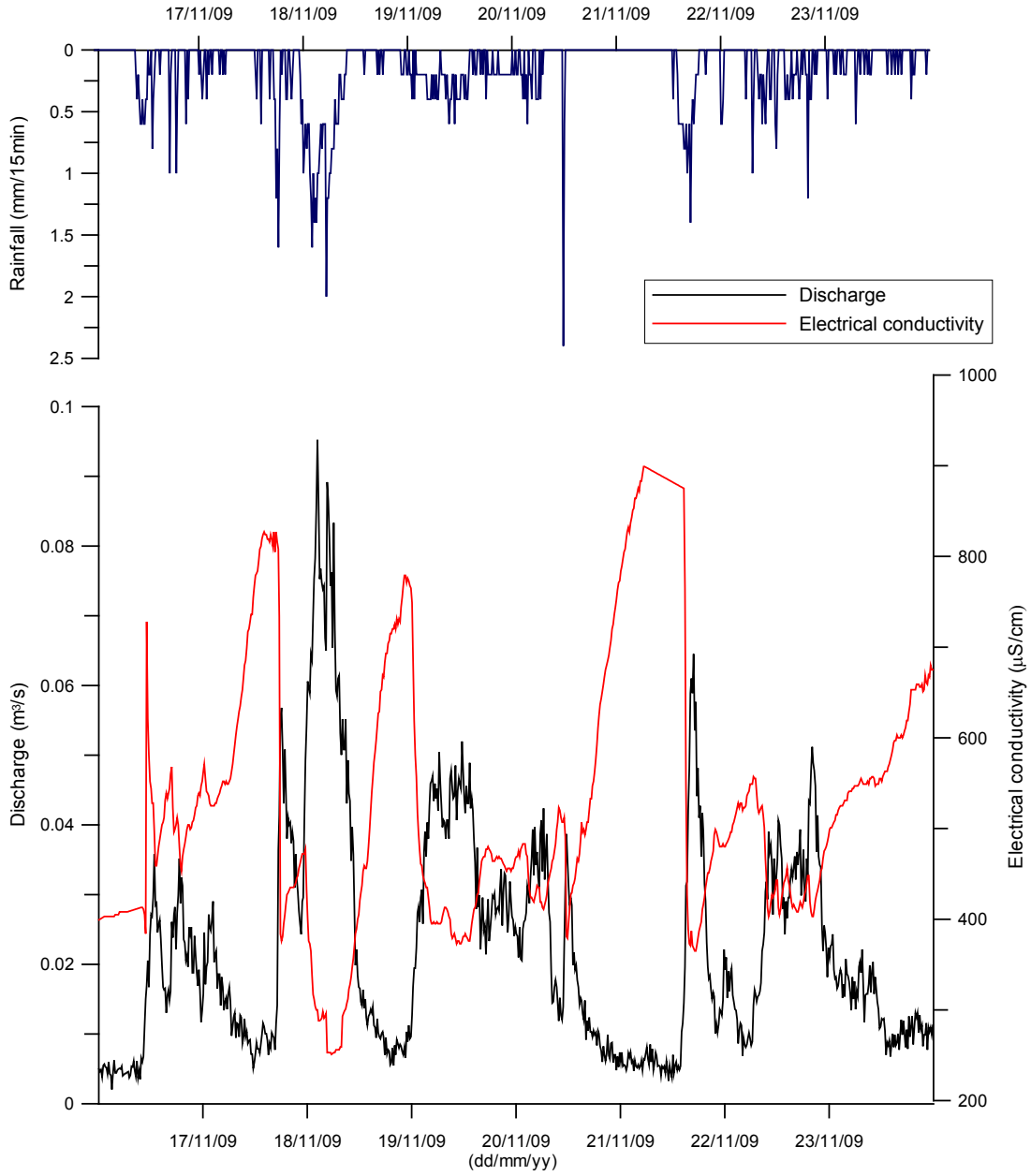

Figure 5-9 *Rainfall, streamflow, and electrical conductivity at the Hollow sub-catchment for the November storm event*

Data from the monitoring show that the EC showed a generally inverse relationship to discharge. While rainfall at the nearby raingauge station had EC values of around

11 µS/cm, with small variations during storm events, the EC in runoff reached extremely high values of 980 ± 20 µS/cm (average = 525 µS/cm). As can be seen from Figure 5-9, during the event the EC drops, due to dilution of the relative high EC pre-event ('old') water with low EC event ('new') water. Before the storm event, the EC was 827 µS/cm and during the storm it dropped to 251 µS/cm. In the case of recessions, an opposite trend occurred. It seems possible that the lower EC values are indicative of the greater influence of runoff from the hillslope whereas the higher EC is related to the higher groundwater supply or pre-event ('old') water. As mentioned in the literature high dissolved mineral concentration represented by an increase of EC might be due to the long residence times allowing reactions between recharged water and soil minerals (Burt and Pinay 2005).

The EC shows a clockwise hysteresis with the lower EC on the descending limb (Figure 5-10) compared with the ascending limb. These results indicate that during the intense storm, discharge increased with flushing effect of rainfall on the EC, while in the case of decreasing discharge, the EC concentrations increase. It seems possible that during flushing, low EC indicates soils with near saturation, while high EC indicates drier conditions.

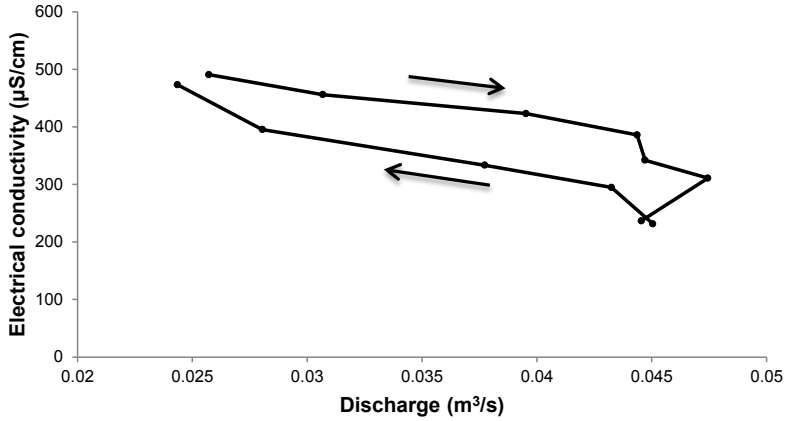

Figure 5-10 *Hysteresis loop of the electrical conductivity plotted against discharge, during the November storm event at the Hollow sub-catchment*

During low flow conditions, there is a high conductivity in the stream water that indicates the high presence of inorganic dissolved solids (nutrients). This can cause triggering of excessive algal growth (algal bloom) or eutrophication.

In general, therefore, it seems that the electrical conductivity is an indicator of the origin of the water for both storm events. It provides information about the hydrological behaviour of specific catchments during stormwater runoff that can affect water bodies

and agricultural activities. Based on this behaviour it is proposed that the EC is a useful natural hydrologic tracer for estimates of surface and subsurface components of flow (event and pre-event water) at the outlet of the sub-catchment scale, because of its low cost, easy monitoring and the immediate assessment of the water composition.

5.3.1 Hydrograph separation at the Hollow sub-catchment

The electrical conductivity (EC) was used to distinguish between event water (overland flow) and pre-event water (baseflow/subsurface flow) according to the procedure of Hugenschmidt et al. (2010).

Chemistry-based hydrochemical separation relies on the principle of mixing where the equations of continuity and mass balance govern the quantity of tracer flow (Ogunkoya and Jenkins 1993). An example of a two-component separation is:

$$Q_t = Q_o + Q_n$$
$$Q_tC_t = Q_oC_o + Q_nC_n$$

where Qt, Qo and Qn (Q in m^3s^{-1}) represent volumes of current stream flow, pre-event water (old water - subsurface water including soil water and/or groundwater) and event water (new water - rainfall, overland flow), respectively, and Ct, Co, and Cn (C in mgl^{-1} or μScm^{-1}) are the corresponding tracer concentrations.

In this study, electrical conductivity values were obtained by continuous measurements with a CTD Diver and by direct field measurements at the outlet of the sub-catchment. As mentioned earlier (Chapter 2, Section 2.1), rainfall has a short residence time and does not make much contact with mineral soils (Burt and Pinay 2005; Weiler et al. 1999). Therefore, it is assumed that the electrical conductivity in the overland flow is similar to that of rainfall (Gremillion 2000). The overland flow and rainfall water samples were collected and analysed in order to test that overland flow and rainfall values were similar and thus represented the same end member in the two-component mixing model.

During the sampling period, samples of baseflow/subsurface flow (pre-event water; water in the stream during periods without rainfall), overland flow and rainfall (both constituents of event water; from a tipping bucket set up on the hillslope) were collected and measured. As the interflow component for the E3 event was not available, and for

the E4 event was not activated, this component could not be included in the separation process.

In this study, the two end-member compositions (event water and pre-event water) were considered from two initial sources: rainwater and baseflow/subsurface flow. The end-members chosen for the two-component hydrograph separation for each storm event are given in Table 5-4. The baseflow/subsurface flow electrical conductivity is an average of baseflow conductivities over a twenty-four hour period prior to the storm event.

Table 5-4 *Electrical conductivity of the event and pre-event water used in the hydrograph separation of discharge in the Hollow sub-catchment*

	Electrical conductivity (µS/cm)		
Event	November 2009 (E3)	January 2010 (E4)	March-April 2010 (E5)
Event water (overland flow)	11	43	11
Pre-event water (baseflow)	819	984	971

The rainfall conductivity value for the November 18th storm event (E3) was 11.0 µS/cm. The average overland flow runoff conductivity was measured as 11.2 µS/cm. This shows a similarity between the average overland flow conductivity and rainfall conductivity value. Because of this similarity and the fact that only one conductivity value can represent event water concentration, the overland flow conductivity data was chosen to represent event water conductivity to define the event water end-member.

During the January 15th, 2010 storm event, the electrical conductivity of the rainfall was 12.0 µS/cm. The average overland flow runoff was 43.4 µS/cm. Because of this difference, the rainfall conductivity was not considered as a significant component.

The average rainfall conductivity value for the March 30th (E4), 2010 storm event was 11.0 µS/cm. The average overland flow runoff conductivity was also 11 µS/cm, which shows the same similarity between overland flow runoff and rainfall conductivities.

The results obtained from the hydrograph separation techniques are presented in Figure 5-11. New water (event-water) runoff is a significant portion of the total runoff for each event. Average new water contributions for all events range from 15 to 22%. The separation was mainly composed of the pre-event water (78%) for the November storm event (E3). These results suggest that they are due to long duration of rainfall and infiltration into soils, which consider two components of flow, the overland and subsurface flow. At the moment when the soil was saturated it produced saturation excess overland flow.

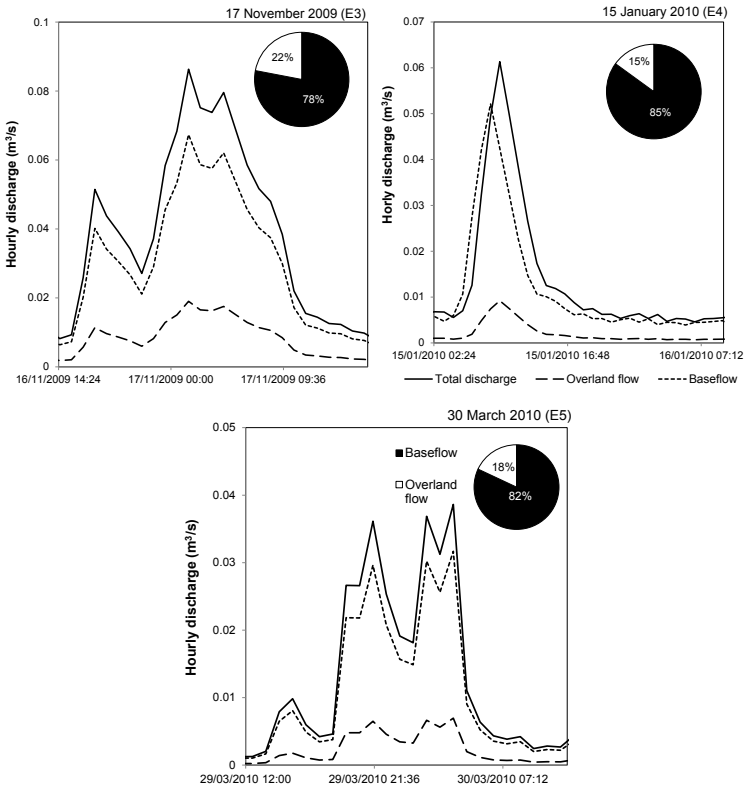

Figure 5-11 *Results of the hydrograph separation for 17 November 2009 (E3), 15 January 2010 (E4) and 30 March 2010 (E5)*

The separation of event 4 (E4) shows the appearance of a baseflow peak prior to the one of total runoff. The overland and the subsurface flow do not peaked at about the same time. The subsurface flow was dominant with 85% and the overland flow with 15%. This observation may be explained by the fact that in January the soil (ground) was frozen, producing the overland flow, with the baseflow peak occurring due to freezing-melting alternations. During melting or thawing, the upper soil layers melt first, allowing infiltration of water and saturation of the soil. Frozen soils do not allow any infiltration, hence produces a very rapid overland flow. The thickness of frozen soil was approximately 18 cm or even deeper according to field observations in lysimeters installed on the hillslope at that depth. Based on the observation that soil was frozen in the sub-catchment during December 2009 to January 2010, it is suggested that the observed overland flow is Hortonian flow rather than saturated excess overland flow. The storm follows a relatively dry period (Table 5-3); the antecedent precipitation total for 7 days prior to the event was low (6 mm).

For the event 5 (E5), the subsurface flow was dominant with 82% and the overland flow with 18%. The antecedent precipitation total for 7 days prior to event 5 was 31 mm. This suggests on comparison to all events that the event water proportion increases with an increase of precipitation depth. In comparison of all events, E3 event experienced the

highest proportions of event water. The smaller events produce more pre-event water due to the importance of mixing between event and pre-event water during the beginning of runoff generation where the pre-event water ranged from 82-85% (E4 and E5) for smaller to 78% for larger events (E3).

The application of the two-component hydrograph separation shows that for all events, the overland flow and subsurface flow are present. However, the overland flow is not the dominant flow process in the sub-catchment during storm events. This finding is in agreement with Ogunkoya and Jenkins (1991) who report that pre-event water contributes the most significant volumes to stream flow during storms where values ranging between 80-95%. This the case in the majority of studies, while several studies show 60% of stream flow during storms to be event water, with maximum contributions of 80% event water (Ogunkoya and Jenkins 1991) The dominant flow process in the Hollow sub-catchment during storm events is subsurface flow.

The amount of overland flow generated by individual storm events is dictated by variables such as the infiltration capacity of the ground, water table height, capillary fringe height, storm magnitude, and storm intensity (Occhi 2009). This author also indicates that the amount of overland flow may be affected even by the amount of time in between storms, which can dictate the rate at which water can permeate the ground water table at infiltration zones.

Linking these findings with Hypothesis 3 (Chapter 1) that was tested over the sub-catchment, it is shown that continuous measurement of variables at the outlet of the sub-catchment can provide adequate estimates of surface and subsurface components. This means that electrical conductivity can be used as a tracer to separate hydrographs at the small scale catchment (sub-catchment, 0.09 km^2), which is consistent with the third hypothesis of this study.

This study does not include the hydrograph separation techniques at the catchment scale (Blind Beck) because no data of electrical conductivity were available as mentioned in the sub-section 4.3.1. Therefore, it was not possible to determine scale effects between catchment and sub-catchment in the amount of runoff and the percentage generated from the overland flow using this method. Consequently, the intention of this study to provide a broader picture on upscaling effects and proportions of event water and pre-event water at each scale was not achieved.

The hydrograph separation techniques using the two-component separation method is likely to be affected by errors related to each of the two end members, and the uncertainty in the measurement of stream values.

The results of the hydrograph separation suggest that overland and subsurface flows both play a significant role in the runoff generation of the sub-catchment, providing major pathways for nutrients. According to this, the question raised at the beginning of this chapter, 'What are the major hydrological pathways in the sub-catchment?' has been answered.

5.4 Stream water quality

The chemistry of major ions (Ca^{2+}, Mg^{2+}, K^{+}, Na^{+}, HCO_3^{-}, Cl^{-}, SO_4^{-2} and NO_3^{-}) in the water of Blind Beck and Hollow stream was studied. One of the primary goals of this study is to evaluate the characteristics of stream nutrients in the water for the Blind Beck and Hollow stream.

As shown in Table 4-6 of Chapter 4, data on five water quality parameters were collected on a monthly basis (one point value) during 2009-2010 year at sites 1, 2, 3, 4 and 5. Stream water was sampled at the weir of the Hollow catchment at site 4 and for all sites (see Figure 4-38), but collection of water samples was not available in January 2010. In addition, another parameter used for the interpretation of water quality was discharge. For all samples, electric conductivity, pH, and the concentrations of K^{+}, Na^{+}, Ca^{2+}, Mg^{2+}, HCO_3^{-}, Cl^{-}, SO_4^{-2} and NO_3^{-} were measured.

Table 5-5 shows the average chemical compositions of rain water. Also, minimum, maximum, and standard deviation of measured ions are included in Table. It can be seen from Table that Cl^{-}, HCO_3^{-} and Na^{+} are the dominant ions in rainwater of Sykeside. The Appendix D1: Table D1-1 provides the full chemical results of rain water, showing that the major ion concentrations were higher in the winter. The average pH of rainfall for the sampling period (August 2009-July 2010) was 6.4, which indicates that rain water samples were slightly acidic in nature. The average electrical conductivity (EC) was 11 µS/cm. The general trend of the abundances of different chemical constituent is as follows:

$$Cl^{-} > Na^{+} > SO_4^{2-} > Ca^{2+} > K^{+} > NO_3^{-} > Mg^{2+}$$

The chemical composition of rain water is dominated by chloride and sodium ions, however, high concentrations of sulphate, calcium and potassium can occur. Sulphate, calcium and potassium are associated with both marine and terrestrial sources.

Table 5-5 *Statistical analysis of chemical composition of rainwater over Sykeside Farm during 2009 – 2010 year (n = 12)*

Rainwater	pH	EC (µS/cm)	Na^+	K^+	Ca^{2+}	Mg^{2+}	HCO_3^-	Cl^-	SO_4^{2-}	NO_3^-
			mg/l							
Min.	5.8	7	1.3	0.4	0.8	0.2	3.3	4.7	1.6	0.3
Mean	6.4	11	2.5	1.0	1.5	0.4	5.0	7.5	2.3	0.9
Max.	7.2	13	5.6	2.0	3.5	0.8	7.7	8.1	3.6	2.8
SD.	0.4	2	1.5	0.5	0.9	0.2	1.5	2.1	0.7	0.8

Min = minimum value, Max = maximum value, SD = standard deviation

Table 5-6 summarises statistical analysis of stream water concentrations from sites 1 to 5. During dry periods (April – July 2010), sampling of water at the outlet of the Hollow sub-catchment was a problem because no water spilled over the weir and the stream was dry with some areas of standing water. Samples with large errors (16 - 40%) were eliminated and not included in this thesis. The full chemical results for the stream water with the Charge Balance Error (CBE) may be found in Appendix D1: Table D1-2 to D1-6.

Table 5-6 *Statistical analysis of chemical composition of stream water for site: 1 to 5 in Blind Beck during 2009 – 2010 year*

Site 1 (n = 16)	pH	Na^+	K^+	Ca^{2+}	Mg^{2+}	HCO_3^-	Cl^-	SO_4^{2-}	NO_3^-
		mg/l							
Min.	7.4	7.4	1.1	54.8	14.3	202.4	10.9	6.0	1.6
Mean	7.9	8.9	2.2	75.0	26.7	285.8	19.3	10.5	4.6
Max.	8.4	14.8	5.9	108.4	34.2	374.2	41.2	20.5	7.2
SD.	0.3	1.8	1.2	14.8	4.6	50.3	7.7	3.6	2.0
Site 2 (n = 16)	**pH**	**Na^+**	**K^+**	**Ca^{2+}**	**Mg^{2+}**	**HCO_3^-**	**Cl^-**	**SO_4^{2-}**	**NO_3^-**
		mg/l							
Min.	7.3	6.1	0.9	50.0	13.8	204.3	10.6	5.7	1.0
Mean	8.0	8.6	2.1	73.6	26.1	287.41	16.8	9.5	4.6
Max.	8.4	18.2	5.6	97.8	32.4	392.8	39.8	12.7	7.4
SD.	0.3	3.0	1.3	17.1	5.1	53.7	7.7	2.0	2.0
Site 3 (n = 16)	**pH**	**Na^+**	**K^+**	**Ca^{2+}**	**Mg^{2+}**	**HCO_3^-**	**Cl^-**	**SO_4^{2-}**	**NO_3^-**
		mg/l							
Min.	7.4	6.7	0.8	53.3	13.3	192.0	11.2	5.8	1.1
Mean	8.0	9.1	2.1	73.0	25.9	278.6	19.1	8.5	4.2
Max.	8.5	19.4	6.5	95.8	30.6	406.1	41.2	11.4	7.3
SD.	0.3	3.4	1.5	13.8	4.9	58.9	8.4	1.8	1.9
Site 4 (n = 9)	**pH**	**Na^+**	**K^+**	**Ca^{2+}**	**Mg^{2+}**	**HCO_3^-**	**Cl^-**	**SO_4^{2-}**	**NO_3^-**
		mg/l							
Min.	6.8	5.4	0.6	37.3	9.8	112.7	8.0	5.0	0.0
Mean	7.2	7.0	1.4	77.2	19.1	272.2	13.0	6.8	1.3
Max.	8.0	8.5	3.0	102.0	24.4	376.2	20.4	9.4	3.5
SD.	0.4	1.1	0.9	27.6	6.4	112.7	5.1	1.7	1.2
Site 5 (n = 16)	**pH**	**Na^+**	**K^+**	**Ca^{2+}**	**Mg^{2+}**	**HCO_3^-**	**Cl^-**	**SO_4^{2-}**	**NO_3^-**
		mg/l							
Min.	7.4	6.8	1.1	59.4	14.4	211.3	11.5	5.8	2.9
Mean	7.9	8.3	1.7	92.9	26.6	340.1	17.3	8.8	7.8
Max.	8.4	10.4	3.6	120.0	34.4	462.2	27.0	16.3	14.6
SD.	0.2	0.9	0.7	16.1	4.5	60.3	4.1	2.5	3.4

Min = minimum value, Max = maximum value, SD = standard deviation

The average pH of stream water was in the range 7.2 – 8.0, indicating slightly alkaline conditions. Potassium concentration values were low, with minimum values ranging from 0.6 to 6.5 mg/l. At site 1, the potassium concentrations in the stream water were high compared to other sites, with the mean potassium concentration of 2.2 mg/l and the maximum concentration of 5.9 mg/l. At site 2 the mean potassium concentration in the samples was 2.1 mg/l, and the maximum concentration was 5.6 mg/l, while at site 3 the mean potassium concentration was 2.1 mg/l and the maximum concentration was 6.5 mg/l. Sodium concentrations in stream water were generally low, the mean concentration ranged from 7.0 to 9.1 mg/l. At site 3 the mean sodium concentration at this site was 9.1 mg/l and the maximum concentration was 19.4 mg/l. Calcium ranged from 37.3 - 120 mg/l and magnesium from 9.8 - 34.4 mg/l. The Ca^{2+} and Mg^{2+} presence reflects the lithology of the catchment (see Chapter 4, Figure 4.4). As can be seen from Table 5-6 all cations and pH were lowest at site 4 (Hollow).

Bicarbonate concentration ranged from 112.7 to 462.2 mg/l. Chloride concentration varied between 8.0 - 41.2 mg/l. Sulphate concentrations varied with sampling location from 5.0 -20.5 mg/l, with the highest value at site 1. This could be due to the vicinity of the farm where ammonium sulphate fertiliser is commonly used. The nitrate values were from 0.0 - 14.6 mg/l, with the highest value at site 5, where nitrate sources are likely to be from agricultural activities. In the interpretation of this data, it must be considered that both manure and fertilisers were applied to cultivated crops of the study area.

Figure 5-12 illustrates the percentage contribution of each ionic constituent to the total ionic mass. The contribution of Ca^{2+} is 51% at site 4 and 56.6% at site 5 of the total ionic mass. The accounted proportion of K^{+} was very low (1.0 - 1.5%).

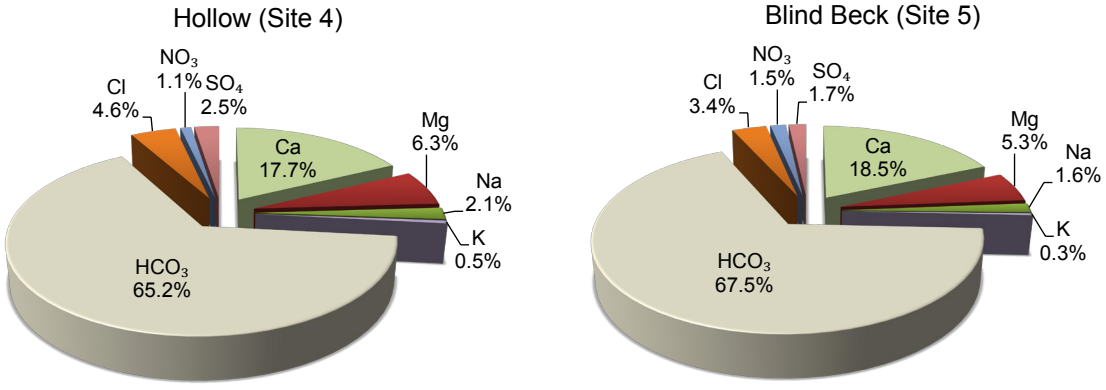

Figure 5-12 *Percentage contribution each ion to total ionic mass*

Water chemistry for all sites is predominantly calcium-bicarbonate-magnesium-chloride type of water with the following ionic sequences:

$$Ca > Mg > Na > K$$

$$HCO_3 > Cl > SO_4 > NO_3$$

Two chemical signatures may be distinguished from the study of the constructed Piper diagram: Ca(Mg)-HCO_3 (stream) and Cl(Na)-HCO_3 (rainwater), as illustrated in Figure 5-13.

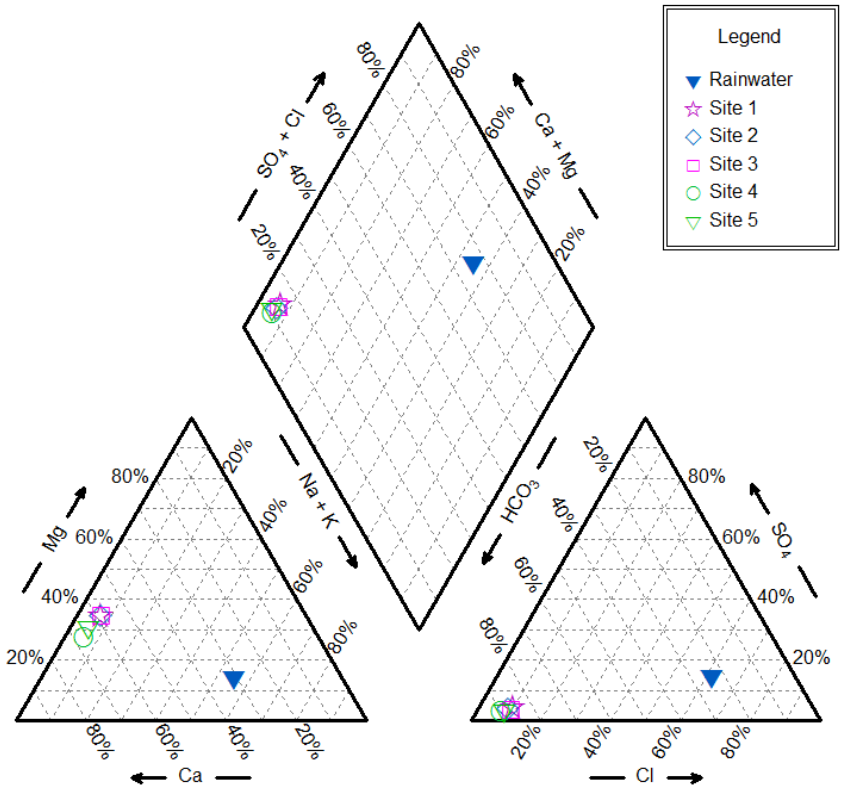

Figure 5-13 *Piper diagram illustrating the major ion compositions in stream water at the Blind Beck catchment (site 5), the outlet of the Hollow sub-catchment (site 4), sites 1, 2, 3 and rainwater*

The average chemical composition of the Blind Beck stream (site 1, 2, 3 and 5), and the Hollow stream (site 4) is very similar but differs from the rainwater which clearly has a very different chemical signature. The stream water at all sites was heavily dominated by bicarbonate ions. The major ions determined in this study are consistent with prior studies in Blind Beck (Ockenden 2010).

In comparison to the Hollow, Blind Beck contains slightly higher concentrations of bicarbonate, calcium and nitrate. These differences could be attributed to variations in bedrock geology such as limestone. The observed slightly high concentrations of nitrate in the Blind Beck stream could be attributed to extensive agricultural activity and crop cultivation, which affected drainage water and had a great influence on stream water

quality (Figure 5-14). The nitrate concentrations are lower at the Hollow sub-catchment as pasture land compared with sites 1, 2 and 3 due to the influence of localised pollution at Sykeside Farm where intensive farming is present. The low concentrations of potassium for both catchments suggests that migration of potassium depends on soil texture and organic matter content of soil, especially pH (Peverill et al. 1999). However, at three sites 1, 2 and 3 there are high levels of potassium in the stream water due to farm pollution. The slightly higher sodium concentrations in the stream water from site 3 may be the result of pollution through a pipe that drains the area in between the two hills, which emerges as a small ephemeral spring that flows into the Beck just 10 m upstream of site 3 (sub-section 4.6.2, Figure 4-41).

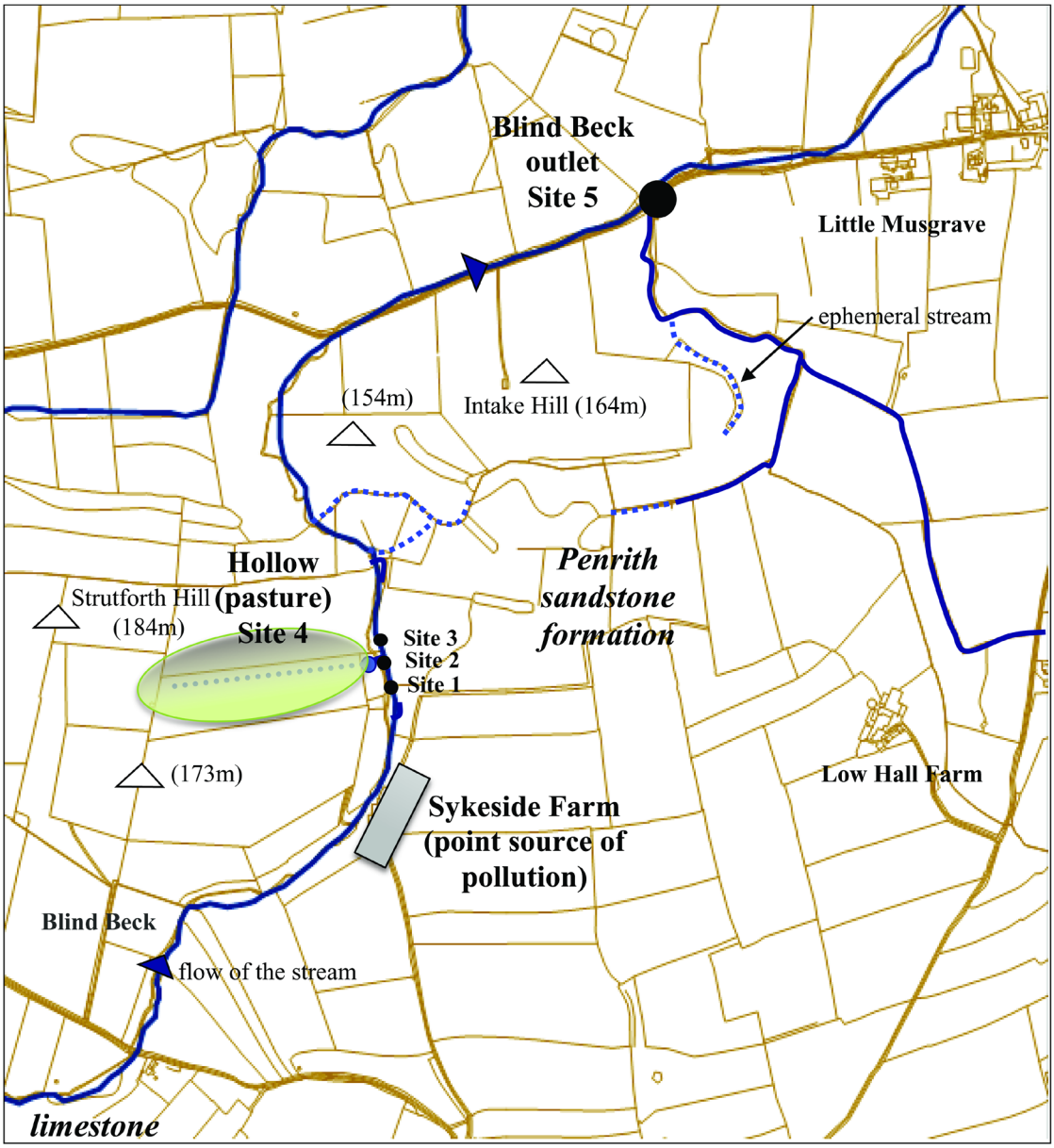

Figure 5-14 *Schematic map of the stream water sampling sites indicating point source pollution and influence of geology*

The Environment Agency's (2006) Groundwater Quality Monitoring Network recorded the same dominant water type in the Upper Eden basin as throughout the Penrith Sandstone aquifer as Ca(Mg)-HCO_3. This shows the same water type as recorded in the water stream at all sites in this study. The geology upstream of the Sykeside Farm contains large quantities of limestone (calcium carbonate) where the stream flows through the limestone stream bed, where bicarbonate ions from the calcite are released, which results in high alkalinity measurements for sampling sites downstream (Figure 5-14). Overall, it became clear that what seemed to be established in the research literature on hydrological pathways of a deeper pathway where the water infiltrates into the limestone and then passes through the sandstone and reaches the stream (Chapter 2, Ockenden 2010) can be in agreement with the results of water quality in this study.

Relationship between ion concentration and discharge

The relationship between the stream water discharge and ion concentration of the Hollow sub-catchment (site 4), and the Blind Beck catchment (site 5) is presented in Figures 5-15 and 5-16.

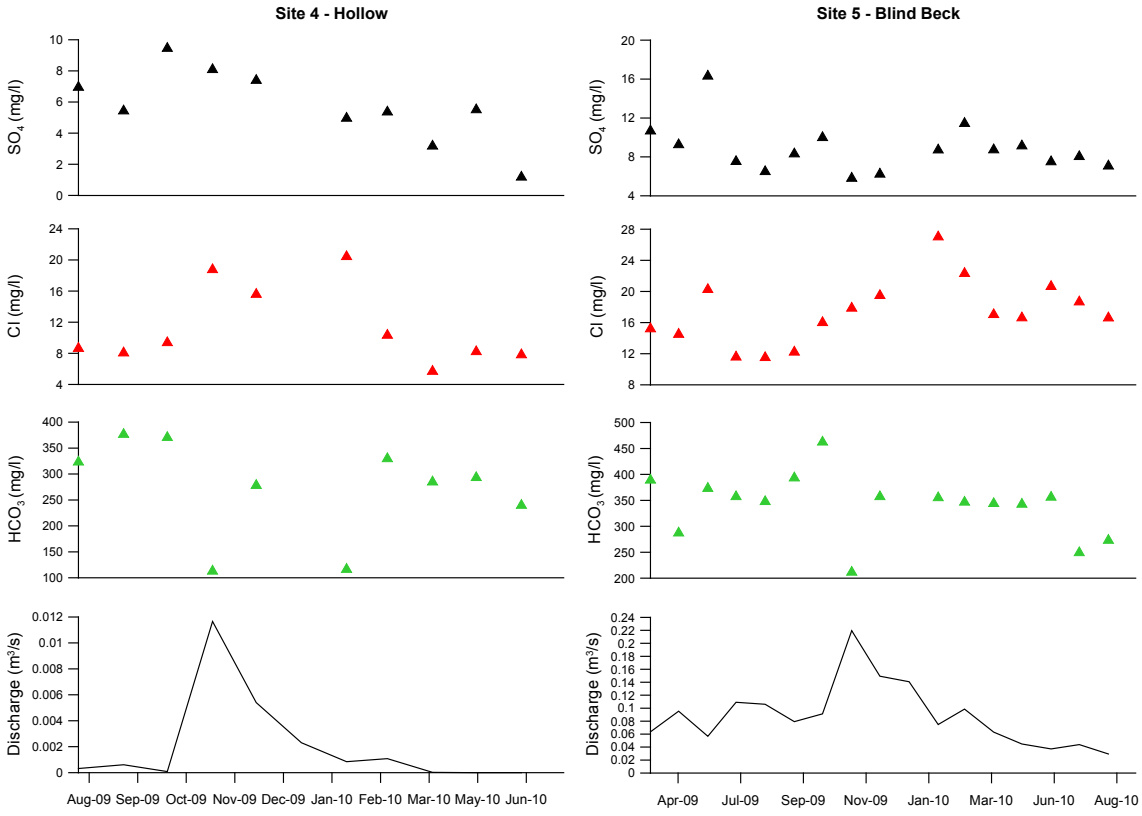

Figure 5-15 *Relationship between water quality variables – anions (monthly means) and discharge (monthly means)*

Among cations, similar behaviour is observed between SO_4^{2-} and Cl^- for both sites. The similar trend was observed between Ca^{2+} and Mg^{2+}; Ca^{2+}, Mg^{2+} and HCO^-_3 for both

stream and Na^{+} with K^{+} for the Blind Beck stream. The HCO^{-}_{3}, Ca^{2+} and Mg^{2+} concentrations are inversely related to discharge, demonstrating a strong dilution effect, while SO_4^{-2} shows less pronounced dilution.

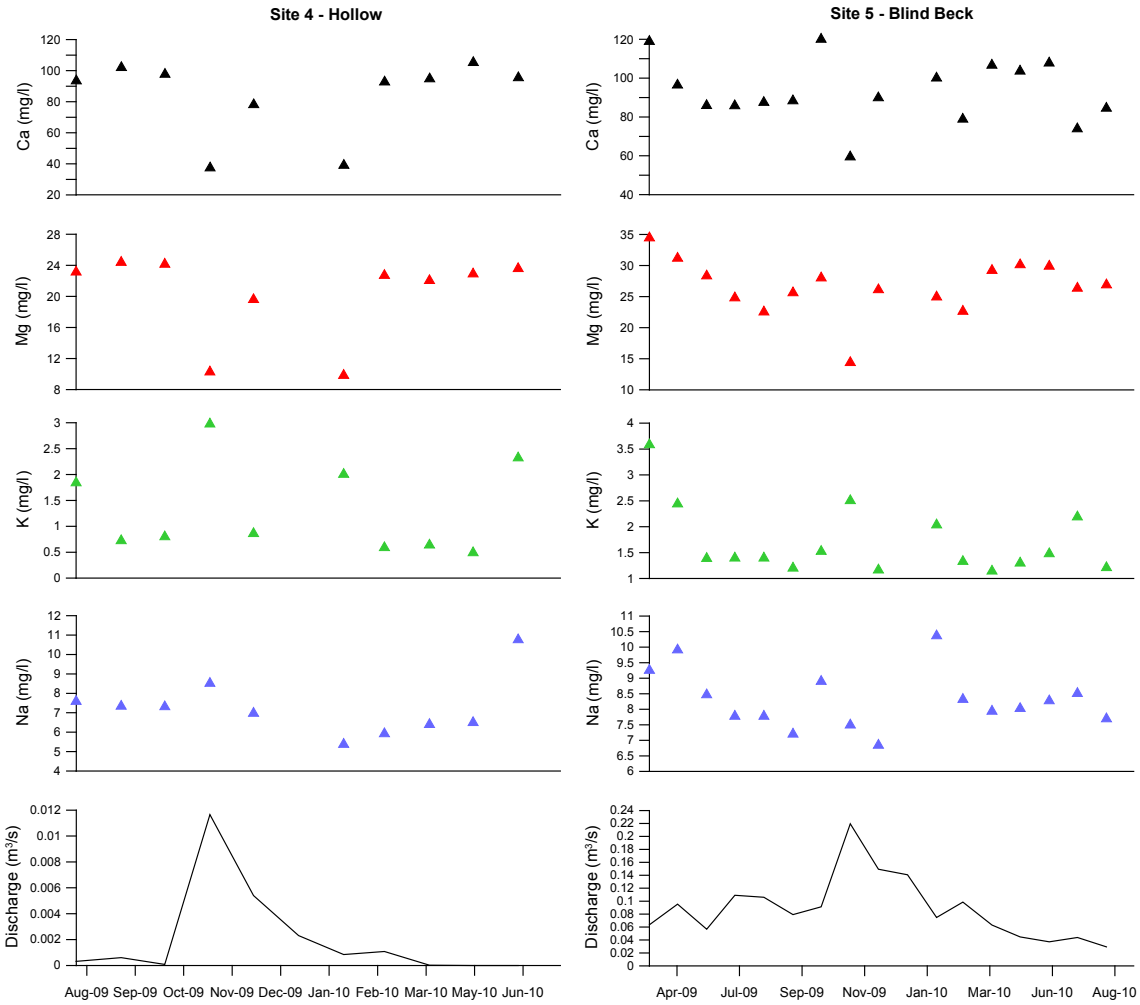

Figure 5-16 *Relationship between water quality variables – cations (monthly means) and discharge (monthly means)*

The chloride concentrations in the stream started to increase during the autumn (Figure 5-15). However, there is a record of high chloride concentration in February that suggests that during snowmelt, chloride stored in the unsaturated zone is flushed into groundwater, which increases its chloride concentration (Lundmark 2005). Therefore, groundwater may be the major source of water in the stream during melting of the snowpack. The water quality of groundwater has not been monitored in this study to justify this statement, but the water quality from the hillslope of the Sykeside Farm in the overland and subsurface flows were investigated and will be discussed in the Chapter 7. HCO_3^{-} concentrations, increasing from August to October, drop in November due to dilution and remain relatively constant from February to June 2010 for the Blind Beck stream. In the case of the Hollow stream, HCO_3^{-} concentration increasing from

August to October, drop in November 2009 due to high stream flow, and also in February 2010, then increase in March. Discharge increased dramatically in November 2009 during the storm event and concentration consequently declined, which is very clearly presented for Ca^{2+}, Mg^{2+} and HCO_3^-.

During the drier months, sulphate accumulates within the soil due to increased rates of oxidation (Heal et al. 2002). Norrström (1995) pointed out that higher rainfall in the autumn re-wets the soil and releases this store of sulphate into the stream with runoff. During the period of lowest discharge, groundwater is expected to be the major ion supplier.

In summary, the behaviour of anions and cations in the stream water is similar for both the catchment and sub-catchment, and are related to discharge. Soulsby et al. (2002) pointed out that the definition of flow concentration relationships is important for modelling and predicting water quality.

Determination of chemical sources at site 4 and 5

Sources of ions and pH in stream water at site 4 and 5 were examined using the correlation matrix. The correlation matrices of all collected samples are given in Table 5-7 and 5-8. It is considered that the correlation is good if $r > 0.3$ and marginal $0.2 < r < 0.3$ at 95% confidence interval ($P < 0.00002$ for site 4 and $P < 0.0002$ for site 5).

Table 5-7 *Correlation matrix of ionic components for the Hollow sub-catchment (site 4)*

	Na	**K**	**Ca**	**Mg**	**HCO_3**	**Cl**	**NO_3**	**SO_4**	**pH**
Na	1.0								
K	0.42	1.0							
Ca	0.0	-0.83	1.0						
Mg	0.05	-0.83	1.0	1.0					
HCO_3	0.05	-0.80	0.98	0.99	1.0				
Cl	-0.05	0.69	-0.93	-0.91	-0.85	1.0			
NO_3	0.07	0.13	-0.23	-0.28	-0.39	-0.04	1.0		
SO_4	0.63	0.29	-0.10	-0.02	-0.06	0.25	-0.39	1.0	
pH	-0.43	-0.70	0.62	0.57	0.49	-0.69	0.26	-0.71	1.0

Table 5-8 *Correlation matrix of ionic components for the Blind Beck catchment (site 5)*

	Na	**K**	**Ca**	**Mg**	**HCO_3**	**Cl**	**NO_3**	**SO_4**	**pH**
Na	1.0								
K	0.63	1.0							
Ca	0.42	0.10	1.0						
Mg	0.39	0.25	0.79	1.0					
HCO_3	0.11	-0.29	0.73	0.45	1.0				
Cl	0.35	-0.02	-0.18	-0.08	-0.27	1.0			
NO_3	0.35	-0.21	0.55	0.36	0.54	0.29	1.0		
SO_4	0.38	0.06	0.22	0.39	0.40	0.17	0.5	1.0	
pH	-0.01	0.02	0.36	0.65	0.22	-0.33	0.20	0.46	1.0

Site 4: Hollow sub-catchment

A significant positive correlation was found between Ca^{2+} and Mg^{2+} (r = 1). This suggests that these cations may have originated from the same source, most likely the soil/rock. Ockenden (2010) observed the highest concentrations of magnesium in the Sykeside boreholes, with the higher concentration in the deeper (18 m) of 35 mg/l than the shallower (6 m) borehole of 30 mg/l. Ockenden suggests an explanatory theory that under low flow conditions, the stream water is derived from regolith zones where there is the most weathering of the bedrock. In that study, Ockenden also identified that during storm events, the water comes mainly from the near surface soil zones where there are lower concentrations of the bedrock minerals because of the shorter contact time between the water and soil.

The significant positive correlation between bicarbonate anion and calcium (r = 0.98), and magnesium (r = 0.99) probably reflects common geological sources. Limestone dissolution is the major controlling factor for calcium and carbonate concentrations in the stream. Bicarbonate shows a good correlation with pH, which means bicarbonate alkalinity and increase of HCO_3^- during weathering originates from soil/atmospheric CO_2. Chloride shows moderate correlation with K^+ (r = 0.69), which may have originated from the application of potassium chloride as the most widely used K^+ fertilizer. The fields at the top of the hill at Sykeside Farm are improved grassland and certainly experienced application of fertiliser/manure. Another source of K^+ can be the substantial amount of leaf/litter decaying organic matter in the stream, which was indeed observed in the field. Chloride showed a significant negative correlation with calcium (r = -0.93), magnesium (r = -0.91) and bicarbonate (r = -0.85). Therefore with increase or decrease in the values of Cl^-, the values of Ca^{2+}, Mg^{2+} and HCO_3^- decreases or increases. The magnesium content of Hollow stream water shows a good positive correlation with pH. A weak correlation between Cl^- and SO_4^{2-} (r = 0.25) could indicate that there is another source of sulphate ions in the sub-catchment than atmospheric inputs. This suggests that the most significant source of Cl^- and Na^+ in stream water is precipitation. Another possible source of chlorine may be released during weathering of sedimentary rocks, such as sandstone (chlorine can occur in the cement) or mudstones.

Site 5: Blind Beck catchment

In the present study for the period from 2009 to 2010 chloride has a strong negative correlation with HCO_3^- (r= -0.27) and Ca^{2+} (r= -0.18). This shows that with increase or

decrease in the values of Cl^-, HCO_3^- and Ca^{2+} also exhibit decrease or increase in their concentrations. Cl^- ions bear a negative correlation with K^+. This indicates that KCl may be absent from water samples. There is also a strong correlation between Ca^{2+} and Mg^{2+} (r = 0.79), and with bicarbonate (r = 0.73). The magnesium content of Blind Beck water varies with pH. The NO_3^- shows a moderate correlation with bicarbonate.

The weathering of the minerals in the bedrock may account for ions found in the stream. The most abundant cation in the stream is Ca^{2+}. The possible source for Ca^{2+} includes weathering of calcite. Calcite weathers with carbonic acid to produce Ca^{2+} and $2HCO_3^-$ according to the following equation:

$$CaCO_3 + H_2CO_3^- > Ca^{2+} + 2HCO_3^-$$

Sulphate (SO_4^{2-}) is most likely derived from the atmosphere. Sulphuric acid reacts with minerals such as calcite to form sulphates according the following reaction:

$$2CaCO_3 + H_2SO_4 \rightarrow 2Ca^{2+} + 2HCO_3^- + SO_4^{2-}$$

According to Drever (1997), magnesium ions result from the weathering of the mineral biotite and kaolinite, a clay mineral:

$$7.3KMg_3AlSi_3O_{10}(OH)_2 + 51CO_2 + 26H_2O = 3.7Al_2Si_2O_5(OH)_4 + 22Mg^{2+} + 7.3K^+ + 51HC_3^- + 15SiSi_2$$

Both sites are characterised by the same source of alkaline water which is represented with a strong correlation between Ca^{2+} and Mg^{2+}, and with bicarbonate.

5.4.1 NO_3 and DOC concentration in the stream water

The marked variations in the nitrate (NO_3^-) and the dissolved organic carbon (DOC) concentration were observed between sites, seasons and months (Figure 5-17). Table 5-9 shows a summary of nitrate (NO_3^-) and dissolved organic carbon (DOC) concentration at sample points (site 1, 2, 3 and 5) along the length of the Blind Beck stream and the outlet of the Hollow sub-catchment (site 4). The mean nitrate concentrations along the length of Blind Beck (site 1 to 3) were fairly constant (4.2 to 4.7 mg/l) except at site 5 where the mean was higher (7.8 mg/l). The NO_3^- concentrations were significantly lower in the stream draining the Hollow sub-catchment, while NO_3 concentrations were higher at sites along the Blind Beck stream. The range of DOC data was very similar between Blind Beck and the stream draining the Hollow sub-catchment (Figure 5-17). Although the mean DOC concentration was slightly larger for the Hollow sub-catchment (13 mg/l) than sites 1, 2, 3 and 5 (12.2-

12.5 mg/l), concentrations were not significantly different between the stream draining the Hollow sub-catchment and sites along the length of the Blind Beck stream. The highest maximum DOC concentration was recorded on site 1 (32.5 mg/l) indicating the impact of the farm. The Appendix D2: Tables D2-1 and D2-2 provide the full NO_3^- and DOC results.

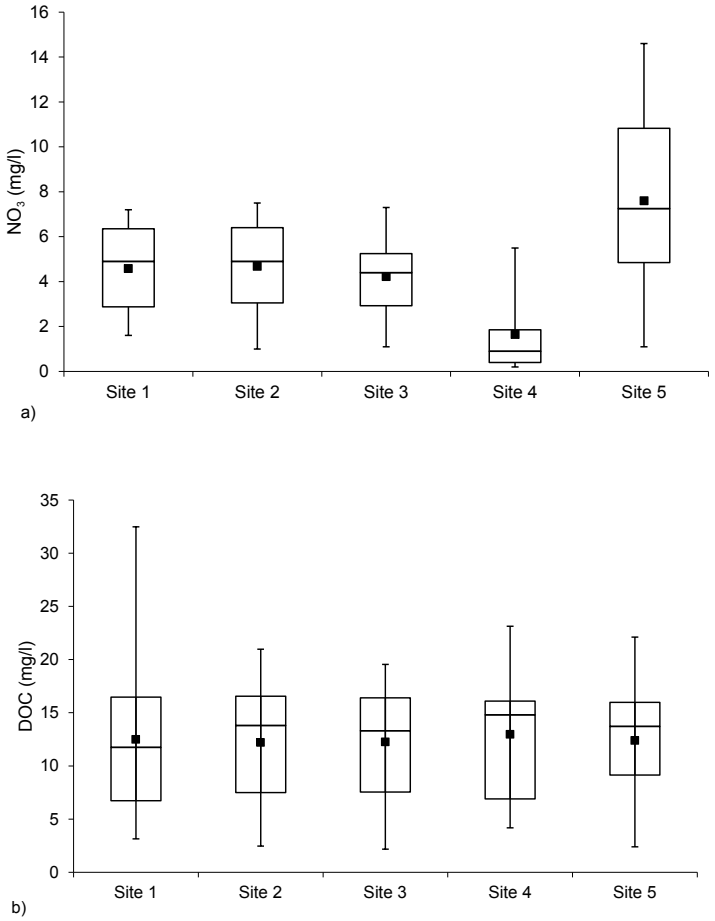

Figure 5-17 *Box plots showing the distribution of average a) nitrate and b) dissolved organic carbon for five sites. Box plots depict the mean (small square within the boxes), median (line within the boxes), 25th and 75th percentiles (lower and upper edges of the boxes), minimum and maximum of the data (lower and upper error bars)*

Table 5-9 *Mean, minimum and maximum NO_3^- and DOC concentrations with standard deviation for Sykeside Farm (site 1, 2 and 3, period April 2009 - Aug 2010), Hollow (site 4, period Aug 2009 - Aug 2010) and Blind Beck (site 5, period April 2009 - Aug 2010)*

Location	Site 1 (n = 16)	Site 2 (n = 16)	Site 3 (n = 16)	Site 4 (n = 10)	Site 5 (n = 16)
	NO_3^- (mg/l)				
Min.	1.6	1.0	1.1	0.2	1.1
Mean	4.6	4.7	4.2	1.6	7.8
Max.	7.2	7.4	7.3	5.5	14.6
SD.	1.9	2.1	2.1	1.9	3.4
	DOC (mg/l)				
Min.	3.1	2.5	2.2	4.12	0.1
Mean	12.5	12.2	12.3	13.0	12.4
Max.	32.5	21.0	19.5	23.1	22.1
SD.	7.6	5.6	5.6	6.8	5.9

Min = minimum value, Max = maximum value, SD = standard deviation

Figure 5-18 shows the relation between the stream water discharge, the monthly point values of the NO_3^- and the DOC concentration for the Hollow sub-catchment (site 4) and the Blind Beck catchment (site 5). For the Blind Beck catchment, the behaviour of nutrients in stream flow is much more complex than for the Hollow sub-catchment.

Along the Blind Beck stream, the lowest monthly point values of the NO_3^- concentrations were observed in July 2010 at site 2 (1.0 mg/l) and the highest concentrations in April 2010 year at site 5 (14.6 mg/l). The nitrate concentrations were zero in the Hollow at site 4 in August 2009, July and August 2010, while the highest concentrations were in April 2010 (5.5 mg/l). However, for both streams, the minimum monthly point values of the DOC concentrations were observed in December 2009, while the maximums were in July 2010. Between April and July 2010, due to dry conditions and no flow at the outlet of the Hollow sub-catchment, water and sediment samples were collected from a stagnant pool in the stream bed that flowed intermittently. This effect is identified in Figure 5-18a by the high monthly point concentration values of the NO_3^- (42.7 mg/l) and the DOC (105 mg/l), suggesting eutrophication. Therefore, these data have not been included in the calculation of the other statistics to avoid skewing of the results. The evidence of eutrophication has been identified during a field visit at the outlet of the Hollow sub-catchment as blue-green algal blooms and foul smell of water. As can be seen in Figure 5-18a, the high DOC levels at the Hollow sub-catchment outlet indicate a stagnant stream system of water that became muddy, cloudy, full of weeds and with a number of insects as the stagnant stream is the favourite breeding ground.

The annual NO_3^- and DOC losses (flux) were estimated as the product of the stream discharge multiplied by the NO_3^- or the DOC concentration (discharge weighted mean concentrations) based on monthly point values. The discharge weighted annual mean NO_3^- concentration based on monthly point values for the Blind Beck catchment was 6 mg/l in 2009 and 10 mg/l in 2010, while for the Hollow sub-catchment in 2010 it was 1.3 mg/l (Table 5-10). Based on the monthly means for discharge and the NO_3^- concentration, the total annual discharge of NO_3 for Blind Beck is estimated at 37 Mg for 2009 and 27 Mg in 2010, while for Hollow the nitrate discharge was 0.08 Mg in 2010 (Table 5-10). The NO_3^- export per unit area is estimated at 4 g NO_3^- m^{-2} (40 kg/ha) in 2009 and 2.9 g/m^{-2} (29 kg/ha) in 2010 for Blind Beck, while the export for the Hollow sub-catchment is 0.88 g NO_3 m^{-2} (8.8 kg/ha).

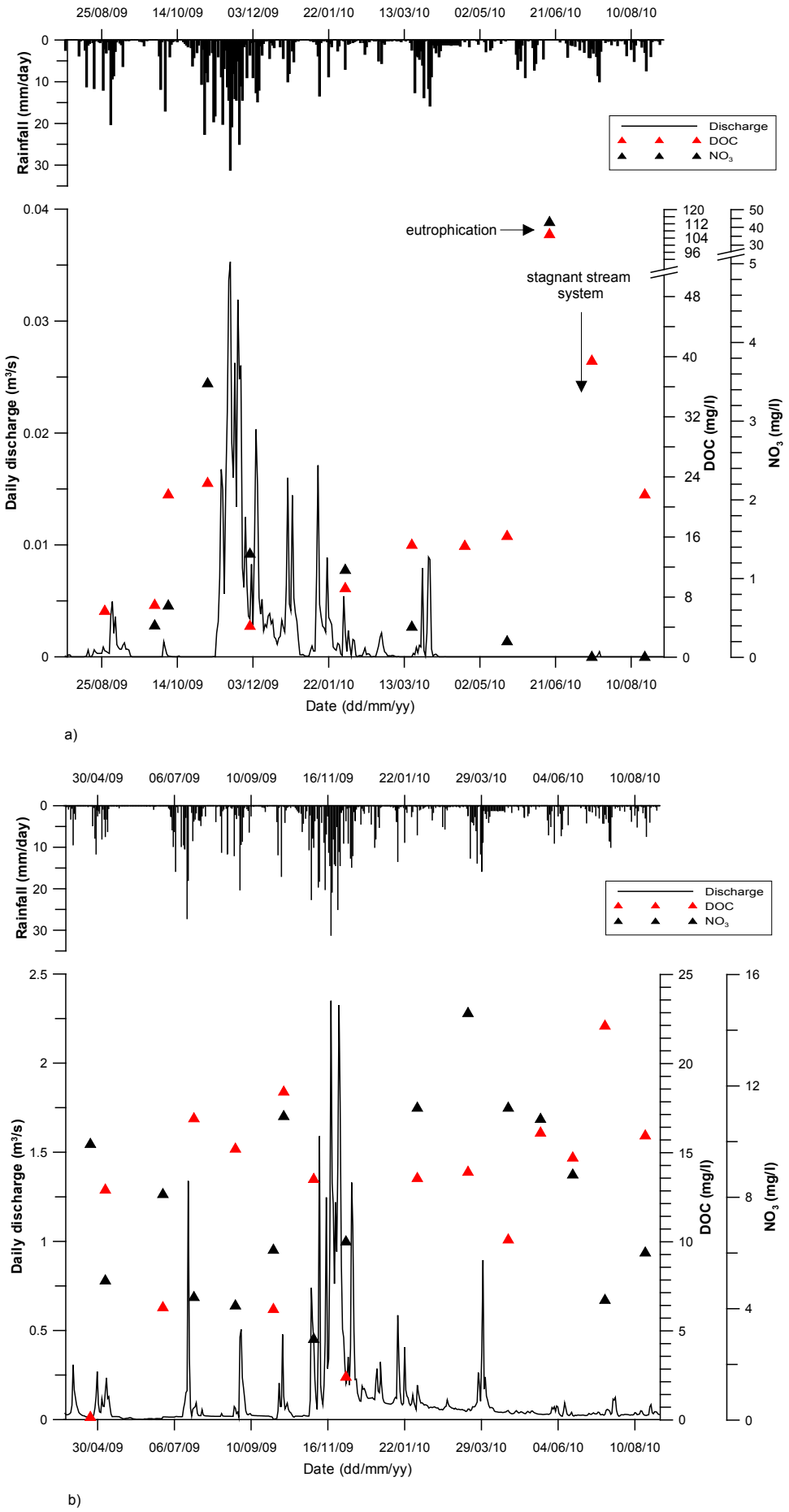

Figure 5-18 *Daily average discharge and stream NO_3^- and DOC concentrations (point values) for a) Hollow sub-catchment (site 4) and b) Blind Beck catchment (site 5)*

Table 5-10 *Estimated annual nitrate (NO_3^-) and dissolved organic carbon (DOC) export for 2009 and 2010 year*

Location	Year	Discharge weighted mean NO_3^- (mg/l)	Annual estimated NO_3 export (Mg/yr)	Area weighted NO_3^- export (g NO_3^- m^{-2}/yr)
Blind Beck	2009	6.0	37	4.0
	2010	10.0	27	2.9
Hollow	2010	1.3	0.08	0.88
Location	**Year**	**Discharge weighted mean DOC (mg/l)**	**Annual estimated DOC export (Mg/yr)**	**Area weighted DOC export (g DOC m^{-2}/yr)**
Blind Beck	2009	9.6	60	6.5
	2010	12.8	36	3.9
Hollow	2010	13.0	0.8	8.8

The discharge weighted annual mean DOC concentration based on monthly point values for the Blind Beck catchment was 9.6 mg/l in 2009 and 12.8 mg/l in 2010, while for the Hollow sub-catchment it was 13 mg/l. The total annual DOC export from the Blind Beck catchment is estimated at 60 Mg in 2009 and 36 Mg in 2010 (Table 5-10). The DOC export per unit area is estimated at 6.5 g m^{-2} (65 kg/ha) in 2009 and 3.9 g m^{-2} (39 kg/ha) in 2010. In 2009, the area weighted annual discharge was almost twice as large as 2010. This is due to climate variability, as 2010 during the summer period was dryer compared with 2009. Table 5-10 gives the annual DOC loss of 8.8 g m^{-2} (88 kg/ha) or 0.80 Mg for the Hollow sub-catchment. The DOC export is largely driven by changes in the stream water volume that is directly affected by dry climate conditions.

The mean nitrate concentrations in this study along the Blind Beck stream are consistent with the findings of Barber (2008). The mean nitrate concentrations in the stream water (sites 1, 2 and 3) of Blind Beck are considered 'very low' (<5 mg/l as NO_3^-) and 'low' for site 5 (EA 2006) and are well below the Nitrate Directives recommended limit of 25 mg/l. Therefore, the naturally occurring levels of nitrate are not harmful to the environment. The highest value of nitrate concentration at the outlet of the Hollow sub-catchment of 42.7 mg/l would be considered as 'very high' (EA 2006), which is the result of eutrophication and pollution. Other authors reported different nitrate levels that could lead to eutrophication. Armstrong and Burt (1993) showed that concentrations of 6.5 mg/l could lead to algal growth (cited in Barber 2008). According to these earlier studies, the concentrations recorded in this study could be considered high enough to cause eutrophication. However, Johnson et al. (2000) indicated that high levels of nitrate (>1 mg/l) are not good for aquatic life. It is widely assumed that nitrite concentrations in freshwaters are negligible (Stanley and Hobbie 1981; Paul and Clarke 1989), and the worldwide average concentration has been estimated to be 1 mg of nitrite/litre (Meybeck 1982; Adeyemo et al. 2008).

Along Blind Beck stream, the nitrate concentration is greater in the downstream site. Barber (2008) found that the average concentration of nitrate increases from 4.85 mg/l at site 1 to 5.51 mg/l below the farmyard. In contrast to earlier findings, this study shows that nitrate concentration decreases from 4.6 mg/l to 4.2 mg/l. However, the observed difference between site 1 and site 3 was not significant. Site 1 is located approximately 150 m downstream from the farmyard, which is possibly a point source of nitrate (Figure 5-14). The relatively high nitrate concentration observed at site 5 could be due to the influence of a small stream that flows past Little Musgrave Farm into Blind Beck 10 m upstream (see Figure 4-38) where Barber (2008) recorded mean nitrate concentration of 16.61 mg/l. Another explanation for higher nitrate is inputs from agricultural land, which is in the line with the report of Commins et al. (1983). Barber (2008) investigated the source of this high nitrate concentration approximately 550 m upstream of the small stream that flows past Little Musgrave Farm. This author claims that the highest concentration is coming from the stream that flows from the south-east past Low Hall Farm, which had a maximum recorded concentration of 19.55 mg/l where it is likely that the N is being leached from the land surrounding this stream.

The nitrate concentrations at the Hollow sub-catchment were on average smaller than the Blind Beck catchment, but still in excess of 25 mg/l nitrate in dry conditions. This may be because the Hollow sub-catchment is under a pasture system dominated by sheep farming where nitrate concentrations leaving agricultural soils are diluted to a some extent. This suggests that water moves through soil and depletes the soil nitrate from soils to stream or groundwater. In the case of higher rainfall, more water passes through the soil, diluting and reducing the average nitrate concentration on its way to stream or groundwater. This may partly explain the lower nitrate concentration at the stream of the Hollow sub-catchment.

In this study, it is not possible to identify actual trends in the NO_3^- and the DOC concentrations without an analysis that requires data over a number of years and a number of factors, otherwise it would lead to misinterpretation of trends.

During the early part of the winter and the spring, nitrate concentrations in the stream water draining the Blind Beck catchment are higher than in the stream of the Hollow sub-catchment. These high values may, in part be due to agricultural influence in the Blind Beck catchment. The nitrate is lost from the land mainly during the winter due to

runoff from saturated land. Increasing trends in nitrate during the winter period is in agreement with Burt et al. (1988) who also found that during the winter the high NO_3^- concentrations combine with high discharge to produce the high NO_3^- loads. Other authors (Burns and Kendall 2002; Pardo et al. 2004; Piatek et al. 2005; Judd et al. 2007) suggested that microbially produced NO_3^- appears to dominate stream NO_3^-, even during the spring snowmelt, when water is flushing quickly through soils.

During the dry conditions, nitrate concentrations in both streams increased as discharge decreased through the summer, in agreement with behaviour reported in the literature (DEFRA 2007b). However, as Figure 5-18a illustrates, nitrate levels in the stream of the Hollow sub-catchment (site 4) increase but drop quickly during dry conditions. With no overland flow for transport, nitrate concentration does not appear in the stream.

The nitrate concentration tends to increase before the November storm event, but after sufficiently high discharges, nitrate concentrations are diluted by the large water influx into the stream. From this point on, there is an inverse relationship between discharge and nitrate concentration observed at both streams. The reason for this increasing of nitrate before a large event was likely due to increased leaching from the soil as mineralization (i.e. release of nutrients from organic matter) by overland flow and shallow subsurface runoff. Vinten and Smith (1993) pointed out that nitrate concentration in a stream water increase in the autumn due to reduced nitrate uptake by plants and the stimulation of microbial nitrification processes by soil drying and wetting cycles. During smaller rain events, nitrate transport into streams of Blind Beck and Hollow seems to be with overland flow that washes nitrate from the fields.

It is interested to note how these nitrate concentrations behaviours change at different locations. During storm events, the pattern of nitrate concentration at the Hollow sub-catchment is similar to that at the Blind Beck catchment. Although nitrate patterns are similar during large rain events, seasonal dry and wet conditions lead to a somewhat different pattern on the two streams (Figure 5-18).

In summary, nitrate losses from the Hollow sub-catchment are smaller than those from the Blind Beck catchment. Table 5-10 shows that the NO_3^- loss from the Hollow sub-catchment has annual nitrate losses of 8.8 kg/ha, while the Blind Beck catchment has losses in the range of 29-40 kg/ha. This is evidence of the importance of intense agricultural influence in determining nitrate concentrations in the Blind Beck stream.

Typically, nitrate concentrations decreased with increasing discharge. Johnes and Burt (1993) estimate that 80% of the annual the N loss occur in the winter and report that, following a dry summer, soils require sometimes a prolonged recharge in the autumn and the early winter before drainage and leaching begins (Barber 2008). According to the results from hydrograph separation in sub-section 5.3.1, it is possible that overland flow and subsurface flow is responsible for the transport of labile nutrients (NO_3^-) into streams during the winter and the autumn months followed by storm events. These are referred to leaching of the NO_3^- concentrated 'old' water. The high level of nitrate observed during the dry season in this study is in agreement with Wolfhard and Reinhard (1998) who concluded that nitrate is usually built up during dry seasons and that high levels of nitrate are only observed during early rainy seasons.

Dissolved organic carbon (DOC)

In many regions, some authors have predicted an increase in stream DOC concentrations due to a warmer and wetter climate (de Wit and Wright 2008; Köhler et al. 2009; Sebestyen et al. 2009; Ågren 2010). The DOC concentrations in the stream system studied are consistent with DOC data reported from small stream catchments in Scotland (Wearing 2008). Previous studies have reported that the DOC concentration in streams generally increased during the storm periods due to the increase of discharge as a major factor controlling the output of organic carbon (Hope et al. 1994). This is consistent with the findings of this study (Figure 5-18) except during very dry summer months and large storm events.

Under the high stream flow, more DOC is generated from the deeper soil layer by subsurface flow than by overland flow. Support for this statement comes from the hillslope experiment for the wet conditions where the soil water solution at 18 cm soil depth had the significantly higher DOC concentration of 27 mg/l than overland flow of 8 mg/l (Chapter 7). The DOC concentrations observation at the hillslope provided evidence that samples from lysimeters located at 10 cm soil depth had a very low DOC concentration during the wet periods (approximately 5 mg/l). Hence, these inputs of soil water solution directly to the stream by overland flow would tend to dilute the DOC concentrations in stream flow. The dilution effects of the precipitation can also decrease the DOC concentration or even flux (Boyer et al. 1997).

However, under low flow conditions, the largest DOC portion is derived from deeper soil layers by subsurface flow where the DOC concentrations are small. The evidence

for this statement is derived from the hillslope experiment during the dry conditions where the DOC concentration of the soil solution at 10 cm soil depth was 32 mg/l, at 18 cm 22 mg/l, and overland flow 13 mg/l. According to Fragalà (2009), the unsaturated zone at Sykeside Farm can be assimilated to a two-layer system composed of topsoil and till (unsorted glacial sediment that it is mixtures of clay, sand, gravel and boulders). A topsoil has a much higher hydraulic conductivity with greater flow compared to the till where it is reduced. As Fragalà (2009: 157) states: "When the infiltration capacity of the till is exceeded water flows laterally through the topsoil, mainly as unsaturated flow. Most of the flow is concentrated in the upper topsoil (subsurface lateral flow), which is the most porous portion of the topsoil and which generally higher water contents". Unfortunately, in this study, the hydraulic conductivity measurements were not considered.

The Blind Beck stream during low flow appears transparent with a low accumulation of dissolved materials that indicates low productivity of humic substances, while during high flows it shows brown colour of water due to high concentration of dissolved organic matter, such as humus (Figure 5-19). The site 2 had the DOC point value of stream water during low flow on April 23, 2009 of 7.2 mg/l and during high flow on November 3, 2009 of 14.7 mg/l. One possible explanation is that during heavy rainfall intensity, rainwater infiltrates vertically through the soil profile, dissolves a large amount of organic carbon in the form of the DOC in the upper soil layer where the DOC is mainly produced, and moves to deeper soil horizons.

It can be concluded that the increased concentrations of the dissolved organic carbon (DOC) in stream draining upland catchment are direct evidence of organic carbon loss from mineral soils.

Figure 5-19 *DOC concentration during a) low and b) high flow of the Blind Beck stream (site 2)*

For the November storm event in both the catchment and the sub-catchment, the overland and subsurface flows contribute to the stream flow. The data from the hillslope field experiment suggest that during the November storm event (E3), subsurface flow dominates the DOC export to the stream (Chapter 7). From November 3 2009, the DOC monthly point value decreased by approximately 17% compared with 1 December 2009 at all sites along Blind Beck (site 1, 2, 3 and 5) and the Hollow stream (site 4). These reductions in the DOC concentration might be due to dilution effects but also losses due to sorption and microbial degradation.

5.5 Nutrients in surface sediments

Surface sediments were collected from the Blind Beck and Hollow stream and analysed for grain size distribution and nutrients such as total organic carbon, and total nitrogen in order to understand the spatial distribution and hydrological effects of nutrients.

5.5.1 Sediment particle size

The stream sediments were found to be mainly sandy gravels at all sampling sites, except at the Hollow sub-catchment outlet (site 4). Sandy gravels are generally composed of ~40% – 60% gravel, 50% (±15%) sand and <1% silt + clay. Sediments at the outlet of the Hollow sub-catchment are mainly composed of a mixture of sand and fines (silt+clay). The distribution of sand, fines and gravel in these sediments are as follows: sand>fines>gravel. The sand compromises about 63-87% of the total sediment fractions and the rest is 3% of gravel and 12% of silt + clay. Sediment texture noticed at site 4 (Hollow sub-catchment) was loamy sand. This suggests sediments transport in runoff from the hillslope, where the soil type was determined as loamy sand at 0-10 cm and 10-20 cm soil depth (Chapter 8). The sediment distribution at the outlet of the Hollow sub-catchment largely depends on the source and texture of soils of the concerned area. Sediment size distribution curves are given in Appendix D3.

5.5.2 Sediment total organic carbon (TOC), total nitrogen (TN) and C/N ratio

The TOC contents in the sediment samples ranged from 0.23 to 2.72wt% with means at each sampling site of 0.50 to 2.08wt% (Table 5-11). The highest TOC values were observed at site 4 (TOC = 1.44 ± 2.72wt%, n = 12) dominated by fine-grained sediments. TOC was very low in the sandy gravels sediments of the Blind Beck stream (0.23 ± 1.26wt%), suggesting the lack of accumulation of organic matter (OM) in this

sediment type. TN varied from 0.02 to 0.44wt% with a mean value of 0.08 to 0.22wt% and a standard deviation of 0.05 to 0.06wt%. The highest TN values were at site 4 (TN = 0.12 ± 0.27wt%, n = 12). The relationship between the mean of TN and TOC is shown in Figure 5-20.

Table 5-11 *Mean concentration and data range of TOC, TN and nutrient ratio*

Location	Site		Mean	Min	Max	SD	n
Sykeside Farm	1	TOC (wt%)	0.50	0.28	1.07	0.25	16
		TN (wt%)	0.09	0.02	0.29	0.05	
		C/N	5.56	14.00	3.69	5.00	
	2	TOC (wt%)	0.71	0.29	1.04	0.27	16
		TN (wt%)	0.08	0.02	0.17	0.05	
		C/N	8.88	14.5	6.12	5.40	
	3	TOC (wt%)	0.57	0.23	1.01	0.18	15
		TN (wt%)	0.08	0.02	0.16	0.05	
		C/N	7.13	11.5	6.31	3.60	
Hollow	4	TOC (wt%)	2.08	1.44	2.72	0.29	12
		TN (wt%)	0.22	0.12	0.44	0.05	
		C/N	9.45	12.00	6.18	5.80	
Blind Beck	5	TOC (wt%)	0.67	0.31	1.26	0.29	16
		TN (wt%)	0.08	0.02	0.24	0.06	
		C/N	8.38	15.5	5.25	4.83	

Min = minimum value, Max = maximum value, SD = standard deviation, n = number of sampled records

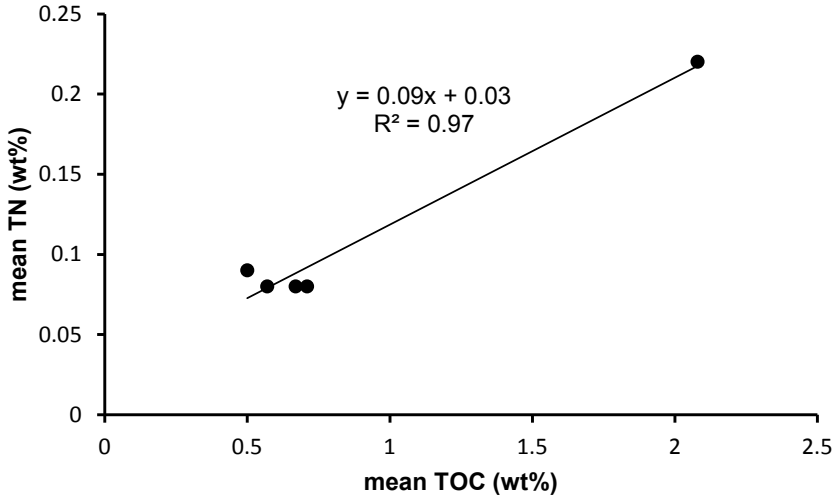

Figure 5-20 *Relationship between TOC (%) and TN (%) contents*

The measured carbon-nitrogen ratios (C/N) in this study varied from 11.5 to 6.31 with mean values for each sampling site of 5.56 to 9.45 and a standard deviation of 5.0 to 5.8 (Table 5-11). The highest C/N ratio was found in sediments at the Hollow sub-catchment outlet (site 4) with a mean value of 9.45, showing that organic fraction of this sediment is mainly of terrestrial origin. This suggests that fine-grained sediments were delivered from the hillslope by runoff processes that will be discussed in the next chapters. The Appendix D4: Tables D4-1 and D4-2 provides the full TOC and TN results for the stream sediments.

The distribution of TOC and TN at the sites along Blind Beck and the outlet of the Hollow sub-catchment are shown as the box plot in Figure 5-21. It visualizes how the sediment TOC and TN concentration changes along the stream. This representation shows spatial differences. It is also useful to see how the presence of the farm affects the sediment TOC content. The upstream site 1 along the Blind Beck stream had the maximum content of TOC and TN content compared to site 2 and 3 but the mean values were not noticeably higher. The maximum TN content then decreased along the stream length to site 3. This suggests the influence of the farm activity. However, sediments at site 4 contained the highest amount of TOC and TN content due to fine-grained sediments where sediment carbon and nutrient concentrations increase with decreasing grain size and had high organic matter. The high total organic carbon (TOC) content in sediments also indicates eutrophication (Folger 1972; EPA 2002). The water quality of the Hollow stream indicates eutrophication due to high nitrate and the DOC concentrations in the stream stagnant water during dry conditions.

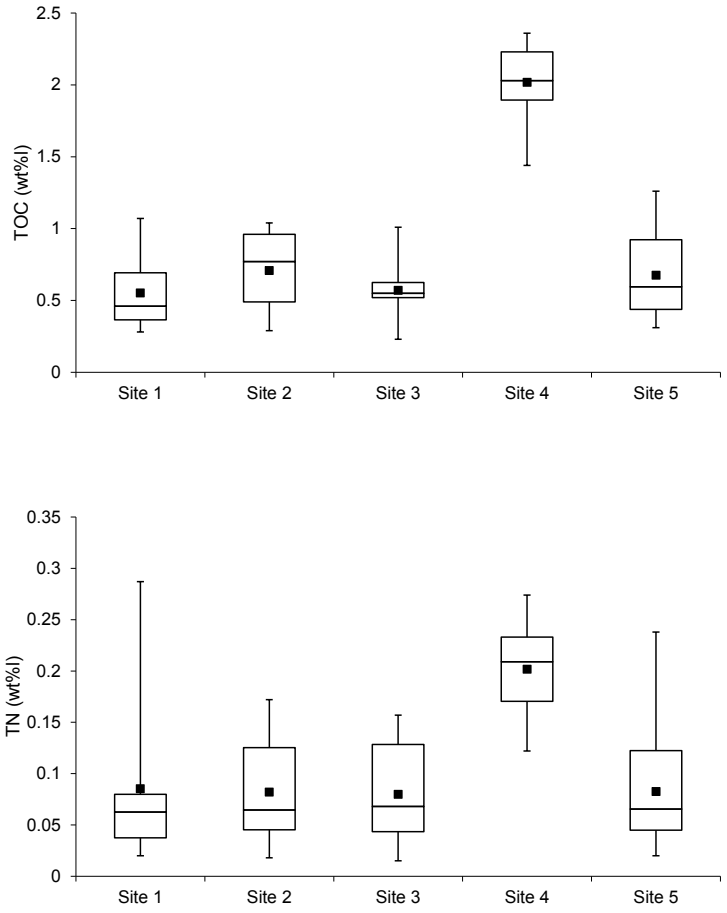

Figure 5-21 *Box plots showing the distribution of average TOC and TN for the years 2009 to 2010, for five sites. The ends of the boxes represent the 25th and 75th percentiles, the bars indicate the lowest and highest values not considered outliers, and the horizontal line shows the median*

The mean content of TN at the Hollow was 2.8 times higher than other sites. TN concentrations for sites 1, 2, 3 and 5 along the Blind Beck stream were similar. At this point it is worth noting that 0.22 wt% of TN demonstrates possible eutrophication.

The source of the sediments and origin of organic carbon is important. It is likely that fine sediments and nutrients were delivered from the hillslope from erosion of topsoil during overland flow, providing sources of both sediments and suspended solids (Figure 5-22). Data on soil core analyses within the hillslope experiments of this sub-catchment showed that the topsoil (0-10 cm) represents the result of humus accumulation that is rich in organic carbon and loamy sand. This soil data together with the main runoff processes on hillslope will be discussed later.

Figure 5-22 *Outlet of the Hollow sub-catchment a) before and b) after sediments delivered from hillslope erosion of topsoil during surface runoff*

Barber (2008) reported that even upstream of site 1 of Sykeside Farm, the stream bed was heavily coated in sediment which suggests that high sediment loads are entering the Beck from other sources in the 7 km^2 upstream catchment (Figure 5-23). He found that at times of increased stream stage, typically following rainfall events, suspended sediment concentrations can increase significantly, particularly at sites 2 and 3 that could be due to mobilisation of sediment from the farmyard or farmland surrounding the Beck, or perhaps from bank erosion.

Figure 5-23 *Sedimentation of Blind Beck upstream of site 1 (source: Barber 2008)*

Nutrient and sediments were affecting the stream, mainly due to farming activities including cattle management and field cultivations. This is the case at Sykeside Farm where cattle were allowed to the stream water at site 1 that cause nutrient pollution problems, partly due to the lack of a riparian zone and the open access to the stream for animals. There is a visual evidence of bank collapse or bank erosion along the Beck (Figure 5-23 and 5-24) and the lack of bank-side vegetation to reduce bank stability. Barber (2008) reported in his study that other sediment sources include the farmyard itself where hard standings (site 1) are very close to the stream. This is consistent with field observations from this study; man-made drainage channels drain the two hills to the west of the farm, providing direct hydrological connectivity between improved grassland and the stream; and also farm vehicles crossing the stream. Figure 5-24 shows where farm vehicles have crossed Blind Beck leaving deep tyre tracks in the bank.

Figure 5-24 *Evidence of farm vehicles crossing Blind Beck and hard standings at site 1*

Bank erosion is prominent due to lack of vegetation that would otherwise provide a binding structure to the soil (Figure 5-25). This area is also easily accessible to animals. It is apparent that land use can alter stream channel geomorphology by catchment runoff and sediment loads. These findings are consistent with Barber (2008).

Figure 5-25 *Bank erosion along Blind Beck at site 3*

The tramlines were made by farm vehicles probably during the wet seasons that run perpendicular to the hillslope and continue right down to the river bank (Figure 5-26).

This can cause the transport of large amounts of sediment and associated pollution/nutrients by overland flow to the stream very quickly. The fields at the top of the hill are improved grassland, and fertiliser or manure applications (Barber 2008).

Figure 5-26 *Field surface degradation and tramlines caused by farm vehicles (site 1) (source: Barber 2008)*

The organic enrichment in sediment observed at the outlet of the Hollow sub-catchment is a sign of environmental deterioration. Sediment organic carbon content has been used as an indicator of enrichment in sediments but the amount of surface area available for carbon adsorption must be considered.

During this study, there were no obvious signs of eutrophication at sites 1, 2, 3 and 5. A photograph from Barber's study (2008) upstream of site 1 (Figure 5-27) shows many stretches of the stream with significant algal blooms, particularly downstream of the farm. Such algal blooms did not affect site 1 during the collection of stream water samples in this study.

Figure 5-27 *Eutrophication of Blind Beck upstream of site 1 (source: Barber 2008)*

Low flows in the dry summer months due to insufficient rainfall, resulted in the accumulation of debris and algal growth in streams due to enrichment of TOC and TN. High organic carbon is considered as a cause of frequent algae blooms, which lead to increased nutrient (nitrogen) loadings into the streams as observed at site 4.

The findings of this sub-section emphasize the need for stream management to focus on small/sub-catchment scales within the context of larger scale catchment management, with the potential for reductions in fine sediment loads that may have an appreciable influence on water quality of stream (eutrophication).

5.6 Summary

There were 5 storm events recorded in 2009-2010, 5 at the Blind Beck catchment and 3 at the sub-catchment. At the sub-catchment scale, the hydrograph separation was clearly able to separate event and pre-event water using electrical conductivity (EC) as a hydrochemical tracer. The hydrograph separation results for each storm event indicate a range of event and pre-event water contributions. For all events, the subsurface flow was the dominant runoff process.

To investigate the characteristics of stream nutrients and the eutrophication process that was observed upstream of site 1 and at the outlet of the sub-catchment/site 4, chemical analyses of water was performed at all sites to determine the water quality status. The differences in ion concentrations in stream water between all five sites are significant and are related to how the geology and agricultural activity of the area dictates the type of water.

This chapter also introduces the role of the nitrate and the DOC and how it varies between sites and seasons. The average NO_3^- concentrations varied among sites, with the Hollow sub-catchment (site 4) having the lowest NO_3^- concentrations and the Blind Beck catchment (site 5) had the highest. The dilution effects on nitrate concentrations appear only with the very high discharge event in November for Blind Beck and the stream of the Hollow sub-catchment. It has been identified that when no precipitation is falling on the sub-catchment and there is no discharge over the weir, the DOC concentrations within the stream are high due to a stagnant stream system. The DOC Concentration is at the highest level in the outlet of the Hollow sub-catchment where significant eutrophication was observed (site 4).

At the Hollow sub-catchment outlet the finest sediment had the highest TOC, suggesting that the hillslope runoff processes were the main driving force in the accumulation of organic matter. The highest C/N ratio (9.45), showing that these sediments are mainly fine-grained, suggesting that they are formed by the transport of sediments by runoff from the hillslope.

Chapter 6. Hydrological behaviour on the hillslope scale

6.1 Introduction

This chapter describes the outcome of the field experiment and monitoring that was conducted to determine the hydrological behaviour in terms of dominant runoff process for different climate conditions at a hillslope of Sykeside Farm. The results have been divided into three periods: a 'dry period' in order to investigate the conditions before enhanced rainfall, a 'wet period' in order to investigate the influence of enhanced rainfall and storm events, and a "transition period" in order to investigate the transition from wet to dry conditions (no enhanced rainfall). A flowchart of the field experiment activities and purpose according to the 'dry', 'wet' and 'transition' period is given in Figure 6-1. During each enhanced rainfall test, additional water from the rainfall collectors is applied continuously to all events. Runoff amounts are monitored during dry, wet and transition periods and recorded at 15 minute intervals.

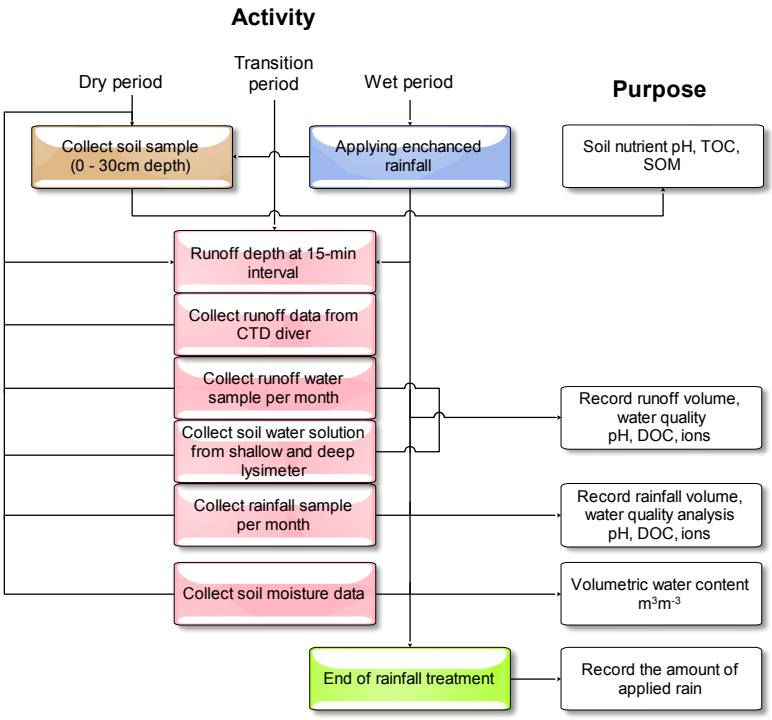

Figure 6-1 *Field experiment activities and purpose according to the 'dry', 'wet' and 'transition' period*

To identify the runoff processes on hillslopes, the soil moisture has to be considered. The soil moisture is of major importance as it has implications for management of water resources, irrigation planning and movement of chemicals/nutrients from land to water (Liu and Zhang 2007). This study investigates the soil moisture at three depths of the top and the bottom of the hillslope. In this chapter, a simple conceptual model based on

soil moisture data is introduced that allows an automated determination of the dominant runoff process on the hillslope.

6.2 The relationship between rainfall, simulated rainfall and runoff

It is apparent that not every drop of water landing on the grass or soil will produce runoff down the guttering drainage pipes of the experimental plots. After rainfall, a thin residue of water will be left on the grass and will eventually evaporate. To minimize this interception loss of water, the grass was cut regularly within the hillslope experimental plots. This helps to reduce one possible source of uncertainty in the water balance of the experimental plots.

Precipitation data were provided from the Hydrolog data base. Potential evapotranspiration (PET) values were calculated using a weather generator as described in sub-section 7.3.2. The average monthly rainfall depth for the 2009 year was 88 mm, and the total rainfall was 1055 mm, while for 2010 until August 19, the average rainfall was 48 mm and total rainfall 381 mm. The field enhanced rainfall tests were conducted from August 6, 2009 to March 18, 2010 (286 days) then again from July 15 to August 19, 2010 (35 days). The enhanced rainfall was applied only at perturbed plots (A and B) (Chapter 4, Figure 4-19).

Between April 1, 2009 and August 18, 2010 a total of 1110 mm of rainfall was measured distributed over 505 days and three significant events (Table 6-1). The maximum daily rainfall intensity was 31 mm/day. Significant snowfall occurred during December 2009, January and February 2010. There were many rainy days per month and the number ranged from 4 in April 2010 to 27 in November 2010.

Table 6-1 *Hydrological statistics of rainfall for the period of record*

Period	Total rainfall (mm)	Max monthly (mm)	Min monthly (mm)	Max intensity (mm/d)	Range rain days (days/mth)
1/4/09 – 17/8/10	1110	308 (November 2009)	1.8 (June 2009)	31	4-27

The enhanced rainfall was applied on perturbed plots A and B to examine the runoff effect and loss of nutrients due to enhanced rainfall. Table 6-2 lists the total natural rainwater applied to runoff plots. The enhanced rainfall experiment was carried out after a three month period of natural rainfall. This period was necessary to make comparisons between plots during natural climate condition before beginning the additional rainfall input.

Table 6-2 *The total of natural rainfall applied to runoff plots during runoff experiment, enhanced rainfall (shaded area)*

Date	Plot type	Perturbed plot	Control plot (natural)
	Plot	A, B	C
	Treatment/Climate condition	Rainfall (mm)	
23/4/2009	Dry	192	192
6/5/2009			
25/6/2009			
22/7/2009	Wet 1	1221	610
6/8/2009			
27/8/2009			
29/9/2009			
8/10/2009			
3/11/2009			
1/12/2009			
2/2/2010			
18/3/2010			
22/4/2010	Transition	154	154
20/5/2010			
17/6/2010			
15/7/2010	Wet 2	148	74
19/8/2010		+30*	
*container	Total	1745 mm	1030 mm

6.2.1 The overland and the subsurface flows at the hillslope plots

The overland flow data are provided from May 2009 to August 2010 with more detailed analyses of the storm events. At the beginning of the experiment, the soil was clearly not saturated. The relationship between the two plots A (perturbed plot) and C (control plot) of the overland flow generated under each rainfall event are shown in Figure 6-2.

Three storm events were selected for detailed analysis and named in following text as E1, E3 and E5 (Table 6-3). Of the three events, the event of 18 November 2009 (E3 in Table 6-3) produced the largest amount of rainfall (46 mm), was the longest in duration, and generated the largest volume of the overland flow on the perturbed plot (18 mm). The control plot, which was only affected by the natural rainfall, produced only 11 mm of overland flow.

Table 6-3 *Some characteristics of measured rainfall and overland flow events*

Event #	Day of the event	Rainfall total (mm)	Overland flow (mm)		Rainfall peak (mm/hour)	Overland flow peak (mm/hour)	
			A	C		A	C
E1	16/7/2009	27	4.8	4.6	4.8	2.1	2.3
E3	17-18/11/2009	46	18.0	11.4	5.2	3.4	1.6
E5	30-31/3/2010	25	8.3	4.4	4.8	1.9	0.6
	Sum	98	30.6	20.4			

A-perturbed plot, C- control (natural) plot

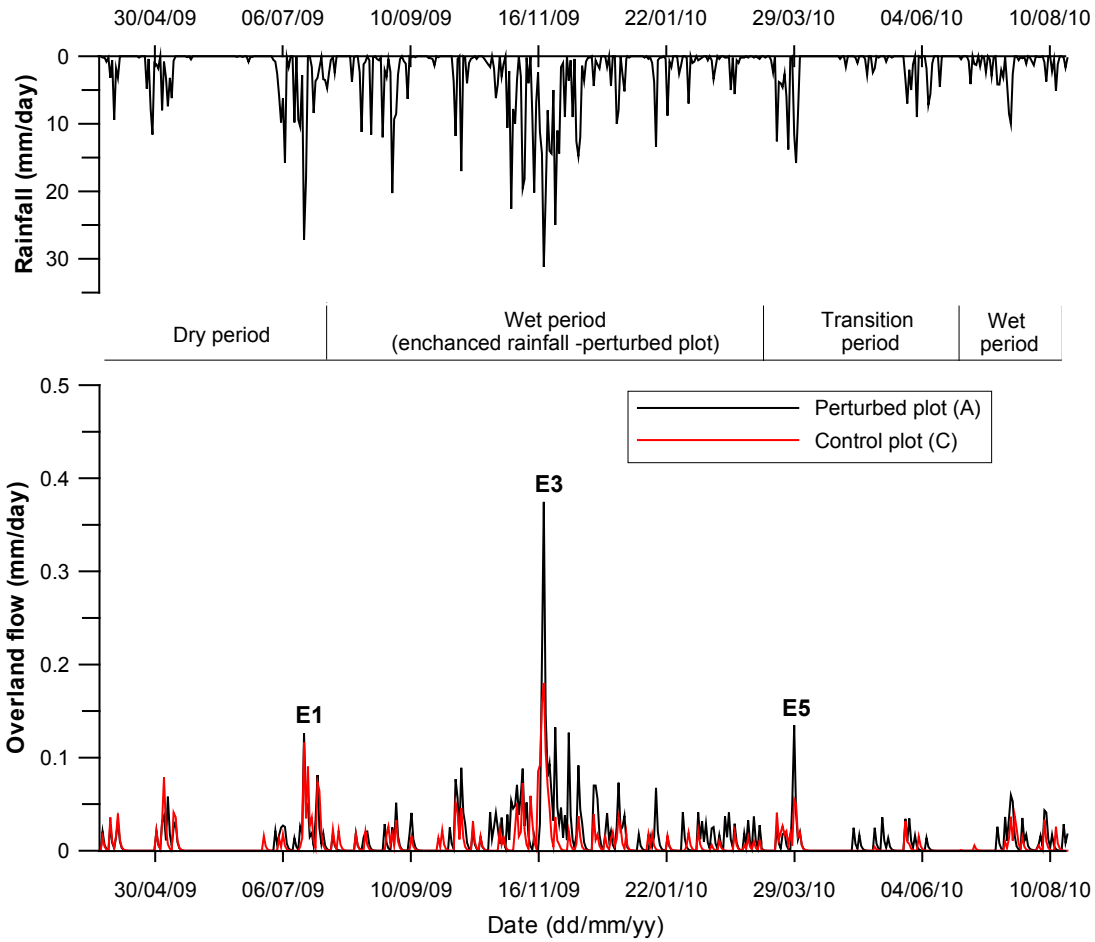

Figure 6-2 *Daily precipitation and overland flow with events measured during 2009 to 2010 year at the hillslope plots*

Total overland flow for the three events accounts for 20.4 mm of precipitation at the control plot, which is equivalent to 21 % of the precipitation that fell during three events (98 mm), and in the case of the perturbed plot, 30.6 mm of total overland flow is equivalent to 31% of the precipitation.

The overland flow based on three storm events is presented in Figures 6-3, 6-4 and 6-5, where two types of hydrograph can be distinguished: hydrograph with one runoff peak and with several peaks of runoff.

16 July 2009 storm event (E1)

Over 27 mm of rain fell on 16 July 2009, which wetted the surface soil layer to saturation and produced the single-day event (Figure 6-3). The event hydrograph at both the perturbed and control plots showed the same behaviour for the same rainfall conditions, with the matching of the time of peak flow, runoff volume and peak flow. This runoff event occurred in the (initial) dry period when enhanced rainfall was not applied on the perturbed plot.

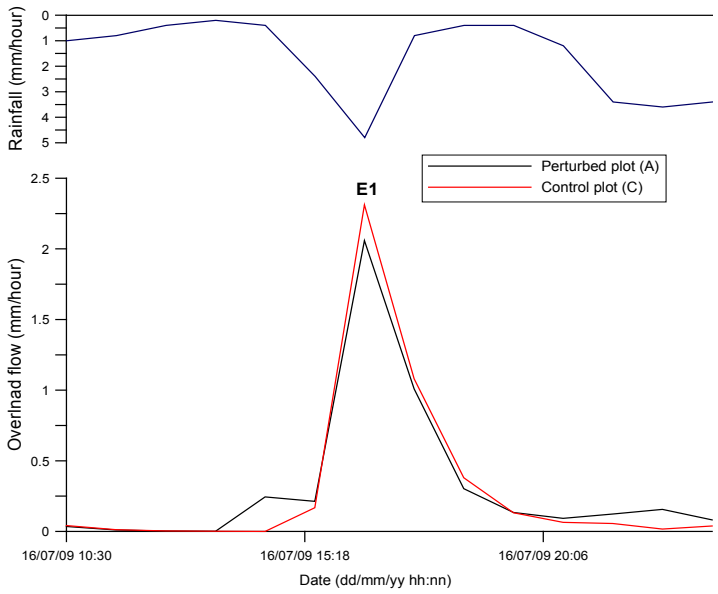

Figure 6-3 *July event (E1) hydrograph for the overland flow*

17-19 November 2009 storm and flood (E3)

The November 2009 storm event (E3) started with high rainfall intensities, which produced a saturation excess overland flow (Figure 6-4). The evidence for this statement is based on the visual field observation and direct observations of the saturated soil during the event. This was the top ranked event in 2009 that produced the major flood in the Hollow sub-catchment, and also in the Upper Eden basin. At the beginning of the event, there were a series of several runoff peaks, and then two distinct sharp peaks with short duration. In the case of the control plot, three runoff peaks with low runoff rate occurred at the beginning of the event, which differs from the perturbed plot. The storm event hydrograph in Figure 6.4 shows also the difference in the main peaks between plots with the higher peaks at the perturbed plot. The runoff peak flow, runoff volume and time to peak all differ between the two plots. The significant differences between the two plots is suggested to be a consequence of different surface soil moisture conditions, permeability or strictly, field saturated hydraulic conductivity K_{fs} and enhanced rainfall input at the perturbed plot. This runoff event occurred in the wet period when the enhanced rainfall was applied on the perturbed plot.

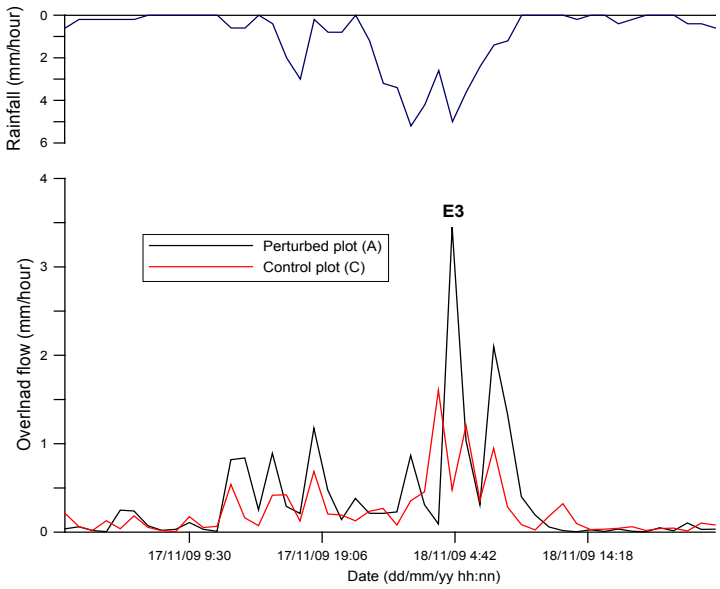

Figure 6-4 *November event (E3) hydrograph for the overland flow*

30-31 March 2010 storm event (E5)

The hydrograph for the March event (E5) has two corresponding runoff peaks at the perturbed plot (Figure 6-5) and one peak at the control plot. The runoff peaks at the perturbed plot are higher than at the control plot. This suggests that there is higher antecedent soil moisture from the previously enhanced rainfall period. This runoff event occurred in the transition period when enhanced rainfall was not applied on the perturbed plot.

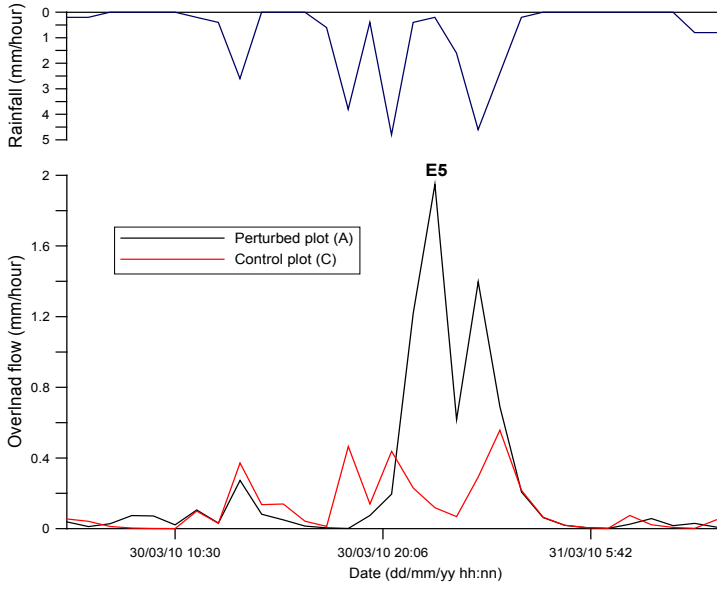

Figure 6-5 *March event (E5) hydrograph for the overland flow*

Compared to the rainfall average in 2009, the rainfall amounts during April to July 2010 were lower. The observations for all hydrographs include rapid rise and fall of overland

flow. The amount or timing of runoff during storm events has been influenced by the rainfall intensity and the antecedent soil moisture. In natural rainfall conditions compared to intensified rainfall, dry soil antecedent conditions are likely to be responsible for the absence of the overland flow. Some storms did, however, generate runoff as shown in Figures above, but with low runoff volume and runoff peaks.

Figure 6-6 illustrates the subsurface flow response observed during different climate conditions for the period 30 September 2009 to 17 August 2010. It is not possible to present the subsurface flow during the initial (dry) conditions because the installation of a subsurface drainage pipe was set up later in the wet condition on 6 August 2009.

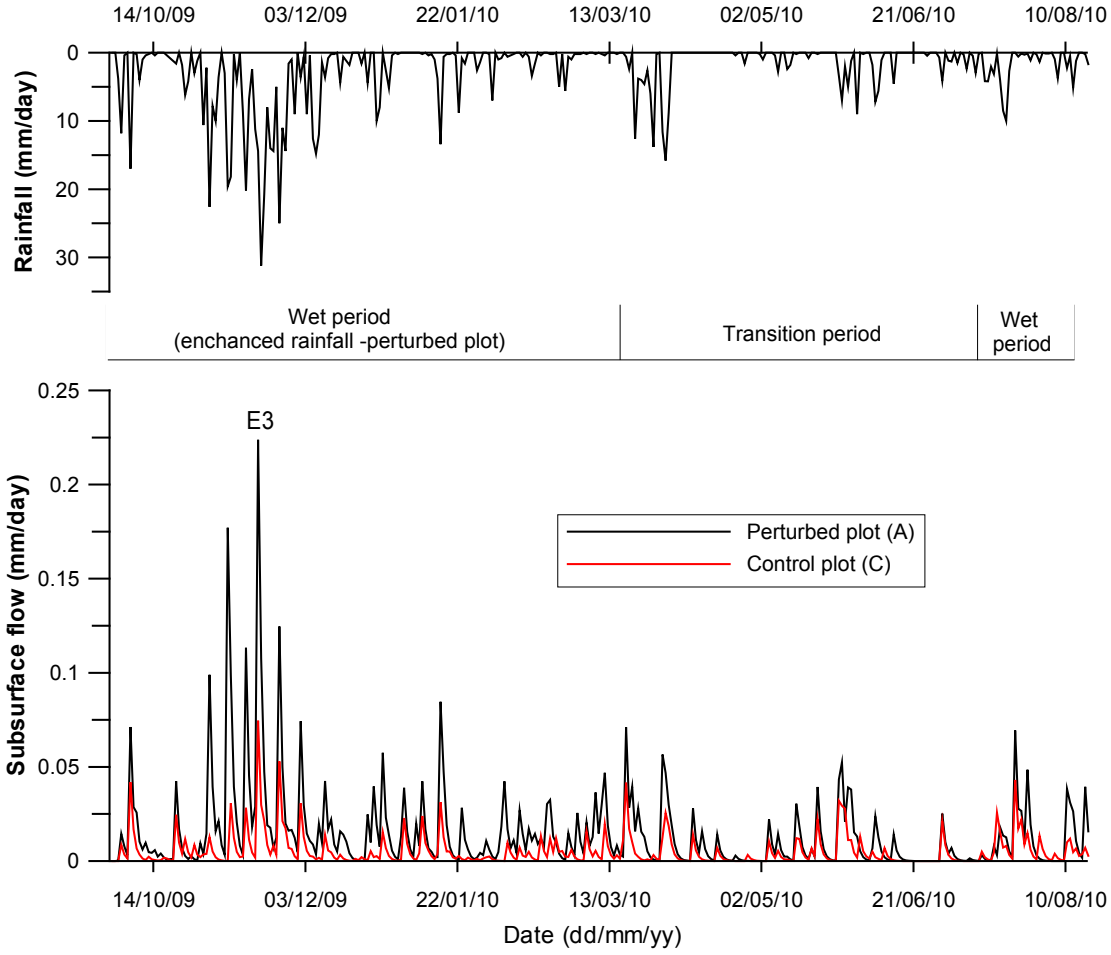

Figure 6-6 *Subsurface flow at the perturbed and control plots*

The results show that the subsurface flow is more significant under the dry (transition period) conditions than under the wet conditions.

The total climate condition overland flow depth was 149 mm for the perturbed plot and 84 mm for the control plot (Table 6-4), representing 8.5% and 8.2% of the total rainfall depth. The percentage of the rainfall that became the overland flow ranging from 6.7 to 10.9% for the perturbed climate conditions and from 6.5 to 10.4% for the natural

climate conditions. The duration of treatments was not the same, therefore comparison between the dry and the wet period is not possible related to the flows. For the dry climate condition, the soil was dry and the rate of the infiltration was high, therefore it produced less the overland flow compared to the wet climate conditions. For the November storm event (#E3), the overland flow dominated at the both plots (Table 6-4). In this case, the soil moisture content was high and the rainfall event occurred over a couple of days, the overland flow represented 39.1% and the subsurface 17.4% of the total rainfall for that event. For this comparison, the same amount of the rainfall was used. This indicates that for this storm event doubling of the rainfall input results 22% change in the overland and 52% in the subsurface flow between the natural and the perturbed conditions. The runoff generation at the hillslope was dominated by the saturated overland flow during the storm events and the role of the saturated soil.

Table 6-4 *Rainfall and flow of the hillslope plots during different climate condition and percentage of rainfall that became flow*

Treatment/ Climate condition	**Rainfall**		**Perturbed plot (A)**				**Control plot (C)**			
	Perturbed plot (A)	Control plot (C)	Overland flow		Subsurface flow		Overland flow		Subsurface flow	
	(mm)	(mm)	(mm)	(%)	(mm)	(%)	(mm)	(%)	(mm)	(%)
Dry (16 weeks)	192	192	21	10.9	N/A	N/A	20	10.4	N/A	N/A
Wet 1 (24 weeks)	1221	610	100	8.2	81	6.6	48	7.9	26	4.3
Transition (17 weeks)	154	154	16	10.4	21	13.6	10	6.5	10	6.5
Wet 2 (34 days)	178	74	12	6.7	12	6.7	6	8.1	7	9.5
Total	1745	1030	149	8.5	114	6.5	84	8.2	43	4.2
Storm event (E3)	46	46	18	39.1	8.0	17.4	11.4	24.8	2.5	5.4

N/A not available

Table 6-4 shows the overland and the subsurface flows of the total flow during the dry period, the first enhanced rainfall period (wet 1), the transition period and the second enhanced rainfall period (wet 2). The rainfall distribution on the plots was also presented in Table. The overland flow comprised 21 mm at the perturbed plot and 20 mm at the control plot during the dry conditions. However, 100 mm (plot A) and 48 mm (plot C) was composed of overland flow during the first enhanced rainfall period (wet 1). The difference in the overland flow between the two plots was not significant during the transition and the second enhanced rainfall period (wet 2). The subsurface flow comprised 81 mm at the perturbed plot and 26 mm at the control plot during the wet 1 condition. The difference in the subsurface flow between the two plots was 5% during the transition and the wet 2 conditions.

The perturbed plot was compared to the control plot through the percentage of the rainfall and flows (Table 6-5). For the 24 weeks of the rain application during the wet period 1, the perturbed plot produced a significantly higher response, with 68% of

rainfall producing the overland flow, while the control plot produced 32%. The similar situation occurred during the second enhanced rainfall event (wet 2) with 34% difference. During the transition period, the difference was 24%. The differences of the subsurface flow between the plots were 52% for the wet 1, 36% for the transition and 26% for the wet 2 conditions.

Table 6-5 *Percentage of rainfall and flow from the perturbed plot compare to the control plot at the hillslope during different climate condition*

Rainfall and flow	Treatment/Climate condition	Plot			Percentage		
		Perturbed plot (A)	Control plot (C)	Total	Perturbed plot (A)	Control plot (C)	Total
Rainfall (mm)	Dry (16 weeks)	214	214	428	50	50	100
	Wet 1 (24 weeks)	1100	550	1650	67	33	
	Transition (17 weeks)	144	144	288	50	50	
	Wet 2 (34 days)	148	74	222	71	29	
Overland flow (mm)	Dry (16 weeks)	21	20	41	51	49	100
	Wet 1 (24 weeks)	100	48	148	68	32	
	Transition (17 weeks)	16	10	26	62	38	
	Wet 2 (34 days)	12	6	18	67	33	
Subsurface flow (mm)	Dry (16 weeks)	N/A	N/A	N/A	N/A	N/A	N/A
	Wet 1 (24 weeks)	81	26	107	76	24	100
	Transition (17 weeks)	21	10	31	68	32	
	Wet 2 (34 days)	12	7	19	63	37	

N/A not available

During the winter period from 1 to 29 January 2010 the subsurface runoff dominated at the event peak (16 January 2010) (Figure 6-7). The reason for this appears to be related to melting or thawing of soils by the time of rain-on-snow event and/or frozen soil water. According to the field observations in lysimeters, the frozen soil water was noticed at a depth of 18 cm on 2 February 2010. It is assumed that the thickness of the frozen soil was approximately at 18 cm soil depth or even deeper. Therefore, the overland flow dominated on 2 February 2010 compared to the subsurface flow, Figure 6-7. This suggests that the overland flow occurs in the winter period during frozen soil as Hortonian overland flow. The comparable results were found in a study of Wilcox et al. (1997) who monitored runoff, both the surface and lateral subsurface of ponderosa pine hillslope in northern New Mexico. They found that the snowpack generated only the overland flow when it melted, while no lateral subsurface runoff was measured.

The enhanced rainfall experiment generated more runoff where the principal reasons for the higher runoff peaks compared with the control plot are suggested to be wetter antecedent soil moisture conditions, the higher rainfall intensity and lower permeability. There was the significantly less the overland flow from the control plot compared to the perturbed plot. Observed differences in the overland flow between plots during the

transition and wet 2 periods were likely reflected by the greater homogeneity of the soil infiltration properties and previous rainfall-runoff events.

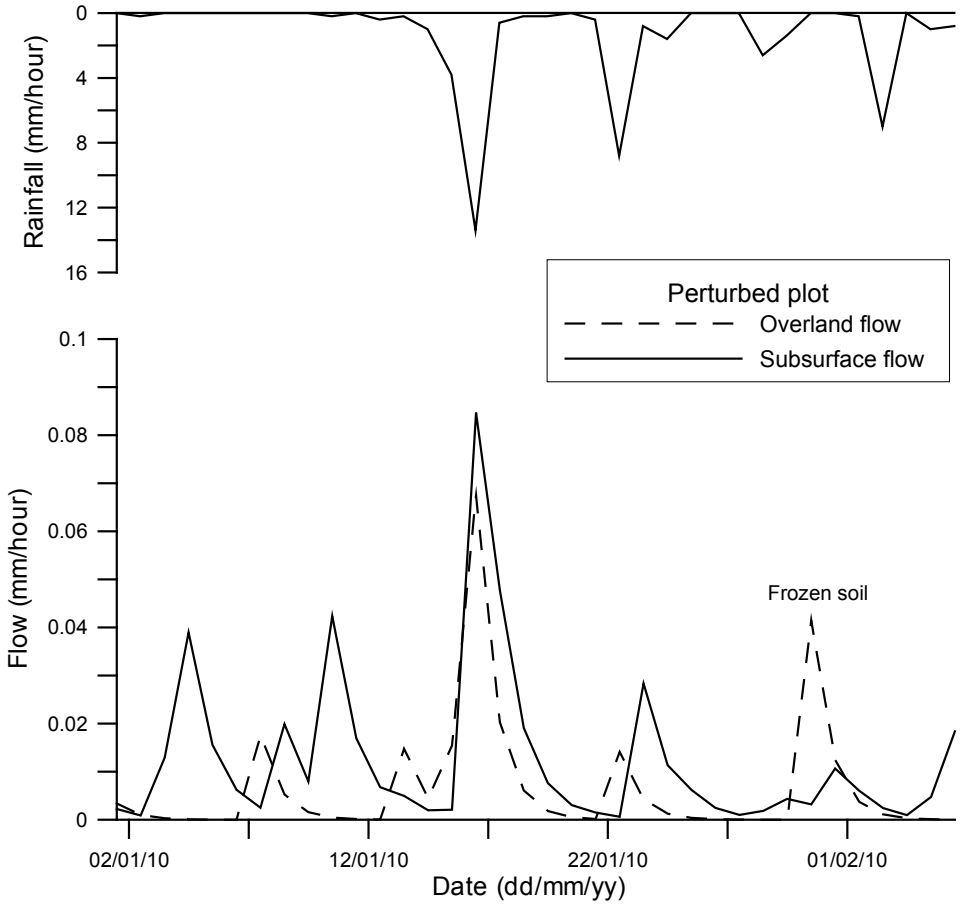

Figure 6-7 *Overland and subsurface flows at the perturbed plot during the winter period*

During the wet 1 period, the overland flow was dominated for the both plots. The results showed that during the transition period or a 'switching' behaviour between the first (wet1) and the second (wet 2) wet seasons, the lateral subsurface flow dominated.

At the hillslope the soil water table was observed at approximately 25 cm below the surface. It is believed that the soil would rapidly become saturated and the saturation overland flow would occur. This is possible due to the high permeability of the loamy sand layer that extends from ground surface to 20 cm. These data are based on laboratory analysis, shown later in Chapter 8. Therefore, this allowed easy infiltration of water into the soil and rise of the soil water table.

An important contributor of labile nutrients from the hillslope to the stream is the overland storm flow. The contributions of the hillslope to the stream flow of the Hollow sub-catchment were quantified through the storm event. It was found that the overland hillslope flow comprised 32% from the perturbed plot and 20% from the control plot of the total catchment storm runoff during the larger November event.

6.3 Soil moisture distribution on the top and the bottom of the hillslope

In order to understand runoff processes at the hillslope and in the catchment, it is necessary to measure internal information, i.e. soil moisture patterns in this case. The soil moisture patterns combined with other existing data give us much insight into runoff processes. Hupet and Vanclooster (2002) mention the soil moisture as another state variable for a range of hydrological processes that act over a variety of spatial and temporal scales.

In this study, the soil moisture was determined in the vadose (unsaturated) zone over three soil depths of 10, 20 and 30 cm at the top and bottom of the hillslope or three soil layers. Bulk density and soil texture were also measured at these depths that have potential for dictating soil moisture patterns (further discussed in Chapter 8). Bulk density was found to be higher in sandy loam at 30 cm than in loamy sand at 10 and 20 cm soil depth. Due to several equipment faults with the soil moisture data logger (DL6), data were available only for the periods from 11 September to 8 October 2009, 6 January to 1 February 2010, 19 February to 18 March 2010, and 26 March to 22 April 2010. The observation had a monthly schedule to download data from August 2009 to July 2010. Part of the data set is missing due to a data file corruption.

The soil moisture time series observed in the field are shown for the three different soil depths in Figures from 6-8 to 6-10. These Figures also present comparisons between the top and the bottom of the hillslope. Volumetric water content was measured at 15 minute intervals. The soil moisture time series suggest a relationship between rainfall events and peaks in soil moisture.

The points below are used as explanations for the soil moisture curves shown in Figures (based on Aquaflex (2005), with modifications by the author):

1) The soil is very dry
2) Rainwater has penetrated to the depth of the Theta Probe sensors
3) Slight drops in moisture could be attributed to short interruptions in the rain event or some rapid drainage of water from the air voids around the sensor, as the soil is wetted
4) There is no further wetting maybe because the soil is saturated and additional water is draining freely past the sensor and through the soil profile

4-5) The soil has remained saturated

5) Excess water draining past the sensor combined with water extraction by the grass has resulted in a net loss of water from the depth at which the sensor is located
6) The rapid decline in water is most likely due to gravity drainage of excess water applied during rain event
7) Movement of water through capillary action and pressure gradients often cause a slight increase in soil water content
8) The slower decline in soil moisture levels is probably due to evaporation
9) A distinct reduction in water usage indicates that the soil moisture is approaching the wilting point, and the plants are beginning to experience significant water stress.

Figure 6-8 shows the differences of the volumetric water content in the upper and lower soil layers. There has been a sharp increase in the soil moisture content on October 3, 2009 at the bottom of the hillslope at a depth of 10 cm. It is clearly shown that the soil moisture at 20 cm depth decreases continually. This suggests a strong drainage process because root extraction is excluded as an option because it is generally very small and near the top of the soil profile. All Figures show 'noise' at 10 cm that is a possible sensitive reflection of the Theta Probe sensors to small changes in the soil moisture content or measurement error. The soil moisture data at 30 cm soil depth in the bottom of the slope were not used in interpretations due to their corruption.

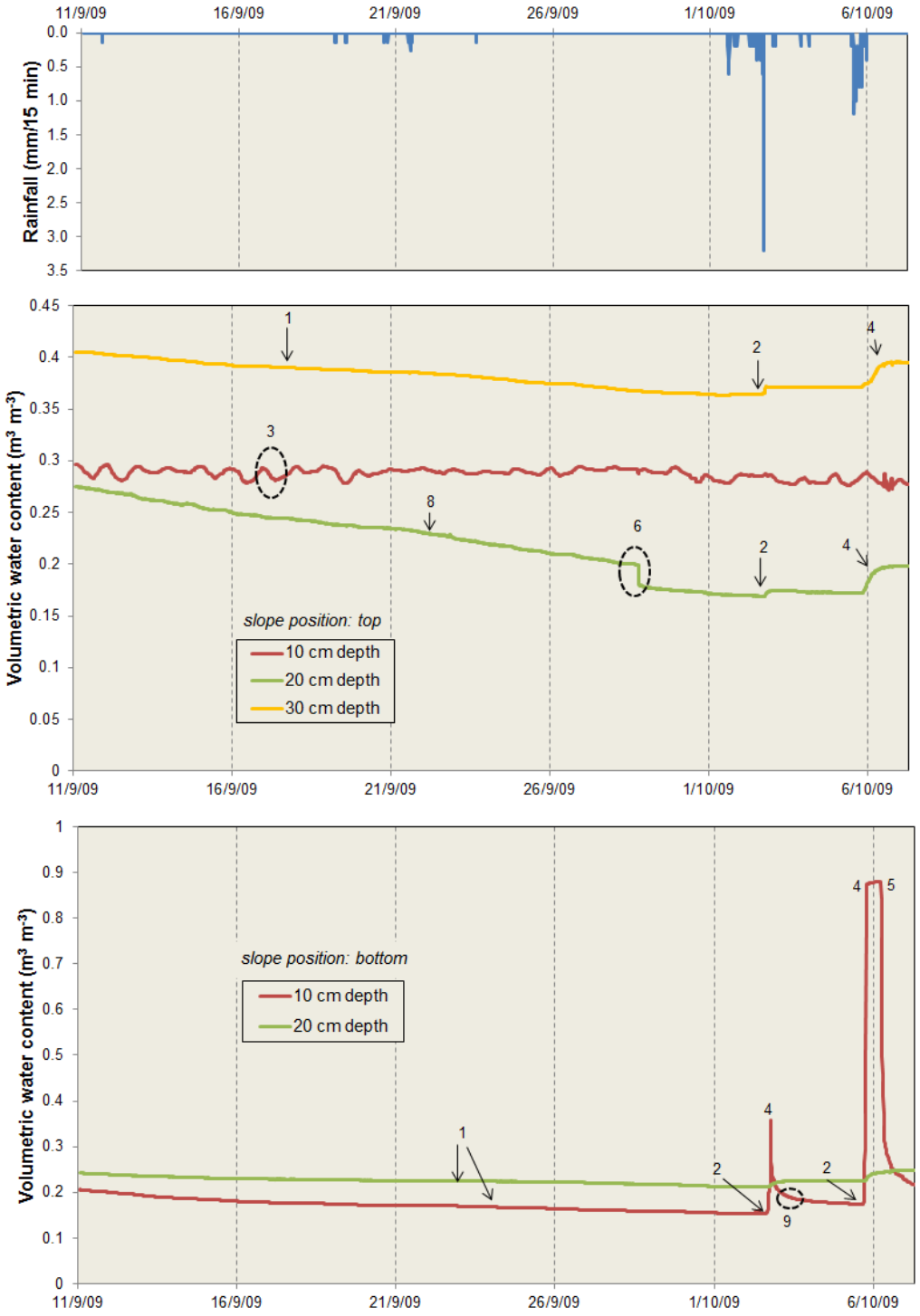

Figure 6-8 *Soil moisture content in the different layers at the top and the bottom of the hillslope and rainfall for the period Sep - Oct 2009*

Figure 6-9 shows an example of one storm realisation in January 2010. The soil moisture peaks are evident due to rainfall inputs at the top of the slope at the depth of 20 cm and much less at 30 cm, while in the bottom of the slope they are only evident at 10 cm depth. Here is also evident noise at 10 cm depth. The periods of noise in the soil moisture data were not used in interpretations.

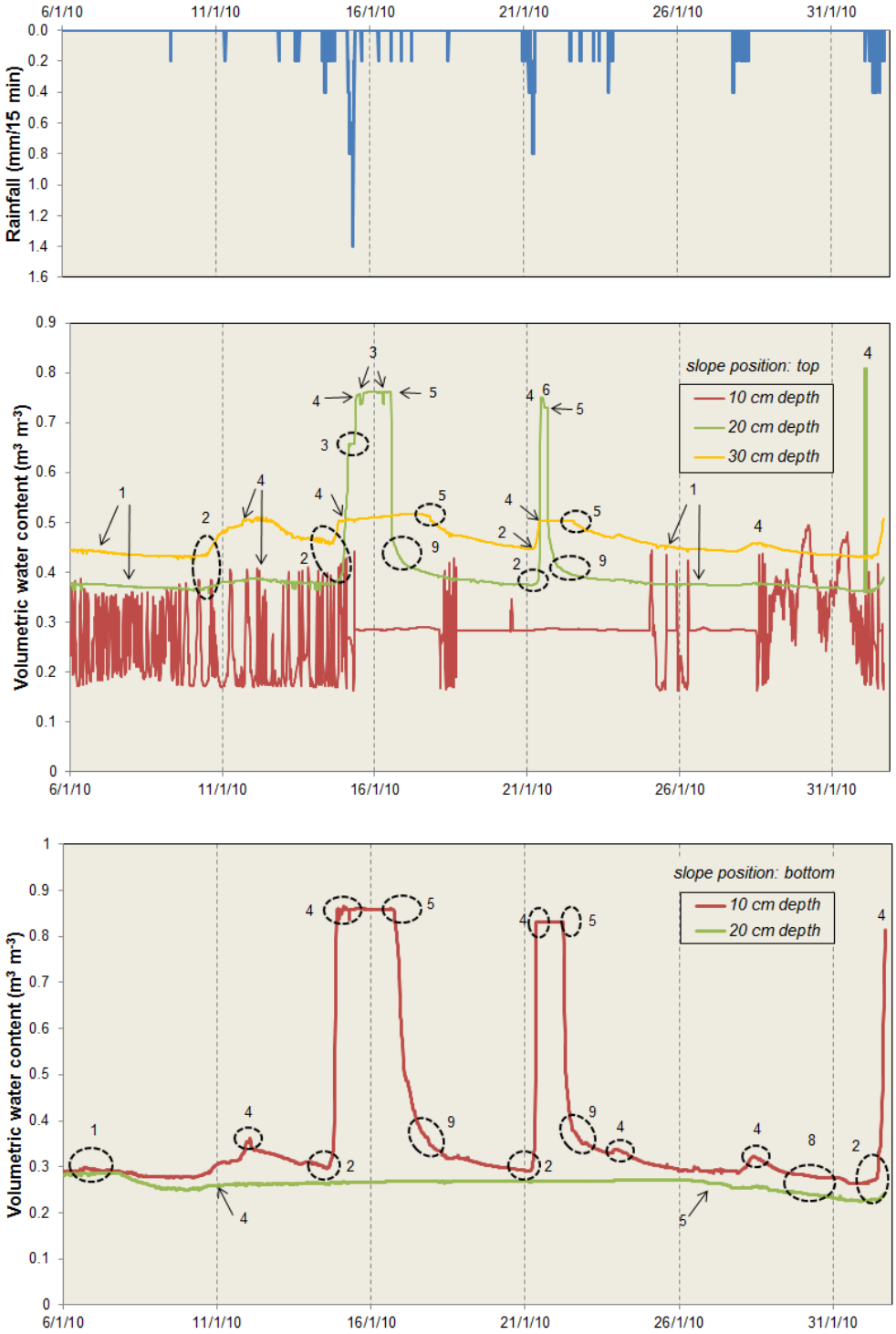

Figure 6-9 *Soil moisture content in the different layers at the top and the bottom of the hillslope and rainfall for the period in January 2010*

The graphs in Figure 6-10 show the spatial changes in soil moisture at the top of the slope at depths of 20 and 30 cm, and in the bottom of the slope at 20 cm depth during snowmelt and moderate rainfall intensity. The Theta Probe at the bottom of the slope at 30 cm soil depth did detect water but only at a very low content. This suggests that the snowmelt process has caused high volumetric content at 20 cm at the hillslope bottom.

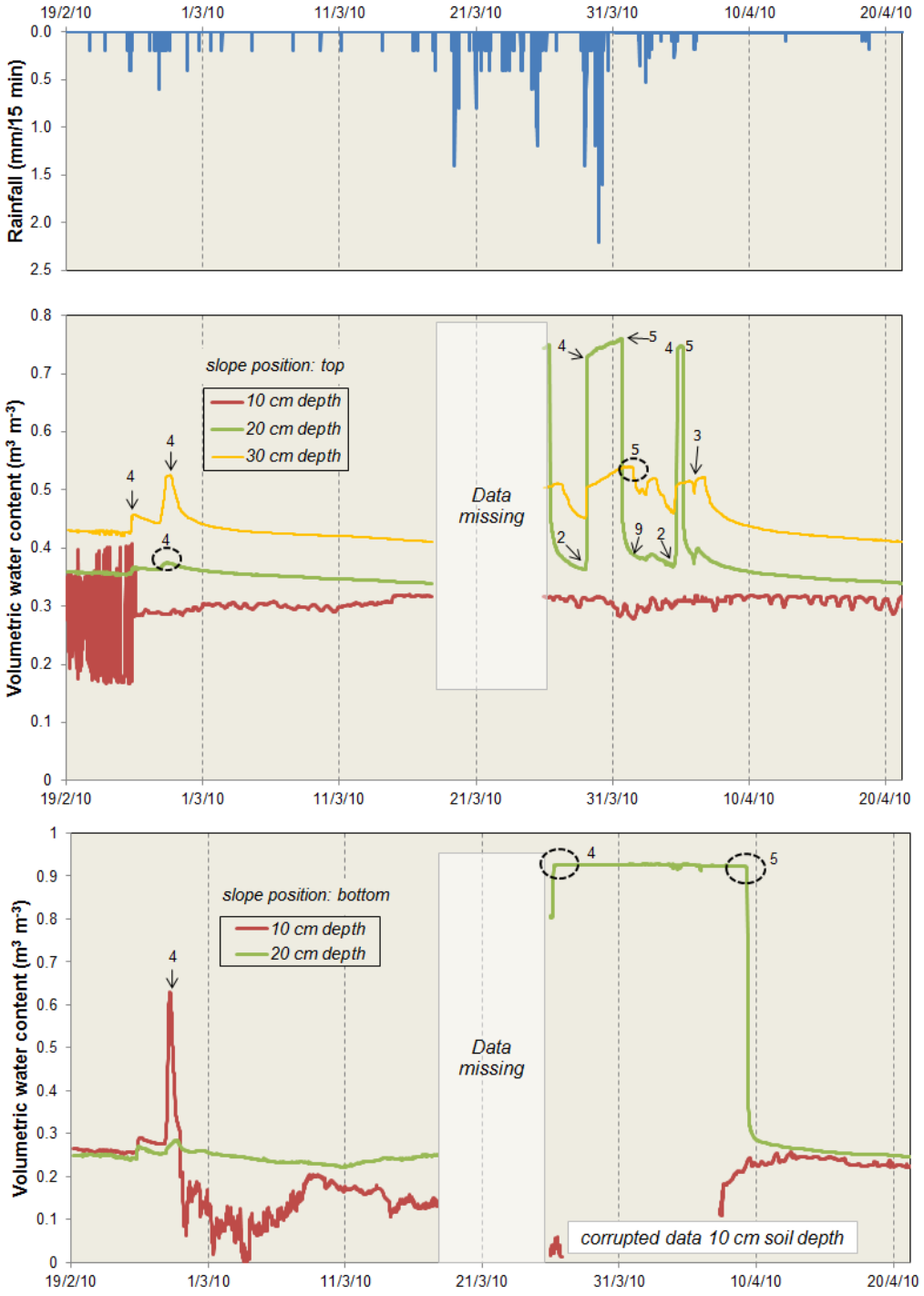

Figure 6-10 *Soil moisture content in the different layers at the top and the bottom of the hillslope and rainfall for the period Feb – April 2010. Gaps in the record denote instrument failure*

From Figures above, the soil moisture above 0.7 m^3m^{-3} indicate that the soil is fully saturated and the overland flow is occurring. This suggests fully saturated soil due to a previous snowmelt event and/or high precipitation input. The snowpack accumulated later and began to melt at the end of February and March with moderately saturated soil where additional rainfall acted as a trigger to produce the overland flow. The soil moisture measured at 10 cm soil depth shows some noise that could influence the

interpretation of the results. Therefore, caution must be applied, as the findings might not be transferable.

The relationship between the soil moisture at 30 cm and the measured subsurface flow at 18 cm allowed the identification of the soil moisture threshold value above which runoff significantly increased (Figure 6-11, Table 6-6). The subsurface flow was low during dry conditions and a sharp increase occurred when the 46% moisture threshold was exceeded at 30 cm.

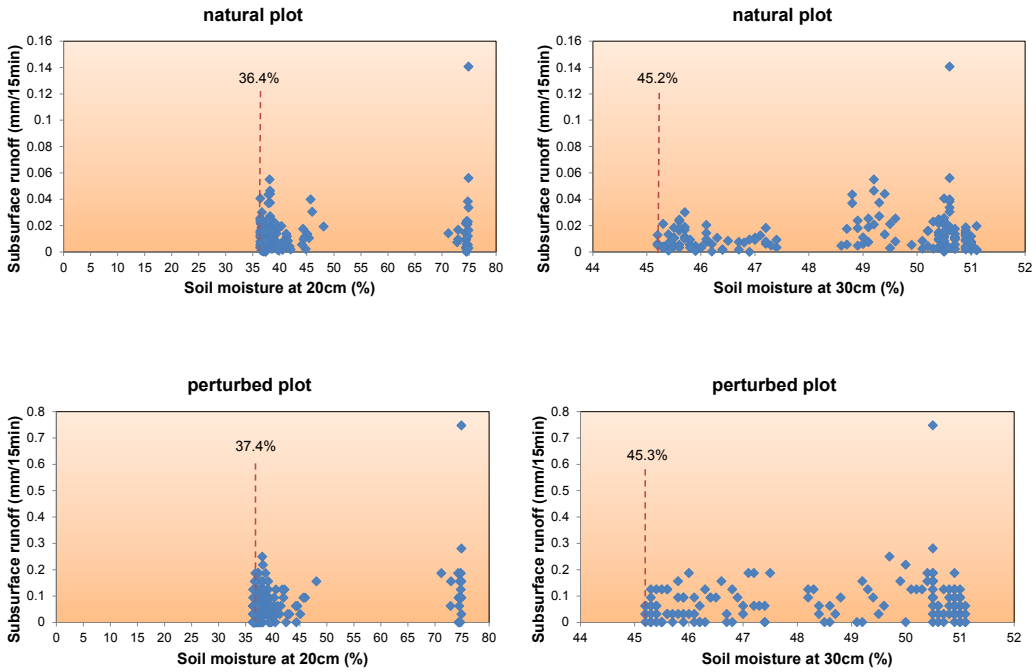

Figure 6-11 *Threshold behaviour in the relationship between the hillslope soil moisture at the top prior to the event and the subsurface flow runoff values. The vertical lines highlight the soil moisture threshold*

Table 6-6 *Threshold behaviour in the relationship between the hillslope soil moisture at the top and bottom prior to the event and the subsurface flow runoff values*

Depth (cm)	Threshold	
	top	bottom
10	~0.33 m^3m^{-3} (33%)	~0.30 m^3m^{-3} (30%)
20	~0.37.4 m^3m^{-3} (38%)	~0.30 m^3m^{-3} (30%)
30	~0.45.3 m^3m^{-3} (46%)	~0.05 m^3m^{-3} (5%)

Moisture contents seem to be the threshold above which major changes occur in the lateral subsurface moisture fluxes runoff. Moisture conditions less than the threshold represent lateral subsurface moisture fluxes and runoff processes under unsaturated conditions or moderately dry soils. In the case of larger threshold values, lateral subsurface moisture fluxes and runoff occurs for soil moisture conditions that are at or near saturation.

Table 6-7 summarises the statistics of soil moisture for several periods. A mean soil moisture ranged from 0.27 to 0.32 m^3m^{-3} at 10 cm depth, from 0.18 to 0.47 m^3m^{-3} at 20 cm depth and from 0.37 to 0.49 m^3m^{-3} at 30 cm depth of soil at the top of the hillslope. In the case of bottom position, the mean soil moisture ranged from 0.13 to 0.79 m^3m^{-3} at 10 cm depth, from 0.23 to 0.89 m^3m^{-3} and at 20 cm depth. The standard deviation decreases with an increase of the mean soil moisture value.

The top of the slope has the highest, while the bottom of the hillslope has relatively low soil moisture content. The mean moisture content decreases, while variation of moisture content along the hillslope profile (top to bottom) increases, resulting in large spatial variability of soil moisture. However, only the wet period is considered, the high soil moisture is at the bottom, and lower at the top of the hillslope. The overall results from this study are in agreement with those of Ockenden (2010) who measured the soil moisture in the Blind Beck catchment on five separate occasions with different antecedent condition to investigate temporal variation.

Soil moisture measurements were not made directly during the storm event (e.g. November 2009) thus, it cannot be possible to determine whether lateral subsurface flow during the storm was related to the shallow or deeper soil moisture pattern. In this study only precipitation depth, gradient, soil bulk density and soil texture were collected but many factors (vegetation, soil hydraulic parameters, land use, etc.) jointly cause the variability of surface moisture to be complicated and cannot be considered only by a single factor.

Table 6-7 *Soil moisture statistics for the top and bottom of the hillslope for three different soil depths*

Occasions/ (conditions)	Slope position	Depth (cm)	Soil moisture			Antecedent rainfall		Rainfall for occasions (mm)
			Mean (m^3m^{-3})	Standard Deviation (m^3m^{-3})	Coefficient of variation	10 days (mm)	40 days (mm)	
11 – 30 Sep 2009 (dry)	top	10*	0.13	0.0	0.01	29	103	3
		20	0.23	0.03	0.13			
		30	0.39	0.01	0.03			
	bottom	10	0.17	0.01	0.07			
		20	0.23	0.01	0.03			
		30	0.04	0.01	0.14			
1 – 8 Oct 2009 (wet)	top	10*	0.28	0.00	0.01	2	73	33
		20*	0.18	0.01	0.06			
		30	0.37	0.01	0.03			
	bottom	10	0.23	0.18	0.75			
		20	0.23	0.01	0.06			
		30	0.03	0.01	0.31			
6 – 31 Jan 2010 (wet)	top	10*	0.27	0.06	0.22	16	111	36
		20	0.41	0.09	0.23			
		30	0.47	0.03	0.06			
	bottom	10	0.38	0.18	0.47			
		20	0.26	0.01	0.04			
		30	0.03	0.01	0.45			
1 – 2 Feb 2010 (wet)	top	10	0.32	0.09	0.29	15	67	7
		20	0.37	0.05	0.14			
		30	0.44	0.02	0.04			
	bottom	10	0.30	0.10	0.34			
		20	0.23	0.00	0.02			
		30	0.03	0.00	0.13			
19 – 28 Feb 2010 (wet)	top	10	0.27	0.05	0.19	7	52	13
		20	0.36	0.01	0.02			
		30	0.45	0.03	0.06			
	bottom	10	0.27	0.08	0.30			
		20	0.26	0.01	0.04			
		30	0.03	0.01	0.21			
1 – 18 March 2010 (dry)	top	10	0.30	0.01	0.02	13	45	2
		20	0.35	0.01	0.02			
		30	0.42	0.01	0.02			
	bottom	10	0.13	0.04	0.33			
		20	0.24	0.01	0.04			
		30	0.03	0.01	0.28			
26 Mar – 10 April 2010 (wet)	top	10	0.31	0.01	0.03	50	70	50
		20	0.47	0.15	0.33			
		30	0.49	0.03	0.06			
	bottom	10	0.23	0.01	0.04			
		20*	0.89	0.14	0.16			
		30	0.06	0.01	0.23			
11 – 22 April 2010 (dry)	top	10	0.31	0.01	0.03	9	88	0.4
		20	0.35	0.01	0.02			
		30	0.42	0.01	0.02			
	bottom	10	0.23	0.01	0.04			
		20	0.26	0.01	0.04			
		30	0.02	0.00	0.20			

* caution applied

6.3.1 Conceptual model of hillslope runoff response based on soil moisture pattern

In this study, a simple conceptual model is proposed by linking the results of soil moisture with observed overland and subsurface flows at the hilslope. This is an attempt to create the model of dominant runoff process within the unsaturated zone. The conceptual model is presented in Figure 6-12 for dry and wet conditions. The highest mean value of water content recorded by Theta Probe soil moisture sensor is indicated by a red arrow and label as I. The possible direction of moving water through the soil is indicated as parallel to the soil water table or topography.

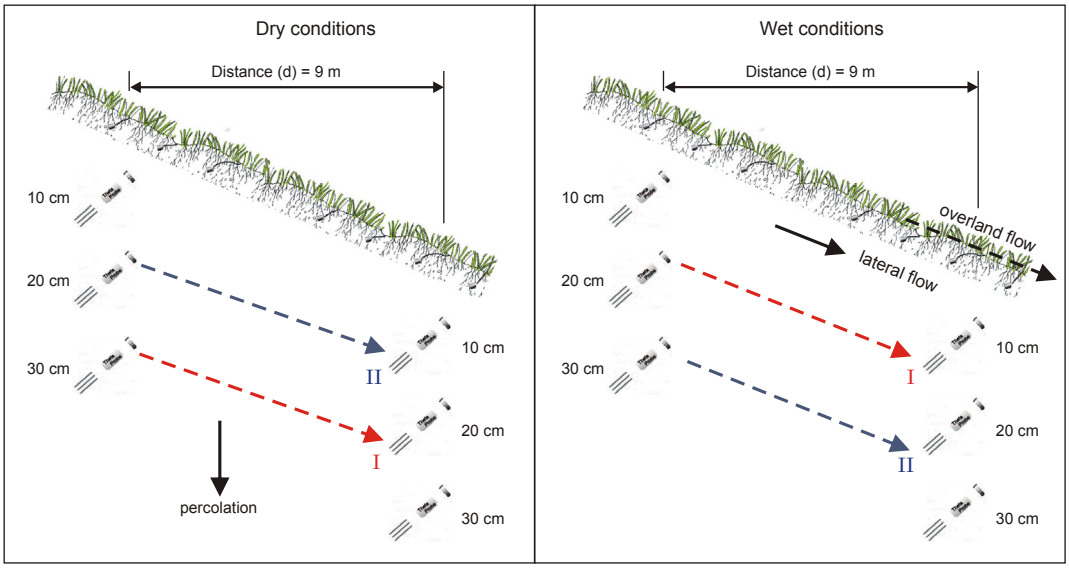

Figure 6-12 *Conceptual model of dominant runoff at the hillslope in dry and wet conditions based on the soil moisture measurements (source: the author)*

Several flow processes were observed during the soil moisture monitoring. These have been classified into dominant (red arrow) and subordinate (blue arrow) flows on the basis of the highest mean soil moisture values. During dry conditions, the highest mean soil moisture value (I) was recorded at the depth of 30 cm at the top and 20 cm at the bottom of the hillslope. Second highest value (II) was at the depth of 20 cm at the top and at 0.10 m of the bottom. During dry conditions, soil moisture is reduced, likely causing a significant reduction in hydraulic conductivity, and it is dominated by vertical flow or percolation to groundwater.

The second model corresponds to the wet period, where the highest mean soil moisture value (I) was recorded at the depth of 20 cm at the top and 10 cm at the bottom of the hillslope. Second highest value (II) was at the depth of 30 cm at the top and at 20 cm of the bottom. The spatial distribution of soil moisture during the wet period was attributed to lateral redistribution of water through the subsurface from top to bottom of the hill as

lateral flow. Increasing of saturation during the intense rainfall could produce the overland flow.

The soil layer at 30 cm at the bottom of the hillslope shows lower soil moisture values. This suggests that for the dry conditions, the lateral subsurface flow occurs as the deep- and shallow-subsurface flow identified as the dominant process at 30 cm and 20 cm soil depth. The absence of significant high values of the soil moisture at 10 and 30 cm depth of the bottom was the key to this interpretation.

It is possible that the soil layer at 30 cm depth is a transition as it remained relatively moist and it has been a source of upward water movement where the water and nutrients are being transferred to the top layer at the bottom of the hillslope. There is no evidence to justify this conceptual model but can be regarded as a hypothesis rather than conclusive evidence.

6.4 Summary

In this study, a field experiment was conducted on a small scale hillslope in the Hollow sub-catchment and aimed to characterize the runoff flow pathways and soil moisture pattern of three soil depths. Representation of possible climate variability in terms of precipitation perturbation on flow at the hillslope has been shown to have effects on the hydrological cycle. For 24 weeks of enhanced rainfall application on the perturbed plot, produced 65 % of overland flow, while the control plot produced 35% of overland flow. The overland flow varied from 14% in dry conditions (before treatment) to more than 64% in the enhanced rainfall conditions of the total measured overland flow. The results have shown that sensitivity of different runoff processes to different types/size of storms can support analysis of impacts of enhanced climate variability. During the winter, the overland flow of runoff was facilitated by frozen soil.

It was found that both the overland and subsurface flows depend on rainfall intensity and seasonal changes in the soil moisture. It is observed that lateral subsurface runoff dominates in the transition period. However, it can occur together with the overland flow in specific conditions such as snowmelt. The shallow and permeable soils detected at the hillslope lead to saturation during storm events to produce the saturated overland flow.

This chapter incorporates a conceptual model of the effect of precipitation and soil moisture on hillslope runoff fluxes. The results indicated that the subsurface saturation is related to soil depth, gradient and soil moisture pattern.

The findings that were significant difference between measurements at plots in this study supports the use of small plots of 2 m^2 to estimate the runoff. Bagayoko (2006) used in his study a short (1 m^2) and long (10 m^2) plots for estimating of overland flow. He observed that the short plot became saturated more quickly than the long plots for the same rainfall depth. It is clear that no matter of size of the plots they will never give a true representation of runoff, as they will always have an edge effect especially on the bottom side where runoff water and sediment would be collected. The advantage of the larger plot is less worry about edge effects. The results from this study showed the overall method to be a valid and reliable tool for monitoring runoff for understanding the hydrological behaviour of dominant runoff process for different climate conditions.

This data has implications for determination of the dominant flow for nutrient and water transport and connectivity of the hillslope to the stream of the sub-catchment. This runoff experiment will be supported together with geochemical analyses later in the study to establish a new concept in the understanding of overland and subsurface hydrological controls on nutrient fluxes.

Chapter 7. Nutrient behaviour at the hillslope scale

7.1 Introduction

The purpose of this chapter is to summarize the water quality results, and the electrical conductivity relationship to flow at a hillslope scale, to test hypotheses 1 and 2 of this study (Chapter 1), and to identify the variation in the dissolved organic carbon (DOC) and the nitrate (NO_3^-) concentrations in overland and subsurface flows. This chapter aims to investigate which of the surface and subsurface hydrological processes within the hillslope are controlling nutrient fluxes, measured in overland flow and soil water solution at 10 cm and 18 cm soil depth representing subsurface flow. In this study, the results from the field and laboratory chemistry analyses are used to identify those climatic and hydrologic variables that best explain variations in the DOC and the nitrate.

7.2 Hillslope water quality

The water quality chemistry results are based on data collected from July 2009 to August 2010. The chemical composition of the soil water solution was studied during 10 months (one wet and one transition period) using lysimeters. The lysimeter pairs consisted of one lysimeter which was placed 10 cm into the soil ("shallow lysimeter") and one which was placed at 18 cm into the soil ("deep lysimeter"). The lysimeters were pumped out every month. The assessment of the soil water chemistry was limited by the lack of water chemical data during the summer period.

The full quality data for all parameters with the use of the Charge Balance Error (CBE) are listed in Tables 1-6 of Appendix E1. To examine the relationship between runoff and variation in chemical concentration, data from runoff water samples were collected as monthly point values.

Table 7-1 summarises the statistical analysis of the overland flow water concentrations of the perturbed and control (natural) plot. During dry periods (May – June 2010), sampling of the flow water at plots was a problem because there was no water in the tipping buckets.

The pH of the overland flow water varied in the range 5.8 - 7.2 indicating slightly acidic to a neutral type of water.

Table 7-1 *Statistical analysis of chemical composition in the overland flow water of the perturbed plot (A) and control plot (C) at hillslope during June 2009 – August 2010*

Perturbed plot (A) (n = 13)	**pH**	**Na^+**	**K^+**	**Ca^{2+}**	**Mg^{2+}**	**HCO_3^-**	**Cl^-**	**SO_4^{2-}**	**NO_3^-**
		mg/l							
Min.	5.8	2.0	1.9	2.2	0.6	3.5	6.4	1.7	0.5
Mean	6.6	4.7	4.5	5.2	1.3	16.0	9.9	4.7	1.8
Max.	7.2	9.5	9.3	8.4	2.7	30.5	17.1	12.3	4.5
SD.	0.4	1.9	2.1	2.2	0.6	9.8	8.7	3.0	1.2
Control plot (C) (n = 13)	**pH**	**Na^+**	**K^+**	**Ca^{2+}**	**Mg^{2+}**	**HCO_3^-**	**Cl^-**	**SO_4^{2-}**	**NO_3^-**
		mg/l							
Min.	5.8	1.1	0.6	0.8	0.2	0.9	4.5	0.9	0.0
Mean	6.6	4.4	3.9	3.2	0.9	11.2	8.7	2.7	1.2
Max.	7.2	7.4	8.0	6.4	1.8	24.7	13.5	5.8	4.0
SD.	0.4	2.2	2.8	2.0	0.5	6.7	3.1	1.4	1.2

Min = minimum value, Max = maximum value, SD = standard deviation

Perturbed plot

The Charge Balance Error (CBE) has been calculated for 11 samples of which 5 had positive CBE and 6 negative CBE (see Appendix E1, Table E1-1). CBE ranged from a minimum of 8.3% to a maximum of 11.6%. If the relative errors are within ±10% they are considered acceptable.

The dominant cation in the overland flow water was Ca^{2+} (2.2 to 8.4 mg/l), followed by Na^+ (2.0 to 9.5 mg/l), K^+ (1.9 to 9.3 mg/l) and Mg^{2+} (0.6 to 2.7 mg/l).

HCO_3^- ranged from 3.5 to 30.5 mg/l, followed by Cl^- of 6.4 to 17.1 mg/l. SO_4^{2-} ranged from 1.7 to 12.3 mg/l and NO_3^- 0.5 to 4.5 mg/l.

The chemical composition of the overland flow water for the perturbed plot is predominantly calcium-bicarbonate-sodium-chloride type of water with the following ionic sequences:

$$Ca > Na > K > Mg$$
$$HCO_3 > Cl > SO_4 > NO_3$$

Control plot

The Charge Balance Error (CBE) has been calculated for 13 samples of which 8 had positive CBE and 5 negative CBE. From the Appendix E1: Table E1-2, CBE ranged from a minimum of 10.6% to a maximum of 11.2%.

The dominant cation was Na^+ (1.1 to 7.4 mg/l), followed by K^+ from 0.6 to 8.0 mg/l. Ca^{2+} ranged from 0.8 to 6.4 mg/l and Mg^{2+} from 0.2 to 1.8 mg/l.

HCO_3^- ranged from 0.9 to 24.7 mg/l, followed by Cl^- of 4.5 to 13.5 mg/l. SO_4^{2-} ranged from 0.9 to 5.8 mg/l and NO_3^- 0.0 to 4.0 mg/l.

The chemical composition for the control plot in the overland flow is predominantly sodium-bicarbonate-potassium-chloride type of water with the following ionic sequences:

$$Na > K > Ca > Mg$$
$$HCO_3 > Cl > SO_4 > NO_3$$

Figure 7-1 illustrates the percentage contribution of each ionic constituent in the overland flow water to the total ionic mass. The highest contribution had HCO_3^- then Ca^{2+} with 32.9% and 10.7% of the total ionic mass of the perturbed plot. For the control plot, HCO_3^- contributed with 31.4% and Ca^{2+} with 8.8%. The proportions of Cl^- and Na^+ are 20.4% and 9.5% of the total ionic mass for the perturbed plot, while for the control plot were 24.6% and 12.5%. The proportion of Mg^{2+} was accounted as very low (~2.5%).

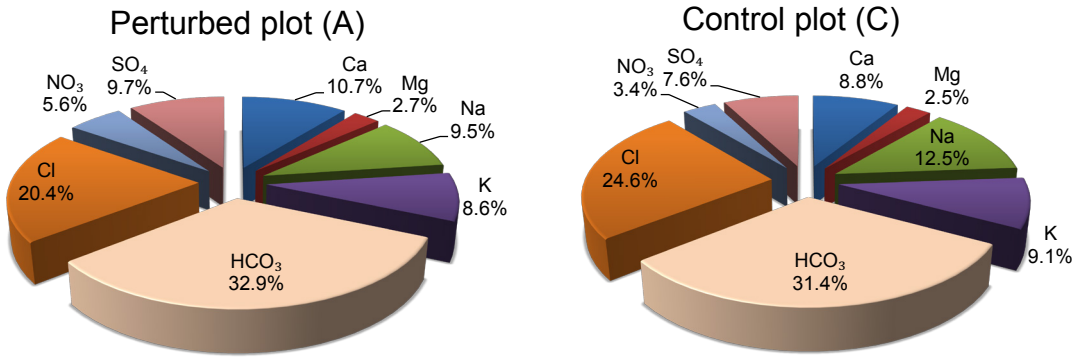

Figure 7-1 *Percentage contribution each ion to total ionic mass in the overland flow water*

Table 7-2 summarises the statistical analysis of the soil water concentrations of the perturbed and control plots, collected at 10 and 18 cm soil depth. The pH of the soil water varied in the range 5.7 - 7.4 indicating slightly acidic to a neutral type.

Perturbed plot – soil water at 10 cm depth

The dominant cation in the soil water at 10 cm soil depth was Ca^{2+} (6.6 to 9.4 mg/l), followed by Na^+ (0.5 to 6.9 mg/l), Mg^{2+} (1.0 to 2.7 mg/l) and K^+ (0.8 to 2.1 mg/l).

HCO_3^- varied from 5.2 to 9.1 mg/l, followed by Cl^- of 1.9 to 16.7 mg/l, SO_4^{2-} from 1.2 to 7.3 mg/l and NO_3^- 0.3 to 5.9 mg/l.

Table 7-2 *Statistical analysis of chemical composition of the soil water (lysimeter sampling) at the both plots during 2009 – 2010 year*

	Soil water at 10 cm depth								
Perturbed plot (A) (n = 5)	**pH**	**Na^+**	**K^+**	**Ca^{2+}**	**Mg^{2+}**	**HCO_3^-**	**Cl^-**	**SO_4^{2-}**	**NO_3^-**
		mg/l							
Min.	6.1	0.5	0.8	6.6	1.0	5.2	1.9	1.2	0.3
Mean	6.5	3.7	1.3	7.4	1.5	6.7	6.2	4.9	2.3
Max.	7.4	6.9	2.1	9.4	2.7	9.1	16.7	7.3	5.9
SD.	0.5	2.3	0.5	1.2	0.7	1.5	18.6	2.5	2.3
Control plot (C) (n =4)	**pH**	**Na^+**	**K^+**	**Ca^{2+}**	**Mg^{2+}**	**HCO_3^-**	**Cl^-**	**SO_4^{2-}**	**NO_3^-**
		mg/l							
Min.	5.7	1.8	0.3	3.8	0.6	3.4	2.1	0.7	0.9
Mean	6.4	2.7	0.4	4.1	0.7	5.7	4.0	3.1	1.4
Max.	7.2	3.5	0.5	4.3	0.7	7.0	5.2	5.9	2.1
SD.	0.6	0.7	0.1	0.2	0.1	1.7	1.4	2.1	0.6
		Soil water at 18 cm depth							
Perturbed plot (A) (n = 10)	**pH**	**Na^+**	**K^+**	**Ca^{2+}**	**Mg^{2+}**	**HCO_3^-**	**Cl^-**	**SO_4^{2-}**	**NO_3^-**
		mg/l							
Min.	5.9	2.1	0.3	2.4	0.5	2.0	1.6	0.9	0.0
Mean	6.4	4.9	0.7	9.4	1.3	8.4	6.3	5.7	1.9
Max.	7.2	11.0	1.4	20.0	2.1	16.9	14.9	13.2	7.5
SD.	0.5	2.9	0.4	5.2	0.6	6.0	4.8	3.9	2.6
Control plot (C) (n =4)	**pH**	**Na^+**	**K^+**	**Ca^{2+}**	**Mg^{2+}**	**HCO_3^-**	**Cl^-**	**SO_4^{2-}**	**NO_3^-**
		mg/l							
Min.	5.8	2.1	0.3	4.1	0.6	1.8	1.7	1.3	0.2
Mean	6.3	2.5	0.4	5.3	0.8	5.1	4.6	3.0	0.5
Max.	7.0	2.9	0.5	6.6	1.0	7.4	7.8	4.8	1.0
SD.	0.5	0.4	0.1	1.3	0.2	2.5	3.2	1.5	0.4

Min = minimum value, Max = maximum value, SD = standard deviation

Control plot – soil water at 10 cm depth

At 10 cm soil depth, the dominant cation was Ca^{2+} (3.8 to 4.3 mg/l), second Na^+ from 1.8 to 3.5 mg/l, third Mg^{2+} from 0.6 to 0.7 mg/l and K^+ from 0.3 to 0.5 mg/l.

Four anions, HCO_3^- dominated in the range of 3.4 to 7.0 mg/l, than Cl^- from 2.1 to 5.2 mg/l, SO_4^{2-} from 0.7 to 5.9 mg/l and NO_3^- 0.9 to 2.1 mg/l.

Perturbed plot – soil water at 18 cm depth

At 18 cm soil depth, Ca^{2+} was dominant cation that ranged from 2.4 to 20.0 mg/l, then Na^+ from 2.1 to 11.0 mg/l. Mg^{2+} ranged from 0.5 to 2.1 mg/l, while K^+ from 0.3 to 1.4 mg/l.

In the case of anions, HCO_3^- ranged from 2.0 to 16.9 mg/l, followed by Cl^- of 1.6 to 14.9 mg/l, SO_4^{2-} from 0.9 to 13.2 mg/l and NO_3^- 0 to 7.5 mg/l.

Control plot – soil water at 18 cm depth

Ca^{2+} was dominant cation that varied from 4.1 to 6.6 mg/l, followed by Na^+ from 2.1 to 2.9 mg/l, Mg^{2+} from 0.6 to 1.0 mg/l and K^+ from 0.3 to 0.5 mg/l.

HCO_3^- ranged from 1.8 to 7.4 mg/l, Cl^- of 1.7 to 7.8 mg/l, then SO_4^{2-} from 1.3 to 4.8 mg/l and NO_3^- from 0.2 to 1.0 mg/l.

The chemical composition of the soil solution collected at 10 and 18 cm soil depth for both plots is the same, predominantly calcium-bicarbonate-sodium-chloride type of water with the following ionic sequences:

$$Ca > Na > Mg > K$$
$$HCO_3 > Cl > SO_4 > NO_3$$

Figure 7-2 illustrates the percentage contribution of ions at 10 and 18 cm soil depth with the highest contribution of HCO_3^- and Ca^{2+} (19.6% and 21.7%) for the perturbed plot. The proportions of HCO_3^- and Ca^{2+} were 25.8% and 18.6% for the control plot, respectively. The proportion of K^+ was accounted as low (1.8 to 3.8%).

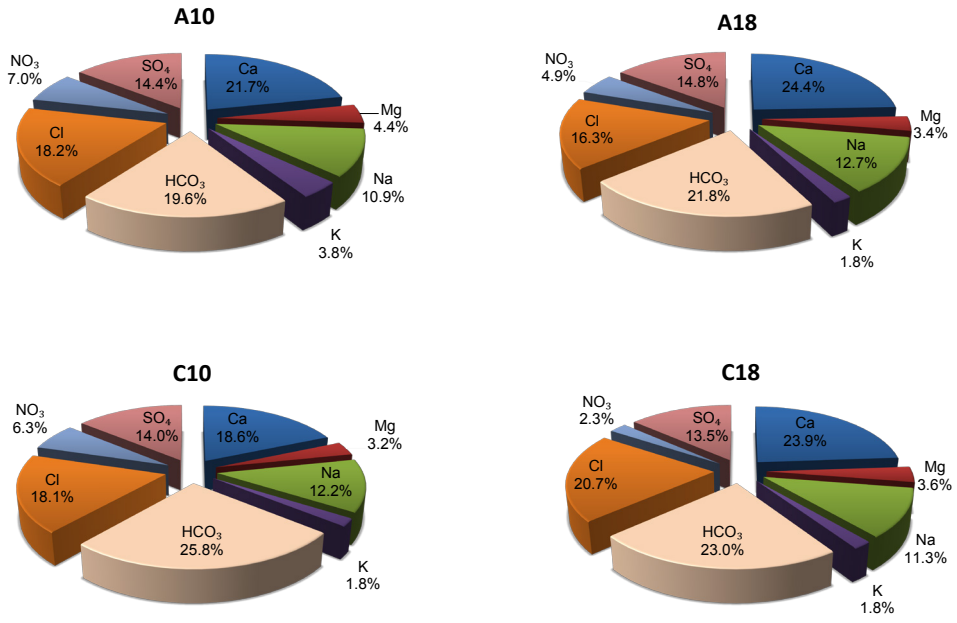

Figure 7-2 *Percentage contribution each ion to total ionic mass of the soil water A: perturbed plot, C: control plot; 10: soil solution at 10 cm depth; 18: soil solution at 18 cm soil depth*

At 18 cm soil depth, the contribution of HCO_3^- and Ca^{2+} was higher for both plots. The proportions of Cl^- and Na^+ were 16.3% and 12.7% for the perturbed plot, while for the control plot were 20.7% and 11.3%. The proportion of K^+ was very low (1.8%). Analysis comparing the mean NO_3^- concentrations for the shallow lysimeter (10 cm) and the deep lysimeter (18 cm) showed that there was the significantly greater the mean NO_3^- concentration in the deep lysimeter for the both plots. For example, O'Reilly et al. (2010) reported that a nitrate concentration of 3.3 mg/l was measured in the lysimeter at the depth of 1.4 m and 0.84 mg/l from the 2.6 m deep well. In this study, the mean

nitrate concentrations were higher under the double rainfall inputs at the perturbed plot (10 cm: 2.3 mg/l; 18 cm: 1.9 mg/l) compared to the control plot under natural rainfall inputs (10 cm: 1.4 mg/l; 18 cm: 0.5 mg/l).

The major ions obtained from chemical analyses of the rainwater, the overland flow water and the soil solution are displayed on a Piper diagram (Figure 7-3). The average chemical composition of the overland flow water and the soil solution had a different chemical signature from the rainwater.

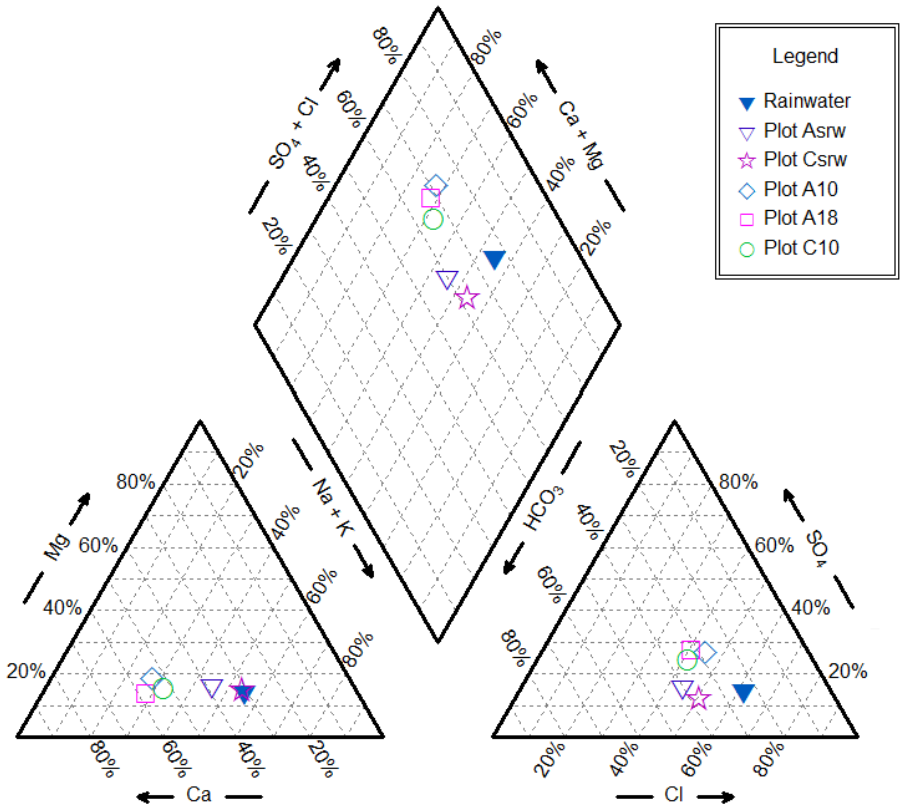

Figure 7-3 *Piper diagram illustrating the major ion compositions in rain, runoff water and soil solution at the control and perturbed plot for total sample days (A: perturbed plot, C: control plot; srw: surface runoff water; 10: soil solution at 10 cm depth; 18: soil solution at 18 cm soil depth)*

The concentration of ions in runoff water was higher than in the rain water (Chapter 5, Table 5-5). There were significant differences in chloride concentrations between the perturbed and the control plot. The highest concentration of chloride in the overland flow water and in the soil water solution of the perturbed plot is likely due to additional inputs of rainwater compared to the control plot under natural rainfall conditions. In general, the highest levels of chloride occurred during the autumn and the winter.

At the hillslope, the linkage between the rainfall water and runoff water chemistry has been observed during the November storm event that is discussed in Section 7.4 with

high conductivity values in the overland flow water at the perturbed plot. For the rest of the events the linkage has not been analysed because an extreme event was needed.

The similar chemical composition of the overland flow water from the perturbed plot was observed with the soil water solution with the following ionic sequences: Ca > Na, while that it is not the case with the control plot (Na > K). The relationship between the chemical composition of the overland flow water from the perturbed plot and the soil solution may be explained by the fact that the mobility of calcium is relatively low, especially compared to cations such as sodium or potassium where loss of Ca^{2+} through leaching is relatively low, especially when it is in the form of lime (Hodges 1995).

Under the saturated water conditions in the soil, the water moves upward and transport nutrients to the upper soil layer where it is most likely to be lost in the overland flow. Several studies have reported a rising water table that transports high nutrient concentrations in the upper soil layer (Hornberger et al. 1994; Boyer et al. 1997; van Verseveld 2007). The major research limitation of this study was the failure to collect and analyse the data of the water table and hydraulic gradient using tensiometers.

From the chemical composition, the major cation in the overland flow water for the perturbed climate conditions is Ca^{2+}, and for the control climate conditions is Na^{+}, while the major anion beside HCO_3^{-} is Cl^{-} for both conditions. Na^{+} and Cl^{-} probably reflect primary recharge from the rain. Since residence time is so short and there is a little contact between the soil and the flowing water, then the solute content in the overland flow will be low and will retain the characteristics of rainfall (Burt and Pinay 2005). Further evidence for this statement is discussed in Section 7.4.

The concentration of potassium ion (K^{+}) was in the same decreasing order: overland flow > soil solution collected at 10 cm > solution collected at 18 cm as reported by Tsai et al. (2010). He also suggested that the highest K^{+} concentration in the overland flow could be attributed to the decomposition of litterfall at soil surface. In Tsai's study, Sposito (1984) and Grimaldi et al. (2004) suggested that lower concentrations of K^{+} ion in soil solution was the result of easily absorbed and reused K^{+} ion by plant roots. The concentration of $Cl^{-}$and Na^{+} for the perturbed plot was in following order: overland flow > solution collected at 18 cm > soil solution collected at 10 cm. For the control plot Cl^{-} ion had the same order as the perturbed plot but for Na ion was: overland flow > soil solution collected at 10 cm > solution collected at 18 cm. Higher content of Cl^{-} and Na^{+} in the overland flow suggests that the rainwater significantly affects the overland flow

and the soil solution chemistry. For the perturbed plot, Ca^{2+} and Na^{+} were dominant cations, while for the control plot Na^{+} and K^{+} were dominant. The concentration of Ca^{2+} ion was in following order: solution collected at 18 cm > soil solution collected at 10 cm > overland flow. The presence of Ca^{2+} reflects the lithology, the source of Na^{+} reflects rain input, while K^{+} reflects lithology or fertilizer input. Comparisons between the concentration of ions in the overland flow and soil solution showed that obviously the lower content of cations and anions in soil solution at 18 cm suggest that the strong leaching effects occur. Mulder and Cresser (1994) reported that the chemistry of soil solution may vary considerably through the year of a given soil horizon, due to (i) a variable composition of infiltration water, (ii) variability in climatic conditions, and (iii) variability in biological activity. Sulphate concentrations changed very little during the observation period at both plots, probably due to sorption within the soil.

Water quality was very good as indicated by the low concentrations of nutrients and no pollution that could percolate into groundwater. Although the number of samples taken before, during and after enhanced rainfall treatment is limited on monthly point value, the data show a marked difference between two climate conditions, the perturbed and unchanged rainfall conditions. The sum of anions and cations (total dissolved solids) was higher for the perturbed climate conditions.

In this study, it was considered that some sources of error or uncertainties can occur, such as: (1) the limitation of sampling number and replication, (2) the difference of spatial distribution of soil properties between the two plots, (3) the input of precipitation and loss as output of evaporation.

The results of the runoff experiment indicate that rainfall and changes in the dominant stormflow pathways were the most significant factors affecting differences in the ion concentrations between the two plots. This study has demonstrated the usefulness of available chemical data for understanding the overland and subsurface flows water quality and important implications for developing appropriate conceptual models.

7.3 Variation in total dissolved organic carbon (DOC) and nitrate (NO_3) concentrations at the hillslope

Dissolved organic carbon (DOC)

Several researchers have investigated the influence of the climatic variables on the DOC concentration, with the primary focus on temperature (Freeman et al. 2001b), and

precipitation (Tranvik and Jansson 2002). An increase in the total dissolved organic carbon (DOC) concentrations in runoff in terrestrial ecosystems has been considered by others. Naden and McDonald (1989) in northern England and Neal et al. (1997) in Wales linked the climatic factors such as increased temperatures and dry periods to the DOC. However, more work is necessary to unravel variations in the DOC concentrations in the overland flow and the soil solution. This is possible by linking the flow to the climatic factors of the dry, wet and transition periods and comparison between the plots. In this section, the data from the field will potentially help to unravel the principal variations of the total dissolved organic carbon relate to the enhanced and the natural rainfall conditions.

The water samples of the runoff were collected as the monthly point values from July 2009 to August 2010. To investigate variations in the DOC concentrations, firstly monthly point values of the DOC concentrations were compared between the two plots, then between the overland and the subsurface flow water.

Figure 7-4a shows the DOC concentration in the overland flow for both plots perturbed (A) and control (C), while the mean concentrations for each season are presented in Table 7-3.

Table 7-3 *Mean concentrations of DOC in the overland flow for the perturbed and control plots separately shown for each season (dry, wet and transition)*

Season	Perturbed plot (A)	Control plot (C)
	DOC (mg/l)	
Dry	17.1	17.6
Wet	9.6	12.4
Transition	14.1	13.8

The DOC for the perturbed plot during the dry period ranged from 15.9 to 18.2 mg/l, the wet period from 8.54 to 11.2 mg/l and the transition period from 9.3 to 22.9 mg/l. For the control plot, the DOC ranged during the dry period from 16.4 to 18.8 mg/l, the wet period from 3.8 to 16.0 mg/l and the transition period from 6.2 to 23.9 mg/l (Appendix E2, Table E2-1). The DOC concentration at the perturbed plot with the intensified rainfall was 23% less than the concentration at the control (natural) plot. From the results, the average DOC concentration tended to be highest in the dry period and the lower in the wet period.

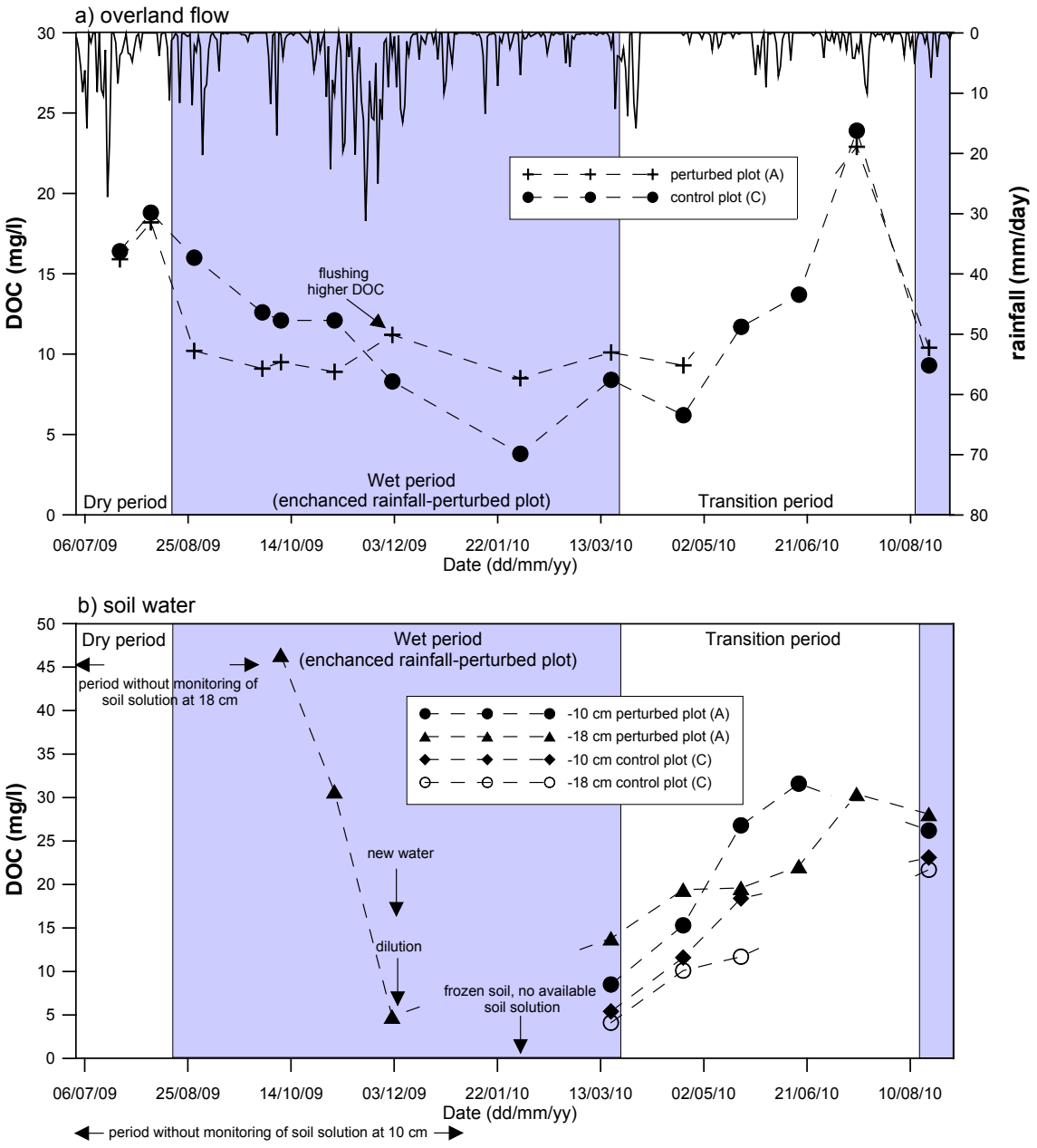

Figure 7-4 *Comparison of DOC concentration in a) overland flow and b) soil solution between plots*

The results corresponding to the DOC export for the whole period of the analysis are reported in Table 7-4. It is clear that the use of the limited number of the soil water samples in this case may present some difficulty in estimating of the DOC and the NO_3^- losses through the subsurface flow. The export of C is estimated at the soil depth of 18 cm where the subsurface flow was monitored. Multiplying the overland flow by the flow-weighted, the DOC concentration showed C loss of 9.7 kg C/ha for the intensified climate condition compared to 5.8 kg C/ha for the unchanged climate conditions. This approach assumes that in the case of the subsurface flow, the C loss was 22 kg C/ha for the intensified climate condition. It was not possible to estimate the C loss through the subsurface flow for the unchanged climate conditions. At the perturbed runoff plot, the

wet period includes the enhanced rainfall and the large flood event in November 2009 that influenced the high losses in the DOC by the overland and the subsurface flows.

Table 7-4 *Amount of C export in runoff*

Period	Total Dissolved Carbon (kg/ha)	Total Dissolved Carbon (mg/l)	Flow (mm)
Perturbed plot – overland flow			
Dry	4.8	17	28
Wet	9.7	9.6	100
Transition	2.6	14	16
Control plot – overland flow			
Dry	4.7	18	26
Wet	5.8	12	48
Transition	1.1	14	8
Perturbed plot – subsurface flow			
Dry	N/A	N/A	N/A
Wet	22	28	80
Transition	4.4	19	23
Control plot – subsurface flow			
Dry	N/A	N/A	N/A
Wet	N/A	N/A	N/A
Transition	1.1	10	11

N/A not available

Before the enhanced rainfall treatment (dry period), the DOC concentrations in the overland flow water between the two plots were not significantly different, but there are differences in the carbon loss during the wet period. Under the enhanced rainfall treatment (wet period) at the perturbed plot, the C losses are lower in the overland flow (9.7 kg/ha) compared with the subsurface flow (22 kg/ha). This indicates enhanced loss of the DOC by the subsurface leaching pathway relative to losses through the overland flow. Worrall et al. (2002) reported that the soil flow paths are the greatest source of DOC to streams, and the flow path which is followed is dependent on the intensity and length of the rainfall, and the time period since the previous rainfall. Stevens et al. (1999) demonstrated that nutrient and cation transport via the subsurface lateral flow varies between hillslope position and rainfall events where environmentally significant amounts of nitrate and dissolved organic carbon moved as the subsurface lateral flow via macrospores.

The DOC concentration in the overland flow generally decreased during the wet period for the both plots due to dilution. At the start of the wet period, the DOC concentration in the overland flow at the perturbed plot showed a lower concentration compared to the control plot (Figure 7-4a). The difference between the two plots of approximately 22% for the wet period can be attributed to the climatic conditions, as on the perturbed plot there was double input of rain that caused the lower DOC concentration and the higher DOC loss. However, surprisingly, the DOC concentration did increase progressively

with the increase in the rate of rainfall input (Figure 7-4). As can be seen from Figure 7-4 during the winter period the relative magnitude of the DOC was changed. This can be explained by the "flushing theory", which suggests that the DOC accumulates underneath the snow during the winter and during the snowmelt waters move through the soil where DOC is rapidly flushed into streams. O'Riley (2012) also supported the "flushing theory" and pointed to a lack of understanding of what controls DOC dynamics during the snowmelt period.

During the dry period, the soil solution from lysimeters was not available for the both plots. As can be seen in Figure 7-4b, the high rainfall events significantly decreased the DOC concentration measured at the soil depth of 18 cm. At the perturbed plot, the DOC concentrations sampled with lysimeters from 10 and 18 cm deep soil over the total observed period ranged from 8.5 to 31.6 mg/l and 4.8 to 46.4 mg/l (Appendix E2, Table E2-2). The DOC concentrations sampled at the control plot (unchanged climate conditions) from 10 cm and 18 cm deep soils showed the DOC concentrations from 5.4 to 23.1 mg/l and from 4.1 to 21.7 mg/l. Overall, the soil solutions were increased during the transition period, and started to decrease in the second wet period. On the hillslope, the concentration of the DOC in the soil solution at 10 cm during the transition period was low compared to the soil solution at 18 cm (decrease with soil depth) where it surprisingly started to increase and was higher than the soil solution at 18 cm. About the case of the DOC concentrations decrease with the soil depth, the literature is in agreement (e.g. Thurman 1985; Allan 2001; Gundersen 2012) where loss of the DOC is attributed to the combination of the three processes; biodegradation, adsorption, and decreasing the concentration of SOM with depth.

In the soil water solution, the DOC originated from the decomposition of the organic matter together by leakage of metabolites from plant and microbial cells (Christ and David 1996; Kalbitz et al. 2000; Yano et al. 2004), and it is removed largely by adsorption in the mineral soil (Qualls and Haines 1992). Figure 7-4b shows for December 2009 the low DOC concentration in the soil solution sampled at 18 cm soil depth. This suggests that during the wet conditions, the 'new' water moves vertically through the soil and dilutes the 'old' water where the soil perched water table may have risen into more permeable shallow subsurface and surface horizons. According to this, the soil perched water table rises, concentrated soil solution is displaced from the deep to the upper soil layer. It was found, as did McGlynn and McDonnell (2003), that the DOC concentration of the hillslope runoff was a mixture of shallow high DOC soil

water and deep low DOC mineral soil water. During the autumn and the winter period, probably most of the DOC infiltrates through the soil vertically and flows laterally through deep soil layer. Taken together, these results suggest that the intensity of rain is an important factor controlling the flushing of the DOC.

Figure 7-4 shows an increase trend in the DOC concentrations during the transition period suggesting a temporary dilution of the soil carbon pool that was released to the overland flow of the previous storm events. The highest DOC concentration in the overland flow was observed after the long dry period in July 2010 during the summer period. This was observed at the field in the tipping bucket that collected the overland flow water at the perturbed plot. The increase of the DOC led to an enhanced water colour similar to dark tea (Figure 7-5). The reason for such an increase is believed to be due to the long dry period and low precipitation that prevents the transport of the DOC to the deeper soil layer, which therefore leads to accumulation of the DOC in the upper soil layer (around 10 cm, 32 mg/l; 18 cm, 22 mg/l). After the dry period, the first intense rain events probably caused slow flow where soil TOC is increasingly flushed through the system, leading to increases in the DOC.

The high DOC concentrations in the overland and the subsurface flows during the transition period were probably the result of the dry climate condition and the low antecedent wetness condition. This suggests a build-up of labile organic material in the upper soil layer because of incomplete decomposition and lack of the flushing.

Figure 7-5 *Water colour of the overland flow in the DOC from the perturbed plot, July 2010*

The different seasonal and climate conditions indicate the significance of variations in the solute signatures for different flow process during the wet or dry periods. The DOC concentration was generally higher during the summer in the overland flow and lower during the winter. These increases during the summer or dry periods have been reported

in many studies (de Wit and Wright 2008; Köhler et al. 2009; Sebestyen et al. 2009; Ågren 2010).

It is concluded from this study that the flushing mechanism generates the higher DOC concentrations during the summer rains (storm) events compared to the wet periods. It is important to understand the factors that influence increasing of the DOC concentration that lead to higher loads of organic matter in the surface water and increasing colouring. This could have implications for drinking water quality in some areas.

Nitrate (NO_3^-)

The effect of climate on the concentration and fluxes of nitrate is studied by many researchers, with the influence of climate for biological, chemical and physical processes which determine N cycling and losses (Howden and Burt 2008, 2009; Jones and Smart 2005; Monteith et al. 2000; Zhang and Schilling 2005; Odoux et al. 2010). For example, Odoux et al. (2010) report in their study that climate can govern two kinds of processes: 1) soil processes related to the mineralisation of organic soil nitrogen, for which soil temperature and wetness are the main climatic drivers - these processes play an important role in leaching rates of nitrate because small imbalances between inorganic nitrogen availability in the soil and biological uptake may lead to marked changes; and 2) hydrological processes, mainly driven by effective rainfall that can couple or uncouple the nitrate supply and its leaching in time and space.

Figure 7-6a shows the NO_3^- concentration in the overland flow for both plots, while the mean concentrations for the each period are presented in Table 7-5. The NO_3^- concentrations in the overland flow are different between seasonal periods (dry, wet and transition period).

Table 7-5 *Mean concentrations of NO_3^- in the overland flow for the perturbed and control plot separately shown for each season (dry, wet and transition)*

Season	Perturbed plot	Control plot
	NO_3^- (mg/l)	
Dry	1.3	1.2
Wet	3.3	3.1
Transition	0.5	0.3

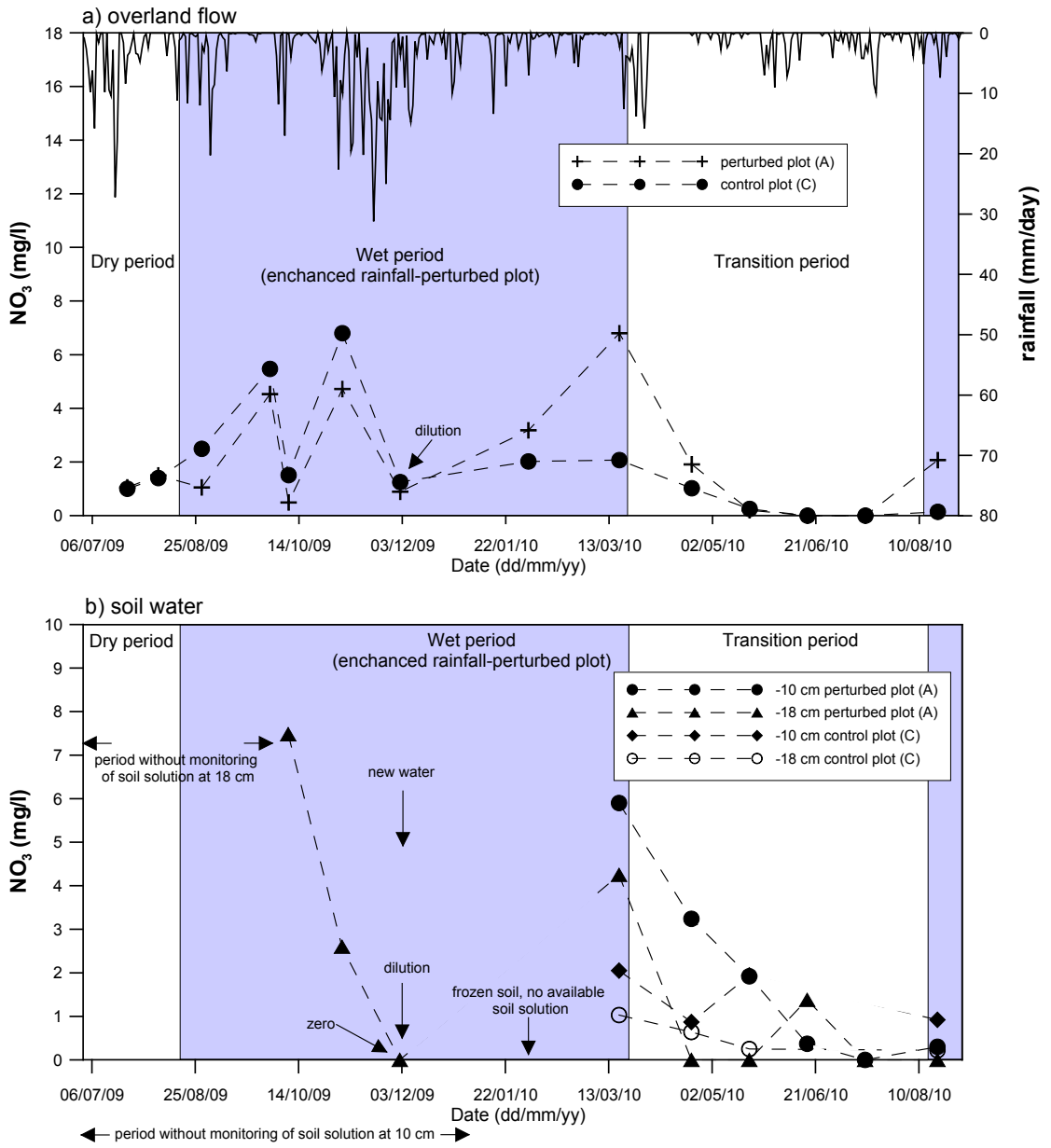

Figure 7-6 *Comparison of NO_3^- concentration in a) the overland flow and b)soil solution between plots*

The NO_3^- in the overland flow of the perturbed plot during the dry period ranged from 1.1 to 1.5 mg/l, during the wet period from 0.5 to 8.0 mg/l and the transition period from 0.2 to 1.9 mg/l. For the control plot, the NO_3^- ranged during the dry period from 0 to 1.4 mg/l, during the wet period from 1.3 to 5.5 mg/l and the transition period from 0 to 2.1 mg/l (Appendix E2, Table E2-1).

The NO_3^- concentrations were generally higher in the wet period, and lower during the dry and the transition period, which is the opposite of the DOC concentration trend. There is also obvious variation in the NO_3^- concentration during the wet period; the high intensity of rain decreased the NO_3^-, while the low intensity increased the NO_3^- concentration. Hodges (1995) report that leaching occurs when inorganic forms of N,

particularly nitrite (NO_2^-) and nitrate (NO_3^-) are solubilized and carried by water through the soil profile or by the overland flow.

The results in the NO_3^- losses corresponding to the whole period of the analysis, and they are reported in Table 7-6. The N loss from the perturbed plot was 3.3 kg N/ha as compared with 1.5 kg N/ha from the control plot during the wet period in the overland flow. As mentioned before it is difficult to estimate the NO_3^- losses through the subsurface flow as the number of the soil solution samples was limited.

Table 7-6 *Amount of N export in flow*

Period	Nitrate (kg/ha)	Nitrate (mg/l)	Flow (mm)
Perturbed plot – overland flow			
Dry	0.4	1.3	28
Wet	3.3	3.3	100
Transition	0.1	0.5	16
Control plot – overland flow			
Dry	0.3	1.2	26
Wet	1.5	3.1	48
Transition	0.02	0.3	8
Perturbed plot – subsurface flow			
Dry	N/A	N/A	N/A
Wet	1.8	3.4	80
Transition	0.09	0.4	23
Control plot – subsurface flow			
Dry	N/A	N/A	N/A
Wet	N/A	N/A	N/A
Transition	0.06	0.5	11

N/A not available

Before the enhanced rainfall treatment (dry period), the NO_3^- concentrations in the overland flow water between two plots are not significantly different. Under the rainfall treatment (wet period), the N losses were higher in the overland than the subsurface flows. This suggests that during the enhanced rainfall treatment more N was available to be lost in the overland flow once the soil was saturated. Furthermore, significant differences in the N loss were found between the perturbed and the control plot that received no enhanced rainfall during the transition period in the overland flow. There is the difference in the nitrate loss between conditions before (dry) and during rainfall (wet) treatment, with more N lost during the wet period in the overland flow. It is suggested that the nitrate export is higher in the subsurface flow during the dry period through leaching. That means that high concentration of the nitrate occurs in the deeper part of the soil. Infiltration of water dilutes nitrate concentration, which is the reason for low concentrations during the wet period in the subsurface flow and high in the overland flow. According to Tables 7-5 and 7-6 the nitrate concentrations do not differ

much between the perturbed and control plots and the difference in loads is a result of the different flows.

In November and December, overall the concentrations were much lower. A dilution phase was evident, but again concentrations increased for the enhanced climate conditions during the wet period. The control plot also indicates the concentration decrease during the storm event with an increase during the wet period but now lower in concentration compared to the perturbed plot. The monthly changes were observed in the NO_3^- concentrations in the soil solution at 10 cm and 18 cm depth for both plots collected from lysimeters (Figure 7-6b). The NO_3^- concentrations at 10 cm depth varied from 0 to 5.9 mg/l for the perturbed plot, and 0.9 to 2.1 mg/l for the control plot. In the case of 18 cm soil depth, the soil water in the NO_3^- concentration varied from 0 to 4.3 mg/l for the perturbed plot, and from 0.2 to 1.0 mg/l for the control plot. The mean values of the NO_3^- concentrations in the soil water collected from the perturbed plot at both depths were higher than collecting those from the control plot. The mean nitrate concentrations in flow are considered as 'very low' (<5 mg/l as NO_3^-) (EA 2006).

In this study, the results showed that nitrate content in the overland flow and the soil water solution collected at 10 and 18 cm depth decreased at the end of the transition period, and increased with the establishment of the rainy season and the second wet treatment (Figure 7-6). During the wet period, the NO_3^- concentrations in the overland flow were higher on the control plot than on the perturbed plot. As a result, at the perturbed plot the soil water concentration in the NO_3^- simply decreases with apparent dilution as rainwater increases.

It is assumed that increased the NO_3^- in the overland flow concentration in the winter was due to high NO_3^- contribution from the melting snowpack that is consistent with findings of Inamdar and Mitchell (2006). These can be explained by several processes in the cycling of nitrogen in snow pack and snowmelt; firstly with the wet and dry deposition of atmospheric nitrogen, and secondly with freeze-thaw cycles that led to increasing nitrogen in the bottom layer of snow pack (Hafich 2010). The process of melting produces water mobilization of solutes downward with a moving wetting front, while freezing process produces an increase of nitrate concentrations at the wetting front (Hafich 2010). Therefore, after several cycles of thawing and freezing, the higher concentrations of nitrate were present in the deeper snow pack layer that led to extreme nitrate concentrations in the first flush of melt water (Kuhn 2001; Hafich 2010). The

nitrogen deposition and the movement occurs above ground in the snow, while in the soil nitrogen cycling by nitrification and mineralization of organic N in soils when N availability exceeds the uptake by micro-organisms and plants. This N mineralization and nitrification produce available pools of the NO_3^- in the soil, which happens in the winter, the early spring, and the autumn when vegetation is dormant (Lepori et. al. 2003, Hafich 2010). Creed and Band (1998) found that the NO_3^- peaks on the rising limb of the hydrograph and attributed this pattern to flushing of the NO_3^- from surface soils by rising water tables. In this study, on April 2010, a rain event shows a dilution trend in the NO_3^- concentration, while it was not apparent for two previous rain events in September and November 2009 (Figure 7-6).

The monthly variations in the NO_3^- concentrations of the soil solutions were very similar for both plots showing an increasing trend during the wet period. During the dry period there was the opposite situation, as the NO_3^- concentration decreased. During the wet period, the NO_3^- was the highest just below the ground surface at approximately 10 cm and then decreased with depth into the soil profile. The soil water concentrations in the NO_3^- during the transition period of June and July were not detected and/or have a zero value for both plots. It is assumed that is due to dry climate conditions.

During the second wet period, the NO_3^- concentration in the overland flow for the perturbed plot slightly increases in comparison to the soil solution. This suggests that large amounts of the NO_3^- may have accumulated in the deeper soil layers during the transition period (a prolonged dry period), and the first significant rains with the soil saturation trigger export of the NO_3^- upward. This statement was based on the field evidence and the results presented later in the text (Chapter 8) that indicates depletion of total nitrogen (TN) at deeper soil layers (20-30 cm) during the wet condition. This finding is in agreement with findings of Ritter and Bergstrom (2001) who found the high concentration of NO_3 both in the overland and subsurface flows due to the large pool of the NO_3^- contained in the soil medium. Iqbal (2006) reported that after irrigation in a field in China, the nitrate concentration leachate of 30 cm soil layer was higher than that of 60 cm, and the concentration of nitrate leaching at the five N treatments through the two depth soil layer came into the same level. This is in agreement with findings from this study.

The DOC and the NO_3^- concentrations in the soil water solution were highest from just below the organic layer at 10 cm and decreased with depth into the soil profile

(Figures 7-4 and 7-6). This is in the line with findings of van Verseveld (2007) which suggests a net release of both the DOC and N from the organic layer with net removal of the DOC and N from solution below the organic layer. Similar to observations of van Verseveld (2007), the upper mineral soil (0-10 cm) was the largest source of the DOC and N, which is also in agreement with findings of Yano et al. (2004).

The flow characteristics of the November flood event (E3) as well as the DOC and the NO_3^- export are summarized in Table 7-7. The other events E1 and E5 were not included here as data were not available for the DOC and the NO_3^-. The values for concentration were calculated using an interpolation method.

To identify how specific hydrological processes control the DOC and the NO_3^- losses during the storm event, the November storm event was chosen. The event extended over one day, 46 mm of precipitation. Table 7-7 shows the DOC as well as the NO_3^- export during the November storm event with the different hydrological pathways for the perturbed plot. For the DOC and the NO_3^- concentrations, estimates are much less certain due to the limited number of the samples and some additional assumptions are made. The DOC and the NO_3^- concentration in flow is assumed to be best described by the interpolation of the flow-only concentrations.

Table 7-7 *Export rates of DOC and NO_3^- during the November storm event at the perturbed (A) and control plot (C)*

Storm event	**E3**
Start date	17.11.2009
End date	18.11.2009
Total precipitation (mm)	46
Overland flow: perturbed plot	
DOC export (kg/ha)	1.6
NO_3^- export (kg/ha)	0.25
Overland flow: control plot	
DOC export (kg/ha)	0.6
NO_3^- export (kg/ha)	0.19
Subsurface flow: perturbed plot	
DOC export (kg/ha)	2.5
NO_3^- export (kg/ha)	0.21
Subsurface flow: control plot	
DOC export (kg/ha)	N/A
NO_3^- export (kg/ha)	N/A

N/A not available

The estimated value of the DOC is generally in line with published data of Smith (2012) who reported the total amount of the DOC exported during the major storm event on 8-11 August 2010 of 2.6 kg/ha during a long-term experiment at the Neal Smith National Wildlife Refuge in Jasper County, Iowa, USA. She did not indicate which flow was dominant. Tang et al. (2011) indicated that the subsurface lateral flow was the dominant

pathway for nitrate export from the hillslope. These authors, however, reported the higher t losses from 1.5 to 2.4 kgN/ha during the observed storm events. Many factors can affect the nitrate leaching such as the soil physical and the chemical properties and the weather conditions. From Table above, the DOC export to surface water is facilitated by the subsurface flow during the storm event, while the NO_3^- export is dominated by overland and subsurface storm flows. McGlynn and McDonnell (2003) report that subsurface storm flow is responsible for the transport of labile nutrients into surface water bodies. The N loss in the overland and the subsurface flows is almost the same. Transport of nutrients is driven by the surface runoff, which is generated from soils that have low infiltration capacity because of high clay content, high water table, surface crusting and/or shallow bedrock (Czapar et al. 2008). They reported that most of the nutrient losses in surface runoff tend to occur in a few rare events that involve large quantities of runoff (Czapar et al. 2008).

The current study has only examined the monthly point values of the DOC and the NO_3^- therefore it was not possible to estimate the correlation between nutrient (C and N) flux and flow. It is hypothesized that the labile nutrient source of the soil solution is preferentially depleted under an intensified hydrological cycle. This hypothesis is consistent with observations on the role of rainfall intensity and seasonality. These results indicate that rainwater easily accesses the soil where it:

1) dilutes the NO_3^- concentration and during storm events also the DOC,
2) washes away the labile nutrients at deeper soil layers by subsurface flow or
3) in the case of intensified rain events results in rising from the soil water table and moving labile nutrients in the upper soil layer.

The results from the November storm events (Table 7-7) support the hypothesis that the subsurface leaching pathway for nutrient losses from the soil will be enhanced relative to losses through overland flows in an intensified hydrological cycle.

7.4 Electrical conductivity relationship to flow

In the field, measured rainfall had an electrical conductivity (EC) of around 11 μS/cm. It is often assumed that the electrical conductivity of precipitation is similar to that of the overland flow runoff (Gremillion et al. 2000). This assumption can be made because the precipitation has a short residence time and little contact with mineral soils (Weiler et al. 1999; Burt and Pinay 2005). Figure 7-7 presents the electrical

conductivity (EC) of the overland flow that was measured in 15 min intervals. It is apparent from this Figure that there is a significant difference between the two climate conditions in the EC values. The EC in the overland flow reached values of 47 µS/cm for the perturbed and 53 µS/cm for the control plot before the November storm event. For the perturbed plot at the start of the event, the EC decreased to 28 µS/cm due to rainfall flushing then increased to 45 µS/cm, while for the control plot the EC continued to decrease until it reached the EC of rainfall (11 µS/cm). The EC of the overland flow from the perturbed plot reached values of 40 µS/cm during peak discharge of the November 2009 flood event with small variations during the storm event. After the event, the water had EC in the range of 33 to 54 µS/cm for the perturbed plot, while the EC for the control plot reached the EC peak of 29 µS/cm on 19 November 2009 and decreased to 11 µS/cm.

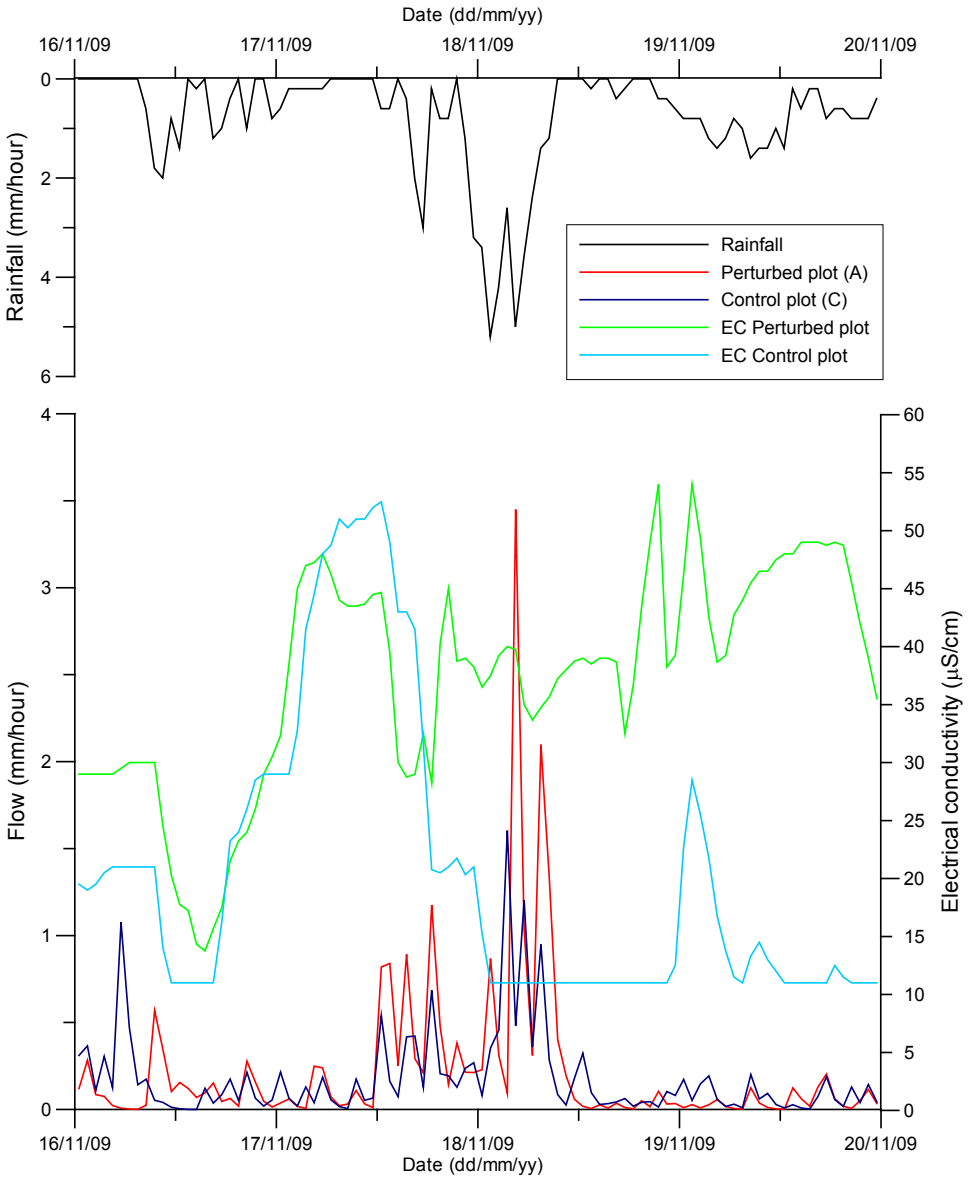

Figure 7-7 *The relationship between overland flow and electrical conductivity during the November 2009 flood event*

A conceptual model of EC flushing is developed for each plot during the storm event and it is presented in Figure 7-8. An increasing conductivity trend was observed in the perturbed plot. The most possible explanation for this increasing trend is that there is a more significant contribution from the runoff rather than from rainfall. It is interesting to note that the EC for the control plot showed increasing and decreasing trends. This suggests the observed decreasing trends reflect the flushing process of rainwater during the rain event and dilution of the total dissolved solids.

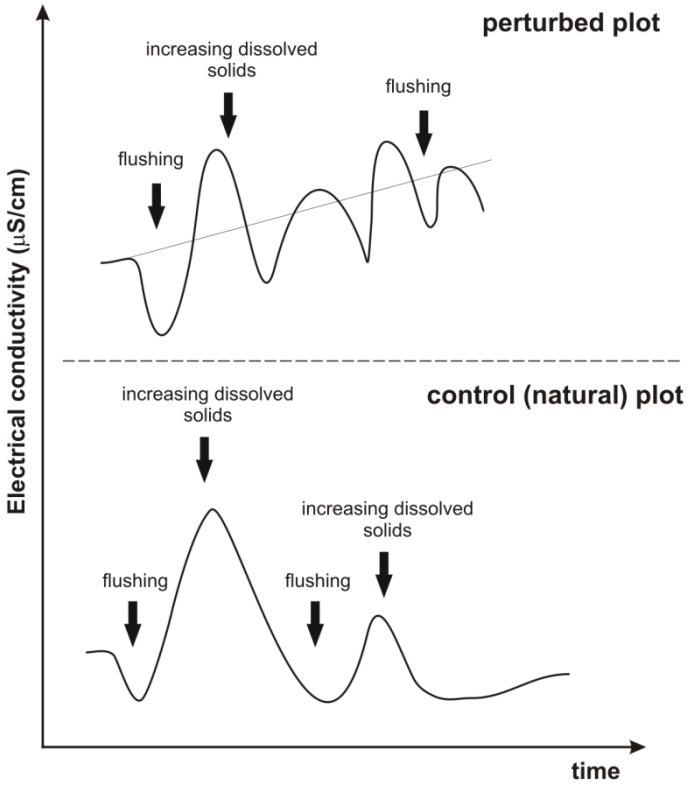

Figure 7-8 *Conceptual model of EC flushing during the storm event*

High values of the electrical conductivity are related to high concentration of dissolved solids. During the storm event, the overland flow transports dissolved material from soils to streams. The overland flow may continue to carry nutrients long after rainfall ends, with low intensity. Langlois and Mehuys (2003) investigated within-storm variations of dissolved nutrient concentrations that were determined in two agricultural fields during four natural rainfall events along with discharge, sediment, antecedent soil water conditions, and nutrient contents. Their results showed that nutrient concentrations increased with time during each event.

The findings of this study suggest that saturation excess overland flow occurred during the largest flood event at the perturbed plot as a result of rain falling on the saturated

plot which, being unable to infiltrate, collects nutrients from the upper soil layer, then runs off downslope and export nutrients (DOC and NO_3^-). The EC at the control plot showed that during large flood events, rainwater flushing nutrients and direct rainwater contributed to the water quality in the overland flow. According to the similarity of the overland flow water and rainfall conductivity values with contribution of increasing dissolved solids in the subsurface flow, it is assumed that mixtures of new and old water indicate the shallow subsurface flow.

The export rate in the DOC and the NO_3^- of the overland flow was smaller for the unchanged climate conditions compared to the intensified conditions (Table 7-7), which is in agreement with the developed conceptual model of the EC flushing during the storm event. The mobilization and transport of nutrients to the stream are driven by the two key factors: soil and hydrological control. The soil is characterized by soil texture, soil structure, nutrient and organic matter status, while hydrological status controls factors indicate whether nutrients are moved or not and which runoff process is dominant in their mobilization to the stream. The finding of this study suggested there are two main runoff processes or pathways: saturation excess overland flow and shallow subsurface flow. The nutrients can be attached to sediment particles in the overland flow or soluble in the subsurface flow. During the mobilization of nutrients their status can be changed in chemical, physical and biological sense before they enter the stream. The nutrient behaviour also depends on the intensity and duration of rainfall, contact between the soil and water, characteristics of the hillslope, land use and grazing intensity.

7.5 Summary

Chapter 7 has improved knowledge of nutrient behaviour at a hillslope scale through water chemistry from samples collected monthly from overland flow and soil solution, with measurement of the DOC and the nitrate concentrations and electrical conductivity of the overland flow.

This study showed that the flushing mechanism generates the higher DOC concentrations during the summer rains (storm) events compared to wet periods. The DOC concentrations were significantly lower during the wet period compared to the dry and the transition period, which is the opposite of the NO_3^- concentration trend. Under the enhanced rainfall treatment (wet period) at the perturbed plot, C losses are lower in

the overland flow compared with the subsurface flow while the N losses were higher in overland than subsurface flows.

It was difficult to estimate the DOC and the NO_3^- export in the subsurface flow due to limited numbers of soil water data. The overland flow was found to be an important feature in the NO_3^- export, while in the case of the DOC the subsurface flow dominated during storm events.

The runoff mechanisms were examined during storm events with electrical conductivity data measured in the field. It was suggested that the two dominant runoff mechanisms at the hillslope scale were (1) saturation excess overland flow and (2) shallow subsurface flow.

Chapter 8. Effects of enhanced rainfall on soil at the hillslope scale

8.1 Introduction

The purpose of this Chapter in the context of different climate conditions is to present i) soil physical and chemical properties, ii) soil carbon and nitrate content and iii) soil C depletion sequence with use of thermal analysis. Sixteen soil cores were used in this study; four of them were from the perturbed (B) and four from the control (C) plot before and after enhanced rainfall or wetting treatment on the soil samples. In the following Tables and Figures, values represent the average of four samples. The soil samples before enhanced rainfall were collected on April 23, 2009 while soil samples after enhanced rainfall were collected on August 19, 2010. Soil samples were also collected on October 8, 2009, but the experimental results did not show a large difference as was expected (data not shown).

Soil samples were taken in dry and wet (during enhanced rainfall test) periods at different depths (10, 20 and 30 cm) from perturbed-sample plot (B) and control plot (C) for analysis of soil nutrients.

8.2 Soil physical properties

Texture

The results of particle size analyses for 'wet' (enhanced rainfall treatment) and 'dry' plots revealed that soils are found to contain more than 80% of sand. The texture of the investigated soils from the perturbed and control plots varied from loamy sand at 0-10 cm and 10-20 cm depth to sandy loam at 20-30 cm depth. A determination is made according to a Particle Size Distribution (PSD) triangle (Chapter 4). Soils are dominated by the sand fraction with 86% in the upper horizons and higher content of finer fractions (silt + clay) at 20-30cm depth (Figure 8-1), which might be due to the translocation of finer particles from the surface soil layers to subsurface layers.

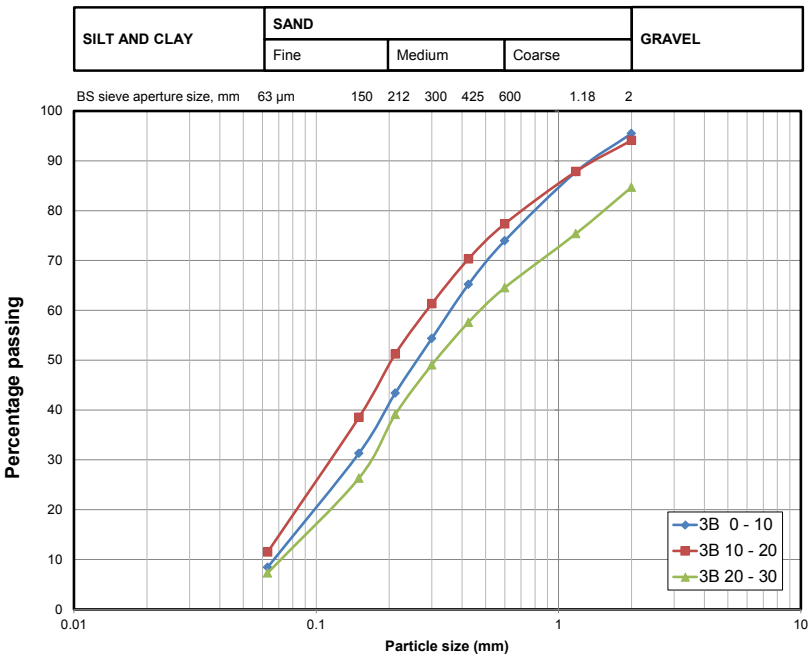

Figure 8-1 *Example of Particle Size Distribution curve for the perturbed plot after wetting*

Bulk density and porosity

The bulk density is dependent on soil texture, the densities of the soil mineral and organic matter. Figure 8-2 shows the density values obtained from the perturbed (B) and control (C) plot. The overall bulk density in the humus horizon varied within the interval 0.60 - 0.83 g/cm^3 with the overall porosity around 60%. According to texture, the loamy sand horizon at the depth of 10 - 20 cm had the bulk density within the interval 1.05 - 1.19 g/cm^3 and the overall porosity 55%. The values of the bulk density in the soil depth of 20 -30 cm are within the interval 1.35 - 1.55 g/cm^3, and those of the overall porosity within the interval 42 - 51%. The bulk density increases with soil depth due to reduced organic matter and aggregation in the subsurface layer compared to the surface layer.

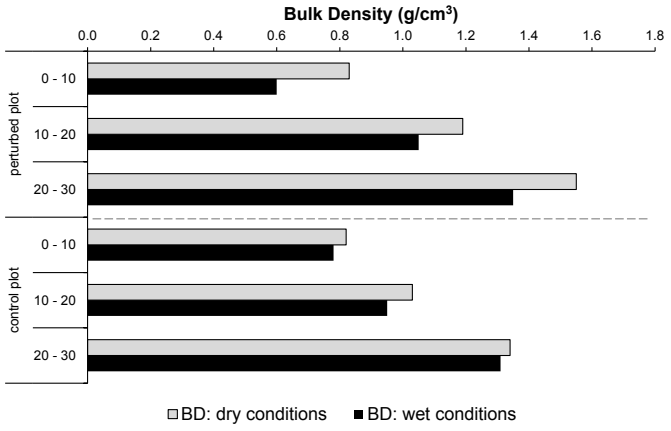

Figure 8-2 *Soil dry bulk density for the dry and wet condition treatments*

In wet condition treatment, the bulk density values are significantly lower compared to dry conditions for the perturbed plot. The additional input of rain indicated as 'wet' treatment on the perturbed plot has significantly affected the soil density and available water capacity of the soil. Soils with lower bulk density have a high proportion of pore space. This suggests that there would be more organic matter content in nutrient-rich soil as a result of the high pore space.

8.3 Soil chemical properties

pH

As can be seen from Figure 8-3, the soil pH of the perturbed and control plots varies with depth. At the perturbed plot without additional rain, soil pH was 6.0, 5.6 and 5.4 at depths of 0-10, 10-20 and 20-30 cm, respectively. The data on the soil pH indicates that soils were found to be moderately to slightly acidic. Soils formed under high rainfall conditions (wet) are more acid than those formed under dry conditions. At lower pH values, reduction reactions take place and vice versa. Therefore, in the process of soil formation, acidity plays a significant role in oxidation-reduction reactions (Dzamic and Stevanovic 2007). The soil acidity is a significant factor in solubility of nutrients in the soil. Lucas and Davis (1961) determined the relationship between pH and availability of important nutrients. They concluded that the ideal pH range (in terms of total nutrient availability) for soil solution is between 5.0 and 6.0.

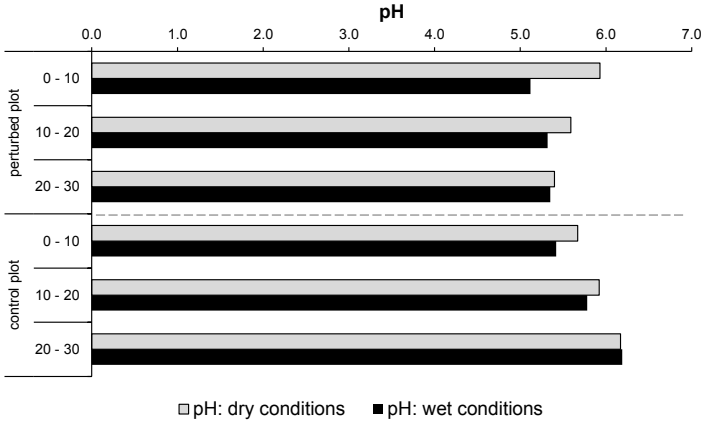

Figure 8-3 *Comparison of the soil pH by depth under dry and wet conditions*

An increase in the pH down the soil profile could be due to leaching of basic cations accumulated in the upper part of the soil profile. Rainfall dissolves nutrients and leaches them from the soil or percolates to deeper soil layers. Nutrient availability varies according to the pH.

Distribution of soil nutrients

Mineral soil was analysed for exchangeable cations by extraction with NH_4NO_3, and total cations by HF. The exchangeable calcium (Ca^{2+}), magnesium (Mg^{2+}) and potassium (K^+) soil values are indicators of the available nutrient level in the soil. The total cations are indicators of weathering-leaching of the soil, showing the extent to which cations have been lost through leaching. Extractable nitrate (NO_3^-) and sulphate (SO_4^{2-}) were also measured by extraction with deionised water.

Adsorptive capacity is one of the most important characteristics of the soil because it reduces leaching of substances from the soil, and so is of great importance for plant nutrition and soil properties.

Exchangeable and total Ca and Mg

Calcium is the major component of lime, dolomite and gypsum. Calcium plays an important role to maintain and increase soil fertility. The soil in which adsorptive complex is saturated with Ca-ion has good physical properties, high adsorption capacity and favourable conditions for the biological and biochemical processes that influence nutrient mobilization from soil reserves (Dzamic and Stevanovic 2007).

Calcium and magnesium are only available to plants in the exchangeable form. Frank (2006a) investigated ideal Ca:Mg:K ratios in soil and he found that considering ratios only of total calcium, magnesium and potassium did not provide a good indicator of available nutrients to plants. He suggested that the exchangeable form of calcium, magnesium and potassium provide better estimate of the soil's ability to provide these nutrients to plants.

The results of the calcium content obtained by the NH_4NO_3 and HF method are presented in Figure 8-4. The exchangeable calcium content of the perturbed plot after enhanced rainfall treatment showed an increased trend at a depth of 0-10 cm of 10%, at the depth of 10-20 cm of 17% and at the depth of 20-30 cm of 9%. The total calcium content of the perturbed plot after enhanced rainfall showed at a depth of 0-10 cm the loss of calcium content of 14%. For the same condition, loss of calcium content was 12% at the depth of 10-20 cm and 12% at the depth of 20-30 cm.

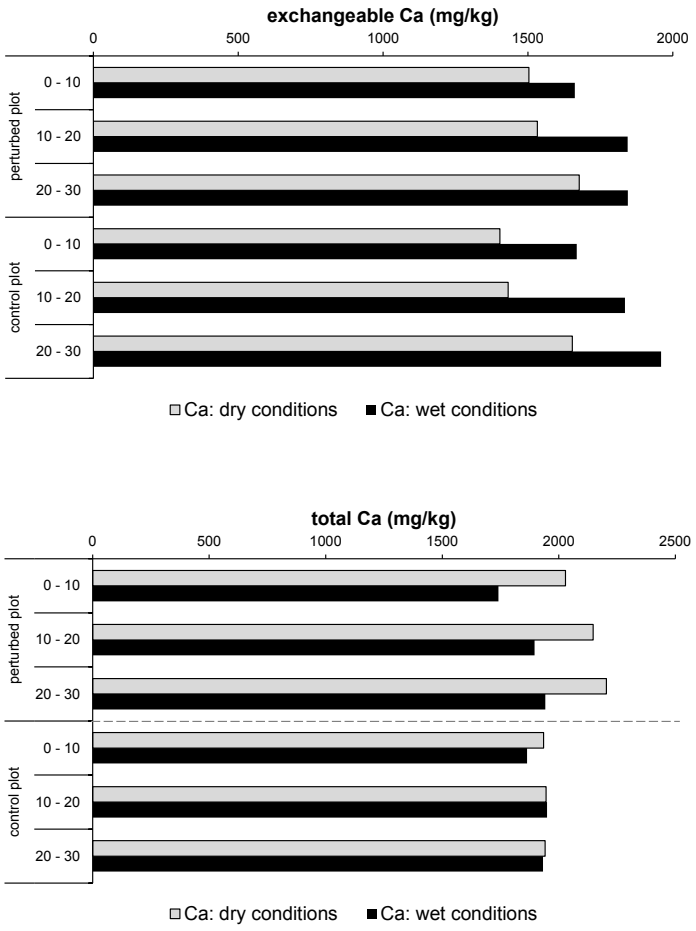

Figure 8-4 *The average content in soil of exchangeable and total calcium*

The content of exchangeable calcium increases with increasing depth. There is a slight increasing trend of total calcium with depth but this trend is not significant. The calcium content of the control plot samples was almost the same for all depths.

Kelling and Schulte (1992) reported that leaching of calcium through soils does not normally occur because of its relatively strong attraction to the surface of clay particles. Calcium is not considered as a leachable nutrient as can be seen in Figure 8-4.

The results obtained from the perturbed plot showed exchangeable Mg loss of 30%, 12% and 4% in 10, 20 and 30 cm soil depth after wetting treatment (Figure 8-5). For the control plot, loss of exchangeable magnesium was 4% and 5% at 10 and 20 cm soil depth, while at depth of 20-30 cm magnesium content was increased for 9%. The total Mg content for the perturbed plot at 0-10 cm soil depth after enhanced rainfall treatment showed 11% of loss (Figure 8-5). The loss of total magnesium content was 7% at the depth of 10-20 cm and 16% at the depth of 20-30 cm. The loss of magnesium was 8% in 0-10 cm depth, an increase of 2% in 10-20 cm and 6% in 20-30 cm soil depth on the control plot.

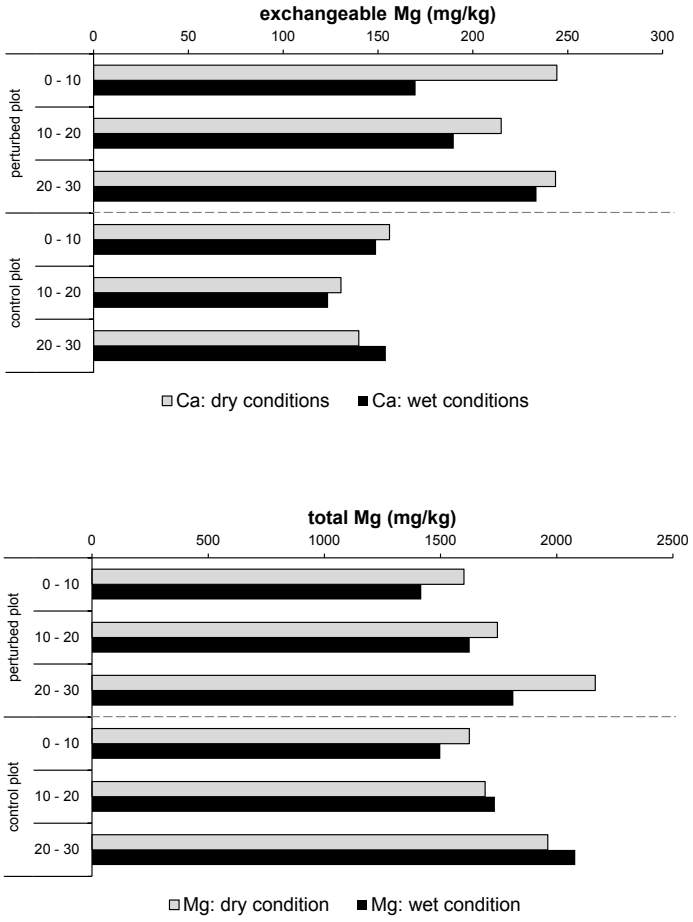

Figure 8-5 *The average content in soil of exchangeable and total magnesium*

The Mg content varies with depth. The results from the perturbed plot were significantly different between dry and wet conditions. The soil calcium and magnesium content is in the range of content found in the literature of Yong at al. (2005). According to some results where no treatment effect was observed as in this study, Schweiger and Amberger (1979) for example calculated average loss of Mg in long term lysimeter experiments of 72 kg/ha in sandy soil and 94 kg/ha in loamy soil. This investigation was carried out in a region with 810 mm of average precipitation.

Exchangeable and total K

The total potassium varies widely in soil, where the total K^+ in the soil is determined by the amount of potassium minerals in the parent material. The potassium minerals during decomposition are transformed into clay minerals (feldspar and mica), where the amount of clay is taken as an indicator of K^+ content. The second source of potassium beside feldspar and mica that makes 98% of potassium unavailable for plants is the nonexchangeable potassium that acts as a reserve source of potassium in the soil and is associated with the 2:1 clay minerals. The third source of potassium is called the

exchangeable potassium or readily available potassium that can be found in layers of clay and it is still very hard for plants to use. However, during wet conditions when the clay holding the potassium becomes wet, readily available potassium is created and it is found on the cation exchange sites or in the soil solution. In this way, potassium is taken up by the plants root system and it is then replaced by the potassium on the exchange sites (McAfee 2008). In summary, soil K^+ exists in four forms in soils: solution, exchangeable, fixed or nonexchangeable, and structural or mineral.

The clay content and types of clay minerals present in the soil strongly affect the behaviour of K^+ in soil, including release, absorption, fixation and leaching (Mengel and Kirkby 1987).

Figure 8-6 shows the rate and direction of reactions between the solution and exchangeable forms of potassium. It indicates whether applied K^+ will be leached into lower horizons, taken up by plants, converted into unavailable forms, or released into available forms (Sparks 2001). Sparks (2001) reports in his study of potassium in soils that the reaction rate between soil solution and exchangeable phases of K^+ is strongly dependent on the type of clay minerals present in the soil (Sivasubramaniam and Talibudeen 1972; Sparks 1980; Sparks and Jardine 1981, 1984) as well of the method employed to measure kinetics of K^+ exchange (Sparks 1989, 1995; Amacher 1991; Sparks et al. 1996; Sparks 2001).

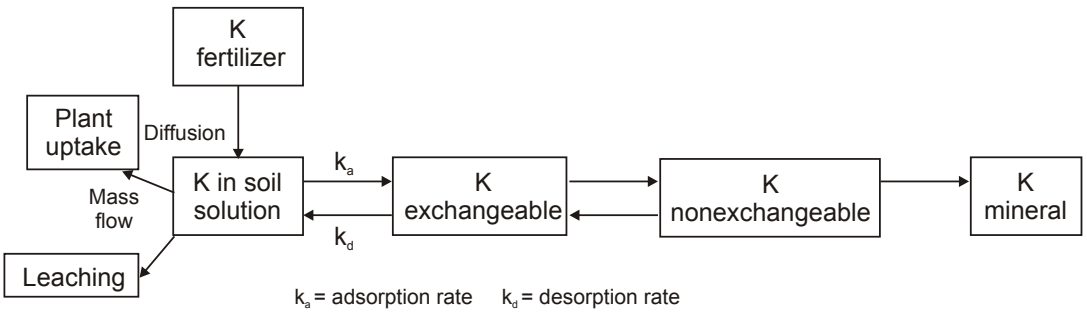

Figure 8-6 *A simple diagrammatic representation of the potassium cycle in soil (source: modified from Sparks and Huang (1985); Mutscher (1995) and modified by the author)*

Many studies have investigated kinetics of K^+ exchange in soils (Sparks and Huang 1985; Sparks 1987; Sparks 2000). For example, Sparks and Jardine (1981) studied K^+ adsorption/desorption on a Matapeake soil from Delaware and they found that potassium desorption was slower than adsorption.

The content of exchangeable K^+ in this study showed the loss of 33% at the 10 cm soil depth after an enhanced rainfall treatment on the perturbed plot. The plot with perturbed

climate conditions did show significant loss (Figure 8-7). A decreasing trend was also recorded at 20 and 30 cm of 34% and 22% K^+ loss. The total K^+ increase with depth that indicates an increase of clay content in the deeper layers of sandy loam and loamy sand as shown in Figure 8-7. Total potassium is an indicator of weathering of the soil, showing the extent to which K^+ has been lost through leaching, erosion of surface soils and removal via plant and animal products (Rayment and Higginson 1992). According to that, the soil test shows 5% of total K^+ loss at the perturbed plot at 0-10 cm soil depth after enhanced rainfall treatment (Figure 8-7). The loss of total potassium content was 2% and 11% at the depth of 20 cm and 30 cm. At the control plot, loss of total potassium was 4% at 10 cm, while at 20 cm and 30 cm soil depth it increased by 3% and 1%. The control plot shows a gain in total K^+ from dry to wet when moving deeper into the soil. The total K^+ varies widely in soil, and therefore soil test values vary greatly (Frank 2006b). Sadusky et al. (1987) reported similar findings of total potassium in loamy sand of Delaware soils, but most of the mineral K^+ was present as K^+ feldspars in the sand fractions. The type of clay minerals present in soils was not investigated as part of this study.

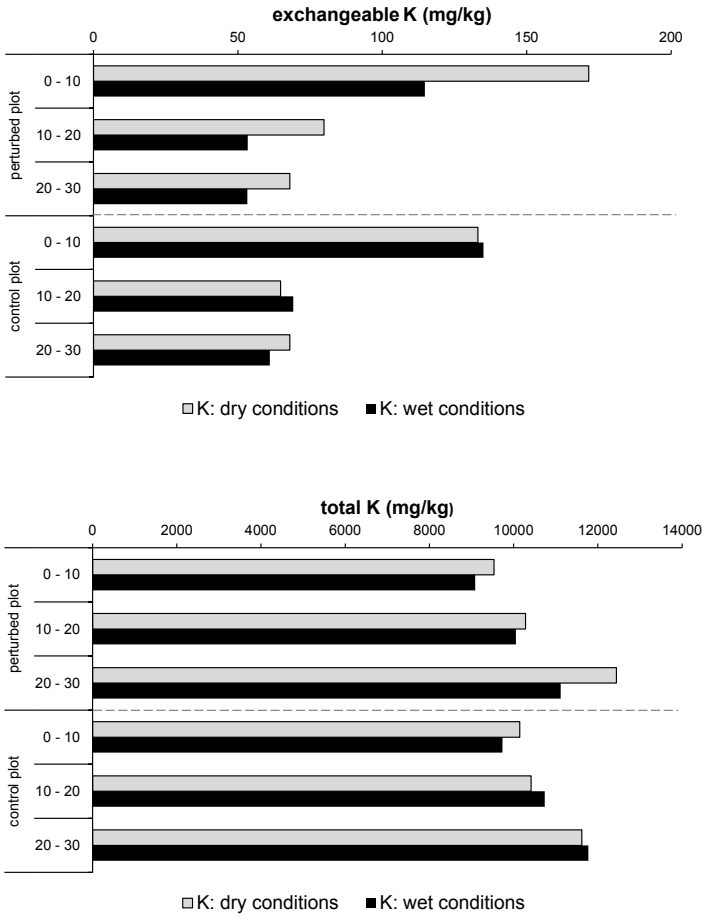

Figure 8-7 *The average content in soil of exchangeable and total potassium*

The K^+ content at all soil depths is in range with those of Allotey et al. (2008) where they measured available exchangeable K^+ levels in soils of clay to silty clay in Ghana in the range from 0.3 to 1.1 cmol/kg. McAfee (2008) reports that excess water can increase the amount of leaching of potassium particularly in sandy soils as opposed to clay type soils with high to very high levels of potassium. This is in agreement with findings in this study of exchangeable K^+ leaching that is expected to have slightly higher leaching in sandy loam and less in loamy sand that contains more percentage of clay minerals.

Sparks (2001) suggests that the amount of clay and soil organic matter (SOM) in the soil strongly influences the degree of potassium leaching. Leaching of K^+ is often a problem in sandy soils, while soils with higher cation-exchange capacity (CEC) have a greater ability to retain added K^+ (Sparks and Huang 1985; Sparks 2001). The content of exchangeable K^+ decreases significantly with increasing depth, while for the total K^+ there is an opposite trend, but this is not significant. For the unchanged climate condition (control plot) at all soil depths, the loss of potassium content was minor which confirmed the influence of additional rainwater at the perturbed plot.

The content of exchangeable Ca^{2+} is up to 10 times higher than those of exchangeable Mg and K^+. The Ca^{2+} and Mg^{2+} is subject to leaching from the surface to deeper soil layers which is in contrast to K^+.

The soil test results suggest that heavy rainfall is a dominant control of nutrient distribution in the soil. The calcium content increases with soil depth. The observed increase can be attributed to hydrological flow paths, with this cation originating from the deep subsurface flow. The exchangeable magnesium and potassium are more vulnerable to leaching during higher rainfall than exchangeable calcium. Low leaching of calcium can be explained by relatively strong attraction to the surface of clay particles. In the K^+ and Mg levels as can be seen from Figures above, significant losses were found at 10 cm soil depth in wet conditions. The leaching differences between cations are probably due to the differing adsorption properties. The results showed that potassium was leached more in comparison with calcium and magnesium at all soil depths. Other authors have also reported significant potassium leaching in sandy and organic soils and in high-rainfall areas (Malavolta 1985; Havlin et al. 1999; Schroth and Sinclair 2003). The loss of exchangeable cations was in the order of K > Mg > Ca.

The decreasing exchangeable K^+ content with the soil depth show the same trend as the organic carbon content (see Figure 8-10), which is in the line with the findings of

Barthold et al. (2007). These authors suggest that exchangeable K^+ is preferentially bound to humic substances where is the high content of exchangeable K^+ in topsoil than in the subsoil. The reason for this is that plant obtains the bulk of their K^+ from the topsoil and that in soils with limited cation content the recycling processes mainly take place in topsoil. In contrast to exchangeable K^+, the exchangeable Ca^{2+} content shows opposite trend.

The total content of nutrient distribution in the soil may reflect the lithology and its mineral composition. Considering this, it is not possible to put any explanation of the mineral composition of the soil that is made of Ca^{2+}, Mg^{2+} and K^+ without mineral soil analysis. After soil leaching, total cation contents had been reduced at all depths at perturbed plot. The order of total cation loss was Ca > Mg > K, which coincided with the experimental results in Chapter 7 of the soil solution collected at the 10 and 18 cm soil depth.

Extractable NO_3^- and SO_4^{-2}

Figure 8-8 illustrates details of soil nitrate conditions before and after rainfall treatment. The NO_3^- content was not detected at 0-10 cm soil depth in dry conditions. After enhanced rainfall treatment, the nitrate content increased at 0-10 cm soil depth. The extractable NO_3^- content between 'dry' and 'wet' conditions at the perturbed plot after enhanced rainfall treatment showed an increased trend at a depth of 0-10 cm, decreasing trend at the depth of 10-20 cm of 65%, and at the depth of 20-30 cm of 46%. The NO_3^- content of the control plot increased 50% in 0-10 cm, while leaching in nitrate content was 11% and 20% at depths 20 and 30 cm.

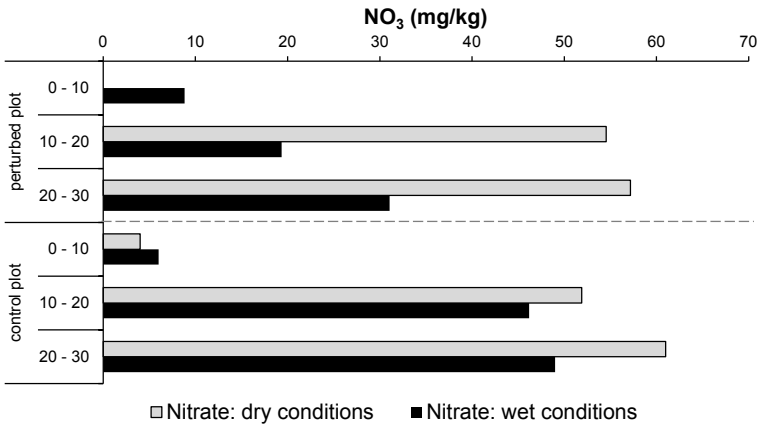

Figure 8-8 *The average content in soil of extractable NO_3^-*

Significant decrease in NO_3^- were found at 20 and 30 cm soil depth under enhanced rainfall treatment. The lower or zero NO_3^- content was found at the surface soil depth (0-10 cm) for both conditions, whereas after the wet conditions increase of nitrate content from the surface downward was detected. The reason can be related to the infiltration of rain that moved nitrate to deeper soil layers, leaching by the subsurface flow or in the case of saturated soil, the rise of the soil water table. In the spring, the content of nitrate is usually low because of unfavourable conditions of nitrifies, while later the content of nitrate increases and then decreases in the autumn (Dzamic and Stevanovic 2007). This suggests that during the autumn when the intensity of rain increases, which is in our case during the wet conditions, the content of nitrate decreases. It is possible that nitrates during dry periods can move upward and may accumulate at the soil surface (Neale 2006). However, if nitrates once have been leached below the root zone, upward movement of large quantities is unlikely, and according to that they are lost to the crop (Hauck 1984). This suggests the absence of the nitrate content in the upper soil layer (0-10 cm) observed in this study (perturbed plot).

In Figure 8-9, soil samples at the perturbed plot after enhanced rainfall treatment showed the loss of sulphate content of 69% at the depth of 0-10 cm. For the same conditions, loss of sulphate content was 70% at the depth of 10-20 cm and 73% at the depth of 20-30 cm. At the control plot, loss of sulphate was 12% in 0-10 cm depth, 9% in 10-20 cm, and at a depth of 20-30 cm 11%.

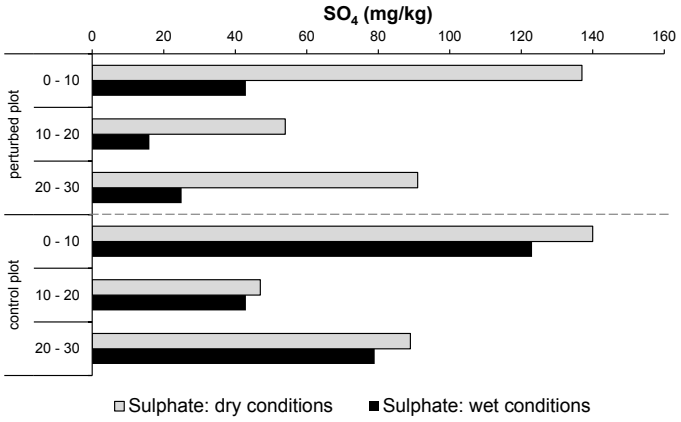

Figure 8-9 *The average content in soil of extractable* SO_4^{-2}

SO_4^{-2} may appear in the soil solution due to mineralization of organic matter and the use of fertilizers which contain sulphur. SO_4 in soils behaves very similar to K^+, being very soluble and readily leached. At all soil depths, losses of sulphate were high. This can be

explained by soil solution that carries nutrients down the soil profile where anions are leached with the equivalent amounts of cations (Schroth and Sinclair 2003). The loss of elements was in order of $SO_4^{-2} > NO_3^-$. Supporting the evidence of the loss of nutrients (Ca^{2+}, Mg^{2+}, K^+, NO_3^-, SO_4^{2-}) was the decrease in percentage of ion contents at mineral soil depths after enhanced rainfall treatment. Among all ions, SO_4^{-2} showed the highest loss and sensitivity to wetness. Ruszkowska et al. (1988) reported leaching losses of calcium, magnesium and sulphur in the lysimeter experiment of (in kg/ha per year): 49-82 kg Ca^{2+}, 15-25 Mg^{2+}, and 21-37 kg SO_4^{-2} from the loamy soil.

The understanding of soil nutrients in relation to farm budgets is useful for describing the nutrient flow within the farming system with minimal leakage of nutrients into the environment.

8.4 Soil carbon and nitrate content

Soil organic carbon (SOC) is an important constituent of soil organic matter (SOM), which indicates soil quality and productivity, and its capacity to affect plant growth as both a source of energy and a trigger for nutrient availability through mineralization (Walpola and Arunakumara 2011). The major factors that have been found to control soil organic carbon beside vegetation, elevation, terrain position and soil texture is climate. The relationship between climatic factors and the carbon and nitrogen contents of soils are well documented in the past. The content of carbon and nitrogen contents of soils increase with increasing rainfall (Sievers and Holtz 1923; Russell and McRuer 1927; Dean 1938). The relationship between climate and soil organic carbon (SOC) have been studied at large and small scales with scale-dependent outcomes (Woldeselassie 2009). At a global scale, it was concluded that SOC generally increases with increasing precipitation and with decreasing temperature for any specific level of precipitation (Post et al. 1982; Jobbagỳ and Jackson 2000; Woldeselassie 2009). In contrast, the same conclusion was drawn at the small scale at the grassland of the US Central Plains (Burke et al. 1989).

The increasing of carbon in soils (i.e. organic matter) is associated with many important productions and environmental benefits including (Liddicoat et al. 2010):

- Improved soil structure,
- Increased soil fertility,
- Increased water holding capacity,

- Increased infiltration capacity,
- Increased water use efficiency - due to reduced moisture loss from runoff, evaporation or deep drainage below the root zone,
- Increased soil biological health resulting in higher nutrient cycling and availability.

The chemical, physical and biological aspects of soil quality are controlled by the soil organic matter (SOM) as a fundamental component of the soil (Chan 2001). The role of soil organic matter in ecosystems has been summarised by various authors (Volk and Loeppert 1982; Charman and Roper 1991; Fisher 1995; Skjemstad, et al. 1998) and include:

- Source of carbon and energy for soil micro-organisms,
- Cation exchange capacity which affects the retention (prevents the leaching of essential plant nutrients), release and availability of plant nutrients,
- Major source of and a temporary sink for plant nutrients (such as N, P and S),
- Improvement in soil buffering capacity, against acidification and toxicities,
- Formation and maintenance of desirable soil structure,
- Improvement of water percolation into and retention by the soil,
- Absorption of solar radiation which influences soil temperatures,
- Ability to stimulate plant growth.

In this study, the total organic carbon (TOC) content at the perturbed plot after enhanced rainfall treatment showed an increased trend of 38% at a depth of 0-10 cm, 22% at the depth of 10-20 cm and 50% at the depth of 20-30 cm (Figure 8-10). In 0 to 10 cm soil layer, the TOC content was significantly larger for wet conditions at the perturbed plot than those at control plot.

Figure 8-10 illustrates the loss in calcium carbonate ($CaCO_3$) content with increase depth. Overall, $CaCO_3$ contents in the soil depth of 0-10 cm, 10-20 cm and 20-30 cm were significantly decreased by 30%, 34% and 20% compared to the initial amount before enhanced rainfall treatment. The loss in calcium carbonate at the control plot was not significant.

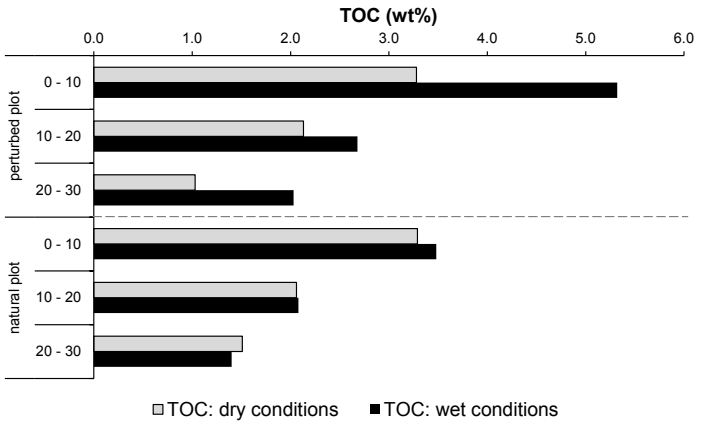

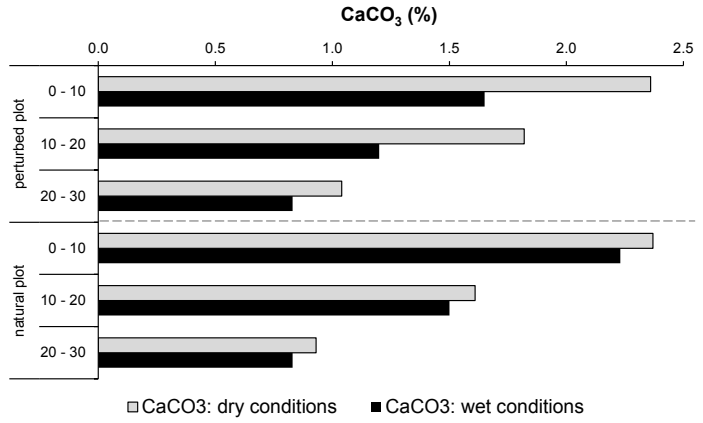

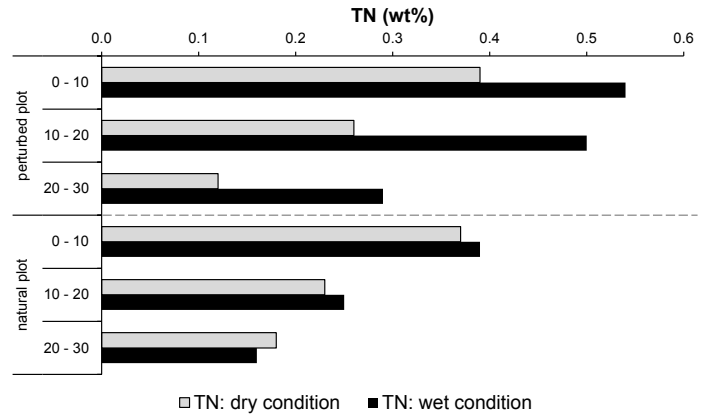

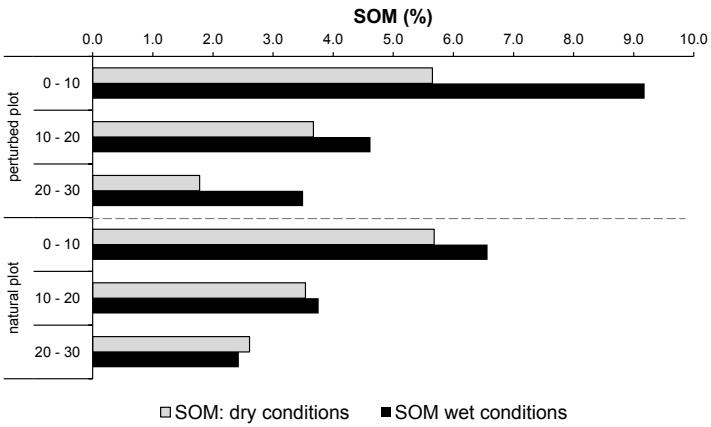

Figure 8-10 *Changes in total organic carbon (TOC), carbonate ($CaCO_3$), total nitrate (TN), and soil organic matter (SOM) content in mineral soil affected by soil depth and enhanced rainfall*

The total N content increased after wetting at 0-10 cm depth by 28%, at 10-20 cm depth by 48% and at 20-30 cm depth by 59% compared to dry conditions as can be seen in Figure 8-10. Total N tended to decrease significantly with depth. This can be due to its direct relationship with carbon and the microbial biomass.

In the plot with perturbed climate conditions, the soil organic matter increased at the 0-10 cm depth by 38% due to enhanced rainfall (Figure 8-10), at 10-20 cm depth 21%, and 49% in 20-30 cm. At the plot with natural climate conditions, SOM was recognized by 14%, 6% at soil depths 0-10 cm, 10-20 cm and decreased by 7% in 20-30 cm.

The amount of soil organic carbon (SOC) that is stored in a soil can be calculated using the equation of Broos and Baldock (2008):

$$SOC\ (t/ha) = depth\ (cm) \times bulk\ density\ (g/cm^3) \times organic\ carbon\ content\ (\%)$$

The amount of soil organic carbon (SOC) that is stored in the soil at 10 cm soil depth was estimated to be 23 t/ha in the dry condition and 32 t/ha in the wet conditions. For example, Dalal and Mayer (1986) reported that the organic carbon increase in virgin soils of 48 kg C/ha for each mm of rainfall compared to 29 kgC/ha per mm of rainfall in cultivated soils.

During dry conditions, decreases were observed in the TOC, TN and SOM content in soil compared to wet conditions. In this study, there was not a direct measurement of temperature effects on C and N in soil, which has a direct effect on the rate of decomposition of organic materials and SOC (Jenkinson 1991). Dalal and Chan (2001) reported that the decomposition of SOC is more rapid in tropical regions than in more temperate regions.

Previous studies have reported that decreases in soil bulk density increase organic carbon and nitrogen levels (Schjonning et al. 1994; Mapa and Gunasena 1995; Haynes and Naidu 1998; Halvorson et al. 1999; Rawls et al. 2003). This is consistent with the findings of this study.

Total organic carbon decreased significantly with increasing soil depth before and after treatment, as expected. The TOC contents increased after enhanced rainfall where rainfall has a driving role on SOC content due to its effect on plant productivity. For the plot under perturbed climate conditions, surface mineral soil (0-10 cm) had a significantly higher value of TOC content than subsurface soil at 10-20 cm and 20-30 cm depth. Dry climate conditions as observed in this study can lead to reduce

microbial biomass activity and nutrient mineralization due to a shortage of energy sources and poor soil SOC (Tanhan et al. 2007). The soil sample with greater TOC will be much better for the growth of plant as well as biomass increase (Anyasi 2012). Dean (1938) showed in his study the relationship of climatic conditions to the carbon and nitrogen contents of Hawaiian soils similar values of total carbon (from 1.32 to 12.82%) and nitrogen (from 0.13 to 0.78%) to values of this study.

Generally, the amount of $CaCO_3$ in the soil was observed to decrease after enhanced rainfall. The results indicate that with increased rainfall, $CaCO_3$ is significantly leached from the soil. The application of additional rainwater on the perturbed plot had significant effects on the distribution of $CaCO_3$. This treatment decreased $CaCO_3$ at all depths. This result may explain by the fact that runoff increased erosion and transport of the soil particles. There is also a possible explanation that after wetting treatment, $CaCO_3$ dissolves allowing Ca^{2+} and HCO_3^- ions to move downwards with the percolating soil water. Calcium carbonate precipitates where the percolation stopped or calcium carbonate can also percolate if the concentration in solution becomes high enough. $CaCO_3$ precipitation is not evenly distributed over the soil.

After rainfall treatment, the wet conditions showed a marked influence on soil TOC, $CaCO_3$, TN and SOM content. These changes can affect the soil C budget, which can be attributed to climate variability. The wet conditions significantly increased TOC, TN and SOM content in the soil to 30 cm depth. The results from this study are largely in agreement with the conclusion of Burke et al. (1989) that rainfall increased C, N and SOM. For example, in semi-arid grassland, Niu et al. (2009) reported that water addition on the soil C could significantly stimulate gross ecosystem productivity. However, Lü et al. (2011) reported that water addition of a 2-year treatment failed to affect the soil C storage because the amount of precipitation is not as important as precipitation distribution as a suggestion by Chen et al. (2009).

Distribution of C and N in the soil profile at the plot scale showed higher content in the surface layer. These findings suggest that in general TN increases with more moisture. As expected, the SOM decreased with depth in both plots. The higher SOM content in the upper soil layers was probably the result of considerable plant residues. There was a significant difference between the two climate conditions. In the case of enhanced rainfall, SOM increased at all depths. In general, therefore, accumulation of organic matter in the soil is greater with more rainfall.

From the results, the soil productivity can be changed by excessive nutrient runoff and intensified rainfall inputs. The findings of C, N and SOM give a better understanding of soil productivity especially for farming management and agrosystems in the future according to climate variability. For the successful implementation of any management practices, research is needed to quantify the impacts of vegetation. Much of this research is still to be carried out.

8.5 Thermal analyses of soil

One of the objectives of this study was to determine changes in the soil quality by assessing the soil C depletion sequence in terms of thermal properties. The TG-QMS-DSC method was necessary to use to support the aims of this study. The soils were isolated from a sequence of 0 to 10 cm depth from the grassland mineral soil, and analysed using thermogravimetry (TG) and differential scanning calorimetry (DSC) before and after enhanced rainfall treatment. To determine the properties of the major components that are released as gas (12 (C), 18 (H_20) and 44 (CO_2 and N_2O)), a quadrupole mass spectrometer (QMS) was also used.

A considerable amount of literature has been published on thermal analyses. These studies indicate the application of thermal analyses techniques by means of determining and examines changes in soil organic matter quality, for instance in clay-associated organic matter isolated from soils in an organic C depletion sequence (Plante et al. 2004), quality under different land use (Lopez-Capel et al. 2005), on tropical soil with forest vegetation from unburnt and burnt cane plantations (Critter and Airoldi 2006), also on coal, charcoal, peat and lignite. However, no research has been found that applied TG-DSC-QMS techniques on the soil in terms of natural and progressive climate condition.

The TG-DSC experiment involves continuous and simultaneous measurement of weight loss (TG) and energy change (DSC) during heating (Lopez-Capel et al. 2005). Thermogravimetry (TG) contributes to understanding the heating effects on soil components such as loss of water, organic matter combustion and clay dehydroxylation, in order to compare the relative abundance of more and less labile carbon sources (Siewert 2004; Miyazawa et al. 2000; Gaál et al. 1994). DSC measures the heat into and out of (endothermic and exothermic) a sample relative to a standard reference as a function of temperature. Initial weight loss is dominated by the exothermic

decomposition of labile aliphatic and carboxyl groups (approx. 300°C) whist exothermic loss of more refractory aromatic C occurs at higher temperatures (approx. 450°C) (Flaig et al. 1975; Schulten and Leinweber 1999; Czimczik et al. 2002). Brown (1988) points out that the weight loss that occurs in these two parts of the heating cycle can be used to compare the relative abundance of more and less labile C, the position of DSC peaks reflecting structure and chemical composition.

Figure 8-11 compares the results before and after enhanced rainfall obtained from thermal analysis. TG-DSC traces of samples before treatment show thermograms typical of those previously reported in the literature (Lopez-Capel et al. 2005). Thermogravimetric mass losses were observed at 200, 350, 500, 800 and 900°C. The TG traces clearly showed single stage decomposition. The total weight losses on the perturbed plot were before wetting 9.32% and after wetting 11.74%, respectively. The maximum energy occurred between 200 and 500°C. The weight loss curves (TG) in Figure 8-11 show that the decomposition of soil organic matter (SOM) increases at 270°C and is completed before 600°C. Release of CO_2-C occurs at temperatures above 500°C (Gaál et al. 1994).

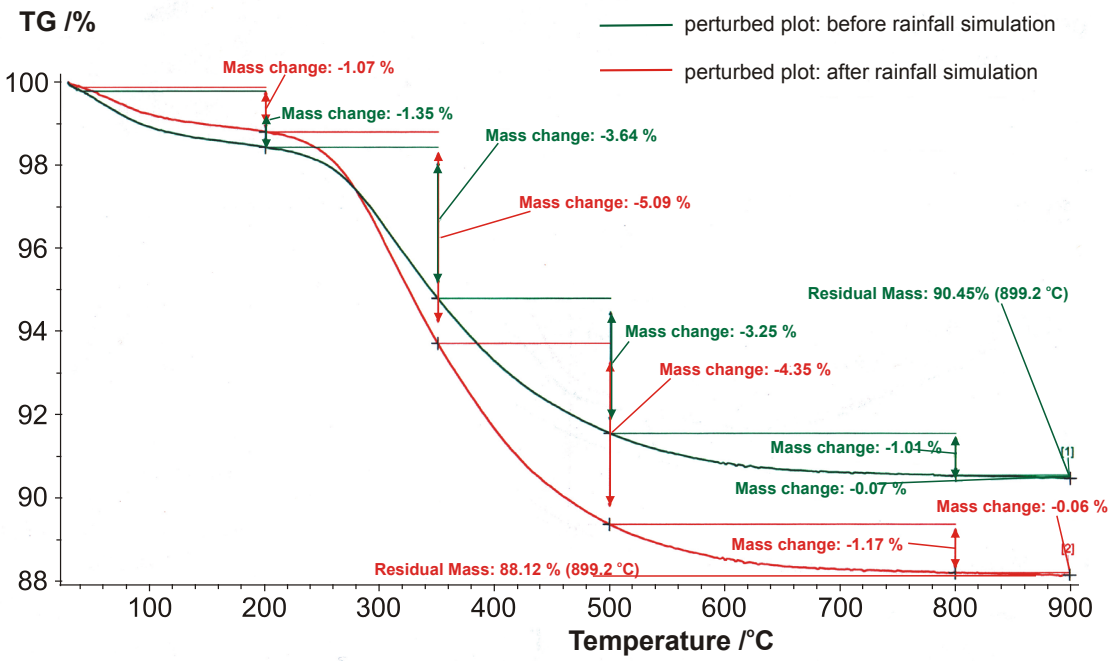

Figure 8-11 *TGS curves of mineral soil sample of 10 cm depth on the perturbed plot before and after enhanced rainfall*

According to Lopez-Capel et al. (2005, 2006), for soil organic matter, weight losses between 250 - 350°C correspond to labile material, 250 - 500°C to recalcitrant, and 500 - 650°C to refractory (organic matter) OM. Following this approach, mineral soil was

subdivided into a thermally labile C pool called OM1 (250 – 350), thermally recalcitrant C pool called OM2 (350 – 500) and a refractory C pool called OM3 (500 – 800), also similar to the approach used by Dell'Abate et al. (2003). The thermogravimetric data for the soil before and after enhanced rainfall are presented in Table 8-1.

Table 8-1 *Thermogravimetry (TG) mass losses in the exothermic region attributed to organic matter oxidation*

Perturbed plot	**Mass losses (%)**			
Enhanced rainfall	OM1	OM2	OM3	Total OM (20-900°C)
Before	3.64	3.25	1.01	9.32
After	5.09	4.35	1.17	11.72

Table 8-2 stability indices (Exo1 – Exo 3) are calculated from the relative percentage of the weight loss according to terminology proposed by Dell'Abate et al. (2000) corresponding to the first exothermic (aliphatic C and carbohydrates predominantly cellulose), second exotherm (aromatic C, predominantly lignin), and third exotherm (aromatic C, refrectory), normalised with respect to the weight loss between 200 and 800°C (Exototal). The values of thermal stability indices indicate the relative abundance of organic materials with different thermal stabilities. Cumulative losses (TG) are scaled to 100%. Arrows show the "threshold" temperature chosen for SOM fractionation.

Table 8-2 *TG parameters summarising: relative weight losses (%) of temperature intervals Exo 1 (200-350°C), Exo 2 (350-500 °C) and Exo 3 (500-800 °C), total weight loss for the temperature interval 200-800°C, composition of TOC by LECO analyser, TOC 1, TOC 2 and TOC 3 mass weight according to temperature intervals*

Treatment	**Exo 1 (%)**	**Exo 2 (%)**	**Exo 3 (%)**	**Exotot (%)**	**TOC (wt%)**	**TOC 1 (wt%)**	**TOC 2 (wt%)**	**TOC 3 (wt%)**	**Exo 1/(Exo2+Exo3)**
Before	46.08	41.14	12.78	7.90	3.28	1.51	1.35	0.42	0.85
After	47.97	41.00	11.03	10.61	5.32	2.55	2.18	0.59	0.92

The DSC traces were characterized by an endothermic reaction between 70 and 82°C due to water release and a range with exothermic reactions between 20 to 900°C (Figure 8-12). These exothermic reactions are positive values of DSC that represents energy release and oxidation of organic matter. In qualitative terms, the DSC thermogram showed for both treatments one sharp exothermic peak at approximately 350°C consistent with analyses of organic matter and humic substances reported in the literature (Lopez-Capel et al. 2005). The maximum DSC values of 0.16 and 0.21 $\mu V mg^{-1}$ before and after wetting were measured at 346°C and 349°C. The gentler slope of the TG thermograms in the 200 and 500°C region reflects the distinction between the beginning and end of DSC peak. As shown in Figure 8-12, the exothermic region of the low-temperature around 300-350°C ascribes to the burning of carbohydrate and other aliphatic compounds.

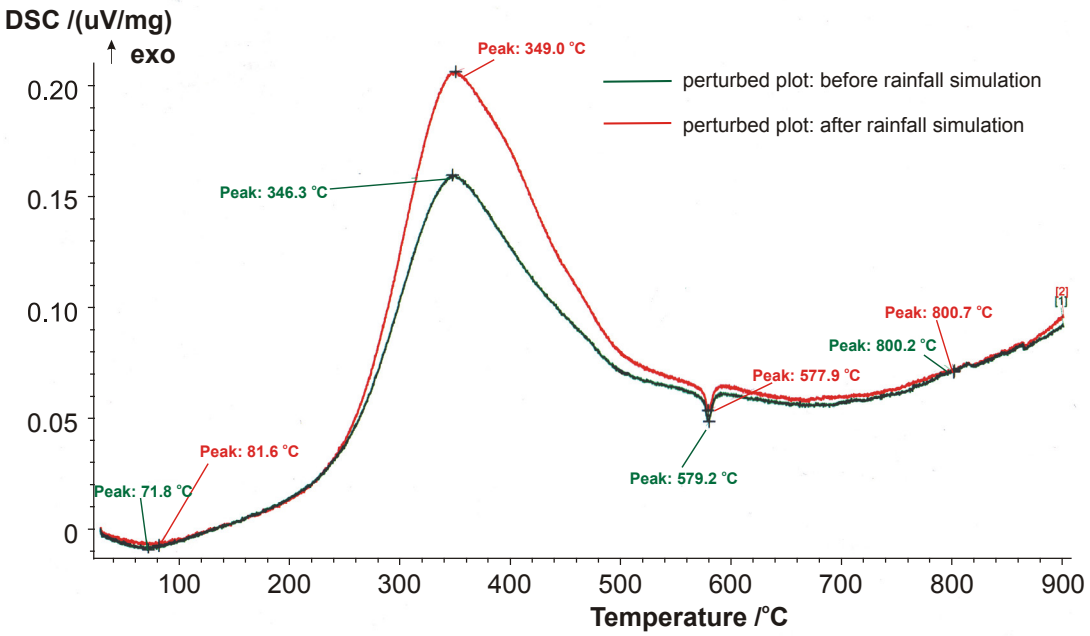

Figure 8-12 *DSC curves of mineral soil sample of 10 cm depth on the perturbed plot before and after enhanced rainfall. Arrows show the "threshold" temperature chosen for SOM fractionation*

Figure 8-13 shows the results for each mass to charge (*m/z*) relationship between soil before and after perturbed climate condition (with enhanced rainfall). The temperature ranges at which the emission profiles lie run from 200°C up to 700°C for m/z=12, 44 with a maximum around 350°C. The main gas species detected in this mineral soil were m/z12 at 351°C and 321-376°C, then m/z18 at 60-75 and 300°C, and m/z44 at 346°C. Emission of carbon (m/z 12) begins at some point between 40 and 200°C and increases up to 351°C, where it tends to decrease. There was a significant difference between the two climate conditions and loss of C of 67%.

During thermal decomposition of water (m/z18), two peaks may be observed. First peak at 60-75°C is observed that may correspond to the evaporation of the water contained in soil. Second one at 300°C is probably due to the breaking down of the groups that contain oxygen, mainly hydroxide (OH) groups, giving rise to the formation of pyrolysis water over a wide range of temperatures. The maximum emission of carbon dioxide (mz44) is observed at 341°C and 361°C. This may indicate carbon decomposition, which can occur at higher temperatures (peak at 500°C).

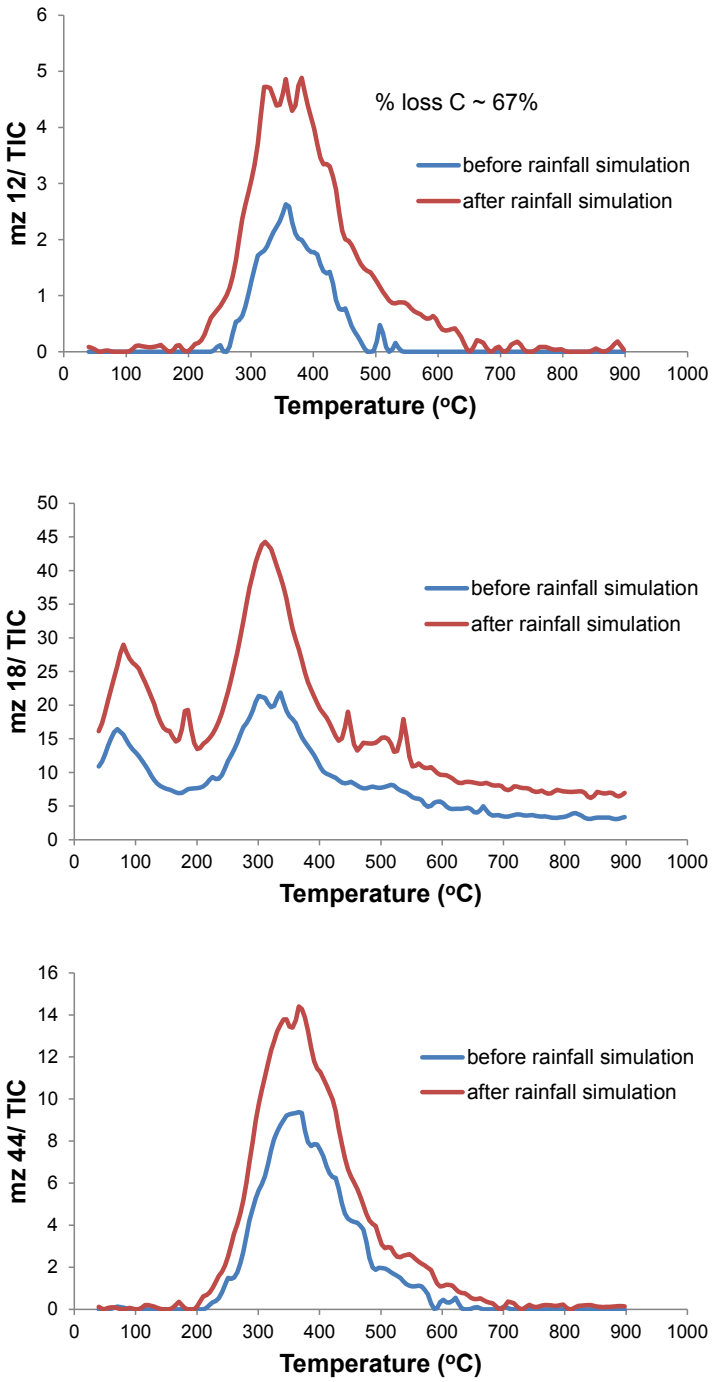

Figure 8-13 *Thermogram of ion currents m/z12, m/z18 and m/z44*

Thermal techniques such as TG, DSC and QMS are rapid and easy way to determine changes in soil and detect an organic C depletion within the soil. Thermal analyses of the soil data show significant difference in the mineral soil under different climate conditions. Intensified rainfall from the perturbed plot resulted in significant carbon depletion due to enhanced storm events attributed to increased rainfall intensity and duration. Thermogravimetric mass loss ratios were greater in the thermally labile (250-300°C) exothermic region than in the more thermally resistant, recalcitrant (350-500°C) exothermic region. Soil organic matter (SOM) decomposition can be represented by

three carbon pools that includes a labile (which includes cellulose (Lopez-Capel et al. 2005), a recalcitrant (including lignin (Leinweber et al. 1992)) and a refractory pool (including chars (Kaloustian et al. 2001)) as well as aromatic carbon (Lopez-Capel et al. 2006). Similarly, the DSC peaks were higher in the exothermic region of 350-500°C. According to this, the higher ratios indicate that the more thermally resistant organic matter has been retained and the more thermally labile organic matter is lost in the soil. Strong evidence of carbon loss was found when coupled quadrupole mass spectrometers was used. The enhanced rainfall treatment of the mineral soil samples removed approximately 67% of the initial organic carbon.

It can be concluded that the thermal analysis results indicates preferential depletion of labile carbon affected by the enhanced rainfall treatment as compared to unchanged climate conditions. The coupled TG-DSC-QMS system allows the proportions of OM pools to be quantified, and demonstrates C changes in soils.

8.6 Summary

Distributions of nutrients in hillslope soils of Sykeside Farm were analysed during dry and wet conditions. Soils from the 0 to 10, 10 to 20 and 20 to 30 cm depth ranges were analysed for: exchangeable and total Ca^{2+}, Mg^{2+} and K^{+}; extractable NO_3^{-} and SO_4^{-2}; TOC, $CaCO_3$, TN and SOM; and the soil C depletion sequence in terms of thermal properties. The results showed: (1) that the nutrients were most concentrated in the topsoil (upper 10 cm), (2) leaching rates of nutrients were in the following order: K > Mg > Ca, (3) SO_4^{-2} in the soil is more vulnerable to leaching during high rainfall than NO_3^{-}, (4) the content of K^{+}, TOC, $CaCO_3$, TN and SOM decreases with increasing soil depth, (5) intensified rainfall conditions resulted in significant carbon depletion based on thermal analysis.

Chapter 9. The role of hillslope hydrology in the process of nutrient mobilisation

9.1 Introduction

In this chapter, conceptual models of runoff generation and changes in DOC and NO_3^- concentrations under dry and wet scenarios on hillslopes are developed based on the findings described in Chapter 7. Parameters including soil moisture, surface slope, soil clay content, vegetation cover and observed flow have been used to develop relationships and understanding of the runoff generation processes at the hillslope scale.

A number of runoff generation concepts have evolved, some already mentioned in the literature review (Chapter 2) that include the partial area concept of Betson (1964), the variable source area concept of Hewlett and Hibbert (1967), Dunne and Black (1970), and the rapid subsurface storm flow concept of Dunne and Leopold (1978), and McDonnell (1990). These concepts differ from each other in terms of source locations of runoff and dominant hydrological flow pathways, which determinant nutrient mobilization and transport in the landscape (Dahlke et al. 2012).

The purpose of this Chapter is to present: i) a conceptual model of runoff generation at the hillslope scale, ii) changes in the DOC and the NO_3^- concentrations under dry and wet scenarios and iii) to establish a method to upscale nitrate loads.

9.2 The conceptual runoff models in unsaturated zone

Different approaches have been developed to describe runoff generation on hillslopes as described in Section 2.1. Conceptual runoff models were made under three soil moisture regimes according to soil depths. For all three models, it is assumed that during the wet season soil water and rain create recharge at the top of the hill along a 9 m length that contributes to the deep soil water storage and flow. The subsurface flow is separated into shallow and deep flow processes.

Model 1: The model is based on analysis of the data for the soil moisture for the dry period. Looking at Table 6-7 in Chapter 6 for the period 11-30 September 2009, the highest mean soil moisture content at the top of hillslope at 30 cm depth was 39%. For the 20 cm soil horizon, saturation at the bottom of the hillslope was 23%. Absence of the soil saturation at the top in 10 cm up to a depth of 20 cm indicates vertical drainage

through the profile probably by flow in micropores or through the soil matrix. Model 1 is presented in Figure 9-1. Based on these results, the shallow and deep lateral subsurface flows are proposed that occurs at 20 and 30 cm of the soil depth. Many research studies have proposed the conceptual understanding of the subsurface flow (SSF) formation (McDonnell 1990, Sidle et al. 2000; Kienzler and Naef 2007) as well as addressing the question of where the subsurface flow occurs (Jones et al. 1997; Scherrer and Naef 2003). During the low or moderate rainfall, water infiltrates vertically through the soil where it accumulates and moves laterally downslope at or very close to the soil surface, which produces the shallow subsurface storm flow. Since the early work of Hursh (1936, 1944), shallow subsurface flow processes have perplexed hydrologists and to some extent are still ignored as a contribution to the storm event response (Michener and Lajtha 2008). Model 1 shows that the subsurface flow is the dominant pathway that can be applied for the dry climate conditions.

Model 2: Turning now to the experimental evidence on the soil moisture for the period 6-31 January 2010 (Table 6-7), the highest mean value of water content can be seen at the top of the slope at 20 and 30 cm soil depth. However, at the bottom of the hillslope there was at the soil depth of 20 and 10 cm.

The soil physical properties (Chapter 8) and field observations (Figure 4-46) show the presence of clay (loam) soils located at a depth of approximately 20 cm and below, indicating that rainwater enters a layer of restricted permeability. When the water content exceeds the storage capacity of the soil it flows laterally downslope and discharges from the hillslope.

Clay soils are layered sediments, usually irregularly structured, and could form clay lenses. It is assumed that this presence of clay soils formed its own soil water table, i.e. a perched soil water table. To assess the evidence behind this assumption, information collected from the field observation during a runoff experiment at the hillslope is used. In the trench, tipping buckets for collecting flow water samples were used to monitor flows during intensive rainfall, and the perched soil water table was identified. The trench was around 30 cm deep, the clay soil layer was visible, and was one-third full of water making a so called “water pool”. It is well known that clay soils in contact with water absorb and increase volume through swelling. According to this, it is possible that the clay soil layer acts as a buffer zone, stores the water and reduces percolation into the groundwater.

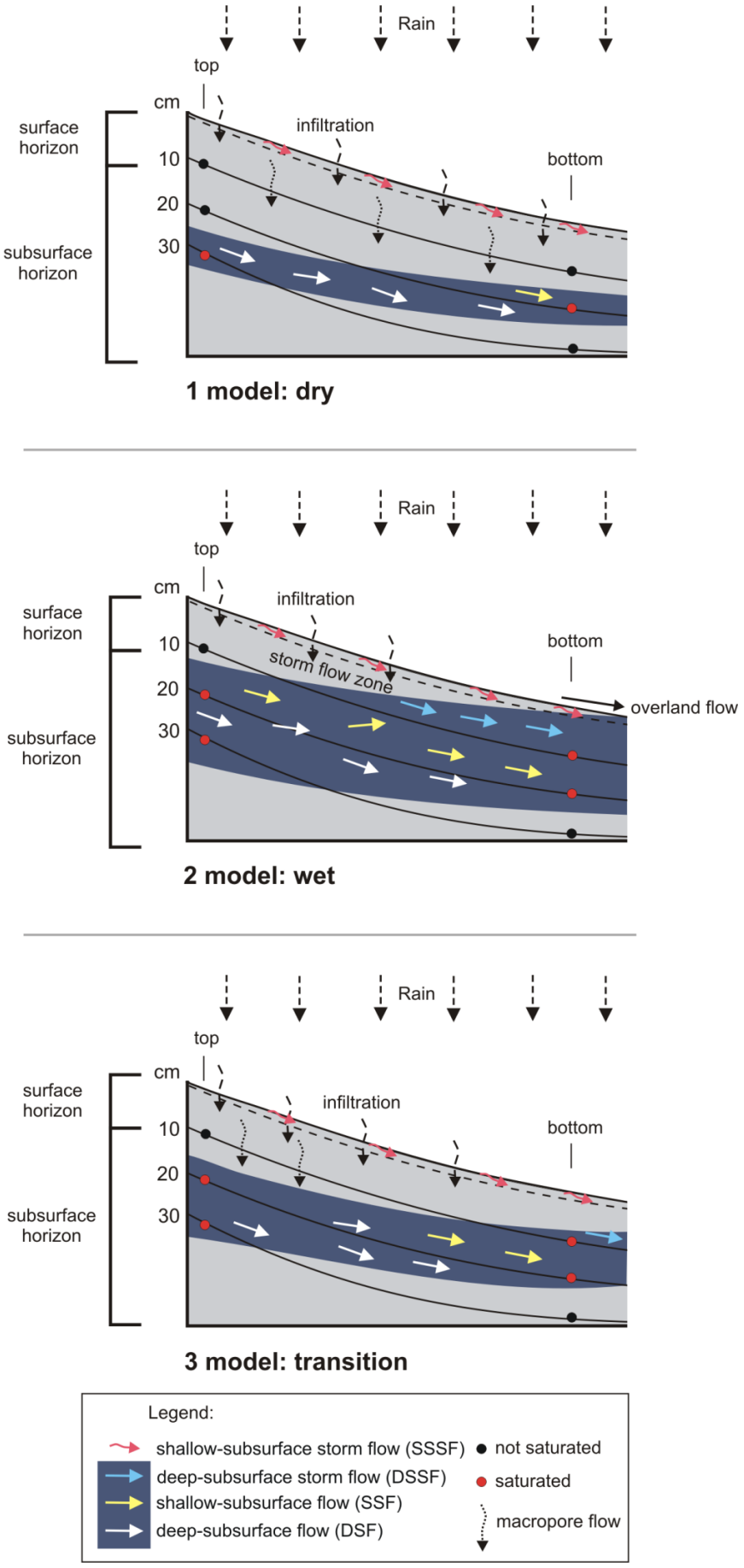

Figure 9-1 *Conceptual model of flow processes at the hillslope within the unsaturated zone*

Based on this evidence, therefore, it seems that that shallow and deep lateral subsurface flows are the dominant pathways, and when saturation increases and the perched soil water table moves upward this produces firstly deep subsurface then shallow subsurface storm flows (Figure 9-1). This aspect of the perched soil water table is shown by the work of Wilson and Luxmoore (1988) and Wilson et al. (1990, 1991) in a small (0.5 ha) upper hillslope sub-catchment of Walker Branch. They reported that a perched water table developed in the upper soil profile in response to moderate-large storms, contribute most of the subsurface storm flow via macropores. When the soil reaches full saturation, excess rainwater does not infiltrate, which then produces the overland flow or a saturation excess overland flow. In summary, the dominant flow during storm events is subsurface and overland and/or saturated excess overland flows.

Attempts are made to relate the findings from hydrograph separation in Section 5.3.1 of the storm event (E3) to soil moisture contents (Chapter 6, Table 6-7) and to this conceptual model. The findings from hydrograph separation are consistent with this runoff process model.

The conceptual Model 2 can be successfully applied for explanation of flow paths within the unsaturated zone during storm events or intensive rainfall.

Model 3: The soil wetness was recorded at the top of the hillslope at 20 and 30 cm depth. At the bottom of the hillslope, the mean soil water content was recorded at 10 cm and 20 cm soil depth, while at 30 cm depth the soil was not saturated based on moisture evidence, Table 6-7 (February 2010). As was previously pointed out in Model 2, the presence of the clay layer indicates lateral subsurface flow, which is also the case here. There are three flow mechanisms identified: deep and shallow subsurface flow and deep storm subsurface flow (Figure 9-1).

The following question was addressed: what is the primary application for this model? It is assumed that this model can fit for low rainfall intensity with short duration. The previous two models are for dry periods and for storm events and this model could fit between them as a transition model from dry to wet conditions.

The major limitation in the conceptual models is that the soil water table measurements are not available. Testing models on situations outside those on which they were developed can provide some significant insights into the limitations of model operation.

According to the soil moisture and chemical composition, a new approach is proposed to select the flow process within mineral soil type under grassland at the hillslope scale. The evidence for this is based on the hillslope water quality (Section 7.2). The five runoff processes are defined:

1) ***saturation excess overland flow*** occurs when the soil is saturated. This flow has the chemical composition of these dominant ions:

$$HCO_3 > Cl > X$$

where X can be one of this ions Ca^{2+}, Mg^{2+} or K^{+}, depending on the mineral composition of soils.

2) ***shallow-subsurface storm flow (SSSF)*** occurs at or very close to the soil surface (at most 3 cm soil depth) with flow laterally through the soil. This flow has the chemical composition of these dominant ions:

$$Na\text{-}Cl \text{ and } Na\text{-}Cl\text{-}HCO_3 > Cl > Na$$

3) ***deep-subsurface storm flow (DSSF)*** occurs approximately at 3 to 15 cm soil depth. Once the soil is saturated at that depth, flow occurs. This flow has the chemical composition of these dominant ions:

$$HCO_3 > Cl > X$$

where X can be one of this ions Ca^{2+}, Mg^{2+} or K^{+}, depending on the mineral composition of soils.

4) ***shallow-subsurface flow (SSF)*** occurs at soil depth of approximately 15 to 25 cm. This is the dominant flow during the dry period but also occurs during rainfall periods. This runoff has the chemical composition of these dominant ions:

$$HCO_3 > Cl > X$$

where X can be one of this ions Ca^{2+}, Mg^{2+} or K^{+}, depending on the mineral composition of soils.

5) ***deep-subsurface flow (DSF)*** occurs on an up-slope part of the hillslope at soil depth of approximately 25 to 35 cm or deeper. This is the dominant flow during dry periods but also occurs during rainfall periods. This flow has the chemical composition of these dominant ions:

$$HCO_3 > X > Y$$

where X and Y can be one of ions, depend on the mineral composition of soils and geology.

Mulholland et al. (1990) investigated the storm hydrogeochemical response at the whole catchment scale. Their results suggest that water chemistry differed considerably between flow paths, and shallow (subsurface) and deep (groundwater) flow paths were important in generating storm stream flow.

Upscaling these runoff models of hydrological behaviour from the hillslope to the Hollow sub-catchment scale, it is possible to explain under which type of runoff models nutrients reach the stream.

9.3 Conceptual model of labile nutrients (DOC and NO_3) flushing

Understanding the flushing mechanism during storm events is important for model development for the prediction of land use change and climate change effects on surface water quality. During storm events or snowmelt, many studies have reported a significant increase in dissolved organic carbon (DOC) and nitrate (NO_3-N) that is attributed to nutrient flushing (Creed et al. 1996; Boyer et al. 1997; McHale et al. 2002; McGlynn and McDonnell 2003; Vanderbilt et al. 2003).

The results shown in previous chapters have been used to develop conceptual models for the export of the labile nutrients (DOC and NO_3^-) from the hillslope to the stream. The models assume that water and solutes are mixed into upper subsurface soil horizons.

To be able to understand the mechanism of nutrient flushing from the hillslope, it is first necessary to explain the source of nutrients (DOC and NO_3^-) within the unsaturated zone and then to link these sources with the main flow processes. In the soil solution nitrate, may originate from organic matter or ammonium. A detailed explanation was given in Chapter 2.

Figure 9-2 gives insight into the DOC concentration in rainwater and flows. The mean DOC concentration was lower in the rainwater and higher in the soil water.

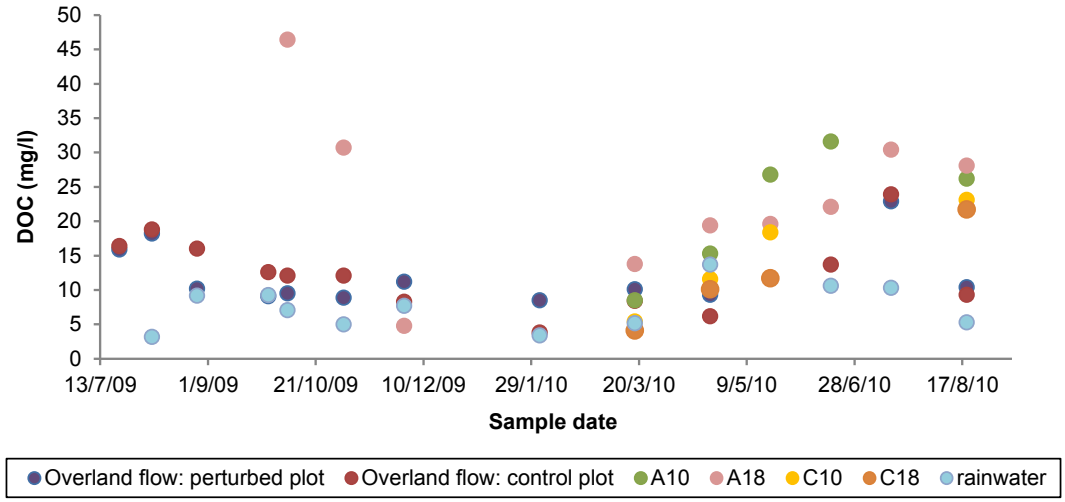

Figure 9-2 *DOC concentration (mg/l) of various compartments at the hillslope. A: perturbed plot, C: control plot; 10: soil solution at 10 cm depth; 18: soil solution at 18 cm soil depth*

During low rainfall or dry periods, the greatest DOC concentrations are suggested to be in the shallow mineral layer at approximately 10 cm depth as shown in Figure 9-3a. The total organic carbon content (Chapter 8) was the highest in the upper soil layer. The evidence for this is based on the soil solution collected and analysed from the field that presented the higher DOC concentration at 10 cm depth (32 mg/l), medium at 18 cm depth (22 mg/l) and low in the overland flow (13 mg/l). The shallow-subsurface flow with deep-subsurface storm flows may facilitate the flushing of the high DOC concentration to the catchment.

Figure 9-3b presents the conceptual model of the DOC flushing during periods of high precipitation intensity of storm events. It suggests that the high DOC concentrations in deep soil layers are due to downward movement of the DOC. The evidence for this is based on the soil solution collected and analysed from the field that presented higher DOC concentration at 18 cm depth (27 mg/l) and low in the overland flow (8 mg/l). According to this, the deep-subsurface flow is attributed to flushing of the high DOC concentration with the shallow-subsurface flow of medium concentration.

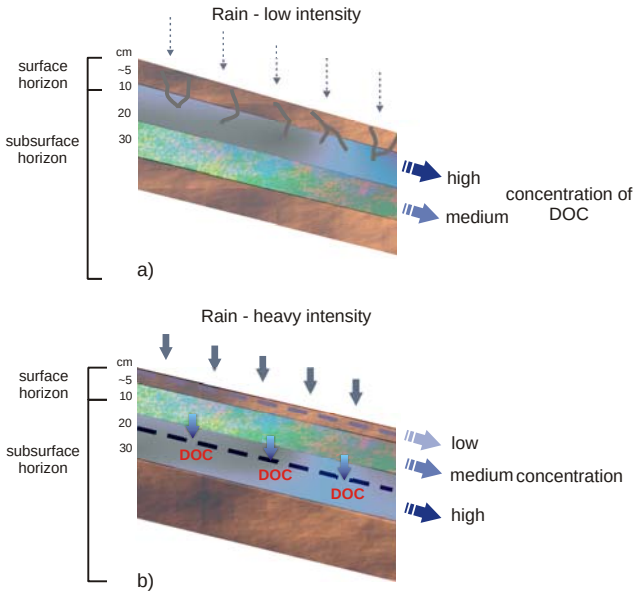

Figure 9-3 *Conceptual model of DOC export during a) low and b) heavy rain intensity*

During low rainfall, the greatest nutrient (NO_3^-) concentrations are likely to be in the deeper mineral layer as shown in Figure 9-4a. As stated previously in Chapter 7, infiltration of low rainwater intensity can transport the NO_3^- to deeper soil layers. The evidence for this is based on the soil solution collected and analysed from the field that presented the higher NO_3^- concentration at 18 cm depth (1.9 mg/l), low at 10 cm depth (0.3 mg/l) and in the overland flow (0.3 mg/l). According to this, the deep-subsurface flow is responsible for flushing of high nitrate concentration to the catchment scale. Heathwaite (1995) indicates that subsurface flow is important for soluble elements such as nitrate for transport to the stream.

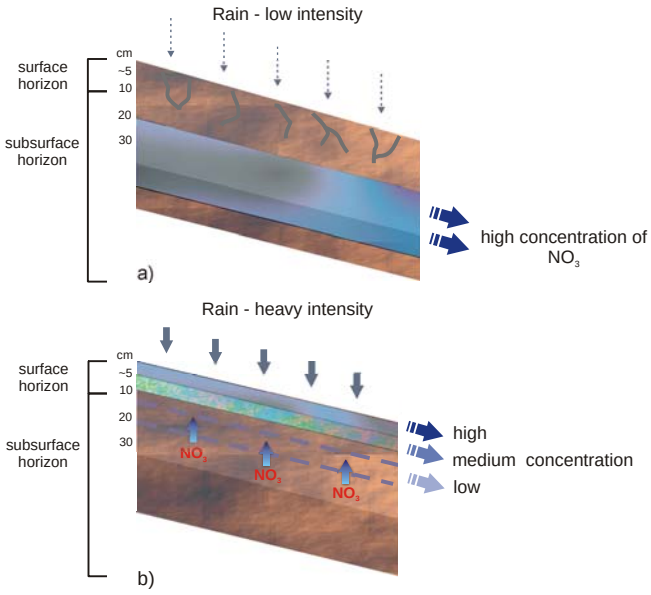

Figure 9-4 *Conceptual model of NO_3^- export during a) low and b) heavy rain intensity*

Under the heavy precipitation and saturation of deeper soil horizons, nitrate may be lost by denitrification, which takes place in an anaerobic condition, below the perched soil water table. In previous sub-sections, the existence of the clay soil layer and the soil perched water table were identified. It is assumed that the soil perched water table may have risen into more permeable shallow subsurface and surface horizons. As the soil perched water table rises, concentrated soil solution is displaced from the deep to the upper soil layer (Figure 9-4b). The soil solution collected and analysed from the field presented the low NO_3^- concentration at 18 cm depth (1.0 mg/l) and higher in the overland flow (2.1 mg/l). The overland and shallow-subsurface storm flows contribute to high nitrate concentration flushing with the deep-subsurface flow of medium concentration from the hillslope to streams.

Van Verseveld et al. (2007) reported in their study that nutrient flushing mechanisms have been explained in the literature by: (1) a rising water table that intersects high nutrient concentrations in the upper soil layer, (2) vertical transport of nutrients, by preferential or matrix flow through the (deeper less bio-active) soil to the soil–bedrock interface and then laterally downslope (Creed et al. 1996; Hill et al. 1999; Buttle et al. 2001), and (3) vertical transport of nutrients and then laterally within the soil profile (Gaskin et al. 1989). As mentioned before, the data of the water table and hydraulic gradient were not available in this study. Therefore, a rising of water table is assumed and conclusions were based on collected the DOC and the NO_3^- concentration in the overland flow and the soil water solution.

The overall findings resulted in the conceptual model of a mechanistic assessment of labile nutrients (DOC and NO_3^-) transport within the mineral soil from the hillslope to the stream of the sub-catchment. This study clearly demonstrated that high concentrations of nutrients under low precipitation intensity and duration have a strong response to the subsurface water quality.

The model presented in this study is consistent with statement of Heathwaite (1995) who suggests that there are two key driving factors at the hillslope in the mobilization and subsequent transport of nutrients to the stream. These two main pathways of nutrient transport are overland or surface flow and subsurface or throughflow. Further, this author reports that nutrients once mobilized, may undergo further physical, chemical or biological transformations along the hillslope hydrological pathway before they enter the stream.

Thus, these models give an overview of hillslope nutrient behaviour during different climate conditions, which is important for implementation of catchment nutrient management plans. It also results in an improved understanding of the sources, flow path and transport mechanisms responsible for the export of the DOC and the NO_3^- from the hillslope to catchment scale.

9.4 Upscaling nitrate from hillslope to sub-catchment and catchment scale

The study covers three nested spatial scales: plot scale (2 m^2) within the hillslope (45 m^2), the sub-catchment (0.09 km^2) and the Blind Beck catchment (9.2 km^2) located in the Upper Eden basin, Cumbria, UK. Sivapalan and Kalma (1995) identified the scale issue as a major unresolved problem in hydrological sciences and it pervades all aspects of catchment hydrology and biogeochemistry (Blöschl 2001). Theoretical investigations into catchment scaling have outpaced field observations and empirical understanding (McGlynn et al. 2003). These authors state that the reason for this is often difficult and expensive measurements, and empiricists often do not know where to sample or indeed how many measurements are necessary to characterize a given catchment (regardless of scale). According to this, field investigations have been conducted most often at the headwater catchment scale and then extrapolated to larger scales (McGlynn et al. 2003).

The nitrate was one of the labile nutrients chosen to represent nutrient conditions across scales. Figure 9-5 reports a box plot (75%, max, mean, min, 25%) distribution of nitrate data for all scales: plots within hillslope, Hollow sub-catchment and Blind Beck catchment. It clearly shows the differences between scales. The average NO_3^- concentration at the catchment was higher than at the sub-catchment and the hillslope. Overall, the average NO_3^- concentrations were low at all sampling sites and did not exceed the water quality limits (> 5 – 10 mg/l) according to the Nitrate Concentration Guide (EA 2006).

In Figure 9-6, the nitrate concentration on the two smaller scales showed remarkably similar behaviour, with a high concentration at high flow rates, while at the catchment there is an opposite trend. A maximum concentration of 14.6 mg/l N was recorded in March 2010 at the Blind Beck catchment that has intensive farming (Figure 9-6). The relatively high nitrate concentration observed at this scale as mentioned before (Chapter 5) suggests the influence of a small stream that flows past Little Musgrave Farm into Blind Beck 10 m upstream, where Barber (2008) recorded a mean nitrate

concentration of 16.61 mg/l. This author suggests that the highest concentration is coming from the stream that flows from the south-east past Low Hall Farm, which had a maximum recorded concentration of 19.55 mg/l, with N being leached from the land surrounding this stream.

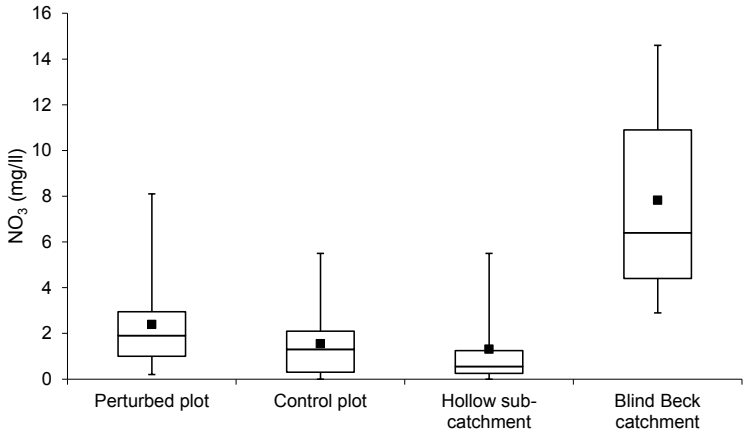

Figure 9-5 *Box plots showing the distribution of average nitrate at three scales: the hillslope, the Hollow sub-catchment and the Blind Beck catchment. The ends of the boxes represent the 25th and 75th percentiles, the bars indicate the lowest and highest values not considered outliers, and the horizontal line shows the median*

These results show that dilution during high flow plays an important role in reducing nitrate concentration to 3 mg/l. This is in agreement with Doležal and Kvítek (2004) who observed a similar effect, and also the study of Floate (2002) who carried out a nutrient pollution assessment of the River Eden and its tributaries at 3 different catchment scales; micro-catchment (1 km^2), mini catchment (10 km^2) and meso-catchment (100 km^2). The study of Floate found dilution effects at the meso-catchment scale, while the micro-catchment sites were the nitrate 'hotspots' and were responsible for the high levels of nitrogen measured at all scales with a maximum concentration of 9.5 mg/l N recorded after a nitrate leaching event in the micro-catchment. Work by Soler (2003) followed a multi-scale approach with samples of nitrate taken in three sub-catchments at micro-, mini, and meso-scales, and found that the results from the multiscale sampling showed that nutrient concentrations were below EC Drinking Water limits for nitrates at all of the sites, and the highest nitrate levels were found in the meso-catchment sites. Mannix (2005) carried out a runoff experiment at Sykeside Farm to attempt to quantify the nitrate concentration that occurs in overland flow before and after land spreading of manure. The results showed high nitrate concentrations at the near surface with peaks in the soil profiles that likely represent flushing downwards of peaks in nitrogen content in the near subsurface which have built up by the end of each summer. This study also involved groundwater sampling from the Great Musgrave

site and surface water sampling at upland and lowland tributaries in the Upper Eden. The lowest nitrate concentrations were found in surface water of the uplands with mid-range values of 0.66 to 1.21 mg/l measured in the meso- and larger micro-scale catchments. In comparison to Soler (2003), nitrate concentrations showed an increase in surface water from nitrate hotspots at micro-catchment sites.

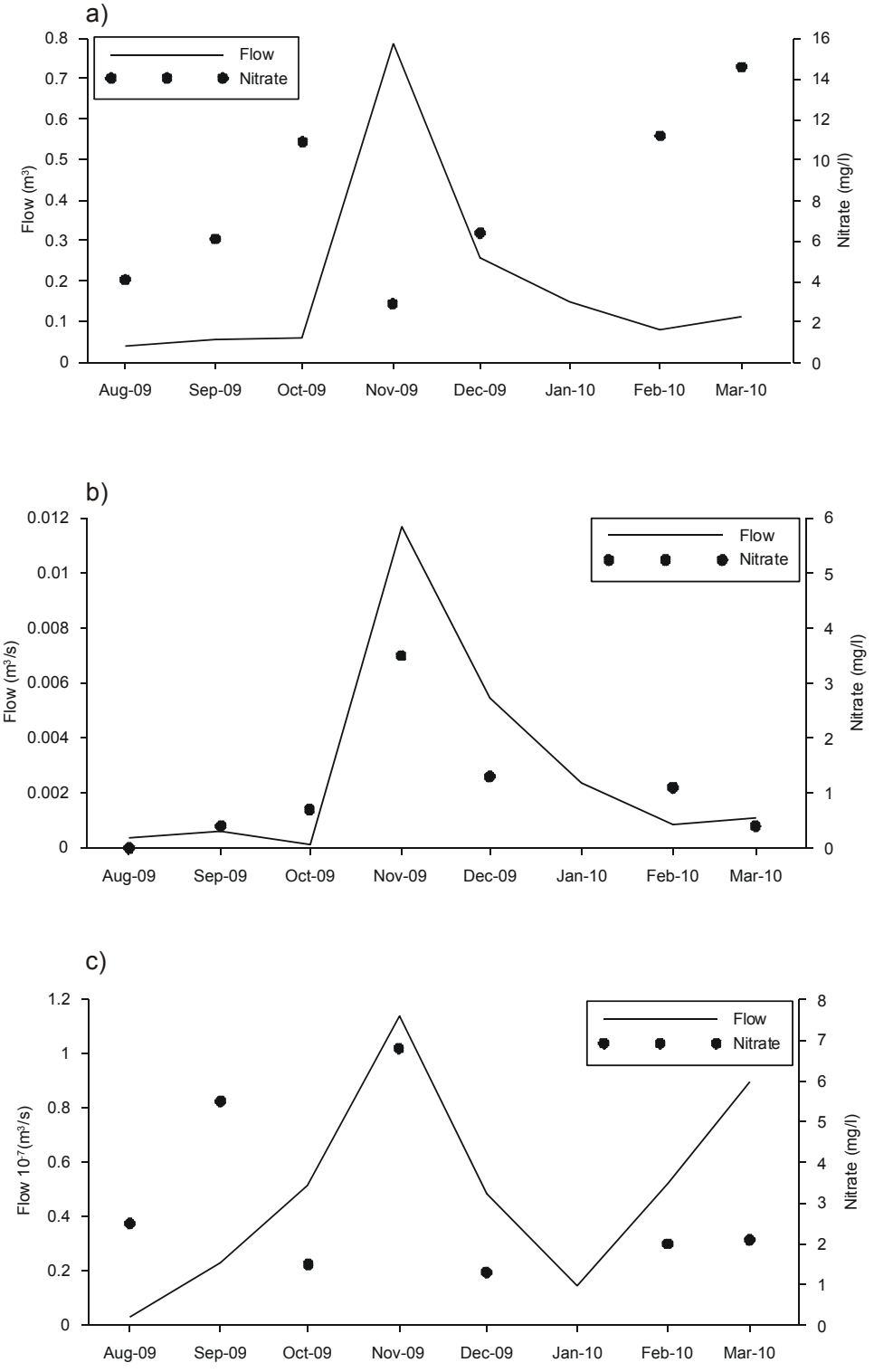

Figure 9-6 *Propagation of the discharge and nitrate concentration signal from: a) Blind Beck catchment (9.22 km^2), b) Hollow sub-catchment (0.09 km^2) and c) the plot within hillslope (2 m^2)*

During the flood event period in November 2009, the maximum flow recorded at the catchment scale (9.22 km^2) was 0.8 m^3/s with a minimum of 3 mg/l nitrate (Figure 9-6a). At the sub-catchment scale (0.09 km^2), the maximum flow recorded was 0.0108 m^3/s with a maximum of 3.5 mg/l nitrate (Figure 9-6b). At the plot scale (2 m^2), the maximum flow was $1.14x10^{-7}$ m^3/s with a maximum of 6.8 mg/l nitrate (Figure 9-6c).

It was possible to estimate nitrate loads across different scales in order to evaluate and predict the eventual effects of agricultural and/or farming on stream water quality. The nitrate load was obtained by multiplying the average concentration by the average flow:

$$Chemical\ load = Concentration\ x\ Flow$$

where: Chemical load = grams per second (g/s) or kilograms per hour (kg/h); Concentration = grams per litre (g/l); Flow rate = cubic metres per second (m^3/s) (in general consisting of only one sample)

The nitrate loads during the extreme November event varied from 2.4 g/s to 0.038 g/s to $7.74x10^{-7}$ g/s from the Blind Beck catchment to the Hollow sub-catchment to the hillslope plot scale. The nitrate concentrations showed an increase from the catchment to sub-catchment to plot scales while the nitrate load showed the opposite trend.

The nitrate loads per hectare were calculated by dividing the chemical load by the area. Of the catchment, sub-catchment and plot scales, greatest nitrate loads per ha were identified at the sub-catchment scale of 0.0042 g/s/ha. High nitrate loading per ha was evident at plot scale of 0.0039 g/s/ha. The nitrate loads per ha at the catchment scale were 0.0026 g/s/ha.

Using the results from this study, nitrate loads can be scaled up to give a prediction of the nitrate load. The ability to use information about nitrate load from discrete areas to predict what conditions may be like in other locations can be very useful (Rudolph et al. 2010). The nitrate load estimated at the plot, sub-catchment and catchment scales can be used to estimate the nitrate load at the sub-catchment and catchment scale through upscaling approach. The simplest approach is to multiply the nitrate load of the plot scale by the area of the sub-catchment divided by the area of the plot scale. This gives the predicted nitrate load of the sub-catchment of 0.035 g/s. If the nitrate load of the plot scale is multiplied by the area of the catchment divided by the area of the plot scale, it gives the predicted nitrate load of the catchment as 3.6 g/s. The upscaled nitrate load from the sub-catchment to the catchment scale is 3.9 g/s. The upscaled nitrate load from the sub-catchment and plot scale to the catchment scale (3.9 g/s and 3.6 g/s) is almost

1.6 times higher than the estimated nitrate load for the catchment (2.4 g/s). This suggests a reduction in nitrate concentration by dilution. A major limitation in the prediction of the nitrate load at the catchment scale does not take into account many factors important at the catchment scale. Such factors include stream dilution effects during high flow and/or intensive farming drainage. The good agreement between the plot and the sub-catchment scale suggests that the plot scale conditions at the hillslope were more similar to the Hollow sub-catchment conditions (land use, soils, landscape, and nitrate management) than conditions at the catchment scale. This is consistent with Mulla et al. (2003) who suggest that the upscaling techniques do not seem to depend on the magnitude of upscaling as on the relative similarity between the smaller unit that is upscaled and the larger unit. It is obvious that types of measurements taken at a point (1 m^2) differ from the measurement made at the hillslope scale (1 ha), in small catchment of 1 km^2 or in large catchment of 1000 km^2 (Heathwaite 2001). Therefore, it should be noted that the upscaling effort required assumptions about the nitrate concentration reduction at the catchment scale. Further steps may include development of a correction factor. Because of a lack of data in terms of the other peaks of the event, the correction factor cannot be developed in this study. However, there is a good area scaling from the plot to sub-catchment but not from the plot and sub-catchment to the catchment.

Guo et al. (2002) recognize many potential sources of error and uncertainty during estimation of nutrient loads. Quinn (2002) stated that scaling-up techniques have been noted internationally as an important area of further research, and Heathwaite (2003) stated that scaling-up is associated with considerable uncertainty. Since data on concentrations is not continuous, it likely shows considerable error. The uncertain parameter is the nitrate concentration on days when no sample was taken. There are no other peaks of the event of similar magnitude to compare this nitrate load with.

9.5 Linking hillslope water chemistry with stream chemistry

The water chemistry results presented in this section are based on data collected from July 2009 to August 2010. Surface and subsurface waters were monitored and sampled on the plots of the hillslope to test runoff generation and stream chemical composition. There was a significant difference between the perturbed and control plots in the overland flow water quality. Linking the flow water quality results from the hillslope to the sub-catchment and catchment scales suggest a different chemical signature

(Figure 9-7). This difference has been studied by researchers, where linking hillslope runoff with stream hydrological conditions (Peters et al. 1995) and chemistry (Hill 1990) showed that the riparian zone may reset hillslope flow paths and chemical signatures (Robson et al. 1992). Comparing the cations, the dominant Ca^{2+} ion suggests that the bedrock geology is probably the main source on water chemistry in the streams. Stream water with the highest overall mean Ca^{2+} and Mg^{2+} concentrations (93 mg/l and 27 mg/l) is Blind Beck. The Ca^{2+} concentrations showed an increase from the plot to sub-catchment and to catchment scales that reflecting the limestone geology. Burns, et al. (1998) reported that differences in the degree of chemical weathering in soil minerals may also be related to flushing frequency.

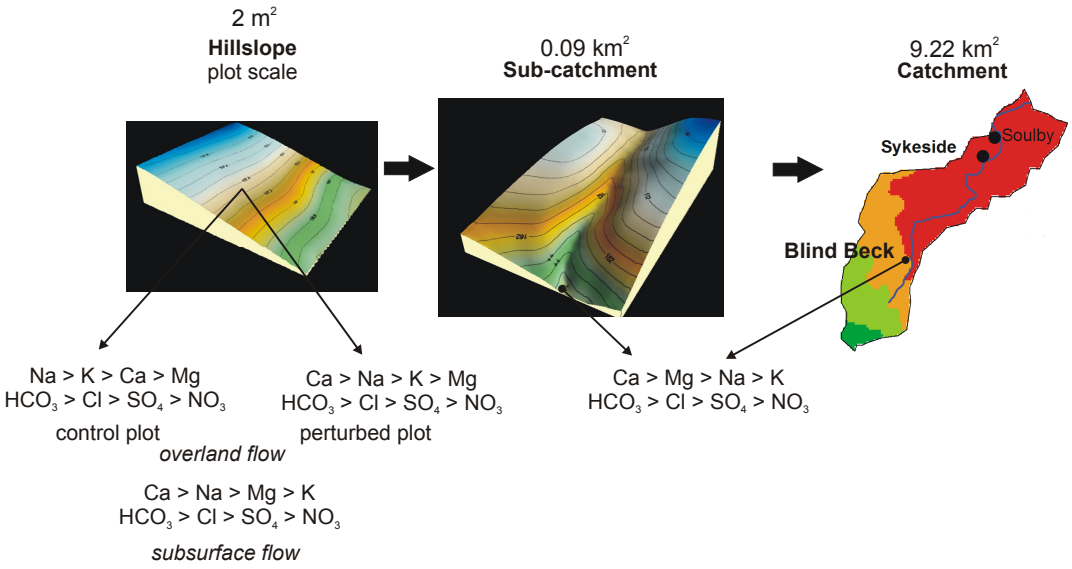

Figure 9-7 *Scale link water quality data*

The results show that there is a significant relationship between the hillslope flow and sub-catchment and/or catchment flow during enhanced rainfall conditions (perturbed plot). However, there is no significant relationship between the overland flow of the hillslope (control plot) and sub-catchment and/or catchment for the normal rainfall conditions. Chemical analyses of the overland flow water samples at plots suggest storm discharge into streams as a mixture of "old" and "new" water that has been transported from the hillslope to the sub-catchment prior to the intensified rainfall event. This suggests that the sub-catchment and catchment may be supplied largely with "old" water. Ockenden (2010) investigated stream water chemistry of Blind Beck using a hydrograph separation based on two end-members: bicarbonate concentration and specific conductivity. For the period September to December 2008, the hydrograph separation for Blind Beck stream indicated 46% ± 8% of "old" water. In this study, the

chemistry of the subsurface flow at the hillslope is more similar to the chemistry of the overland flow of the perturbed plot within the hillslope than the catchment scale. There have been relatively few studies of chemical evolution on hillslopes because of the complexity in deriving chemical models of subsurface flow at the hillslope scale (Bishop et al. 1990; Wilson et al. 1991; Burns et al. 1998). By contrast, most studies and models of water chemistry have been focused at the catchment scale (Cosby et al. 1985; Hooper et al. 1990; Wolford et al. 1996). The chemical signature of soil water in the hillslope differs from the chemistry of riparian water where all hillslope water must pass through the riparian zone before reaching the stream (Katsuyama and Ohte 2005).

To be able to fully represent the linkages between the hillslope and the catchment water chemistry, this study needs to consider groundwater and riparian zone chemistry with their contribution to the stream. As a consequence of this limitation, the linkages described in this thesis are not crucial.

9.6 Summary

This chapter described the development of a conceptual model of runoff and nutrient flushing from the hillslope to the catchment scale. The model accounts for both the overland (specifically saturation-excess overland and lateral subsurface mechanisms of runoff production. The effect of soil moisture on subsurface flows and the development of areas of saturated soils are accounted for.

Nutrient flushing at the hillslope scale was assessed for low and intense rainfall conditions, and it is concluded that different flushing mechanisms occurred during these two conditions. The following flushing mechanisms are proposed: (1) during low rainfall or dry periods, the shallow-subsurface flow with deep-subsurface storm flows may facilitate the flushing of high concentration of the DOC, (2) during heavy rainfall, the deep-subsurface flow is attributed to flushing of the high DOC concentration, (3) during low rainfall, the deep-subsurface flow is responsible for flushing of high nitrate concentration to the catchment, and (4) during heavy rainfall, the overland and shallow-subsurface storm flows are contributed to high nitrate concentration flushing to the catchment.

In this chapter, the best results for nitrate loads upscaling to the sub-catchment scale (0.09 km^2) were obtained from the plot scale (2 m^2) within the hillslope scale (45 m^2), rather than from the plot and sub-catchment scale to the catchment scale (9.22 km^2).

This is because the plot scale conditions at the hillslope were more similar to the Hollow sub-catchment conditions (land use, soils, landscape, nitrate management) than conditions at the catchment scale. Upscaling predictions of the nitrate load were reasonably good. The potential errors need to be considered during monitoring of data and uncertainty of the nitrate concentration on days when no sample was taken.

Analysis of ions showed that the concentrations of most ions were highest in the Blind Beck stream. Compared to other sites, Blind Beck had a high Ca^{2+} and Mg^{2+} concentration that indicates more effect on rock weathering in the stream water. The sub-catchment and catchment may be supplied largely with "old" water. One of the main limitations highlighted within this chapter concerns lack of groundwater and riparian zone chemistry data.

As with all the work undertaken in this thesis, there are alternative approaches, methods and/or modelling that may be suited to the work carried out here. Therefore, Chapter 9 also presents an exploration of the work presented in this study by critically considering what has been achieved as well as developing ideas for future work.

Chapter 10. Application of SHETRAN for simulation of hydrological and nitrate processes at catchment, sub-catchment and hillslope scales

10.1 Introduction

In this chapter, a distributed physically based hydrological model SHETRAN is used to simulate runoff generation, soil moisture and nitrate storage and transport in the Blind Beck catchment and the Hollow sub-catchment. The modelling approach will help to improve understanding of the hydrological components of the water balance at both the catchment and hillslope scale, and how they behave over different scales.

This chapter begins with the introduction of the model and the input data, including the maps that were created to run the model. Parameter calibration and validation of the model is presented, and the model results of runoff, soil moisture and nitrate are analysed and discussed.

10.2 The chosen model

French and Deelstra (2003) gave a list of the following four factors as important to consider when choosing a suitable model:

- Time needed to set up a specific model, data availability
- Cost of commercial software, technical support
- Need for knowledge (input data, programming knowledge)
- Model availability/development.

The following questions are addressed when considering the SHETRAN model for research purposes:

- Is the model available (time and money)?
- Who else uses the SHETRAN model and their experience?
- Is it possible to have the technical support in time?
- Is the SHETRAN model under continuous revision?
- What are the model inputs data requirements, model parameters, model structure and output results?
- What would be the time and space resolution of input data?

As mentioned in the fourth Chapter 4, Section 4.9, the SHETRAN model has been developed at the Newcastle University and considering the selection factors and questions listed above, it is selected for the simulation of hydrological processes at the catchment and hillslope scale. In this study, SHETRAN is used as the hydrological model. The detailed information about the model can be found in the corresponding user's manuals and websites (http://research.ncl.ac.uk/shetran).

In this study the SHETRAN model was applied to the Blind Beck catchment (9.22 km^2), Hollow sub-catchment (0.09 km^2) and hillslope (45 m^2) scales. A manual calibration and validation procedure was performed in order to account for hydrological differences across scale.

10.3 Model setup

This section discussed the application of the SHETRAN model for the Blind Beck catchment, the Hollow sub- catchment and the hillslope.

A Geographical Information System (GIS) tool was applied in this study to shape the geomorphological features of the catchment. ArcGIS 10.1 software was used in this research to prepare, analyse and represent data for particular the catchment and the sub-catchment.

10.3.1 Model setup for Blind Beck catchment

A Digital Elevation Model (DEM) was used to define the physical characteristics of the catchment area and to derive different additional datasets that collectively describe the drainage pattern of the catchment.

Delineation of the Upper Eden basin was completed with ArcGIS. The use of readily available 50 m resolution DEM of the Upper Eden basin constructed by Walsh (2004) allows the procedure to be easily replicated. The catchment grid delineation process relies on the hydrology tool in the main menu of the ArcGIS Spatial Analysis tool to define watersheds and stream networks shown in Figure 10-1. Preparation for running the Watershed processing feature includes running the fill, the flow direction, the sink, the flow accumulation and the stream functions. The watersheds may now be delineated with the Watershed function in ArcGIS. This function utilizes the flow direction surface to identify all cells flowing out of the specific outlet. The flow direction raster and the

outlet or feature pour point data were used as input to the watershed function in ArcGIS. Each cell has an outlet point called a pour point that indicates the location where water would flow out of the cell. The created catchment is in a grid format and it is represented as a polygon. The Blind Beck catchment area was extracted from the Upper Eden basin by use of a mask function. The mask function eliminates the undesired area of an image by multiplying the source image by the mask image that contains two values 1 for preserved areas and 0 for undesired areas.

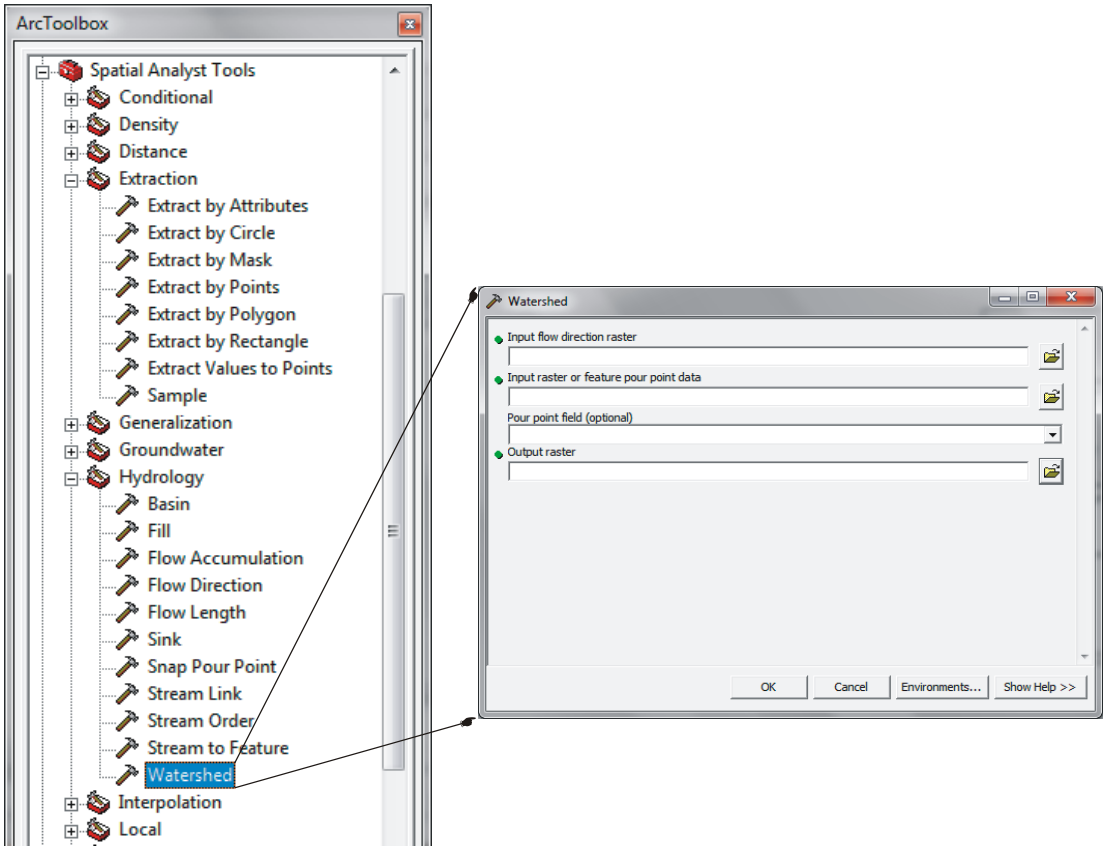

Figure 10-1 *Illustration of main menu of Arc Spatial Analysis tools and Watershed function*

To change the grid size, the 50 m DEM was aggregated to a grid cells of 100 m x 100 m size with the generalization tool in ArcGIS spatial analysis using aggregate function (Figure 10-1). The resultant rectangular raster grid (100 m, 100 m) had 56 rows and 48 columns. Within this raster grid, the catchment area was defined by 922 cells that comprise the active model domain for the overland plane. Figure 10-2 shows the map or shape of the Blind Beck catchment, which would be the border of the counted values for computation, any value of the model variables and parameters outside this domain will be ignored. Figure 10-2 shows the tops of the columns in plain view and stream channel network lies along the edges of the surface finite difference cells.

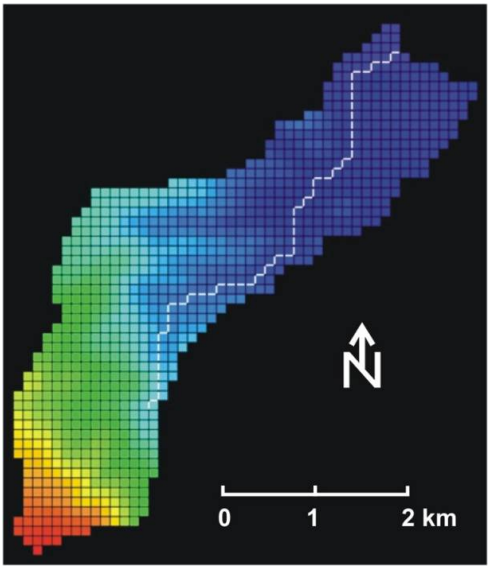

Figure 10-2 *SHETRAN mesh (100 m grid resolution) and elevations for the Blind Beck catchment. The stream channels run along the edge of the grid squares (colours have no significance)*

10.3.2 Model setup for Hollow sub-catchment

For the Hollow sub-catchment, the TIN as the result of GPS points of the sub-catchment (described in the subsection 4.2.2) was converted into raster format, using TIN-to-Raster-conversation function in 3D Analyst module of ArcGIS, and the resultant GRID format of the sub-catchment is shown in Figure 10-3. The GRID resolution was set as 10 metres in this transformation from vector (TIN) to raster (GRID) format. In a second step, the masking function was used to cut out only the Hollow sub-catchment. The raster (GRID) presents grid cells of 10 x 10 m cell size of DEM.

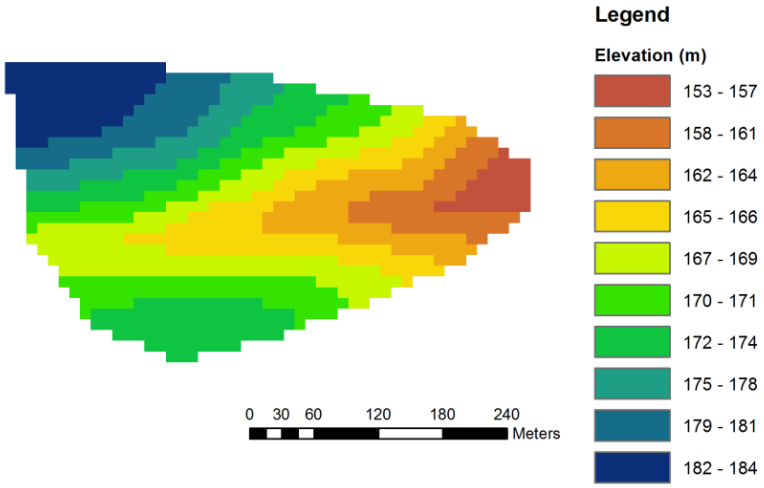

Figure 10-3 *GRID maps of Hollow sub-catchment. The maps are composed of raster cells of 10 m by 10 m area*

The resultant rectangular raster grid (10 m, 10 m) had 29 rows and 49 columns, and the sub-catchment was defined by 944 cells. A shape of the sub-catchment is shown in

Figure 10-4 which would be the border of the counted values for computation, and any value outside of the model would be ignored.

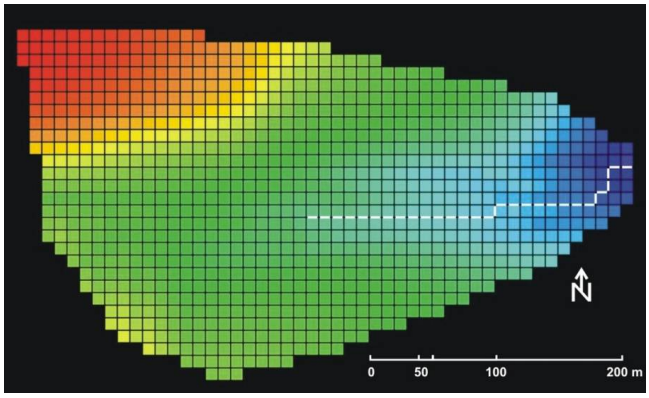

Figure 10-4 *SHETRAN mesh (10 m grid resolution) and elevations for the Hollow sub-catchment. The stream channels run along the edge of the grid squares (colours have no significance)*

10.3.3 Model setup for hillslope

The model summarized here was accompanied by an extensive field study. The model was "physically based" in the sense that its parameters have a physical meaning and can be derived from field measurements or experiments. The conceptual model represents the hillslope as a rectangular storage element of length L and depth D. The hillslope was assumed to be composed of three parallel soil layers of depth h, of nearly the same characteristics. The two-dimensional version of the hillslope model was developed with the hillslope sequence taken from the top of the hillslope down to the lower slopes (45 m long).

The location of the cross-section through the Hollow sub-catchment (Figure 10-5) was prepared in ArcGIS using DEM to estimate the elevation of the top of the hillslope down to lower slope. Once the estimation was performed, the resulting elevation data were exported to Excel to produce a cross-section of the hillslope (Figure 10-6).

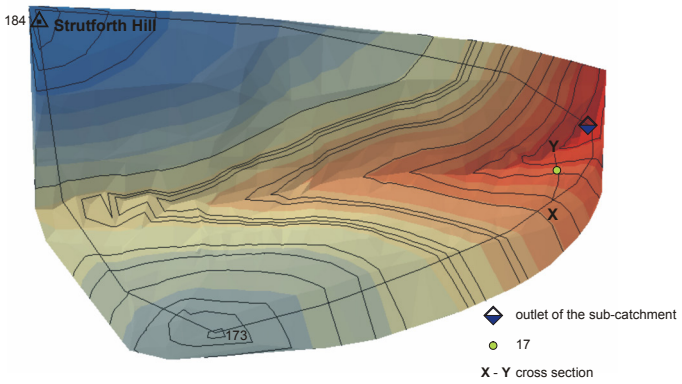

Figure 10-5 *Location of a cross - section through the Hollow sub-catchment*

The hillslope model was broken into 45 grid cells (Figure 10-6) where each grid had the reference of level depth, soil and vegetation parameters.

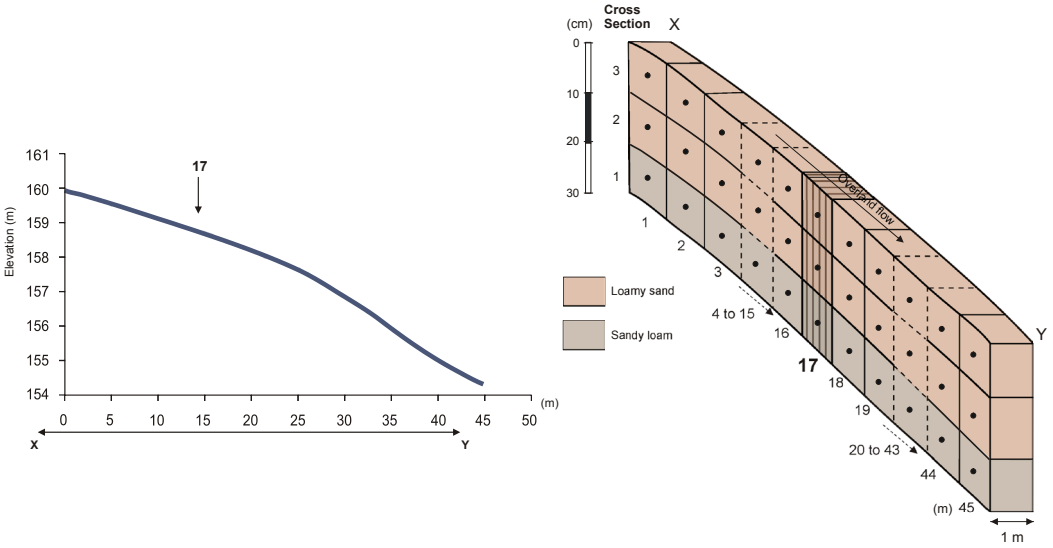

Figure 10-6 *A cross-section X-Y of the hillslope profile. The instrumented runoff plots are highlighted with 17*

The thickness of soil layer was fixed at 10 cm which was considered appropriate to describe processes such as lateral subsurface flow and nutrient leaching. The bottom layer of the calculated soil column was numbered by 1 with layers increases upwards to the top layer numbered by 3.

The lower boundary of the soil profile was governed by the presence of a gravity drained bottom boundary condition and a lateral flow boundary at the top. A schematic illustration of the soil profile is shown in Figure 10-7. A two-dimensional (horizontal/vertical) version of the model was developed. In the unsaturated soil matrix, water movement of the hillslope was approached by approximating the Richard's equation.

The characteristic hillslope model represented water movement along a two-dimensional section of soil down to a stream weir. All parameters were assumed to be uniform within each model cell. The lateral subsurface inflow was assumed to enter the hill at the top and producing lateral subsurface outflow (Figure 10-7) where downslope entering the stream weir. Percolation was assumed as gravity drainage with no physical connection with the groundwater.

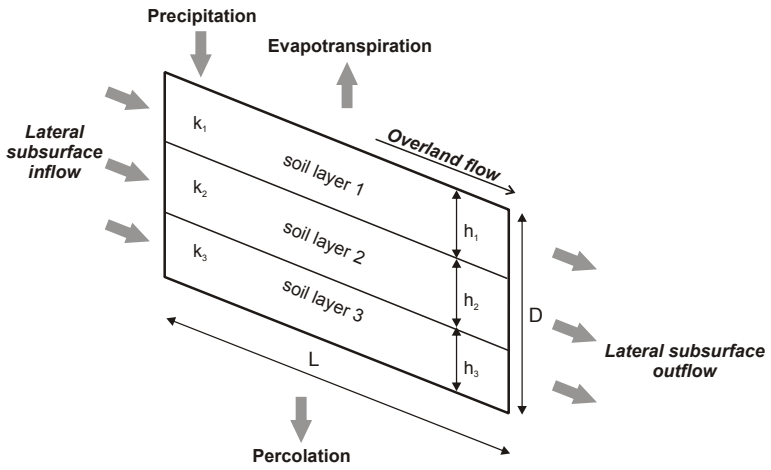

Figure 10-7 *Conceptual hydrological hillslope 2D model (length L, hydraulic conductivity k_{1-3}, thickness of soil profile D, thickness of layer h_{1-3})*

10.3.4 SHETRAN input files

The basic data sets required to develop the SHETRAN model inputs are: topography, climatic data (rainfall and potential evapotranspiration), land use and soil.

Topography

Blind Beck: The 50 m DEM of the Upper Eden basin after aggregation as described above was used to represent the land elevation of the Blind Beck catchment in the model. The 100 m DEM and MASK files were prepared as input files in the SHETRAN model.

Hollow: The 10 m raster (GRID) was used to represent the land elevation of the Hollow sub-catchment in the model. The raster (GRID) was converted to ASCII format. In the processing stage of data input during the implementation of the model runs, the 10 m DEM and MASK were prepared as input files.

Precipitation

Rainfall time series (mm/hour) are a compulsory input data in the SHETRAN model for the entire studied period. Hourly rainfall data were obtained from the Hydrolog data base. The selected period for the catchment was from 01/01/2008 to 31/08/2010, and for the sub-catchment 01/06/2009 to 17/08/2010.

Potential evapotranspiration (mm/day)

Daily potential evapotranspiration (PET) values are required by SHETRAN, which was calculated using a weather generator. The weather generator (WG) can generate

precipitation and other variable data at a given location on a map interface system. The main reason to use the weather generator for PET is due to the problems with the CHASM AWS that resulted in no available data. The potential evapotranspiration (PET) was calculated using a FAO-modified (Food and Agriculture Organisation of the United Nations) version of the Penman method. The Penman-Monteith form of the combination equation is:

$$ET = \frac{\Delta(R_n - G) + \rho_a c_p \frac{(e_s - e_a)}{r_a}}{\Delta + \gamma\left(1 + \frac{r_s}{r_a}\right)}$$

where: Rn = the net radiation, G = the soil heat flux, (es - ea) represents the vapour pressure deficit of the air, ρa = the mean air density at constant pressure, cp = the specific heat of the air, Δ = the slope of the saturation vapour pressure temperature relationship, γ = the psychrometric constant, and rs and ra = the (bulk) surface and aerodynamic resistances.

More details and the formula used to calculate the PET by the WG can be found in the papers by Ekström et al. (2007) and Kilsby et al. (2007). Kilsby et al. (2007) describe the general approach taken in the weather generator that is more sophisticated than Neyman-Scott point process model (Cowpertwait 1991) (for current climate condition, as future climate condition are ignored) as:

- Observed data of rainfall and other weather variables used to define current climate,
- Weather generator model based on a regression relation between daily climatic variables and daily rainfall: parameterised using current climate data, and then applied for future climates, using future factored daily climate variable statistics,
- Software implementation using a map viewer linked to a spatial database allowing the flexible selection of areas for generation of the series.

Figure 10-8 shows schematic of the operation of the weather generator described by Kilsby at al. (2007).

Daily rainfall data sets from the Sykeside raingauge (sub-catchment) were selected as input to the weather generator to generate daily weather variables from which potential evaporation was extracted. Using the GIS interface on the weather generator, the local catchment was selected which contained the selected raingauge. The advantage of using data obtained from the weather generator is that it allows a larger spatial coverage of the PET data.

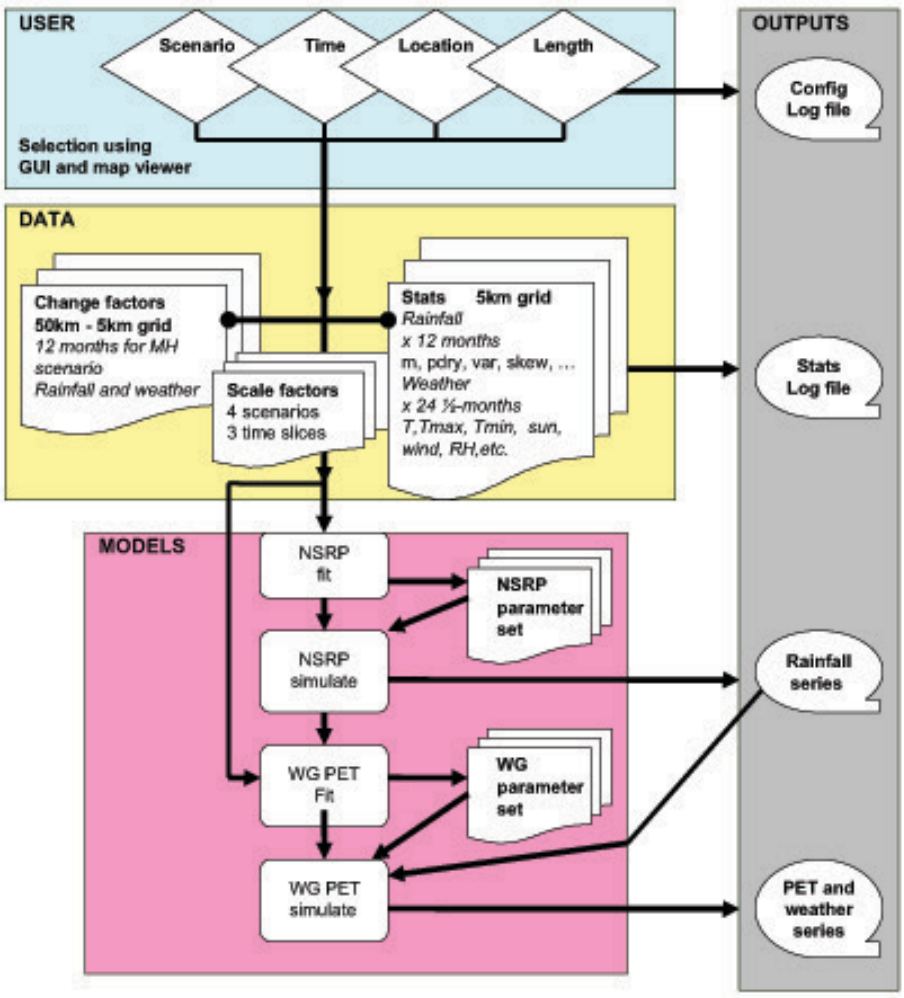

Figure 10-8 *Schematic of operation of the weather generator including map viewer (source: Kilsby et al. 2007)*

Land use

A land use map provided spatial distribution of major land cover classes within the catchment area and affects the hydrology in the model including dependant parameters such as: root density function (RDF) and the actual/potential evapotranspiration function as a function of soil water potential.

The source of the land use map is the Land Cover Map of Great Britain 1990. The area of the Blind Beck catchment was extracted from this map using ArcGIS. More detail is given in Chapter 4.

A set of parameters was used in the evapotranspiration component of the SHETRAN model: soil moisture tension, canopy resistance, leaf area index, maximum rooting depth, AE/PE at field capacity. The values of these parameters were based on literature reported values or supplied with the SHETRAN model.

Vegetation related parameters

In the computation of the actual ET and interception used for preliminary runs in this study, parameter values for grass were proposed and presented in Table 10-1. For preliminary runs of the model, the values of these parameters were assumed not to vary during the simulations.

Table 10-1 *Vegetation properties for the hillslope model*

Properties/Vegetation type	Grass	Reference
Canopy storage capacity (mm)	1.5	Rutter (1975)
Leaf area index	6	supplied with SHETRAN
Maximum rooting depth (m)	1	supplied with SHETRAN
AE/PE at field capacity	0.6	Shuttleworth (1993)

The proposed initial values for the hillslope model were just starting point values, which were adjusted during calibration process.

Soil types

The soil map of the Upper Eden basin was available from Newcastle University, UK. The area of the Blind Beck catchment was extracted from the Upper Eden basin. The HOST Classification (The Macaulay Institute 2008) was used to classify soils for the sub-catchment. The soils map consists of five soil types (Figure 4-7). For the modelling in this study, physical properties of the soil were used: saturated hydraulic conductivity, porosity, residual water content, specific storage and the parameters for the van Genuchten soil characteristics (α and n). The values of these parameters were based on literature reported values or supplied with the SHETRAN model. The overall soil depth modelled was selected to be 2 m but within this, the focus was primarily on the shallow soil horizons.

Hillslope

The soil type of the different soil layers at the hillslope were based on the soil samples collected from the field. The particle size distribution analyses and the soil texture triangle were used to classify the texture class. The proposed initial values of the soil water content at saturated conditions (porosity) of the different soil layers were estimated taking into account ranges of values reported in the literature, Table 10-2 (Freeze and Cherry 1979).

Field measurements did not include saturated conductivity. Thus, the initial values of saturated hydraulic conductivities for loamy sand and sandy loam textures were based on literature reported values (Rawls et al. 1982) for representative physical properties of

soils by texture as shown in Table 10-2. The initial value of residual water content assumed for loamy sand (0.075) and sandy loam (0.098) is reported by Freeze and Cherry (1979). Table 10-2 gives the soil parameters used for the hillslope simulation.

Table 10-2 *The initial soil parameters for unsaturated zone used in the hillslope model simulation*

Properties/Layers	Layer 1	Layer 2	Layer 3	Reference
Soil type	Loamy sand	Loamy sand	Sandy loam	lab measured using PSD
Layer depth (cm)	10	20	30	field measured
Saturated Water Content (porosity)	0.37	0.37	0.412	Freeze and Cherry (1979)
Residual Water Content	0.075	0.075	0.098	supplied with SHETRAN
Saturated Conductivity (m/day)	1.467	1.467	0.622	Rawls et al. 1982
van Genuchten-α (cm^{-1})	$1.99x10^{-2}$	$1.99x10^{-2}$	$1.44x10^{-2}$	supplied with SHETRAN
van Genuchten-n	1.793	1.793	1.736	supplied with SHETRAN

10.3.5 Measured discharge

Stream flow data were collected at one gauging station within the catchment at the Blind Beck stream, and at the outlet of the sub-catchment. The stream flow data were disaggregated from a 15 minute interval to mean hourly intervals in order to compare with simulated hourly flow data from the model.

Measured flow data at a plot scale were the only available data at the hillslope scale. The runoff data were collected for the period from April 2009 to August 2010 at the plot scale of the hillslope.

10.4 Hydrological model calibration and validation

The effectiveness of hydrological models depends both on how well the model is calibrated and how it performs during validation (Ajami et al. 2004; Bekoe 2005). The calibrated model should be tested against an independent set of measured data, which is commonly used as model validation. The practice in hydrological modelling is to divide available time series data into two sets (Klemes 1986). According to that one set is used for calibration and the remaining data used for validation.

Once the model has been set up, the next step is to calibrate the model in order to adjust measured discharge with simulated. The parameters were manually optimised by trial-and-error. The quality of each set of parameters for which the SHETRAN model was run was tested using calibration statistics and visual inspection of the hydrographs.

Madsen (2000) noted that for a proper evaluation of the calibrated model, it is necessary to translate the overall calibration objective into more operational terms. With this observation, he noted that the following objectives should be considered for proper evolution of the calibration model (Madsen 200:278):

1) "a good agreement between the average simulation and observed catchment runoff volume (i.e. a good water balance)
2) a good overall agreement of the shape of the hydrograph
3) a good agreement of the peaks with respect to timing, rate and volume
4) a good agreement for low flows".

SHETRAN was manually calibrated by estimating of various parameters in order to understand their relevance and also was gain control over mean annual water balance, as suggested by Santhi et al. (2001).

10.4.1 Calibration parameters

The SHETRAN model is most sensitive to external inputs of precipitation and potential evapotranspiration (PET). However, these weather inputs are typically not adjusted during calibration. Within the model, the annual water balance is usually most sensitive. Table 10-3 shows the key model parameters used in the calibration process in the SHETRAN model to which the simulations are most sensitive. In the Blind Beck catchment and Hollow sub-catchment the model was calibrated using 5 parameters to fit the model results to the measured values. For parameters that were calibrated are given a brief explanation in this section.

Table 10-3 *Calibrated parameters*

Parameter	Description
Kx, Ky, Kz	Saturated hydraulic conductivity (m/day)
θ_{sat}	Volumetric saturated soil water content (porosity)
θ_{res}	Volumetric residual water content
n	van Genuchten n parameter
α	van Genuchten α parameter (cm^{-1})

Saturated hydraulic conductivity

This calibration parameter is an essential parameter for understanding soil hydrology. The saturated conductivity (K_{sat}) is the rate of discharge per unit area through a saturated medium. It varies considerably in soils from less than 0.01 m/day in clay soils to over 100 m/day in gravel alluvium.

The hydraulic conductivity ($K_{x,y,z}$) in a soil is greatest when the soil is saturated ($\theta = \theta_{sat}$), while as the soil dries out the larger pores spaces no longer hold any water, the conductivity is confined to the smaller pore spaces and the hydraulic conductivity decreases.

The saturated conductivity values are defined for each soil and rock in the x, y and z directions and given in SHETRAN Data Requirements, Data Processing and Parameter Values report.

Volumetric saturated soil water content (porosity)

The volumetric saturated soil water content is by definition the moisture content when all pore space is occupied by water. However in the real world it is not 100% of the soil porosity occupied by water, because there is always air trapped in micro pores. The value of the porosity for soil range from 0.3 (30%) in sand soil to 0.6 (60%) in clay soil. Coarse-textured soils tend to be less porous than fine-textured soils.

Volumetric residual water content

This calibration parameter (degree of saturation or volumetric water content and soil suction) defines the residual state condition of soil and represents one location along the soil-water characteristic curve. Residual water content can be associated with the immobile water present within a dry soil profile in films on particle surfaces in the interstices between particles, and within soil pores.

Van Genuchten parameters

The van Genuchten parameters **α** and **n** (van Genuchten 1980) together with the saturated moisture content and the residual moisture content fully describe the soil-water potential (θ) and the soil-water content (Ψ) relationship of unsaturated soils and fractured rock. The van Genuchten's soil water retention curve model (van Genuchten 1980) is described by:

$$\frac{\theta - \theta_r}{\theta_s - \theta_r} = [1 + (\alpha|h|)^n]^{-m}$$

where: θ = the volumetric water content (cm^3cm^{-3}), θr = the residual water content (cm^3cm^{-3}), θs = the saturated water content (cm^3cm^{-3}), h = the water pressure (kPa), α = a scaling parameter that is inversely proportional to mean pore diameter (cm−1), n = the soil water characteristic curve index (shape parameter of the curve), and m = 1 − 1/n. θr and θs can be measured directly. α and n = fitted parameters.

10.4.2 Model Performance

Model performance was evaluated with an hourly discharge time step for the entire available record. Two statistical performances were used: the goodness-of-fit measures were a coefficient of determination (R^2 coefficient), and a Nash-Sutcliffe efficiency (NSE) (Nash and Sutcliffe 1970).

The R^2 measure is the coefficient of determination, which describes how much of the variance between the two variables is described by a linear fit.

$$R^2 = \frac{[\sum_{t=1}^{T}(Q_m^t - \overline{Q_m})(Q_o^t - \overline{Q_o})]^2}{\sum_{t=1}^{T}(Q_m^t - \overline{Q_m})^2 \sum_{t=1}^{T}(Q_o^t - \overline{Q_o})^2}$$

where: Q_o = observed discharge, Q_m = modelled discharge, Q_o^t = observed discharge at time t

The R^2 values can range from 0 to 1. The higher a value of R^2, the more useful the model is. The value of 1 for the R^2 is the best, while the value of 0 means that none of a variance measured data is replicated by the model prediction. Henriksen et al. (2003) suggests that R^2 value > 0.85 is excellent for a hydrological model, values between 0.65 and 0.85 are very good, 0.50-0.65 are good, 0.20-0.50 are poor and < 0.20 are very poor (Whitehead 2005).

The Nash-Sutcliffe model efficiency coefficient is often used to assess a prediction efficiency of the hydrological models (Nash and Sutcliffe 1970). It is given by the formula:

$$NSE = 1 - \frac{\sum_{t=1}^{T}(Q_o^t - Q_m^t)^2}{\sum_{t=1}^{T}(Q_o^t - \overline{Q_o})^2}$$

The Nash-Sutcliffe efficiencies range from negative infinity to 1. The value of 1 (NSE=1) corresponds to a perfect match of modelled discharge to the observed data. The closer the model efficiency is to 1, the more satisfactory the model is. The simulation results were considered to be good if NSE ≥0.75, and satisfactory if 0.36 ≤ NSE ≤ 0.75 (van Liew and Garbrecht 2003). Liden and Harlin (2001) and Andersen et al. (2001b) state that a good simulation should have an NSE between 0.5 and 0.95.

Table 10-4 shows the calendar for the calibration and validation (split-sample test) for the catchment and sub-catchment. The model was run for a period of time (warm up) until the storage reaches a representative value. The SHETRAN model needs an adaptation period to read in the initial data input and to warm up until calculation equilibrium.

Table 10-4 *Calibration and validation calendar*

Site	Warm-up	Calibration	Validation
Blind Beck	01/01/2008 – 31/08/2008	01/09/2008 – 31/08/2009	01/09/2009 – 31/08/2010
Hollow	01/05/2008 – 31/05/2009	01/06/2009 – 07/01/2010	08/01/2010 – 17/08/2010

The hydrologic models were first calibrated by adjusting model parameters until the simulated and measured annual water budgets were in good agreement. Then, the intensity and arrival time of individual events were calibrated. This process was repeated until the simulated results closely represent the measured flow patterns and magnitude.

10.4.3 Calibration and validation for the Blind Beck catchment

The SHETRAN model was calibrated using the parameters mentioned in the previous section. The model was calibrated for the certain period until the parameters were consistent with the model input and output and the calculated discharge curve was close to the measured flow. Table 10-5 reports calibrated values for the Blind Beck catchment. These parameters were adjusted manually to produce the highest possible R^2 and ENS for the calibration year and therefore the same values were used to simulate the validation period.

Table 10-5 *Calibrated soil parameter values*

Parameter	Description	Soil layer	Value
Kx, Ky, Kz	Saturated hydraulic conductivity (m/day)	1	1.1140
		2	0.1830
		3	0.6220
		4	5.0400
		5	0.0050
θ_{sat}	Volumetric saturated soil water content (porosity)	1	0.5440
		2	0.4520
		3	0.4120
		4	0.3520
		5	0.1800
θ_{res}	Volumetric residual water content	1	0.3260
		2	0.0930
		3	0.0980
		4	0.0660
		5	0.0500
n	van Genuchten n parameter	1	1.4430
		2	1.6810
		3	1.7360
		4	1.8470
		5	2.0000
α	van Genuchten α parameter (cm^{-1})	1	0.0046
		2	0.0052
		3	0.0144
		4	0.0120
		5	0.0120

The hourly calibrated simulated stream flow of the Blind Beck catchment is shown in Figure 10-9. Period from 1/09/2009 to 31/08/2010 have been used to validate the Blind Beck catchment. The hourly validated simulated stream flow of the Blind Beck is shown, respectively, in Figure 10-10.

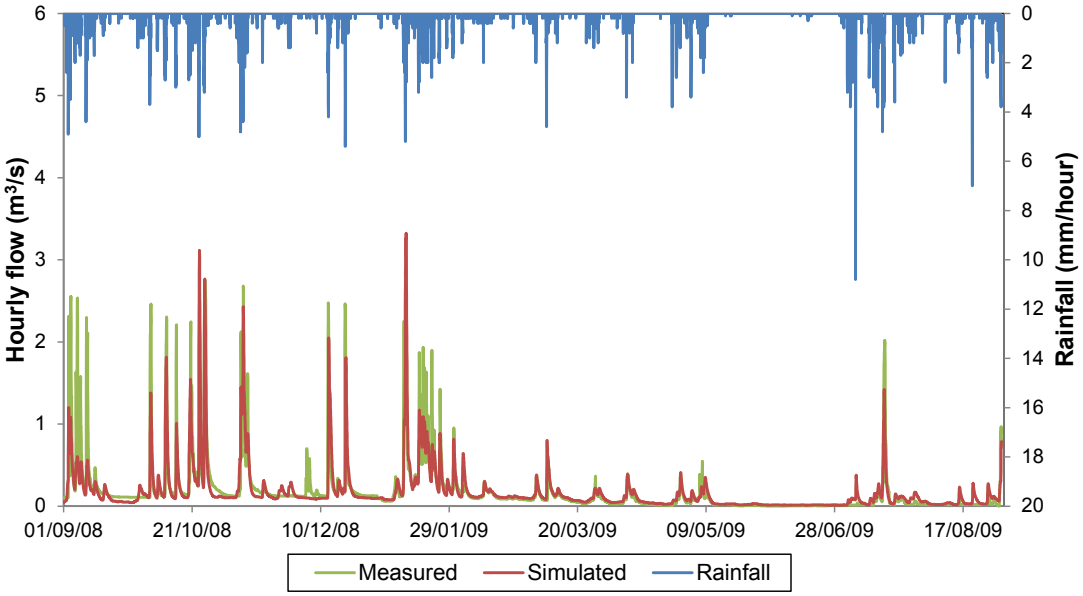

Figure 10-9 *Hourly calibrated simulated stream flow for the Blind Beck catchment*

The hydrograph of the measured and the simulated flow show that is not possible to achieve the best match of the entire shape of hydrographs throughout the simulation period. SHETRAN tends to underpredict some of the high flow periods, in particular those that happened in autumns and winters 2008 and 2009. For the calibration in 2008 and 2009 (Figure 10-9) the model overpredicted very high peak flows. Figure 10-10 shows that the November storm peak flows were underpredicted by SHETRAN during the validation period. However, the visual representations show that the model overpredicted the higher peak flow during the November storm event. In the 2010 simulation, hourly stream flow was overpredicted by the model for most of the time series.

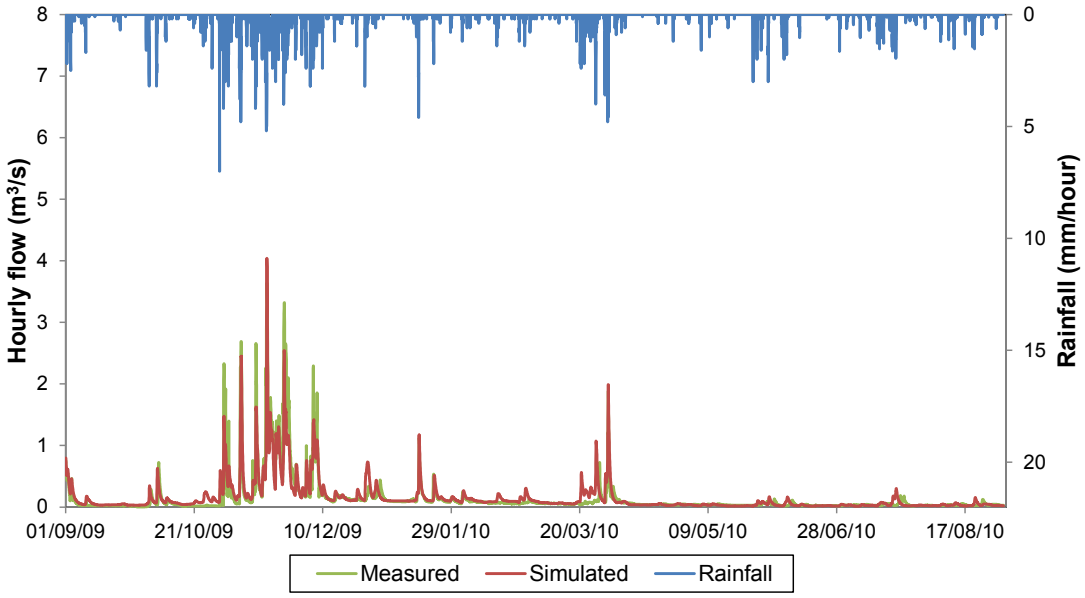

Figure 10-10 *Hourly validated simulated stream flow for the Blind Beck catchment*

Table 10-6 presents the summary statistics of the calibration and validation results. The performance efficiency (R^2) value for simulated versus measured hourly stream flow for the catchment was 0.74 for the calibration period and 0.84 for the validation period. According to Henriksen et al. (2003) the R^2 value falls into the range of very good model. The hourly calibration and validation NSE was 0.74 and 0.83 indicating satisfactory and good the model results according to NSE criteria of van Liew and Garbrecht (2003).

Table 10-6 *Calibrated and validated model performance statistics for hourly stream flow simulations in the Blind Beck catchment*

Dataset	Statistical test	Units	Blind Beck	Model Performance
Calibration	R^2	-	0.74	very good
	NSE	-	0.74	satisfactory
Validation	R^2	-	0.84	very good
	NSE	-	0.83	good

To provide a measure of model accuracy, average hourly model predicted and observed flows were compared through a regression analysis shown in Figure 10-11. The regression analysis indicates that the closer the data comes to the 45° angle line, the better the two data sets match. The analysis suggests that most of the flows were well correlated, with the modelled flows slightly over predicted in the validation period.

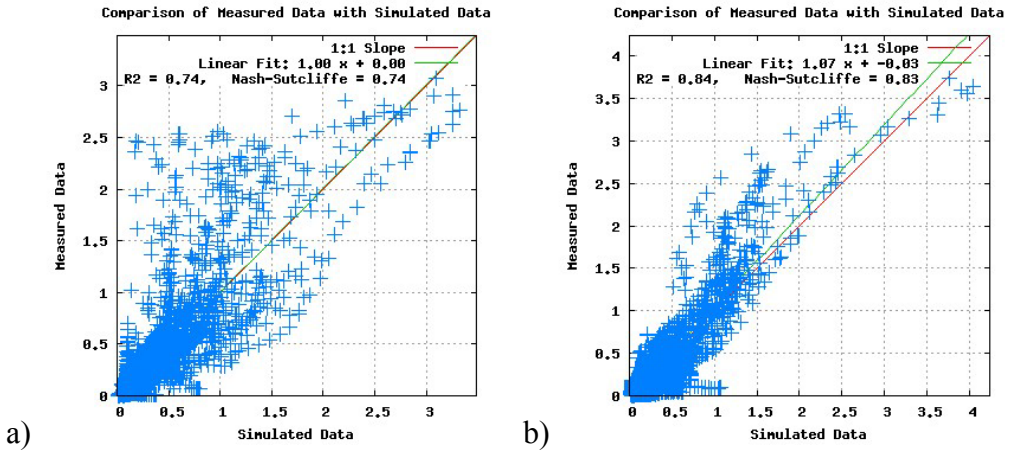

Figure 10-11 *Regression analysis of simulated and measured average hourly flows (m^3/s) during a) calibration period and b) validation period of the Blind Beck catchment (red line: line of equal value; green line: best-fit line)*

Another useful measure is an evaluation of model performance with respect to monthly variation. Figure 10-12 illustrates the variation of the measured and simulated flow by month. This graph indicates that the model slightly overpredicted stream flow from August to October 2009, from December 2009 to April 2010 and underpredicted flow during November 2009 month.

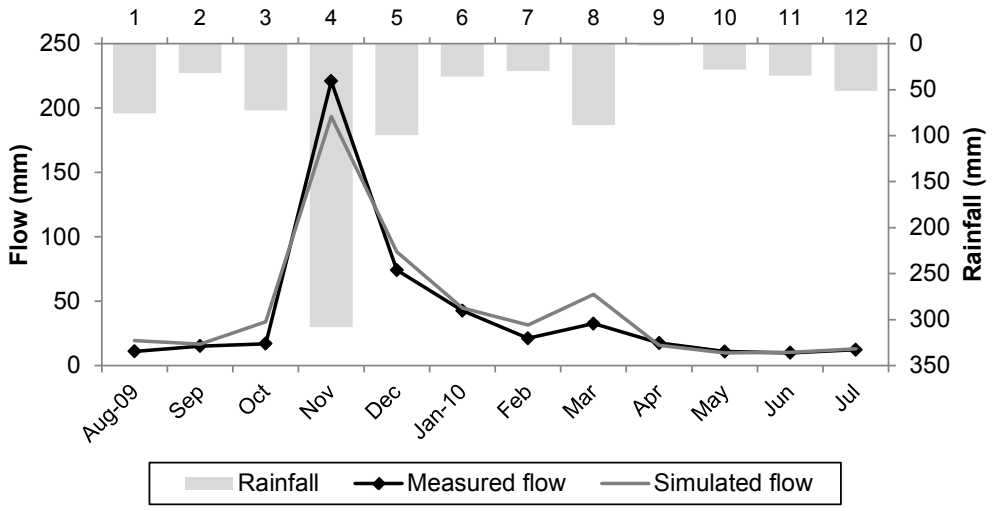

Figure 10-12 *Monthly variation of the simulated and the measured flow during calibration and validation of the Blind Beck catchment*

In addition, to the graphs above, flow duration curves of simulated and measured flows were compared to ensure that all flow regime trends were captured in the model. The graphs below give an overview of duration curves for calibration and validation periods. Figure 10-13 shows that the simulated flow duration curve in the calibration period follows the trends of the measured flow duration curve during most flow regimes.

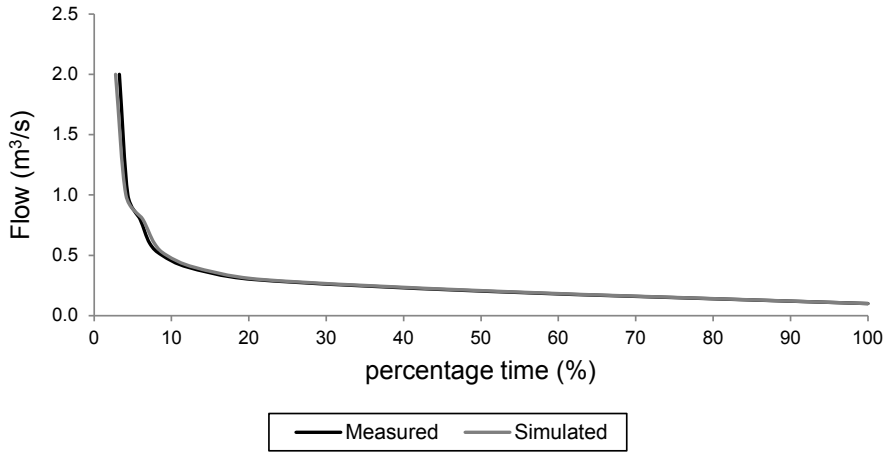

Figure 10-13 *Flow duration curves at Blind Beck for the calibration period*

The flow duration curves for measured and simulated hourly stream flows closest match for the most part for the validation period (Figure 10-14). Only some flows were overestimated by the model. From the results, it can be concluded that flow duration curves give relatively good results.

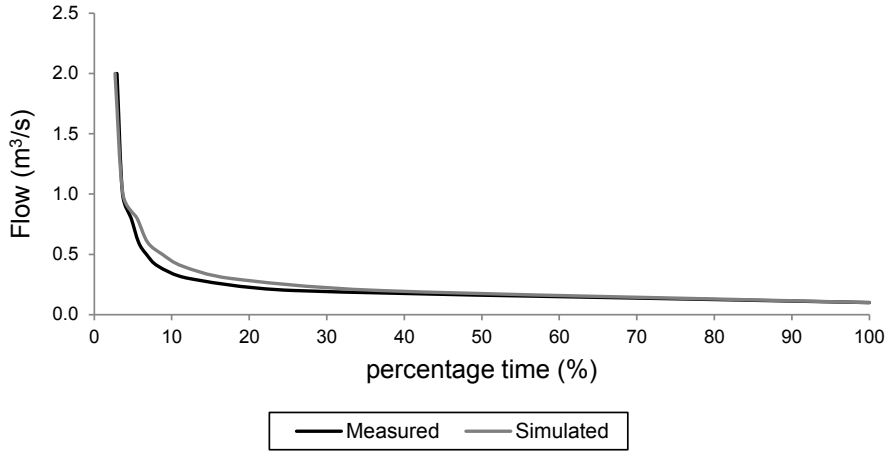

Figure 10-14 *Flow duration curves at Blind Beck for the validation period*

The observed comparisons of annual runoff volumes in Table 10-7 indicate that the simulation accuracy is different in the calibration and validation period. Total runoff for the calibration period was undersimulated by volume error of -0.8%. The total runoff for the validation was slightly overestimated by the model (9.8%). The % volume errors for the calibration and the validation period are less than ±10%, indicating a very good model for annual runoff.

Table 10-7 *Summary of annual simulated and observed runoff volumes (m^3)*

Calibration				**Validation**			
Year	OBS	SIM	ERR	Year	OBS	SIM	ERR
1/9/2008-31/8/2009	1611	1598	-0.8	1/9/2009-31/8/2010	1241	1362	9.8

SIM = Simulated, OBS = Observed, ERR = 100 x (SIM – OBS)/OBS %

Visual comparison of simulated and measured stream flow during the calibration and validation period shows that the model performed well in terms of the rainfall and flow relationships. Overall, a limitation of the simulation is to model the flow peaks adequately. Most of estimated peaks are lower than the measured. Except for large events, the hourly measured and simulated stream flow during the calibration and validation periods match reasonably well (e.g. for the July 2009 (E1) event simulation = 1.35 m^3/s and measurement = 1.72 m^3/s, while for the major flood event in November 2009 (E3) simulation = 4.04 m^3/s and measured = 3.64 m^3/s). It can be noticed that for the spring seasons the model gives better results than the winter periods. As seen from the presented graphs, the parameters that are found in the calibration process fit well for the validation process. The model gives better results for the validation than the calibration period according to R^2 = 0.84 and Nash–Sutcliffe efficiency = 0.83.

The calibration and validation results show that SHETRAN is reasonably able to predict the total discharge within the Blind Beck catchment, with all percentage errors falling below 10%. The model performance statistics show a range in model accuracy but the majority of the statistics reflect a good to very good overall performance. The measured and simulated annual mass balances agree well for 2008-2009 but differ for 2009-2010; Table 10-15 shows the overall balance.

10.4.3.1 Storm event simulation for Blind Beck stream

The final step in model calibration and validation is to examine the representation of individual storm hydrographs in both time periods. For the period 2009-2010 three storm events were incorporated within the SHETRAN model run (November 2009, January 2010 and March 2010). The graphs of the measured and simulated flow for the storm events (E3, E4 and E5) are presented in Figure 10-15.

The simulated and measured peak flows, time to peak flows, runoff volumes and percentage differences (errors) of the respective measured and simulated values are given in Table 10-8.

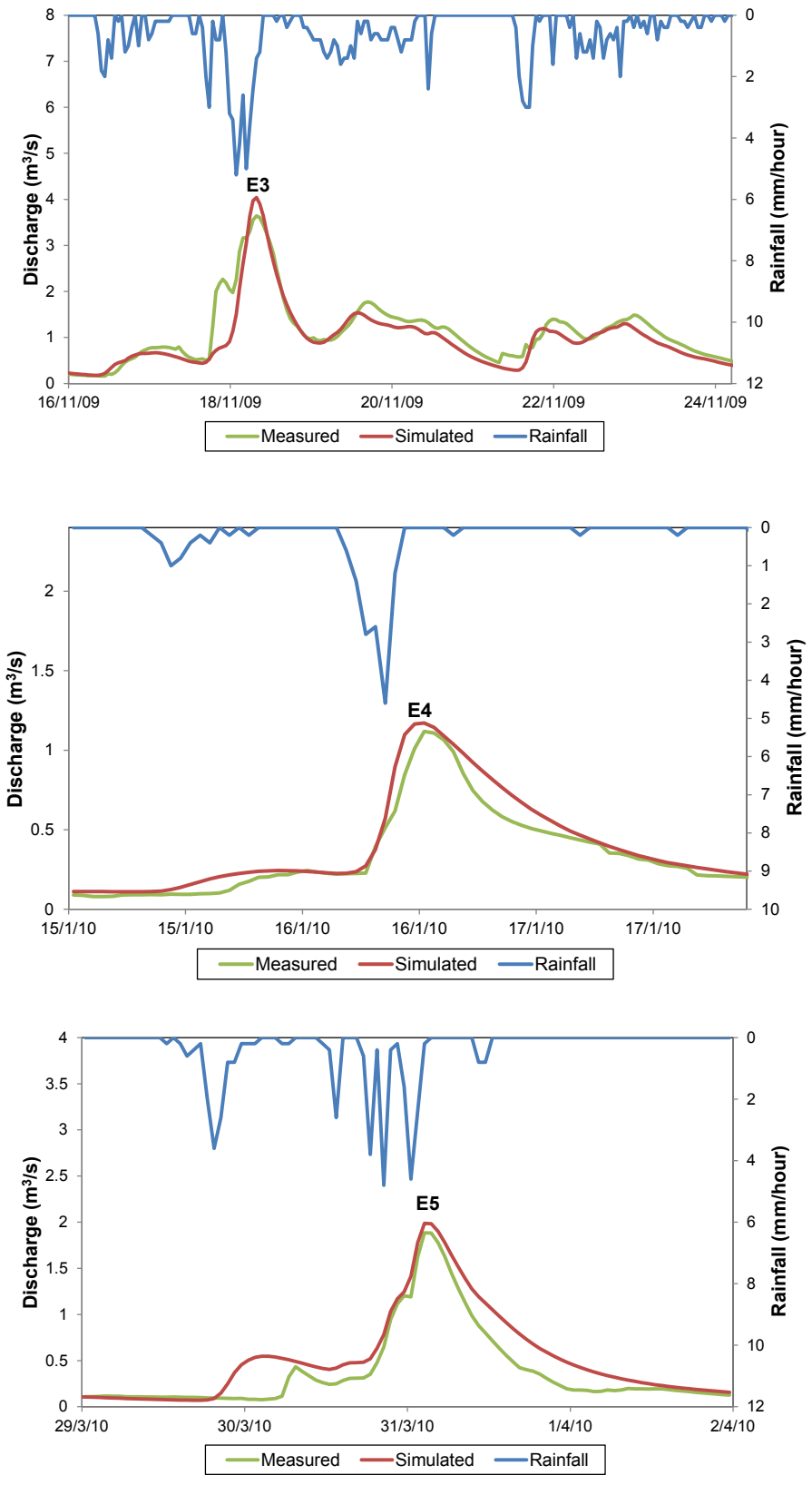

Figure 10-15 *Measured and simulated flow of Blind Beck stream flow during storm events: E3, E4 and E5*

Table 10-8 *Comparisons of measured and simulated SHETRAN hourly continuously peak flows, time to peaks and runoff volumes of three storm events of Blind Beck stream flow*

Period	SHETRAN hourly continuous simulation			
	Parameter (unit)	Simulated	Measured	Percentage error (%)
E3: November 16 – 21, 2009	Peak flow (m^3/s)	4.04	3.64	11
	Time to peak (h)	8	8	0
	Runoff volune (mm)	57.4	65.5	-12
E4: January 15 -17, 2010	Peak flow (m^3/s)	1.17	1.12	4
	Time to peak (h)	5	6	-17
	Runoff volune (mm)	11.3	9.7	16
E5: March 29 – April 1, 2010	Peak flow (m^3/s)	1.99	1.88	6
	Time to peak (h)	27	27	0
	Runoff volune (mm)	14.0	19.5	-28

As can be seen from Table above, negative runoff volume errors indicate underpredictions. In the case of time to peaks errors, the negative one indicating arrival of simulated peaks generally too early. The two storm event hydrographs, E3 and E4 predicted the time to peak more accurately. As can be seen from Figure 10-15, hydrograph, peak flow and runoff volume of the main flood event in November 2009 (E3) could be simulated in the Blind Beck catchment by the SHETRAN model. From Figure it is clear that simulated flood hydrographs do not differ much from the measured one.

The model efficiencies for each of the five storm hydrographs were calculated and are summarized in Table 10-9.

Table 10-9 *Storm event model performance statistics for hourly stream flow simulations of the Blind Beck catchment*

Statistical test	Units	E3	E4	E5	Model performance
R^2	-	0.80	0.96	0.87	very good to excellent
NSE	-	0.72	0.89	0.76	satisfactory to good

E3: 16 – 21 November 2009

The November storm event was the largest flood event to be recorded by the instrumentation during the 2009 year. Figure 10-15 presents the first case of the multi-day event. The model matched the time of peak flow and peak flow prediction correctly. The simulated hydrograph had a rising limb in reasonable agreement but with the simulated curve falling off less steeply which probably does not represent the slow release of groundwater to the stream after the storm event. The corresponding NSE was 0.72 and R^2 was 0.80 (Table 10-9). Thus, the simulated results for the November event are considered satisfactory to very good.

E4: 15 - 17 January 2010

The storm event model predicted the peak flow and runoff volume for the simulation period. A long tail of the simulated hydrography was most likely due to release temporary groundwater storage. This model performed the best according to the statistical results as indicated by the R^2 value of 0.96 and NSE value of 0.89.

E5: 29 March - 1 April 2010

Another pair of closely spaced rainfall events occurred during the period 29 March - 1 April 2009. On a rising limb, the measured and simulated hydrograph showed a pronounced "knee". The time flow peaks did match the measured flow. There was a good fit between the simulated and measured values. The descending hydrograph limb of measured data shows a step. The simulated results for this event are excellent to good (R^2 = 0.87 and NSE = 0.76).

The models were simulated with an NSE of > 0.5. Overall, the best modelling result is for the January event (E4). Predicted flow at hourly time intervals successfully captured the timing of peak flow and was well simulated for storm events. E3 and E5 storm events show that the model is satisfied according to the Nash-Sutcliffe Efficiency (NSE) criteria. According to the R^2 value, the hydrological model is good. Model prediction of storm event peaks is generally very good.

10.4.4 Calibration and validation for the Hollow sub-catchment

The model comparisons are performed for both the calibration and validation periods. The specific comparisons of simulated and measured values include:

- Hourly time series of flow (m^3/s),
- Annual runoff volumes (m^3/s),
- Storm event periods, e.g. hourly values (m^3/s).

Parameter adjustments focused primarily on saturated hydraulic conductivity, porosity, residual water content and van Genuchten parameter changes, as a function of soils to obtain reasonable overall water balances. Table 10-10 reports calibrated values for the Hollow sub-catchment. The soil type of different soil layers at the Hollow sub-catchment were estimated as: clay, silt loam and sandy loam. Following model calibration, model validation was performed to test the calibrated parameters for a second time period, without further model adjustment.

Table 10-10 *Parameters used in model calibration for the three soil types used to characterize the sub-catchment*

Parameter	Description	Soil class	Value
Kx, Ky, Kz	Saturated hydraulic conductivity (m/day)	clay	0.0140
		silt loam	0.452
		sandy loam	0.6220
θ_{sat}	Volumetric saturated soil water content (porosity)	clay	0.4440
		silt loam	0.4520
		sandy loam	0.4120
θ_{res}	Volumetric residual water content	clay	0.3260
		silt loam	0.0630
		sandy loam	0.0980
n	van Genuchten n parameter	clay	1.443
		silt loam	1.681
		sandy loam	1.7360
α	van Genuchten α parameter (cm^{-1})	clay	0.0458
		silt loam	0.0515
		sandy loam	0.0144

Visual observations (Figure 10-16) for the hourly simulation were that the shape of the hydrograph produced from simulating sub-catchment was good visually in terms of patterns of peaks, the onset of the rainy season and dry seasons, but that the timing of these peaks and rainy seasons were not coinciding with the measured stream flow. Most of simulated peaks are lower than the measured.

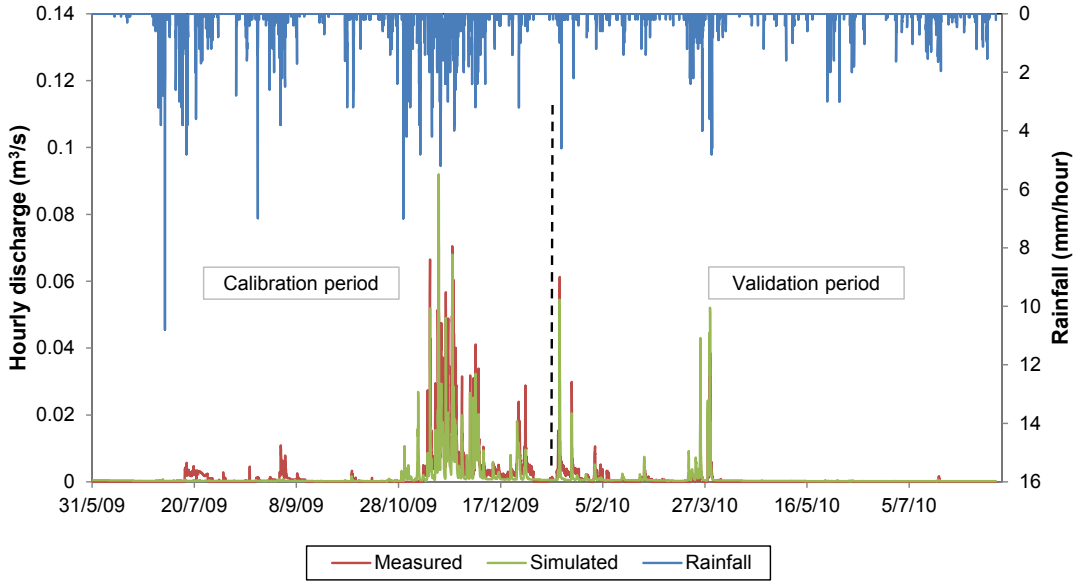

Figure 10-16 *Hourly calibrated and validation simulated stream flow for the Hollow sub-catchment*

The hourly calibrated and validated simulations of stream flow from the Hollow sub-catchment are shown in Figure 10-16 and the performance statistics are displayed in Table 10-11. The period from 8/01/2010 to 17/08/2010 has been used to validate the Hollow sub-catchment. For the flow validation, good results were achieved for the dry and wet periods. The hourly hydrograph show one large flood event, 15-19 November

2009 in the calibration period and two events 15-17 January 2010 and 30 March – 1 April 2010 in the validation period.

Table 10-11 *Calibrated and validated model performance statistics for hourly stream flow simulations in the Hollow sub-catchment*

Dataset	Statistical test	Units	Hollow	Model performance
Calibration	R^2	-	0.83	very good
	NSE	-	0.78	good
Validation	R^2	-	0.73	very good
	NSE	-	0.70	satisfactory

For the Hollow sub-catchment, hourly measured and simulated stream flows events match quite well during the calibration resulting in hourly NSE of 0.78. The hourly validation NSE was 0.70. The hourly calibration and validation R^2 were 0.83 and 0.73. These show that the calibrated model satisfied the Nash-Sutcliffe Efficiently (NSE) criteria ≥ 0.5. The R^2 value falls into the range of very good model.

To provide a measure of model accuracy, average hourly the model simulated and measured flows were compared through a regression analysis for the calibration and validation period and shown in Figure 10-17. The analysis suggests that the flows were overpredicted in the calibration and underpredicted in the validation period.

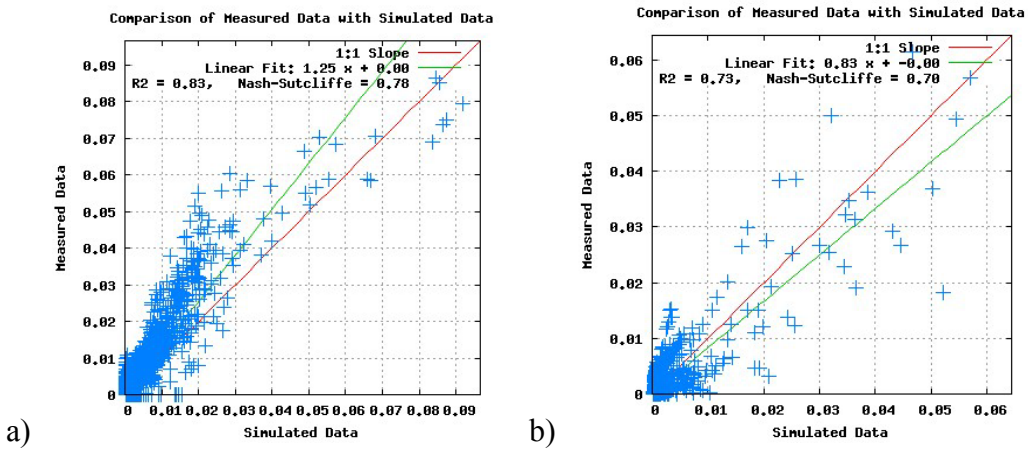

a) b)

Figure 10-17 *Regression analysis of simulated and measured average hourly flows (m^3/s) during a) calibration period and b) validation period of the Hollow sub-catchment (red line: line of equal value; green line: best-fit line)*

Figure 10-18 illustrates the monthly variation of the measured and simulated flow. The model slightly underpredicted stream flow from August to September, overpredicted in October then underpredicted from November 2009 to February 2010, and from March to July overpredicted flow.

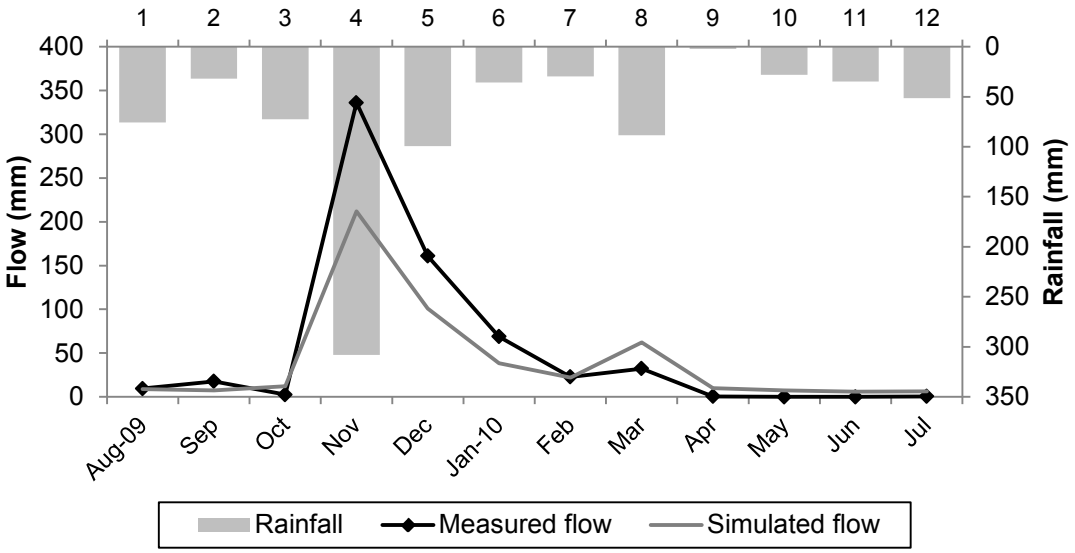

Figure 10-18 *Monthly variation of the simulated and measured flow during calibration and validation of the Hollow sub-catchment*

The observed comparisons of annual runoff volumes in Table 10-12 indicate that the simulation accuracy is different in the calibration and validation period. Total runoff for the calibration period was underestimated by -34%. The total runoff for the validation was overestimated by the model (27%). The % volume errors for the calibration and validation period (Table 10-12) are higher than ±10%. This confirms that the model is a good to a fair for the calibration and validation mean annual flow. This larger difference was probably caused by uncertainties in the rainfall data, no flow over the weir during dry months and short period of data.

Table 10-12 *Summary of annual simulated and observed and observed runoff volumes (m^3)*

Calibration				**Validation**			
Year	OBS	SIM	ERR	Year	OBS	SIM	ERR
1/6/2009-7/1/2010	13.8	9.2	-34	8/1/2010-17/8/2010	3.0	3.8	27

SIM = Simulated, OBS = Observed, ERR = 100 x (SIM – OBS)/OBS %

The calibration and validation results show that SHETRAN is reasonably able to predict total runoff within the Hollow sub-catchment. Despite the time series of available flow data being relatively short by hydrological standards, the Hollow model was both calibrated and validated with an NSE of > 0.5. The extreme event of November 2009 was also well represented. The simulated values for the extreme event is 0.092 m^3/s while the measured value was 0.080 m^3/s. However, the simulated and measured annual mass balances are not in good agreement for the calibration and validation (errors in annual runoff of -34% and 27%); Table 10-17 shows the overall balance.

10.4.4.1 Storm event simulation for Hollow stream

For the period 2009-2010 three storm events were incorporated within the SHETRAN model run (November 2009, January 2010 and March 2010) and presented in Figure 10-19. In order to receive an overall "feel" for how well the SHETRAN model performed on a sub-catchment, the simulated hydrographs were visually compared with the measured hydrographs.

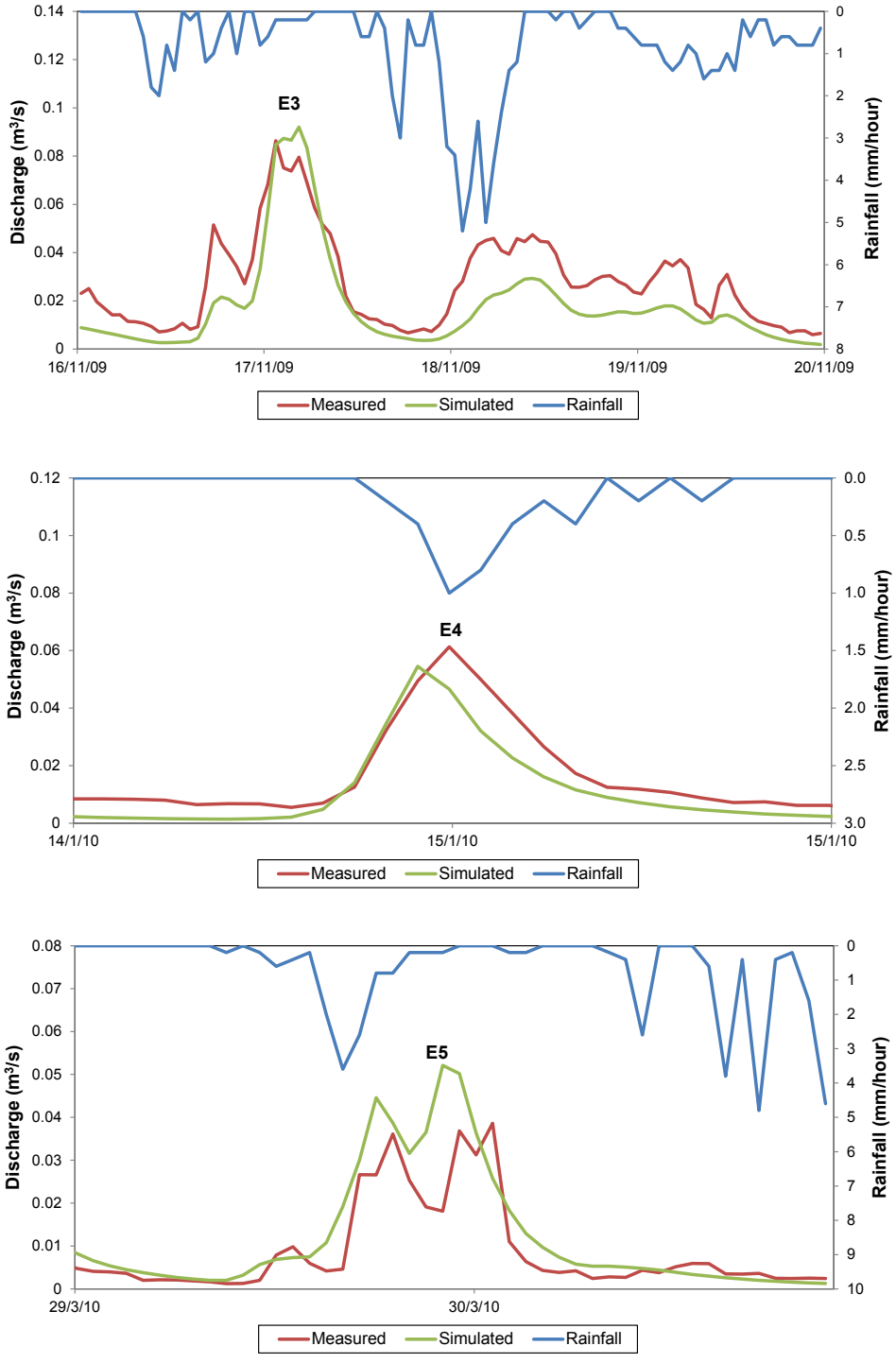

Figure 10-19 *Measured and simulated flow in the Hollow catchment during storm events (E3, E4 and E5)*

The simulated and measured peak flows, time to peak flows, runoff volumes and percentage difference (errors) of the respective measured and simulated values are given in Table 10-13.

Table 10-13 *Comparisons of measured and simulated SHETRAN hourly continuously peak flows, time to peaks and runoff volumes of three storm events of the Hollow sub-catchment flow*

Period	SHETRAN hourly continuous simulation			
	Parameter (unit)	Simulated	Measured	Percentage error (%)
E3: November 16 – 24, 2009	Peak flow (m^3/s)	0.092	0.086	7
	Time to peak (h)	25	25	0
	Runoff volume (mm)	68.40	105.51	-35
E4: January 15 - 17, 2010	Peak flow (m^3/s)	0.055	0.061	-10
	Time to peak (h)	8	9	-11
	Runoff volume (mm)	11.62	17.43	-33
E5: March 30 – 1 April, 2010	Peak flow (m^3/s)	0.052	0.038	37
	Time to peak (h)	24	25	-4
	Runoff volume (mm)	21.29	15.99	33

In the case of time to peaks errors, all events except E3 showed negative errors indicating advanced simulated peak arrivals. Amongst the three hydrographs, peak flow and runoff volume of the main flood event in November 2009 (E3) were the most accurate.

The model efficiencies for each of the three storm hydrographs were calculated are summarized in Table 10-14.

Table 10-14 *Storm event model performance statistics for hourly stream flow simulations in the Hollow sub-catchment*

Statistical test	Units	E3	E4	E5	Model performance
R^2	-	0.82	0.90	0.81	very good to excellent
NSE	-	0.52	0.76	0.56	satisfactory to good

E3: 15 – 19 November 2009 flood event

The 15 – 19 November 2009 were multi-day storm events that result in flood with 0.086 m^3s^{-1} peak flow. Both the measured and simulated hydrographs start to rise at the same time and have "knee" in the rising limb. The SHETRAN model did a good job of simulating the measured hydrograph. The performance efficiency (R^2) value for the simulated versus measured storm event (E3) flow for the sub-catchment was 0.82 and NSE 0.52. This confirms that the model is very good to satisfactory.

E4: 15 January 2010 event

The simulated and measured hydrographs only had one sharp peak. The simulated hydrograph was shifted so that it forecasted a slightly earlier peak flow rate than was measured. Both of hydrographs had a quick rising and falling limb. The measured peak was considerably higher than the simulated one. The SHETRAN model did a good job

of simulating the measured hydrograph, however it showed a time shift to the left of approximately one hour.

E5: 30 March 2010 event

Although the simulated peak flow was higher than the measured value, there is generally good agreement between the measured and simulated hydrographs. The simulated hydrograph falls off more slowly than the measured hydrograph. The measured and simulated hydrographs have similar shapes. The SHETRAN model did a good job of simulating the measured hydrograph shape, however it did not perform as well around the hydrograph peak.

Overall, the % difference in storm peaks reflecting a good simulation of storm peaks. The Nash-Sutcliffe Efficiency (NSE) criteria ≥ 0.5 is a good for the E4 storm event. For the same event, the R^2 value falls into the range of excellent for a hydrological model according to Henriksen et al. (2003). For the storm events E3 and E5 according to R^2 value it falls into the range of very good model, while according to the Nash-Sutcliffe Efficiency criteria to satisfactory model. According to statistical analysis of storm events, the best result is achieved for the storm event in January 2010 (E4).

10.4.5 Interpretation of results

It can be concluded that the calibration and validation results show that SHETRAN is reasonably able to predict total runoff within the Blind Beck catchment and the Hollow sub-catchment. The Nash and Sutcliffe efficiencies (NSE) for all two calibration sites are also comparable with other UK SHETRAN models. Wilkinson (2009) achieved best NSE values of 0.81 for Great Musgrave (222 km^2), 0.82 for Temple Sowerby (616 km^2) and 0.93 Smardale (36 km^2) that include four different storm events.

In comparison to studies carried out in other countries, the NSE values attained in the UK are relatively similar. Bathurst et al. (2011) obtained an ENS value of 0.85 for the Pejibaye catchment in Costa Rica (131 km^2), 0.92 for the Panamá and 0.81 for the Lise catchment in Ecuador (10 km^2), 0.84 for the forested condition and 0.91 for the logged condition for the La Reina catchment in Chile (0.35 km^2), and 0.83 (outlet), 0.78 (Martial sub-catchment) and 0.76 (Godoy sub-catchment) in Argentina (12.9 km^2).

It is important to consider the range of uncertainty revealed in the model calibration and validation relative to specific uses of the model. There is uncertainty regarding the

model's ability to accurately predict high flow peaks. The uncertainty within the SHETRAN model is reflected in the November flood event by underpredict the flood peak for both the catchment and the sub-catchment. However, this uncertainty is not always constant throughout the model simulation for the catchment. For the sub-catchment, there is a constant uncertainty of over- and underpredicted storm peak flows and also an advanced peak arrival in the storm peak. According to this, an assumption is made that the model uncertainties are constant and it is likely produced by the rainfall within the model.

There is uncertainty within the sub-catchments by underestimating runoff during the autumn and the winter months. This can result in less runoff being generated in the model. This can be seen in the model output for the calibration period for the sub-catchment. However, the validation period generates more simulated runoff during the spring and the summer periods than the autumn and the winter periods, which is shown for the both the catchment and the sub-catchment scale. Therefore, as with the previous point, this is a result of the uncertainty of rainfall input and it is known to be constant.

The fit between hourly measured and simulated stream flows was checked graphically by plotting the flow duration curves. General agreement between the measured and simulated flow duration curves indicates adequate calibration and validation over the range of the flow conditions simulated.

For the sub-catchment, goodness of fit measures indicated a reasonably good fit between the measured and simulated stream flow during the calibration and validation with good representation of the general flow pattern and hourly hydrograph.

It is expected that the better simulations are often for the larger scales and events and the largest differences tend to be for the smaller scales and smaller events. The simulated flows were slightly better simulated for the catchment scale than for the sub-catchment scale. This suggests application of rainfall data derived outside of the sub-catchment (see sub-section 4.5.4).

The simulated and measured annual mass balances are in reasonable agreement for the catchment scale but for the sub-catchment, it is a good to a fair. This suggests uncertainty of the measured flow at the outlet of the sub-catchment.

The overall shape of the storm event hydrographs was very well captured; however, the sub-catchment overpredicted peak flow for the E3 and E5 events and underpredicted for

the E4 event. The storm simulations are generally in the range of a good, although some are very good. Thus, the model shows a clear consistency between the rainfall and the resulting runoff. The baseflow are modelled correctly, showing the catchment and the sub-catchment wetness levels.

10.4.6 Hillslope model performance

In this study, the modelling techniques consider the fate of runoff from a 45 m hillslope. The simulated hillslope runoff is presented in Figure 10-20. There was no measured runoff at the hillslope scale and the runoff was estimated using a model based on physical parameters. All input parameters were determined by field and laboratory measurements.

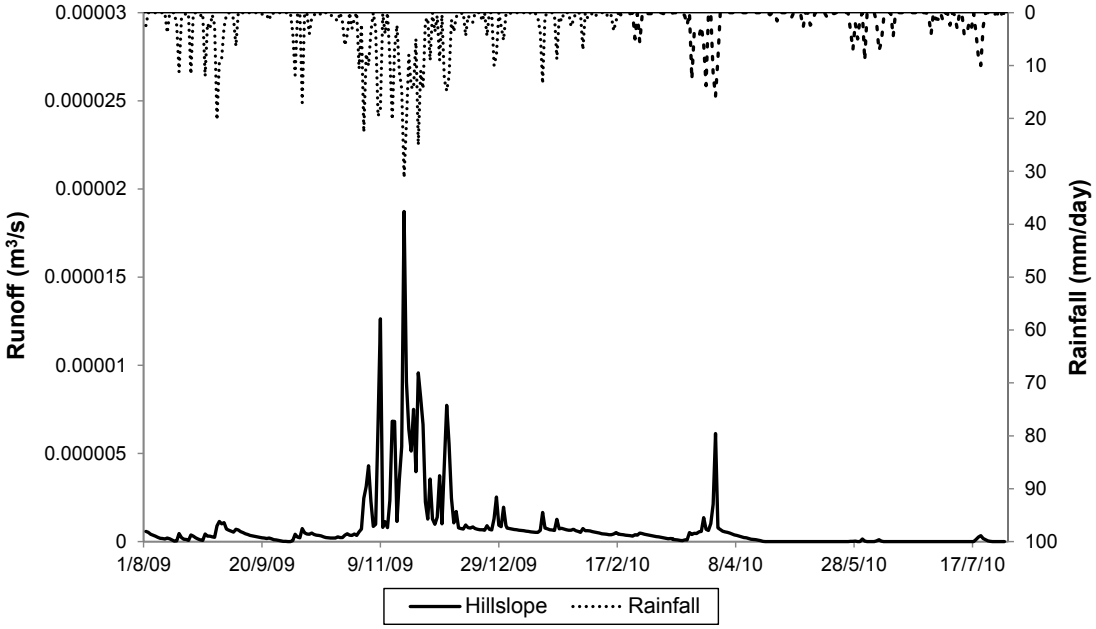

Figure 10-20 *Simulated hillslope runoff*

The model was manually calibrated. Due to the lack of runoff data, the model could not be calibrated in a traditional sense. To calibrate the model, measurement data of soil moisture were used. The soil moisture was measured with Theta Probes in three different depths (10, 20, 30 cm) as discussed in Section 6.3. Due to a failure of the measuring system the soil moisture data are only available from September 11 to October 8, 2009, January 6 to February 1, 2010, February 19 to March 18, 2010, and March 26 to April 22, 2010. The possible measurement errors were taken into account when using this data for the model calibration.

The reasonable agreement has been achieved between field observations and the model by adjusting the saturated water content parameter θsat with the final value of 0.4 for the hillslope. It appears, however, that the modelled runoff for the hillslope is realistic.

During calibration, there were observed variations in some parameters of the soil that can cause large changes in the runoff at the hillslope. It was found that the soil moisture was an important factor for evaluating criteria.

The peaks in the hydrograph are well simulated, as well for size as for time of occurrence. The hourly hillslope responses at the peak of the November flood event. The runoff is seen to make up a small volume of the total runoff, becoming important only in the most intense period of storm event. The runoff is generated as a rapid flow response.

It can be concluded that hydrograph, peak flow and runoff volume of the main flood event in November 2009 as well as of the three following small events could be simulated by the hillslope model, so the hillslope model is suitable for use in climate impact analysis.

To demonstrate the usefulness and performance of the hillslope model, modelled rainfall and runoff patterns were assessed at 100 random selected samples for 30-year time slices and the results were analysed statistically to assess the effects of climate change on rainfall and runoff at the hillslope scale. This will be discussed in the next chapter.

10.5 Discussion of uncertainties

Any application of a hydrological model has some level of uncertainty. Three main sources of uncertainties in the SHETRAN modelling process could be distinguished:

1) Input parameters
2) Model assumptions and
3) Measured data.

These are briefly described here.

10.5.1 Input parameters

The SHETRAN model for the Upper Eden basin was originally developed in Walsh, (2004). Thus, input data used a 50 m DEM of the Upper Eden basin constructed by Walsh (2004) which was aggregated to a 100 m DEM.

As rainfall data were available from the field measurements in the sub-catchment the uncertainties related to this data are low. However, due to a failure of the raingauge, more uncertainties are related to the rainfall data for 2009 and 2010, because data from raingauges outside the sub-catchment had been used as model input. These rainfall daily data sets were selected as input to the weather generator from which potential evaporation was extracted, to help reduce the uncertainty.

The spatial distribution of the land use was taken from the Land Cover Map of Great Britain 1990. Due to detailed spatial distribution of major land cover classes the quality of the map is very good.

The vegetation parameters were available from studies of Rutter (1975) and Shuttleworth (1993). Leaf area index and maximum rooting depth were taken from SHETRAN library values. As these are not directly measured, the uncertainty caused by these parameters may be quite high.

Soil physical parameters were available from literature sources or from SHETRAN library values. The uncertainty related to these parameters therefore may also be fairly high.

10.5.2 Model assumptions

There are uncertainties related to how the simulation processes are represented in the model. These are difficult to quantify, and assessment of the influence of these on the results is beyond the scope of this study. The uncertainties related to the simulation processes may arise from the assumptions used in the model.

10.5.3 Measuring data

In general, all measurements contain measurement errors, which have to be taken into account while using this data for calibration and validation. The discharge was calculated based on continuous water level measurements and a stage-discharge

relationship for each gauge. Although this method is related with uncertainties, it is the standard method for discharge measurements, because other methods for continuous discharge measurements are not available.

The discussion of the uncertainties showed that uncertainties exist at all levels. Often it is not possible to determine which uncertainties cause the deviation between simulated and measured variables.

10.6 Water balance

Hydrological models have become useful tools in water resources planning and managements, providing a capability to analyse quantity and quality of stream flow and a hillslope runoff.

The components of the (sub) catchment water balance include precipitation and change in storage ΔS while the output comprises the actual evapotranspiration E_{act} and the stream discharge Q at the outlet of the (sub) catchment.

$$P - ET - Q = \Delta S$$

where: P = precipitation [L/T], ET = evapotranspiration [L/T], Q = stream discharge at the outlet of the catchment [L/T], ΔS = change of storage [L]

In a general form, the long term water balance of the hillslope can be written as:

$$A \cdot \Delta S_{soil} = (P + Q_{in}) - \left(ET + Q_{out} + R_s + R_p\right) \cdot \Delta t$$

where: A = area of the hillslope [m^2], ΔS_{soil} = change in soil water storage [mm]

Inputs:

P = precipitation [mm/hr], Q_{in} = lateral subsurface inflow [m^3/hr]

Outputs:

ET = evapotranspiration [mm/day], Q_{out} = lateral subsurface outflow [m^3/hr], R_s = overland flow [mm], R = recharge losses (downward vertical flow) = percolation [mm]

Δt = time interval [hr]

10.6.1 Water balance for the Blind Beck catchment

The monthly rainfall and runoff for the Blind Beck catchment for the period 2009-2010 are shown in Table 10-15. The hourly values of rainfall and runoff (simulated discharge) were aggregated to the monthly values. This would provide a better insight into the long-term rainfall-runoff relationship at the Blind Beck catchment. The highest

rainfall was in November (308.2 mm) while the lowest value was in April (2.2 mm). The monthly runoff values were higher in the winter period while lower in the summer period. The highest measured runoff value was in November of 220.9 mm and the lowest in June of 9.9 mm.

As can be seen from Table 10-15, the months from October to January and March have positive storage values while the remaining months are negative. The negative monthly water balance indicates that water was being lost from storage.

Table 10-15 *Water balance of the observed and simulated stream flow in the Blind Beck catchment, August 2009 to July 2010*

Month	Precipitation (P) (mm)	Evapotranspiration (ET) (mm)	Measured discharge (mm)	Simulated discharge (mm)	Change in storage - measured (ΔS) (mm)	Change in storage - simulated (ΔS) (mm)
Aug	75.8	69.4	11.0	19.4	-4.6	-13
Sep	31.9	44.1	15.2	16.6	-27.4	-28.8
Oct	72.4	24.7	17.0	34.1	30.7	13.6
Nov	308.2	9.5	220.9	193.5	77.8	105.2
Dec	99.4	6.2	74.2	88.3	19	4.9
Jan	35.8	9.1	42.7	44.8	-16	-18.1
Feb	29.6	13.0	21.2	31.6	-4.6	-15
Mar	88.6	32.2	32.6	55.2	23.8	1.2
Apr	2.2	55.4	17.6	15.7	-70.8	-68.9
May	28.2	75.8	10.9	9.9	-58.5	-57.5
Jun	34.7	70.6	9.9	10.3	-45.8	-46.2
Jul	51.4	65.1	12.3	13.0	-25.98	-26.68
Annual	858.2	475.1	485.5	532.4	-102.38	-149.3

Table 10-16 shows the water balance on the annual basis and the difference between the simulated and measured discharge data. These differences were compared to the rainfall and to the measured discharge with a computed percentage difference. For the annual period, the difference between the simulated and the measured runoff as a proportion of the annual rainfall were 5.5%. This indicates that the simulated values of annual runoff are good compared to the measured. The error in runoff as a proportion of the measured annual runoff (discharge) was 9.7%.

Table 10-16 *Annual water balance components at the Blind Beck catchment. P = rainfall, ET = evapotranspiration, Q_s = simulated discharge, Q_m = measured discharge and ΔS is change in storage*

Year	P – ET - Q_s = ΔS	Q_m (mm)	$Q_s - Q_m$ (mm)	%($Q_s - Q_m$) to P	%($Q_s - Q_m$) to Q_m
2009-2010	858.2-475.1-532.4 = -149.3	485.5	46.9	5.5	9.7

The change in the annual water balance is negative, which suggests that the water being lost from the storage.

10.6.2 Water balance for the Hollow sub-catchment

The total monthly rainfall and runoff in the Hollow sub-catchment for the period 2009-2010 are shown in Table 10-17. The highest rainfall is in November with a value of 308.2 mm while the lowest value was in April with a value of 2.2 mm. The total monthly runoff values were higher in the winter period but lower in the summer period. The highest simulated runoff value was in November of 212.1 mm and the lowest in June of 5.9 mm.

Table 10-17 *Water balance of the measured and simulated stream flow in the Hollow sub- catchment, August 2009 to July 2010*

Month	Precipitation (P) (mm)	Evapotranspiration (ET) (mm)	Measured discharge (mm)	Simulated discharge (mm)	Change in storage - measured (ΔS) (mm)	Change in storage - simulated (ΔS) (mm)
Aug	75.8	69.4	9.5	9.0	-3.1	-2.6
Sep	31.9	44.1	17.6	7.5	-29.8	-19.7
Oct	72.4	24.7	2.5	12.1	45.2	35.6
Nov	308.2	9.5	336	212.1	-37.3	86.6
Dec	99.4	6.2	160.8	100.9	-67.6	-7.7
Jan	35.8	9.1	68.9	38.4	-42.2	-11.7
Feb	29.6	13.0	22.8	22.1	-6.2	-5.5
Mar	88.6	32.2	32.3	62.0	24.1	-5.6
Apr	2.2	55.4	0.6	10.0	-53.8	-63.2
May	28.2	75.8	0.0	7.5	-47.6	-55.1
Jun	34.7	70.6	0.0	5.9	-35.9	-41.8
Jul	51.4	65.1	0.6	6.2	-14.28	-19.88
Annual	858.2	475.1	651.6	493.7	-268.48	-110.6

As can be seen from Table 10-17, just two months have a positive storage value while the remaining months negative. These negative values of storage indicate that water was being lost from the storage.

Table 10-18 shows the water balance on an annual basis and the difference between the simulated and measured discharge data. The difference between the simulated and the measured runoff as a proportion of the annual rainfall had very high percentage. This indicates that the simulated values of runoff are quite far from the measured. The error in runoff as a proportion to the measured annual runoff (discharge) had also a relatively high percentage error.

Table 10-18 *Annual water balance components at the Hollow sub-catchment. P = rainfall, ET = evapotranspiration, Q_s = simulated discharge, Q_m = measured discharge and ΔS is change in storage*

Year	P – ET - Q_s = ΔS	Q_m (mm)	$Q_s - Q_m$ (mm)	%($Q_s - Q_m$) to P	%($Q_s - Q_m$) to Q_m
2009-2010	858.2-475.1-493.7 = -110.6	651.6	-157.9	18.4	24.2

The uncertainty in the water balance was reflected by the uncertainty in annual stream discharge for the weir with high temporal-resolution recording capacitance devices of

5% (Winter 1981; Lesack 1993; Genereux 2005). Allen et al. (1989) reported the standard errors of 0.36 mm/day for the monthly reference Penman-Monteith ET estimates.

Tables 10-17 and 10-18 show the water balance on the annual basis and difference between the simulated and measured discharge data. These negative values of storage indicate that water was being lost from the storage. It shows that losses exceed precipitation in most of the months in the year 2009-2010, which makes it a deficit year. The water balance calculations show for the Blind Beck catchment that, October to December and March are found to be surplus months. For the Hollow sub-catchment, surplus months are October and November for the simulated discharge, while October and March for the measured discharge.

The simulation results obtained in this study show that the availability of water in the catchment and the sub-catchment scale, on a monthly time scale, is useful for decision making and the effective utilization of water. For example, these results are useful in agricultural planning, groundwater modelling and vulnerability studies.

10.6.3 Water balance for the hillslope

Figure 10-21 presents a diagram of the main aspects of water balance and estimated fluxes from the SHETRAN model simulation for one year at the slope section (1 m wide by 45 m long).

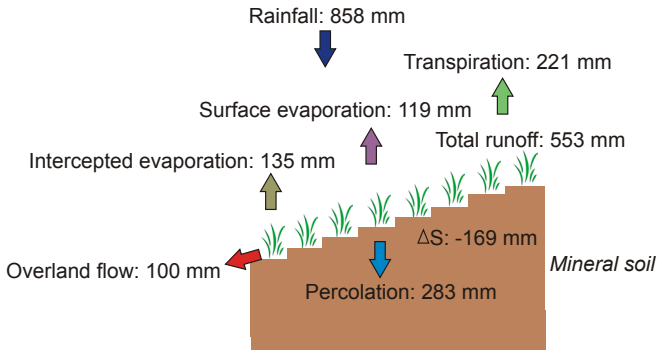

Figure 10-21 *Estimated water balance components at the hillslope, August 2009 to July 2010 (ΔS: change in soil water storage)*

A mass balance of water within the hillslope from the SHETRAN model is estimated for the entire year as:

$$Rainfall = overland\ flow + E + infiltrated\ water$$

and

$$E = intercepted\ evaporation + surface\ evaporation + transpiration$$

$$Infiltration = \Delta Storage + Q$$

$$Q = percolation + lateral\ subsurface\ outflow$$

where: ΔStorage = the change in soil moisture in the unsaturated zone, Q = defined as the estimated sum of percolation, and lateral subsurface outflow

The subsurface flow and percolation are the largest water losses from the hillslope.

The net inputs to the unsaturated storage are produced by rainfall and lateral subsurface inflow where lateral subsurface inflow was calculated by the model, so it can be regarded as negligible in the equation. As output, discharge at the hillslope scale, which includes overland flow, lateral subsurface outflow and percolation was difficult to separate. Focusing on the hillslope, equation can be re-written as follows:

$$Rainfall = overland\ flow + E + percolation$$

The monthly rainfall and simulated discharge values have been compared by taking the monthly totals for the period August 2009 – July 2010. This provides better insight into the long-term rainfall-runoff relationship at the hillslope. The hourly values of rainfall and runoff (simulated discharge) were aggregated to the monthly values.

The total monthly rainfall and runoff of the hillslope for the period August 2009 - July 2010 is shown in Figure 10-22. The highest rainfall was in November with a value of 308.2 mm while the lowest value was in April with a value of 2.2 mm. The total monthly runoff values were higher in the autumn and the winter period while lower in the summer period as shown also for the (sub) catchment. The highest runoff value was in November of 279.5 mm and the lowest in May of 0.1 mm. The highest overland flow values were in November of 90.8 mm and the lowest was zero.

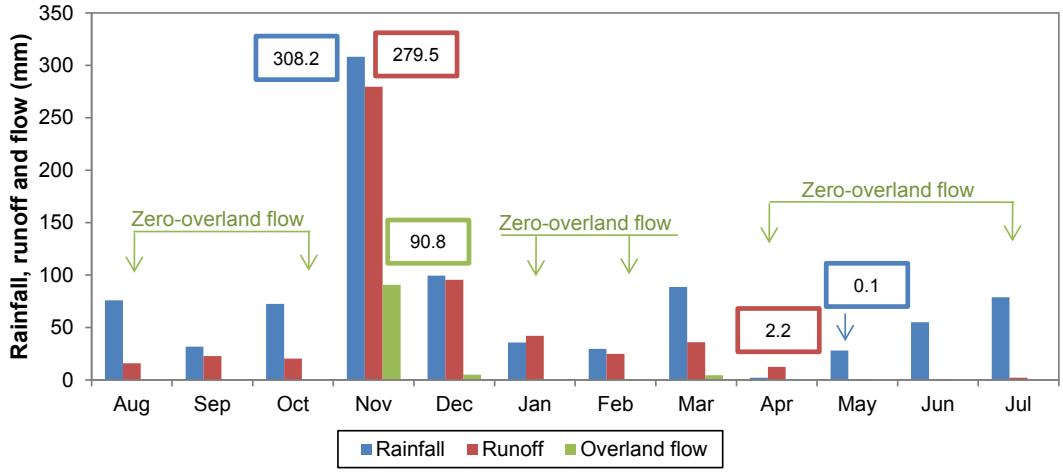

Figure 10-22 *The total monthly rainfall and runoff of the hillslope (Aug 2009 - July 2010)*

The simulated overland flow occurred in response to precipitation event, in November, December and March.

The monthly water balance for the period August 2009 - July 2010 is shown in Table 10-19. As can be seen from Table, three months have a positive storage value while the remaining months negative. There was a net change in soil storage of -169.4 mm. These negative values of storage indicate that water was being lost from the soil storage and draining the hill out over the year.

Table 10-19 *Water balance of the simulated flow at the hillslope, August 2009 to July 2010*

Month	Rainfall (P) (mm)	Evapotranspiration (ET) (mm)	Simulated runoff (Q) (mm)	Change in storage -simulated (ΔS) (mm)	Losses = P - Q
Aug	75.8	69.4	15.8	-9.4	60
Sep	31.9	44.1	22.8	-35	9.1
Oct	72.4	24.7	20.4	27.3	52
Nov	308.2	9.5	279.5	19.2	28.7
Dec	99.4	6.2	95.6	-2.4	3.8
Jan	35.8	9.1	42.1	-15.4	-6.3
Feb	29.6	13.0	24.9	-8.3	4.7
Mar	88.6	32.2	36.0	20.4	52.6
Apr	2.2	55.4	12.5	-65.7	-10.3
May	28.2	75.8	0.1	-47.7	28.1
Jun	34.7	70.6	0.7	-36.6	34
Jul	51.4	65.1	2.1	-15.8	49.3
Annual	858.2	475.1	552.5	-169.4	305.7

The term losses are used as difference between rainfall and net runoff (incorporating soil water storage contributions), therefore the following equation is:

$$Losses = P - Q$$

The total rainfall for the period August 2009 – July 2010 was 858 mm while the total annual runoff is 553 mm that consequently gives losses of 306 mm per year. Factors contributing to uncertainty in the hillslope storage changes include soil moisture content measurement by the Theta Probes.

The hillslope model has provided additional insight into hydrological processes operating in the Hollow sub-catchment. The model provides results for the hillslope runoff, overland flow and water balance. A conceptual hillslope model was designed to produce a model structure with processes and parameters that can be closely linked to the plot scale model.

10.7 Model simulation and interpretation of results

10.7.1 Model simulation results for soil moisture

The knowledge of the spatial distribution of the soil moisture is essential to support assessment of the quality, accuracy and applicability of the SHETRAN model prediction in the subsurface with calibration/validation against measured data.

Knowledge of the soil moisture is important as it has considerable influence on many hydrological (e.g. runoff and flood forecasting) and pedogenic processes (Western et al. 2004), and on the water and energy balances of land surfaces (Qui et al. 2001; di Domenico et al. 2006). In recent years, there has been increasing attention on spatial distribution of the soil moisture (Famiglietti et al. 1998; Starks et al. 2006) because it is widely recognized that improving our knowledge and understanding of the soil moisture and the processes underpinning its spatial and temporal distribution is critical (Wilson et al. 2003; Martinez et al. 2008).

In order to estimate the soil moisture there is methods that can be classified into three main groups: (1) ground based measurement; (2) estimation based on remote sensing; and (3) estimation via simulation models (Grayson and Western 1998; Martinez et al. 2008). In this study, a modelling approach was used to examine the spatial and temporal distribution of soil moisture (soil depth up to 2 m) and comparison of measured with observed data. This study is focused on obtaining estimates of soil moisture at the catchment and sub-catchment scales.

Blind Beck catchment

For the presentation of the soil moisture maps, two images were chosen: one in the middle of the summer dry period (30 June 2009) and one during flood event (24 November 2009) to test the sensitivity of the modelling approach. The spatially distributed soil moisture simulation output of the SHETRAN model is illustrated in Figure 10-23. A very small rainfall event of about 0.1 mm occurred 10 days before 30 June, while 10 days before 24 of November of the same year, rainfall was intensified with a heavy rainfall of about 146 mm. Rainfall appears to be well correlated with the observed temporal soil moisture trends, with wet conditions in the autumn, followed by the drying period in the spring and the summer, before the large flood event and soil wetting in 2009.

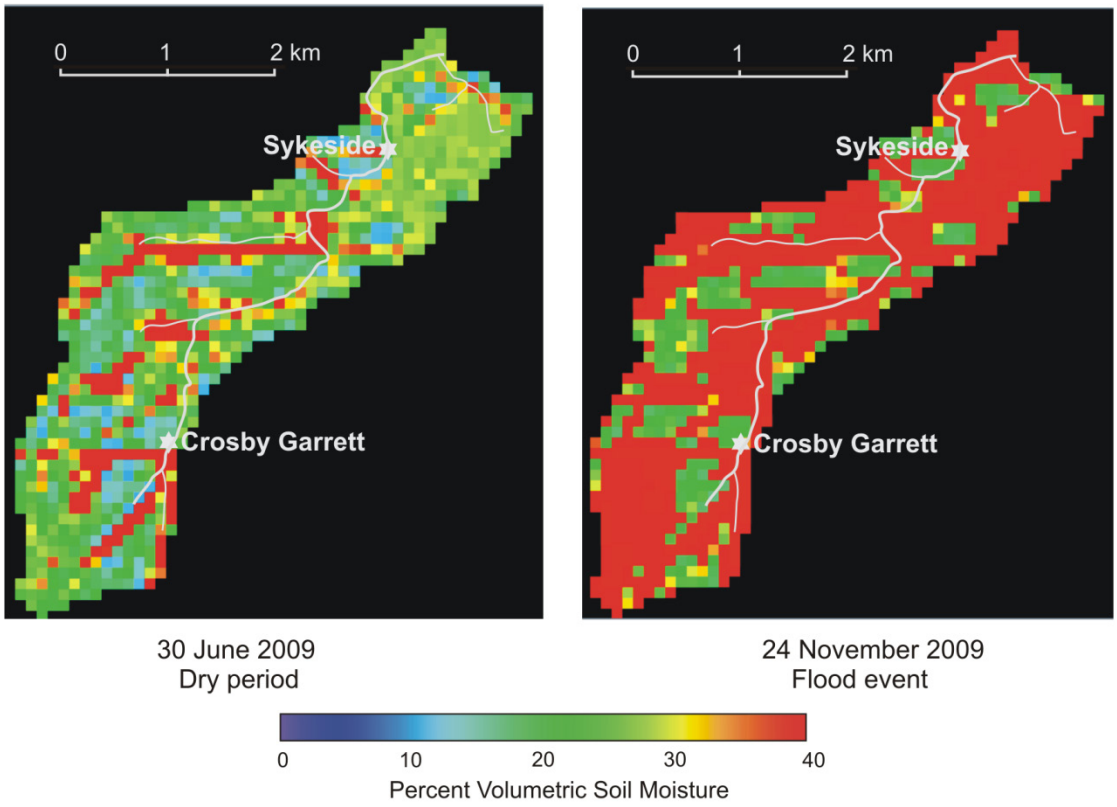

Figure 10-23 *Soil moisture maps derived with the SHETRAN model for two days in 2009 for the Blind Beck catchment*

The light bluish colours on the maps representing a low level of moisture across the entire catchment except for streams and valley areas, where the colour is reddish representing the relatively higher level of soil moisture. Table 10-20 gives a statistical summary of the soil moisture data produced by the SHETRAN. The average soil moisture value ranged from 0.27 to 0.37 m^3m^{-3}. The maximum value for both days were 0.40 m^3m^{-3}.

Table 10-20 *Mean, minimum and maximum soil moisture content with standard deviation*

Date	Soil moisture (m^3m^{-3})			
	Mean	Min	Max	SD
30 June 2009	0.27	0.11	0.40	0.08
24 November 2009	0.37	0.18	0.40	0.07

Min = minimum value, Max = maximum value, SD = standard deviation

A visual assessment of the catchment indicates that the distribution of the near-surface soil moisture depends on topography (Burt and Butcher 1985), soils (Hawley et al. 1983), vegetation (le Roux et al. 1995) and land use. Ockenden (2010) found for the Blind Beck catchment that the pasture sites are clearly much wetter than their woodland sites (mean soil moisture ranged from 0.50 to 0.56 m^3m^{-3} in pasture compared to 0.41 to 0.50 m^3m^{-3} for woodland site). The wetness and dryness patterns agree very much with

expectations, where the driest places are at higher elevations whereas the wettest regions are typically at lower elevations during wet conditions.

The soil moisture change between both days is clearly visible in both images. The Blind Beck catchment shows the highest mean soil moisture in November of 2009 respectively due to the large flood. During the dry period, soil moisture decreases, mainly due to prolonged evaporation losses and relatively low precipitation. The significant low soil moisture contents could lead to agronomic and environmental consequences. The reduction in grass growth rate that the results from water-stress decreases the efficiency of nitrogen uptake by the grass, which in turn requires fertiliser nitrogen applications during the spring and the summer periods to be reduced accordingly (Allen et al. 1998; Coulter 2001).

The simulated soil moisture values were compared with the field measurement from previous study for the same catchment. According to the results of soil moisture measurements, Ockenden (2010) found that most of the sites had mean soil moisture content from 0.4 m^3m^{-3} to 0.56 m^3m^{-3} (i.e. close to saturation) that is in agreement with data from this study.

Hollow sub-catchment

Figure 10-24 shows the spatially distributed soil moisture maps output of SHETRAN simulation for the Hollow sub-catchment, represented by the HDFVIEW. On June 30, 2009 was no visual evidence of runoff response at the catchment outlet. However, wet areas or saturated areas (red) for the stream and valley area were simulated. Another qualitative observation was when the catchment ‘‘wets-up’’ during the flood period (November 24, 2009). The dominant red colours in maps representing a high level of moisture extended across the entire catchment. The maps of these data sets show a good contrast between soil moisture conditions near saturated and saturated.

The simulated mean soil moisture value for 30 June was 0.30 m^3m^{-3}. When including the flood information, the soil moisture tends to increase, which is shown in Figure 10-24 for 24 November 2009. This indicates the saturated soil with a value of 0.41 m^3m^{-3}. It is clear from the simulated results that lower part of the sub-catchment has the highest, while the upper part relatively low soil moisture content.

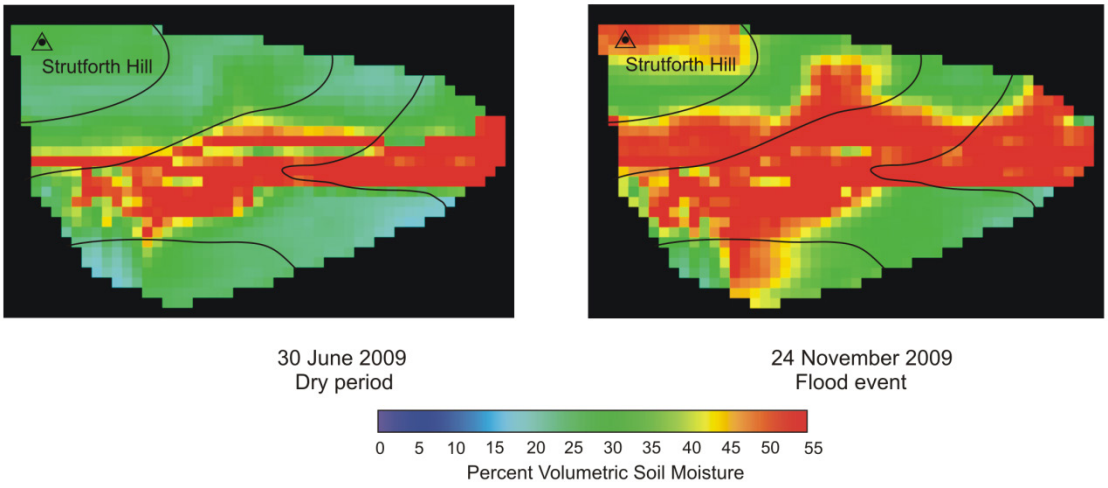

Figure 10-24 *Soil moisture maps derived with the SHETRAN model for two days in 2009 for the Hollow sub-catchment*

The validation of the spatial soil moisture was carried out by comparing the simulated soil moisture content with measured at three depths (10 cm, 20 cm and 30 cm) at the hillslope of the Hollow sub-catchment (Section 6.3). The agreement between simulated and measured soil moisture data at the depth of 0-30 cm was good (Table 10-21). There are three variables that combine to identify each soil moisture measurement and its corresponding simulated value; namely the day on which it was taken, and the position and depth. These data points were at a depth of 30 cm and at the top of the hillslope. Comparing the field soil moisture measurements to the estimates from the simulated model, the R^2 was 0.7 m^3m^{-3} (Figure 10-25).

Table 10-21 *Comparison of the measured soil moisture contents against the values simulated by SHETRAN*

Period	Mean (m^3m^{-3})	
	Measured	Simulated
11 – 30 Sep 2009	0.39	0.37
1 – 8 Oct 2009	0.37	0.37
6 – 31 Jan 2010	0.47	0.53
1 – 2 Feb 2010	0.44	0.53
19 – 28 Feb 2009	0.45	0.52
1 – 18 March 2010	0.42	0.51
26 Mar – 10 April 2010	0.49	0.50
11 – 22 April 2010	0.42	0.47

The comparisons of the mean measured (the actual value measured in the field) versus simulated (the corresponding values simulated by the SHETRAN model) soil moisture contents are arranged according to each of these variables. These measurements were plotted against each other with the line of equality (Figure 10-25). A line of equality is shown along which all values would be expected to lie in the presence of perfect agreement. Clearly, this was not the case, as most of soil moisture values fall above the line of equality (dashed line).

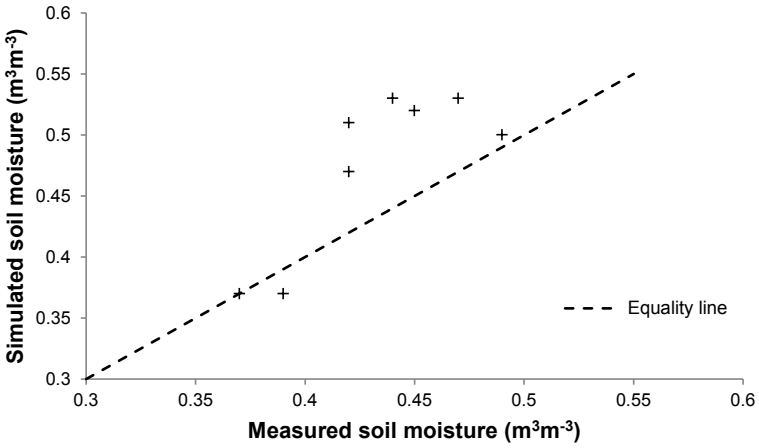

Figure 10-25 *Scatterplot, with line of equality, for measured versus simulated soil moisture using the SHETRAN model*

In this study, the spatial and seasonal comparison was made of the soil moisture. The level of wetness and dryness can provide information to the hydrologist about the spatial distribution of processes in the catchment.

10.7.2 Modelling nitrate

The benefit of using the computer nitrate model is the ability to compare and quantify the effect of different rainfall patterns on the spatial soil distribution and the nitrate transformation within the stream.

A nitrogen transformation model, the Nitrate Integrated Transformation (NITS) component for SHETRAN was used to complete the modelling of nitrate. This has been integrated within SHETRAN's solute transport component, so the concentrations of the nitrogen species are simulated for every finite-difference cell, and are updated, along with water flow and nitrate transport, every time step (Birkinshaw and Ewen 2000a). The distributed model has the capability of predicting the spatial pattern of nitrate within the catchment as well as nitrate stream flux. In addition, this system allows the simulation of nitrate generation, leaching, transport through the subsurface and discharges via seepage areas into surface waters and transport through river networks (Birkinshaw and Ewen 2000a). The SHETRAN model encompasses both the hydrological processes, which control the availability of nitrate in the soil and the stream nitrate concentration. The purpose of N simulations is to indicate transport pathways related to runoff mechanisms using spatial model outputs and time series of export concentrations. SHETRAN nitrate modelling has been used to a small catchment at Slapton Wood Devon, UK that the simulated results for nitrate concentrations and

leaching load, which agree well with existing measurements (Birkinshaw and Ewen 2000b). From this study, it is concluded that SHETRAN should be a powerful, practical and useful tool for studying nitrate pollution problems.

In order to avoid too many assumptions data available from the fieldwork were used based on the stream nitrate concentration and the soil nitrate content. From previous modelling there is also considerable knowledge within catchments, previous experience and literature that was used to make the nitrate model (Birkinshaw and Ewen 2000a). Considering the available data of N in the soil and stream concentration collected from the field, some basic assumptions and limitations were made in order to simplify the construction of the model:

- Nitrogen fertilizer was ignored as it not monitoring in the field
- Nitrate leaching and subsurface transport to groundwater were ignored
- Plant uptake was ignored
- Organic, ammonium N pool and process within were ignored
- Atmospheric deposition is assumed to 1.21 g N m^{-3}.

SHETRAN was used here to simulate nitrate transport in the Blind Beck catchment. This was carried out as a validation test against field measurements of soil and the stream nitrate concentrations as applied the Slapton Wood catchment. Figure 10-26 shows the spatial distributed maps of the nitrate in soil (soil depth up to 2 m) for the Blind Beck catchment, represented by the HDFVIEW. The nitrate concentration in the soil ranged from 0.9 mg/l to 7 mg/l in the wet season whereas in the dry season, the nitrate concentration ranged from 8 mg/l to 20 mg/l. The high nitrate content during June could be attributed to the influence of the dry season. The low nitrate content in the soil is the result of precipitation. High rainfall, with 380 mm from October-November 2009, favoured leaching losses of the nitrate from soils.

The simulation results for the stream nitrate concentrations of the Blind Beck catchment are shown in Figure 10-27 with indication of storm events (#E3 to E5). These results illustrate the ability of the model to simulate trends in the stream nitrate concentrations for the Blind Beck catchment.

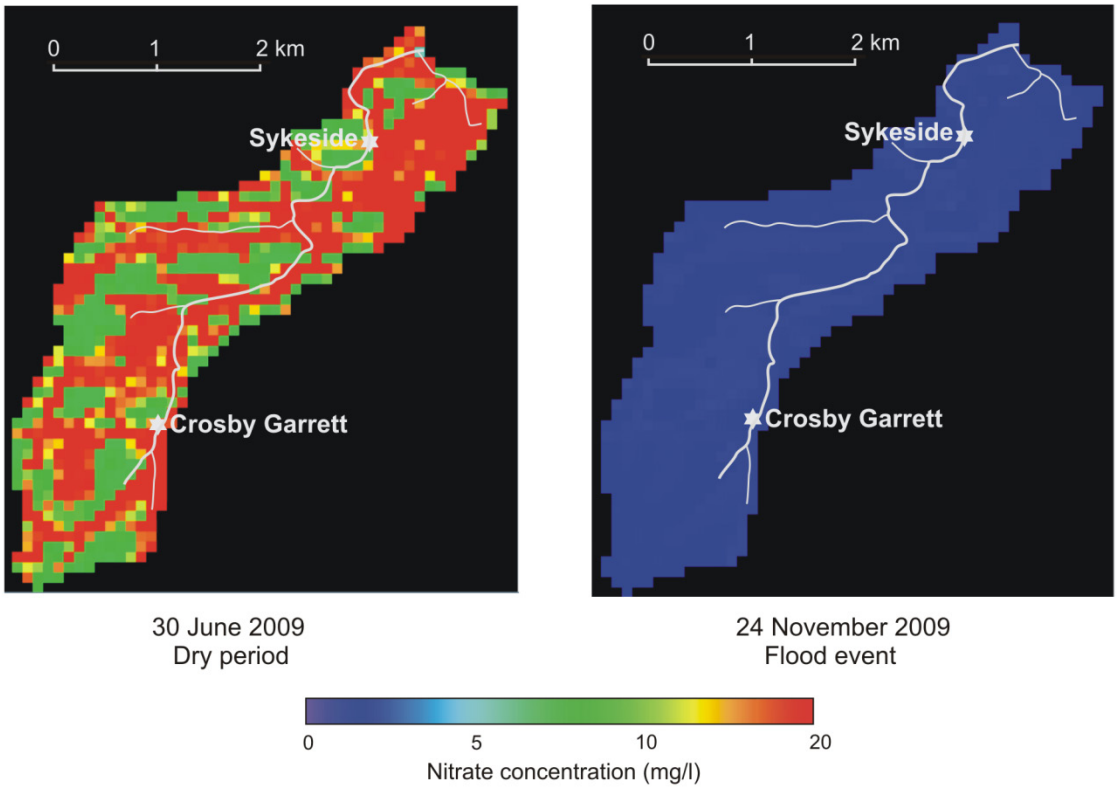

Figure 10-26 *Soil nitrate maps derived with the SHETRAN for the Blind Beck catchment*

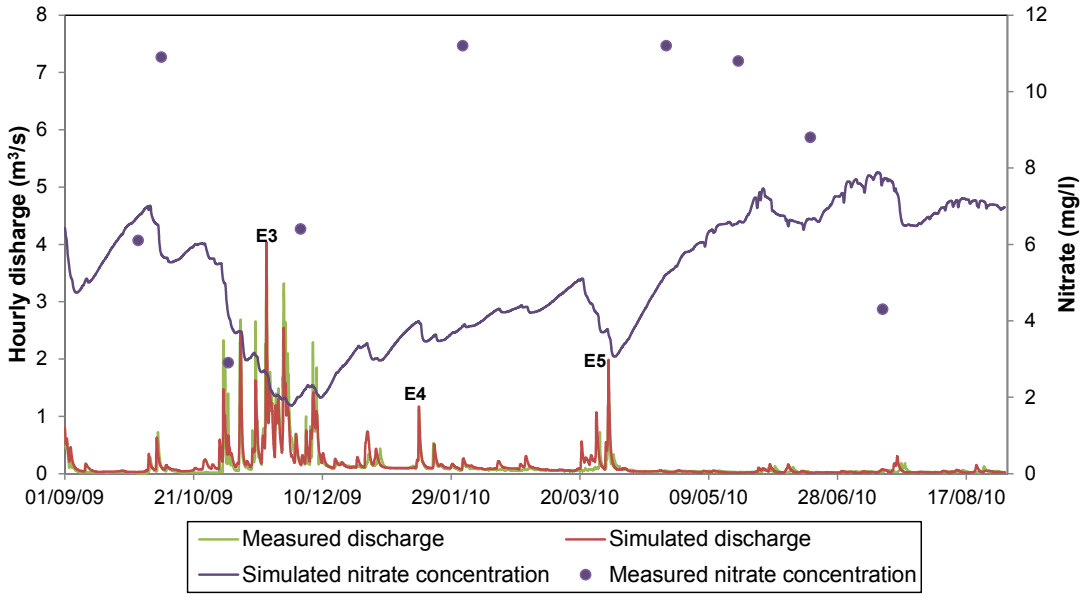

Figure 10-27 *Stream discharge and simulation of nitrate concentrations for the Blind Beck catchment*

The model was not able to fit the measured nitrate concentrations. The monthly point measured values are generally high compared to the low simulated values, although due to the relatively long time between sampling there were not enough field measurements to verify the model adequately well.

During the November 2009 storm event (E3), the peak discharge reached 3.6 m^3/s, while the stream water nitrate concentration reached the minimal 1.8 mg/l likely due to the intensive depletion of the nitrate pool in soils during rainfall events. During the second rainfall event in January 2010 (E4), the stream water nitrate concentration fluxes were higher than during the first rainfall event (Figure 10-27). During this event, the stream water nitrate concentration decreased and increased very sharply from 1.8 mg/l to more than 3.8 mg/l. The overall decreases of the nitrate concentrations in the falling limbs of the hydrographs can be associated with high portions of 'new' water in the total discharge which contained the lower nitrate concentration.

Figure 10-28 shows the spatial distributed maps of the nitrate in the soil as output of the SHETRAN simulation for the Hollow sub-catchment. The nitrate concentration in the soil ranged from 7.7 mg/l to 21 mg/l in the dry season whereas in the wet season, the nitrate concentration ranged from 0.9 mg/l to 2.9 mg/l.

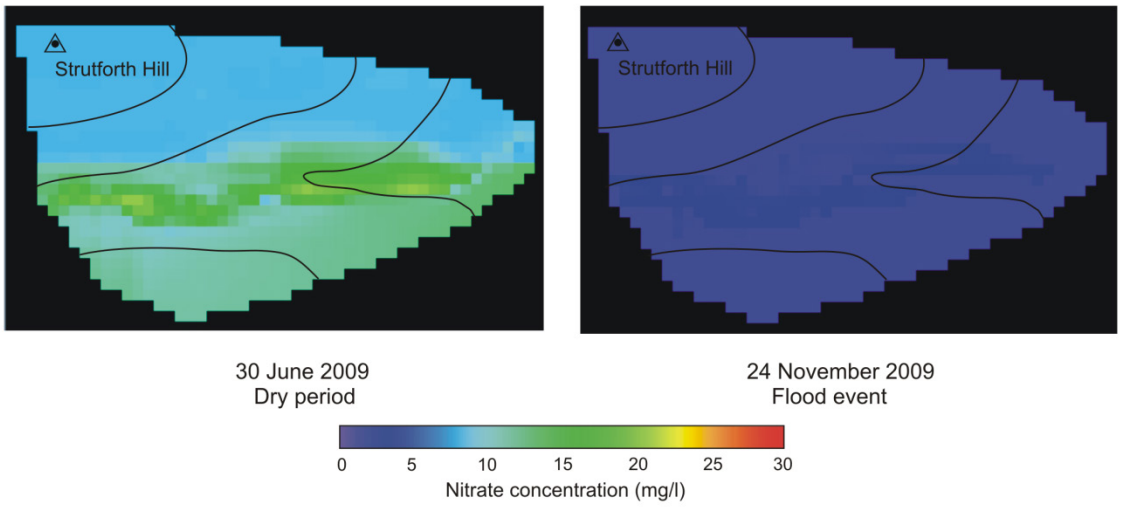

Figure 10-28 *Soil nitrate maps derived with the SHETRAN for the Hollow sub-catchment*

The highest nitrate concentration occurred on 30 June 2009 (10.4 mg/l), while the lowest was 24 November 2009 (1.1 mg/l). The high nitrate content during June is likely due to the influence of the dry season and lack of rainfall. From the results of the soil nitrate presented in Chapter 8, Figure 8-8, that in dry conditions the nitrate concentration is higher in the deeper soil layers and decreased during the wet is in agreement with simulated findings.

The simulation results for the stream nitrate concentrations at the outlet of the Hollow sub-catchment are shown in Figure 10-29. Figure shows that the simulated nitrate concentrations are much higher than the measured ones. The model overpredicted the

nitrate concentration for the Hollow stream related to the monthly point measured values. These results illustrate the ability of the model to simulate trends in the stream nitrate concentrations for the Hollow sub-catchment.

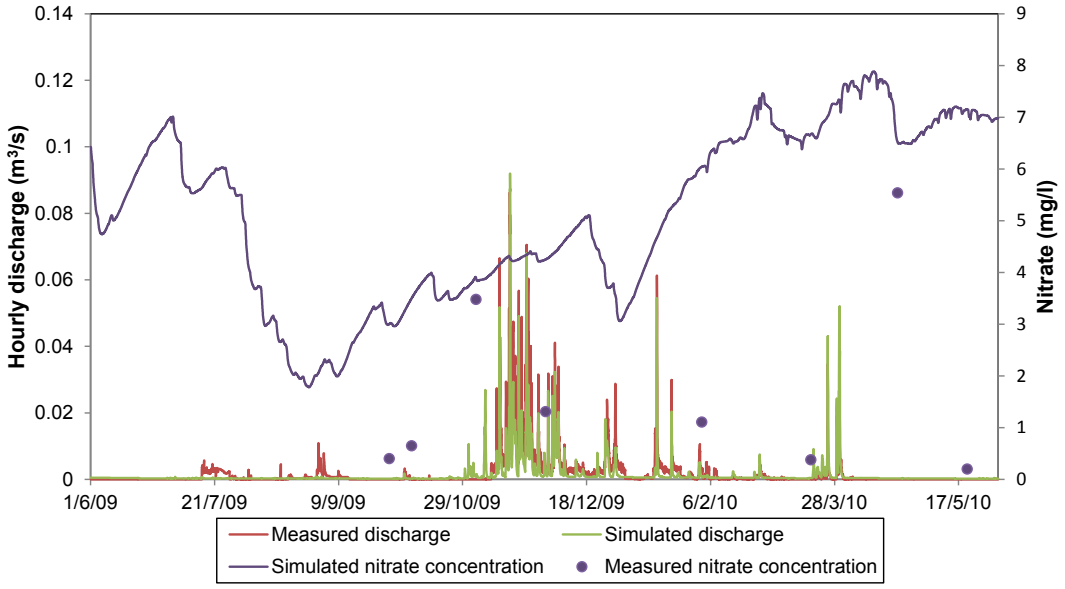

Figure 10-29 *Stream discharge and simulation of nitrate concentrations at the outlet of the Hollow sub-catchment*

For both scales, the low soil content of the nitrate during the wet period and higher during the dry is consistent with our findings at the hillslope (see Figure 8-8). The low soil nitrate concentrations are likely due to heavy rain that infiltrates into soil and flushes the nitrate out of the vadose zone into deeper soil layers, percolating to groundwater, leaching by subsurface flow or/and moving from the soil water table to the ground surface. From the spatial distribution map of the soil nitrate concentration, it can be seen that the highest soil nitrate concentrations occur during the dry period.

If the soil moisture maps are linked with the nitrate concentration maps for the same date, it can be seen that high soil level moisture coincides with low level of the nitrate concentration and opposite. In theory, the soil nitrate tends to accumulate in the spring and decrease during the summer due to crop uptake.

The stream water nitrate concentration is often used as an index of water quality. As the result of nitrate simulation, the concentration of the nitrate increases as water flow decreases, with apparent dilution. This finding is in agreement with other authors (Olsen 2003; DEFRA 2007b). Also, Poor and McDonnell (2007) found that in the agricultural catchment, nitrate concentrations decreased with increasing flow rates during storm events. Comparison with field data of Blind Beck and Hollow stream shows reliable the

simulation results. Based on the measured concentrations from previous events this decrease in nitrate in stream flow was expected.

There is not enough data available at the catchment and sub-catchment scale to support the detailed and physically based approach in this study. Furthermore, the uncertainty of the input parameters and the simulation outputs there was not investigated. This should be taken into account when making decisions based on the use of these models. However, the overall spatial and nitrate flux were simulated satisfactorily with the SHETRAN model. The results show that the model is suitable for prediction of the spatial distribution and flux of nitrate for extremely wet and dry seasons.

10.7.3 Catchment, sub-catchment and hillslope scale linkages of simulated flow

Hydrological modelling is being carried out at spatial scales ranging from plot scale to global scale and a variety of scaling theories has been developed (e.g. Blöschl and Sivapalan (1995) and Beven 1995). The scaling theories consider different spatial scales for single processes.

The simulations have been carried out for the hillslope as well as for the catchment and sub-catchment by the SHETRAN model. Figure 10-30 presents comparison and quantifying of the flow proportion that is changing across scales. The model represents the characteristics of the fast flow response to rainfall in the (sub) catchment and the hillslope. On a daily time step, there is almost no lag between rainfall and flow at the outlet. The hillslope responds to storm very differently from the (sub) catchment scale. These comparisons show the nature of rapid runoff at the smaller scale with the more baseflow at the hillslope scale. The scale affects the hydrological characteristics of the drainage area. Most of the precipitation on the hillslope scale tends to runoff quickly because there is little time or area for infiltration. On the large scale, travel distances are much longer, water storage may decrease flow peaks, precipitation has more time to infiltrate, and runoff reaches the (sub) catchment outlet more slowly after peak rainfall than at a small scale.

The modelling results within the catchment, sub-catchment and hillslope do show the runoff peak for the storm event in November, the same trends but different runoff rate and volume (Figure 10-30). This reflects the fact of scale, where the catchment (9.22 km^2) is much larger than the sub-catchment (0.09 km^2) and hillslope (45 m^2). The peak flow is higher for the catchment (0.56 m^3/s) than sub-catchment (0.03 m^3/s) and

hillslope (1.87·10-5 m^3/s) but the peak per unit area is relatively lower for the catchment (0.06 $m^3/s/km^2$) compared to the sub-catchment (0.33 $m^3/s/km^2$) and hillslope (0.45 $m^3/s/km^2$). This is partly related to the areal properties of the storm event, to infiltration losses and to the longer time required for the total catchment to contribute to the peak runoff (time of concentration).

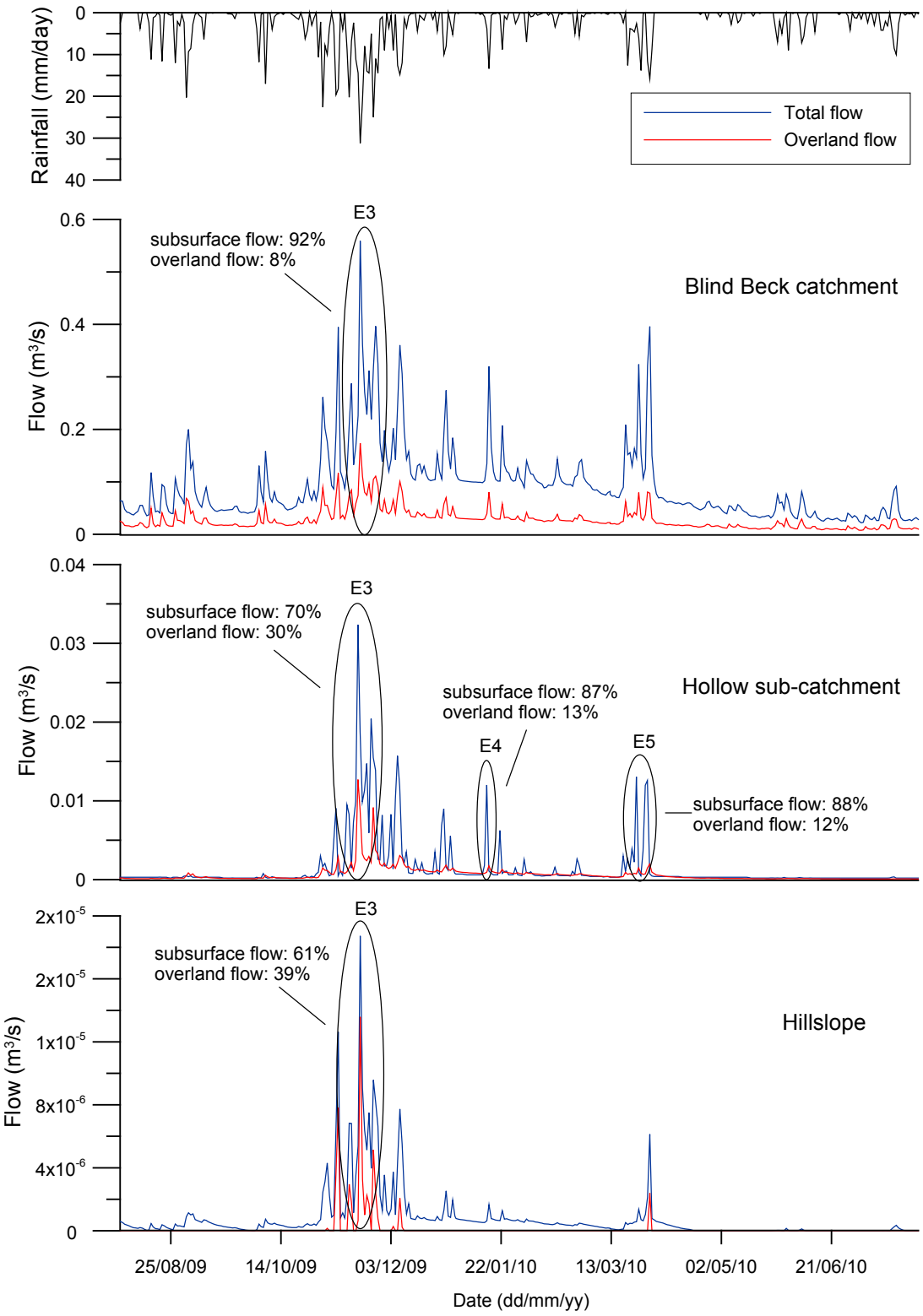

Figure 10-30 *Comparison of simulated discharge at the catchment, sub-catchment and hillslope scales (E3-E5: storm event)*

Figure 10-30 shows the simulated hydrological components of the total, the overland and the subsurface flows. The baseflow from the daily simulation for the November flood event (E3) is estimated to be approximately 92% of the total flow for the Blind Beck catchment. The modelling results indicate that the subsurface flow contributes to the runoff generation of the Blind Beck catchment, but no data are available to verify the modelling details in this particular aspect. However, the field measurement with EC tracer was applied at the outlet of the Hollow sub-catchment as described in sub-section 5.3.1. The model for the Hollow sub-catchment provides a split of the total storm flow into 30% overland and 70% subsurface flow for the November flood event (E3). The corresponding proportions for the E4 event in January are 13% overland flow and 87% subsurface/baseflow. For the event (E5) in March, the simulated results in Figure 10-30 demonstrate that the subsurface/ baseflow is 88% of the total flow, and the overland flow is 12%, respectively. Compared to the measured flow and applied hydrochemical separation, this is well in agreement with the simulated separation of the total flow. The overland flow proportion in the hillslope flow was a minor component of the flow with 39% of the subsurface contributions. Many researchers (Neal and Rosier 1990; Sklash 1990; McDonnell 2003; Kirchner 2003) demonstrated through field monitored experiments that the most part of the hillslopes runoff production comes from the subsurface, reaching often percentages around 80% of total runoff. This is in agreement with the simulated subsurface flow of the hillslope from this study.

The scaling behaviour of the runoff generation was limited by current data. Only the plot scale was fully conducted and measured for both the overland and the subsurface flows. The preliminary simulated result on scale effect is that the runoff coefficient at the catchment was smaller (0.37) than at the sub-catchment (0.57) and the hillslope scale (0.64). The results show that the November flood event runoff coefficients are highest at the hillslope scale, while lowest at the catchment scale. Wainwright and Parsons (2002) and Cerdan et al. (2004) has been examined the scale dependency of runoff coefficients to a plot and a catchment area and they both identified a significant decrease in the runoff coefficient as area increases. This is in agreement with the results from this study. The main cause of runoff coefficients decreasing with the increasing catchment area is probably due to long time of the surface runoff travelling to the outlet, the more rainfall amount needed for runoff generation or more infiltration amount for the larger catchment (Feng and Li 2008).

The subsurface flow increased moving from the hillslope scales to larger scales, while the overland flow decreased moving from small scales to larger. This indicates that hypothesis 4 which states that subsurface flow increase relative to overland flow with increase of scale is correct.

10.8 Summary

Modelling of the Blind Beck catchment and the Hollow sub-catchment using the SHETRAN model has been undertaken and the results shown by means of model performance, calibration and validation. The SHETRAN model results showed that hydrographs and the water balance were simulated adequately within an acceptable range for the calibration and validation phases.

During the modelling, the performance criteria used for appraising of the model performance were undertaken with a coefficient of determination (R^2 coefficient), and a Nash-Sutcliffe efficiency (NSE) for hourly predicted flows. The criteria of Henrikson et al. (2003) for R^2 was followed as R^2 value > 0.85 is excellent, values between 0.65 and 0.85 are very good, 0.50-0.65 are good, 0.20-0.50 are poor and < 0.20 are very poor. For the NSE, the results were considered to be good if NSE $\geq$0.75, and satisfactory if $0.36 \leq NSE \leq 0.75$ (van Liew and Garbrecht 2003). The fit for the catchment and sub-catchment is generally good, with R^2 values (on hourly flows) in the range of 0.73 to 0.84 and Nash-Sutcliffe Efficiency coefficients in the range of 0.70 to 0.83. Therefore, the model calibration and validation tests are judged to be successful. The statistics show that the SHETRAN performed satisfactorily in predicting average hourly discharges.

The individual simulated hydrographs for the catchment showed a very good modelling results for the January event (E4) of Blind Beck. The event (E4) is likely due to influence of rain-on-snow event incorporating snowmelt. The winter 2009-2010 in the UK was unusually cold with heavy snowfall and record low temperatures (see Appendix C1 and C2). The snow was observed during December and January but almost of all the snow melts at the end of February and the beginning of March. The event (E4) was modelled with rainfall only and the presence of the snowpack was not taken in account, so the simulation appears to be good based on an assumption that snowmelt played little or no part in the observed runoff generation. The SHETRAN model shows variations between storm events, with better performance for the January event (E4) for the

Hollow sub-catchment. The error in the peak flow rate simulation was much larger for the spring event than it was in the autumn and the winter events. The modelling results of individual storm event show overall a decreased simulated discharge.

A limitation of the models is a poorer performance of simulating low flows at the catchment scale. Based on the observed rainfall and other hydrological data, the water balance for all three scales was modelled. The models were evaluated for 2009 to 2010, from which there was found to be a deficit year for all scales. The catchment and sub-catchment annual water balances showed little differences in overall stream discharge. The change in the annual water balance was negative, which suggested that water was being lost from storage.

Spatially distributed soil moisture values in the Blind Beck catchment declined during the midsummer periods. Evidence from the soil moisture field measurements show that the soil moisture at the 10 cm below soil ground dried significantly during dry conditions, although soils at a greater depths at 20 and 30 cm remained saturated. Comparisons were made between measured and simulated soil moisture data at three depths at the hillslope of the Hollow sub-catchment. The agreement between simulated and measured soil moisture soil at the depth of 0-30 cm was good.

The simulated soil nitrate concentrations generally show high accumulation of nitrate in the dry season, whereas in the wet season they were low. Simulating the spatial distribution of the soil nitrate can provide important information for control of the spread of nitrate leaching to groundwater.

The model supports the hypothesis that with increases of scale, subsurface flow increase relative to overland flow.

Chapter 11. Future scenarios in term of climate variability

11.1 Introduction

Recent extreme weather events such as the autumn UK floods (e.g. 18 November 2009) have attracted attention to the possible impacts of climate change on agricultural land. Evidence from climate models (e.g. Frei et al. 1998, 2006; Ekström et al. 2005) suggests that warming may lead to an intensification of the hydrological cycle and increases in both mean and heavy rainfall (Fowler et al. 2006).

This Chapter presents how the distributed hydrological hillslope model developed in Chapter 10 was used with projected climate change scenarios to assess how runoff is likely to change in the future. Firstly, a review of the climate change modelling approach will be introduced (Section 11.2) with the methodology of deriving climate change projections for the UK. Then the methodology of deriving of climate change projections with a suitable climate change scenario will be described. The impact of this scenario upon climatological variables such as precipitation regime will be assessed. Application of the emission scenarios to a hillslope model and the impact on runoff, will be analysed.

11.2 Climate change modelling and possible future scenarios

In the selection of climate change models, it is important to select a model with the ability to simulate future climate conditions and impacts on the runoff regime for a particular case study at a hillslope scale.

General Circulation Models (GCMs) can provide time series of climate variables globally, accounting for the effects of greenhouses gases in the atmosphere (Ghosh and Mujumdar 2008). The GCMs provide predictions of climate variables at larger spatial scales reasonably well, but perform relatively poorly at smaller space and time scales (Bates 1998). However, they remain relatively coarse in resolution and are unable to resolve significant sub-grid scale features (Grotch and MacCracken 1991) such as topography, clouds and land use. In order to solve these problems, the modelling community has focused on improving techniques to "downscale" these scenarios using a sequence of models to translate these global scenarios to regional and local impacts. To make predictions at regional and local scales, Limited Area Models (LAMs) or dynamic downscaling has been developed in which a fine computational grid over a

limited domain is nested within the coarse grid of a GMC (Jones et al. 1995). This approach is complicated in design with a high computational cost (Ghosh and Mujumdar 2008) in the sense that expanding the region or moving to a slightly different region requires redoing the entire experiment (Crane and Hewitson 1998). A statistical downscaling process is another approach that involves deriving empirical relationships that transform large scale features of the GCM (Predictors) to regional scale variables (Predictands) such as precipitation and streamflow (Ghosh and Mujumdar 2008). In the statistical downscaling are three implicit assumptions (Hewitson and Crane 1992): "(i) the predictors are variables of relevance and are realistically modelled by the host GCM; (ii) the empirical relationship is valid also under altered climatic conditions; (iii) the predictors employed fully represent the climate change signal" (Ghosh and Mujumdar 2008). Statistical downscaling methodologies consist of three categories (Murphy 1999; Wilby et al. 2004): weather generators, weather typing and transfer functions.

Regional Climate Models (RCMs) were developed historically as physically based downscaling tools, in which the limited-area climate model was driven by time-dependent lateral boundary data, either from an analysis or from a coarser-meshed general circulation model (Vidale et al. 2003). Regional Climate Models (RCMs) are commonly used to downscale GCM simulations from the global scale to the regional.

Although both RCMs and GCMs include the representation of hydrology, they generally do not resolve the hydrological cycle at a level of detail that is suitable for hydrological applications (Bergström et al. 2001). They are also subject to systematic biases, particularly for precipitation (Varis et al. 2004), the primary variable that dominates in most hydrological regimes. For this reason, hydrological models are generally used to interpret the climate scenario results from climate models.

Covey et al. (2003) mentioned many sources of uncertainty that have to be considered during the estimation of climate change impacts. Global Climate Model (GCM) uncertainty consists of two sources: structure and parameterisation scheme. In the case of using Regional Climate Model (RCM) data, Déqué et al. (2007) highlighted that the sources of uncertainty increase, as outputs are influenced by RCM resolution, numerical scheme, physical parameterizations and the forcing boundary conditions. Reaney and Fowler (2008) investigated the uncertainty present in studies considering the hydrological impacts from climate change (Figure 11-1). They considered that results

from the emission rates of greenhouse gases produce the major uncertainty but this is determined by society through polices and behaviour (Reaney and Fowler 2008).

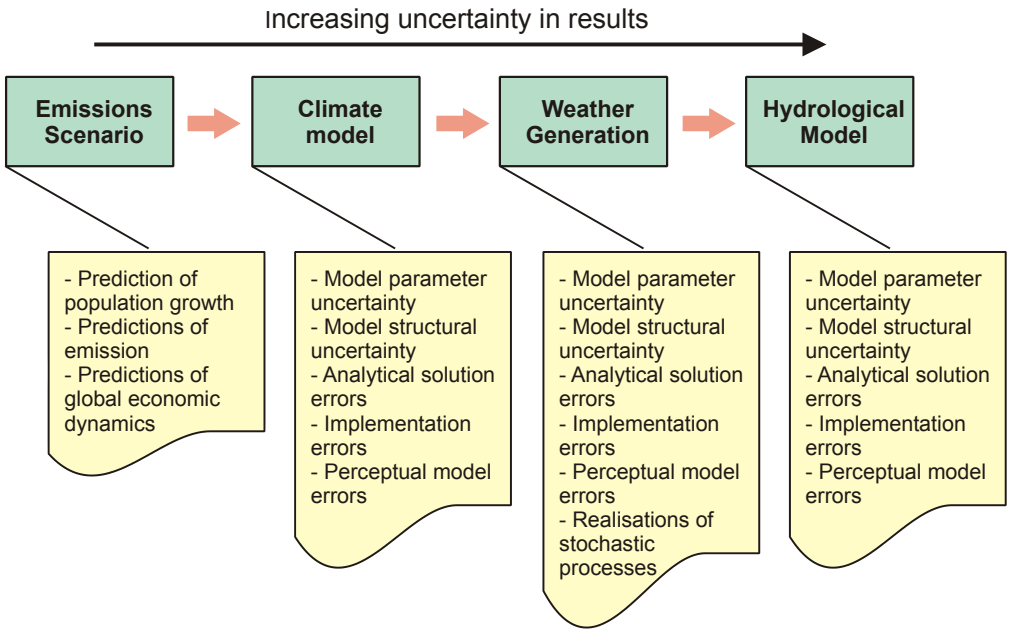

Figure 11-1 *Sources of uncertainty in studies considering hydrological impacts from predicted climatic change (source: Reaney and Fowler 2008; modified by the author)*

A climate-change prediction (or projection) is the change between a model simulation of recent climate (generally 1961-1990) and the model climate prediction for a period (for example, 2071-2100) in the future, under a specific emissions scenario (Jenkins and Lowe 2003).

11.3 Weather Generators

A weather generator is a statistical method of creating projections of future climate variables. There are two fundamental types of daily weather generators based on daily precipitation: Markov chain approach (Hughes et al. 1993; Hughes and Guttorp 1994; Hughes et al. 1999; Mehrotra and Sharma 2005) and the spell-length approach (Wilks 1999). Kilsby et al. (2007) point out that previous weather generators have used simple rainfall models based on either Markov chains (Richardson 1981) or empirical distributions of wet or dry spells (Semenov and Brooks 1999; Kilsby et al. 2007). However, a stochastic weather generator model such as that of Kilsby et al. (2007) and also used in the UKCP09 weather generator generates a synthetic time series of rainfall, temperature, humidity, potential evapotranspiration and sunshine amount. The stochastic approach means that the state of the system at one time does not completely determine the state at the next time (Jones et al. 2009).

The general motivation for using the weather generator is to provide synthetic series of unlimited length (Hulme et al. 2002) or the possibility of infilling missing values by imputation (i.e., sampling missing observations from their conditional distribution given the available observations, see Yang et al. 2005; Semenov et al. 1998). The computational efficiency of this method allows for multi-model probabilistic projections or other impact assessments (Jones et al. 2009).

Weather generators have been used in many different impact studies. For example, Hobson (2005) used a technique to couple a k-nearest stochastic weather generator and Precipitation-Runoff Modelling System (PRMS) basin model to simulate historic streamflow statistics and provide a framework for forecasting flows in the Upper Truckee River Watershed. Walsh and Kilsby (2007) used the UKCIP02 climate scenarios to produce climate sequences for the catchment flow regime affecting Atlantic salmon in the Eden catchment. In this study, the outputs from the UKCIP02 were used as the input series of the SHETRAN model, which subsequently generates flows to represent the climate in the 2080s. Fowler et al. (2008) developed a model to combine different projections of change in climate and flow statistics from multiple RCMs into single probabilistic estimates. They used the stochastic weather generator (SWG) downscaling approach to produce catchment scale climate change scenarios for the River Eden in northwest England. A simplified and calibrated version of the Arno hydrologic model (Todini 1996) was used to produce 1000 synthetic 30-year daily flow sequences.

In this study, in order to estimate future climate conditions at the local scale, weather generator models from the UKCP09 weather generator were used. UKCP09 contains a weather generator which is able to output both daily and consistent hourly weather data on a 5 km grid over the UK for the historic period (1961-1990) and future time slices in decadal steps from the 2020s up to the 2080s (with each encompassing a separate thirty year period) (Jones et al. 2009). These are described in further detail in the next section.

11.4 UKCP09 Methodology

The latest probabilistic projections from the United Kingdom Climate Impacts Program (UKCP09) can be used to produce probabilistic future weather sequences over the UK (UK Climate Projections 2009). Based on the UKCP09 probabilistic change factors over land, a stochastic climate change weather tool has been produced by Newcastle

University to generate weather files with either a daily or hourly time series (Jones et al. 2009).

UKCP09 provides climatic information for three emission scenarios: low, medium and high that are related to greenhouse gas emissions levels - SRES B1, SRES A1B and SRES A1FI scenarios in the IPCC Special Report on Emission Scenarios (SRES) (Nakicenovic et al. 2000). A scenario is not a prediction of the future, it is a coherent, internally consistent and plausible description of a possible future state of the world (Parry and Carter 1998). The UKCP09 weather generator provides seven different thirty-year time periods: 2020s (2010-2039), 2030s (2020-2049), 2040s (2030-2059), 2050s (2040-2069), 2060s (2050-2079), 2070s (2060-2089) and 2080s (2070-2099). The image outputs that can be used to visualise the UKCP09 probabilistic climate projections are presented as Probability Distribution Function (PDF) plots. These help at single estimates to be defined, justified and placed in the context of alternative outcomes.

The UKCP09 WG is based around a stochastic model that simulates future precipitation sequences. The UKCP09 weather generator then uses this daily precipitation sequence as the primary variable while other variables are created using mathematical and statistical relationships with daily precipitation and the previous day's values of other climate variables. The daily observed baseline climate (1961 – 1990) is used to calibrate the weather generator rainfall model. This model is applied across a 25 km grid, while the addition of a 5 km grid for the weather generator allows for changes in local topology and it is based on observations, which have been spatially interpolated onto the same 5 km grid but does not give any further climate information outside the 25 km grid.

The weather generator outputs nine daily variables: mean total precipitation, minimum temperature, maximum temperature, vapour pressure, relative humidity, sunshine hours, potential evapotranspiration (PET), direct radiation and downward diffuse radiation. The hourly temporal resolution contains seven output variables: mean total precipitation, mean temperature, vapour pressure, relative humidity, sunshine hours, direct radiation and downward diffuse radiation.

In summary, the UKCP09 weather generator is able to generate daily and consistent hourly weather data on a 5 km grid over the UK for the historic period (1961-1990) and

future time slices in decadal steps from the 2020s up to 2080s. More details on the UKCP09 weather generator can be found in UK Climate Projections 2009.

11.5 Methodology of deriving climate change projections

In this study, climate change modelling was performed using the UKCP09 weather generator data (WG). Firstly, the emission scenarios medium (SRES A1B) and high (SRES A1FI) were selected because result in the medium and highest increases in global-mean temperature by 2100. Emissions scenario A1B is based on the assumption of very rapid future economic growth, technological developments with fossil fuel use. Scenario A1FI assumes only very rapid future economic growth and fossil fuel use. It was decided to assess climate change in the 2020s (2010-2039) and the 2050s (2040-2069) for monthly temporal averages. The use of these two time slices avoids the use of data with high uncertainty for 2080s period and to consider the results on scientific (2050s) and shorter-term management (2020s) time scale. In the next step, the 5 km grid point of the weather generator was selected that covers the study site. The option for random sampling of model variants was selected and the weather generator was run for 100 randomly selected samples of the input parameters. The time frequency of weather generator output was hourly and daily. The duration of each weather generator run was set to 30 years. The random number seed generator was selected to be 1. The run of 100 randomly selected samples for 30 years produced 100 30 year stochastic simulations of the baseline period (1961-1990) and another 100 of the future scenario climate period. In each simulation, precipitation (P) and mean potential evaporation (PET) were output.

11.5.1 Climate change and runoff scenarios

Available data

The monthly baseline 1961-1990 averages for rainfall were provided by the UKCP09 weather generator. The climate change scenarios obtained from the weather generator were prepared in the form of hourly time scale for precipitation and daily time scale for PET. They consist of 100 different realisations of a possible future climate scenario with each realisation consisting of a thirty-year time series. For each WG 100 30-year climate scenarios were produced for each of the SRES A2 and SRES A1FI emissions scenarios.

After the calibration and validation of the SHETRAN model carried out for the hillslope, the hourly future climate variables (P and PET) for the 2020s and 2050s period were input to SHETRAN and used to examine changes in flow. All the simulations were based on an hourly time step.

11.6 Results of future climate model runs

11.6.1 Analysis of monthly rainfall projections

Future climate conditions at the hillslope were estimated by applying the corresponding climate change scenarios for the observed climate baseline as detailed in the previous section.

The mean monthly rainfall data for the 2020s and 2050s time slices, and for the medium (M) and high (H) emission scenarios (A1B and A1FI) are illustrated in Figure 11-2. These monthly series are the average of 100 rainfall series of each scenario.

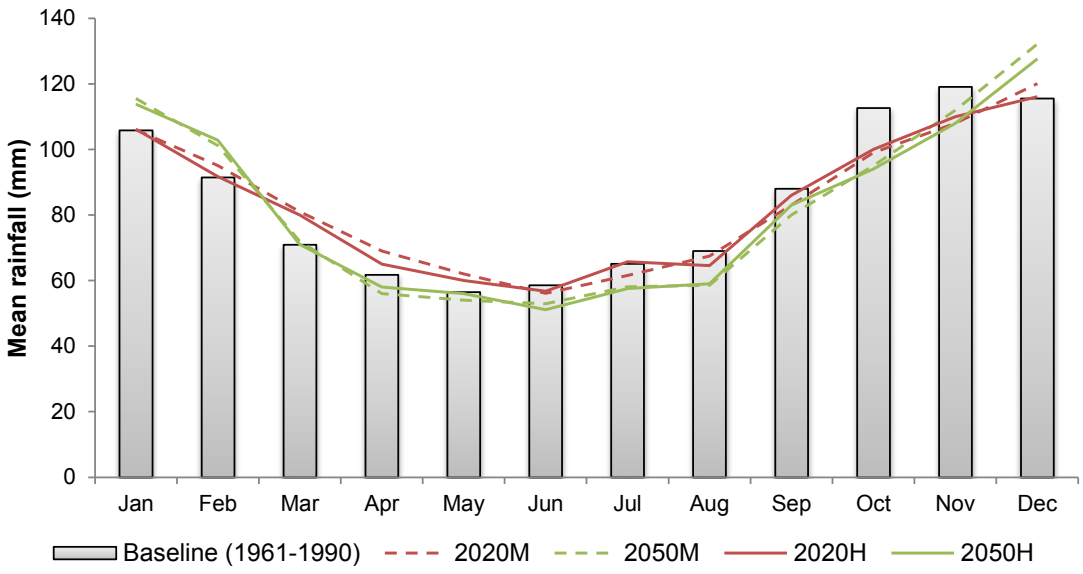

Figure 11-2 *Comparison of mean monthly rainfall for the baseline and UKCP09 scenarios*

Comparison between the UKCP09 scenarios and the baseline showed that rainfall is projected to increase from January to April, decrease from May to September and to increase from October to December. The scenario shows mostly higher rainfall except for April to September. Seasonally, mean projected rainfall was higher in the autumn and the winter, while less in the spring and the summer. The largest changes are projected for the High scenario between the 2020s and 2050s. Rainfall is higher during July for the 2020-High than for the 2050-High. Rainfall is significantly lower from June

to September and higher from October to April for the 2040-2069 period than for the 2010-2039 period.

Annual rainfall for the baseline period was 1014 mm. The baseline and future rainfall for the each emission scenario were compared (Table 11-1). For the A1B scenario, the average annual rainfall in the 2020 centred period (2010-2039) was 0.6% less than for the baseline. For the A1FI scenario, there was 1.2% reduction. By 2050, rainfall reductions were much larger for the A1FI scenario than for the A1B scenario. Average annual rainfall for the 2050-centred period (1040-2069) was approximately 2.6% and 3.2% less than the baseline for the A1B and A1FI scenarios respectively. However, for the A1FI scenario, the rainfall reduction to 2020 was smaller than it was for 2050, at approximately 1.2% compared with 3.2%.

Table 11-1 *Mean annual rainfall for the A1B and A1FI climate scenarios, reported for baseline and future periods*

Period	Baseline	A1B (Medium)		A1FI (High)	
		Rainfall (mm)	% Change from baseline	Rainfall (mm)	% Change from baseline
(1961-1990)	1014		-		-
2020 (2010-2039)		1008	-0.6	1002	-1.2
2050 (2040-2069)		988	-2.6	982	-3.2

Table 11-2 compares the average winter (DJF) and the summer (JJA) rainfall for the baseline (1961-1990) and climate change projections (2020 and 2050). The UK Climate Projections for the 2020s and 2050s show that a trend toward wetter winters and drier summers. More specifically, an average rainfall increase in the winter for the Medium and High emissions scenario of between 0.4% and 2.7% for the 2020s, and 10.0% to 11.6% for the 2050s. Summer rainfall was highest in the baseline period (1961-1990), was lower in 2020 and lower still in the 2050 period. By 2050, rainfall reductions were much larger for the Medium and High scenarios than for the 2020.

Table 11-2 *Comparison of baseline and climate projectors for the winter and the summer rainfall*

	Baseline	Rainfall (mm)				% Change from baseline			
		2020M	2050M	2020H	2050H	2020M	2050M	2020H	2050H
Winter (DJF)	317	321	349	314	344	2.7	11.6	0.4	10.0
Summer (JJA)	193	185	170	187	168	-4.0	-11.7	-2.9	-12.8

11.6.2 Runoff results of future climate model runs

The runoff results are the average of the SHETRAN simulations for each emission scenario (A1B and A1FI). It has been analysed for the mean annual and monthly runoff

assessed at two 30-year time-slices between 2020 and 2050 and the baseline period (1961-1990). Projected and baseline runoff have been compared.

Figure 11-3 shows the monthly runoff projected for the 2020s and 2050s under the High and Medium emission scenarios and the baseline (1961-1990) period. Simulations of the future runoff predict increases in the autumn and the winter, and decreases in the summer runoff. The following runoff results are the average of 100 simulations for each emission scenario.

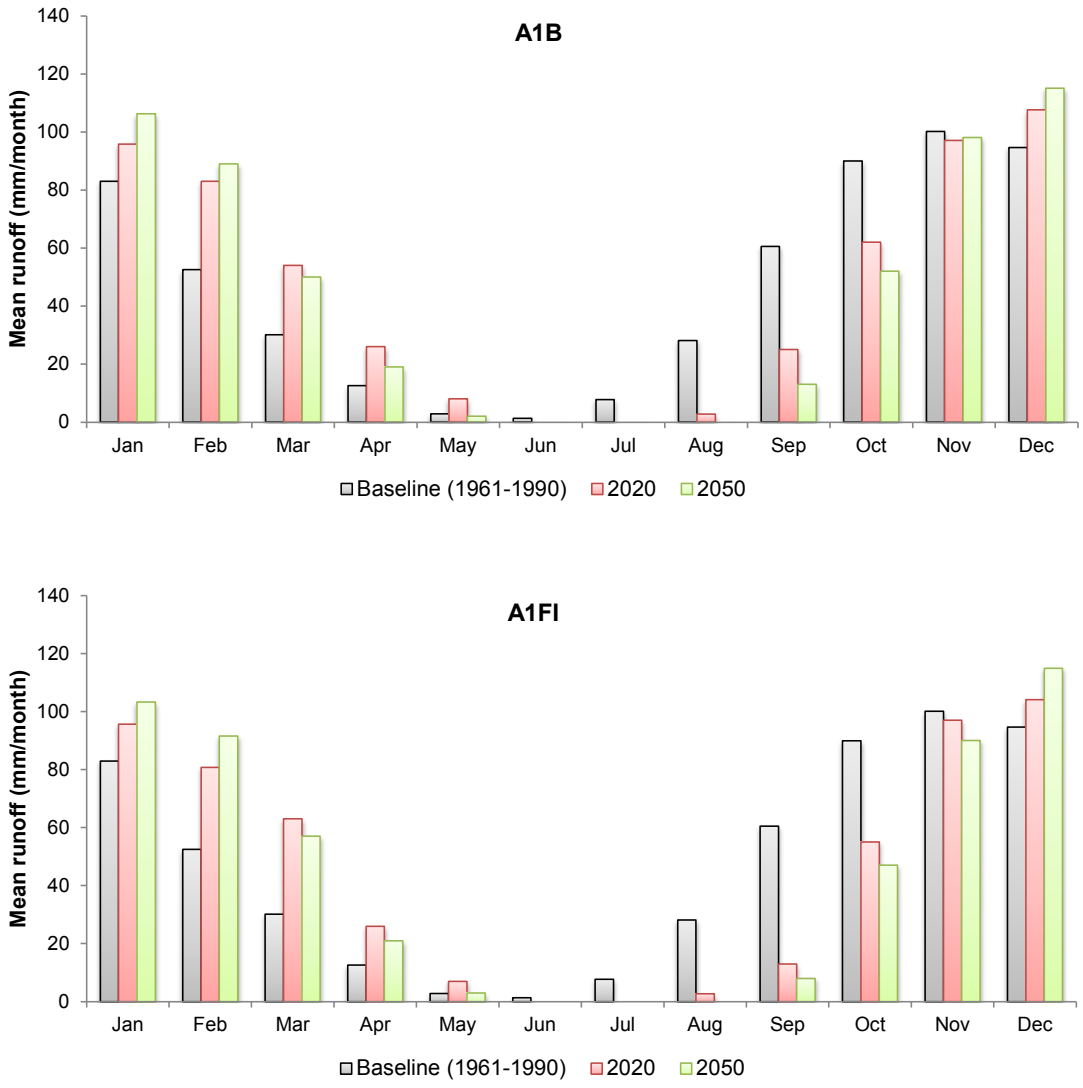

Figure 11-3 *Mean monthly runoff for the hillslope for the A1B and A1FI climate scenario*

According to the climate change projections, an increase relative to the summer and a significant decrease compared to the historical observations in the long-term mean monthly runoff can be expected from August to December for the 2010-2039 period and from September to December for the 2040-2069 period. For the months June and July a decrease in the long-term mean monthly runoff is expected for both periods and also in

the month of August for the 2040-2069 period. The projected runoff for the A1FI scenario in the 2020s is lower than for the 2050s from December to May. This effect is also evident for the A1B scenario where the projected runoff for the 2020s was lower than for the 2050s from November to March. The highest increase in mean runoff at the hillslope is projected to occur in December for both time periods and both scenarios.

The mean annual runoff for each emission scenarios for the future periods compared to the baseline period are shown in Table 11-3. The largest decrease in runoff was found for the A1FI scenario by 2050 of 4.8%. The runoff reduction was similar to the A1B scenario by 2050 and A1FI by 2020 at 3.4%. However, it appears that runoff for the A1B scenario by 2020 was 0.4% less than the baseline period.

Table 11-3 *Mean annual runoff for the A1B and A1FI climate scenarios, reported for baseline and future periods*

Period	Baseline	A1B (Medium)		A1FI (High)	
		Runoff (mm)	% Change from baseline	Runoff (mm)	% Change from baseline
(1961-1990)	563		-		-
2020 (2010-2039)		561	-0.4	544	-3.4
2050 (2040-2069)		544	-3.4	536	-4.8

Table 11-4 compares the average winter and the summer runoff for the baseline and climate projectors (2020s and 2050s) under the Medium and High emission scenarios. The changes show wetter winters and drier summers. More specifically, an average runoff increase in the winter for the High and Medium emissions scenario of 22 and 24% for the 2020s, and 35 to 37% for the 2050s. By 2050, runoff reductions are much larger for both scenarios than for the 2020. This indicates lack of runoff in the summer months.

Table 11-4 *Comparison of baseline and climate projectors for the winter and the summer runoff*

	Baseline	Runoff (mm)				Percentage difference			
		2020M	2050M	2020H	2050H	2020M	2050M	2020H	2050H
Winter (DJF)	230	286	310	280	310	24	37	22	35
Summer (JJA)	37	3	0	3	0	-92	-100	-92	-100

The mean monthly runoff results for each emission scenario are shown in Table 11-5. An increase in monthly runoff can be expected in November and/or December, and in April and May for the 2040-2069 period under A1B and A1FI emission scenarios and the 2010-2039 period under both scenarios. The highest relative increase in the mean monthly runoff for the 2010-2039 period in comparison with the baseline period can occur in May under the A1B scenario (+100%) and in April under the A1FI scenario

(+94%). In the case of the 2040-2069 period, the highest increase can be assumed to be in April under the A1B scenario (+80%) and in March under the A1FI scenario (+96%).

Table 11-5 *Mean monthly runoff for the A1B and A1FI climate scenarios, reported for baseline and future periods*

Month	Runoff	% Change from baseline			
		2020		2050	
	Baseline (mm)	A1B	A1FI	A1B	A1FI
January	83	15	15	28	24
February	53	58	54	69	74
March	30	70	63	77	96
April	13	91	94	80	84
May	3	100	91	20	17
June	1	-100	-100	-100	-100
July	8	-100	-100	-100	-100
August	28	-90	-90	-100	-10
September	61	-63	-61	-75	-83
October	90	-35	-35	-39	-46
November	100	-6	-8	1	-10
December	95	14	-10	27	21

A decline in the long-term mean monthly runoff may occur from June to November and/or December for the 2020s period under both emission scenarios and the 2050s period under the A1FI scenario. The extreme decrease in monthly runoff could occur in June and July for the 2020s and 2050s period under the High and Medium emission scenarios, i.e. -100. This decrease in runoff can be caused by a decrease in rainfall exactly in these months (Figure 11-2).

11.7 Projected changes in rainfall and runoff patterns

For this study the weather generator (WG) 100 30-year climate series were produced for each of medium (SRES A1B) and high (SRES A1FI) scenarios, which means the other possible scenarios, such as Low-Medium and Low-High remains unstudied. For the modelling study, focus is given on the fate of runoff at a hillslope scale.

For both future periods mean monthly rainfall is projected to decrease for all emission scenarios except for the months of February and December, and including January for the 2050s. The projected change in the rainfall pattern has a direct impact on the runoff at the hillslope. A projected increase in runoff can be attributed to the projected increase in rainfall from September to December (Figure 11-3). The most extreme projected decrease in monthly runoff during June and July for both periods, and additionally in August for the 2040-2069 period, due to decrease in rainfall during these months. This suggests the absence of antecedent soil moisture that directly depends on the rainfall of the previous months to produce flow. The results indicate a projected reduction in the

future runoff during the summer period and an increase during the winter period. This is consistent with the findings of Walsh and Kilsby (2007) who found the same trend for the River Eden catchment above at Temple Sowerby (area 600 km^2), in the northern UK.

The rainfall patterns of the future climate conditions may gradually lead to a critical reduction in the soil moisture for the hillslope of a catchment during the summer months and consequently to the total lack of the catchment's deep subsurface flow. The effect of increased climate variability on water storages at the hillslope depends on the hydrologic processes of rainfall. The low runoff simulated for the scenario period would potentially cause drought which would have effects on stream ecology (eutrophication, blooming of algae, watercolour) while on the other hand simulated high runoff would cause more floods (erosion of stream banks, lower accessibility of fields) which would have some effect on agriculture. The evidence of the climate change impact is seen during the summer 2010 where low runoff increase the DOC and the nitrate concentration in stream of the Hollow sub-catchment that cause the problems in stream such as eutrophication. These future changes would depend on change in future rainfall, runoff volume and runoff peak. In the Eden basin, floods are normally considered as a serious problem, as they often have an impact on agriculture fields, infrastructure and buildings. What this work does not consider, is the application of the weather series to the catchment and sub-catchment model and the impact on stream flow that could reveal much about the frequency and magnitude of peak flows, low, high flows and extreme floods.

The propagation of uncertainties and errors with modelling future climate changes on runoff is amplified during the hydrological modelling. The results of this climate change modelling are likely affected by the uncertainty of hydrological modelling and processes to model as shown in Figure 11-1 and described by Reaney and Fowler (2008). The two emission scenarios used in this study ranged from medium (A1B) to high (A1FI) are based on the future greenhouses gas emission which represented a great deal of uncertainty as to how these will develop in the future. The scenarios do not represent actual predictions but do represent projected future climate data. By taking more climate change scenarios into account, it is possible to give a better impression of the results. Nevertheless, the results of this study are believed to be responsible for the purpose of estimating approximate runoff from the hillslope within the historical data and future changes in runoff for the range of specified climate scenarios.

The data in this study are useful in projecting future water availability and can be used to support management changes. The potential impact of climate change is a significant consideration for decision making at large scales.

11.8 Summary

This research assesses the effects of climate change on rainfall and runoff at a hillslope scale. Modelled rainfall and runoff patterns were assessed for 100 randomly generated samples for 30-year time slices representing the following timeframes:

- 1961-1990 baseline
- 2020 centred future period (2010-2039)
- 2050 centred future period (2040-2069)

The emission scenarios medium (SRES A1B) and high (SRES A1FI) were selected for the simulations. Projected rainfall series for these two emission scenarios were applied to the SHETRAN hydrological model for the hillslope. In terms of seasonal changes, future projections of change in rainfall indicate an increase during the winter months with decreases during the summer. By the 2020s between 0.6 % and 1.2 % less rainfall is expected under the medium and high emission scenarios. By the 2050s rainfall reduction is expected to fall between 2.6 % (medium emission) and 3.2 % (high emission). The monthly mean runoff is seen to decrease from June to November and/or December with an extreme decrease in June and July, and increase from November and/or December to May. The projected increase in mean runoff is predominantly through increases in the winter and the spring runoff, while monthly mean runoff in the summer and the autumn are projected to remain the same or to decrease.

These results provide an assessment of direct climate change impacts on runoff at the hillslope scale in the range of medium to high emission scenarios. This work should be extended to the catchment and sub-catchment scales, and to simulate the impacts of climate change upon carbon and nitrate water quality.

Chapter 12. Conclusions

12.1 Introduction

The aim of the work presented in this study was to provide a new understanding of surface and subsurface hydrological controls on nutrient fluxes within mineral soils at the hillslope and catchment scale in Cumbria (UK), and how these are possibly influenced by future climate variability. Based on the findings, a new conceptual understanding was developed of the role of runoff on nutrient fluxes within mineral soils of the unsaturated zone, and applied to a larger scale. The overall methodology has been integrated in the form of field experiments and sampling, laboratory analysis and modelling. The hillslope runoff experiment was conducted on two hillslope runoff plots to identify runoff processes and to quantify nutrient fluxes, one under perturbed (i.e. enhanced rainfall) conditions, and the other as the control plot. Hydrochemical separation was carried out to provide quantitative information of storm and seasonal runoff pathways at the outlet of the sub-catchment. The modelling approach included development and testing of numerical flow and transport models, and simulation of possible impacts of precipitation variability on runoff.

In the first section of this chapter, the main findings of this study are presented with respect to the initial four objectives. Concluding remarks are given with regard to the key hypotheses. In the last section, recommendations for further study are presented.

12.2 Main thesis findings

Objective 1: Identification and quantification of runoff processes at the catchment and hillslope scales using field experiments.

It was hypothesized that hydrochemical flow separation using continuous measurement of variables at the catchment outlet could provide quantitative estimates of surface and subsurface components of flow at the catchment scale (**Hypothesis 3**). This hypothesis was addressed by the application of two-component hydrograph separation on three high to moderate intensity rainfall events in the Hollow sub-catchment to evaluate the dominant storm runoff generation processes. Electrical Conductivity (EC) was used as a continuous tracer in combination with stream discharge data. Hydrograph separation indicates that storm flow was largely composed of pre-event water that is a significant portion of the total runoff for each event. Average pre-event water contributions for all

events range from 78% to 85%. The current study was unable to determine hydrochemical separation at the outlet of the Blind Beck catchment because no data of continuously monitored electrical conductivity were available. Hydrochemical flow separation has been shown to be an effective tool for separating runoff at the outlet of the sub-catchment.

At the plot scale (2 m^2) observations are extrapolated to the hillslope transect determining the hydrological role of nutrient and water mobilization within the unsaturated zone. The examination of the hydrological behaviour at the hillslope during runoff experiments was based on analysis of enhanced rainfall and three rain storm events that show significant runoff differences. Analyses of runoff for different climate conditions within the unsaturated zone suggested: i) overland flow varied from 14% in dry conditions (before treatment) to more than 67% in the enhanced rainfall conditions of the total measured overland flow, ii) lateral subsurface flow dominates hillslope runoff during the transition period and iii) overland flow occurs in the winter during periods of frozen soil as Hortonian flow. The enhanced rainfall experiment produced 68% of overland flow over the longer term as compared to the natural climate condition control plot with 32% overland flow.

Objective 2: Determination of hydrological controls on soil C and N storage and transport using geochemical analyses.

The runoff hillslope experiment was used to help us to understand the effects of rainfall and runoff on soil properties under various climate conditions. In this study for the first time is used TG-DSC-QMS method to give an estimation of carbon loss during change of climate conditions. These observations beg the question: How and why soil carbon is declining? This method provides the significant results of 67% C loss in the wet condition. From the author's point and based on the results the TG-DSC-QMS method may serve as a valid tool to estimate carbon loss. During the wet period, the significant changes in TOC content (38%) were in the upper soil layer with increasing of TOC (Section 8.4). For the same conditions, the TN increased with significant changes of 59% observed in deeper soil layers (20-30 cm). The amount of soil organic carbon (SOC) that is stored in the soil at 10 cm soil depth was estimated to be 23 t/ha in the dry condition and 32 t/ha in the wet conditions. Declining of soil organic carbon is accelerating by the removal of soil organic matter. The main key for the declining of soil carbon is a significant influence of rainfall intensity and duration.

Objective 3: Construction of a conceptual model of storages and fluxes of water and nutrients from the hillslope to the catchment scales.

A conceptual model of the EC flushing was being developed for each plot during the storm event (Section 7.4, Figure 7-8). It was found an increasing trend of the total dissolved solids in the perturbed plot during an intensified rainfall event that suggested additional contributions from runoff than rainfall. The electrical conductivity measured at a control plot for the extreme storm event (November 2009) showed the flushing mechanism of the rain and dilution of the total dissolved solids. Based on these data, the saturation excess overland flow occurred during the large flood event at the perturbed plot. It is the result of rain falling on the saturated plot which, being unable to infiltrate, collect nutrients from the upper soil layer, runs off downslope and export labile nutrients (DOC and NO_3^-). The DOC and the NO_3^- export in the overland flow were smaller for the unchanged climate conditions compared to the intensified conditions. These findings support a conceptual model of water and nutrient flushing from the hillslope.

The runoff water samples were collected on a monthly basis from the perturbed and control plots at the hillslope scale. The DOC export to surface water is facilitated by the subsurface flow under perturbed, while the export of the NO_3^- is dominated by the overland flow under perturbed conditions. The enhanced rainfall treatment in the overland flow reduced the DOC concentration 1.7 times, while increasing the NO_3^- concentration 2.5 times. For the observed period in intensified rainfall conditions, the mean DOC exported from the perturbed plot was 9.7 kg/ha in the overland flow, and 22 kg/ha in the subsurface flow. In contrast, nitrate exports were larger in the overland than in the subsurface flow. The mean nitrate loss was 3.3 kg/ha in the overland flow, and 1.8 kg/ha in the subsurface flow. The results do partially support the hypothesis that the subsurface leaching pathway for nutrient losses from soil are enhanced relative to losses through surface flows under an intensified hydrological cycle predicted for continued global warming (**Hypothesis 1**). This hypothesis is not supported by the NO_3^- as shown that the dominant flow in the nitrate loss was the overland flow. The DOC export to surface water is facilitated by the subsurface flow during the large November storm event, while the NO_3^-export is dominated by the overland and subsurface storm flows, which do support listed hypothesis. Therefore, in order to apply this hypothesis in full other storm events should also be considered to validate these findings.

It is concluded that the export of C and N from the hillslope to a greater degree depends on the rainfall intensity and duration. Based on this data, understanding about the leaching process has been improved for determining changes in the carbon and nitrogen balance in the soil. These observations supported a new conceptual model of nutrient flushing from the hillslope scale.

The novel conceptual models for the export of the labile nutrients (DOC and NO_3^-) from the hillslope to the stream were developed. These models represent a new approach of where water and nutrients travels (e.g. soil depth), how it travels (e.g. surface or subsurface flow), when it travels (e.g. storm events), and where it is transported (e.g. streams).

The conceptual runoff generation models have been developed for the hillslope, presents flow pathways for dry, transition and wet periods. During the dry period, the subsurface flow dominates, while during the wet period shallow and deep lateral subsurface flow are the dominant pathways. Overall, it is concluded that main transport of delivering nutrients (DOC and NO_3^-) to the streams is intensified by rainfall events. The hypothesis that labile nutrient source of the soil solution is preferentially depleted under an intensified hydrological cycle is correct (**Hypothesis 2)**. This depletion is based on dominant runoff process occurring within the unsaturated zone, the role of rainfall (duration and intensity) and seasonality.

Objective 4: Development and testing of numerical flow and transport models, and application of models using probabilistic future weather projections (UKCP09) to simulate possible impacts of precipitation variability on runoff.

The hydrological models (Chapter 10) have been developed to address the initial hypothesis that with increases of scale increases subsurface flow relative to overland flow (**Hypothesis 4)**. A modelling approach was used to quantify the runoff proportion and to test the significance of scale.

The hydrological model has been successfully developed and calibrated to represent hydrological processes in the catchment and the sub-catchment. The statistics describing the fit of the hourly predicted flows, including R^2, and Nash-Sutcliffe coefficient of efficiency (E_{NS}) – a very good model according to Henriksen et al. (2003). The satisfactorily performance of the model shows the model is reasonably capable for prediction of runoff. The behaviour of the catchment differs from the behaviour of the

sub-catchment in dry periods; no discharge in the sub-catchment. Evaluation on performance of runoff simulation shows the results are consistently better at small scale than catchment, which indicates that SHETRAN model is suitable for small-scale hydrological modelling. The possible uncertainties in the modelling process could be attributed to input parameters, model assumptions and measuring data for the model validation.

The hillslope model aimed to capture the significant hydrological responses in storm events. A good relationship in the hydrographic shapes was found between the hillslope and sub-catchment scale. Furthermore, hydrograph observed at smaller scale reproduce rapid runoff, and the more baseflow – dominant runoff at the catchment scale.

It was hypothesised that with increases of scale increases subsurface flow relative to the overland flow, which is supported by the results of modelling approach. Moving from hillslope scale to sub-catchment and catchment scale, subsurface flow increased with a larger proportion at the catchment scale.

The model satisfactorily simulated spatial nitrate concentration for a heavy storm event at both catchment scale and sub-catchment scale in agreement with field measurement data. In the light of these results, SHETRAN demonstrated its ability to satisfactorily simulate runoff and nitrate across different scales.

To estimate climate impacts on runoff, projected rainfall and potential evaporation series for two emission scenarios were applied to the hillslope hydrological model for the 2010-2039 and 2040-2069 period. The emission scenarios of medium (A1B) and high (A1FI) greenhouse gas emission were selected. The seasonal pattern in hillslope runoff is expected to change giving significantly higher runoff during the winter and decrease during the summer. The most dramatic change in hydrological regime is predicted by a lack of runoff during the summer (June and July). Decreases in the mean rainfall between 0.6% and 2.6% for the 2020 and 2050 period of the A1B emission scenario are modelled to decrease annual runoff 0.4% and 3.4 %. For the A1FI emission scenario, a decrease in rainfall between 1.2% and 3.2% is modelled to decrease annual runoff by 3.4% for the 2020 period and by 4.8% for the 2050 period. An increase in monthly runoff can be expected in November and/or December, and in April and May for the 2040-2069 period under A1B and A1FI emission scenarios and the 2010-2039 period under both scenarios. This increase could be caused by an increase in the rainfall during the whole year except for the summer months (June and July) for the both

periods under High (A1FI) and Medium (A1B) emission scenarios. The monthly mean runoff is seen to decrease from June to November and/or December with an extreme decrease in June and July, and increase from November and/or December to May. The projected increase in mean runoff is predominantly through increases in the winter and the spring runoff, while monthly mean runoff in the summer and the autumn are projected to remain the same or to decrease.

This study has improved our understanding of the dominant role of hydrological control on nutrient flux under different climate conditions. The data in this study are useful in projecting future water availability and can be used to make management changes. The potential impact of climate change is a significant consideration for decision making on large scales.

12.3 Recommendations

Due to the fixed time limit set for this study the following recommendations are given for further research:

- more detailed investigation of the runoff generation that could include a three-component hydrograph separation at the outlet of the catchment. It is recommended to make use of other tracers to support separation of runoff components.
- research should also be undertaken to investigate the nutrient data beyond the Blind Beck catchment and to determine biological nutrient response. More information on the concentration of phosphorus, dissolved oxygen (DO), suspend sediments and turbidity in stream water would give additional information on the water quality. More broadly, research is also needed to determine the water quality of groundwater and estimate possible contribution to the stream water.
- automatic samplers for water quality need to be installed at different points along the stream so that storm events can be captured without dependence on manual sampling and based on high resolution detailed measurements, to allow nutrient fluxes to be estimated more accurately.
- soil moisture levels should be measured at various locations within the catchment at different soil depths to establish how different topography and soils respond to rainfall.

- other sources of soil organic carbon (SOC) depletion such as microbes, climate change (warming and drying) and erosion should be investigated to get a broader picture of the main drivers of carbon losses.
- the SHETRAN modelling should be improved by automatic calibration. Further modelling of nitrate should include simulation of nitrate leaching to groundwater.
- climate change simulations should be considered for the catchment scale, including also assessment on nitrate and carbon loads in the stream. It would also be interesting to assess the effects of climate change on sediments.
- a comparison of findings could be made for other sites with different soil types (e.g. peat), climate, geology, geometry and vegetation. It is recommended that future research be undertaken at a wider scale using the methodology of this study.

Chapter 13. References

Abbott, M.B., J.C. Bathurst, J.A. Cunge, P.E. O'Connell and J. Rasmussen (1986a). An introduction to the European Hydrological System – Systeme Hydrologique Europeèn, SHE. 1: Hystory and physolophy of a physically-based, distributed modelling system. Journal of hydrology, 87: 45-49.

Abbott, M.B., J.C. Bathurst, J.A. Cunge, P.E. O'Connell and J. Rasmussen (1986b). An introduction to the European Hydrological System – Systeme Hydrologique Europeèn, SHE. 2: Structure of a physically-based, distributed modelling system. Journal of hydrology, 87: 61-67.

Ackers, P., W.R., White, J.A. Perkins and A.J.M. Harrison (1978). Weirs and Flumes for Flow Measurement, Chichester, New York, Brisbane and Toronto: John Wiley and Sons Ltd.

Adams, R., S.M. Dunn, R. Lunn, R. Mackay and J.R. O'Callaghan (1995). Assessing the performance of the NELUP hydrological models for river basin planning. Journal of Environmental Planning and Management, 38(1): 53-76.

Adamson, J.K., W.A. Scott and A.P. Rowland (1998). The dynamics of dissolved nitrogen in a blanket peat dominated catchment. Environmental Pollution 99:69-77.

Addiscott, T.M., A.P. Whitmore and D.S. Pawlson (1991). Farming, Fertilizers and the Nitrate Problem. CAB International, Wallingford: 176.

Adeyemo, O.K., O.A., Adedokun, R.K. Yusuf and E.A. Adeleye (2008). Global NEST Yournal, 10(3): 326-336.

Ågren, M. Haei, S. Köhler, K. Bishop and H. Laudon (2010). Long cold winters give higher stream water dissolved organic carbon (DOC) concentrations during snowmelt. Biogeosciences Discussions, 7: 4857–4886.

Aiken, G. and E. Cotsaris (1995). Soil and hydrology: their effect on NOM. Journal of the American Water Works Association, 87(11): 36-45.

Ajami, N.K., H. Gupta, T. Wagener and S. Sorooshian (2004). Calibration of a semi-distributed hydrologic model streamflow estimation along a river system. Journal of Hydrology, 298: 112-135.

Allan, J.D. (2001). Stream Ecology, structure and function of running waters. Dordrecht: Kluwer academic publishers.

Allen, R.G., M.E. Jensen, J.L. Wright and R.D. Burman (1989). Operational Estimates of Reference Evapotranspiration. Agronomy Journal, 81: 650-662.

Allen, R.G., L.S. Pereira, D. Raes and M. Smith (1998). Crop evapotranspiration. Guidelines for computing crop water requirements. FAO, Irrigation and Drainage Paper, 56.

Allotey, D.F.K., R.D. Asiamah, C.D. Dedzoe and A.L. Nyamekye (2008). Physico-chemical properties of three salt-affected soils in the Lower Volta basin and

management strategies for their sustainable utilization. West African Journal of Applied Ecology, 12.

Amacher, M.C. (1991). Methods of obtaining and analyzing kinetic data. In: Sparks, D.L., Suarez, D.L. (eds.), Rates of Soil Chemical Processes. Soil Science Society of America Journal, Madison, WI, 19–59.

Andersen, H.E., M.L. Pedersen, O. Jorgensen and B. Kronvang (2001a). Analysis of the Hydrology and Flow of Nitrogen in 17 Danish Catchments. Water Science and Technology, 44(7): 63-68.

Andersen, J., J.C. Refsgaard and K.H. Jensen (2001b). Distributed hydrological modelling of the Senegal River Basin-model construction and validation. Journal of Hydrology, 247: 200-214.

Anderson, M.G. and T.P. Burt (1982). The role of throughflow in storm runoff generation: an evaluation of a chemical mixing model. Earth Surface Processes and Landforms, 7: 565–74.

Anyasi, R.O. (2012). Growth of Chromolaena odorata (Siam weed) in two soil samples studied under greenhouse condition. Scholarly Journal of Agricultural Science, 2(10): 253-262.

Aquaflex (2005). Interpreting an AQUAFLEX Soil Moisture Meter Graph.
Available at:
http://www.streatsahead.com/Pages/Aquaflex%20Menu.htmlreat%20Instruments%20%20%20Moisture%20Meter,%20Analyzer%20&%20Moisture%20Control.htm(Accessed : April 2011).

Armstrong, A.C. and T.P. Burt (1993). Nitrate Losses from Agricultural Land, in: Burt, T.P., A.L. Heathwaite and S.T. Trudgill (eds.), Nitrate: Processes, Patterns and Management. John Wiley and Sons Ltd, Chichester, UK, 239-268.

Arnell, N. (2002). Hydrology and Global Environmental Change. Pearson Education Limited, Essex, UK.

Atkinson, T.C. (1978). Techniques for measuring subsurface flow on hillslopes. In: Kirkby, M.J. (eds.), Hillslope Hydrology. John Wiley, Chichester, UK.

Bagayoko, F. (2006). Impact of land-use intensity on evaporation and surface runoff: Processes and parameters for eastern Burklina Faso, West Africa. Ecology and Development Series No. 40.

Barber, N. (2008). The Application of a Farm Integrated Runoff Management (FIRM) Plan to Sykeside Farm, Cumbria: A Scoping Study. School of Civil Engineering and Geosciences. Newcastle University. MSc Thesis.

Barthold, F.K., R.F. Stallard and H. Elsenbeer (2007). Soil nutrient–landscape relationships in a lowland tropical rainforest in Panama, Forest Ecology and Management. Elsevier Science. Article in press.

Bates, B.C, S.P. Charles and J.P Hughes (1998). Stochastic downscaling of numerical climate model simulations. Environ Modelling and Software, 13: 325–31.

Bathurst, J.C. (2001). Experimental design task force: Site selection report for the EA, E. A. (2007). Review of the 2007 summer floods. Environment Agency. Eden/Irthing catchments (unpublished report). Newcastle Upon Tyne, Newcastle University**,** 150.

Bathurst, J.C., J. Ewen, G. Parkin, P.E. O'Connell and J.D. Cooper (2004). Validation of catchment models for predicting land-use and climate change impacts: 3. Blind validation for internal and outlet responses. Journal of Hydrology, 287(1-4): 74-94.

Bathurst, J.C., S.J. Birkinshaw, F. Cisneros, J. Fallas, A. Iroumé, R. Iturraspe, M.G. Novillo, A. Urciuolo, A. Alvarado, C. Coello, A. Huber, M. Miranda, M. Ramirez and R. Sarandón (2011). Forest impact on floods due to extreme rainfall and snowmelt in four Latin American environments 2: Model analysis. Journal of Hydrology, doi:10.1016/j.jhydrol.2010.09.001

Battarbee, R.W., M. Kernan, D.M. Livingstone, U. Nickus, P. Verdonschot, D. Hering, B. Moss, R.F. Wright, C.D. Evans, J.O. Grimalt, R.K. Johnson, E. Maltby, C. Linstead and R.A. Skeffington (2008). Freshwater ecosystem responses to climate change: the Euro-limpacs project, p. 313-354, In P. Quevauviller, et al. (eds.), The Water Framework Directive - Ecological and Chemical Status Monitoring. John Wiley and Sons Ltd, Chichester, UK.

Bekoe, E.O. (2005). Application of a hydrological model in a data-poor tropical West African catchment: a case study of the Densu Basin of Ghana. Institute of Water and Environment. Cranfield University at Silsoe. PhD Thesis.

Bergström, S., B. Carlsson, M. Gardelin, G. Lindström, A. Pettersson and M. Rummukainen (2001). Climate change impacts on runoff in Sweden - assessments by global climate models, dynamical downscaling and hydrological modelling. Climate Research, 16: 101-112.

Bertilsson, S. and J.B. Jones (2003). Supply of dissolved organic matter to aquatic ecosystems: autochthonous sources in Aquatic ecosystems: interactivity of dissolved organic matter. Findlay, S.E.G. and R.L. Sinsabaugh (eds.), Elsevier Science, New York: 26-59.

Betson, R.P. (1964). What is basin runoff? Journal of Geophysical Research, 69: 1541-42.

Beven, K. (1995). Linking parameters across scales: subgrid parameterizations and scale dependent hydrological. Hydrological Processes, 9: 507–25.

Bier, A.F. (2004). Investigating runoff generation processes in a small forested headwater catchment using artificial tracers. The Faculty of Graduate Studies. Geography. The University of British Columbia, Vancouver. MSc thesis.

Birkinshaw, S.J. and J. Ewen (2000a). Nitrogen transformation component for SHETRAN catchment nitrate transport modelling. Journal of Hydrology, 230: 1–17.

Birkinshaw, S.J. and J. Ewen (2000b). Modelling nitrate transport in the Slapton Wood catchment using SHETRAN. Journal of Hydrology, 230: 18–33.

Birkinshaw, S.J., P. James and J. Ewen (2010). Graphical User Interface for Rapid Set-up of SHETRAN Physically-Based River Catchment Model. Environmental Modelling and Software, 25: 609-610.

Bishop, K.H., H. Grip and A. O'Neill (1990).The origins of acid runoff in a hillslope during storm events, Journal of Hydrology, 116, 35–61.

Blöschl, G. and M. Sivapalan (1995).Scale issues in hydrological modeling - a review, Hydrological Processes, 9(3-4): 251-290, 1995.

Blöschl, G. (2001). Scaling in hydrology. Hydrological Processes, 15: 709– 711.

Bohté, R., M.L. Mul, T.A. Bogaard, H.H.G. Savenije, S. Uhlenbrook and T.C. Kessler (2010). Hydrograph separation and scale dependency of natural tracers in a semi-arid catchment. Hydrology and Earth System Sciences Discuss, 7: 1343-1372.

Bonell, M. (1993). Progress in the understanding of runoff generation dynamics in forests, Journal of Hydrology, 150: 217–275.

Bonell, M. (1998). Selected challenges in runoff generation research in forests from the hillslope to headwater drainage basin scale. Journal of the American Water Resources Association, 34: 765-785.

Borken, W. and E. Matzner (2009). Reappraisal of drying and wetting effects on C and N mineralization and fluxes in soils. Global Change Biology, 15:808-824.

Bouraoui, F. L. Galbiati and G. Bidoglio (2002). Climate change impacts on nutrient loads in the Yorkshire Ouse catchment (UK). Hydrology and Earth System Sciences, 6(2): 197–209.

Boyer, E.W., G.M. Hornberger, I.C.E. Bencala and D.M. McKnight (1997). Response characteristics of DOC flushing in an alpine catchment. Hydrological Processes, 11(12): 1635-1647.

Brooks, R.H. and A.T. Corey (1964). Hydraulic properties of porous media. Hydrology Papers 3. Colorado State University, Fort Collins.

Broos, K. and J. Baldock (2008). Building soil carbon for productivity and implications for carbon accounting in 2008. South Australian GRDC Grains Research Update.

Brown, M.E. (1988). Introduction to thermal analysis: Techniques and applications. Chapman and Hall, London.

BSI (1981) Methods of measurement of liquid flow in open channels. Weirs and flumes. Method using thin-plate weirs (BS3680- 4a:1981).

Burke, I.C., C.M. Yonker, W.J. Parton, C.V. Cole, K. Flach and D.S. Schimel (1989). Texture, climate, and cultivation effects on soil organic content in U.S. grassland soils: Soil Science Society of America Journal, 53: 800-5.

Burns, D.A. (2005). What do hydrologists mean when they use the term flushing? Hydrological Processes, 19: 1325–1327.

Burns, D.A., R.P. Hooper, J.J. McDonnell, J. Freer, C. Kendall and K. Beven (1998). Base cation concentrations in subsurface flow from a forested hillslope—the role of flushing frequency. Water Resources Research, 34: 3535–3544.

Burns, D.A. and A.C. Kendall (2002). Analysis of delta N-15 and delta O-18 to differentiate NO_3) sources in runoff at two basins in the Catskill Mountains of New York. Water Resources Res, 38:1051.

Burt, T.P. (1979). The relationship between throughflow generation and the solute concentration of soil and stream water. Earth Surface Processes, 4: 257-266.

Burt, T.P. (1986). Runoff processes and solutional denudation rates on humid temperate hillslopes. In Trudgill, S.T., editor, Solute processes, Chichester: Wiley: 193–249.

Burt, T.P. (1989). Storm runoff generation in small catchments in relation to the flood response of large basins. In Beven K.J. and P.A. Carling (eds.), Floods. Chichester: Wiley: 11–36.

Burt,T.P. (1992). The hydrology of headwater catchments. In Calow, P. and G.E. Petts, (eds.), The Riurs Handbook, 1: 3 -28.

Burt, T.P. and D.P. Butcher (1985). Topographic controls of soil moisture distribution. Journal of Soil Science 36: 469-486.

Burt, T.P., B.P. Arkell, S.T. Trudgill and D.E. Walling (1988). Stream nitrate levels in a small catchment in south west England over a period of 15 years. Hydrological Processes, 2: 267-284.

Burt, T.P., A.L. Heathwaite and S.T. Trudgill (1993). Nitrate: Processes, Patterns and Management. John Wiley and Sons, Inc., New York, Chapters 5 and 10.

Burt, T.P. and G. Pinay (2005). Linking hydrology and biogeochemistry in complex landscapes. Progress in Physical Geography, 29(3): 297–316.

Butcher, A.S., A.R. Lawrence, C. Jackson, J. Cunningham, E. Cullis, K. Hasan and J. Ingram (2003). Investigation of rising nitrate concentrations in groundwater in the Eden valley, Cumbria: Scoping study. Environment Agency R and D Report NC/00/24/14.

Buttle, J.M. (1994). Isotope hydrograph separations and rapid delivery of pre-event water from drainage basins. Progress in Physical Geography, 18: 16–41.

Buttle, J.M., S.W. Lister and A.R. Hill (2001). Controls on runoff components on a forested slope and implications for N transport. Hydrological Processes, 15(6): 1065–1070.

Centre for Ecology and Hydrology, Land Cover Map of Great Britain (1990). Available at: http://www.ceh.ac.uk/LandCoverMap1990.html (Accessed: June 2008).

Cerdan, O., Y. Le Bissonnais, G. Govers, V. Leconte, K. van Oost, A. Couturier, C. King and N. Dubreuil (2004). Scale effects on runoff from experimental plots to catchments in agricultural areas in Normandy. Journal of hydrology, 299: 4–14.

Chan, K.Y. (2001). Soil organic carbon and soil structure: implications for the soil health of agrosystems. In: 'Soil Health. The Foundation of Sustainable Agriculture', Proceeding of a workshop on the importance of soil health in agriculture, Ed R. Lines-Kelly, Wollongbar Agriculture Institute, NSW, pp. 126-133.

Charman, P.E.V. and M.M. Roper (1991). Soil organic matter. In: 'Soils-their properties and Mangement: a Soil Conservation Handbook for New South Wales', (eds.), P.E.V. Charman and B.W. Murphy. Sydney University Press, Australia, pp. 206-214.

Chen, S.P., G.H. Lin, J.H. Huang and G.D. Jenerette (2009). Dependence of carbon sequestration on the differential responses of cosystem photosynthesis and respiration to rain pulses in a semiarid steppe. Glob Change Biology, 15: 2450–2461.

Christ, M. and M.B. David (1996). Dynamics of extractable organic carbon in Spodosoil forest floors. Soil Biology and Biochemistry, 28: 1171-1179.

Cirmo, C. and J.J. McDonnell (1997). Linking the hydrologic and biogeochemical controls of nitrogen transport in near-stream zones of temperate-forested catchments: a review. Journal of Hydrology, 199: 88-120.

Cole, J.J., Y.T. Prairie, N.F. Caraco, W.H. McDowell, L.J. Tranvik, R.G. Striegl, C.M. Duarte, P. Kortelainen, J.A. Downing, J.J. Middelburg and J. Melack (2007). Plumbing the global carbon cycle: Integrating inland waters into the terrestrial carbon budget, Ecosystems, 10: 171-184.

Commins, K.A., M. Alouso, P. Lopez and M. Comelles (1983). Limnology of Ciallocanta Lake, Argon, North Eastern Spain. Hydrobiology, 105: 207-239.

Cory, R.M., S.A. Green and K.S. Pregitzer (2002). Dissolved organic matter concentration and composition in the forests and streams of Olympic National Park, Wa, Biogeochemistry, 67: 269-288.

Cosby, B. J., G.M. Hornberger, J.N. Galloway and R.F. Wright (1985). Modeling the effects of acid deposition: Assessment of a lumped parameter model of soil l water and streamwater chemistry, Water Resources Research, 21: 51-63.

Coulter, B.S. (2001). Editor. Nutrient and Trace Element Advice for Grassland and Tillage Crops. Teagasc, Johnstown Castle Research Centre, Wexford.

Covey, C., K.M. Achuta Rao, U. Cubasch, P. Jones, S.J. Lambert, M.E. Mann, T.J. Phillips and K.E. Taylor (2003). An overview of results from the Coupled Model Intercomparison Project. Global Planet Change, 37: 103-133.

Cowpertwait, P.S.P. (1991). Further developments of the Neyman-Scott clustered point process for modelling rainfall. Water Resources Research, 27: 1431-1438.

Crane, R.G. and B.C. Hewitson (1998). Doubled CO_2 precipitation changes for the Susquehanna Basin: down-scaling from the genesis general circulation model. International Journal of Climatology, 18: 6576.

Creed, I.F, L.E. Band, N.W. Foster, I.K. Morrison, J.A. Nicotson, S. Semkin and D.S., Jeffries (1996). Regulation of nit:rate-N release from temperate forests: a test of the N flushing hypothesis. Water Resources Research, 32(11): 3337-3354.

Creed, I.F. and L.E Band (1998). Export of nitrogen from catchments within a temperate forest: Evidence for a unifying mechanism regulated by variable source area dynamics. Water Resources Research, 34.

Critter, S.A.M. and C. Airoldi (2006). Thermal analysis of brazilian tropical soils originating from different sources. Journal of Brazilian Chemical Society 17(7): 1250-1258.

Cronan, C.S. and G.R. Aiken (1985). Chemistry and transport of soluble humic substances in forested basins of the Adirondack Park, New York, Geochimica et Chosmochimica Acta, 49: 1697-1705.

Crosson, P. (1985). Impact of erosion on land productivity and water quality in the United States: 217–236. In S. El-Swaify et al. (eds.), Soil erosion and conservation. The Soil Conservation Society of America, Ankeny, IA.

CSIRO Huon Estuary Study Team (2000). Huon Estuary Study: Environmental Research for ntegrated Catchment Management and Aquaculture. Project No. 96/284, Final Report to the Fisheries Research and Development Corporation: 285.

Czapar, G.F., J.M. Laflen, G.F. McIsaac and D.P. McKenna (2008). Effects of Erosion Control Practices on Nutrient Loss. in UMRSHNC (Upper Mississippi River Sub-basin Hypoxia Nutrient Committee). 2008. Final Report: Gulf Hypoxia and Local Water Quality Concerns Workshop. American Society of Agricultural and Biological Engineers, 117-127.

Czimczik, C.I., C.M. Preston, M.W. I. Schmidt, R.A. Werner and E.D. Schulze (2002). Effects of charring on mass, organic carbon, and stable carbon isotope composition of wood. Organic Geochemistry, 33: 1207–1223.

Dahlke, H.E., Y.M. Easton, S.W. Lyon, M. T. Walter, G. Destouni and T. Steenhuis (2012). Dissecting the variable source area concept – Subsurface flow pathways and water mixing processes in a hillslope. Journal of Hydrology, 420–421: 125–141.

Dalal, R.C. and R.J. Mayer (1986). Long-term trends in fertility of soils under continuous cultivation and cereal cropping in Southern Queensland. II total organic carbon and its rate of loss from the soil profile. Australian Journal of Soil Research, 24: 281-292.

Dalal, R.C. and K.Y. Chan (2001). Soil organic matter in rainfed cropping systems of Australian cereal belt. Australian Journal of Soil Research, 39: 435-464.

Dalva, M. and T.R. Moore (1991). Sources and sinks of dissolved organic carbon in a forested swamp catchment. Biogeochemistry, 15: 1-19.

Danielson, R.E. and P.L. Sutherland (1986). Porosity. In Methods of Soil Analysis, Part 1. Physical and Mineralogical Analysis. A. Klute (eds.), SSSA, Madison, WI:. 443-461.

Darcy, H. (1856). Les fontaines publiques de la ville de Dijon, Dalont, Paris.

Davies, J.J.L., A. Jenkins, D.T. Monteith, C.D. Evans and D.M. Cooper (2005). Trends in surface water chemistry of acidified UK Freshwaters, 1988-2002. Environmental Pollution 137:27-39.

Dawson, J.J.C., M.F. Billett, C. Neal and S. Hill (2002). A comparison of particulate, dissolved and gaseous carbon in two contrasting upland streams in the UK. Journal of Hydrology, 257: 226-246.

Dawson, J.J.C., C. Soulsby, D. Tetzlaff, M. Hrachowitz, S.M. Dunn and I.A. Malcolm (2008). Influence of hydrology and seasonality on DOC exports from three contrasting upland catchments, Biogeochemistry, 90: 93-113.

Dean, L.A. (1938). The Effect of Rainfall on Carbon and Nitrogen Contents, and Carbon-Nitrogen Ratios of Hawaiian Soils. Soil Science Society of America Journal, 2: 455-459.

DEFRA (2007a). The Government's Strategic Review of diffuse water pollution from agriculture in England. Paper 1: Agriculture and water: a diffuse pollution review. Available at:
http://www.defra.gov.uk/environment/water/quality/diffuse/agri/reports/dwpa01a.htm (Accessed: April 2008).

DEFRA (2007b). Diffuse nitrate pollution from agriculture – strategies for reducing nitrate leaching. Supporting paper D3 for the consultation on implementation of the Nitrates Directive in England. ADAS report.
Available at:
http://archive.defra.gov.uk/environment/quality/water/waterquality/diffuse/nitrate/documents/consultation-supportdocs/d3-inventory-measures.pdf (Accessed: February 2008).

DEFRA (2008). Available at:
http://www.defra.gov.uk/corporate/consult/soilstrategy/index.htm (Accessed: September 2008).

DEFRA (2009). Safeguarding Our Soils: A strategy for England. September 2009. DEFRA, UK (http://www.defra.gov.uk/environment/quality/land/soil/documents/soil-strategy.pdf)

De Laat, P.J.M. (2005). Workshop on Hydrology. Lecture note. UNESCO-IHE, Delft. The Netherlands.

Dell'Abate, M.T., S. Canali, A. Trinchera, A. Benedetti and P. Sequi (2000). Thermal method of organic matter maturation monitoring during composting process. Journal of Thermal Analysis and Calorimetry,. 61: 389-396.

Dell'Abate, M.T., A. Benedetti and P.C. Brookes (2003). Hyphenated techniques of thermal analysis for characterisation of soil humic substances. Journal of Separation Science 26, 433440.

Déqué, M., D.P. Rowell, D. Lüthi, F. Giorgi, J.H. Christensen, B. Rockel, D. Jacob, E. Kjellström, M. de Castro and B. Van den Hurk (2007). An intercomparison of regional climate simulations for Europe: assessing uncertainties in model projections. Clim. Change, 81: 53-70.

De Wit, H.A. and R.F. Wright (2008). Projected stream water fluxes of NO_3 and total organic carbon from the Storgrama headwater catchment, Norway, under climate change and reduced acid deposition. Ambio, 37(1): 56-63.

Di Domenico, A., G. Laguardia and M. Fiorentino (2006). Capturing critical behaviour in soil moisture spatio-temporal dynamics. Advances in Water Resources, 30(3): 543–554.

Dinçer, T. (1968). The use of oxygen-18 and deuterium concentrations in the water balance of lakes. Water Resources Research, 14: 6.

Djorovic, M. (1980). Slope effect on runoff and erosion. In M. De Broodt and D. Gabriels (eds.), Assessment of erosion, Wiley-Interscience, Chichester, 215-225.

Dodge, R. (2001). Water measurement manual: A guide to effective water measurement practices for better water management. United States, Interior Dept., Bureau of Reclamation.

Doležal, F. and T. Kvítek (2004). The role of recharge zones, discharge zones, springs and tile drainage systems in peneplains of Central European highlands with regard to water quality generation processes. Physics and Chemistry of the Earth, 29: 775-785.

Drever, J.I. (1997). The geochemistry of natural waters: 3rd edition Prentice Hall, Upper Saddle River, New Jersey.

Dunne, T. and R.D. Black (1970). An experimental investigation of runoff production in permeable soils. Water Resources Research, 6: 478–90.

Dunne, T. and L. Leopold (1978). Water in Environmental Planning. W.H. Freeman and Co., New York.

Dzamic, R. and D. Stevanovic (2007). Agrochemistry. II edition. Faculty of Agriculture. Partenon, Belgrade (in Serbian).

Edina Digimap. Available at: http://edina.ac.uk/digimap (Accessed: March 2008)

Edwards, W. and L. Owens (1991). Large storm effects on total soil erosion. Journal of Soil Water Conservation, 46:75–78.

Ekström, M., H.J. Fowler, C.G. Kilsby and P.D. Jones (2005). New estimates of future changes in extreme rainfall across the UK using regionalclimate model integrations. 1. Future estimates and use in impactstudies. Journal of Hydrology, 300: 234–251.

Ekström, M. P.D. Jones, H.J. Fowler, G. Lendernik, T.A. Buishand and D. Conway (2007). Regional climate model data used within the SWURVE project. 1: Projected changes in seasonal patterns and estimation of PET. Hydrolology and Earth Systems, 11(3): 1069-1083.

Engelund, F. and E. Hansen (1967). A monograph on sediment transport in alluvial streams. Teknish Forlag, Copenhagen, Denmark.

Engler, A. (1919). Untersuchungen über den Einfluss des Waldes auf den Stand der Gewässer, 12. Kommissionsverlag von Beer and Cie, Zürich, 626 pp. in Wieler et al. 2005.

Enriquez, S., C.M. Duarte and K. Sand-Jensen (1993). Patterns in decomposition rates among photosynthetic organisms: the importance of detritus C:N:P content. Oecologia, 94: 457-471.

Environment Agency (2006). North West General Quality Assessment (GQA) 2006, Available at: http://environment-agency.wales.gov.uk/regions/northwest/346910/347005/440418/445438/?version=1&lang=_e (Accessed: November 2007).

EPA (U.S. Environmental Protection Agency) (2002). Mid-Atlantic Integrated Assessment (MAIA) Estuaries 1997.

EPA (U.S. Environmental Protection Agency) (2012). Nitrates.
Avaliable at:
http://water.epa.gov/type/rsl/monitoring/vms57.cfm (Accessed: May 2012).

Evans, C.D., D.T. Monteith and D.M. Cooper (2005). Long-term increases in surface water dissolved organic carbon: Observations, possible causes and environmental impacts. Environmental Pollution, 137:55-71.

Ewen, J., G. Parkin and P.E. O'Connell (2000). SHETRAN: distributed river basin flow and transport modeling system. Journal of Hydrologic Engineering, 5(3): 250-258.

Ewen, J., J. C. Bathurst, G. Parkin, P.E. O'Connell, S.J. Birkinshaw, R. Adams, R. Hiley, C.G. Kilsby and A. Burton (2002). SHETRAN: Physically-based distributed river basin modelling system. In: Mathematical Models of Small Basin Hydrology and Applications, V.P. Singh and D.K. Frevert (eds.), Water Resources Publications LLC: 43-68.

Famiglietti, J.S., J.W. Rudnicki and M. Rodell (1998). Variability in surface moisture content along a hillslope transect: Rattlesnake Hill, Texas, J. Hydrol., 210: 259 – 281.

FAO (2006). Guidelines for soil description. Fourth edition. Food and agriculture organization of the united nations. Rome, Italy.

Fawcett, R.S. (2005). A Review of BMPs for Managing Crop Nutrients and Conservation Tillage to Improve Water Quality. Edited by Tim Smith (2005). Conservation Technology Information Centre (CTIC), West Lafayette, I N, USA.

Feddes, R.A., P. Kowalik, S.P. Neuman and E. Bresler (1976). Finite difference and finite element simulation of field water uptake by plants. Hydrological Sciences Bulletin, 21: 81–98.

Feng, P. and J. Z. Li (2008). Scale effects on runoff generation in meso-scale and large-scale sub-basins in the Luanhe River Basin. Hydrology and Earth System Sciences Discussions, 5: 1511–1531.

Fierer, N.G. and J.E. Gabet (2002). Carbon and Nitrogen Losses by Surface Runoff following Changes in Vegetation. Journal of Environmental Quality, 31: 1207–1213.

Figueiredo, E.E. and J.C. Bathurst (2007). Runoff and sediment yield predictions in a semiarid region of Brazil using SHETRAN. Prediction in Ungauged Basins: PUB Kick-off. IAHS Publication: 309.

Fisher, R.F. (1995). Soil organic matter: clue and conundrum: In: 'Carbon Forms and functions in Forest Soils'. Soil science Society of America. W.W. McFee and J.M. Kelly (eds.), CRC Inc. Madison, USA, 594: 1-11.

Fitzhugh, R.D., C.T. Driscoll, P.M. Groffman, G.L. Tierney, T.J. Fahey and J.P. Hardy (2001). Effects of soil freezing disturbance on soil solution nitrogen, phosphorus, and carbon chemistry in a northern hardwood ecosystem. Biogeochemistry, 56:215-238.

Flaig, W., H. Beutelspacher and E. Rietz (1975). Soil components. J.E. Gieseking, Springer-Verlag New York.

Floate, C. (2002). Nutrient pollution in rural systems. University of Newcastle Upon Tyne. Unpublished MSc thesis.

Flühler, H. and K. Roth (2004). Physik der Ungesättigten Zone. Skript zur Vorlesung Bodenphysik and der ETH Zürich, Version 2004.1. Zürich, CH.

Folger, D.W. (1972). Characteristics of estuarine sediments of the United States: U.S. Geological Survey Prof. Paper, 742: 94.

Ford, T.E., S.A. Ford, M.A. Lock and R.J. Naiman (1990). Dissolved organic carbon concentrations and fluxes along the Moisie River, Quebec. Freshwater Biology, 24: 35-42.

Fowler, H.J., S. Blenkinsop, A.P. Smith, M. Ekstrom and C.G. Kilsby (2006). BHS, 9th National Hydrology Symposium, Durham, UK.

Fowler, H.J., C. Tebaldi and S. Blenkinsop (2008). Probabilistic estimates of climate change impacts in flows in the River Eden, Cumbria. BHS, 10th National Hydrology Symposium, Exeter, UK.

Foy, R.H. (2005). The Return of the Phosphorus Paradigm: Agricultural Phosphorus and Eutrophication, in: Sims, J. T. and A.N. Sharpley (eds.), Phosphorus: Agriculture and the Environment, American Society of Agronomy, Wisconsin, USA, 911-939.

Fragalà, F.A. (2009). Assessment of local recharge through glacial and alluvial deposits in the Upper Eden valley, UK. School of Civil Engineering and Geosciences. Newcastle University. PhD Thesis.

Frank, K.D. (2006a). Calcium and Magnesium. Part I. Fertility Principles In:."EC06-155 Nutrient Management for Agronomic Crops in Nebraska" Ferguson, R.B. (2006). Historical Materials from University of Nebraska-Lincoln Extension. Paper 1711.

Frank, K.D. (2006b). Potassium. Part I. Fertility Principles In:."EC06-155 Nutrient Management for Agronomic Crops in Nebraska" Ferguson, R.B. (2006). Historical Materials from University of Nebraska-Lincoln Extension. Paper 1711.

Fraser, C.J.D., N.T. Roulet and T.R. Moore (2001). Hydrology and dissolved organic carbon biogeochemistry in an ombrotrophic bog. Hydrological Processes, 15: 3151-3166.

Freeman, C., C.D. Evans, D.T. Monteith, B. Reynolds and N. Fenner (2001a). Export of organic carbon from peat soils. Nature, 412:785.

Freeman, C., N. Ostle and H. Kang (2001b). An enzymic 'latch' on a global carbon store - A shortage of oxygen locks up carbon in peatlands by restraining a single enzyme. Nature, 409:149.

Freeman, C., N. Fenner, N.J. Ostle, H. Kang, D.J. Dowrick, B. Reynolds, M.A. Lock, D. Sleep, S. Hughes and J. Hudson (2004). Export of dissolved organic carbon from peatlands under elevated carbon dioxide levels. Nature, 430:195-198.

Freese, C., S. Lorentz, P. le Roux, J. van Tol and D. Vermeulen (2011). A description and quantification of hillslope hydrological processes in the Necf, Weatherley catchment. 15th SANCIAHS National Hydrology Symposium. Science and practice for sustainable water resources management, Rhodes University, Grahamstown, Greece.

Freeze, R.A. (1972). Role of subsurface flow in generating surface runoff: 2. Upstream source areas. Water Resources Research, 8: 1271-83.

Freeze, R.A. and J.A. Cherry (1979). Groundwater. Prentice-Hall, Inc. Englewood Cliff, New Jersey.

Frei, C., C. Schär, D. Luthi and H.C. Davies (1998). Heavy precipitation processes in a warmer climate. Geophys. Res. Lett., 25: 1431-1434.

Frei, C., R. Schöll, S. Fukutome, J. Schmidli and P.L. Vidale (2006). Future change of precipitation extremes in Europe: An intercompariosn of scenarios from regional climate models. J. Geophys. Res., 111.

French, H.K. and J. Deelstra (2003). Modelling at Jordforsk. Objectives and overview of present and potential models. Jordforsk – Norwegian Institute for Agricultural and Environmental research, pp. 49, Ås, Norway.

Futter, M.N., R.C. Helliwell, M. Hutchins and J. Aherne (2009). Modelling the effects of changing climate and nitrogen deposition on nitrate dynamics in a Scottish mountain catchment. Hydrology Research, 40:153-166.

Gaál, F., I. Szöllősy, M. Arnold and F. Paulik (1994). Determination of the Organic Matter, Metal Carbonate and Mobile Water in Soils. Simultaneous TG, DTG, DTA and EGA Techniques, Journal of Thermal Analysis, 42: 1007-1016.

Gaskin, J. W., J.W. Dowd, W.L. Nutter and W.T. Swank (1989). Vertical and lateral components of soil nutrient flux in a hillslope. Journal of Environmental Quality, 18(4): 403–410.

Gburek, W.J. and A.N. Sharpley (1998). Hydrologic Controls on Phosphorus Loss From Upland Agricultural Basins. Journal of Environmental Quality, 27: 267-277.

Genereux, D.P., M.T. Jordan and D. Carbonell (2005). A paired-watershed budget study to quantify interbasin groundwater flow in a lowland rain forest, Costa Rica. Water Resources Research 41, W04011.

Ghosh, S. and P.P. Mujumdar (2008). Statistical downscaling of GCM simulations to streamflow using relevance vector machine. Advances in Water Resources 31: 132–146.

Gifford, G. and F. Busby (1973). Loss of particulate organic materials from semiarid basins as a result of extreme hydrologic events. Water Resources Research, 9: 1443–1449.

Gottschalk, L. and R. Weingartner (1998). Distribution of peak flow derived from a distribution of rainfall volume and runoff coefficient, and a unit hydrograph, Journal of Hydrology, 208: 148-162.

Gowariker, V., V.N. Krishnamurthy, S. Gowariker, M. Dhanorkar, K. Paranjape and N. Borlaug (2009). The Fertilizer Encyclopedia. Wiley, John and Sons.

Gravier, J. (2004). Soil Erosion Evaluation in the Eden. University of Newcastle upon Tyne. Unpublished MSc Thesis.

Grayson, R.B. and A.W. Western (1998). Towards areal estimation of soil water content from point measurements: time and space stability of mean response. Journal of Hydrology 207: 68–82.

Grebmeir, J.M., C.P. McRoy and H.M. Feder (1988). Pelagic-benthic coupling on the shelf of the northern Bering and Chukchi Seas. I. Food supply source and benthic biomass. Marine Ecology Progress Series, 48: 57-67.

Gremillion, P., A. Gonyeau and M. Wanielista (2000). Application of alternative hydrograph separation models to detect changes in flow paths in a basin undergoing urban development. Hydrological Processes, 14: 1485– 1501.

Grieve, I.C. (1984). Concentrations and annual loading of dissolved organic matter in a small moorland stream. Freshwater Biology, 14: 533-537.

Grieve, I.C. (1994). Dissolved organic carbon dynamics in 2 streams draining forested catchments at Loch Ard, Scotland. Hydrological Processes, 8: 457-464.

Grieve, I.C. and R.L. Marsden (2001). Effects of forest cover and topographic factors on TOC and associated metals at various scales in Western Scotland. Science of the Total Environment, 265: 143-151.

Grimaldi, C., M. Grimaldi, A. Millet, T. Bariac and J. Boulegue (2004). Behaviour of chemical solutes during a storm in a rainforested headwater catchment. Hydrological Processes, 18: 93-106.

Grotch, S. and M. MacCracken (1991) The use of general circulation models to predict regional climate change. Journal of Climate, 4: 284–303.

Gundersen, C.B. (2012). Biodegradation and Characterization of Dissolved Organic Matter (DOM) along the Flowpath of a N-saturated Subtropical Forested Catchment in China. Department of chemistry, University of Oslo. MSc Thesis.

Guo, Y., M. Markusa and M. Demissie (2002). Uncertainty of nitrate-N load computations for agricultural watersheds. Water Resources Research, 38 (10): 1185.

Gustard, A. (1992). Analysis of river regimes. In The Rivers Handbook, Calow, P. and G.E. Petts (eds.), Blackwell Scientific: Oxford, 1: 29-47.

Hafich, K. (2010). Nitrogen Cycling in the Snowmelt Process: Effects on Episodic Acidification of Alpine Streams. EPS 415/Crossey.

Halvorson, A.D., C.A. Reule and R.F. Follett (1999). Nitrogen fertilization effects on soil carbon and nitrogen in a dryland cropping system. Soil Science Society of America Journal, 63, 912–917.

Hargreaves, K.J., R. Milne and G.R. Cannell (2001). UK Emissions by Sources and Removals by Sinks due to Land Use, Land Use Change and Forestry Activities, Chapter 4: Carbon balance of afforested peatland in Scotland. Department of the Environment, Transport and the Regions, Global Atmosphere Division.

Hatch, D., K. Goulding and D. Murphy (2002). Nitrogen, in: Haygarth, P.M. and S.C. Jarvis (eds.), Agriculture, Hydrology and Water Quality. CAB International, Wallingford, UK: 7-27.

Hauck, R.D. (1984). Nitrogen in Crop Production. Madison, Wisconsins: American Society of Agronomy. Crop Science Society of America. Soil Science Society of America.

Havlin, J.L., J.D. Beaton, S.L. Tisdale and W.L. Nelson (1999). Soil fertility and fertilizers. 6th (eds.), Prentice Hall. Upper Saddle River, NJ.

Hawley, M.E., T.J. Jackson and R.H. McCuen (1983). Surface soil moisture variation on small agricultural watersheds. Journal of Hydrology 62: 179-200.

Haygarth, P.M. and S.C. Jarvis (2002). Agriculture, hydrology, and water quality. CABI Publishing. UK.

Haynes, R.J. and R. Naidu (1998). Influence of lime, fertilizer and manure applications on soil organic matter content and soil physical onditions: a review. Nutrient Cycling in Agroecosystems, 51: 123–137.

Heal, K.V., P.E. Kneale and A.T. McDonald (2002). Manganese in runoff from upland catchments: temporal patterns and controls on mobilization. Hydrological Sciences-Journal, 47: 5.

Heathwaite, A.L. (1995). Sources of eutrophication: hydrological pathways of catchment nutrient export. Man's Influence on Freshwater Ecosystems and Water Use (Proceedings of a Boulder Symposium, July 1995). IAHS Publ. no. 230.

Heathwaite, A.L. (2001). Modelling Nutrient Export from Agricultural Land: Approaches, Scales and End-Users. International congress on modelling and simulation, Modsim 2001. The Australian National University, Canberra.

Heathwaite, A.L. (2003). Making process-based knowledge useable at the operational level: a framework for modelling diffuse pollution from agricultural land. Environmental Modelling and Software 18: 753-760.

Heathwaite, A.L., T.P. Burt and S.T. Trudgill (1993). The Nitrate Issue: a Question of Scale, in: Burt, T.P., Heathwaite, A.L. and S.T. Trudgill (eds.), Nitrate: Processes, Patterns and Management. John Wiley and Sons Ltd, Chichester, UK: 3-22.

Henriksen, H., L. Troldborg, P. Nyegaard, T. Sonnenborg, J. Refsgaard and B. Madsen (2003). Methodology for construction, calibration and validation of a national hydrological model for Denmark, Journal of Hydrology, 280: 52-71.

Hewitson, B.C. and R.G. Crane (1992). Large-scale controls on local precipitation in tropical Mexico. Geophys Res Lett, 19(18): 1835–8.

Hewlett, J.D. (1961). Basin management. In Report for 1961 Southeastern Forest Experiment Station, US Forest Service, Asheville, North Carolina: 62–66.

Hewlett, J.D. and A.R. Hibbert (1963). Moisture and energy conditions within a sloping soil mass during drainage. Journal of Geophysical Research, 68: 1081-1087.

Hewlett, J.D. and A.R. Hibbert (1967). Factors affecting the response of small watersheds to precipitation in humid regions. In: Sopper, W.E. and H.W. Lull (eds.), Forest Hydrology. Pergamon Press, Oxford.

Hill, A.R. (1990). Ground water flowpaths in relation to nitrogen chemistry in the near-stream zone. Hydrobiologia, 206: 39-52.

Hill, A.R., W.A. Kemp, J.M. Buttle and D. Goodyear (1999). Nitrogen chemistry of subsurface storm runotf on forested Canadian Shield hillslopes. Water Resources Research, 35(3), 811-821.

Hobson, A.N. (2005). Use of a stochastic weather generator in a basin model for streamflow simulation. Department of Civil, Environmental and Architectural Engineering. University of Colorado. MSc Thesis.

Hodges, S.C. (1995). Soil Fertility Basics, Soil Science Extension North Carolina State University certified Crop Advisor Training, 2-75.

Hofer, M. (2007). Water fluxes along a boreal hillslope in northern Sweden under current and possible future climate conditions. Diploma thesis. Department of Geography, University of Zurich.

Hooper, R.P., N. Christophersen and N.E. Peters (1990). Modelling streamwater chemistry as a mixture of soilwater end-members - An application to the Panola mountain catchment, Georgia, U.S.A., J. Hydrol., 116, 321 – 343.

Hope, D., M.F. Billett and M.S. Cresser (1994). A review of the export of carbon in river water: Fluxes and processes. Environmental Pollution, 84: 301–324.

Hope, D., M.F. Billett, R. Milne and T.A.W. Brown (1997). Exports of organic carbon in British rivers. 217 Hydrological Processes, 11: 325-344.

Hornberger, C.M., K.E. Bencala and D.M. McKnight (1994). Hydrological controls on dissolved organic carbon during snowmelt in the Snake River near Montezuma, Colorado. Biogeochemisrry, 25(3): 147-165.

Horton, R.E. (1933). The role of infiltration in the hydrological cycle. Transactions, American Geophysical Union, 14: 446-60.

Horton, R.E. (1945). Erosional development of streams and their drainage basins: hydrophysical approach to quantitative morphology. Bulletin of the Geological Society of America, 56: 275-370.

Howden, N.J.K. and T.P. Burt (2008). Temporal and spatial analysis of nitrate concentrations from the Frome and Piddle catchments in Dorset (UK) for water years

1978 to 2007: evidence for nitrate breakthrough ? Science of the Total Environment, 407: 507–26.

Howden, N.J.K. and T.P. Burt (2009). Statistical analysis of nitrate concentrations from the Rivers Frome and Piddle (Dorset, UK) for the period 1965–2007. Ecohydrology, 2: 55–65.

Hruška J, P. Kram, W.H. McDowell and F. Oulehle (2009). Increased Dissolved Organic Carbon (DOC) in Central European Streams is Driven by Reductions in Ionic Strength Rather than Climate Change or Decreasing Acidity. Environmental Science and Technology, 43: 4320-4326.

Hugenschmidt, C., J. Ingwersen, W. Sangchan, Y. Sukvanachaikul, S. Uhlenbrook and T. Streck (2010). Hydrochemical analysis of stream water in a tropical, mountainous headwater catchment in northern Thailand. Hydrology and Earth System Sciences Discussions, 7: 2187-2220.

Hughes, J.L., L.A. Eccles and R.L. Malcolm (1974). Dissolved Organic Carbon (DOC), an Index of Organic Contamination in Ground Water Near Barstow, California. Ground Water, 12(5): 283–290.

Hughes, J.P, D.P. Lettenmaier and P. Guttorp (1993). A stochastic approach for assessing the effect of changes in synoptic circulation patterns on Gauge precipitation. Water Resources Research, 29(10): 3303–15.

Hughes, J.P. and P. Guttorp (1994). A class of stochastic models for relating synoptic atmospheric patterns to regional hydrologic phenomena. Resources Research, 30(5): 1535–46.

Hughes, J.P, P. Guttorp, S.P. Charles (1999). A non-homogeneous hidden Markov model for precipitation occurrence. Journal of Applied Statistics, 48(1): 15–30.

Hulme, M., G.J. Jenkins, X. Lu, J.R. Turnpenny, T.D. Mitchell, R.G. Jones, J. Lowe, J.M. Murphy, D. Hassell, P. Boorman, R. McDonald and S. Hill (2002). Climate Change Scenarios for the United Kingdom: The UKCIP02 Scientific Report, Tyndall Centre for Climate Change.

Hupet, F. and M. Vanclooster (2002). Intraseasonal dynamics of soil moisture variability within a small agricultural maize cropped field. Journal of Hydrology, 261: 86–101.

Hursh, C.R. (1936). Storm-water and adsoption. Transactions of the American Geophysical Union, 17: 863-870.

Hursh, C.R. (1944). Subsurface flow. Transactions of the American Geophysical Union, 25: 743-746.

Inamdar, S.P and M.J. Mitchell (2006). Hydrological and topographical controls on storm-event exports of dissolved organic carbon (DOC) and nitrate across catchment scales. Water Resources Research: 42.

IPCC (Intergovernmental Panel on Climate Change) 2001. Climate Change 2001, The Scientific Basis. Cambridge University Press, New York.

Iqbal, M.T. (2006). Study on Vertical and Lateral Leaching of Nitrate from a Wheat Field in China. Turk J Agric For 30.

Jansson, M., L. Persson, A.M. De Roos, R.I. Jones and L.J. Tranvik (2007). Terrestrial carbon and intraspecific size-variation shape lake ecosystems. Trends in Ecology and Evolution, 22: 316–322.

Jardine, P.M., N.L. Weber and J.F. Mccarthy (1989). Mechanisms of dissolved organic carbon adsorption on soil. Soil Science Society of America Journal, 53: 1378-1385.

Jenkins, G.J. and J. Lowe (2003). Handling uncertainties in the UKCIP02 scenarios of climate change. Hadley Centre technical note, 44.

Jenkins, G.J., M.C. Perry and M.J. Prior (2008). The climate of the United Kingdom and recent trends. Met Office Hadley Centre, Exter, UK.

Jenkinson, D.S. (1991). The Rothamsted long-term experiments: are they still of use? Journal of Agronomy, 83: 2.

Jobbagỳ, E.G. and R.B. Jackson (2000). The vertical distribution of soil organic carbon and its relation to climate and vegetation. Ecological Applications, 10: 423-436.

Johnes, P.J. and T.P. Burt (1993) Nitrate in Surface Waters. In T. P. Burt, A. L. Heathwaite and S. T. Trudgill (eds.), Nitrate: Processes, Patterns and Controls, Wiley: 269-317.

Johnson, D.W, W. Cheng and I.C. Burke (2000). Biotic and abiotic nitrogen retention in a variety of forest soils. Soil Science Society of America Journal, 64: 1503–1514.

Jones, J.A.A., J.M. Richardson and H.J. Jacob (1997). Factors controlling the distribution of piping in Britain: a reconnaissance. Geomorphology, 20: 289–306.

Jones, A.L. and P.L. Smart (2005). Spatial and temporal changes in the structure of groundwater nitrate concentration time series (1935–1999) as demonstrated by autogressive modelling. J Hydrol., 310: 201–15.

Jones, P.D, J.M. Murphy and M. Noguer (1995). Simulation of climate change over europe using a nested regional-climate model, I: assessment of control climate, including sensitivity to location of lateral boundaries. Q.J.R. Meteorological Society, 121: 1413–49.

Jones, P.D., C.G. Kilsby, C. Harpham, V. Glenis and A. Burton (2009). UK Climate Projections science report: Projections of future daily climate for the UK from the Weather Generator. University of Newcastle, UK. ISBN 978-1-906360-06-1.

Judd, K. E, L.E. Gene and P. M. Groffman (2007). High nitrate retention during winter in soils of the Hubbard Brook Experimental forest. Ecosystems. DOI: 10.1007/s10021-007-9027.

Kaipainen, H., Ä. Bilaletdin, T. Frisk and A. Paananen (2008). The Impact of Climate Change on Nutrient Flows In the Catchment of River Kokemäenjoki. BALWOIS 2008 – Ohrid, Republic of Macedonia.

Kalbitz, K., S. Solinger, J. H. Park, B. Michalzik and E. Matzner (2000). Controls on the dynamics of dissolved organic matter in soils: a review. Soil Science, 165: 277-304.

Kaloustian, J., A.M. Pauli and J. Pastor (2001). Kinetic study of the thermal decompositions of biopolymers extracted from various plants. Journal of Thermal Analysis and Calorimetry, 63: 7–20.

Kaplan, L.A. and J.D. Newbold (1993). Biogeochemistry of dissolved organic carbon entering streams. In: Ford, T.E. (eds.), Aquatic Microbiology: An Ecological Approach. Blackwell Science, Malden, MA, 139–165.

Katsuyama, M. and N. Ohte (2005). Effects of bedrock permeability on hillslope and riparian groundwater dynamics in a weathered granite catchment. Water resources research, 41.

Kazmierczak, A. and J.Carter (2010). Adaptation to climate change using green and blue infrastructure: A database of case studies. Report.

Kelling, K.A. and E.E. Schulte (1992). Soil and applied calcium. University of Wisconsin-Extension, 2523: 1-2.

Kendall, C. and J.J. McDonnell (1998). (eds.), Isotope Tracers in Catchment Hydrology. Elsevier Science B.V., Amsterdam: 839.

Kerven, G.L., N. W Menzies and M.D. Geyer (2000). Soil carbon determination by high temperature combustion. A comparison with dichromate oxidation procedures and the influence of charcoal and carbonate on the measured value. Communications in Soil Science and Plant Analysis, 31: 1935-1939.

Kienzler, P.M. and F. Naef (2007). Subsurface storm flow formation at different hillslopes and implications for the "old water paradox". Hydrological Processes, in press.

Kienzler, P.M. and F. Naef (2008). Temporal variability of subsurface stormflow formation. Hydrology and Earth System Sciences, 12: 257–265.

Kilsby, C.G., P.D. Jones and A. Burton, A.C. Ford, H.J. Fowler, C. Harpham, P. James, A. Smith and R.L. Wilby (2007). A daily weather generator for use in climate change studies. Enviromental modelling and software, 22: 1705-1719.

Kirchner, J.W. (2003). A double paradox in catchment hydrology and geochemistry. Hydrological processes, 17: 871–874.

Kirkby, M.J. and R.J. Chorley (1967). Throughflow, overland flow, and erosion. Int. Assoc. Hydrological Sciences Bulletin 12(3): 5–21.

Kirkby, M.J. (1978). Editor. Hillslope Hydrology. John Wiley and Sons, Chicester.

Kirkby, M.J. (1988). Hillslope runoff processes and models. Journal of Hydrology, 100 (1-3): 315-339.

Kirschbaum, M.U.F. (1999). Will changes in soil organic carbon act as a positive or negative feedback on global warming? Biogeochemistry, 48: 21-51.

Kleinman, P.J. A., M.S. Srinivasan, C.J. Dell, J.P. Schimidt, A.N. Sharpley and R.B. Bryant (2006). Role of rainfall intensity and hydrology in nutrient transport via surface runoff. Journal of Environmental Quality, 35: 1248-1259.

Klemes, V. (1986). Operational testing of hydrological simulation models. Hydrol. Sci. J., 31(1): 13-24.

Köhler, S.J., I. Buffam, H. Laudon and K. Bishop (2008). Climate's control of intra-annual and inter-annual variability oftotal organic carbon concentration and flux in two contrasting boreal landscape elements. Journal of Geophysical Research, 113, G03012, doi:10.1029/2007JG000629.

Köhler, S.J., I. Buffam, J. Seibert, K.H. Bishop and H. Laudon (2009). Dynamics of stream water TOC concentrations in a boreal headwater catchment: Controlling factors and implications for climate scenarios. Journal of Hydrology, 373: 44–56.

Kuhn, M. (2001). The nutrient cycle through snow and ice, a review. Aquatic Sciences 63: 150-167.

Land Inforamtion Systems (LandlS). Available at: http://www.landis.org.uk/data/nmtopsoiltexture.cfm (Accessed: April 2013).

Langlois, J. L. and G.R.Mehuys (2003). Intra-Storm Study of Solute Chemical Composition of Overland Flow Water in Two Agricultural Fields. Journal of Environmental Quality, 32(6): 2301-2310.

Leinweber, P., H.R. Schulter and C. Horte (1992). Differential thermal analysis, thermogravimetry and pyrolysis-field ionisation mass spectrometry of soil organic matter in particlesize fractions and bulk soil samples. Thermochimica Acta, 194: 175–187.

Lepori, F., A. Barbieri and S.J. Ormerod (2003). Causes of episodic acidification in alpine streams. Freshwater Biology, 48: 175-189.

Le Roux, X., T. Bariac and A. Mariotti (1995). Spatial partitioning of the soil water resource between grass and shrub components in a West African humid savanna. Oecologia, 104: 147-155.

Lesack, L.F.W. (1993). Water Balance and Hydrologic Characteristics of a Rain Forest Catchment in the Central Amazon Basin. Water Resources Research, 29 (3): 759-773.

Liden, R. and J. Harlin (2001). Analysis of conceptual rainfall-runoff modelling performance in different climates. Journal of Hydrology, 238: 231-247.

Liddicoat, C., A. Schapel, D. Davenport and E. Dwyer (2010). Soil Carbon and climate change. PIRSA Discussion Paper, June 2010.

Liu, G. and J.H. Zhang (2007). Spatial and temporal dynamics of soil moisture after rainfall events along a slope in Regosols of southwest China. Hydrological processes, 21(20): 2778-2784.

Longobardi, A., P. Villani, R.B. Grayson and A.W. Western (2003). On the relationship between runoff coefficient and catchment initial conditions. Proc., MODSIM 2003

International Congress on Modelling and Simulation, Modelling and Simulation Society of Australia and New Zealand Inc., Townsville, Australia, 2: 867-872.

Lopez-Capel, E., S. Sohi, J.L. Gaunt and D.A.C. Manning (2005). Use of thermogravimetry–differential scanning calorimetry to characterize modelable soil organic matter fractions. American Journal of Soil Science Society, 69: 136–140.

Lopez-Capel, E., J.M.R.Arranz, F.J. G. Vila, J.A G. Perez and D.A.C. Manning (2006). Elucidation of different forms of organic carbon in marine sediments from the Atlantic coast of Spain using thermal analysis coupled to isotope ratio and quadrupole mass spectrometry. Organic Geochemistry, 37: 1983–1994.

Lowrance, R. and R. Williams (1988). Carbon movement in runoff and erosion under simulated rainfall conditions. Soil Science Society of America Journal, 52: 1445–144.

Lucas, R.E. and J.F. Davis (1961). Relationships between pH values of organic soils and availabilities of 12 plant nutrients. Soil Science, 92: 171–182.

Lundmark, A. (2005). Modelling the impacts of deicing salt on soil water in a roadside environment. KTH, Land and water Resources Enginner, Stockholm.

Lundquist, E.J., L.E. Jackson and K.M. Scow (1999). Wet-dry cycles affect dissolved organic carbon in two California agricultural soils. Soil Biology and Biochemistry, 31:1031-1038.

Lü, F.M., X. T. Lu, W. Liu, X. Han, G.M. Zhang, D.L. Kong and X.G. Han (2011). Carbon and nitrogen storage in plant and soil as related to nitrogen and water amendment in a temperate steppe of northern China. Biology and Fertility of Soils, 47: 187-196.

The Macaulay Institute, Hydrology of Soil Types (HOST). Available at: http://www.mluri.sari.ac.uk/host/index.html. (Accessed: December 2009).

Madsen, H. (2000). Automatic calibration of conceptual rainfall–runoff model using multiple objectives. Journal of Hydrology, 235: 276–288.

MAFF (1986). The analysis of agricultural materials. Reference Book 427. 3rd edition. HMSO. 248pp.

Malavolta, E. (1985). Potassium status of tropical and subtropical region soils. In'Potassium in Agriculture'. (Ed. RD Munson): 163-200. ASA and SSSA, Madison, WI USA.

Malcom, R.L. and J.A. Leenheer (1973). The usefulness of organic carbon parameters in water quality investigations. Institute of Environmental Sciences: 336-340.

Mannix, A. (2005). The source and fate of nitrates in the Upper Eden Catchment. University of Newcastle Upon Tyne. Unpublished MSc thesis.

Mapa, R.B. and H.P.M. Gunasena (1995). Effect of alley cropping on soil aggregate stability of a tropical Alfisol. Agrofor. Syst. 32, 237–245.

Martinez, C., G.R. Hancock, J.D. Kalma and T. Wells (2008). Spatio-temporal distribution of near-surface and root zone soil moisture at the catchment scale. Hydrological Processes, 22: 2699– 2714.

Mash, H., P.K. Westerhoff, L.A. Baker, R.A. Nieman and M. Nguyen (2004). Dissolved organic matter in Arizona reservoirs: assessment of carbonaceous sources, Organic Geochemistry, 35: 831-843.

Matzner, E. and W. Borken (2008). Do freeze-thaw events enhance C and N losses from soils of different ecosystems? A review. European Journal of Soil Science, 59:274-284.

Mayes, W.M., C.L. Walsh, J.C. Bathurst, C.G. Kilsby, P.F. Quinn, M. Wilkinson, E., A.J. Daugherty and P.E. O'Connell (2006). Monitoring a flood event in a densely instrumented catchment, the Upper Eden, Cumbria, UK, Water and Environment Journal, 20: 217–226.

McAfee, J. (2008). Potassium, A Key Nutrient for Plant Growth. Department of Soil and Crop Sciences:
http://jimmcafee.tamu.edu/files/potassium%20a%20key%20nutrient%20for%20plant%20growth.pdf

McDonnell, J.J. (1990). A rationale for old water discharge through macropores in a steep, humid catchment. Water Resour. Res., 26 (11): 2821–2832.

McDonnell, J.J. (2003). Where does water go when it rains? Moving beyond the variable source area concept of rainfall-runoff response. Hydrological Processes, 17: 1869-1875.

McDowell, W.H. (1998). Internal nutrient fluxes in a Puerto Rican rain forest. Journal of Tropical Ecology, 14: 521-536.

McDowell, W.H. and G.E. Likens (1988). Origin, composition, and flux of dissolved organic carbon in the Hubbard Brook Valley. Ecological Monographs, 58: 177-195.

McGlynn, B.L. and J.J. McDonnell (2003). Role of discrete landscape units in controlling catchment dissolved organic carbon dynamics. Water Resources Research, 39(4): 1090.

McGlynn, B.L., J.J. McDonnell, M. Stewart and J. Seibert (2003). On the relationships between catchment scale and streamwater mean residence time. Hydrological Processes, 17: 175–181.

McGlynn, B.L., J.J. McDonnell, J. Seibert and C. Kendall (2004). Scale effects on headwater catchment runoff timing, flow sources, and groundwater-streamflow relations. Water Resources Research. doi:10.1029/2003WR002494.

McGuire, K.J., J.J. McDonnell, M. Weiler, C. Kendall, B.L. McGlynn, J.M. Welker and J. Seibert (2005) The role of topography on catchment-scale water residence time. Water Resources Research, 41:W05002.

McHale, M.R, J.J. McDonnell, M.J. Mitchell and C.P. Cirmo (2002). A field-based study of soil water and groundwater nitrate release in an Adirondack forested basin. Water Resources Research, 38(4): 1031.

McKnight, D.M., G.M. Hornberger, K.E. Bencala and E.W. Boyer (2002). In-stream sorption offulvic acid in an acidic stream: a stream-scale transport experiment. Water Resources Research, 38(1).

Mehrotra, R. and A. Sharma (2005). A nonparametric nonhomogeneous hidden Markov model for downscaling of multi-site daily rainfall occurrences. Journal of Geophysical Research - Atmos, 110(D16): 16108.

Mengel, K. and E.A. Kirkby (1987). Principles of Plant Nutrition. 4th Ed.International Potash Institute, Basel, Switzerland.

Messer, T. (1980). Soil erosion measurements on experimental plots in Alsace vineyards (France). In M. De Broodt and D. Gabriels (eds.), Assessment of erosion, Wiley-Interscience, Chichester, 455-462.

Met Office (Meteorological Office) (2012). UK actual and anomaly maps. Available at: http://www.metoffice.gov.uk/climate/uk/summaries/anomacts (Accessed: September 2012).

Meybeck, M. (1982). Carbon, nitrogen and phosphorus transport by World Rivers, American Journal of Science, 282: 401–450.

Michaelides, K., D. Lister, J. Wainwright and A.J. Parsons (2009). Vegetation controls on small-scale runoff and erosion dynamics in a degrading dryland environment, Hydrological Processes, 23: 1617-1630.

Michener, R. and K. Lajtha (2008). Stable Isotopes in Ecology and Environmental Science. 2nd Edition, John Wiley and Sons.

Miyazawa, M., M.A. Pavan, E.L. Oliveira, M. Ionashiro and A.K. Silva (2000). Gravimetric determination of soil organic matter. Brazilian Archives of Biology and Technology, 43: 475.

Monaghan, R.M., R.J. Paton, L.C. Smith and C. Binet (2000). Nutrient loss in drainage and surface runoff from a cattle-grazed pasture in Southland. Proceedings of the New Zeeland Grassland association, 62: 99-104.

Monteith, D.T., C.D. Evans and B. Reynolds (2000). Are temporal variations in the nitrate content of UK upland freshwaters linked to the North Atlantic Oscillation? Hydrological Processes, 14:1745-1749.

Monteith, D.T., J.L. Stoddard, C.D. Evans, H.A. de Wit, M. Forsius, T. Høgåsen, A. Wilander, B.L. Skjelkvåle, D.S. Jeffries, J. Vuorenmaa, B. Keller, J. Kopácek and J. Vesely (2007). Dissolved organic carbon trends resulting from changes in atmospheric deposition chemistry. Nature, 450: 537-541.

Moore, T.R. and R.J. Jackson (1989). Dynamics of dissolved organic-carbon in forested and disturbed catchments, Westland, New Zealand .2. Larry River. Water Resources Research, 25: 1331-1339.

Morris, D., H. Zagarese, C.E. Williamson, E.G. Balseiro, B.R. Hargreaves, B. Modenutti, R. Moeller, C. Queimalinos (1995). The attenuation of solar UV radiation in lakes and the role of dissolved organic carbon. Limnology and Oceanography 40(8): 1381–1391.

Mulder, J. and M.S. Cresser (1994). Soil and Soil Solution Chemistry. Biogeochemistry of Small Catchments: A Tool for Environmental Research. Edited by B. Moldan and J.Cerny. John Wiley and Sons Ltd.

Mulholland, P.J., G.V. Wilson and P.M. Jardine (1990). Hydrogeochemical response of a forested watershed to storms: effects of preferential flow along shallow and deep pathways. Water Resources Research, 26: 3021-3036.

Mulla, D. J., P. H. Gowda, A. S. Birr and B. J. Dalzell (2003). Estimating nitrate-N losses at different scales in agricultural watersheds. Ch. 17, In: Y. Pachepsky, D. Radcliffe, and M. Selim, (eds.), Scaling Methods in Soil Physics. CRC Press. Boca Raton, FL.

Murphy, J.M. (1999). An evaluation of statistical and dynamical techniques for downscaling local climate. Journal of Climate, 12: 2256–84.

Mutscher, H. (1995). Measurement and Assessment of Soil Potassium. IPI Research Topics 4. International Potash Institute, Basel, Switzerland.

Naden, P.S. and A.T. McDonald (1989). Statical modelling of water colour in the uplands: The Upper Nidd catchment. Environmental Pollution, 60: 141-163.

Nakicenovic, N., J. Alcamo, G. Davis, B. de Vries, J. Fenhann, S. Gaffin, K. Gregory, A. Grübler, T.Y. Jung, T. Kram, E.L. La Rovere,L. Michaelis, S. Mori, T. Morita, W. Pepper, H. Pitcher, L. Price, K. Riahi, A. Roehrl, H.H. Rogner, A. Sankovski, M. Schlesinger, P. Shukla, S. Smith, R. Swart, S. van Rooijen, N. Victor and Z. Dadi (2000). IPCC Special Report on Emissions Scenarios. Cambridge University Press, Cambridge, United Kingdom and New York, NY, USA. 599pp.

Nash, J.E. and J.V. Sutcliffe (1970). River flow forecasting through conceptual models 1. A discussion of principles. Journal of Hydrology, 10: 182-190.

Nash, D., D. Halliwell and J. Cox (2002). Hydrological mobilization of pollutants at field/slope scale: 225–242. In P.M. Haygarth and S.C. Jarvis (eds.), Agriculture, hydrology, and water quality, CABI Publ., Wallingford, UK.

Nasr, A. (2004). Modelling of phosphorus loss from land to water: a comparison of SWAT, HSPF and SHETRAN/GOPC for three irish catchments. Thesis submitted to the Department of Civil Engineering. Univesity College Dublin for the degree of PhD.

Neal, C. and P.T.W. Rosier (1990). Chemical studies of chloride and stable oxygen isotopes in 2 conifer afforested and moorland sites in british uplands. Journal of Hydrology, 115: 269–283.

Neal, C., J. Wilkinson, M. Neal, M. Harrow, H. Wickham, L.Hill and C. Morfitt (1997). The hydrochemistry of the headwaters of the River Severn, Plynlimon. Hydrology and Earth System Sciences, 1: 583-617.

Neale, B.D. (2006). Effects of Fertilizer Application and Cutting Interval on Nitrate Accumulation in Bermudagrass. Thesis submitted to the Department of Agriculture, University of Tennessee at Martin for the degree of MSc in Agricultural Operations.

Nilsson, M., J. Sagerfors, I. Buffam, H. Laudon, T. Eriksson, A. Grelle, L. Klemedtsson, P. Weslien and A. Linderoth (2008).Complete carbon budgets for two years of a boreal oligotrophic minerogenic mire. Global Change Biology, 14: 1-16.

Niu S.L, H.Y. Yang, Z. Zhang, M.Y. Wu, Q. Lu, L.H. Li, X.G. Han and S.Q. Wan (2009). Non-additive effects of water and nitrogen ddition on ecosystem carbon exchange in a temperate steppe. Ecosystems, 12: 915–926.

Norrström, A.C. (1995) Concentration and chemical species of iron in soils from groundwater/surface water ecotones. Hydrological Sciences Journal, 40(3): 319–329.

Ocampo, C.J., C.E. Oldham, M. Sivapalan and J.V. Turner (2006). Hydrological versus biogeochemical controls on catchment nitrate export: a test of the flushing mechanism. Hydrological Processes, 20 (20): 4269-4286.

Occhi, M. (2009). Sources of Stream Discharge in the North East and North West Branches of the Anacostia Watershed: Unpublished manuscript.

Ockenden, M.C. (2010). Identification of catchment runoff processes as a basin for defining water quality protection zones. Lancaster University. PhD thesis.

Odoux, C.G., P. Aurousseau, P. Durand, L. Ruiz and J. Molenat (2010). The role of climate on inter-annual variation in stream nitrate fluxes and concentrations. Science of the Total Environment, 408: 5657–5666.

Ogunkoya, O.O. and A. Jenkins (1991). Analysis of runoff pathways and flow contributions using deuterium and stream chemistry, Hydrological Processes, 5: 271-282.

Ogunkoya, O.O. and A. Jenkins (1993). Analysis of storm hydrograph and flow pathways using a three-component hydrograph separation model, Journal of Hydrology, 142: 71-88.

Olsen, L. (2003). Selected Applications of Hydrologic Science and Research in aryland, Delaware, and Washington, D.C., 2001-2003. USGS Fact Sheet FS-126-03.

O'Reilly, A.M., N.B. Chang, M.P. Wanielista and Z. Xuan (2010). Identifying biogeochemical processes beneath stormwater infiltration ponds in support of a new best management practice for groundwater protection. GQ10: Groundwater Quality Management in a Rapidly Changing World (Proc. 7th International Groundwater Quality Conference held in Zurich, Switzerland).

O'Riley, J.L. (2012). Dissolved Organic Carbon Dynamics During the Snowmelt Period in a Small Urban Watershed. Graduate Masters Theses. Paper 120.

Pardo, L.H, C. Kendall, J. Pett-Ridge and C.C.Y. Chang (2004). Evaluating the source of streamwater nitrate using delta N-15 and delta O-18 in nitrate in two basins in New Hampshire, USA. Hydrological Processes, 18: 2699–712.

Park, J., J. Lee, S. Kang and S. Kim (2007). Hydroclimatic controls on dissolved organic matter (DaM) characteristics and implications for trace metal transport in Hwangryong River Basin, Korea, during a summer monsoon period. Hydrological Processes, 21: 3025-3034.

Parkin, G., G. O'Donnell, J. Ewen, J.C. Bathurst, P.E. O'Connell and J. Lavabre (1996). Validation of catchment models for predicting land-use and climate change impacts. 2. Case study for a Mediterranean catchment. Journal of Hydrology, 175: 595-613.

Parkin, G. (2000). Catchment Hydrology and Sustainable Management (CHASM), The Eden Catchment. I. report, Newcastle University.

Parry, M. and T. Carter (1998). Climate Impact and Adaptation Assessment. Earthscan Publications Ltd., London, UK.

Paul, E.A. and F.E. Clarke (1989). Soil microbiology and biochemistry. Academic Press, Inc., San Diego, California.

Peters, D.L., J.M. Buttle, C.H. Taylor and B.D. Zazerte (1995). Runoff production in a forested shallow soil. Canadian Shield basin. Wat. Resour. Res., 31: 1291-1304.

Peuravuori, J. and H. Pihlaja (1989). Isolation and fractionation of humic substances in lake waters, in Humic substances in the aquatic and terrestrial environment, 33, B. Allard, H. Borén and A. Grimvall, (eds.), Springer-Velag, Linköping: 9-36.

Peverill, K.I., L.A. Sparrow and D.J. Reuter (1999). Soil Analysis: An Interpretation Manual. CSIRO PUBLISHING, Australia.

Piatek, K.B, M.J. Mitchell, S.R. Silva and C. Kendall (2005). Sources of nitrate in snowmelt discharge: Evidence from water chemistry and stable isotopes of nitrate. Water, Air, and Soil Pollution, 165: 13–35.

Pimentel, D. and N. Kounang (1998). Ecology of soil erosion in ecosysotems. Ecosystems, 1: 416–426.

Pinder, F.G. and J.F. Jones (1969). Determination of the groundwater component of peak discharge from the chemistry of total runoff. Water Resources Research, 5(2): 438-445.

Plante, A.F., C. Chenu, M. Balabane, A. Mariotti and D. Righi (2004). Peroxide oxidation of clay-associated organic matter in a cultivation chronosequence. European Journal of Soil Science, 55: 471–478.

Poor, C.J. and J.J. McDonnell (2007). The effect of land use on stream nitrate dynamics. Journal of Hydrology, 332: 54–68.

Post, W.M., W.R. Emanuel, P.J. Zinke and A.G. Stangenberger (1982). Soil carbon pools and World Life Zones. Nature, 298: 156-159.

Puckett, L.J., T.K. Cowdery, P.B. McMahon, L.H. Tornes and J.D. Stoner (2002). Using chemical, hydrologic and age dating analysis to delineate redox processes and flow paths in the riparian zone of a glacial outwash aquifer-stream system. Water Resources Research, 38(8).

Qualls, R.G. and B.L. Haines (1992). Biodegradability of dissolved organic matter in forest throughfall, soil solution, and stream water. Soil Science Society of America Journal, 56: 578-586.

Qui, Y., B. Fu, J. Wang and L. Chen (2001). Soil moisture variation in relation to topography and land use in a hillslope catchment of the Loess Plateau, China. Journal of Hydrolology, 240: 243–63.

Quinn, P. (2002). Models and monitoring: scaling-up cause-and-effect relationships in nutrient pollution to the catchment scale. In 'Agricultural effects on ground and surface waters: research at the edge of science and society. Proceedings of an international symposium, Wageningen, Netherlands, October 2000'. Wallingford UK. (eds.) Steenvoorden, J., Claessen, F. and Willems, J.) pp. 397-403. (IAHS Press) Radke, L.C. (2002). Catchment clearing impacts on estuaries. AUSGEO News, 65: 6-7.

Rawitz E., E.T. Engman and G.D. Cline (1970). Use of mass balance method for examining the role of soils in controlling basin performance. Water Resources Research, 6: 1115– 1123.

Rawls, W.J, D.L. Brakensiek and K.E. Saxton (1982). Estimation of soil Water Properties. Trans. ASAE, 25: 1316-1320.

Rawls, W.J., Y.A. Pachepsky, J.C. Ritchie, T.M. Sobecki and H. Bloodworth (2003). Effect of soil organic carbon on soil water retention. Geoderma 116, 61–76.

Rayment, G.E. and Higginson, F.R. (1992). Australian Laboratory Handbook of Soil and Water Chemical Methods. Inkata Press, Melbourne.

Reaney, S.M. and H.J. Fowler (2008). Uncertainty estimation of climate change impacts on river flow incorporating stochastic downscaling and hydrological model parameterisation error sources. Proceedings of the British Hydrological Society 10th National Hydrology Symposium. Exeter, 15-17th September 2008.

Reid, K. (2006). Soil Sampling and Analysis for Managing Crop Nutrients. Factsheet. Ministry of agriculture, food and rural affairs, Ontario.

Richards, L.A. (1931). Capillary conduction of liquids through porous mediums, Physics, 1: 318-333.

Richardson, C.W. (1981). Stochastic simulation of daily precipitation, temperature, and solar radiation. Water Resources Research, 17: 182-190.

Ritter, W.F. and L. Bergstrom (2001). Nitrogen and water quality. p. 59-90. In W.F. Ritter and A. Shirmohammadi (eds.), Agricultural Nonpoint Source Pollution: Watershed Management and Hydrology. Lewis Publishers, Boca Raton, FL.

Rivera-Monroy, V.H. and R.R. Twilley (1996). The relative role of denitrification and immobilisation in the fate of inorganic nitrogen in mangrove sediments (Terminos Lagoon, Mexico). Limnology and Oceanography, 41: 284-296.

Robson, A.R., K. Beven and C. Neal (1992). Towards identifying sources of subsurface flow: a comparison of components identified by physically based runoff model and those determined by chemical mixing techniques. Hydrological Processes, 6: 199-214.

Rowell, D.L. (1994). Soil science. Methods and applications. Longman Scientific and Techical, Harlow, Essex, UK.

Rudolph, D.L., B.Jr.Conant, L.E. Bekeris, J. Cole, S.K. Frey, J.T. Koch and M.R. Sousa (2010). Monitoring of Selected Hog Farms to Assess the Impacts of Implemented BMPs Resulting From the Nutrient Management Act. A Research Project Conducted for: Ontario Pork. Department of Earth and Environmental Sciences University of Waterloo Waterloo, Ontario.

Russell, J.C. and W.G. McRuer (1927). The relation of organic matter and nitrogen content to series and type in Virgin Grassland soils. Soil Science, 24: 421-452.

Ruszkowska M., M. Warchoowa, Z. Rebowska, S. Sykut and M. Kusio (1988). Nutrient balance in a lysimeter experiment (1981-1985). II. Balance of calcium, magnesium and sulphur. Pamietnik Puawski, 91: 235-250.

Rutter, A.J., K.A., Kershaw, P. C. Robins and A. J. Morton (1971/1972). A predictive model of rainfall interception in forest I. Derivation of the model from observations in a plantation of Corsican Pine. Agricultural and Forest Meteorology: 9: 367-384.

Rutter, A.J., A.J. Morton and P.C. Robins (1975). A predictive of rainfall interception in forest II. Generalization of the Model and Comparison with Observation in some Coniferous and Hardwood Stands. Journal of Applied Ecology, 12: 367-380.

Sadusky, M.C., D.L.Sparks, M.R. Noll and G.J. Hendricks (1987). Kinetics and mechanisms of potassium release from sandy soils. Soil Science Society of America Journal, 51: 1460-1465.

Santhi, C., J.G. Arnold, J.R. Williams, W.A. Dugas, R. Srinivasan and L.M. Hauck (2001). Validation of the SWAT model on a large river basin with point and nonpoint sources. Journal of American Water Resourources Association, 37(5): 1169-1188.

Scherrer, S. and F. Naef (2003). A decision scheme to identify dominant flow processes at the plotscale for the evaluation of contributing areas at the catchments-scale. Hydrological Processes, 17(2): 391–401.

Schimel, J., T.C. Balser and M. Wallenstein (2007). Microbial stress-response physiology and its implications for ecosystem function. Ecology, 88:1386-1394.

Schjonning, P., B.T. Christensen and B. Carstensen (1994). Physical and chemical-properties of a sandy loam receiving animal manure, mineral fertilizer or no fertilizer for 90 years. European Journal of Soil Science, 45, 257–268.

Schroth, G. and F.L. Sinclair (2003). Trees, Crops and Soil Fertility. Concepts and research methods. CABI Publishing.

Schulten, H.R. and P. Leinweber (1999). Thermal stability and composition of mineral-bound organic matter in density fractions of soil. European Journal of Soil Science, 50: 237–248.

Schumacher, B.A. (2002). Methods for the determination of total organic carbon (TOC) in soils and sediments. Ecological Risk Assessment Support Center. US. Environmental Protection Agency: 23.

Schweiger, P. and A. Amberger (1979). Mg-Auswaschung und Mg-Bilanz in einem langjährigen Lysimeterversuch. Z. Acher-und Pflanzenbau, 148: 403-410.

Sebestyen, S.D., E.W. Boyer and J.B. Shanley (2009). Responses of stream nitrate and DOC loadings to hydrological forcing and climate change in an upland forest of the northeastern United States. Journal of Geophysical Research, 114: G02002.

Selby, M.J. (1993). Hillslope Materials and Processes. Oxford University Press, Oxford.

Semenov, M.A., R. Brooks, E. Barrow and C. Richardson (1998). Comparison of the WGEN and LARS-WG stochastic weather generators for diverse climates. Climate Research, 10: 95-107.

Semenov, M.A. and R.J. Brooks (1999). Spatial interpolation of the LARS-WG stochastic weather generator in Great Britain. Climate Research, 11: 137-148.

SHETRAN Hydrological model. Available at: http://research.ncl.ac.uk/shetran/ (Accessed: March 2008).

Shuttleworth, W.J. (1993). Evaporation. In Maidment, D.R. (eds.), Handbook of Hydrology. McGraw-Hill, New York, Chapter 4.

Sidle, R.C., Y. Tsuboyama, S. Noguchi, I. Hosoda, M. Fujieda and T. Shimizu (2000). Stormflow generation in steep forested headwaters: A linked hydrogeomorphic paradigm. Hydrological Processes, 14: 369 – 385.

Sievers, F.J. and H.F. Holtz (1923). The influence of precipitation on soil composition and soil organic matter maintenance. Wash. Agr. Expt. Sta. Bull., 176.

Siewert, C. (2004). Rapid screening of soil properties using thermogravimetry. Soil Science Society of America Journal, 68: 1656–1661.

Sivapalan, M. (2003). Process complexity at hillslope scale, process simplicity at the basin scale: is there a connection? Hydrological Processes, 17: 1037-1041.

Sivapalan, M and J.D. Kalma (1995). 1: Scale problems in hydrology: contributions of the Robertson workshop. In Scale Issues in Hydrological Modeling, Kalma, J.D. and M. Sivapalan (eds.), Wiley: Chichester, UK. 1–8.

Sivasubramaniam, S. and O. Talibudeen (1972). Potassium-aluminum exchange in acid soils. I. Kinetics. J. Soil Sci., 23: 163--176.

Skinner, G.R. B., R. Thomas, M. Taylor, M. Sellarajah, S. Bolt, S. Krett and A. Wright (1997). Thyroxine should be tried in clinically hypothyroid but biochemically euthyroid patients. British Medical Journal, 314: 1764.

Skjemstad, J.O., L.J. Janik and J.A. Taylor (1998). Non-living soil organic matter: what do we know about it? Australian journal of Experimental Agriculture, 38: 667-680.

Sklash, M.G. (1990). Environmental isotope studies of storm and snowmelt runoff generation. In: Anderson, M.G. and T.P. Burt (eds.), Process Studies in Hillslope Hydrology: 401–435.

Slaymaker, O. (1991). Field experiments and measurements programs in geomorphology. Vancouver University of British Columbia Press.

Sleutel, S. (2005) Carbon sequestration in crop land soils: recent evolution and the potential of alternative management options. Ghent University. Department of Soil Management and Soil Care. PhD thesis.

Smith, T.E. (2012). Effects of native perennial vegetation buffer strips on dissolved organic carbon in surface runoff from an agricultural landscape. Iowa State University, Ames, Iowa. MSc thesis.

Soil Association (2009). Soil Carbon and Organic Farming. A review of the evidence on the relationship between agriculture and soil carbon sequestration, and how organic farming can contribute to climate change migration and adaptation. UK

Soil Survey Lab Staff (1996). Soil Survey Laboratory Manual. USDA, Washington, D.C. Soil Survey Investigations Report Number, 42(3).

Soler, M.J. (2003). Nutrient pollution evaluation in the River Eden. University of Newcastle Upon Tyne. Unpublished MSc thesis.

Solheim, A.L., K. Austnes, T.E. Eriksen, I. Seifert and S. Holen (2010). Climate change impacts on water quality and biodiversity. Background Report for EEA European Environment State and Outlook Report 2010. Europian Enviromental Agency, ADS/06/001-Water, Prague.

Sørbotten, L.E. (2011). Hill slope unsaturated flowpaths and soil moisture variability in a forested catchment in southwest China. Norwegian University of Life Sciences, Department of Plant and Environmental Sciences. MSc thesis.

Soulsby, C., C. Gibbins, A.J. Wade, R. Smart and R. Helliwell (2002). Water quality in the Scottish uplands: a hydrological perspective on catchment hydrochemistry. Science of the Total Environment, 294: 73 –94.

Soulsby C, P. Rodgers, R. Smart, J. Dawson and S. Dunn (2003). A tracer-based assessment of hydrological pathways at different spatial scales in a mesoscale Scottish catchment. Hydrological Processes, 17: 759-777.

Sparks, D.L. (1980). Chemistry of soil potassium in Atlantic Coastal Plain soils: A review. Commun. Soil Sci. Plant Anal. 11: 435-449.

Sparks, D.L. (1987). Potassium dynamics in soils. Advances in Soil Science, 6: 1-63.

Sparks, D.L. (1989). Kinetics of Soil Chemical Processes. Academic Press, San Diego, CA.

Sparks, D.L. (1995). Environmental Soil Chemistry. (eds.), Geoderma, 67: 1–140.

Sparks, D.L. (2000). Bioavailability of soil potassium, D-38-D-52. In M.E. Sumner (eds.), Handbook of Soil Science, CRC Press, Boca Raton, FL.

Sparks, D.L. (2001). Dynamics of K in Soils and Their Role in Management of K Nutrition. Department of Plant and Soil Sciences, University of Delaware, Newark, Delaware 19717-1303. Event: IPI PRII K in nutrient management for sustainable crop production in India, New Delhi, India.

Sparks, D.L., D.C. Martens and L.W. Zelazny (1980). Plant uptake and leaching of applied and indigenous potassium in Dothan soils. Agronomy Journal, 72: 551-555.

Sparks, D.L. and P.M. Jardine (1981). Thermodynamics of potassium exchange in soil using a kinetics approach. Soil Science Society of America Journal, 45: 1094-1099.

Sparks, D.L. and P.M. Jardine (1984). Comparison of kinetic equations to describe K-Ca exchange in pure and in mixed systems. Soil Science, 138: 115-122.

Sparks, D.L. and P.M. Huang (1985). Physical chemistry of soil potassium. In R.D. Munson (eds.), Potassium in agriculture. American Society of Agronomy, Madison, WI., 201-276.

Sparks, D.L., S.E Fendorf, I.V. Toner and C.V. Carski (1996). Kinetic methods and measurements. In: Sparks, D.L. (eds.), Methods of Soil Analysis: Chemical Methods. SSSA Book Ser. No. 5, American Society of Agronomy, Madison, WI, 1275–1307.

Sposito, G. (1984). The future of an illusion-ion activities in soil solutions. Soil Science Society of American Journal, 48: 531-536.

Srinivasan, K., S. Muruganandan, J. Lal, S. Chandra, S.K. Tandan and V.R. Prakash (2001). Evaluation of anti-inflammatory activity of Pongamia pinnata leaves in rats. Journal of Ethnopharmacology, 78(2-3): 151-157.

Stanley D.W. and J.E. Hobbie (1981). Nitrogen cycling in a North Carolina coastal river. Limnology and Oceanography, 26: 30–42.

Starks, P.J, G.C. Heathman, T.J. Jackson and M.H. Cosh (2006). Temporal stability of soil moisture profile. Journal of Hydrology, 324: 400–411.

Stevens, D.P., J.W.Cox and D.J. Chittleborough (1999). Pathways of phosphorus, nitrogen, and carbon movement over and through texturally differentiated soils, South Australia. Australian Journal of Soil Research, 37(4): 679–693.

Striffler, W.D. (1965). The selection of experimental watersheds and methods in distributed forest areas. Proceedings of the Symposium of Budapest on Representataive and Experimental Areas, IAHS, 66: 464-473.

Tang, J., B. Zhang, C. Gao and H. Zepp (2011). Subsurface lateral flow from hillslope and its contribution to nitrate loading in the streams during typical storm events in an agricultural catchment. Hydrology and Earth System Scienced Discussusion, 8: 4151-4193.

Tanhan, P, M. Kruatrachue, P. Pokethitiyook and R. Chaiyarat (2007). Uptake and accumulayion of cadmium, lead and zinc by siam weed [Chromlaena odorata (L) King and Robinson]. Chemosphere, 68: 323-329.

Tardy, Y., V. Bustillo and J.L. Boeglin (2004). Geochemistry applied to the basin survey: hydrograph separation, erosion and soil dynamics. A case study: the basin of the Niger River, Africa. Applied Geochemistry, 19: 469-518.

Tardy, Y., V. Bustillo, C. Roquin, J. Mortatti and R. Victoria (2005). The Amazon. Bio-geochemistry applied to river basin management. Part I. Hydro-climatology, hydrograph

separation, mass transfer balances, stable isotopes, and modelling. Applied Geochemistry, 20: 1746-1829.

Taylor, G. (2003). "Geology from rail journeys: the Settle-Carlisle Railway.Geology Today, 19(4): 143-148.

Theta Probe, Soil Moisture Sensor (1999). TYPE ML2x, User Manual, ML2x-UM-1.21. Delta-T Devices Ltd., 128 Low Road, Burwell, Cambridge, CB5 0EJ, England.

Thomann, R.V. (1972). Systems analysis and water quality measurement. Environmental Research and Application. Inc., New York.

Thurman, E.M. (1985). Organic geochemistry of natural waters, Martinus Nijhoff/Dr W. Junk Punlishers, Dordrecht.

Tierney, G.L., T.J. Fahey, P.M. Groffman, J.P. Hardy, R.D. Fitzhugh and C.T. Driscoll (2001). Soil freezing alters fine root dynamics in a northern hardwood forest. Biogeochemistry 56:175-190.

Tipping, E., C. Woof, E. Rigg, A.F. Harrison, P. Ineson, K. Taylor, D. Benham, J. Poskitt, A.P. Rowland, R. Bol and D. D. Harkness (1988). Climatic influences on the leaching of dissolved organic matter from upland UK moorland soils, investigated by a field manipulation experiment. Environment International, 25: 83-95.

Tischendorf, W.G. (1969). Tracing Stormflow to Varying Source Area in Small Forested Basin in the Southeastern Piedmont. University of Georgia, Athens, Georgia. Ph.D. thesis.

Tischendorf, L.C. (2002). Catchment clearing impacts on estuaries. AUSGEO News, 65: 6-7.

Tockner, K.U. Uehlinger and C.T. Robinson (2009). Rivers of Europe. Amsterdam; London: Academic Press.

Todini, E. (1996). The ARNO rainfall-runoff model. Journal of Hydrology, 175: 339–382.

Tranvik, L.J. and M. Jansson (2002). Climate change -Terrestrial export of organic carbon. Nature, 415: 861-862.

Tromp-van Meerveld, H.J., A.L. James, J.J. McDonnell and N.E. Peters (2008). A reference data set of hillslope rainfall-runoff response, Panola Mountain Research Basin, United States. Water Resources Research, 44.

Tsai, C.C., P.C. Chen and Z.S. Chen (2010). Soil solution chemistry and elemental balance of Fushan natural hardwood forest ecosystem in Taiwan. 19th World Congress of Soil Science, Soil Solutions for a Changing World. Brisbane, Australia.

Twilley, R.R., J. Cowan, T. Miller-Way, P.A. Montagna and B. Mortazavi (1999). Benthic nutrient fluxes in selected estuaries in the Gulf of Mexico, pp 163-209 In Bianchi, T.S., Pennock, J.R. and R.R. Twilley (eds.), Biogeochemistry of Gulf of Mexico Estuaries, John Wiley and Sons, Inc.

UK Climate Projections (2009). Available at: http://www.defra.gov.uk/publications/2011/03/28/pb13274-uk-climate-projections-090617/ (Accessed: December 2010).

University of Newcastle Upon Tyne (2000). CHASM: Catchment Hydrology And Sustainable Management. Available at: http://research.ncl.ac.uk/chasm/

USEPA (1999). Protocol for Developing Nutrient TMDLs. EPA 841-B-99-007. Office of Water (4503F), United States Environmental Protection Agency, Washington D.C. 135 pp.

Vanderbilt, K.L., K. Lajtha and F.J. Swanson (2003). Biogeochemistry of unpolluted forested watersheds in the Oregon Cascades: temporal patterns of precipitation and stream nitrogen fluxes. Biogeochemistry, 62: 87–117.

Van Genuchten, M.Th. (1980). A closed-form equation for Predicting the Hydraulic Conductivity of Unsaturated Soils. Soil Science Society of America Journal, 44: 892-898.

Van Liew, M.W. and J. Garbrecht (2003). Hydrologic simulation of the Little Washita river experimental basin using SWAT. Journal of the American Water Resources Association, 39(2): 413–426.

Van Verseveld (2007). Hydro-biogeochemical coupling at the hillslope and catchment scale. Oregon State University. PhD Thesis.

Varis, O., T. Kajander and R. Lemmelä (2004). Climate and water: from climate models to water resources management and vice versa. Climatic Change, 66: 321-344.

Vidale, P.L., D. Luthi, C. Frei, I. Seneviratne and C. Schär (2003). Predictability and uncertainty in a regional climate model. Journal of Geophysical Research, Atmos 108, Art. No.–4586.

Vinten, A.J.A. and K.A. Smith (1993). Nitrogen cycling in agricultural soils. In Burt, T.P., A.L. Heathwaite and S.T. Trudgill (eds.), Nitrate: Processes, patterns, and management. John Wiley and Sons, West Sussex, UK: 39-74.

Volk, B.G. and R.H. Loeppert (1982). Soil organic matter. In: 'Handbook of Soils and Climate in Agriculture', V. J. Kilmer and A.A. Hanson(eds.), CRC Press, Inc. Boca Raton, Florida.

Wainwright, J. and A.J. Parsons (2002). The effect of temporal variations in rainfall on scale dependency in runoff coefficients. Water Resources Research, 38 (12): 1271.

Walpola, B.C. and K.K.I.U. Arunakumara (2011). Carbon and nitrogen mineralization of a plant residue amended soil. The effect of salinity stress. Bangladesh Journal of Scientific & Industrial Research, 46(4): 565-572.

Walsh, C.L. (2004). Simulation and Analysis of River Flow Regimes: Implications for Sustainable Management of Atlantic Salmon (Salmo salar) Under Climate Change. School of Civil Engineering and Geosciences. Newcastle Upon Tyne, Newcastle University.

Walsh, C.L. and C.G. Kilsby (2007). Implication of climate change on flow regime affecting Atlantic salmon. Hydrology and Earth System Sciences, 11(3): 1127-1143.

Wearing, C.L. (2008). Changes in fluxes of dissolved organic carbon (DOC) from small catchments in central Scotland. The School of Biological and Environmental Sciences. University of Stirling. PhD Thesis.

Weiler, M., S. Scherrer, F. Naef and P. Burlando (1999). Hydrograph Separation of Runoff Components Based on Measuring Hydraulic State Variables, Tracer Experiments, and Weighting Methods: International Association of Hydrologic Science,. 258: 249-255.

Weiler M., J.J. McDonnell, I. Tromp-van Meerveld and T. Uchida (2005). Subsurface stormflow runoff generation processes. In Encyclopedia of Hydrological Sciences, Anderson M.G. (eds.), John Wiley and Sons Ltd, 1719 – 1732.

Western, A.W, S-L. Zhou, R.B. Grayson, T.A. McMahon, G. Blöschl and D.J Wilson (2004). Spatial correlation of soil moisture in small catchments and its relationship to dominant spatial hydrological processes. Journal of Hydrology, 286: 113–134.

Weyman, D.R. (1973). Measurements of the downslope flow of water in a soil. Journal of Hydrology, 20: 267-288.

Whitehead, J.C. (2005). Environmental Risk and Averting Behavior: Predictive Validity of Revealed and Stated Preference Data. Environmental and Resource Economics, 32:301-316.

Wicks, J.M. and J.C. Bathurst (1996). SHESED: a physically based, distributed erosion and sediment yield component of the SHE hydrological modelling system. Journal of Hydrology, 175: 213-238.

Wilby, R. L, S. P Charles, E. Zorita, B. Timbal, P. Whetton and L. O. Mearns (2004). The guidelines for use of climate scenarios developed from statistical downscaling methods. Supporting material of the Intergovernmental Panel on Climate Change (IPCC), prepared on behalf of Task Group on Data and Scenario Support for Impacts and Climate Analysis (TGICA).
<http://ipccddc.cru.uea.ac.uk/guidelines/StatDown_Guide. pdf.

Wilcox, B.P., B.D. Newman, D. Brandes, D.W. Davenport and K. Reid (1997). Runoff from a semiarid ponderosa pine hillslope in New Mexico. Water Resources Research, 33(10): 2301-2314.

Wilkinson, M. E. (2009). A multiscale nested experiment for understanding and prediction of high rainfall and flood response spatial behaviour in the Eden Catchment, Cumbria, UK. School of Civil Engineering and Geosciences. Newcastle University. PhD Thesis.

Wilks, D.S. (1999). Multisite downscaling of daily precipitation with a stochastic weather generator. Climate Research, 11: 125–36.

Wilson, D.J, A.W. Western, R.B. Grayson, A.A. Berg, M.S. Lear, M. Rodell, J.S. Famiglietti, R.A Woods and T.A. McMahon (2003). Spatial distribution of soil moisture over 6 and 30cm depth, Mahurangi river catchment, New Zealand. Journal of Hydrology, 276: 254– 274.

Wilson, G.V. and R.J. Luxmoore (1988). Infiltration, macroporosity and mesoporosity distributions on forested watersheds. Soil Science Society of America Journal, 52: 329-335.

Wilson, G.V., P.M. Jardine, R.J. Luxmoore and J.R. Jones (1990). Hydrology of a forested watershed during storm events. Geoderma, 46: 119-138.

Wilson, G.V., P.M. Jardine, R.J. Luxmoore, L.W. Zelazny and D.E. Todd (1991). Hydrogeochemistry processes controlling subsurface transport from an upper subcatchment of Walker Branch during storm events. 1. Hydrologic transport processes. Journal of Hydrology, 123: 297-316.

Winter, T.C. (1981). Uncertainty in Estimating the Water Balance of Lakes. Water Resources Bulletin (AWRA), 17 (1): 82-115.

Woldeselassie, M.K. (2009). Soil Organic Carbon and Site Characteristics in Aspen and Evaluation of the Potential Effects of Conifer Encroachment on Soil Properties in Northern Utah. Utah State University, MSc thesis.

Wolfhard, S. and B. Reinhard (1998). The heterogeneity of runoff and its significance for water quality problems. Hydrological Sciences Journal, des Sciences Hydrologiques, 43: 103-113.

Wolford, R.A., R.C. Bales and S. Sorooshian (1996). Development of a hydrochemical model for seasonally snow-covered alpine watersheds: Application to Emerald Lake watershed, Sierra Nevada, California. Water Resources Research, 32: 1061 – 1074.

WMO (2008). Climate.
Available at: http://www.wmo.int/pages/prog/wcp/COP16QAvariability.php
(Accessed: May 2008).

Worrall, F., T.P. Burt, R.Y. Jaeban, J. Warburton and R. Shedden (2002). Release of dissolved organic carbon from upland peat. Hydrological Processes, 16: 3487-3504.

Worrall, F., T.P. Burt and J. Adamson (2006). The rate of and controls upon DOC loss in a peat catchment. Journal of Hydrology, 321: 311-325.

Yalin, M.S. (1963). An expression for bed-load transportation. Journal of Hydrology, 89: 221-250.

Yang, C., R.E. Chandler, V. Isham and H.S. Wheater (2005). Spatial-temporal rainfall simulation using Generalized Linear Models. Water Resources Research, 41, W11415.

Yano, Y., K. Lajtha, P. Sollins and B.A. Caldwell (2004). Chemistry and seasonal controls on the dynamics of dissolved organic matter in a coniferous old-growth stand in the Pacific Northwest, USA. Biogeochem., 71: 197-203.

Yong, J., Z. Yu-Ge, L. Wen-Ju and Q. Li (2005). Pedogenic and anthropogenic influence on calcium and magnesium behaviors in stagnic anthrosols. Scinece Press, Beijing, 15(3): 341-346.

Younger, P.L. and C.A. Milne (1997). Hydrostratigraphy and hydrogeochemistry of the Vale of Eden, Cumbria, UK. Proceedings of the Yorkshire Geological Society, 51(4): 349-366.

Yusop, Z., I. Douglas and A.R. Nik (2006). Export of dissolved and undissolved nutrients from forested catchments in Peninsular Malaysia, Forest Ecology and Management, 224: 26-44.

Zhang, Y.K. and K. Schilling (2005). Temporal variations and scaling of streamflow and baseflow and their nitrate–nitrogen concentrations and loads. Advances in Water Resources, 28: 701–10.

Appendices

Appendix A1 Geology Map Upper Eden basin

Appendix A2 Land Cover Map Upper Eden basin

Appendix A3 HOST Classification (The Macaulay Institute 2008)

Appendix B Open pit at the Hollow sub-catchment

Appendix C1 UK maps for December 2009 and January 2010

(including mean temperature, mean daily minimum temperature, days of ground frost and days of snow lying)

Appendix C2 UK map of recorded snow depths at 0900 GMT on Thursday 7 January 2010

Appendix D1 Analysis of major ions in rain water and stream water within Blind Beck and Hollow

Appendix D2 Analysis of NO_3^- and DOC in stream water within Blind Beck and Hollow

Appendix D3 Sediment size distribution curves

Appendix D4 Analysis of TOC and TN in sediments within Blind Beck and Hollow

Appendix E1 Analysis of major ions in the overland and subsurface flow within the hillslope

Appendix E2 Analysis of DOC and NO_3^- in the overland and subsurface flow within the hillslope

Appendix A1 Geology Map Upper Eden basin

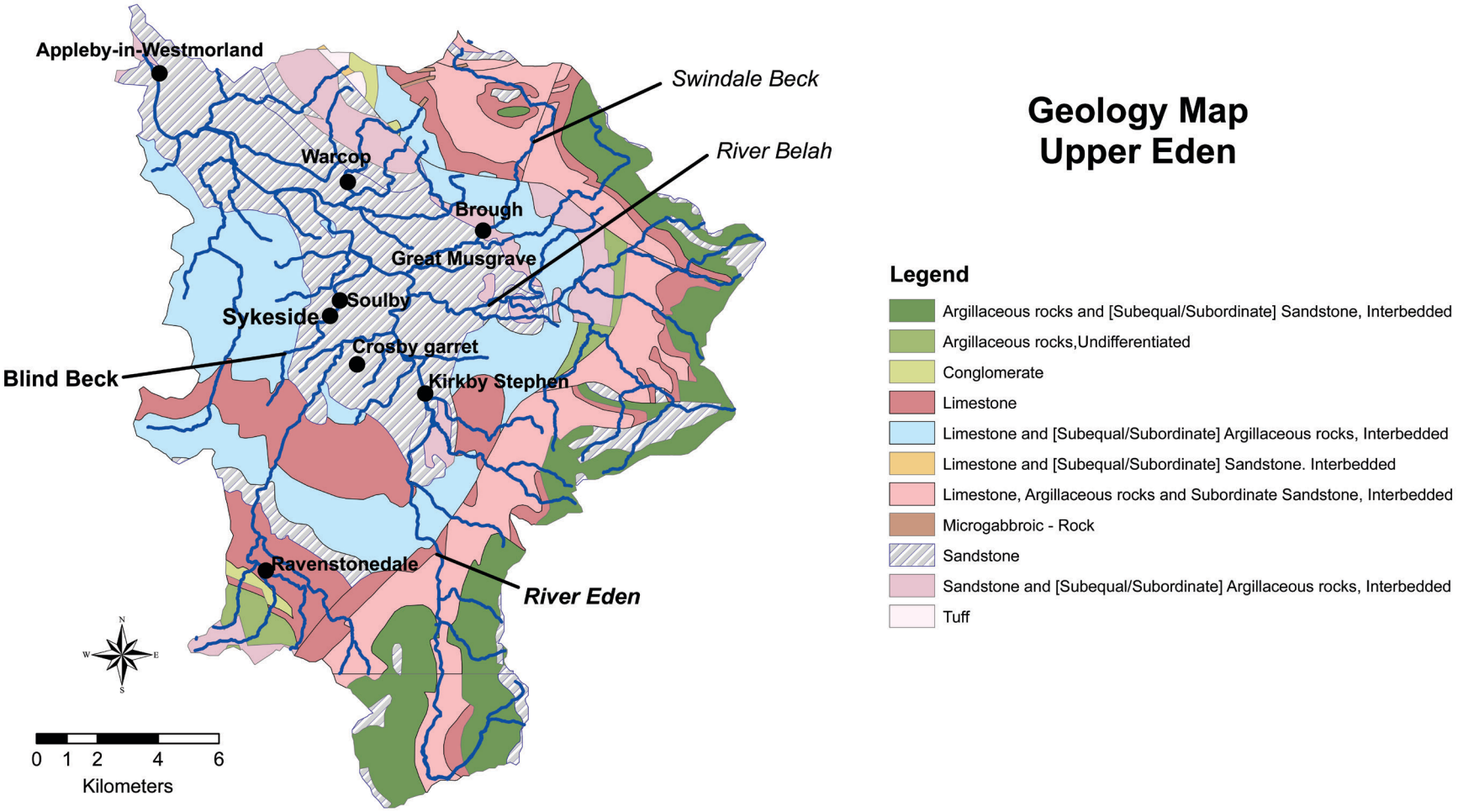

Appendix A2 Land Cover Map Upper Eden basin

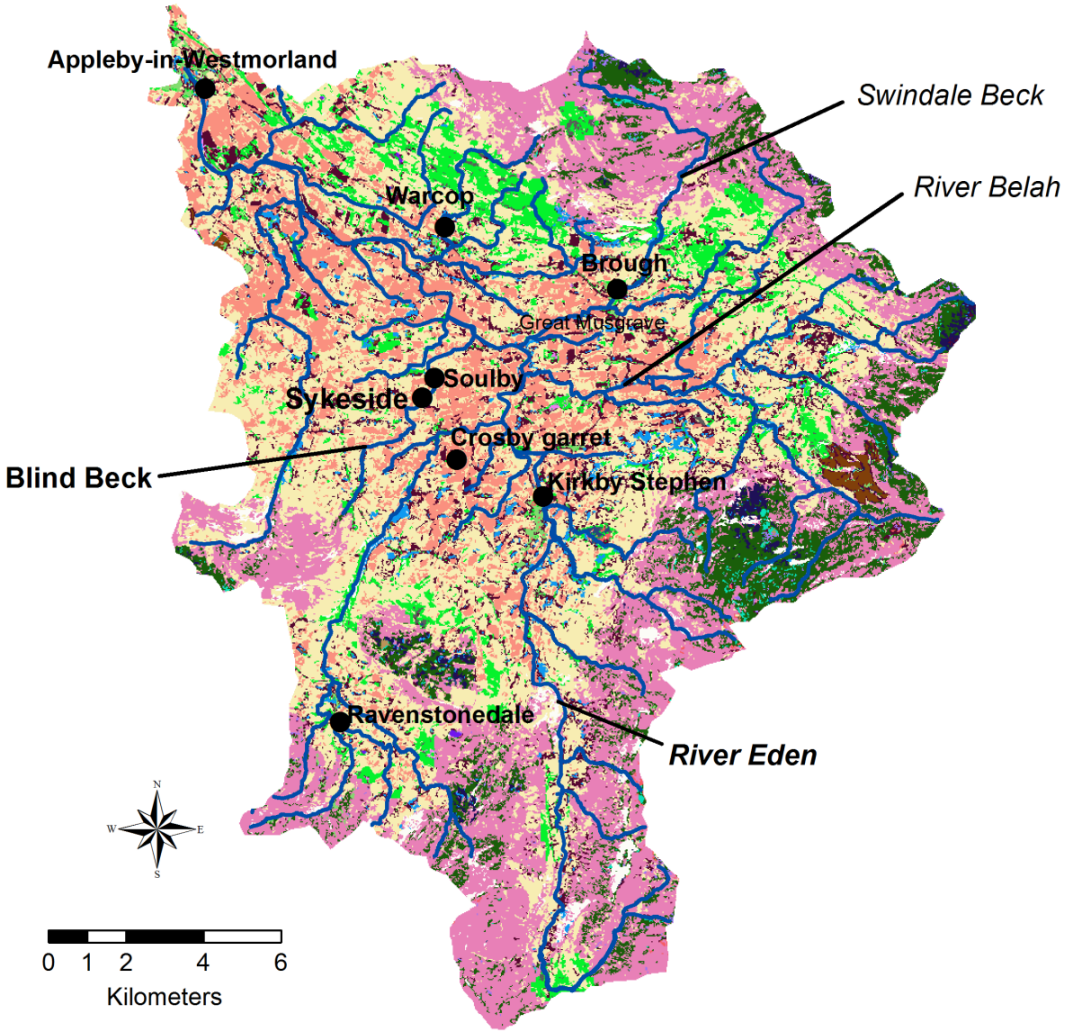

Appendix A3 HOST Classification (source: The Macaulay Institute 2008)

HOST Class	Description of HOST Class
4	**Geology**: hard fissured Dalradian, Cambrian or Ordovician limestones or sandstones. Some well weathered intrusive and metamorphic rocks (England and Wales only). **Landforms**: Limestone region - Few areas of true Karst, predominantly undulating with ridges (eg Lismore), rocky knolls or craggy outcrops on steep-sided valleys. Much of the land has been extensively glaciated. Sandstone region - varies from gently undulating lowlands (e.g. Black Isle) with few rock outcrops to the rock-dominated hill tops of Sutherland and Caithness. In Shetland, the topography can be very rocky with a stepped appearance or strongly undulating lowlands. **Soils**: freely drained (wetness class I) brown earths, humus-iron podzols, brown and podzolic rankers, brown rendzinas and lithosols. They are often shallow. **Vegetation**: semi-natural grasslands and herb-rich heather moorland in the uplands to arable, improved pastures, coniferous plantation and occasionally broadleaved woodlands in the lowlands. **Flow**: flow in substrate is mainly through rock fissures though some rock is porous.
5	**Geology**: fluvioglacial sands and gravels or windblown sands, some coarse morainic drift. **Landforms**: quite variable includes a raised beach, windblown links and dunes (Culbin, Tentsmuir and Gullane) as well as high level river terraces (in Scotland at least) and the parallel roads of Glen Roy. The fluvioglacial deposits can be either moundy with long sinuous ridges or gently sloping outwash plains (e.g. around Forres in North-east Scotland). **Soils**: freely drained (wetness class I) humus-iron podzols and brown earths with brown calcareous soils, calcareous regosols, alluvial sands and gravel, and regosols. Found throughout Scotland but primarily south and east of the Great Glen. **Vegetation**: varies from natural marram grassland through heather moorland to coniferous plantation but the dominant land use is arable and permanent pasture. **Flow**: flow through these soils and substrates is largely laminar and intergranular.
6	**Geology**: loamy textured drift underlain by porous rocks such as sandstones. They are found throughout the lowlands of Scotland but most extensively in the east, Caithness and Sutherland. **Landforms**: the landforms associated with this class are highly variable from undulating non-rocky lowlands, valley sides and hilltops. The land has a wide range of slopes and is occasionally rocky and there are also localised areas of moundy moraine. The class ranges in altitude from virtually sea level to around 700 m. **Soils**: freely drained (wetness class I) brown earths and humus-iron podzols with some subalpine podzols. **Vegetation**: ranges from cultivated arable land in the lowlands through heather moorland, rough grasslands and semi-natural woodland. **Flow**: microporous with by-pass flow common along major structural cracks.

HOST Class	Description of HOST Class
8	**Geology**: alluvial deposits. **Landforms**: alluvial areas in close proximity to rivers. **Soils**: immature free and imperfectly drained, loamy textured alluvial soils (wetness class I-III). **Vegetation**: often intensively cultivated. **Flow**: these soils are underlain by a fluctuating groundwater table generally within two metres, by-pass flow common.
10	**Geology**: alluvial deposits and saltings. **Landforms**: found in low lying areas around lochs, between fluvioglacial mounds, along rivers and on raised beaches. Also saltings and dune slacks. **Soils**: poorly drained alluvial soils and mineral ground water gleys (wetness class IV). Saline alluvial soils below the high-water mark which are periodically inundated by the sea. **Vegetation**: varies from the halophytic marsh species of the saltings, rush pastures, and sedge mires to permanent pasture and intensive agriculture where the level of the water table can be controlled.
15	**Geology**: hummocky and slope moraines, coarse to medium textured till. Soft rock geologies. **Landforms**: valley moraines depression and receiving sites, ice-scoured landscapes with rock knolls and pockets of drift, some stepped topography, foot slopes, till embayment's, spring lines and concave slopes. **Soils**: peaty gleys, peaty podzols and peaty rankers on porous rock types (wetness class V and VI). **Vegetation**: permanent and rush pastures, commercial forestry, bog heather moorland and molinia grassland, flush sites with mosses, rushes and sedges.
17	**Geology**: loamy textured drift drifts overlying hard, coherent rock at depths greater than one metre, colluvium and loose, frost-shattered debris. **Landforms**: gentle to strongly undulating, steep, rocky and non-rocky valley sides and foothills, moraines, boulder lobes and stone strips of mountain top environments. Ranges in altitude from virtually sea level to over 900 metres. **Soils**: freely drained brown earths, humus-iron podzols, subalpine soils, some brown magnesian soils and alpine soils. **Vegetation**: cultivated arable lands of the lowlands, coniferous plantations, semi-natural woodland, heather moorland, rough grasslands and the wind clipped moorland and heath reminiscent of the fringes of the arctic tundra including alpine azalea, lichens and sedges.

HOST Class	Description of HOST Class
24	**Geology**: fine to medium textured lodgement till (formerly boulder clay), glaciolacustrine and estuarine deposits. **Landforms**: undulating till plains with occasional drumlin swarms, till embayments and some steep sided valleys. Gently undulating or level. The estuarine silts and clays form a specific and distinct landform associated with the Rivers Tay, Forth and Cree and are known as the Carse lands. **Soils**: non-calcareous mineral gleys with wetness class III or IV. **Vegetation**: cultivated with arable and dairying being a prominent farming system in the lowlands, locally, semi-natural Molinia grassland, rush pasture, broadleaved woodland and conifer plantation.
26	**Geology**: fine-textured lodgement till (formerly boulder clay), glaciolacustrine and estuarine deposits. **Landforms**: lowland depressions, gently undulating hill ground some steeper valley sides. **Soils**: peaty gleys (wetness class V to VI). **Vegetation**: with semi-natural vegetation including rush pasture, Molinia bog and heather moorland.
29	**Geology**: unconfined, umbrageous, climatic peat deposits. **Landform**: undulating land with gentle slopes including mountain plateaux on slopes < 15o. Associated with a great many landform unit throughout Scotland. **Soils**: blanket peats (organic soils) often more than 1 metre deep. **Vegetation**: either semi-natural moorland, Molinia-dominated bog scrub or conifer plantation.

Appendix B Open pit at the Hollow sub-catchment

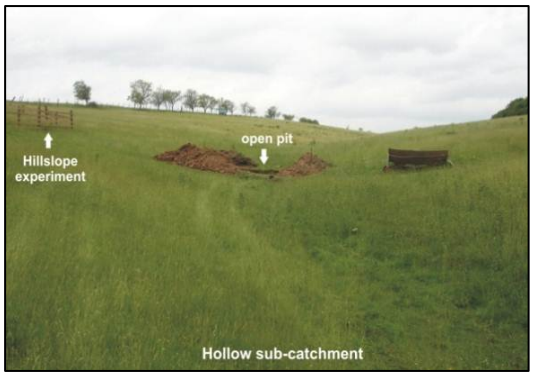

Appendix C1 UK maps for December 2009 and January 2010 (including mean temperature, mean daily minimum temperature, days of ground frost and days of snow lying) (source: Met Office, 2012)

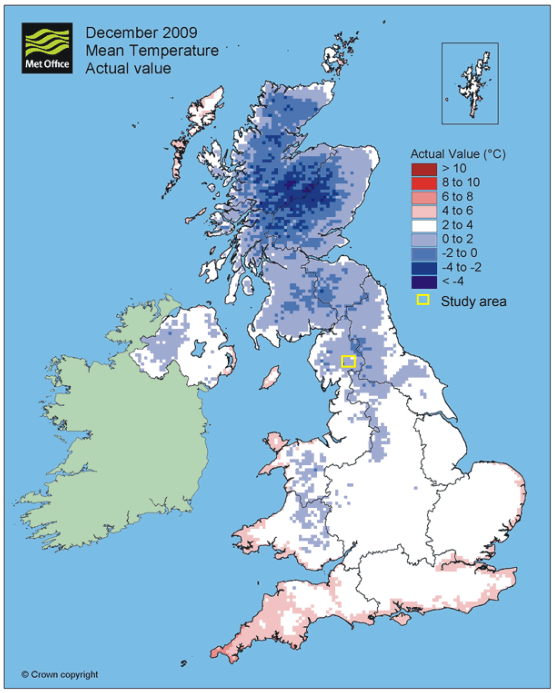

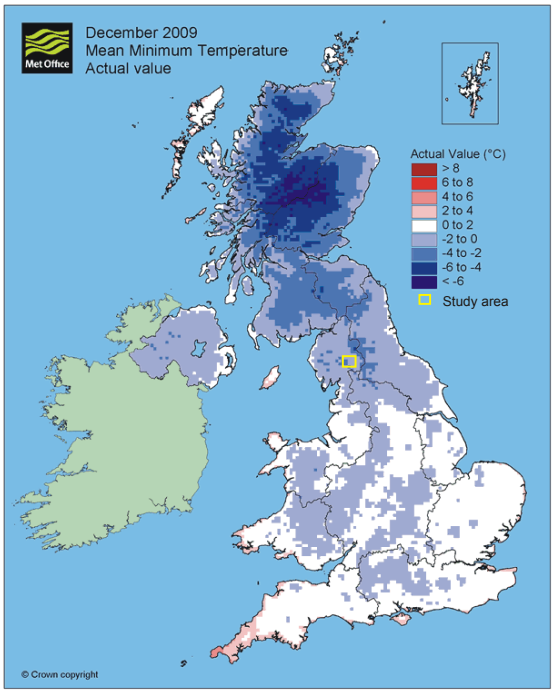

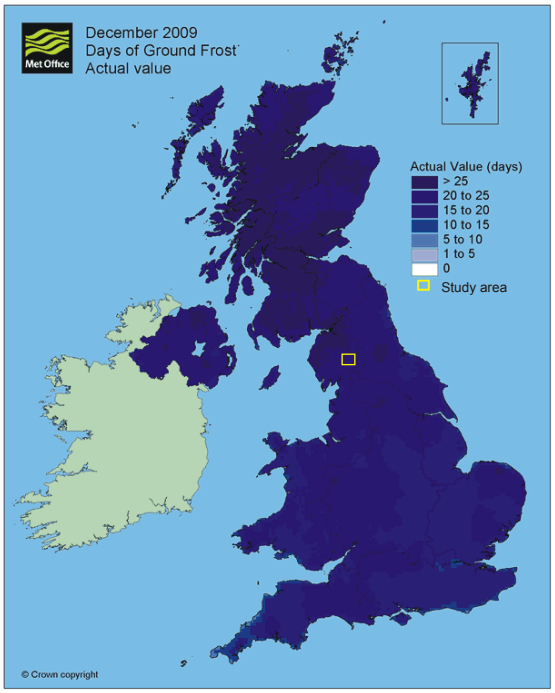

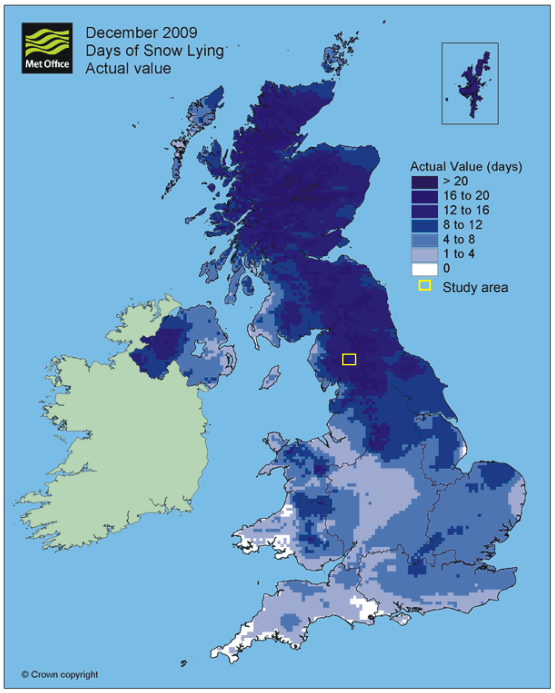

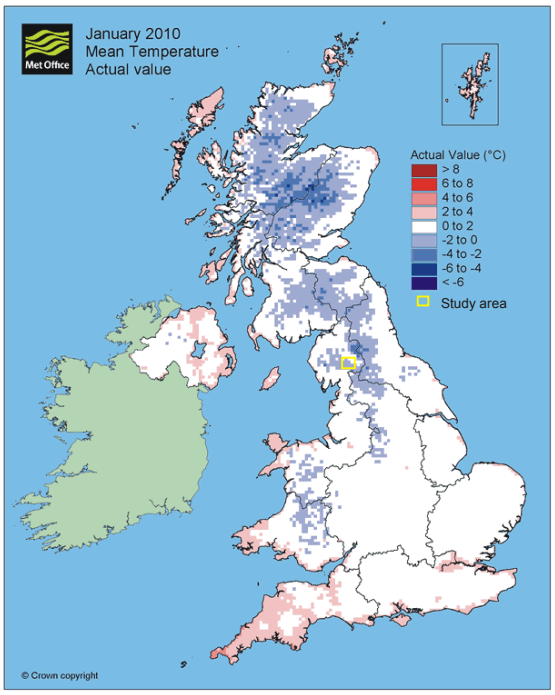
January 2010
Mean Temperature
Actual value
Actual Value (°C)
> 8
6 to 8
4 to 6
2 to 4
0 to 2
-2 to 0
-4 to -2
-6 to -4
< -6
Study area
© Crown copyright

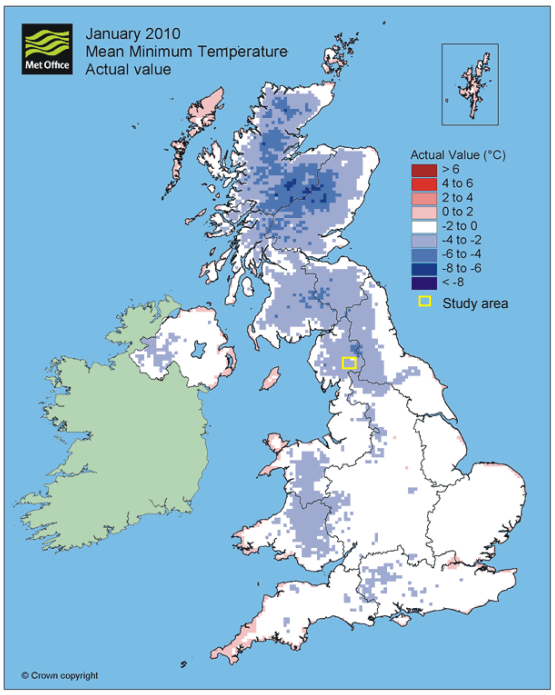
January 2010
Mean Minimum Temperature
Actual value
Actual Value (°C)
> 6
4 to 6
2 to 4
0 to 2
-2 to 0
-4 to -2
-6 to -4
-8 to -6
< -8
Study area
© Crown copyright

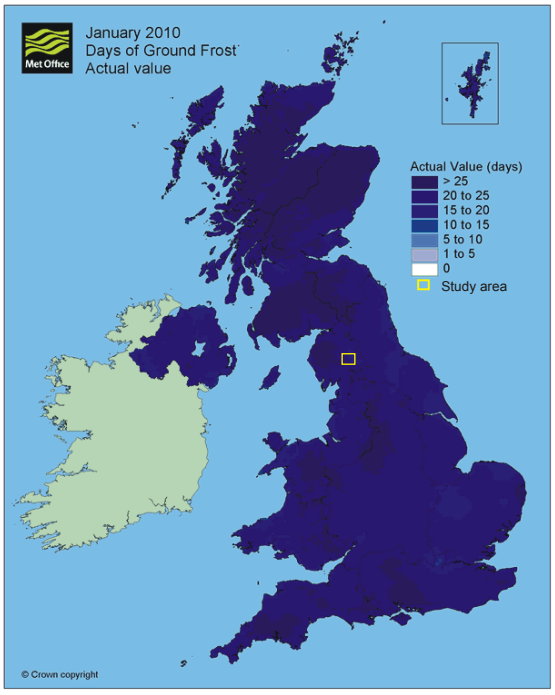
January 2010
Days of Ground Frost
Actual value
Actual Value (days)
> 25
20 to 25
15 to 20
10 to 15
5 to 10
1 to 5
0
Study area
© Crown copyright

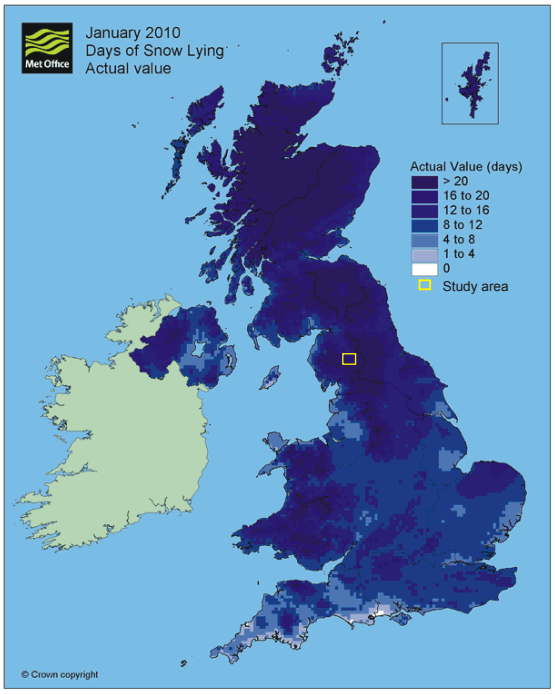
January 2010
Days of Snow Lying
Actual value
Actual Value (days)
> 20
16 to 20
12 to 16
8 to 12
4 to 8
1 to 4
0
Study area
© Crown copyright

Appendix C2 UK map of recorded snow depths at 0900 GMT on Thursday 7 January 2010 (source: Met Office, 2012)

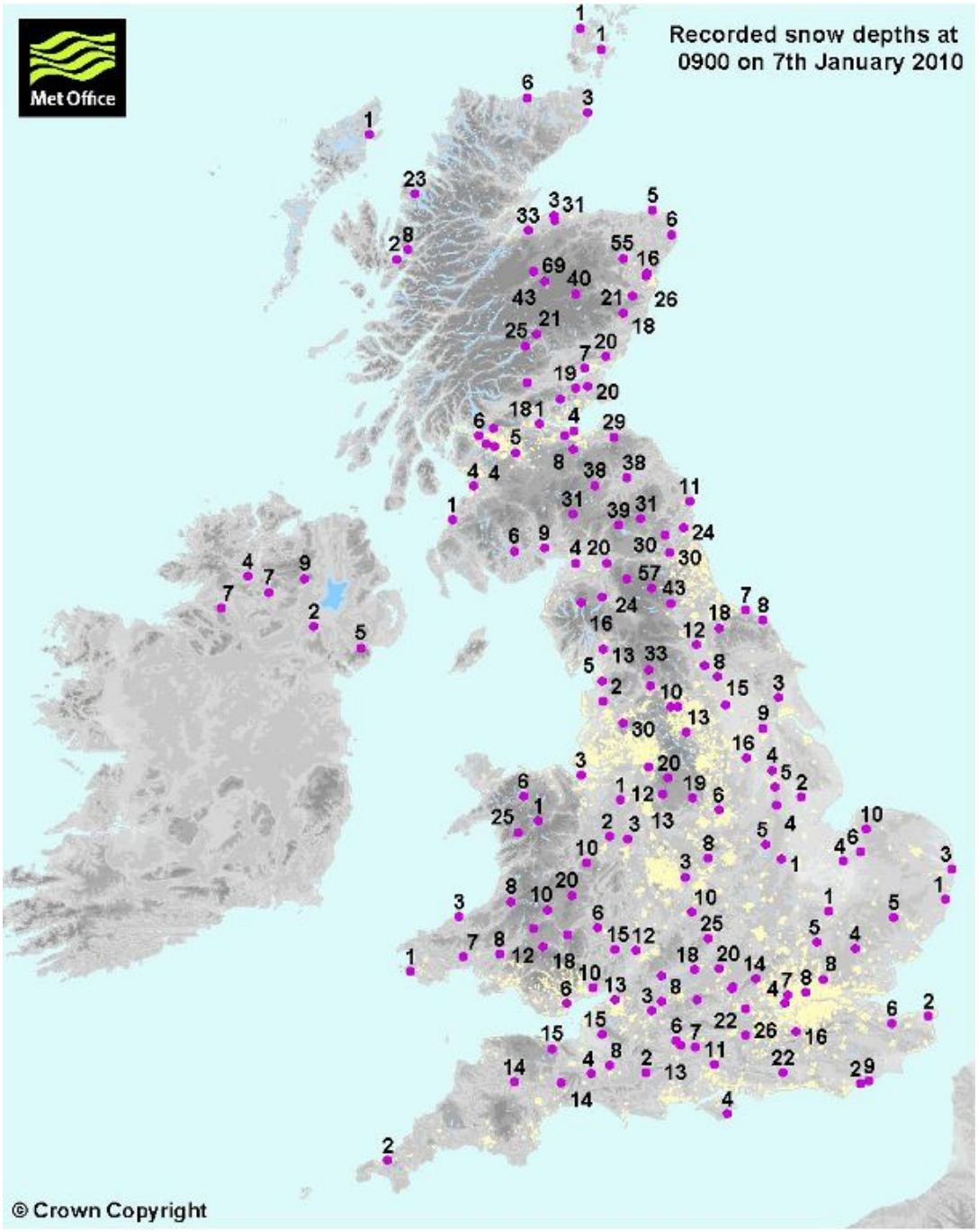

Appendix D1 Analysis of major ions in rain water and stream water within Blind Beck and Hollow

Table D1-1 Summary of rain water results

Date	pH	Na^+	K^+	Ca^{2+}	Mg^{2+}	Cl^-	SO_4^{2-}	NO_3^-	DOC
		mg/l							
6/8/09	6.3	4.0	1.4	1.6	0.3	6.7	3.6	0.9	3.2
29/9/09	6.2	1.3	0.9	1.8	0.4	8.1	1.7	0.5	9.2
8/10/09	6.3	2.2	0.8	0.8	0.3	6.0	1.6	0.4	9.3
3/11/09	6.3	2.8	0.8	3.6	0.8	5.9	2.1	0.9	7.1
1/12/09	5.8	5.0	0.5	0.9	0.5	20.0	2.4	0.4	5.0
2/2/10	7.1	5.6	1.6	0.8	0.3	6.5	3.5	0.8	7.7
18/3/10	6.0	2.7	0.8	1.0	0.4	5.1	3.6	2.8	3.4
22/4/10	6.5	2.5	0.7	0.8	0.2	5.9	1.6	0.9	5.2
20/5/10	N/A	1.3	1.0	1.2	0.3	N/A	N/A	N/A	13.7
17/6/10	N/A	N/A	N/A	N/A	N/A	N/A	N/A	N/A	N/A
15/7/10	6.2	1.8	2.0	2.8	0.8	6.6	1.8	0.3	10.6
19/8/09	6.5	1.0	1.0	0.8	0.2	3.3	1.0	0.5	10.3

N/A not available

Table D1-2 Summary of stream water results at sampling site 1

Date	pH	Na^+	K^+	Ca^{2+}	Mg^{2+}	HCO_3^-	Cl^-	SO_4^{2-}	NO_3^-	Charge balance
		mg/l								%
23/4/09	8.37	8.6	3.5	83.4	34.2	323.8	13.3	9.3	6.3	10.9
06/5/09	8.11	9.6	6.0	92.4	30.3	330.0	17.2	10.6	5.6	10.6
25/6/09	8.37	8.5	1.9	54.8	28.2	280.7	17.7	10.6	3.2	0.9
22/7/09	7.65	8.5	1.7	73.9	23.0	320.4	13.6	8.1	4.0	1.1
27/8/09	7.86	8.1	1.7	80.4	21.3	316.8	10.9	6.0	2.4	4.2
29/9/09	7.51	8.4	1.3	91.0	29.8	324.3	13.8	10.9	6.5	10.1
8/10/09	7.77	8.5	1.6	108.4	29.1	374.2	16.6	14.4	4.5	8.2
3/11/09	7.63	9.3	2.8	57.0	14.3	219.4	16.9	6.2	2.8	2.9
1/12/09	7.78	7.5	1.4	82.4	26.0	343.7	19.7	9.0	6.7	0.9
2/2/10	7.60	14.8	3.1	77.3	23.4	295.3	41.2	8.5	5.5	1.9
18/3/10	7.72	9.0	1.5	74.4	28.8	257.0	25.5	11.9	7.1	10.3
22/4/10	7.89	7.7	1.1	73.9	27.7	271.1	17.2	9.3	7.2	9.5
20/5/10	7.95	8.4	1.7	70.2	30.5	255.6	16.8	20.5	5.3	10.7
17/6/10	8.05	9.6	5.9	92.4	30.3	330.0	17.2	10.6	5.6	10.6
15/7/10	7.35	11.5	2.7	57.9	25.4	202.4	32.1	13.9	1.6	10.0
19/8/10	8.0	8.1	1.6	57.6	29.4	229.3	17.5	10.4	1.7	11.67

Table D1-3 Summary of stream water results at sampling site 2

Date	pH	Na^+	K^+	Ca^{2+}	Mg^{2+}	HCO_3^-	Cl^-	SO_4^{2-}	NO_3^-	Charge balance
		mg/l								%
23/4/09	8.40	8.7	4.0	71.6	29.5	309.9	16.4	12.7	7.4	4.5
06/5/09	8.2	10.7	5.6	93.4	30.5	339.6	16.9	10.7	5.1	10.1
25/6/09	8.37	7.5	1.5	49.9	25.8	276.0	18.2	12.0	4.9	-3.7
22/7/09	7.87	7.5	1.6	55.8	17.3	289.0	14.2	7.9	4.0	-7.9
27/8/09	7.86	7.1	1.3	76.6	20.9	305.2	10.6	6.0	2.3	3.72
29/9/09	7.68	7.0	1.0	94.9	29.7	324.4	13.6	10.2	6.1	11.1
8/10/09	7.83	9.4	2.0	97.8	28.0	332.8	14.8	10.9	4.2	10.7
3/11/09	7.30	7.2	2.4	58.1	13.8	204.3	16.9	5.7	3.2	4.9
1/12/09	7.98	6.5	1.1	84.7	25.9	341.5	20.6	10.4	7.1	1.3
2/2/10	7.61	18.2	3.3	87.4	24.6	295.3	39.8	11.4	6.2	7.1
18/3/10	7.99	7.9	1.2	97.5	32.4	339.6	25.1	11.9	7.0	8.8
22/4/10	8.12	6.9	0.9	73.0	27.7	262.7	15.0	8.9	5.5	11.06
20/5/10	8.2	7.9	1.5	60.6	29.3	228.1	18.6	10.0	5.0	12.2
17/6/10	8.3	7.8	1.6	55.5	31.0	218.9	27.2	7.9	1.3	11.4
15/7/10	7.6	6.1	1.3	65.8	26.5	225.3	16.3	7.0	2.6	9.7
19/8/10	8.0	6.1	1.3	65.8	26.5	245.3	16.3	7.0	2.6	10.5

Table D1-4 Summary of stream water results at sampling site 3

Date	pH	Na^+	K^+	Ca^{2+}	Mg^{2+}	HCO_3^-	Cl^-	SO_4^{2-}	NO_3^-	Charge balance
		mg/l								%
23/4/09	8.1	4.7	4.8	81.4	30.6	304.6	14.7	9.7	4.7	11.3
06/5/09	8.3	9.0	6.5	87.4	28.5	300.4	17.1	10.9	5.1	10.9
25/6/09	8.5	7.8	1.6	53.3	27.5	267.5	16.6	10.0	3.1	1.9
22/7/09	7.9	7.5	1.6	78.2	23.9	328.3	12.0	7.6	3.7	2.5
27/8/09	7.9	6.8	1.3	78.8	20.9	310.0	11.2	6.2	2.4	3.6
29/9/09	7.7	7.3	1.1	88.8	29.1	325.2	12.4	8.6	6.2	9.2
8/10/09	7.9	19.4	2.4	95.8	28.4	406.1	14.3	10.6	4.1	4.4
3/11/09	7.4	7.3	2.4	56.5	13.4	206.5	18.2	5.9	3.9	2.6
1/12/09	7.9	6.7	1.1	83.4	25.8	351.7	14.1	5.8	5.0	1.8
2/2/10	7.7	14.1	3.0	77.6	23.3	290.3	41.2	8.7	5.6	2.3
18/3/10	8.1	7.7	1.2	80.7	29.1	256.5	25.0	11.4	7.3	12.7
22/4/10	8.2	6.8	0.8	65.9	25.1	239.3	16.5	8.9	7.0	9.6
20/5/10	8.3	7.6	1.2	65.3	30.1	245.7	16.6	8.7	4.7	12.4
17/6/10	8.5	7.67	1.6	54.2	28.8	210.2	26.1	7.4	1.2	11.2
15/7/10	7.7	24.2	2.7	54.3	24.2	192.0	34.3	8.1	1.1	10.3
19/8/10	8.0	7.2	1.2	62.7	26.3	233.9	15.1	6.7	2.3	11.8

Table D1-5 Summary of stream water results for at sampling site 4 (Hollow)

Date	pH	Na^+	K^+	Ca^{2+}	Mg^{2+}	HCO_3^-	Cl^-	SO_4^{2-}	NO_3^-	Charge balance
		mg/l								%
27/8/09	7.2	7.6	1.8	93.4	23.1	322.9	8.6	6.9	0.0	9.98
29/9/09	7.5	7.3	0.7	102.0	24.4	376.2	8.1	5.4	0.4	6.60
8/10/09	7.0	7.3	0.8	97.6	24.1	370.4	9.4	9.4	0.7	4.73
3/11/09	6.8	8.5	3.0	37.3	10.3	112.7	18.8	8.1	3.5	9.72
1/12/09	7.2	7.0	0.9	78.1	19.6	277.9	15.6	7.4	1.3	6.09
2/2/10	6.9	5.4	2.0	39.0	9.8	116.1	20.4	5.0	1.1	7.80
18/3/10	8.0	5.9	0.6	92.7	22.7	329.5	10.3	5.4	0.4	9.81
22/4/10	**8.0**	**6.4**	**0.6**	**94.7**	**22.0**	**284.5**	**5.7**	**3.2**	**5.5**	**15.67**
20/5/10	**7.8**	**6.5**	**0.5**	**105.2**	**22.9**	**293.0**	**8.2**	**5.5**	**0.2**	**17.84**
17/6/10	**7.9**	**10.8**	**2.3**	**95.4**	**23.6**	**239.5**	**7.8**	**1.2**	**0.0**	**26.85**
15/7/10	**7.1**	**20.6**	**9.9**	**162.9**	**21.0**	**141.8**	**15.2**	**264.0**	**42.7**	**39.50**

Table D1-6 Summary of stream water results at sampling site 5

Date	pH	Na^+	K^+	Ca^{2+}	Mg^{2+}	HCO_3^-	Cl^-	SO_4^{2-}	NO_3^-	Charge balance
		mg/l								%
23/4/09	8.0	9.25	3.58	118.9	34.4	388.8	15.2	10.7	9.9	12.7
06/5/09	8.1	9.9	2.4	96.39	31.2	287.0	14.5	9.3	5.0	5.7
25/6/09	8.2	8.5	1.4	85.9	28.3	372.9	20.3	16.3	8.1	-0.9
22/7/09	7.9	7.7	1.4	85.8	24.8	357.0	11.6	7.5	4.4	2.2
27/8/09	7.9	7.8	1.4	87.5	7.8	347.5	11.5	6.5	4.1	2.9
29/9/09	7.8	7.2	1.2	88.3	7.2	393.1	12.2	8.3	6.1	-1.4
8/10/09	7.7	8.9	1.5	120.0	8.9	462.2	16.0	10.0	10.9	1.8
3/11/09	7.4	7.5	2.5	59.4	7.5	211.3	17.9	5.8	2.9	4.7
1/12/09	7.9	6.8	1.2	89.8	6.8	357.0	19.5	6.2	6.4	2.4
2/2/10	7.5	10.4	2.0	100.0	10.4	354.9	27.0	8.7	11.2	4.1
18/3/10	7.8	8.3	1.3	78.8	8.3	346.4	22.3	11.4	14.6	-4.6
22/4/10	8.0	7.9	1.1	106.6	7.9	343.7	17.0	8.7	11.2	11.2
20/5/10	7.9	8.0	1.3	103.6	8.0	342.3	16.6	9.1	10.8	10.9
17/6/10	7.9	8.3	1.5	107.7	8.3	355.9	20.6	7.5	8.8	10.7
15/7/10	7.7	8.5	2.2	73.9	8.5	249.0	18.7	8.0	4.3	10.1
19/8/10	7.8	7.7	1.2	84.5	26.9	282.8	16.5	7.1	6.0	11.9

Appendix D2 Analysis of NO_3^- and DOC in stream water within Blind Beck and Hollow

Table D2-1 Summary of nitrate in stream water results at sampling site 1 to 5

Date	1	2	3	4	5
	NO_3^- (mg/l)				
23/4/09	6.3	7.4	4.7	N/A	9.9
06/5/09	5.6	5.1	5.1	N/A	5.0
25/6/09	3.2	4.8	3.1	N/A	8.1
22/7/09	4.0	4.0	3.7	N/A	4.4
27/8/09	2.4	2.3	2.4	0.0	4.1
29/9/09	6.5	6.1	6.2	0.4	6.1
8/10/09	4.5	4.2	4.1	0.7	10.9
3/11/09	2.8	3.2	3.9	3.5	2.9
1/12/09	6.7	7.1	5.0	1.3	6.4
2/2/10	5.5	6.2	5.7	1.1	11.2
18/3/10	7.1	7.0	7.3	0.4	14.6
22/4/10	7.2	5.5	7.0	5.5	11.2
20/5/10	5.3	5.0	4.7	0.2	10.8
17/6/10	1.7	1.3	1.2	0.0	8.8
15/7/10	1.6	1.0	1.1	**42.7**	4.3
19/8/10	2.9	2.6	2.3	N/A	6.0

N/A not available; 4: Hollow; 5: outlet Blind Beck catchment

Table D2-2 Summary of DOC in stream water results at sampling site 1 to 5

Date	1	2	3	4	5
	DOC (mg/l)				
23/4/09	5.0	7.2	3.5	N/A	N/A
06/5/09	4.6	5.6	5.6	N/A	12.9
25/6/09	7.0	6.9	10.9	N/A	6.3
22/7/09	13.9	18.4	19.4	N/A	16.9
27/8/09	6.9	7.6	7.7	6.11	15.2
29/9/09	6.2	7.8	12.8	4.12	6.2
8/10/09	10.9	16.4	14.7	1.5	3.5
3/11/09	12.6	14.7	13.8	18.4	13.5
1/12/09	3.1	2.5	2.2	6.9	2.4
2/2/10	10.0	8.2	7.1	9.1	2.4
18/3/10	18.8	18.5	17.3	0.4	13.9
22/4/10	13.6	12.9	11.5	14.8	10.1
20/5/10	20.0	17.0	18.2	16.1	16.1
17/6/10	19.3	15.6	16.1	**105.9**	14.7
15/7/10	32.5	21.0	19.5	**39.4**	22.1
19/8/10	15.7	15.1	15.9	15.9	10.4

N/A not available; 4: Hollow; 5: outlet Blind Beck catchment

Appendix D3 Sediment size distribution curves

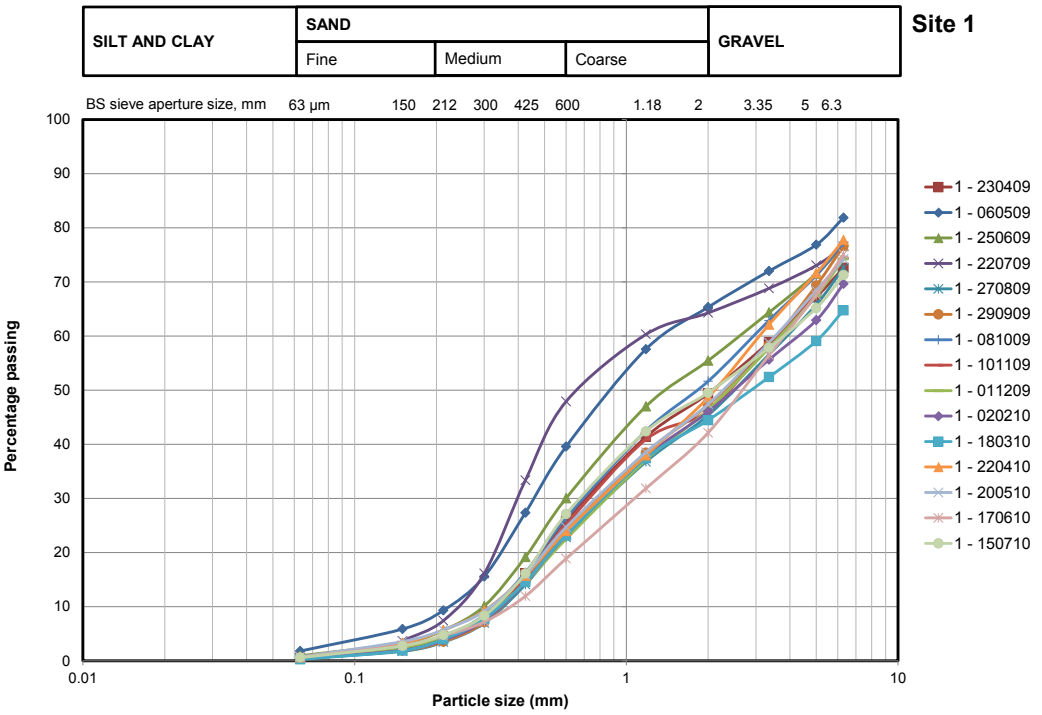

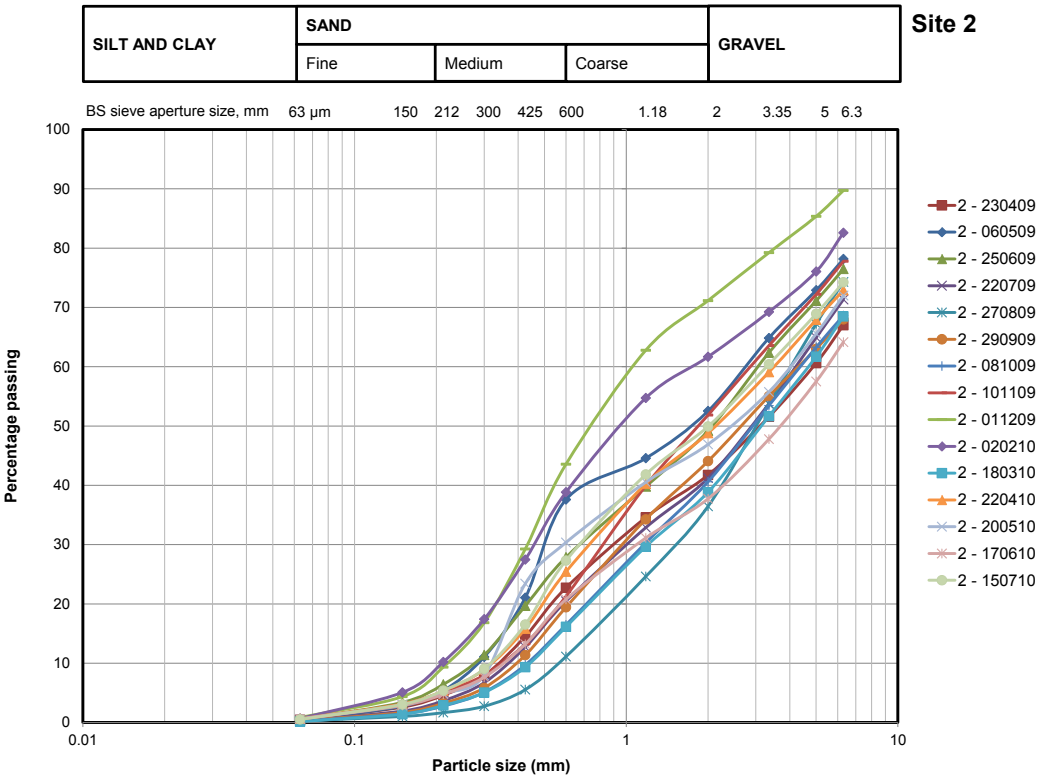

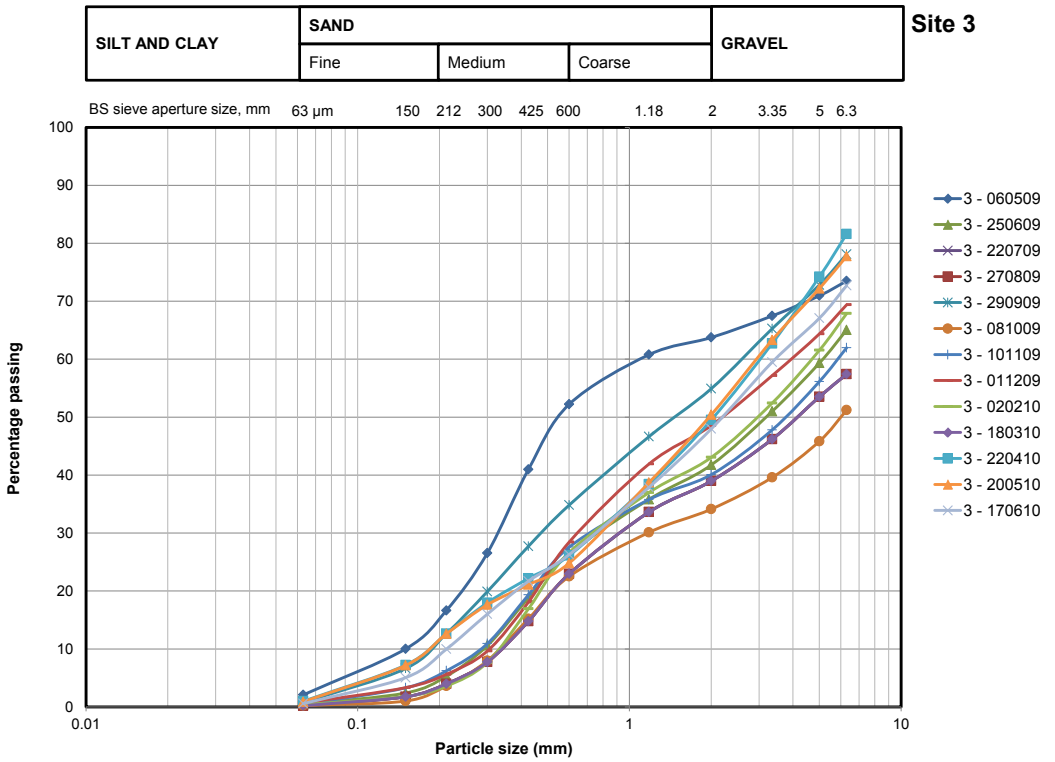
SILT AND CLAY
SAND
Fine
Medium
Coarse
GRAVEL
Site 3
BS sieve aperture size, mm
63 µm
150
212
300
425
600
1.18
2
3.35
5
6.3
Percentage passing
Particle size (mm)
3 - 060509
3 - 250609
3 - 220709
3 - 270809
3 - 290909
3 - 081009
3 - 101109
3 - 011209
3 - 020210
3 - 180310
3 - 220410
3 - 200510
3 - 170610

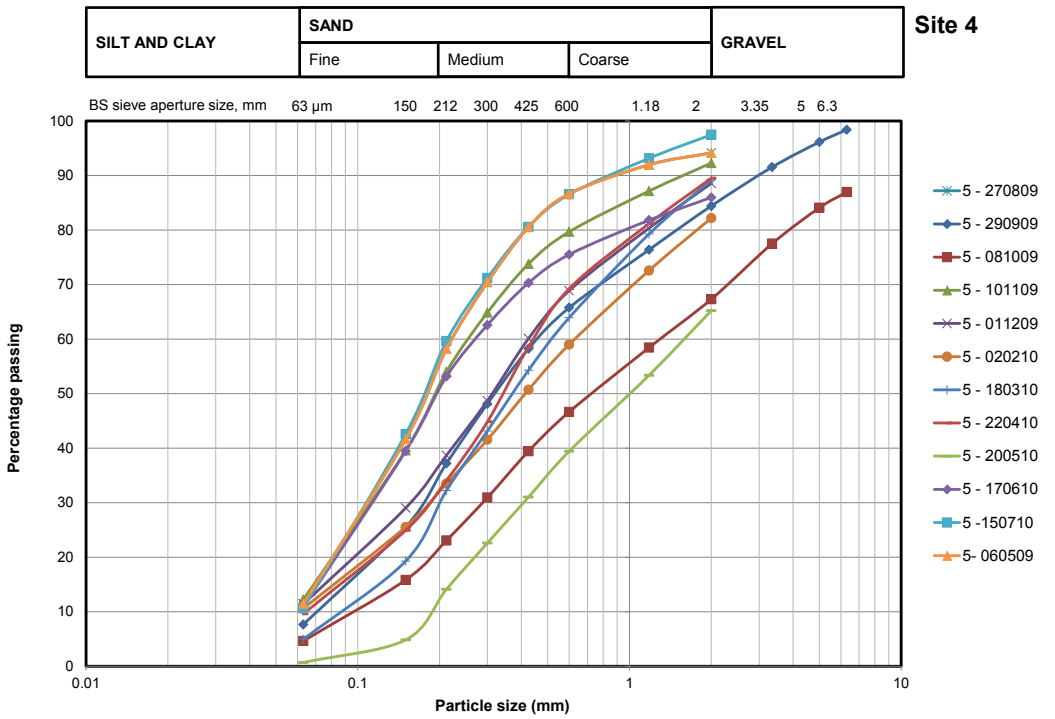
SILT AND CLAY
SAND
Fine
Medium
Coarse
GRAVEL
Site 4
BS sieve aperture size, mm
63 µm
150
212
300
425
600
1.18
2
3.35
5
6.3
Percentage passing
Particle size (mm)
5 - 270809
5 - 290909
5 - 081009
5 - 101109
5 - 011209
5 - 020210
5 - 180310
5 - 220410
5 - 200510
5 - 170610
5 -150710
5- 060509

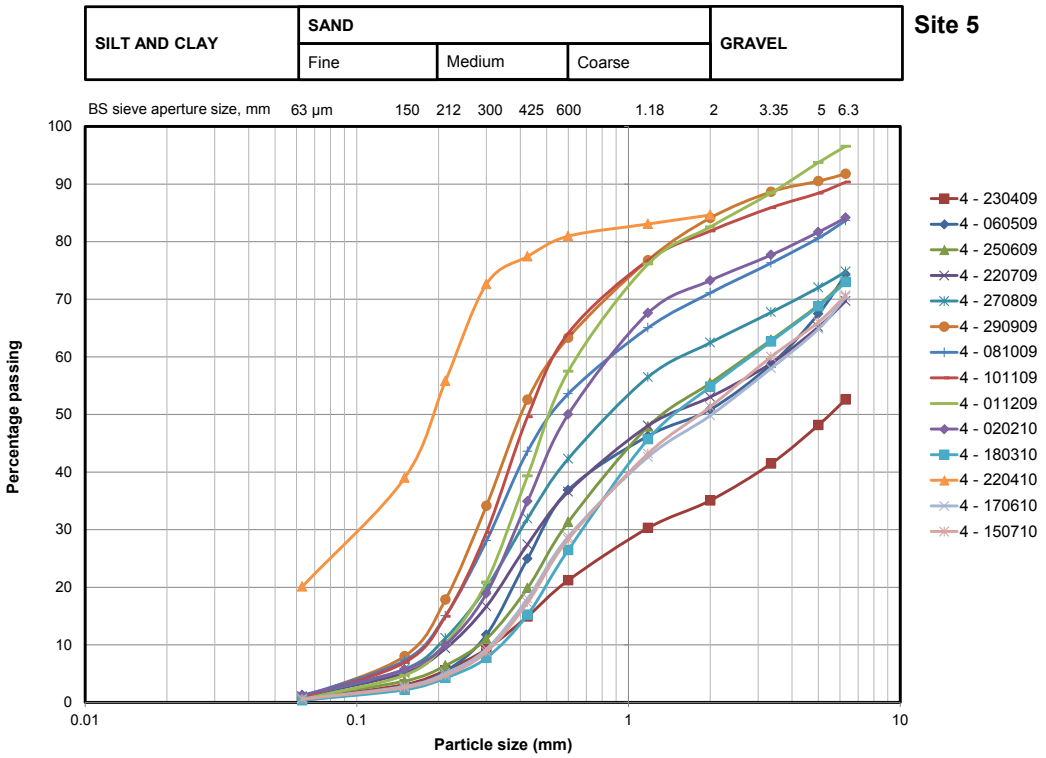
SILT AND CLAY
SAND
Fine
Medium
Coarse
GRAVEL
Site 5
BS sieve aperture size, mm
63 µm
150
212
300
425
600
1.18
2
3.35
5
6.3
Percentage passing
Particle size (mm)
0.01
0.1
1
10
4 - 230409
4 - 060509
4 - 250609
4 - 220709
4 - 270809
4 - 290909
4 - 081009
4 - 101109
4 - 011209
4 - 020210
4 - 180310
4 - 220410
4 - 170610
4 - 150710

Appendix D4 Analysis of TOC and TN in sediments within Blind Beck and Hollow

Table D4-1 Summary of TOC in sediments at sampling site 1 to 5

Date	1	2	3	4	5
	TOC (wt%)				
23/4/09	0.31	0.37	N/A	N/A	0.36
06/5/09	0.41	0.37	0.66	N/A	0.31
25/6/09	0.33	0.30	0.23	N/A	0.53
22/7/09	0.28	0.29	0.32	N/A	0.43
27/8/09	0.58	1.01	0.55	1.44	0.64
29/9/09	0.56	0.59	0.61	2.03	0.44
8/10/09	0.37	0.61	0.54	1.68	0.59
3/11/09	0.47	1.03	0.59	1.99	0.50
1/12/09	0.35	0.99	1.01	2.35	0.34
2/2/10	0.37	0.77	0.47	2.36	1.01
18/3/10	0.45	0.53	0.50	2.06	0.60
22/4/10	0.90	0.87	0.78	1.80	0.84
20/5/10	1.07	0.95	0.64	2.25	0.93
17/6/10	0.90	1.04	0.54	2.02	0.92
15/7/10	0.82	0.77	0.55	2.21	1.09
19/8/10	0.65	0.82	0.56	N/A	1.26

N/A not available; 4: Hollow; 5: outlet Blind Beck catchment

Table D4-2 Summary of TN in sediments at sampling site 1 to 5

Date	1	2	3	4	5
	TN (wt%)				
23/4/09	0.05	0.05	0.05	N/A	0.05
06/5/09	0.03	0.03	0.03	N/A	0.03
25/6/09	0.03	0.03	0.03	N/A	0.03
22/7/09	0.06	0.06	0.06	N/A	0.06
27/8/09	0.05	0.05	0.05	0.16	0.05
29/9/09	0.04	0.04	0.04	0.21	0.04
8/10/09	0.08	0.08	0.08	0.23	0.07
3/11/09	0.12	0.12	0.12	0.23	0.08
1/12/09	0.14	0.14	0.14	0.27	0.14
2/2/10	0.07	0.07	0.07	N/A	0.07
18/3/10	0.06	0.06	0.06	0.27	0.06
22/4/10	0.02	0.02	0.02	0.24	0.02
20/5/10	0.12	0.12	0.12	0.18	0.13
17/6/10	0.14	0.14	0.14	0.12	0.12
15/7/10	0.15	0.15	0.15	0.13	0.14
19/8/10	0.17	0.17	0.17	0.18	0.24

N/A not available; 4: Hollow; 5: outlet Blind Beck catchment

Appendix E1 Analysis of major ions in the overland and subsurface flow within the hillslope

Table E1-1 Summary of the overland flow water results for the perturbed plot (A)

Date	pH	Na^+	K^+	Ca^{2+}	Mg^{2+}	HCO_3^-	Cl^-	SO_4^{2-}	NO_3^-	Charge balance
		mg/l								%
22/7/09	7.1	5.8	3.5	7.0	1.4	30.5	8.3	4.4	1.0	-2.1
6/8/09	6.6	4.6	4.1	3.7	1.0	11.9	7.8	12.3	1.5	-9.8
29/9/09	6.4	3.6	3.3	4.6	1.1	15.7	7.1	3.9	4.5	-4.5
8/10/09	6.2	5.3	9.3	6.7	1.8	22.9	14.6	6.1	0.5	1.4
3/11/09	5.8	3.6	2.7	2.9	0.7	3.5	7.6	2.3	2.7	8.3
1/12/09	6.5	9.5	5.3	8.4	2.7	20.5	15.9	5.8	0.9	-11.1
2/2/09	7.2	5.0	2.7	5.4	1.6	17.2	17.1	2.5	3.2	-11.6
18/3/09	6.7	4.3	3.2	3.7	1.0	10.8	6.4	2.8	1.2	10.4
22/4/09	6.9	4.0	1.9	2.2	0.6	6.41	9.8	3.4	1.9	-11.5
20/5/09	N/A	N/A	N/A	N/A	N/A	N/A	N/A	N/A	N/A	N/A
17/6/09	N/A	N/A	N/A	N/A	N/A	N/A	N/A	N/A	N/A	N/A
15/7/09	6.9	3.5	6.0	8.4	1.6	26.3	7.7	6.3	0.6	3.9
19/08/09	6.5	2.0	4.5	3.9	1.1	10.3	7.0	1.7	2.1	6.02

N/A not available

Table E1-2 Summary of the overland flow water results for the control plot (C)

Date	pH	Na^+	K^+	Ca^{2+}	Mg^{2+}	HCO_3^-	Cl^-	SO_4^{2-}	NO_3^-	Charge balance
		mg/l								%
22/7/09	6.3	6.9	8.0	6.4	1.8	24.7	11.3	2.5	0.0	11.2
6/8/09	6.0	6.0	5.6	5.2	1.4	19.3	11.3	4.7	1.4	3.8
29/9/09	6.7	5.7	6.2	3.9	1.0	11.7	10.2	2.5	2.5	7.8
8/10/09	6.7	5.7	7.3	2.1	0.8	14.6	12.0	3.1	1.5	-4.9
3/11/09	6.6	6.6	5.4	2.7	1.0	10.2	11.4	3.6	4.0	1.1
1/12/09	5.8	7.4	3.4	1.1	0.4	8.3	7.7	2.1	1.3	9.14
2/2/09	7.2	4.5	1.7	0.8	0.4	5.6	8.2	1.5	2.0	-10.6
18/3/09	6.3	2.5	1.0	2.5	0.6	5.2	7.0	2.6	2.1	-10.6
22/4/09	7.0	1.6	0.6	1.1	0.2	0.9	4.5	1.1	1.0	-5.5
20/5/09	6.7	1.1	1.3	4.9	1.1	9.6	4.5	5.8	0.3	5.9
17/6/09	6.8	1.2	0.7	1.6	0.5	5.4	4.5	0.9	0.0	-9.9
15/7/09	6.3	4.8	6.3	5.7	1.6	18.5	13.5	2.6	0.0	2.7
19/08/09	6.9	2.7	2.7	3.4	1.1	11.0	6.8	1.9	0.1	3.8

N/A not available

Table E1-3 Summary of the subsurface flow water results (10 cm) for the perturbed plot

Date	pH	Na^+	K^+	Ca^{2+}	Mg^{2+}	HCO_3^-	Cl^-	SO_4^{2-}	NO_3^-
		mg/l							
18/3/09	6.2	6.9	1.3	9.4	1.8	6.8	16.7	4.9	5.9
22/4/09	6.2	0.5	1.5	7.4	2.7	6.8	4.6	7.2	3.2
20/5/09	7.4	3.9	1.1	6.7	1.1	9.1	5.4	7.3	1.9
17/6/09	6.4	4.2	2.1	7.0	1.1	5.6	2.4	3.9	0.4
15/7/09	N/A	N/A	N/A	N/A	N/A	N/A	N/A	N/A	N/A
19/08/09	6.1	3.0	0.8	6.6	1.0	5.2	1.9	1.2	0.3

N/A not available

Table E1-4 Summary of the subsurface flow water results (18 cm) for the perturbed plot

Date	pH	Na^+	K^+	Ca^{2+}	Mg^{2+}	HCO_3^-	Cl^-	SO_4^{2-}	NO_3^-
		mg/l							
21/10/09	6.1	10.9	1.4	10.7	1.9	6.9	12.1	7.6	7.5
3/11/09	5.9	4.9	0.5	9.8	1.7	5.3	4.6	5.6	4.1
11/11/09	6.2	5.6	1.2	11.3	2.0	16.2	5.5	5.2	1.2
1/12/09	6.1	5.2	0.9	10.6	1.8	10.8	5.0	5.4	2.6
2/2/09	6.0	2.5	0.6	2.4	0.4	2.9	2.9	0.9	0.0
18/3/09	5.9	3.4	0.4	10.0	1.4	3.2	9.5	6.6	4.3
22/4/09	6.2	7.0	0.4	7.4	1.5	7.7	14.9	13.2	0.0
20/5/09	7.2	2.2	0.3	3.6	0.6	5.8	1.6	2.5	0.2
17/6/09	7.0	2.5	0.3	20.0	0.9	16.9	4.2	8.3	1.4
15/7/09	7.1	7.5	1.1	13.7	2.1	16.9	N/A	N/A	0.0
19/08/09	5.7	2.1	0.3	5.0	0.7	2.0	1.6	0.9	0.0

N/A not available

Table E1-5 Summary of the subsurface flow water results (10 cm) for the control plot

Date	pH	Na^+	K^+	Ca^{2+}	Mg^{2+}	HCO_3^-	Cl^-	SO_4^{2-}	NO_3^-
		mg/l							
18/3/09	6.3	3.0	0.4	4.2	0.7	5.7	5.0	2.8	2.1
22/4/09	6.3	2.4	0.3	3.8	0.6	6.8	3.7	3.1	0.9
20/5/09	7.2	3.5	0.4	4.1	0.7	7.0	5.2	5.9	1.9
17/6/09	N/A	N/A	N/A	N/A	N/A	N/A	N/A	N/A	N/A
15/7/09	N/A	N/A	N/A	N/A	N/A	N/A	N/A	N/A	N/A
19/08/09	5.9	1.8	0.5	4.3	0.7	3.4	2.1	0.7	0.9

N/A not available

Table E1-6 Summary of the subsurface flow water results (18 cm) for the control plot

Date	pH	Na^+	K^+	Ca^{2+}	Mg^{2+}	HCO_3^-	Cl^-	SO_4^{2-}	NO_3^-
		mg/l							
18/3/09	6.2	2.9	0.5	6.1	1.0	6.3	7.8	3.4	1.0
22/4/09	6.1	2.8	0.3	6.6	1.0	6.5	7.0	4.8	0.6
20/5/09	7.0	2.1	0.3	4.1	0.5	7.4	2.0	2.5	0.2
17/6/09	N/A	N/A	N/A	N/A	N/A	N/A	N/A	N/A	N/A
15/7/09	N/A	N/A	N/A	N/A	N/A	N/A	N/A	N/A	N/A
19/08/09	5.8	2.1	0.4	4.2	0.6	1.8	1.7	1.3	0.2

N/A not available

Appendix E2 Analysis of DOC and NO_3^- in the overland and subsurface flow within the hillslope

Table E2-1 Summary of DOC and NO_3^- in the overland flow water

Date	Perturbed plot	Control plot	Perturbed plot	Control plot
	DOC (mg/l)		NO_3^- (mg/l)	
22/7/09	15.9	16.4	1.1	1.0
06/8/09	18.2	18.8	1.5	1.4
27/8/09	10.2	16.0	1.1	2.5
29/9/09	9.1	12.6	4.5	5.5
8/10/09	9.5	12.1	0.5	1.5
3/11/09	8.9	12.1	4.7	6.8
1/12/09	11.2	8.3	0.9	1.3
2/2/10	8.5	3.8	3.2	2.0
18/3/10	10.1	8.4	8.1	2.1
22/4/10	9.3	6.2	1.9	1.0
20/5/10	N/A	11.7	0.2	0.3
17/6/10	N/A	13.7	N/A	0.0
15/7/10	22.9	23.9	N/A	0.0
19/8/10	10.4	9.3	2.1	0.1

N/A not available

Table E2-2 Summary of DOC and NO_3^- in soil water solution

Date	Perturbed plot		Control plot		Perturbed plot		Control plot	
	10 cm	18 cm	10 cm	18 cm	10 cm	18 cm	10 cm	18 cm
	DOC (mg/l)				NO_3^- (mg/l)			
8/10/09	Not measured	46.4	Not measured	Not measured	Not measured	7.5	Not measured	Not measured
3/11/09		30.7				2.6		
1/12/09		4.8				0.0		
2/2/10		N/A				N/A		
18/3/10	8.5	13.8	5.4	4.1	5.9	4.3	2.1	1.0
22/4/10	15.3	19.4	11.6	10.1	3.2	0.00	0.9	0.6
20/5/10	26.8	19.6	18.4	11.7	1.9	0.2	1.9	0.3
17/6/10	31.6	22.1	N/A	N/A	0.3	1.4	N/A	N/A
15/7/10	N/A	30.4	N/A	N/A	0.0	0.0	N/A	N/A
19/8/10	26.2	28.1	23.1	21.7	0.3	0.0	0.9	0.2

N/A not available